Springer Transactions in Civil
and Environmental Engineering

T. G. Sitharam
Amarnath M. Hegde
Sreevalsa Kolathayar *Editors*

Geocells

Advances and Applications

Springer

Springer Transactions in Civil and Environmental Engineering

Springer Transactions in Civil and Environmental Engineering (STICEE) publishes the latest developments in Civil and Environmental Engineering. The intent is to cover all the main branches of Civil and Environmental Engineering, both theoretical and applied, including, but not limited to: Structural Mechanics, Steel Structures, Concrete Structures, Reinforced Cement Concrete, Civil Engineering Materials, Soil Mechanics, Ground Improvement, Geotechnical Engineering, Foundation Engineering, Earthquake Engineering, Structural Health and Monitoring, Water Resources Engineering, Engineering Hydrology, Solid Waste Engineering, Environmental Engineering, Wastewater Management, Transportation Engineering, Sustainable Civil Infrastructure, Fluid Mechanics, Pavement Engineering, Soil Dynamics, Rock Mechanics, Timber Engineering, Hazardous Waste Disposal Instrumentation and Monitoring, Construction Management, Civil Engineering Construction, Surveying and GIS Strength of Materials (Mechanics of Materials), Environmental Geotechnics, Concrete Engineering, Timber Structures.

Within the scopes of the series are monographs, professional books, graduate and undergraduate textbooks, edited volumes and handbooks devoted to the above subject areas.

More information about this series at http://www.springer.com/series/13593

T. G. Sitharam · Amarnath M. Hegde ·
Sreevalsa Kolathayar
Editors

Geocells

Advances and Applications

Springer

Editors
Prof. T. G. Sitharam
Department of Civil Engineering
Indian Institute of Technology
Guwahati (IITG)
Guwahati, Assam, India

Amarnath M. Hegde
Department of Civil and Environmental Engineering
Indian Institute of Technology Patna
Patna, Bihar, India

Sreevalsa Kolathayar
Department of Civil Engineering
National Institute of Technology Karnataka
Mangalore, Karnataka, India

ISSN 2363-7633 ISSN 2363-7641 (electronic)
Springer Transactions in Civil and Environmental Engineering
ISBN 978-981-15-6094-1 ISBN 978-981-15-6095-8 (eBook)
https://doi.org/10.1007/978-981-15-6095-8

This Springer imprint is published by the registered company Springer Nature Singapore Pte Ltd.
The registered company address is: 152 Beach Road, #21-01/04 Gateway East, Singapore 189721, Singapore

Preface

Geocells are three-dimensional expandable panels made of high-density polymers. Nowadays, these materials are extensively used in the various geotechnical engineering applications, namely foundations, pavements, railways, embankments, slopes and retaining walls. These futuristic materials can provide cost-effective and sustainable solutions to existing soft soil problems. With the application of the geocells which are growing at the rapid rate, it is necessary to summarize all the important findings till date in the form of a book. This book covers the past findings and the current state of the art related to geocell with the inclusion of the sufficient number of case studies. The chapters are contributed by the renowned experts from the different countries. The contents are designed to provide all the relevant geocell-related information to the academicians, students and the practising engineers. Incidentally, this book happened to be the first book on the geocell technology till date.

In total, this book comprised 18 chapters related to geocells. These chapters have been presented in two parts. The first part contains the chapters covering the introduction, current state of the art, and design and construction practices of the geocell technology. It also contains various contributory chapters covering the different applications of the geocells in the form of foundations, embankment, railways, pavements, machine foundations, protection of buried pipelines, etc. The second part covers the chapters related to the use of the natural fibres like bamboo, coir and areca leaves in the geocell technology and its applications. At the end, a list of leading geocell manufacturers has been provided for the benefit of users.

I would like to express my gratitude to my co-authors, Dr. Amarnatha Hegde and Dr. Sreevalsa Kolathayar, for their fantastic efforts in bringing out this unique book on geocells. I would also like to express my gratitude to all the authors who responded positively and contributed their chapters on time. I also place on record my thanks to all my students who contributed indirectly to the wealth of the knowledge on geocells.

Guwahati, India
June 2019

Prof. T. G. Sitharam

Contents

Editors and Contributors

About the Editors

Prof. Dr. T. G. Sitharam is the Director of Indian Institute of Technology Guwahati and Senior Professor in the Department of Civil Engineering, Indian Institute of Technology Guwahati (IITG). He was the founder Chairman of the Center for Infrastructure, Sustainable Transport and Urban Planning (CiSTUP) at IISc. He is presently the Chairman of the AICTE South Western Zonal Committee, Regional office at Bengaluru and President of the Indian Society for Earthquake Technology (ISET). He is the founder President of the International Association for Coastal Reservoir Research (IACRR). He was a Visiting Professor at Yamaguchi University, Japan, University of Waterloo, Waterloo, ON, Canada; University of Dalhousie, Halifax, Canada; and ISM Dhanbad, Jharkhand. Prof. Sitharam has obtained his BE(Civil Engg) from Govt BDT College of Engineering from Mysore University, India in 1984, Masters in Civil Engineering from Indian Institute of Science, Bangalore in 1986 and Ph.D. in Civil Engineering from University of Waterloo, Waterloo, Ontario, Canada in 1991 in the area of geomechanics. Further, he was a Research Scientist at center for earth sciences and engineering, University of Texas at Austin, Texas, USA until 1994. Over the last 25 years, he has carried out seismic microzonation of urban centers in India and developed innovative technologies in the area of seismic hazard, liquefaction, fracturing and geotechnical applications, leading to about 500 technical papers, Ten books, four patents, 125 consulting projects and two startup companies. He is the chief editor of two international journals (International Journal of Geotechnical Earthquake Engineering from IGI Global and Chief editor, Springer Transactions in Civil and Environmental Engineering). Prof. TG Sitharam has guided 30 Ph.D. students, 25 post-doctoral students, 35 M Tech students and presently he has 8 doctoral students working with him.

Dr. Amarnath M. Hegde is working as Assistant Professor in the Department of Civil and Environmental Engineering at Indian Institute of Technology Patna. He obtained his Ph.D. from Indian Institute of Science Bangalore, in 2015. Previously, Dr. Hegde has held the short term research positions at University of Milan Bicocca in Italy, UPC, Barcelona Tech in Spain and National University of Singapore. Before Ph.D, he has also worked as a geotechnical Engineer in Keller Ground Engineering India Pvt. Ltd in Mumbai for two years. He completed his M. Tech from Indian Institute of Technology Bombay and B. Tech from BVBVET Hubli in Karnataka. Dr. Hegde has published one book and more than 50 research papers in reputed International/national journals and conferences. He is a life member of several professional organizations. Currently, Dr. Hegde is a member of the Technical Committee on Reinforced Fill Structures (TC-218), International Society of Soil Mechanics and Geotechnical Engineering (ISSMGE) UK. He is also the member of Technical Committee on 'Geosynthetics' of Geo-Institute of American Society of Civil Engineers. He is the recipient of the prestigious Young Engineers Award in Civil Engineering Discipline by Institution of Engineers (India) in 2017. He has also received the prestigious Marie Curie Fellowship by European Union consecutively for two terms. Apart from these, Dr. Hegde has also received IGS-Prof. Leonard's award for best Ph.D thesis in geotechnical Engineering. He has also received several best paper awards and travel grants from the reputed organizations. He is the reviewer of the several leading International journals in the field of geotechnical engineering and sustainable construction practices.

Dr. Sreevalsa Kolathayar pursued M.Tech from IIT Kanpur, Ph.D. from Indian Institute of Science (IISc) and served as International Research Staff at UPC BarcelonaTech Spain. He is presently Assistant Professor in the Department of Civil Engineering, National Institute of Technology Karnataka, Surathkal, India. Dr. Sreevalsa has authored three books and over 60 research papers. He is Editorial Board member of two International Journals and acts as a reviewer for many leading international journals. His research interests include Seismic Hazard Assessment, Local Site effects, Liquefaction, Disaster Risk Reduction, Sustainable construction, Geogrids and Geocells, and Water geotechnics. He served as Chairman of Students Council at IISc and Adviser to Think India, a national forum of students from premier Institutes in India. He is currently the Secretary Indian chapter of International Association for Coastal Reservoir Research (IACRR), and Executive Committee Member of Indian Society of Earthquake Technology. In 2017, The New Indian Express honored Dr. Sreevalsa with the Edex award: 40 under 40 - South India's Most Inspiring Young Teachers. He is the recipient of ISET DK Paul Research Award from Indian Society of Earthquake Technology, IIT Roorkee in 2018. He is in the roster of two technical committees of ASCE Geo-Institute. He received "IEI Young Engineers Award" by The Institution of Engineers (India), in recognition of his contributions in the field of Civil Engineering.

About the Contributors

Dr. K. Balan had B.Sc. (Engg.) from University of Kerala in 1982, had Ph.D. from IIT Delhi in 1996 and worked as a faculty in the Directorate of Technical Education, Government of Kerala since 1986 and retired as Professor in civil engineering from College of Engineering Trivandrum. He served as Managing Director of Kerala State Coir Corporation Ltd., Alappuzha, as the first Director of National Coir Research and Management Institute, Trivandrum. He worked as the R&D Manager of Alyaf Industrial Company (Geotextile Manufacturing Company), Kingdom of Saudi Arabia. He is a former Director of Centre for Engineering Research and Development (CERD), APJ Abdul Kalam Technological University, Kerala.

He has published more than 150 papers in reputed international and national journals and conferences. He is bestowed with "Life Time Achievement Award" from Indian Chapter of International Geosynthetics Society for the contributions made in the development of geotextiles in India, especially coir. Indian Society for Technical Education has conferred the national award of "Best Engineering College Teacher from Kerala". He has published two books on coir geotextiles and one book on design engineering. He has contributed chapters on natural geotextiles in various books. He is President of Indian Geotechnical Society, Trivandrum Chapter. He is a technical member in the Expert Committee for Pattissery Earth Dam, Government of Kerala. He is a member of the Sub-group of Rural Roads Committee (H-5) of IRC for use of coir geotextiles in construction of rural roads.

Dr. Arghadeep Biswas is Assistant Professor in the Department of Civil Engineering of Jalpaiguri Government Engineering College (Established on 1961). He has received doctoral degree from the Indian Institute of Technology Guwahati (IIT Guwahati) and pursued postgraduation from the Indian Institute of Technology Kharagpur (IIT Kharagpur) in geotechnical engineering, after his graduation from Jadavpur University in civil engineering. His research area focused on "ground improvement techniques" emphasizing the "geocell-reinforced foundations". He has demonstrated his expertise and contribution on geocell-reinforced systems through a number of publications. Dr. Biswas is actively involved in national and international societies concerned with civil engineering, especially geotechnical engineering. He is also an active reviewer to several international and national journals and conferences of repute. In addition to academics, he is also an active consultant in the area of geotechnical engineering.
e-mail: arghadeep.biswas@gmail.com

Dr. Kaustav Chatterjee is Assistant Professor in the Department of Civil Engineering of IIT Roorkee since 20 June 2016. He has pursued his M.Tech. and Ph.D. from IIT Bombay and postdoctoral research from Graduate School of Agriculture, Kyoto University, Japan. He has worked extensively in the field of dynamic analysis of pile foundations in liquefiable and non-liquefiable soil and published research papers in excellent peer-reviewed journals. His research interest

includes geotechnical earthquake engineering, foundation engineering, soil dynamics, ground improvement, among others. He is a recipient of University Gold Medal and Debjani Dasgupta Memorial Gold Medal in B.Tech. from West Bengal University of Technology; Best Ph.D. Thesis award from IIT Bombay; Prof. G. A. Leonard's Best Ph.D. Thesis Award from Indian Geotechnical Society (IGS), New Delhi, for calendar years 2015 and 2016; Prof. John Carter Award for Young Researchers from International Association for Computer Methods and Advances in Geomechanics (IACMAG), USA; and IGS-Kochi Chapter YGE Best Paper Biennial Award—2018 on Deep Foundations. At present, he is supervising three Ph.D. and two M.Tech. students, and three M.Tech. students have already graduated. He is a member of various professional societies like Indian Geotechnical Society, Indian Society of Earthquake Technology, International Society for Soil Mechanics and Geotechnical Engineering, American Society of Civil Engineers and The Indian Science Congress Association.
e-mail: kchatfce@iitr.ac.in

Dr. Sujit Kumar Dash is currently Professor in the Department of Civil Engineering, Indian Institute of Technology Kharagpur, India. He is a geotechnical engineer by profession and obtained Ph.D. for his work on geocell-reinforced foundations, in the year 2001, from the Indian Institute of Technology Madras. He was a visiting fellow at the Technical University of Munich, Germany, and University of Wollongong, Australia. He has received the German Academic Exchange Service Fellowship and the Australian Endeavour Research Fellowship. He has published more than 80 papers in various journals and peer-reviewed conference proceedings. His papers on geosynthetics and allied construction products have received the Indian Geotechnical Society best paper award.

Dr. Sakdirat Kaewunruen has extensive industry experience in the fields of structural, civil and railway track engineering both in industry and in academia. With over 14 years in rail industry and regulatory environments prior to joining academia in 2014, he has a wide variety of specializations, including rail engineering, track design, track components, structural and geotechnical engineering, maintenance and construction. He is a chartered engineer in both civil and structural colleges, and has research and practical experience internationally in railway systems and infrastructure engineering. His professional work had involved many industry projects worth over £5 billion and has supervised/participated in railway research projects worth over £8 million (in Australia, UK, Japan, USA, Sweden, China, Malaysia and Thailand). His industry and research work has won him numerous international and domestic awards. A few recent awards include Stephenson's Best Paper Award (2017), Institute of Structural Engineers Midlands' Research Award (2016) and Japan Society for the Promotion of Sciences Long-term Fellowship (2015–2016). He has membership in EU-Cost Actions: TU1404 (Towards the next generation of standards for service life of cement-based materials and structures), CA15125 (Designs for noise reducing materials and structures), CA15202 (Self-healing as preventive repair of concrete structures) and

TU1409 (Mathematics for industry network). He is the UK Principal Scientist in ISO and BSI standard committees for railway sleepers (using concrete, plastic and composite materials) and recycling of rolling stocks. He successfully coordinates EU-funded RISEN and is a CI of S-CODE. He is also a committee member of Concrete Society Midlands and is Chief Editor of Frontiers in Transportation and Transit Systems.

Lt. Col. Anand Kumar has done his B.Tech. from College of Military Engineering, Pune, in 2004, and M.Tech. in geotechnical engineering from IIT Roorkee during 2016–2018. He is serving in Corps of Engineers of Indian Army and has been associated with different combat engineering works. He has worked extensively on improving trafficability in desert terrain using geocells. His research areas involve geosynthetics and cold weather concreting.
e-mail: anand_engrs@rediffmail.com

Gholamhosein Tavakoli Mehrjardi Ph.D. is Assistant Professor of experimental soil mechanics at Kharazmi University. His research interests include geosynthetics reinforcement, buried pipelines, recycled materials, slope stability, transportation geotechnics, physical modelling and laboratory testing. He conducted his doctoral project at K.N. Toosi University of Technology on the protection of buried pipes under heavy cyclic loading by using geocell and recycled rubbers, bringing about an efficient protecting system which the major deformations plummeted. The main part of his Ph.D. thesis was carried out at Nottingham Transportation Engineering Centre in University of Nottingham. Furthermore, Gholamhosein has been working on a plenty of numerical simulations by the use of different software, notably FLAC, Plaxis, GeoSlope and ANSYS.

Dr. A. Murali Krishna is a faculty member in the Department of Civil Engineering at the Indian Institute of Technology (IIT) Guwahati, since 2008. He obtained doctoral degree from the Indian Institute of Science Bangalore, M.Tech. from IIT Kanpur and B.Tech. from Sri Venkateswara University, Tirupati. His research interests include earthquake geotechnics; geosynthetics and ground improvement; site characterization; and numerical and physical modelling of geotechnical structures. He supervised six doctoral students and 22 Master's students. He co-authored nearly 160 publications of technical papers in international/national journals and conference/seminar proceedings including book chapters. He is a recipient of BRNS Young Scientist Research award, BOYSCAST fellowship and HERTAGE fellowship. He is an executive member of ISRM, India, and ISET. He is also a member of TC 203 of ISSMGE, since 2011. He organized national and international workshops and short courses. He is a reviewer for several national and international journals.

Dr. Asha M. Nair has completed her Ph.D. from the Indian Institute of Science, Bangalore, in civil engineering. In her research, she has investigated the behaviour of geosynthetic-reinforced soil-aggregate systems under static, repeated and dynamic loads. Post Ph.D., she served as a senior research fellow in the Indian Institute of Science and was involved in establishing fatigue testing facility in the

Department of Civil Engineering at IISc. She has obtained her M.Tech. from the National Institute of Technology, Calicut, Kerala, and B.Tech. from T.K.M College of Engineering, Kollam, Kerala. She has received gold medals for academic excellence in the B.Tech. course. She has also secured second rank in University of Kerala for B.Tech. course and stood first in Calicut University for M.Tech. course too. She has received merit scholarships from Kerala government for her academic performance in matriculation and higher secondary examinations. She is a life member of Indian Geotechnical Society, Indian Roads Congress and an associate member of ASCE. She has participated in many national and international conferences and has published papers in peer-reviewed national and international journals.

Dr. Sanjay Nimbalkar (Ph.D., MIEAust, CPEng, NER) completed his Bachelor of Civil Engineering from University of Pune, India. He obtained M.Tech. and Ph. D. in the field of geotechnical engineering from the Indian Institute of Technology Bombay, India. He is currently working as a lecturer in the School of Civil and Environmental Engineering at the University of Technology Sydney, Australia. In the past, he has worked as a research fellow in the ARC Center of Excellence for Geotechnical Sciences and Engineering, Australia. He is a chartered professional engineer and involved in a number of contract research, testing and consultancy projects in Australia and India. He has published a number of research papers in peer-reviewed journals and conference proceedings. He is the recipient of Institution of Civil Engineer's (ICE) Thomas Telford Premium Award 2014 for the best paper in the category of ground improvement. He is a member of International Society of Soil Mechanics and Geotechnical Engineering (ISSMGE), Australian Geomechanics Society (AGS), including other technical societies of Engineers Australia. He has received certificates of excellence and outstanding contribution in reviewing from many SCI-indexed journals. He serves on the editorial board of various international journals including Transportation and Transit Systems, International Journal of Geosynthetics and Ground Engineering, among others.
e-mail: Sanjay.Nimbalkar@uts.edu.au

Mr. S. B. Prasath was a M.Tech. student in the Department of Civil Engineering at the Indian Institute of Technology Guwahati. Currently, he is working as Assistant Professor in Bannari Amman Institute of Technology, Sathyamangalam, Tamil Nadu. He completed his Bachelor's degree in the Department of Civil Engineering from Anna University. He has 4 years of field experience in the construction of high-rise buildings and industrial buildings. His research interests include performance of ground improvement and geosynthetic applications to pavements.

Piyush Punetha is a Ph.D. research scholar at the University of Technology Sydney (UTS), Australia. His present research is in the field of railway tracks for the high-speed trains. He holds a Bachelor's degree (B.Tech.) in civil engineering from Kumaon Engineering College (KEC), Dwarahat, India, and a Master's degree (M.Tech.) in building engineering and disaster mitigation (BEDM) from the

Academy of Scientific and Innovative Research (AcSIR), New Delhi, India. He worked as Senior Research Fellow in CSIR-Central Building Research Institute (CSIR-CBRI) Roorkee, India, for two years, during which he was involved in several projects related to slope-stability assessment, seismic isolation of structures, liquefaction mitigation, development of innovative foundation for temporary structures, soil–geosynthetic interaction, etc. He is a University Silver Medallist in civil engineering during his Bachelor's degree. He has research publications in reputed peer-reviewed international journals and conferences. He received the Best Paper Award in 6th Indian Young Geotechnical Engineers Conference (6IYGEC-2017), organized by NIT, Trichy, India. His research interests include railway geotechnics, geotechnical earthquake engineering, disaster mitigation, soil–geosynthetic interaction, ground improvement, bio-engineering and constitutive modelling.
e-mail: Piyush.Punetha@student.uts.edu.au

Dr. Vijay Kumar Rayabharapu completed his B.Tech. in civil engineering in 2006 from Kakatiya Institute of Technology and Science, Telangana, India.

He completed his M.S. in civil engineering in 2007 from Florida International University (FIU), Miami, Florida, USA.

He completed his Ph.D. in civil engineering in 2016 from the Indian Institute of Technology Hyderabad (IITH), Hyderabad, Telangana, India.

He has a total working experience of about 10 years which include 9 years of teaching and 1 year of industry.

His research includes studies in geotechnical and transportation engineering using geosynthetics, and his areas of expertise include pavement geotechnics, ground improvement, soil stabilization, instrumentation and energy-efficient materials.

In his sanctioned research project, he is Principal Investigator for the DST project titled "Identification and Demonstration of Cost effective technologies to Maximize Habitat Energy Self-Sufficiency" and was sanctioned for Rs. 2.5 crores on 17 January 2018 in collaboration with IIT Delhi and IIT Roorkee with Rs. 96.35 lakhs for BVRIT Narsapur.

He has authored about 30 international and national journals and conferences.

He is presently working as Associate Professor in the Department of Civil Engineering at B V Raju Institute of Technology, Narsapur, Medak, Telangana.

Dr. Sireesh Saride Ph.D., is currently Professor in the Department of Civil Engineering, Indian Institute of Technology Hyderabad. His expertise and research interests are in the area of pavement geotechnics, geosynthetics and ground improvement. He has graduated from JINT College of Engineering, Kakinada, in 2000, and earned his Master's integrated Ph.D. from the Indian Institute of Science, Bengaluru, in 2006. Prior to joining IIT Hyderabad in 2010, he was a postdoctoral research fellow at the University of Texas at Arlington, during 2006–2010. He has published more than 170 referred journals, conference articles and technical reports. He is currently serving as Associate Editor for the *Journal of Materials in Civil*

Engineering, ASCE and *Journal of Ground Improvement* (ICE). He is a member of American Society of Civil Engineers (ASCE), Institute of Civil Engineers (ICE), Transportation Research Board (TRB); and a life member of Indian Geotechnical Society (IGS) and Indian Roads Congress (IRC).
e-mail: sireesh@iith.ac.in

Mr. Yitzchak Schary, MLA, B.Sc. is a product and training manager at PRS GeoTechnologies, a leading producer of geocell solutions, for more than 10 years, responsible for geocell subject matter expertise and communicating this knowledge internally and externally via all types of formats, media, methods and forums. His areas of interest include geocell technology, product applications, R&D, knowledge management and sustainability. He has served as a consultant for the Ministry of Environment, submitting Israel's national reports to the UN Committee on Sustainable Development, worked as a landscape architect in the private sector and has experience in technical communications and product development of computer-aided design (CAD) for architecture and in other hi-tech industries. He has a Master's of Landscape Architecture from Cornell University, NY, was a visiting Lady Davis Fellow at the Technion—Israel Institute of Technology and has a B.Sc. in Environmental Science from Union College, Schenectady, NY.

Akshay Pratap Singh is a research scholar in the Department of Civil Engineering, Indian Institute of Technology Roorkee, India. He has completed his M.Tech. from the Indian Institute of Technology (Banaras Hindu University) Varanasi, India. He is a member of several professional bodies, including Indian Geotechnical Society, International Society for Soil Mechanics and Geotechnical Engineering, Institution of Engineers (India) and American Society of Civil Engineers. He has worked in the area of reinforced soil and presently working in embedded sheet pile walls.
e-mail: apcl4.dce2017@iitr.ac.in

Professor Seyed Naser Moghaddas Tafreshi graduated from Amirkabir University of Technology with a Ph.D. in geotechnical engineering in 2000. In September 2000, he began his academic career as an assistant professor in the Department of Civil Engineering at K.N. Toosi University of Technology. He has also done one-year (2008–2009) research work at Nottingham Transportation Engineering Centre (NTEC) at the University of Nottingham. He was promoted to the rank of full Professor in 2013.

The main focus of his researches has been in the area of geosynthetic-reinforced beds under monotonic, repeated and dynamic loading using physical modelling, laboratory testing and partly by numerical modelling and analytical methods. He has also been working on the protection of buried pipes, pavement roads, footings, retaining wall, etc. using geosynthetics reinforcement, recycled materials and EPS geofoam material.

Mrs. Divya Viswanath is a postgraduate in geotechnical engineering (M.Tech.) from Visveswaraya Technological University and is currently pursuing Ph.D. She is a civil engineering professional with 3 plus years of industry experience and 5 years of teaching experience. She has been a faculty in CMRIT since 2014 and has guided various B.Tech. student projects in the areas related to geotechnical engineering. She has done her graduation in civil engineering from Mahatma Gandhi University, Kerala. She is a lifetime member of Indian Geotechnical Society. She has completed foundation course on STAAD PRO and is an Autodesk-certified AutoCAD professional. She has also attended and presented papers in national and international conferences.

Contributors

M. N. Asha CMR Institute of Technology, Bengaluru, Karnataka, India

K. Balan Rajadhani Institute of Engineering and Technology, Trivandrum, Kerala, India

Arghadeep Biswas Department of Civil Engineering, Jalpaiguri Government Engineering College, Jalpaiguri, India

Kaustav Chatterjee Indian Institute of Technology Roorkee, Roorkee, India

Sujit Kumar Dash Department of Civil Engineering, Indian Institute of Technology Kharagpur, Kharagpur, India

V. Divya CMR Institute of Technology, Bengaluru, Karnataka, India

Renuka Sai Gadekari Department of Civil Engineering, Amrita Vishwa Vidyapeetham, Coimbatore, India

Akash Gupta Department of Civil Engineering, Indian Institute of Science, Bangalore, India

Amarnath M. Hegde Department of Civil and Environmental Engineering, Indian Institute of Technology Patna, Patna, India

Sakdirat Kaewunruen The University of Birmingham, Birmingham, UK

Sreevalsa Kolathayar Department of Civil Engineering, National Institute of Technology Karnataka, Mangaluru, Karnataka, India

Anand Kumar Indian Institute of Technology Roorkee, Roorkee, India

Seyed Naser Moghaddas Tafreshi Faculty of Civil Engineering, K.N. Toosi University of Technology, Tehran, Iran

A. Murali Krishna Department of Civil and Environmental Engineering, Indian Institute of Technology Tirupati, Tirupati, India

Sanjay Nimbalkar University of Technology Sydney, Sydney, NSW, Australia

S. B. Prasath Department of Civil Engineering, Indian Institute of Technology Guwahati, Guwahati, India

Akshay Pratap Singh Indian Institute of Technology Roorkee, Roorkee, India

Piyush Punetha University of Technology Sydney, Sydney, NSW, Australia

Vijay Kumar Rayabharapu BV Raju Institute of Technology, Narsapur, Telangana, India

Sireesh Saride Indian Institute of Technology, Hyderabad, Telangana, India

Yitzchak Schary PRS Geo-Technologies, Tel Aviv, Israel

T. G. Sitharam Department of Civil Engineering, Indian Institute of Technology Guwahati (IITG), Guwahati, Assam, India

Gholamhosein Tavakoli Mehrjardi Department of Civil Engineering, Faculty of Engineering, Kharazmi University, Tehran, Iran

Hasthi Venkateswarlu Department of Civil and Environmental Engineering, Indian Institute of Technology Patna, Patna, India

Chapter 1
Geosynthetics Overview

Amarnath M. Hegde

Abstract The geosynthetics are one of the popular and major reinforcement materials in civil engineering construction practices. Geosynthetics are known for offering economical, technically efficient, and environmentally friendly solutions for complex problems. The effective utilization of geosynthetics in civil engineering practice depends on fundamental aspects of the reinforcement material. The present chapter provides a brief overview of the geosynthetics including different categories, properties, and functions of geosynthetics. Further, the evolution, applications, and reinforcement mechanisms of cellular confinement systems have been described.

Keywords Geosynthetics · Functions · Geocell evaluation · Reinforcement mechanisms · Applications

List of notations

The following notations are used in the present chapter:

B	Footing width (m)
C_r	Apparent cohesion (kPa)
D	Equivalent diameter of the geocell pocket opening (m)
D_r	Depth of the reinforcement (m)
I_f	Improvement factors (dimensionless)
q_r	Bearing pressure of the reinforced bed (kPa)
q_o	Bearing pressure of unreinforced bed (kPa)
q_{ult}	Ultimate bearing capacity (kPa)
T	Tensile strength of the basal geogrid material (kN/m)

A. M. Hegde (✉)
Department of Civil and Environmental Engineering, Indian Institute of Technology Patna, Patna 801106, India
e-mail: ahegde@iitp.ac.in

T. G. Sitharam et al. (eds.), *Geocells*, Springer Transactions in Civil and Environmental Engineering,
https://doi.org/10.1007/978-981-15-6095-8_1

α Horizontal angle of the tensional force (degrees)
β Load dispersion angle (degrees)
σ_1 Normal stress (kPa)
σ_3 Confining stress (kPa)
σ_h Hoop stress (kPa)
$\Delta\sigma_3$ Increase in the confining stress (kPa).

1.1 Introduction

The method of modifying the in situ soil behavior for supporting the geotechnical structure is known as ground improvement. In ancient times, foundation engineers had the following limited options for the construction of the project over the problematic soil.

(1) avoiding the site location
(2) excavate and replace with the quality material
(3) design the foundation according to the existing soil conditions.

Over the years, the improvements in the field of geotechnical engineering have provided viable and economical solutions for strengthening the in situ soil to support any type of structure. This advancement helps us to design the foundation as per the choice of the designer and the proposed project.

1.1.1 Ground Improvement Techniques

The rapid urbanization, industrialization in the twenty-first century, the construction of problematic soils has become inevitable. As a result, ground improvement techniques have become popular for their wide range of applications in different soil conditions. The necessity of adopting such techniques at the site is as follows:

(1) Enhancing the shear strength and bearing capacity of the soil
(2) Reduces the distortion of soil under the applied stresses (stress–strain modulus increases)
(3) Control the deformations or settlements
(4) Accelerate the rate of consolidation
(5) Prevent detrimental (chemical or physical) changes due to environmental conditions (drying/wetting; thawing/freezing)
(6) Provide lateral stability
(7) Filling the void spaces below the ground surface
(8) Increase resistance to liquefaction.

Based on the methodology followed for improving the ground, the ground improvement techniques are majorly categorized into five types, as listed below:

(1) Mechanical modification
(2) Hydraulic modification
(3) Physical and chemical modification
(4) Modification by inclusion and confinement
(5) Others.

The major function of the above-mentioned methods is to strengthen the soil as per the requirement. However, in practice, there are a wide variety of techniques used for modifying the existing ground. The schematic representation of the various practical methods of ground improvement is shown in Fig. 1.1.

The some of the ground improvement techniques meant for densifying the in situ soil conditions. In few other techniques, additives are used for modifying the soil

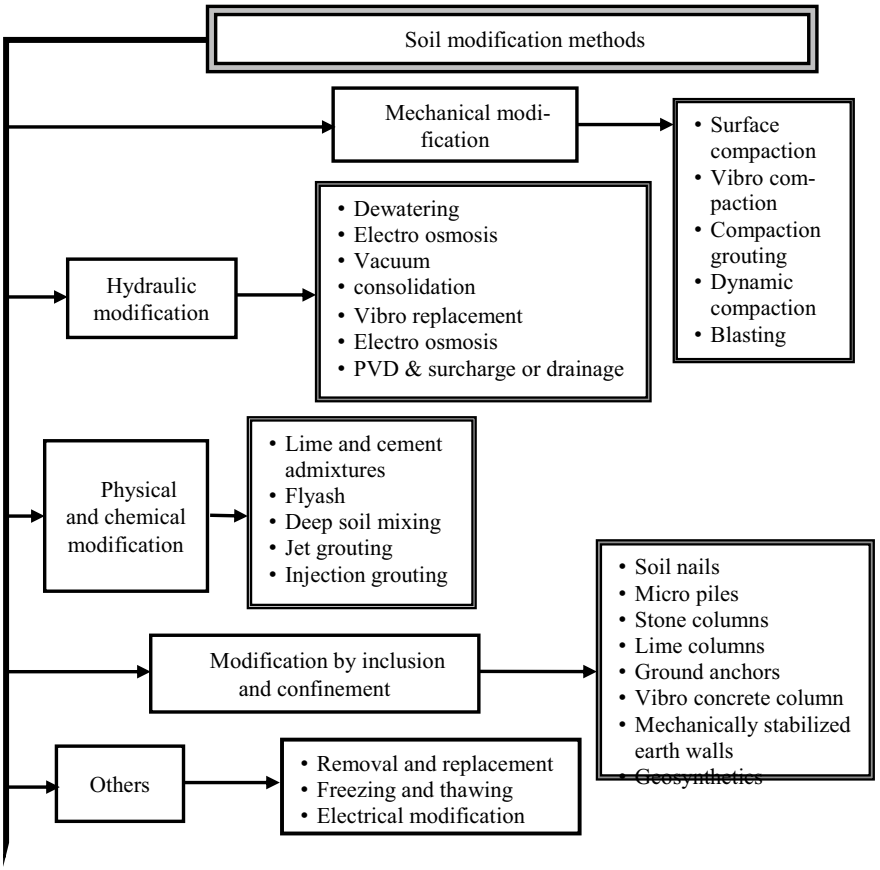

Fig. 1.1 Summary of practical soil modification techniques

behavior. These techniques are helpful in altering the shrinkage and swelling behavior of soft clays. Among the various methods, geosynthetics have become popular reinforcement materials in the modern era of ground improvement. Hence, more emphasis is provided on geosynthetics in the following sections.

1.1.2 Geosynthetics Overview

Geosynthetics are man-made products manufactured from natural or artificial products for enhancing the engineering behavior of soil. The natural products include coir, jute, and hemp. The polymeric materials and metallic strips are coming under the artificial products. The geosynthetics can be used to reinforce the soil, rock, or any other type of geomaterial. In general, the term geosynthetics has been derived from two distinct phrases, namely, geo and synthetics. The first term geo refers to the earth and the synthetics refers to the man-made product. Thus, the generic term geosynthetics is assigned to these materials. The geosynthetics are planar (in the form of sheets, and strips) and three-dimensional in nature. The commonly used polymeric materials for manufacturing the geosynthetics include polypropylene, polyethylene, polyester, polystyrene, polyvinyl chloride, polyamide, etc. The numerous advantages offered by geosynthetics have increased their usage significantly from the past few decades. The benefits of such polymeric products are as follows:

- Geosynthetics offer viable and cost-effective solutions to various challenging problems in the field of geotechnical engineering.
- Use of geosynthetics in construction invariably results in faster constructions.
- Offer sustainable solutions–Permits the use of locally available materials in the construction.
- Unskilled labor can be sufficient.
- The heavy machinery does not require for the installation.

The wide variety of geosynthetics products are available in the market to serve the various functions. A brief overview of the different types of geosynthetics are described following the section.

1.1.2.1 Categories of Geosynthetics

As per the method of manufacturing, the geosynthetics are categorized into various types. The broad range of familiar geosynthetics products includes geotextiles, geogrids, geomembranes, geonets, geocomposites, geocells, geofoams, geopipes, geotubes, geobar, geomat, geomesh, geofabric, geonatural, geostrip, geomatress, electrokinetic geosynthetic, and geosynthetic clay liner. The brief description of the above-mentioned polymeric products are explained below:

Geotextiles

Geotextiles are made of synthetic materials like silk, cotton, and wool instead of natural materials. Thus, these materials less susceptible to biodegradation. The geosynthetics are sheet-like products and the appearance looks like regular fabric. These materials are permeable and flexible in nature due to the presence of synthetic fibers. The geotextiles are manufactured to permit the drainage across their manufactured plane and within the thickness. Based on the manufacturing process, geotextiles are classified into woven, non-woven, knitted, and stitch-bonded geotextiles.

Woven geotextiles:

These geotextiles are manufactured through a conventional weaving process in the form of regular textile nature. The majority of geotextiles are of woven type, and the first developed products from the synthetic fibers. The woven geotextiles have the characteristic appearance of two sets of parallel yarns or threads. The yarn running along the length is called wrap and the one perpendicular direction is called weft.

Non-woven geotextiles:

The continuous or short-staple fiber can be used for manufacturing the non-woven geotextiles. These geosynthetics are formed by bonding the fibers together through mechanical, thermal, and chemical techniques. This process is also known as mechanical interlocking or chemical or thermal bonding of fibers. The thickness of the chemically-bonded non-woven geosynthetics is relatively high as compared to the thermally-bonded non-Wovens. The large quantity of polymer filament is required for providing adequate bonding between the yarns in the case of chemical bonding.

Knitted Fabrics:

These types of geosynthetics are manufactured by using the method called knitting. According to this process, a series of loops of yarn are interlocked together to make geosynthetics.

Stitch-Bonded Geotextiles:

These geotextiles are formed by stitching the yarns or fibers together.

Geogrid

Geogrid is a polymeric and planar product consisting of a regular open network of integrally connected tensile elements or ribs. These ribs are connected at the joints in the same plane through the extrusion, interlacing, or bonding. The opening between transverse and longitudinal ribs is known as aperture. The size of the opening is large enough to provide interlocking with the surrounding soil particles. The major application of the geogrid product is reinforcing the soil. Further, the extruded geogrids are categorized into three types, namely, uniaxial, biaxial, and triaxial geogrids. The brief description of the different types of geogrids is illustrated below.

Uniaxial Geogrid:

These products are manufactured by stretching the regularly punched polymer sheet in a longitudinal direction. Thus, it possesses a higher tensile capacity in the longitudinal direction than the transverse direction. Some of the major applications of the uniaxial geogrid include retaining walls, construction of embankment extensions, dams, and the waste landfills.

Biaxial Geogrid:

These products are manufactured by stretching of regularly punched polymer sheets in both the longitudinal and the transverse directions. Hence, it offers similar tensile capacity in both the longitudinal and the transverse directions. The major applications of the biaxial geogrid include ground reinforcement, road bases, and railway trackbed stabilization. In addition, the biaxial geogrid exhibits higher stiffness and interlocking capabilities than uniaxial geogrids.

Triaxial geogrid:

These are the advanced geogrid products among the different types of geogrids. They are specifically designed for the trafficked surfaces. It is manufactured by the orientation of punched polypropylene sheet in multiple, and equilateral directions to establish its triangular apertures. These geogrids can offer high radial stiffness throughout the 360 degrees. The recent applications of the triaxial geogrid include railway projects (improving the bearing capacity), airport pavements over soft soil, and highways.

Geonet

These are open grid-like polymeric products manufactured by intercepting the two different directional ribs at two different planes. The network of geonet looks like a sheet with the high in-plane porosity to transmit a large quantity of fluid. The configuration of geonet is majorly different from the geogrid in terms of aperture size and the plane of the location of ribs. The apertures of the geonet are in the shape of a diamond. Whereas, the apertures of the geogrid are square, rectangular, and triangular in shape, and ribs are located in the same plane. In addition, the thickness of geonet is relatively larger than the geogrid reinforcement. The geonets are also referred to as geospacers. The geonets are majorly categorized into two types namely, bi-planar and tri-planar geonets. The brief description of the types of geonets are explained below.

Bi-planar Geonet:

These are the synthetic drainage materials, used to transmit the gases and fluid flow uniformly in both the directions. These are the most commonly used geonets, and generally manufactured with the high-density polyethylene (HDPE) resin.

Tri-planer Geonet:

These are the much-advanced version of geonets, designed for transmitting the fluid or gas under many field conditions. It consists of centralized HDPE ribs with the diagonally placed bottom and top ribs for enriching the geometric stability of geonet.

Geomembranes

These are flexible, continuous, and relatively impervious geosynthetics products made of one or more synthetic materials. It can be used as a gas or fluid barrier due to its impermeable nature. The important applications of the geomembranes include canal lining, landfill lining, and tunnel lining.

Geocomposites

These are manufactured by combining the two different types of geosynthetics to obtain the dual advantage of synthetic materials. Some of the general combinations include geotextile-geogrid, geotextile-geonet, geonet-geomembrane, geosynthetic clay liner (GCL), and prefabricated geocomposite drains or prefabricated vertical drains (PVDs).

Geosynthetic clay liners (GCLs):

These are geocomposites manufactured by incorporating the bentonite clay layer in between a top and bottom geotextile layer or geotextile and bentonite bonded to a geomembrane or single layer of geotextile. The geotextile encased clay liners are often needle-punched or stitched through the bentonite core to increase internal shear resistance. These are commonly used in landfill liner applications often in conjunction with a geomembrane.

Prefabricated vertical drains (PVDs):

These are composed of prefabricated plastic sheets encased by a geotextile layer for accelerating the consolidation process of soft clays. The PVDs are also called as prefabricated geocomposite drains or wick drains.

Geocell

It is a three-dimensional geosynthetic product formed by interconnecting the strips of polymeric sheets in a cellular fashion. The interconnected cells are infilled with the granular materials to facilitate the rigid base for supporting the various loading conditions. It helps to distribute the buildup loads over a larger area under static and cyclic loading conditions. The major application of the geocells include foundations, pavements, buried lifelines, embankments, steep slopes, and retaining walls. In addition, the cellular confinement systems (geocells) are also used for erosion control purposes. As of now, three forms of geocell reinforcement were vividly used in various practical applications as shown in Fig. 1.2.

It includes handmade geocells, geocell with perforations, and non-perforated geocell. The handmade geocell is composed of interconnected geogrid or some other synthetic materials through the bodkin joints. Whereas the polymeric sheets are thermally welded or glued in the case of polymeric geocell reinforcements. It may be perforated or non-perforated.

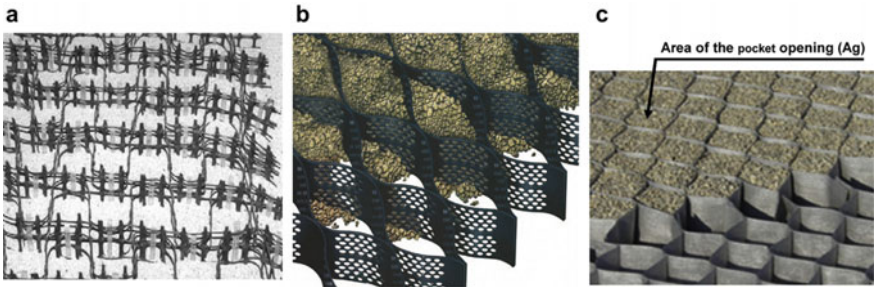

Fig. 1.2 Typical geocell reinforcing elements **a** handmade geocells with perforations (Dash et al. 2003), **b** perforated geocell (Bathurst and Jarrett 1998), and **c** non-perforated flexible geocell (Moghaddas Tafreshi and Dawson 2012)

Geofoam

These are lightweight and low-density network of gas-filled or closely spaced expanded version of the polystyrene foam material. It can be used for thermal insulation applications. It is also useful to reduce the earth's pressure against rigid walls due to its compressive nature.

Geopipes

These are solid-wall or perforated synthetic pipes placed under the ground surface and backfilled.

Geotube

These are large size and oval-shaped tubes manufactured from geotextile fabric and filled with sediment. It is used for dewatering process and shoreline protection.

Geobar

It is a polymeric material in the form of a bar.

Geoblanket

It is a biodegradable and a permeable polymeric product. It is used on slopes where vegetation is possible, thereby protecting the slopes.

Electrokinetic geosynthetic

It is a mesh made from a metal wire stringer and coated with a conductive polymer. It resembles a reinforcing geomesh, and available in the form of sheets, strips, and tubes. In addition to electrical conduction, it also provides drainage, filtration, and reinforcement functions.

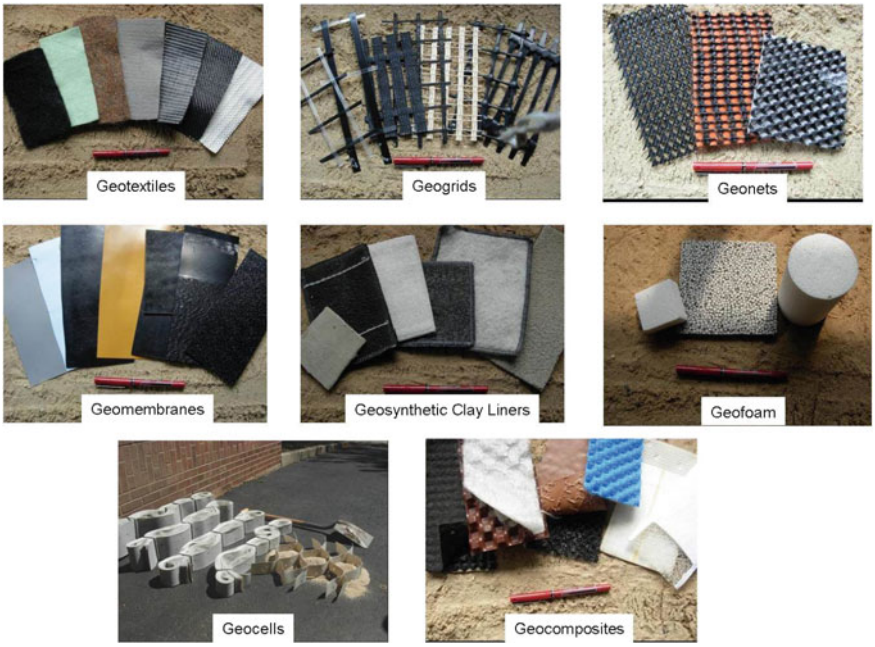

Fig. 1.3 Types of geosynthetics (sourced from Koerner 2012)

Geomat

It is a three-dimensional polymeric structure made of bonded filaments, which are permeable in nature. It is used as a reinforcement to roots of grass and small plants, which, in turn, provides permanent erosion control.

Geomatress

These are three-dimensional, and permeable geosynthetic structure, which is filled with soil or concrete after placing over a soil layer to prevent erosion. The photographs of the different forms of geosynthetics are shown in Fig. 1.3.

1.1.2.2 Properties of Geosynthetics

As discussed earlier, geosynthetics are polymer-based products. The behavior of these products may vary from plastic to viscoelastic. The level of performance is associated with various parameters like temperature, type of load, and the duration of the application of load, etc. Thus, it is necessary to understand the basic properties of geosynthetics to understand their suitability to perform a set of functions. The different properties of geosynthetics are categorized into six major groups. The schematic representation pertaining to the various geosynthetics properties is shown in Fig. 1.4.

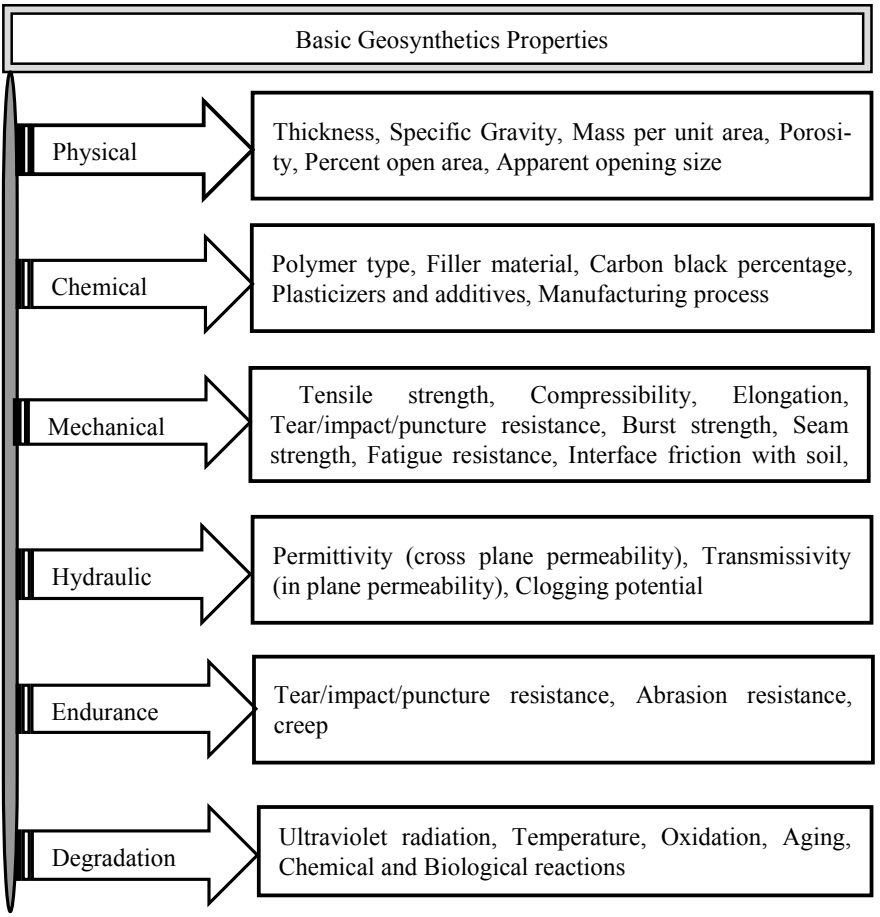

Fig. 1.4 Summary of parameters defines the behavior of geosynthetics

The physical and chemical properties are important to assess the nature and type of geosynthetics product. The strength and deformation characteristics of the geosynthetics are investigated through mechanical properties. These properties help to understand the performance of geosynthetics under different loading conditions without tearing, yielding, puncturing, and slipping at the soil-geosynthetic interface. Hydraulic properties are useful in quantifying the amount of water that can flow through the geosynthetics through the in-plane and cross-plane directions. Endurance properties suggest that the creep behavior and construction survivability of geosynthetics. Whereas, the degradation properties useful for assessing the change in performance of geosynthetics with time (for example, exposure to oxidation or ultra-violate rays in sunlight for longer duration may affect its performance).

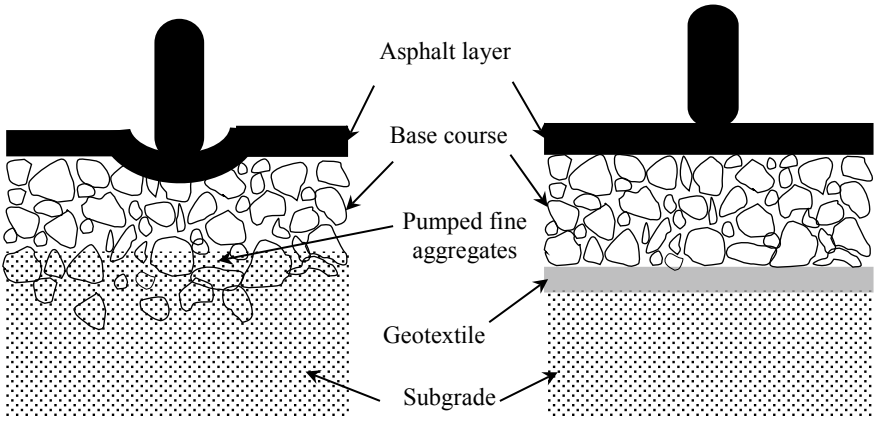

Fig. 1.5 Separation function of geosynthetics

1.1.3 Geosynthetics functions

Nowadays, the application of geosynthetics in various geotechnical projects is increasing at a rapid rate by the virtue of offering a wide variety of functions. However, the selection of geosynthetic products for a particular application majorly depends upon the functional requirements of the project. Sometimes, a combination of geosynthetic products can be used, if the project functions are multi-objective. Hence, the present section briefly introduces the functions offered by geosynthetics. The functions of geosynthetics are majorly categorized into six types as described in the following sections.

1.1.3.1 Separation

The process of preventing the intermixing of two distinct geomaterials is called separation. The geosynthetics are used to separate the two layers of soil that have different particle size distributions. For example, geotextiles are used to prevent road base materials from penetrating into the underlying soft subgrade soils. It helps to maintain the integrity of the design thickness of pavement layers. The geotextile as a separator helps to prevent the pumping of fine-grained subgrade soils into the permeable granular road bases. The schematic representation of the separation function of geosynthetics is shown in Fig. 1.5.

1.1.3.2 Filtration

Geosynthetics can allow water to pass across the plane to retain or prevent the soil particles. The geosynthetics acts similar to a sand filter and allow water to pass

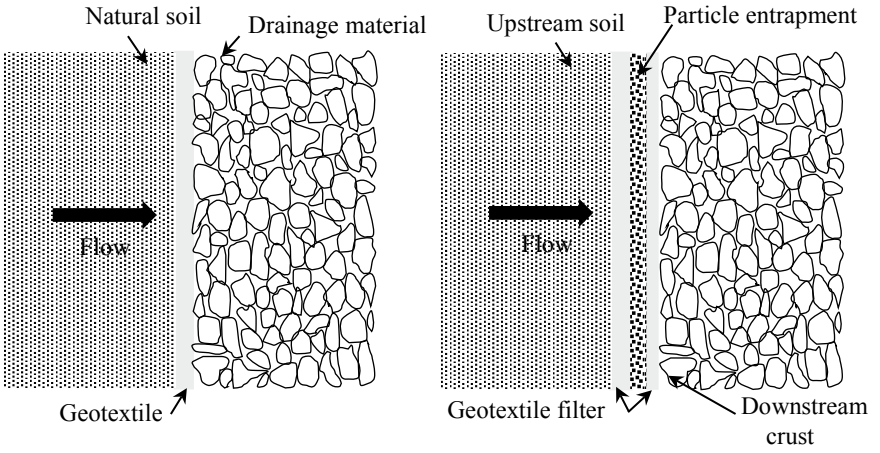

Fig. 1.6 Filtration

through the soil by retaining the upstream soil particles. For example, geotextiles are used to prevent the soil particles from migrating into pipes or drainage aggregates by allowing the flow through the system. Geotextiles are also used below the rip rap and other armor materials in riverbank and coastal protection systems to prevent soil erosion. The schematic representation of the filtration function of geosynthetics is shown in Fig. 1.6.

1.1.3.3 Drainage

The purpose of drainage is to permit the water to pass along its plane, which in turn enhances the consolidation process of the soft soils. The geosynthetic can act as a drain to carry fluids through the less permeable soils. Generally, the geotextiles are used to dissipate pore water pressures at the base of roadway embankments. The geocomposite drains have been designed to control the high flow conditions. These materials are used as a slope interceptor drains, pavement edge drains and retaining wall, and abutment drains. The prefabricated vertical drains (PVDs) are used to accelerate the consolidation of soft cohesive foundation soils under the preload fills and embankments. The schematic representation of the drainage function is shown in Fig. 1.7.

1.1.3.4 Reinforcement

The major function of reinforcement is to improve the strength and stability of soil by imparting the tensile strength of the soil. The geosynthetics can act as a reinforcement element within a soil mass to enrich the stress distribution and controlling

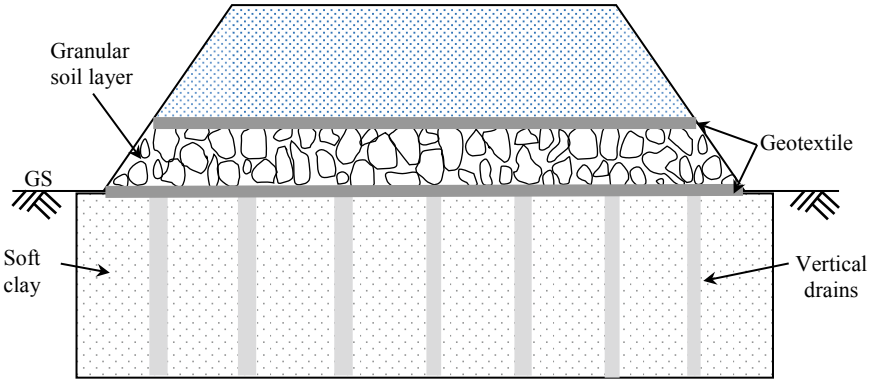

Fig. 1.7 Drainage

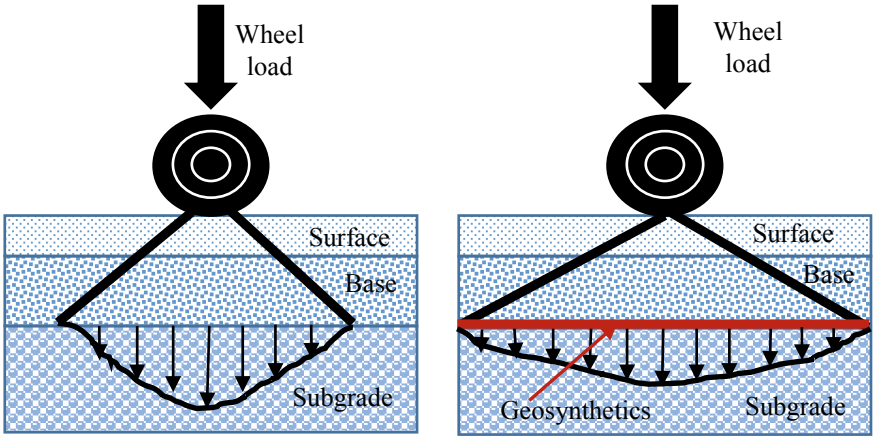

Fig. 1.8 Reinforcement

the deformation behavior of the unreinforced soil. In general, geogrids are used to increase the tensile strength of a soil mass in various applications of geotechnical engineering. The schematic representation of the reinforcement function is shown in Fig. 1.8.

1.1.3.5 Protection (Cushion)

The process of controlling or preventing the local damage of a primary (geosynthetics) element by using the geotextile or a geotextile-related product is known as protection. The major purpose of the protection function is to protect the geosynthetics from the perforation and abrasion. In practice, the geotextile layer is used as a cushion over the geomembrane in order to reduce or prevent the damage of

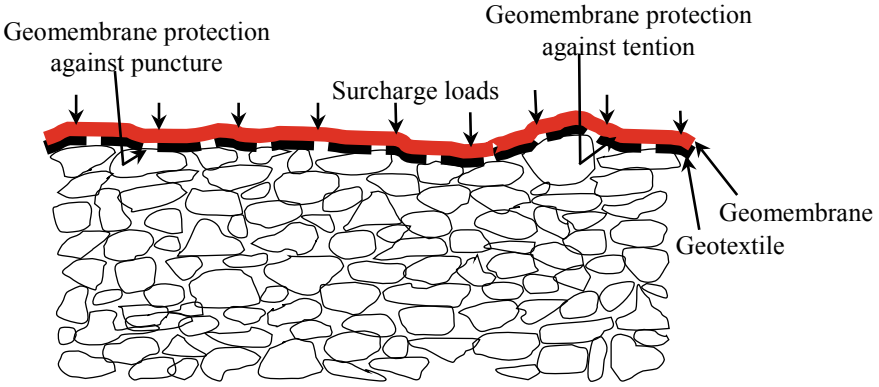

Fig. 1.9 Protection

geomembrane during the construction. The schematic representation of the protection function of reinforcement is shown in Fig. 1.9.

1.1.3.6 Barrier (Waterproofing)

The process of limiting or preventing the flow of gases or liquids is called as a barrier function. The specific type of geosynthetics products can be used as an impermeable and noise barrier. In practice, the geomembranes, geosynthetic clay liners (GCLs), field-coated geotextiles and thin-film geotextile composites are used as a barrier material. It is the major function in various practices for waste containment, encapsulation of swelling soils, and the asphalt pavement overlays. The performance of the geosynthetic barrier is greater than or equal to the performance of the thick soil layer. Thus, the utilization of these products is increased in various construction projects. These products also offer economical, robust, and safer designs for the barrier function. The schematic representation of the barrier function is shown in Fig. 1.10.

1.1.3.7 Erosion Control

The process of reducing or preventing the erosion of soil from the surface runoff and rainfall conditions is known as erosion control. The schematic representation of the erosion control function is shown in Fig. 1.11.

Generally, lightweight geosynthetic mats and temporary geosynthetic blankets are placed over the exposed soil surface for preventing the erosion of soil. In addition, geotextile silt fences are used to remove suspended soil particles from the runoff water. The biodegradable fibers are also used for manufacturing the erosion control mats The summary of primary function offered by various geosynthetics products is

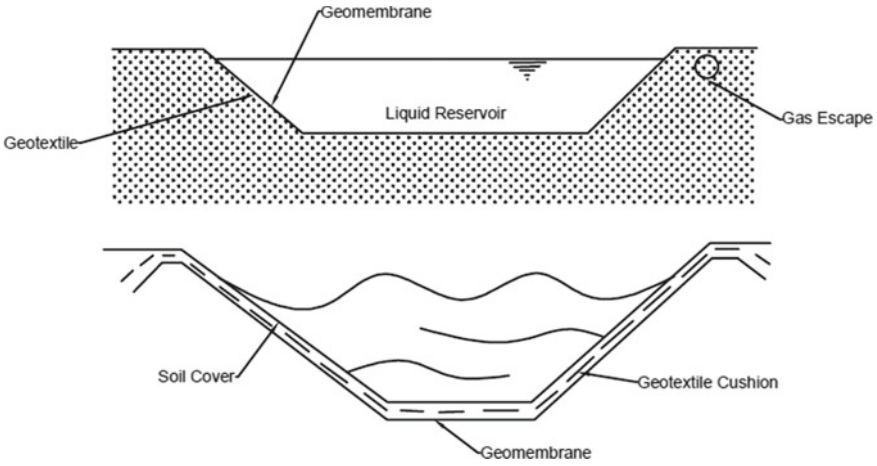

Fig. 1.10 Barrier

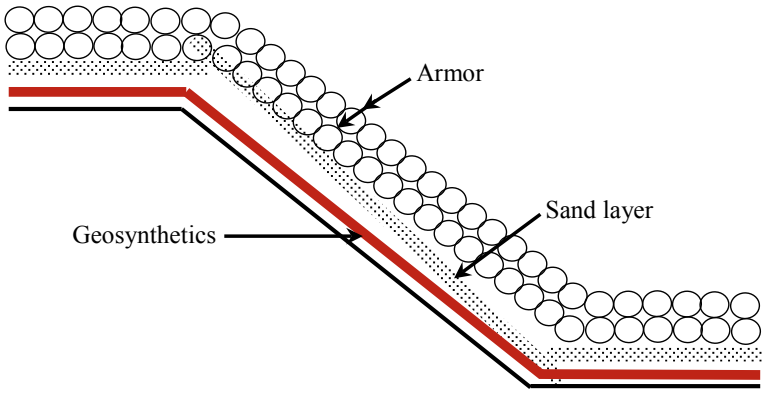

Fig. 1.11 Erosion control

listed in Table 1.1. In addition, the important design parameters need to be considered for serving the various functions of geosynthetics in various civil applications were summarized in Table 1.2.

1.1.4 Geosynthetics in Soil Reinforcement

The major purpose of the geosynthetics in the perspective of the reinforcement function is to enrich the tensile behavior of the soil (material with strong compressive characteristics). As a result, the composite material (soil and geosynthetic) attains both the tensile and compressive strength. The reinforcement function majorly depends

Table 1.1 Summary of the functions served by various geosynthetics products

Types of geosynthetics	Reinforcement functions						
	Separation	Filtration	Drainage	Reinforcement	Protection	Barrier	Erosion control
Non-woven geotextile	*	*	*	*	*		
Woven geotextile	*	*		*			
Geogrid				*			
Geonet			*		*		
Geomembranes						*	
Geosynthetic clay liners						*	
Prefabricated vertical drains			*				
Geocells				*			*
Geofoam				*			
Geocomposites	*	*	*	*	*	*	*
Geobags							*
Geomats			*	*			
Geopipe		*	*				
Gabions				*			

Table 1.2 Summary of essential design parameters for different geosynthetics applications

Applications geosynthetics parameters	Unpaved roads	Railways	Hydraulic construction	Drainage	Embankment	Retaining wall	Containement	Tunnel	Sports field
Tensile elongation (%)	*	*	*	*	*		*	*	
Puncture resistance (N)	*	*		*	*		*	*	*
Drop test	*		*		*				
Effective opening size (mm)	*	*	*	*	*				*
Thickness (mm)	*	*	*	*	*	*	*	*	*
Permeability in the plane, K_h (cm/sec)	*			*	*	*	*	*	
Permeability normal to the plane, K_v (cm/sec)	*	*	*	*	*	*			*
Tear resistance (N)			*						
Tensile strength (kN/m)						*			

(continued)

Table 1.2 (continued)

Applications geosynthetics parameters	Unpaved roads	Railways	Hydraulic construction	Drainage	Embankment	Retaining wall	Containement	Tunnel	Sports field
Burst pressure resistance (kN/m^2)							*		

Note *indicates the primary function/parameter of geosynthetics

on the transference of tensile stresses from soil to geosynthetics through the induced frictional force between them. The major parameters influence the reinforcement function of the geosynthetics are tensile strength, interface shear strength, and the tensile modulus (Pinto and Cousens 2000). The tensile strength helps to resist the tensile stresses transferred from the soil. For soil–geosynthetics interaction problems, interface shear strength is the significant parameter. It is responsible for the transference of stresses from soil to geosynthetics. The tensile modulus helps to maintain the total deformation of the composite material within the allowable limits of the soil.

Initially, the function of reinforcement was divided into two types, namely, tensile element and the tensioned membrane (Fluet 1988). The tensile member is able to support the planar load as shown in Fig. 1.12a. The planar and normal loads can be supported in the case of the tensioned membrane as shown in Fig. 1.12b.

Later, Koerner (1998) and Jewell (1996) revealed that the geosynthetics works as a tensile member due to anchorage and shear mechanisms between the soil and reinforcement. Thus, they have suggested three different mechanisms, namely, shear, anchorage, and tensioned membrane for the soil reinforcement function. Shearing is also referred to as sliding, which occurs due to the sliding of soil particles over the geosynthetic. Anchorage is known as pullout and occurs due to the pullout action of geosynthetics from the soil. The membrane mechanism is attributed due to the deformation of geosynthetics under the applied normal load.

Currently, the reinforcement with geosynthetics has been well accepted for the construction of various structures all over the world. The soil reinforced structures are divided into two groups, namely, load supported and earth structures (Bonaparte et al. 1985). The load supported structures are stable for supporting their own weight and not enough to carry the external load. It includes foundations, pavement, and railway applications. The earth structures are not stable for supporting their own weight and sometimes it is necessary to support the external loads. It includes steep slopes, retaining walls, and embankments. In this section, more emphasis is provided on the reinforcement function of geosynthetics in improving the behavior of foundation beds.

The reinforcement mechanism of geosynthetics in increasing the ultimate bearing capacity of the foundation is shown in Fig. 1.13. Das et al. (1998) considered three components for illustrating the bearing capacity of a reinforced soil system. (1)

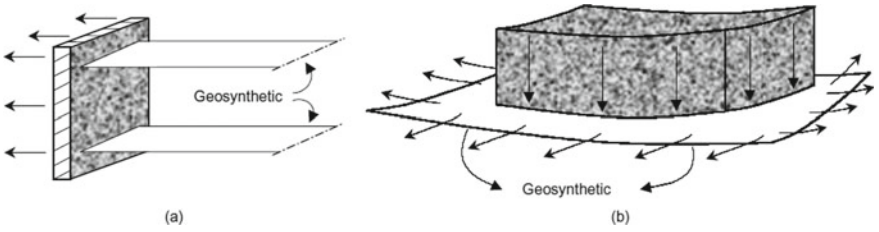

Fig. 1.12 Reinforcement function of geosynthetics: **a** tensile member; and **b** tensioned membrane. *Sourced* from Fluet (1988)

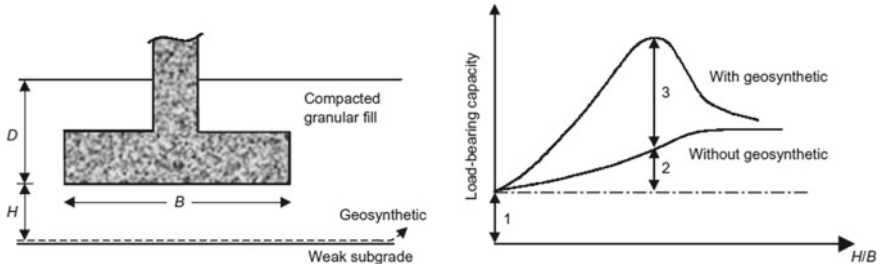

Fig. 1.13 Variation in ultimate bearing capacity of the foundation bed with and without geosynthetics. *sourced* from Das et al. (1998)

ultimate bearing capacity of the existing subgrade soil, (2) contribution of bearing capacity due to the compacted granular fill (without geosynthetics), and (3) ultimate bearing capacity in the presence of geosynthetics. The results revealed that the most beneficial effect of reinforcement (30% increase in bearing capacity) was found at 0.6 times the width of the foundation under the footing.

Later, Hegde and Sitharam (2015a, b, c, d) highlighted the potential benefits of geocell reinforcement in improving the bearing capacity of foundation beds. The findings suggested that the advantages of geocell are more and it improves the shear strength response of the infill material due to its confinement mechanism.

1.1.5 Evolution of Cellular Confinement

The concept of reinforcing the soil with natural materials like bamboo is known to humankind for centuries. There are many instances in history of using timbers in road construction a few 1000 years ago. Even in the construction of the Great Wall of China, a mixture of clay and gravel reinforced with the tamarisk branches have been used. The modern concept of soil reinforcement is derived from the pioneering work of Henry Vidal in the development of the reinforced earth (Bathurst and Karpurapu 1993; Rajagopal et al. 1999; Zhang et al. 2006; Chen et al. 2013; Vidal 1966). However, systematic studies on the reinforced beds have started with the pioneering work of Binquet and Lee (1975). Subsequently, many researchers have reported the beneficial effect of soil reinforcement in improving the bearing capacity of the soil (Akinmusuru and Akinbolade 1981; Fragaszy and Lawton 1984; Guido et al. 1986). The development in the area of geosynthetics over the years has led to the invention of different geosynthetic products such as geotextiles, geonets, geogrids, geocells, geocomposites, etc. Out of which, geocells and geogrids are the most preferred products to reinforce the soil. These products have completely replaced the conventional type of reinforcement such as metal strips and steel bars.

Geocells are three-dimensional expandable panels made of high-density polymers. It was originally developed by the US army corps of engineers in the early

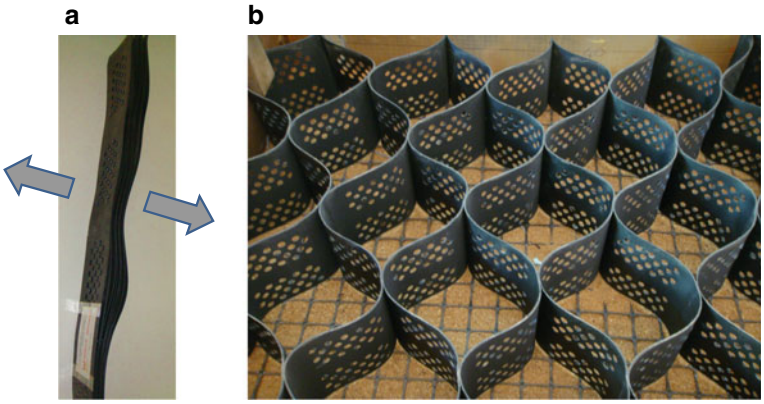

Fig. 1.14 Photograph of the geocell: **a** folded; **b** expanded

1970s for military applications. Afterword, the use of geocells in the civil engineering application is reported by many researchers (Rajagopal et al. 1999; Rea and Mitchell 1978; Mitchell et al. 1990; Bush et al. 1990; Dash et al. 2001). Nowadays, reinforcing the soil in the form of the cellular mattress is showing its efficacy in the fields of highway and embankment construction. Figure 1.14 shows the typical photograph of the geocell.

On the other hand, the traditionally available techniques for improving the weak soils are generally deep foundation techniques. Deep foundations being very expensive, more economical solutions are constantly sought after. In recent years, ground improvement techniques like vibro stone columns and prefabricated vertical drains have gained popularity for their wide range of applications in soft soils. However, engineers and scientists are constantly looking for new techniques, which are faster and cheaper to ground improvement techniques. Hence, the geocell applications are increasing at a rapid rate and are widely used in many geotechnical engineering applications.

1.1.6 Application of Geocells

As discussed in the preceding sections, the general applications of the geocell include foundations, embankments, pavements, earth retaining structures, and erosion control. Figure 1.15 shows the schematic representation of different geocell applications. In addition to these general applications, new applications of the geocells are also coming up nowadays. One of such new and emerging application is the protection of buried pipelines using the geocells.

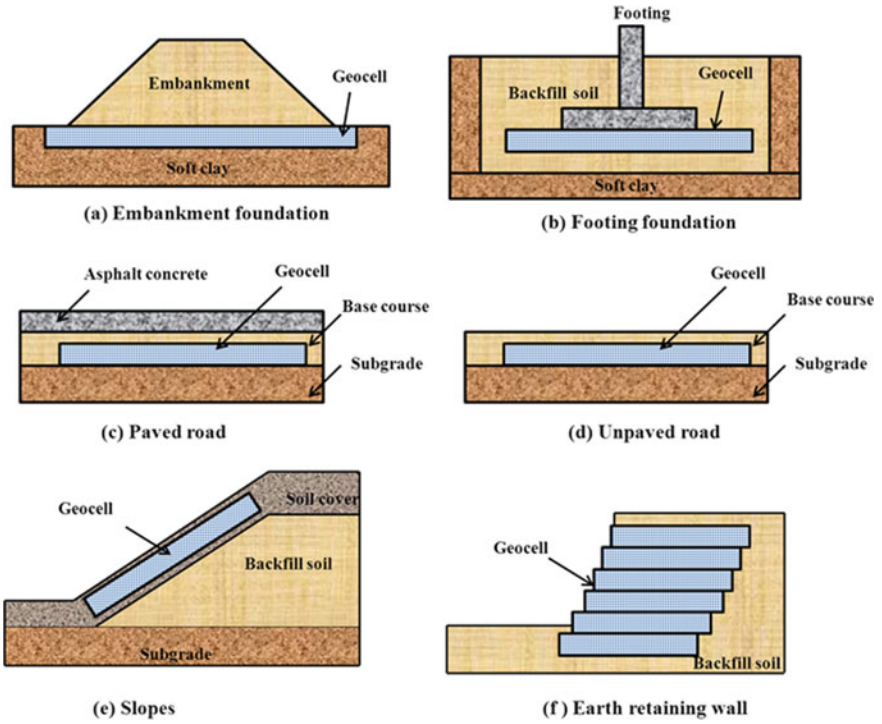

Fig. 1.15 Different applications of geocells

1.1.7 Advantages of Cellular Confinement

The use of geocells has clear advantages over traditional reinforcement techniques. Some of the key advantages of using the geocells are listed below.

- Geocells are the only geosynthetics product, which has three-dimensional structure.
- They are easily transported as flat strips. Hence, the logistics for large quantities is not at all a problem.
- Geocells are easy to install and do not require skilled labors.
- They can be installed in all weather conditions.
- Generally, the infill material has to be granular in nature. However, other type of materials such as recycled materials also can be used.
- Geocells are cost-effective.
- Geocells are environmentally friendly and will not leave any carbon footprint.
- Geocells are durable and no major maintenance is required during its life span.

1.1.8 Reinforcement Mechanism

In recent years, geocell is one of the increasingly used geosynthetics product in various geotechnical engineering applications. Some of the major applications include foundations, pavements, retaining walls, slope stability analysis, and embankments. The geocells have an added advantage than the planar reinforcements by the virtue of its three-dimensional nature. In addition, these products are offering cheaper, faster, sustainable, and environmentally friendly solutions for complex geotechnical problems. It was majorly attributed due to the unique reinforcement mechanism offered by the geocell reinforcement.

Mitchell et al. (1990) (Dash et al. 2004) identified several possible failure modes of sand-filled square-shaped paper grid cells. It includes, (i) cell penetration into the soft subgrade below; (ii) bursting of the cell when the infill material exerts stresses exceeding the bursting strength; (iii) buckling of the cell wall due to insufficient lateral restraint for the cell wall and the cell walls are directly loaded; (iv) bearing capacity failure by shear failure of the underlying soft subgrade; (v) Bending failure of the soil-geocell composite behaving like a slab, caused by excessive wheel load; (vi) durability failure caused by prolonged exposure to the environment; and (vii) excessive rutting caused by a large number of load repetitions. Lateral confinement, increased bearing capacity, and tensioned membrane effect were identified as the major reinforcement mechanisms for geotextile reinforcement (Giroud 1986). Understanding of these mechanisms originated from static plate load tests, but later research has been focused on these mechanisms under cyclic loading. Giroud and Noiray (1981; Giroud et al. 1984) modified the Giroud (1986) design method for geogrid-reinforced unpaved roads by considering these mechanisms. The parameters used in the Giroud and Noiray (1981; Giroud et al. 1984) method include the geometry of road structures, traffic axles and loads, rut depth, properties of base course and subgrade materials, and geogrid properties. The geocell-reinforced bases exhibit tensile strength, bending resistance, and shear strength, and intercept the failure planes from the subgrade (Zhou and Wen 2008). Based on the previous research (Hegde and Sitharam 2015a, b, c, d), the reinforcement mechanisms offered by a geocell reinforcement were observed as:

- Confinement effect
- Tensioned membrane (beam) effect
- Stress distribution.

1.1.8.1 Confinement Effect

Due to the three-dimensional structure, the geocell can provide lateral confinement to the soil particles within the cells as shown in Fig. 1.16. The geocell provides the vertical confinement in two ways: (1) the friction between the infill material and the geocell wall, and (2) the geocell-reinforced base acts as a mattress to restrain the soil from moving upward and outside the loading area. Gourc et al. (2001) carried out

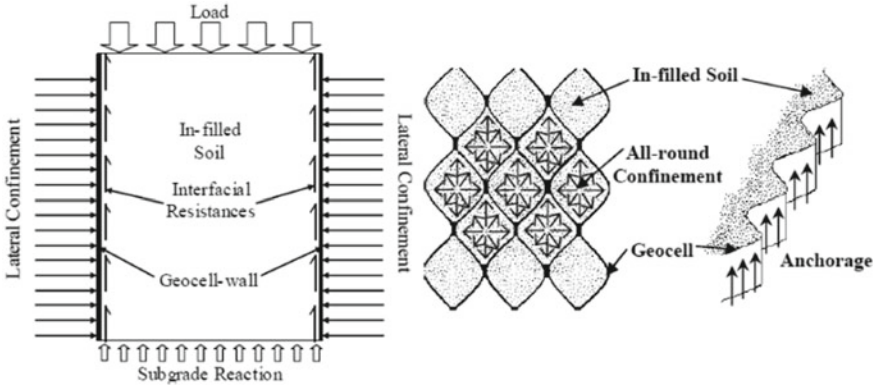

Fig. 1.16 Confinement mechanism of geocell reinforcement. *sourced* from Biswas and Krishna (2017)

compression tests to explain the confinement effect and used finite element analysis to verify the results. Han et al. (2008) investigated the load transfer mechanism between infill and geocell by carrying out both experimental and numerical studies on the behavior of geocell-reinforced sand under a vertical load. The studies showed that geocells could increase the elastic modulus and bearing capacity of the reinforced sand by providing confinement to the infill material. Mhaiskar (1992) identified the hoop stress in the geocell wall as the most significant contributing factor toward resisting loads and suggested a geocell with higher modulus and less extensibility be desired.

1.1.8.2 Tensioned Membrane (Beam) Effect

The beam effect or tensioned membrane is referred to as the tension developed in the curved geocell-reinforced mattress to resist the vertical load (Rajagopal et al. 1999; Zhou and Wen 2008; Demir et al. 2014). However, to mobilize the tensioned membrane effect the pavement structure must deform significantly (Giroud and Noiray 1981). As the geocell-reinforced section is stiffer than the surrounding soil, the curved surface exerts upward reaction and reduces the net stress applied to the subgrade. Douglas (1997) suggested that the concept of coefficient of subgrade reaction, originally intended for monotonic loading, can be successfully extended to linear, repeated-load behavior also. The schematic view of the lateral resistance mechanism is shown in Fig. 1.17.

1.1.8.3 Stress Distribution

Figure 1.18 shows the schematic representation of the vertical stress dispersion mech-

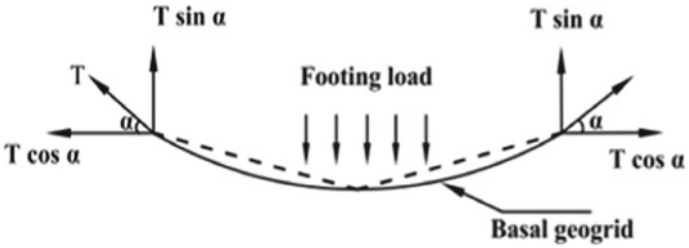

Fig. 1.17 Membrane mechanism *sourced* from Sitharam and Hegde (2013)

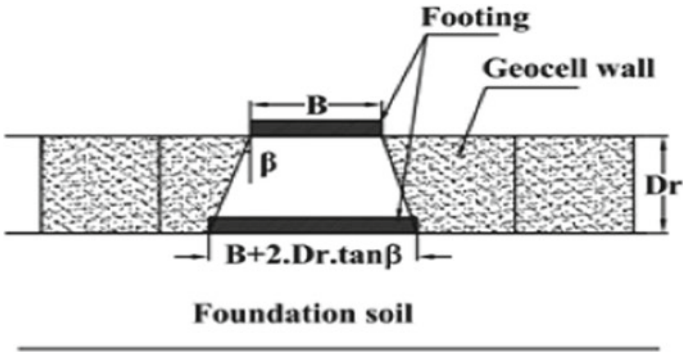

Fig. 1.18 Vertical stress dispersion. *sourced* from Sitharam and Hegde (2013)

anism in the geocell-reinforced foundation beds. Mhaiskar (1992) indicated that a dense infill provides a higher load-carrying capacity and geocell reinforcement distributes the load over a wider area.

Wayne et al. (1998) also pointed out that the planar geosynthetics reinforced bases can distribute the applied load to a wider area as compared to the unreinforced base. Higher bearing capacity can be achieved with a smaller thickness of geocell-reinforced bases (Zhang et al. 2006). The inclusion of the geocell and the confinement effect would increase the stiffness of the reinforced base. The wider stress distribution contributed by geocell reinforcement reduces the stress at an interface between the base and the subgrade and increases the bearing capacity of the foundation.

1.1.9 Summary

The use of geosynthetics in various infrastructure projects has been attracting urban developers and contractors due to its various benefits. In this chapter, the fundamental aspects of geosynthetics such as geosynthetics types, essential properties, and their

suitability in different applications were presented. In addition, a brief description of the advantages and reinforcement mechanisms of the geocell was described.

References

Akinmusuru JO, Akinbolade JA (1981) Stability of loaded footings on reinforced soil. J Geotech Geoenv Eng, 107(ASCE 16320 Proceeding)

Bathurst RJ, Jarrett PM (1988) Large scale model tests of geo-composite mattresses over peat subgrades. Transp Res Rec 1188:28–36

Bathurst RJ, Karpurapu R (1993) Large scale triaxial compression testing of geocell reinforced granular soils. Geotech Test J 16(3):296–303

Binquet J, Lee LK (1975) Bearing capacity tests on reinforced earth slabs. J Geotech Eng Division ASCE 101(12):1241–1255

Biswas A, Krishna AM (2017) Geocell-reinforced foundation systems: a critical review. Int J Geosynth Ground Eng 3(2):17

Bonaparte R, Holtz RD, Giroud JP (1985) Soil reinforcement design using geotextiles and geogrids. In: Proceedings of the symposium on geotextile testing and design engineering, Los Angeles, pp 69–116

Bush DI, Jenner CG, Bassett RH (1990) The design and construction of geocell foundation mattresses supporting embankments over soft ground. Geotext Geomembr 9:83–98

Chen RH, Haung YW, Haung FC (2013) Confinement effect of geocells on sand samples under triaxial compression. Geotext Geomembr 37:35–44

Das BM, Maji A, Shin EC (1998) Foundation on geogridreinforced sand: effect of transient loading. Geotext Geomembr 16(3):151–160

Dash SK, Rajagopal K, Krishnaswamy NR (2001) Strip footing on geocell reinforced sand beds with additional planar reinforcement. Geotext Geomembr 19:529–538

Dash SK, Rajagopal K, Krishnaswamy NR (2004) Performance of different geosynthetic reinforcement material in sand foundations. Geosynth Int 11(1):35–42

Dash SK, Sireesh S, Sitharam TG (2003) Model studies on circular footing supported on geocell reinforced sand underlain by soft clay. Geotex Geomembr 21:197–219

Demir A, Yildiz A, Laman M, Ornek M (2014) Experimental and numerical analyses of circular footing on geogrid-reinforced granular fill underlain by soft clay. Acta Geotech 9(4):711–723

Douglas RA (1997) Repeated-load behaviour of geosynthetic-built unbound roads. Can Geotech J 34(2):197–203

Fluet JE (1988) Geosynthetics for soil improvement: a general report and keynote address. In: Proceedings of the Symposium on Geosynthetics for Soil Improvement, Tennessee, U.S.A, pp 1–21

Fragaszy RJ, Lawton E (1984) Bearing capacity of reinforced sand subgrades. J Geotech Eng 110(10):1500–1507

Giroud JP (1986) From geotextiles to geosynthetics: a revolution in geotechnical engineering. In: Proceedings of the 3rd International Conference on Geotextiles, Vienna, vol 1, pp 1–18

Giroud JP, Noiray L (1981) Geotextile-reinforced unpaved road design. J Geotech Eng Div ASCE 107(GT9):1233–1254

Giroud JP, Ah-Line A, Bonaparte R (1984) Design of unpaved roads and trafficked areas with geogrids. In: Proceedings of the symposium on polymer grid reinforcement, London, pp 116–127

Gourc JP, Arab R, Giroud H (2001) Calibration and validation of design methods for geosynthetic-reinforced retaining structures using partial factors. Geosynth Int 8(2):163–192

Guido VA, Chang DK, Sweeney MA (1986) Comparison of geogrid and geotextile reinforced earth slabs. Can Geotech J 23(4):435–440

Han J, Yang X, Leshchinsky D, Parsons RL (2008) Behaviour of geocell reinforced sand under a vertical load. J Transpo Res Board 2045:95–101
Hegde A, Sitharam TG (2015a) Effect of infill materials on the performance of geocell reinforced soft clay beds. Geomech Geoeng Int J 10(3):163–173
Hegde A, Sitharam TG (2015b) Use of bamboo in soft ground engineering and its performance comparison with geosynthetics: experimental studies. J Mater Civ Eng ASCE 27(9):04014256
Hegde A, Sitharam TG (2015c) Joint strength and wall deformation characteristics of a single cell geocell subjected to uniaxial compression. Int J Geomech (ASCE) 15(5):04014080
Hegde A, Sitharam TG (2015d) 3-dimensional numerical modelling of geocell reinforced sand beds. Geotext Geomembr 43:171–181
Jewell RA (1996) Soil Reinforcement with Geotextiles, Construction Industry Research and Information Association. CIRIA Special publication, London, p 123
Koerner RM (1998) Designing with Geosynthetics, 4th edn. Prentice Hall, Englewood Cliffs, New Jersey
Koerner RM (2012) Designing with Geosynthetics, vol 1, 6th edn. Xlibris Corporation, USA
Mhaiskar SY, Mandal JN (1992) Soft clay subgrade stabilization using geocells. In: Grouting, soil improvement and geosynthetics, ASCE. (Biswas et al. (2017)), pp 1092–1103
Mitchell JK, Seed RB, Seed HB (1990) Kettleman hills waste landfill slope failure. I: liner-system properties. J Geotech Eng 116(4):647–668
Moghaddas Tafreshi SN, Dawson AR (2012) A comparison of static and cyclic loading responses of foundations on geocell-reinforced sand. Geotex Geomembr 32:55–68
Pinto MIM, Cousens TW (2000) Effect of the foundation quality on a geotextile-reinforced, brick-faced soil retaining wall. Geosynth Int 7(3):217–242
Rajagopal K, Krishnaswamy NR, Madhavi Latha G (1999) Behaviour of sand confined with single and multiple geocells. Geotext Geomembr 17:171–181
Rea C, Mitchell JK (1978) Sand reinforcement using paper grid cells. ASCE Spring Convention and Exhibit, Preprint 3130, Pittsburgh, PA, 24–28 April
Sitharam TG, Hegde A (2013) Design and construction of geocell foundation to support embankment on soft settled red mud. Geotext Geomembr 41:55–63
Vidal H (1966) La Terre Armee', Annals of" L'Institut Technique de Batiment et des Travaux Public". Serie Materiaux 30:223–224
Wayne MH, Han J, Akins K (1998) The design of geosynthetic reinforced foundations. Proceedings of Geosynthetics in Foundation and Erosion Control Systems, ASCE Geotechnical Special Publication 76:1–18
Zhang MX, Javadi AA, Min X (2006) Triaxial tests of sand reinforced with 3D inclusions. Geotext Geomembr 24:201–209
Zhou H, Wen X (2008) Model studies on geogrid-or geocell-reinforced sand cushion on soft soil. Geotext Geomembr 26(3):231–238

Chapter 2
Cellular Confinement Systems: Characterization to Field Assessment

Amarnath M. Hegde

Abstract In the last few years, the use of geocell reinforcements in various infrastructural projects has gained importance due to its positive benefits. Due to an increased use of geocells in the infrastructure projects, there exists an expansive scope for further research to understand the material better. Hence, the present chapter provides the wide spectrum of knowledge about the geocell reinforcement ranging from characterization to the field implementation. The chapter has been broadly divided into different sections covering detailed characterization, reinforcement mechanisms, design methods, analytical solutions, and the construction practices. The brief summary about the various factors, which influence the behavior of geocell reinforced system, is presented. Further, a detailed note about the field installation procedure and the equipment requirement has been discussed.

Keywords Geocell · Characterization · Design guidelines · Influencing parameters · Construction practices

List of Notations

B	Footing width (m)
C_r	Apparent cohesion (kPa)
D	Equivalent diameter of the geocell pocket opening (m)
D_r	Depth of the reinforcement (m)
E_i	Initial tangent modulus of the geocell layer (kPa)
I_f	Improvement factors (dimensionless)
K_p	Coefficient of passive earth pressure (dimensionless)
K_r	Young's modulus parameter of the geocell reinforced sand (dimensionless)

A. M. Hegde (✉)
Department of Civil and Environmental Engineering, Indian Institute of Technology Patna, Patna 801106, India
e-mail: ahegde@iitp.ac.in

T. G. Sitharam et al. (eds.), *Geocells*, Springer Transactions in Civil and Environmental Engineering,
https://doi.org/10.1007/978-981-15-6095-8_2

K_e	Young's modulus parameter of the unreinforced sand (dimensionless)
k_1, k_2, k_3	Resilient modulus parameters (dimensionless)
M	Secant stiffness of the geocell (kN/m)
M_r	Resilient modulus (kPa)
n	Modulus exponent (dimensionless)
N_{limit}	Limiting number of cycles (dimensionless)
P	Active earth pressure (kPa)
p_a	Atmosphere pressure (kPa)
q_r	Bearing pressure of the reinforced bed (kPa)
q_o	Bearing pressure of unreinforced bed (kPa)
q_{ult}	Ultimate bearing capacity (kPa)
R_a	Surface roughness (μm)
S_o	Settlement of the unreinforced foundation bed (m)
S_r	Settlement of the reinforced bed (m)
T	Tensile strength of the basal geogrid material (kN/m)
α	Horizontal angle of the tensional force (degrees)
β	Load dispersion angle (degrees)
σ_1	Normal stress (kPa)
σ_3	Confining stress (kPa)
σ_h	Hoop stress (kPa)
$\Delta\sigma_3$	Increase in the confining stress (kPa)
ξ_a	Axial strain (percentage)
ψ	Dilation angle (degrees)
θ	Bulk stress (kPa)
τ_{oct}	Octahedral shear stress (kPa)
ν_g	Poisson's ratio of geocell (dimensionless)
ε_h	Hoop strain (percentage)
ε_3	Percentage radial strain (percentage)
ε_c	Circumferential strain (percentage)
ε_l	Volumetric strain (percentage)

List of Abbreviations

CTE	Coefficient of thermal expansion
ECA	Equivalent composite approach
ESCR	Environmental stress-cracking resistance
HDPE	High-density polyethylene
NPA	Novel polymeric alloy
OIT	Oxidative induction time
PRS	Percentage reduction in the footing settlement

2.1 Introduction

Geocell is considered as cost-effective, environmentally friendly, durable, and easy to use. It can be used in all weather conditions without any major maintenance. General applications include foundations, embankments, pavements, earth retaining structures, and erosion control. Nowadays, the geocell applications are growing at the rapid rate due to its proven advantages over traditional techniques. As the geocell applications are growing at the rapid rate, it is very high time to understand its potential benefits for the successful implementation of future projects. This chapter provides the comprehensive knowledge related to cellular confinement system. The efficacy of geocell reinforcement has been demonstrated through four major sections. It includes detailed characterization, laboratory model studies, analytical studies, numerical studies, and case studies-cum-full-scale studies. The idea is to enrich the knowledge on geocell technology. In addition, the emphasis is given on the influencing parameters, which affect the function of geocell reinforced systems. Figure 2.1 represents the outline of the discussion carried out in the present chapter.

2.2 Geocell Characterization

A detailed characterization of any material is essential before its use. The general geocell characterization includes the determination of its cell dimensions, aspect ratio, strip thickness, density, surface area, tensile strength, and seam strength. In addition, the knowledge about advanced properties of the geocells such as creep reduction factors, durability to UV degradation, and allowed strength for design of 50 years is essential in the design of the geotechnical structures involving geocells. The design of the geocell for extreme environment and varying temperature conditions demands the determination of the properties like environmental stress-cracking resistance (ESCR), coefficient of thermal expansion (CTE), and oxidative induction time (OIT). In the load support applications, surface characteristics of the geocells play an important role in deciding its performance. Generally, the geocell possesses a unique cup-shaped texture on its surface. Figure 2.2a shows the SEM image of the surface texture. These textures are responsible for the roughness of the surface. The surface roughness is responsible for the interface friction between the material and the soil. Higher the surface roughness, higher is the interface friction. The surface roughness (R_a) can be quantified using the optical profilometer (Hegde and Sitharam 2015).

Figure 2.2b shows the typical surface roughness profile of the geocell material. When subjected to varying degrees of temperature, moisture, pressure, or other stress, the geocells must retain their original dimensions (dimensional stability). If the geocell loses its original dimensions, it can weaken the confinement and compaction leading to degradation or failure of a structure. The simplest way of measuring the dimensional stability is by means of the coefficient of thermal expansion (CTE). The

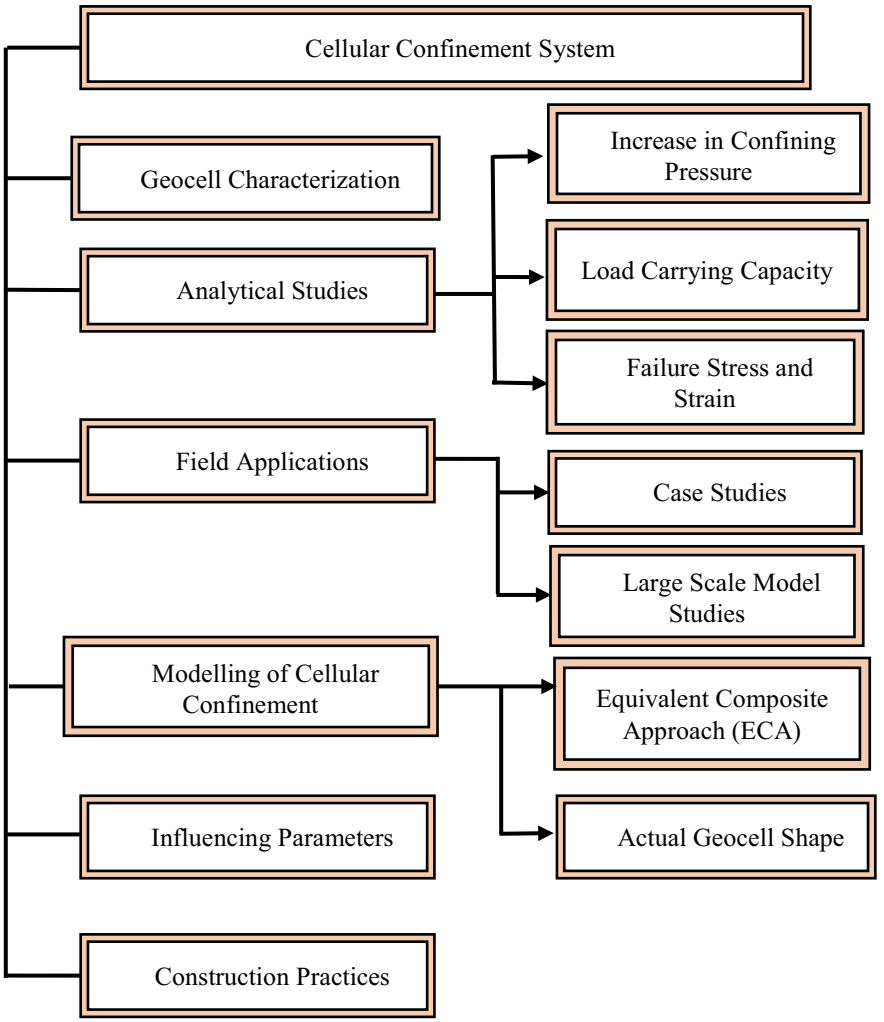

Fig. 2.1 Outline of the research about cellular confinement systems. *Sourced* from Hegde (2017)

low value of the CTE indicates the high-dimensional stability. The recent Neoloy geocells made from reinforcing the nanofibers in a polyolefin are chemically very stable and are having the CTE less than 80 Ppm/°C. Table 2.1 lists the typical properties of the geocells and the reference standards used in the determination of the same.

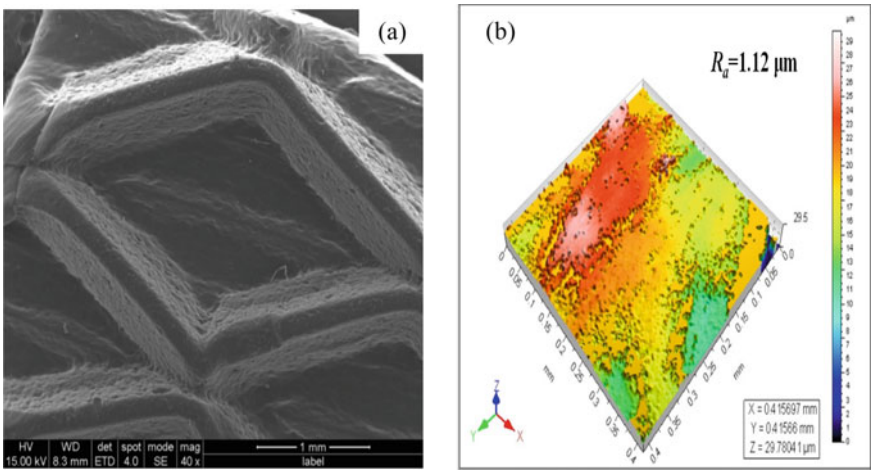

Fig. 2.2 Geocell surface characteristics: **a** SEM image; **b** roughness profile. *Sourced* from Hegde (2017)

2.3 Development and Illustrations of Design Equations

The present section describes about the design equations used to quantify the various improved parameters of the foundation bed in the presence of geocell reinforcement.

2.3.1 Increase in Confining Pressure

The increase in the confining pressure due to the provision of the geocell can be estimated using the formulations provided in the literature. There are separate equations available for the calculation of the increase in the confining pressure in case of the static and cyclic loading conditions. Bathurst and Karpurapu (1993) and Rajagopal et al. (1999) provided the formulation for the static loading conditions. The improvement in the strength and the stiffness of the soil reinforced with the geocells was studied through the triaxial tests. Bathurst and Karpurapu (1993) carried out a series of large-scale triaxial tests on 200 mm high isolated geocell specimen. From the test results, the significant improvement in the apparent cohesion was observed in the presence of geocell reinforcement. Rajagopal et al. (1999) conducted the triaxial compression tests on granular soil encased in a single and multiple geocells. Both geocell reinforced and unreinforced samples exhibited same frictional strength, but significant increment in apparent cohesion (C_r) was observed in the reinforced case as shown in Fig. 2.3.

In figure, the small circle refers to the Mohr circle of the unreinforced soil. Due to the provision of geocell reinforcement, the confining stress increases from σ_3

Table 2.1 Typical properties of the NPA geocells. *Courtesy* Hegde (2017)

Properties	Values	Units	Test methods
Density	0.95	g/cm^3	ASTM D1505 (2010)
Strip thickness	1.53 (±10%)	mm	ASTM D5119 (2012)
Tensile strength	>20	N/mm	PRS method[a]
Diameter of the hole on the surface	10	mm	N/A
Percentage open area on the surface	16	%	N/A
Allowed strength for design of 50 years	>8	kN/m	ASTM D6992 (2009)[b]
Creep reduction factor	>2.7		ASTM D6992 (2009)[c]
Environmental Stress-Cracking Resistance (ESCR)	>3000	hr	ASTM D1693 (2015)
Coefficient of Thermal Expansion (CTE)	<80	Ppm/°C	ISO 11359-2 (TMA) (1999) ASTM E831 (2014)[d]
Durability to UV Degradation	>250	Minutes	ASTM D5885 (2015) (High pressure oxidative induction time (HPOIT) at 150 °C, 3,500 kPa)
Oxidative induction Time (OIT)	>100	min	ISO 11357-6 (2006), ASTM D3895 (2014) (OIT at 200 °C, 25 kPa)
Flexural Storage Modulus at sample temp: 30 °C 45 °C 60 °C 75 °C	 >750 >650 >550 >300	MPa	ISO 6721-1 (2011) ASTM E2254 (2013)

[a]Test sample cut from cell seam to seam measured at strain rate 20%/min, 23 °C
[b]Allowed strength to reach 10% creep strain max for 50 years at 23 °C
[c]Creep (deformation) reduction factor for 50 years at 23 °C
[d]CTE measurement range from −30 °C to +30

to $\sigma_3 + \Delta\sigma_3$ due to which the ultimate normal stress increases to σ_1 from σ_{1u}. The intermediate circle in the figure indicates the Mohr circle corresponding to this state. The same ultimate stress can also be represented with the larger Mohr circle, which has a confining pressure of σ_3 with an apparent cohesion of C_r (Rajagopal et al. 1999). Researchers observed that the geocell reinforcement imparts apparent cohesive strength even to the cohesion less soil. Further, Zhang et al. (2006) opined that inclusion of 3D reinforcement increases both apparent cohesion and the angle of internal friction of the soil.

As suggested by Rajagopal et al. (1999), the induced apparent cohesion of the geocell-soil composite layer can be calculated using Eqs. (1) and (2).

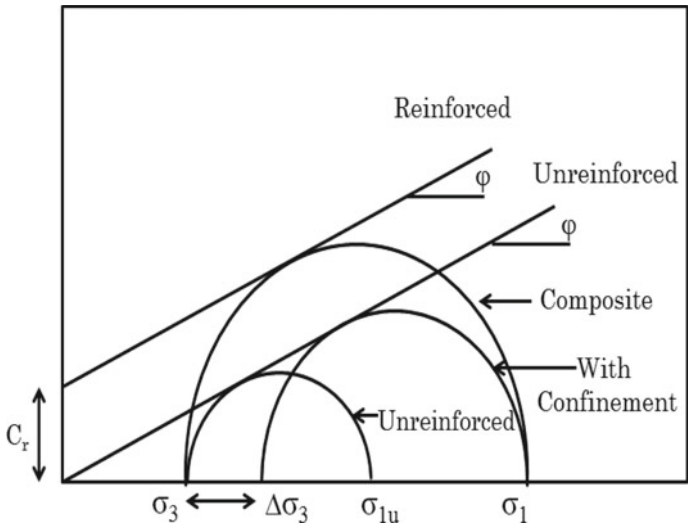

Fig. 2.3 Mohr circle for calculation of the apparent cohesion for geocell-soil composite. *Sourced* from Hegde (2017)

$$\Delta\sigma_3 = \frac{2M}{D}\left[\frac{1-\sqrt{1-\xi_a}}{1-\xi_a}\right] \tag{1}$$

where M is the secant modulus of the geocell material calculated corresponding to the axial strain of ξ_a in the tensile stress–strain response; D is the equivalent diameter of the geocell pocket opening. The increment in the apparent cohesion (C_r) due to the increase in the confining pressure can be given by,

$$C_r = \frac{\Delta\sigma_3}{2}\sqrt{K_p} \tag{2}$$

where K_p is the coefficient of passive earth pressure. The above equation was actually originated from the rubber membrane theory developed by Henkel and Gilbert (1952) to correct the effects of stiff rubber membrane in triaxial tests. The equivalent stiffness of the geocell-soil composite can be related to the stiffness of the unreinforced soil, secant modulus of the geocell material, and the interaction parameter (which represents the interaction, in case of multiple cells) as suggested by Madhavi Latha (2000) below.

$$K_r = K_e + 200M^{0.16} \tag{3}$$

where K_r is the Young's modulus parameter of the geocell reinforced sand and K_e is the Young's modulus parameter of the unreinforced sand. The Young's modulus parameter (K_e) in the Eq. (4) corresponds to the modulus number in the hyperbolic model proposed by Duncan and Chang (1970). The equivalent initial tangent modulus

of the geocell layer is then determined using the equation suggested by Janbu (1963) to relate the stiffness of the soil to the confining pressure as given below.

$$E_i = K_r P_a \left(\frac{\sigma_3}{P_a} \right)^n \tag{4}$$

where E_i is the initial tangent modulus of the geocell layer, σ_3 is the confining pressure acting at the midlevel of the geocell layer, P_a is the atmospheric pressure, K_r is the Young's modulus parameter of geocell layer determined using Eq. (3), and n is the modulus exponent of the unreinforced soil.

Later, Chen et al. (2013) carried out the triaxial compression tests on the geocell reinforced sand. In their study, the researchers have used the different shapes of the geocells, viz. circular, rectangular, and the hexagonal. Out of all the tested shapes of the geocells, the circular shape was found most effective in increasing the apparent cohesion. In addition, the effect of number of cells on the performance of reinforced sand was examined. It was observed that the earth resistance and horizontal pressure increased with the increase in the number of cells. The schematic representation of the reinforced soil sample with the increase in the number of geocell pockets are shown in Fig. 2.4. The number of the cells (i.e., nc= 1, 2, 3, and 4 cells) were varied in the triaxial apparatus of diameter 100 mm. It was noticed that the performance of the soil was improved significantly with the increase in the number of geocell pockets. It was attributed due to the apparent cohesion between the infill material and geocell interface without affecting the internal friction resistance of the soil material (Rajagopal et al. 1999).

It was also reported that the rate of improvement in shear strength of the reinforced soil was maximum when the number of cells increased to three, and the improvement was marginal with the further increase in number of cells. It was justified that the increasing number of cells, increased the ratio of the confined area of the soil over

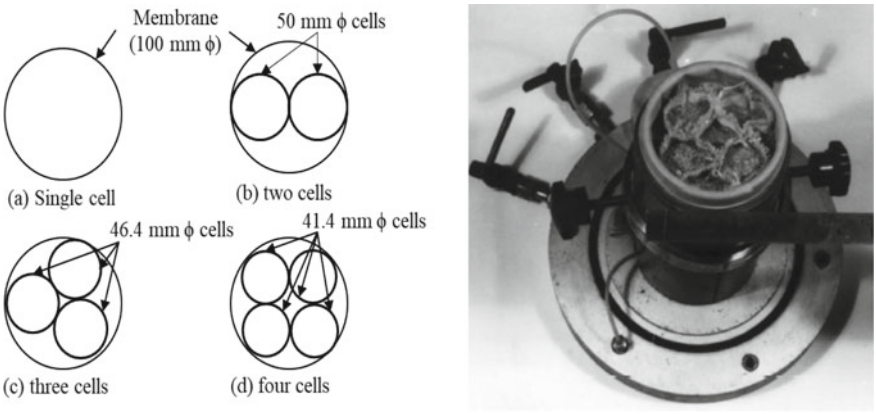

Fig. 2.4 Schematic of cells used in the triaxial tests. *Modified* after Rajagopal et al. (1999)

Table 2.2 Summary of triaxial studies related to the geocells. *Courtesy* Hegde (Hegde 2017)

Researcher	Specimen size	Geocell material/size/number of cells	Confining pressure (kPa)
Bathrust and Karpurapu (1993)	350 mm dia. and 700 mm height	Polyethylene/ 200 mm dia/ single cell with varying aspect ratio	10, 25, 50, 75 and 100
Rajagopal et.al (1999)	100 mm in dia and 200 mm in height	Geotextile/ varying dia/ single as well as multiple	100, 150 and 200
Zhang et al. (2006)	61.8 mm dia and 135 mm height	Galvanized iron sheet/ 4 cm dia/single and double	50, 100, 150 and 200
Chen at al. (2013)	70 mm dia and 140 mm height; 150 mm dia and 300 mm height	High density Polyethylene (HDPE)/ varying dia/ single as well as multiple	50 kPa, 100 kPa and 200

the total area of the triaxial cell, which in turn improved the stiffness of the soil and enhances specimen behavior (Rajagopal et al. 1999). It indicated that increasing the number of cells from three to four did not improve the area of confined soil, thereby did not observe the significant improvement. The summary of the research activities related to triaxial studies on the geocells was summarized in Table 2.2.

Indraratna et al. (2015) proposed an equation to determine the increase in the confining pressure ($\Delta\sigma_3$) due to the provision of the geocell subjected to repeated loading. Researchers have formulated the equation based on the repeated load triaxial test results as represented below.

$$\Delta\sigma_3 = \frac{M}{D}\left[-\frac{\Delta\sigma_3}{M_{r,1}} + \frac{\sigma_1 - (\sigma_3 + \Delta\sigma_3)}{M_{r,2}}\right] \times \left(\frac{\varepsilon_o}{\varepsilon_r}\right) e^{(-\rho/N_{\text{lim}it})\beta} \left(\frac{1+\sin\psi}{1-\sin\psi}\right) \quad (5)$$

where D is the diameter of the sample; M is the tensile stiffness of the geocell (in force/length); σ_3 is the confining stress in the triaxial test; σ_1 is the vertical stress in the triaxial test; ψ is the dilation angle; M_{r1} is the resilient modulus during the stage at which confining stress was increased from σ_3 to $\sigma_3 + \Delta\sigma_3$. M_{r2} is the resilient modulus during the stage at which confining stress was increased from σ_3 to $\sigma_3 + \Delta\sigma_3$; $(\varepsilon_o/\varepsilon_r)$, ρ and β are the permanent deformation parameters of the granular material. N_{limit} is the limiting number of cycles. The resilient modulus (M_r) is calculated using the equations below.

$$M_r = k_1 P_a \left(\frac{\theta}{p_a}\right)^{k_2} \left(\frac{\tau_{\text{oct}}}{p_a} + 1\right)^{k3} \quad (6)$$

where k_1, k_2, and k_3 are resilient modulus parameters of the material; p_a is atmospheric pressure; θ is the bulk stress; and τ_{oct} is the octahedral shear stress. The resilient

modulus M_{r1} is determined using the Eq. (6) with

$$\theta = \sigma_3 + 2(\sigma_3 + \Delta\sigma_3) \tag{7}$$

$$\tau_{\text{oct}} = \frac{\sqrt{2}}{3}\Delta\sigma_3 \tag{8}$$

The resilient modulus M_{r2} is determined using the Eq. (6) with

$$\theta = \sigma_1 + 2(\sigma_3 + \Delta\sigma_3) \tag{9}$$

$$\tau_{\text{oct}} = \frac{\sqrt{2}}{3}[\sigma_1 - (\sigma_3 + \Delta\sigma_3] \tag{10}$$

Similarly, Indraratna et al. (Indraratna et al. 2015) proposed equation for determining the additional confinement due to the provision of geocell subjected to cyclic loading. The additional confinement offered by the geocell was computed using the hoop tension theory. The following equation was given.

$$\Delta\sigma_3 = \frac{2M}{D}\frac{\left[(1-\nu_g)(k+\nu_g)\right]}{(1+\nu_g)(1-2\nu_g)}(-\varepsilon_3) \tag{11}$$

where $\Delta\sigma_3$ is additional confining stress in each pocket; D is the diameter of an equivalent circular area of the geocell pocket; M is the mobilized modulus of the geocell; ν_g is the Poisson's ratio of geocell; k is the ratio between ε_c and ε_3; ε_3 is the percentage radial strain; ε_c percentage circumferential strain.

2.3.2 *Load Carrying Capacity*

Koerner (1998) proposed the analytical solution to estimate the bearing capacity of the geocell reinforced foundation beds. This method attributes the increase in bearing capacity of the geocell reinforced soil to the lateral resistance effect developed due to the interfacial friction between soil and cell wall. Presto (2008) had developed a bearing capacity equation for the geocell reinforced sand. The equation was developed based on the empirical design methods of the unpaved road over the soft subgrade. Zhao et al. (2009) opined that the increase in the bearing capacity of the geocell reinforced soil is mainly due to three mechanisms: (a) lateral resistance effect, (b) vertical stress dispersion effect, and (c) membrane effect. Further, Zhang et al. (2010) proposed simple bearing capacity equations for geocell supported embankment over the soft soil. This method considers only vertical stress dispersion mechanism and the membrane mechanism. The summary of the bearing capacity equations provided by different researches are presented in Table 2.3.

Table 2.3 Summary of the studies related to bearing capacity calculations of geocell reinforced soil. *Courtesy* Hegde (2017)

References	Mechanisms considered	Bearing capacity equations	Parameters
Koerner (1998)	Lateral resistance effect	$P_r = 2p\tan^2(45-\varphi/2)\tan\delta + cN_cS_c + qN_qS_q + 0.5\gamma BN_\gamma S_\gamma$	P_r = bearing capacity of the reinforced soil (kPa); p = applied pressure on geocell mattress (kPa) φ = friction angle of the soil used to fill the geocell pockets (degrees) δ = interface shear angle between the cell wall and the filling soil (degrees) c = cohesion of the soil (kPa) q = surcharge load (kPa) B= width of the applied pressure system (m) γ = unit weight of the soil (kN/m^3) N_c, N_q, N_γ = bearing capacity factors (dimensionless) S_c, S_q, $S_{\gamma\,=}$ shape factors (dimensionless)
Pestro (2008)	N/A	$P_r = 2\frac{h}{d}k_a\sigma_{\text{vm}}\tan\delta + C_uN_c$	P_r = bearing capacity of the reinforced soil (kPa); h/d = geocell aspect ratio (dimensionless); k_a = coefficient of active earth pressure (dimensionless); σ_{vm} = average vertical stress (kPa); δ = interface shear angle between the cell wall and the filling soil (degrees) C_u = subgrade shear strength (kPa); N_c = bearing capacity coefficient (dimensionless);

(continued)

Table 2.3 (continued)

References	Mechanisms considered	Bearing capacity equations	Parameters
Zhang et al. (2010)	Vertical stress dispersion and membrane mechanisms	$P_r = p_s + \frac{2h_c \tan\theta_c}{b_n} p + \frac{2T \sin\alpha}{b_n}$	P_r = bearing capacity of the reinforced soil (kPa); p= applied pressure on geocell mattress (kPa) b_n = width of the uniform load (m); h_c = height of the geocell reinforced cushion θ_c = dispersion angle of the geocell reinforcement (degrees) T = tensile force in geocell reinforcement (kN/m) α = horizontal angle of the tensional force T (degrees)
Avesani Neto et al. (2013)	Confinement effect, stress dispersion effect and the membrane effect	$P_r = P_u + 4\frac{h}{d} k_o pe \tan\delta + (1-e)p$	P_r = bearing capacity of the reinforced soil (Pa); P_u = bearing capacity of unreinforced soil (Pa); h/d = geocell aspect ratio(dimensionless); k_a = coefficient earth pressure at rest (dimensionless); p = load at the top of the geocell mattress (Pa); e = stress redistribution effect (dimensionless) δ = interface shear angle between the cell wall and the filling soil (degrees)

(continued)

Table 2.3 (continued)

References	Mechanisms considered	Bearing capacity equations	Parameters
Sitharam and Hegde (2013)	Lateral resistance effect, vertical stress dispersion and membrane mechanisms	$P_r = P_u + 2P\tan^2(45-\varphi/2)\tan\delta + P_r\left(1-\frac{B}{B+2D_r\tan\beta}\right)+\frac{2T\sin\alpha}{B}$	P_r = Bearing capacity of the geocell reinforced soil (kPa) P_u = Bearing capacity of the unreinforced soil (kPa) P = applied pressure on the geocell mattress (kPa) φ = friction angle of the soil used to fill the geocell pockets (degrees) δ = interface shear angle between the cell wall and the filling soil (degrees) B= footing width (m); D_r = depth of the reinforcement (m) β = load dispersion angle degrees) T = tensile strength of the basal geogrid material (kN/m) α = horizontal angle of the tensional force T (degrees) B_g =width of the basal geogrid (m); S =footing settlement measured at the surface (m)

Similarly, Sitharam and Hegde (2013) proposed a method to estimate the increase in the load carrying capacity of the geocell reinforced soft clay beds by considering all the three mechanisms proposed by Zhao et al. (2009). This model is based on the hypothesis that the lateral resistance effect and the vertical stress dispersion effect are contributed by the geocell while the membrane effect is originated by virtue of basal geogrid.

Koerner (1998) opined that the lateral resistance effect originate due to the interaction between the geocell surface and the infill soil. The interaction leads to the development of the additional shear strength at the interface, which will enhance the bearing capacity of the geocell reinforced soil. The vertical stress dispersion mechanism is also called as the wide slab mechanism. This mechanism was first observed by Binquet and Lee (1975). Schlosser et al. (1983) extended this mechanism to the strip footing resting on the reinforced soil beds. Subsequently, many researchers have reported the wide slab mechanism in their studies (Huang and Tatsuoka 1988, 1990; Takemura et al. 1992). In addition, the presence of a wide slab mechanism in the geocell reinforced foundation bed was justified by the findings of (Dash et al. 2001, 2001; Sitharam and Sireesh 2004, 2005) through 1-g model tests. They observed that the interconnected cells form a panel that acts like a large slab that spreads the applied load over an extended area leading to the overall improvement in the performance of the foundation soil. Footing of width B resting on the geocell reinforcement behaves as if the footing of width $B + \Delta B$ resting on soft soil at the depth of D_r (where D_r is the depth of the reinforcement) and β is the load dispersion angle that varies between 30^o and 45^o.

The membrane effect mechanism is contributed by the vertical component of the mobilized tensile strength of the planar reinforcement (Zhang et al. 2010). Sitharam and Hegde (2013) observed that membrane mechanism originated due to the resistance offered by the soil reinforcement to the bending. When the vertical load is applied on the combination of the geocell and the geogrid, the deformed shape of geogrid is generally parabolic in nature. However, if the footing dimension is very small as compared to the geogrid dimension, then it resembles the triangular shape. Similarly, Avesani Neto et al. (2013) also derived the bearing capacity equation for the soil reinforced with the geocells. In their formulation, the bearing capacity equation of the geocell reinforced soil was obtained by summing up the bearing capacity of the unreinforced soil and the bearing capacity improvement caused by geocells.

2.3.3 Failure Stresses and Strains

When a vertical load is applied to the geocell-soil composite, the mobilization of horizontal stresses takes place in the infill material. The horizontal stress, thus developed imparts the active earth pressure on the cell wall. The active earth pressure on the cell wall generates Hoop stress within the wall and the passive earth pressure on the adjacent walls (Emersleben and Meyer 2008). Hence, the confinement effect of the geocell is based on three main mechanisms: active earth pressure within loaded

cell, passive earth pressure in the adjacent cells and the Hoop stress within the cell wall (Emersleben and Meyer 2008, 2015). The different stresses developed in the geocell walls under the action of compression loads are shown in Fig. 2.5.

The Hoop stress will lead to the deformation of the cell wall. The cell wall deformations can be measured in terms of Hoop strains and the volumetric strains. Hegde and Sitharam (2015) developed the expression for the Hoop stress, Hoop strain and the volumetric strains in the geocell surface using the theory of thin cylinder formulations. Figure 2.6 represents the stresses acting on the surface of the deformed geocell as reported by Hegde and Sitharam (2015).

The only half portion of the geocell was considered by the researchers in the formulation due to the symmetry. P is the active earth pressure exerted by the infill soil on the geocell wall. Researchers have considered the a small element of length, l on the periphery of the geocell, making an angle $d\theta$ with the center to obtain the

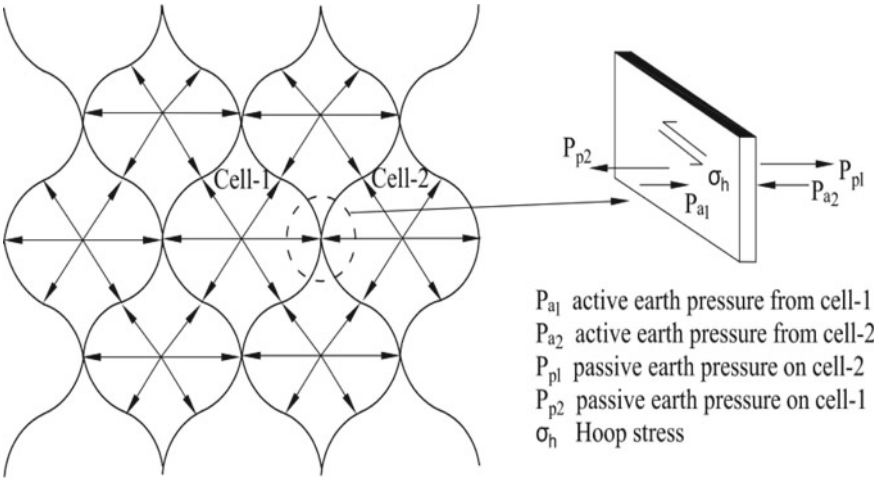

Fig. 2.5 Stresses in expanded geocells under compression loading. *Sourced* from Hegde and Sitharam (2015)

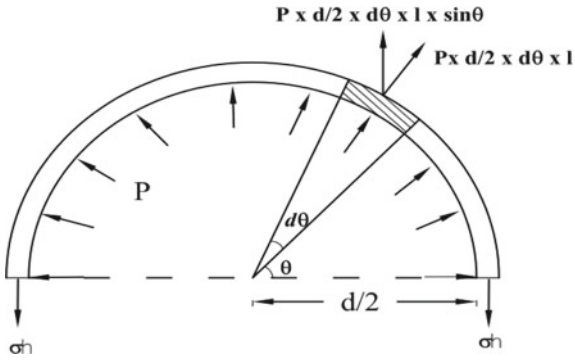

Fig. 2.6 Stresses acting on the surface of the geocell. *Sourced* from Hegde and Sitharam (2015)

Table 2.4 Expressions for the calculation of stresses and strains on geocell surface. *Courtesy* Hegde (Hegde 2017)

Entity	Expression	Parameters
Hoop stress	$\sigma_h = \frac{P \times d}{2 \times t}$	σ_h = Hoop stress on geocell; ε_h =Hoop strain; $\varepsilon_{v=}$ volumetric strain; P = active earth pressure exerted by the infill soil on the geocell wall; E =Young's modulus; d= diameter of the geocell pocket; μ = Poisson's ratio; t= thickness of the geocell
Hoop strain	$\varepsilon_h = \frac{P \times d \times (2-\mu)}{4 \times t \times E}$	
Volumetric strain	$\varepsilon_v = \frac{P \times d}{4 \times t \times E}(5 - 4\mu)$	

expression for Hoop stress (σ_h), Hoop strain (ε_h) and volumetric strain (ε_l). Table 2.4 lists the expression for the Hoop stress, Hoop strain, and the volumetric strains on the geocell surface.

These expressions can be used to evaluate the stresses and strains on the geocell. By knowing the possible load from the superstructure, basic physical parameters (d & t), and elastic parameters (E & μ) of the geocell, the stresses and strains on the geocell can be evaluated. The geocell design can be optimized to keep these stresses and strains within desired limits of failure. The limiting strain value reported by the Hegde and Sitharam (2015) was in the range of 1.3%.

2.3.4 *Bearing Capacity Improvement and Reduction in Settlement*

The majority of reported studies have focused on evaluating the overall performance of the foundation bed in the presence of geocells. The overall performance of the foundation bed can be quantified in terms of the increase in bearing capacity and reduction in the settlement. These parameters can be expressed in terms of dimensionless parameters, namely, bearing capacity improvement factors (I_f) and the percentage reduction in the footing settlement (PRS) respectively (Dash et al. 2003; Madhavi Latha and Somwanshi 2009; Saride et al. 2009; Hegde and Sitharam 2013, 2015). The bearing capacity improvement factor is defined as,

$$I_f = \frac{q_r}{q_o} \tag{12}$$

where q_r is the bearing pressure of the reinforced bed at a particular settlement and q_o is the bearing pressure of unreinforced bed at the same settlement. Bearing capacity improvement factor is similar to the bearing capacity ratio reported by Binquet and Lee (1975). When the ratio is beyond the ultimate bearing capacity of the unreinforced bed, the ultimate bearing capacity (q_{ult}) is used instead of q_o. The improvement

factor depends on the various parameters such as foundation soil properties, geocell material, infill soil properties, and the aspect ratio of the geocells. Further, for a particular type of geocell and the soil, the improvement factor even varies with the settlement of the bed. On an average, the improvement factor for Neoloy geocells varies in the range of 4–6 (Chen et al. 2013). However, some researchers have reported the values even up to 9 for different test bed conditions. Table 2.5 summarizes the values of the improvement factor reported by the various researchers for the different test conditions.

Similarly, the PRS is defined as,

$$\text{PRS} = \left(\frac{S_o - S_r}{S_o}\right) \times 100 \tag{13}$$

Table 2.5 Value of the improvement factor reported by the various researchers. *Courtesy* Hegde (Hegde 2017)

Researchers	Type of reinforcement	Type of soil bed	Type of infill soil	Improvement factors (max)
Dash et al. (2001)	Geocells made from geogrid	Sand (RD = 70%)	Sand	8
Dash et al. (2003)	Geocells made from geogrid	Clay(C_u = 3.1 kPa)	Sand	5.4
Sitharam and Sireesh (2005)	Geocells made from geogrid	Sand (RD = 70%)	Sand	9.5
Sitharam and Sireesh (2005)	Geocells made from geogrid	Clay (C_u = 5.6 kPa)	Sand	5.5
Madhavi Latha and Somwanshi (2009)	Geocells made from geogrid	Sand (RD = 70%)	Sand	4.75
Sireesh et al. (2009)	Geocells made from geogrid	Clay(C_u = 10 kPa)	Sand	4.9
Hegde and Sitharam (2013)	Neoloy geocell	Sand (RD = 70%)	Sand	3.2
Hegde and Sitharam (2013)	Neoloy geocell	Clay(C_u = 5 kPa)	Sand	6
Hegde and Sitharam (2015)	Neoloy geocell with basal geogrid	Clay(C_u = 10 kPa)	Silty clay	8
Hegde and Sitharam (2015)	Neoloy geocell with basal geogrid	Clay(C_u = 10 kPa)	Sand	10
Hegde and Sitharam (2015)	Neoloy geocell with basal geogrid	Clay(C_u = 10 kPa)	Aggregate	12

RD Relative density; C_u Undrained cohesion

where S_o is settlement of the unreinforced foundation bed corresponding to its ultimate bearing capacity and S_r is the settlement of the reinforced bed corresponding to the ultimate bearing capacity of the unreinforced bed. Generally, the double tangent method is used to estimate the ultimate load bearing capacity. In this method, the ultimate bearing capacity is determined by drawing the two tangents; one at the early part of the pressure-settlement curve and the another at the latter part. Hegde and Sitharam (2015) reported the PRS value more than 70% in the clay bed reinforced with the geocells.

2.4 Field Applications

2.4.1 Case Studies

Bush et al. (1990) reported the construction of the geocell reinforced embankments in soft clay in UK. Researchers had used the geocell of height 1 m with local soil as the infill material. With the geocells, about 33% lesser settlements were observed after 4 years when compared to systems with horizontal layers of reinforcement. Further, the cost savings of more than 31% were observed due to the provision of geocells. Cowland and Wong (1993) presented the case history of the construction of the 10 m high road embankment supported on the geocell reinforced soft clay deposit. Two layers of the geocell mattress were used to support the two separate embankments of 300 and 200 m long each. The geocell was coupled with the wick drains to support the embankment. In overall, the satisfactory performance of the geocell was observed in the project. Sitharam and Hegde (2013) discussed the design and construction of the geocell supported embankment in soft settled red mud in Lanjigarh, Orissa in India. The consolidated red mud was having an average SPT-N value of 12. The embankment of 3 m height and 20 m wide and 680 m long was supported on the geocell foundation. Figure 2.7 shows the schematic view of the geocell supported embankment in Lanjigarh. Over 15,000 m^2 of embankment base was stabilized using geocell foundation. The foundation work was completed within 15 days using locally available labors and the equipment. The excellent performance of the geocell was observed without any cracks, seepage or settlements in the embankments.

Emersleben and Meyer (2008) reported the use of geocells in the reconstruction of the roads for a stretch of 500 m near the city of Hannover in Germany. The geocell was placed directly below the asphalt layer. Researchers evaluated the satisfactory performance of the geocells through various field tests. Kief et al. (2011) presented the application of polyester based geocells in the pavement construction near Chennai, India. Researchers used the NPA geocells to reinforce the pavement section. Researchers opined that the geocells can be used in the upper pavement, directly under asphalt. Rajagopal et al. (2014) reported the field performance of the geocell reinforced road section in India. The reported road section was constructed on the black cotton soil. Initially, the black cotton soil was treated with the lime and

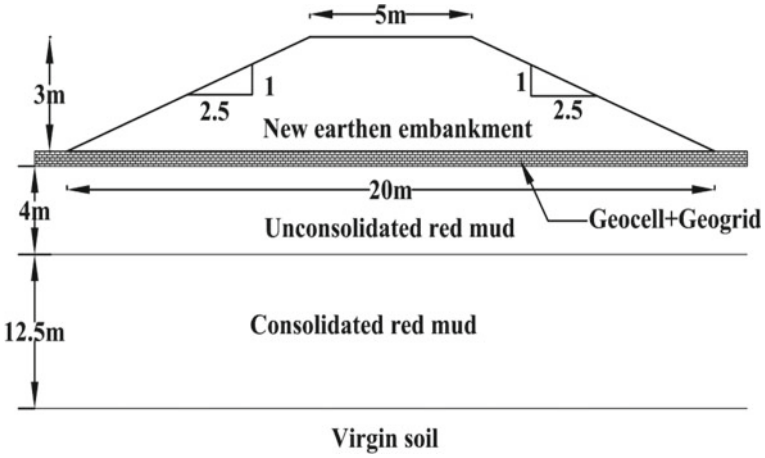

Fig. 2.7 Schematic representation of the geocell supported embankment. *Sourced* from Hegde (2017)

the geocell reinforcement of 150 mm thick was placed above the soil. The geocell pockets were filled with the good quality granular materials. As compared to the unreinforced road section in the same area, the geocell reinforced road sections maintained the uniform surface even after three seasons of heavy rainfall. Pokharel et al. (2010) reported the use of the geocells in the construction of the unpaved roads in the region of northern Alberta and northern British Columbia. The Neoloy geocells of 150 mm height were used in these projects. A significant reduction in the rut depth was observed in the presence of geocells.

2.4.2 Field Tests and Large-Scale Model Tests

Emersleben and Meyer (2008) conducted the field plate load tests and the falling weight deflectometer tests on the pavement reinforced with geocells. Researchers observed the 50% reduction in the vertical stress due to the provision of the geocell reinforcement. The falling weight deflectometer measurements revealed that the 15% reduction in the deflection of the road section. Han et al. (2011) conducted the full scale moving load tests to evaluate the effect of geocell reinforcement on the recycled asphalt pavement (RAP). A test pit of dimension 6.1 m × 4.9 m × 1.8 m was dug and the subgrade consisted of the clay was prepared. Above the compacted subgrade, a layer of Neoloy Polymeric Alloy (NPA) geocell was placed and the cell pockets were filled with the RAP. Researchers observed that the geocell reinforcement improves the performance of unpaved RAP sections by widening the stress distribution angle and reducing the rut depth. Yang et al. (2012) conducted the accelerated pavement tests (APT) on the unpaved roads with geocell reinforced sand bases. Four sections of

the unpaved roads were constructed at the APT facility of dimension 6.1 m × 4.9 m × 1.8 m made of concrete. Out of four sections, the two sections were unreinforced sections with aggregate cover at the top and the other two sections were geocell reinforced sections with different height of the geocell. Researchers observed the substantial reduction in the rut depth in the presence of geocells.

The summary of the previous studies related to field tests, large-scale model tests, and the case studies related to geocells is listed in Table 2.6. Tavakoli Mehrjardi et al. (2013) carried out the full-scale model tests to study the efficacy of the geocell reinforcement in protecting the buried pipeline under the action of repeated load.

The tests were conducted in a concrete box of dimension 6.2 m × 2.5 m × 1.5 m. Test bed was prepared using the sandy soil in their study. In the test bed, a trench of 0.5 m width was excavated and the PVC pipe of 160 mm diameter was

Table 2.6 Field tests, large-scale model tests and the case studies related to geocells. *Courtesy* Hegde (Hegde 2017)

Researchers	Type of soil	Type of geocell	Type of test	Application type	Test size/foot print area
Field test/ Large scale model tests					
Emersleben and Meyer (2008)	Soft soil	HDPE	Field plate load test	Pavements	2 m × 2 m × 2 m
Han et al. (2011)	Clay	Neoloy Polymeric Alloy (NPA)	Moving wheel load tests	Pavement	6.1 m × 4.9 m × 1.8 m
Yang et al. (2012)	Clay	Neoloy Polymeric Alloy (NPA)	Moving wheel load tests	Pavement	6.1 m × 4.9 m × 1.8 m
Tavakoli Mehrjardi et al. (1996)	Sand	Non-woven geotextile cells	Large-scale plate load test	Protection of buried pipeline	6.2 m × 2.5 m × 1.5 m.
Tanyu et al. (2013)	Aggregates	HDPE	Large-scale cyclic plate load test	Pavement	3 m × 3 m × 3.5 m
Moghaddas Tafreshi et al. (2014)	Sand	Non-woven geotextile cells	Field cyclic plate load tests	Pavement	2 m × 2 m × 0.7 m
Case studies					
Cowland and Wong (2008)	Soft clay	HDPE geogrid cells	N/A	Embankment	300 m × 200 m, 2 nos.
Sitharam and Hegde (2013)	Red mud	Neoloy Polymeric Alloy (NPA)	N/A	Embankment	680 m × 20 m
Kief et al. (2011)	Clay	Neoloy Polymeric Alloy (NPA)	N/A	Pavement	500 m

placed. Repeated load was applied to the test bed with the help of a circular footing. Researchers observed the 35% reduction in the pipe strain in the presence of the geocell reinforcement as compared to unreinforced case. Tanyu et al. (2013) carried out the series of large-scale cyclic plate load tests on the geocell reinforced aggregate bases. Tests were conducted in a test facility with a 3 m × 3 m × 3.5 m reinforced concrete pit. HDPE geocell was used in their study to reinforce the aggregate bases.

Researchers observed the 30–50% reduction in the plastic deflection of the working platforms, 40–50% improvement in the resilient modulus of the subbase and twofold increment in the modulus of subgrade reaction of the bed due to the presence of geocells. Similarly, Moghaddas Tafreshi et al. (2014) carried out a series of field cyclic plate load tests to assess the efficacy of the geocells in improving the performance of pavements. Tests were carried out in a pit of 2 m × 2 m × 0.7 m using a 300 mm diameter rigid steel plate. Researchers observed that the use of the combined geocell and rubber soil mixture layers is more effective than geocell layers alone. Apart from the load tests on the geocells, Guo et al. (2015) carried out the outdoor field vegetation tests to investigate the effect of geosynthetic reinforcement on vegetation. Nowadays, in rural areas, geocells have been used to stabilize the unpaved shoulders to accommodate temporary vehicle loads. However, there was a concern about the vegetation growth in such geocell reinforced sections. The test section of each 1.5 m × 1.5 m with different base and top soil combinations was prepared by reinforcing with the HDPE geocells. Perennial rye-grass seeds were planted and its growth was monitored up to a year. No evidence of geocell reinforcement limiting vegetation growth in unpaved shoulders was found in their study.

2.5 Modeling of Cellular Confinement

As discussed in the preceding sections, the unique advantage of the geocell is its confinement. To evaluate and enrich the understanding about this mechanism, it is indeed of additional design approaches apart from the laboratory investigation. The present section briefly discusses the developed methods for modeling the geocell reinforced system.

2.5.1 Modeling Techniques

This section highlights the two- and three-dimensional methods for simulating the geocells. The numerical methods are helpful for the reader to visualize and understand the reinforcement mechanism of geocell in distributing the stresses and controlling the deformation under the foundation. The numerical methods require less time to analyze the problem as compared to the field studies.

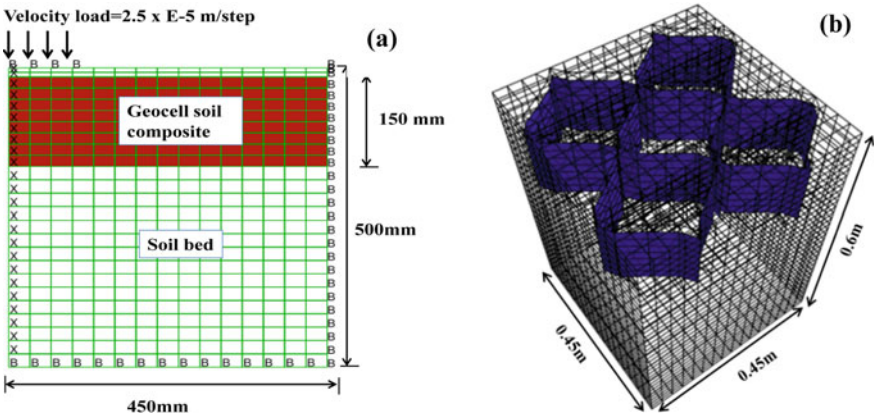

Fig. 2.8 Geocell model: **a** ECA approach; **b** actual shape of geocells. *Sourced* from Hegde and Sitharam (Yang et al. 2010)

2.5.1.1 Equivalent Composite Approach (ECA)

The equivalent composite approach (ECA) is the simplest method of modeling the geocells in the two-dimensional framework. The ECA was adopted by many of the researchers in the past to model the geocells (Bathurst and Karpurapu 1993; Rajagopal et al. 1999). In this approach, the geocell in-filled with sand is modeled as the composite soil layer with improved strength and stiffness parameters. The improved strength and elastic properties of the geocell-soil composite are determined using the formulation illustrated in the Sect. 3.1 using the Eqs. (1)–(4). Figure 2.8a shows the typical ECA numerical model for geocells.

2.5.1.2 Actual Shape 3D Model

Though the ECA offers a simple way of modeling the geocells in two-dimensional framework, it has certain limitations as reported by Hegde and Sitharam (2015). Firstly, it overestimates the bearing capacity of the geocell reinforced foundation beds. Also, it cannot handle the situation, if the combinations of reinforcements are provided (e.g., combination of geocell and geogrid); which is very common practice in the field. In addition, the ECA is applicable only to the geocells with the aspect ratio in between 0.5 and 2.1 (Bathurst and Karpurapu 1993). In order to overcome these limitations, more realistic approach of modeling the geocells has been practiced in the recent studies. The recent trend is to model the geocells in three-dimensional framework by considering its actual shape. However, this approach is slightly complex due to the honeycomb shape of the geocells. Due to this reason, different researchers have used simplified shapes to the geocell pockets.

The numerical simulation of single cell geocell subjected to uniaxial compression was carried out by Han et al. (2008) in FLAC^{3D}. Due to the difficulty in modeling the actual shape, the cell was modeled as the square box in their study. For similar reasons, Hegde and Sitharam (2015) used the circular shaped pocket geometry in their study. Researchers observed the deviation in the experimental and numerical pressure-settlement response. The deviation in the result was attributed due to the shape of the geocell pocket used in the study. Saride et al. (2009) used the square shaped geocell pocket while modeling the multiple cell geocell in FLAC^{3D}. The similar approach was also used by Ling et al. (2009) while modeling geocell reinforced ballast system in ABAQUS. However, Yang et al. (2010) modeled the actual shape (i.e., 3D honeycomb shape) of the single cell geocell, in their study. Hegde and Sitharam (2015a, b) made an attempt to model the real shape of the multiple cell geocells by considering the actual curvature of its pocket. In their study, the foundation soil, infill soil, and the geocell materials were assigned with three different material models to simulate the real case scenario. A photograph of the single cell was taken, and it was digitized to obtain the actual curvature of the cell. The co-ordinates were deduced from the curvature, and the same were used in the FLAC^{3D} to model the actual shape of the geocell (Hegde and Sitharam 2015). Figure 2.8b shows the typical numerical model of the geocells considering the actual shape. Table 2.7 presents the summary of the numerical studies on geocells.

Hegde and Sitharam (2015) compared the vertical stress distribution below the footing for unreinforced and the geocell reinforced soils as shown in Fig. 2.9a–b. In case of unreinforced bed, the uniform pressure bulb of circular shape was observed. The pressure bulb was found to disperse up to the depth of 1.6B (where B is the width of the footing). In geocell reinforced case, the pressure bulb of irregular shape was observed. However, the bulb was confined within geocell pocket and found to spread in lateral direction. The geocells distribute the load into the wider areas below the footing as compared to unreinforced bed (Hegde and Sitharam 2015).

2.6 Influencing Parameters

The several researchers have reported about the various influencing parameters, which affect the performance of geocell reinforced system through laboratory, field, and analytical studies. It was observed that the geocell response significantly depends upon the geometry, placement, formation pattern, the modulus of the geocell, and type of infill and foundation material. The present section provides the optimum details of various parameters to achieve the maximum potential benefits of geocell at the practice. Primarily, the subgrade strength is one of the major factors for the strength of geocell reinforced foundation bed. The model studies of (Biswas and Krishna 2017; Rai et al. 2012; Zhou and Wen 2008) revealed that the geocell can get maximum support from the stiff subgrades. Hegde and Sitharam (2016) highlighted the improvement in performance of the geocell system in the presence of the additional basal geogrid layer. The influence of different infill materials on the behavior of

Table 2.7 Summary of the numerical studies related to geocells. *Courtesy* Hegde (2017)

Researchers	Approach adopted to model geocell	Software program	Type of study
Mhaiskar and Mandal (1996)	ECA with Drucker-Prager model	3D/ANSYS	Geocell reinforced clay bed with sand infill supporting rectangular footing
Bathurst and Knight (1998)	ECA with Duncan-Chang model	2D/GEOFEM	Geocell reinforced sand over steel conduit
Madhavi Latha and Rajagopal (2007)	ECA with Mohr Coulomb model	2D/GEOFEM	Geocell supported embankment on clay subgrade
Han et al. (2008)	Square shape with Mohr Coulomb model for sand and linear elastic model for geocell	3D/FLAC^{3D}	Single cell supporting rectangular footing
Madhavi Latha et.al (2008)	ECA with Duncan-Chang model	2D/GEOFEM	Geocell reinforced sand supporting strip footing
Madhavi Latha et.al (2009)	ECA with Duncan-Chang model	2D/GEOFEM	Geocell reinforced sand supporting strip footing
Madhavi Latha and Somwanshi (2015)	ECA with Duncan-Chang model	3D/FLAC^{3D}	Geocell reinforced sand supporting a square footing
Saride et al. (2009)	Square shape with Mohr Coulomb model for clay and sand and linear elastic model for geocell	3D/FLAC^{3D}	Geocell reinforced clay supporting a circular footing

(continued)

Table 2.7 (continued)

Researchers	Approach adopted to model geocell	Software program	Type of study
Yang et al. (2010)	Honeycomb shape with Duncan- Chang model for sand and linear elastic model for geocell	3D/FLAC^{3D}	Single cell supporting circular footing
Hegde and Sitharam (2013)	ECA with Mohr Coulomb model	2D/FLAC^{2D}	Geocell reinforced sand and clay bed supporting square footing
Hegde and Sitharam (2015)	ECA with Mohr Coulomb model	2D/FLAC^{2D}	Geocell reinforced clay with different infill material
Hegde and Sitharam (2015)	Circular shape with Mohr Coulomb model for infill material and linear elastic model for geocell	3D/FLAC^{3D}	Single cell supporting circular footing
Hegde and Sitharam (2015)	Honeycomb shape with Mohr Coulomb model for sand and linear elastic model for geocell	3D/FLAC^{3D}	Geocell reinforced sand bed supporting square footing
Hegde and Sitharam (2015)	Honeycomb shape with Modified Cam Clay for clay, Mohr Coulomb model for sand and linear elastic model for geocell	3D/FLAC^{3D}	Geocell reinforced clay bed supporting square footing

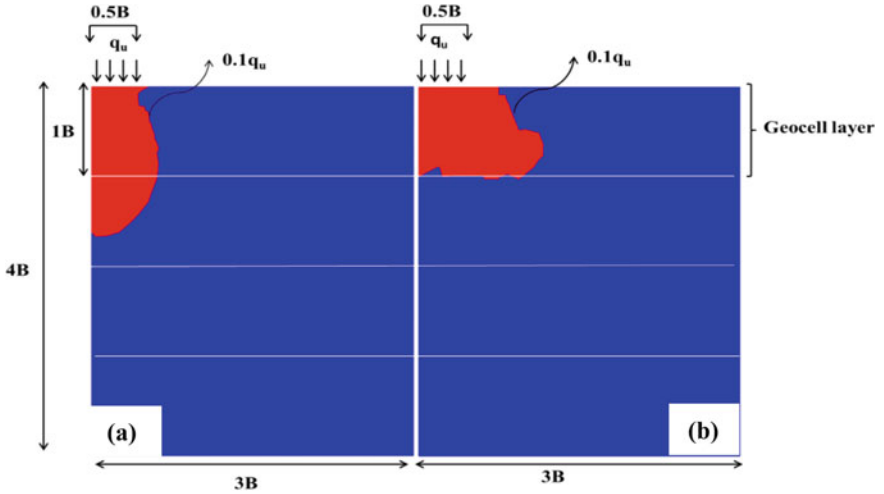

Fig. 2.9 Pressure bulbs corresponding to 0.1 q_u: **a** unreinforced; **b** geocell reinforced. *Sourced* from Hegde and Sitharam (2015)

the geocell system was investigated (Hegde 2015). From the findings, it was noticed that the maximum increase in bearing capacity was observed with the increase in friction angle of infill material. The various studies (Hegde and Sitharam 2015; Bush et al. 1990; Zhou and Wen 2008) have reported the similar findings. Figure 2.10 shows the schematic representation of the geometry of geocell reinforced system.

Davarifard and Tafreshi (2015) studied the performance of multilayered geocell reinforced foundation bed. The results revealed that the significant increase in performance of the bed with the increase in the number of geocell layers. Hegde and Sitharam (2017) studied the behavior of foundation bed reinforced with the geocell made with three different types of materials. The results revealed that the overall

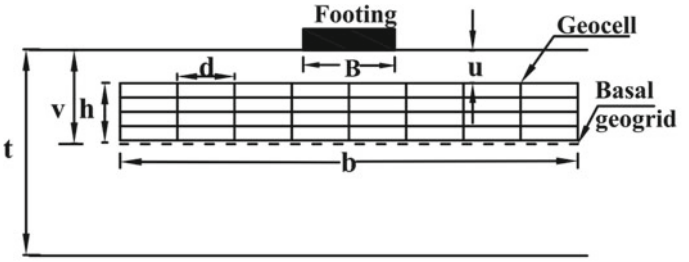

Fig. 2.10 Schematic representation of the geocell reinforced foundation bed

Table 2.8 Summary of influencing parameters on the performance of geocell reinforced foundations

Reference	Footing shape	Influencing parameter	Variation in parameter	Optimum value/details	BCR
Dash et al. (2001)	Strip	Depth of placement of geocell	0*B*, 0.1*B*, 0.25*B*, 0.5*B*, 0.75*B*, 1*B*, and 1.5*B*	0.1*B*	4
Latha et al. (2007)	Strip	Width of geocell	1*B*, 2*B*, 6*B*, and 1*B*	4-6*B*	–
Sireesh et al. (2009)	Circular	Height of geocell	0.6*D* to 3.6*D* with an increment of 0.6*D*	1.5-2*D*	4
Dash et al. (2004)	Circular	Pocket size	1.2*D*, 1.5*D*, and 2.7*D*	0.8*D*	7
Moghaddas Tafreshi and Dawson (2010)	Strip	Height of geocell	H/B = 0.33, 0.66, 1, and 1.33	1.33*B*	3
Hegde and Sitharam (2015)	Strip	Type of infill material	Red soil, sand, and aggregate	Aggregate	13
Hegde and Sitharam (2017)	Strip	Type of geocell material	Geocell made with geogrid, neoloy, and bamboo materials	Bamboo	5.5

[*] *D* is the diameter of the circular footing

performance increases with the increase in modulus of reinforcement material. Dash et al. (2001) studied the effect of formation pattern on the behavior of geocell reinforced system. In overall, three types of patterns, namely, square, diamond, and chevron patterns were considered. From the findings, the superior performance was observed in the case of chevron pattern geocell reinforcement. The summary of the optimum values of different influencing parameters was summarized in Table 2.8.

2.7 Construction Practices

2.7.1 Standard Construction Practices

The field installation of the geocell reinforced structures consists of three major steps, namely, subgrade preparation, installation, and filling of geocell pockets with the infill material. The brief description about the each step is illustrated in the following subsections:

2.7.1.1 Subgrade Preparation

(1) The first and prime step is to prepare the existing site. It should be free from all the organic and foreign matter.
(2) It is indeed to meet the design specifications (geometry, soil compaction, grade etc.) for supporting the proposed project. It can be achieved through proper rolling and other conventional techniques.
(3) The existing soil does not meet the requirements, it should be excavated and replaced with the suitable quality of soil.
(4) Finally, the site should be free of voids and undulations.
(5) A basal geogrid layer (typically biaxial type) is spread out over the leveled ground. If the foundation soil is very soft then a thin layer of granular soil is spread over it. The major functions of the base geogrid layer are to provide a platform for the geocell mattress, and to support the constructional movement.
(6) A minimum overlap of 300 mm is allowed between the adjacent rolls of geogrid layer.

2.7.1.2 Installation or Deployment of Geocell Reinforcement

(1) Decide the site segment and place the collapsed form of the geocell reinforcement over the corresponding segment.
(2) Before the installation of geocell mattress, a series of permanent or temporary wooden stacks (metal anchors) erected over the ground.
(3) The edge cells of the geocell reinforcement are hooked over the stacks, and stretch it up to a maximum coverable area and allowed some time for the relaxation of the reinforcement.
(4) Later, additional stacks will be placed along the perimeter for the complete expansion of the each pocket of the geocell reinforcement. The adjacent sections of the geocell are connected with the help of screw sets.
(5) If it is not possible to install the stacks at the site (presence of rocky strata), an installation frame will be used for the placement of a geocell mattress over the subgrade.

2.7.1.3 Infilling the Geocell Pockets and Its Compaction

(1) Initially, the geocell mattress is filled with good quality granular material with high permeability to facilitate the drainage.
(2) The cells should be filled at least 75 mm above its surface to protect from the damage during construction.
(3) The filling sequence is to fill two rows of cells to half height before filling the first one to full height. The system is continued, always ensuring that no cell is filled to the full height before its neighboring cell is at least half filled to avoid any potential distortion of the geocell structure as shown in Fig. 2.11.

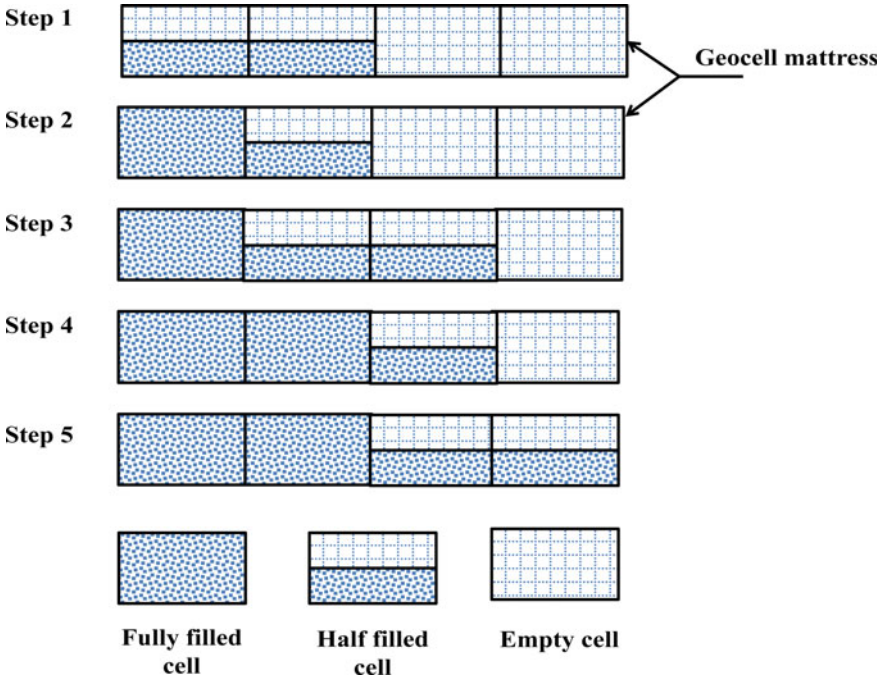

Fig. 2.11 Sequence of filling the geocell mattress

(4) The granular material inside the geocell pocket is either compacted manually by a vibratory hand operated plate compactor or using the vibro floatation technique.
(5) Finally, it is necessary to compact the each and every panel of the geocell reinforced system in accordance with the requirement or specifications. Sometimes, water may be added to the infill material for achieving the required compaction.

2.7.2 Equipment and Accessories Requirement

The brief overview about the various equipment used from the placement of geocell to the compaction of infill material is described in the present section.

(1) Wooden stacks or metal anchors: Useful for stretching the geocell panels over the leveled ground surface. In addition, useful for holding the individual geocell panels in their expanded location while infilling the geocell reinforcement.
(2) Pneumatic staplers, or ties, or screw sets, or rivets: Useful for combining the adjacent panels of the geocell reinforcement.
(3) Front-end loader or dump truck: Useful for dropping the infill material into the geocell pockets from the required height.

(4) Shovels or a bulldozer blade: Useful for pushing the fill material into the pockets of the geocell reinforcement.
(5) Roller compactor: Used to compact the filled cells of the geocell reinforcement.

2.7.3 Precautions and Measures

(1) The suggested sequence of filling the geocell pockets is essential to follow for avoiding the distortion and bending of the geocell reinforcement.
(2) Never allow any equipment to drive over the unfilled area. In addition, always overfill the cells slightly minimum of 50 mm to allow for consolidation.
(3) The excessive drop-height might hurt the cells (Drop-height <1 m is suggested).

2.8 Summary

The use of geocells in various infrastructure projects has been attracting urban developers and contractors due to its various benefits. In this chapter, the various research activities covering the wide spectrum of application related to geocell was described. This chapter has covered the numerous studies related to geocells such as experimental, numerical, and field implementation methods. Further, the detailed description about the developed mechanisms for designing the geocell reinforced systems was presented. In overall, the present chapter would be useful as a primary design guide for the researchers and the practitioners.

References

ISO 6721-1 (2011) Plastics-determination of dynamic mechanical properties. Part 1: general principles. Geneva
ASTM D1505 (2010) Standard test method for density of plastics by the density-gradient technique. ASTM International, West Conshohocken, PA
ASTM D1693 (2015) Standard test method for environmental stress-cracking of Ethylene plastics. ASTM International, West Conshohocken
ASTM D3895 (2014) Standard test method for oxidative-induction time of polyolefins by differential scanning calorimetry. ASTM International, West Conshohocken, PA
ASTM D5199 (2012) Standard test method for measuring the nominal thickness of geosynthetics. ASTM International, West Conshohocken, PA
ASTM D5885 (2015) Standard test method for oxidative induction time of polyolefin geosynthetics by high pressure differential scanning calorimetry. ASTM International, West Conshohocken, PA
ASTM D6992 (2009) Standard test method for accelerated tensile creep and creep-rupture of geosynthetic materials based on time-temperature superposition using the stepped isothermal method. ASTM, West Conshohocken, PA
ASTM E2254 (2013) Standard test method for storage modulus calibration of dynamic mechanical analysers. ASTM International, West Conshohocken, PA

ASTM E831 (2014) Standard test method for linear thermal expansion of solid materials by thermomechanical analysis. ASTM International, West Conshohocken, PA
Avesani Neto JO, Bueno BS, Futai MM (2013) A bearing capacity calculation method for soil reinforced with a geocell. Geosynth Int 20(3):129–142
Bathurst RJ, Karpurapu R (1993) Large scale triaxial compression testing of geocell reinforced granular soils. Geotech Test J 16(3):296–303
Bathurst RJ, Knight MA (1998) Analysis of geocell reinforced soil covers over large span conduits. Comput Geotech 22(3/4):205–219
Binquet J, Lee LK (1975) Bearing capacity tests on reinforced earth slabs. J Geotech Eng Div ASCE 101(12):1241–1255
Biswas A, Krishna AM (2017) Geocell-reinforced foundation systems: a critical review. Int J Geosynth Ground Eng 3(2):17
Bush DI, Jenner CG, Bassett RH (1990) The design and construction of geocell foundation mattresses supporting embankments over soft ground. Geotext Geomembr 9:83–98
Chen RH, Haung YW, Haung FC (2013) Confinement effect of geocells on sand samples under triaxial compression. Geotext Geomembr 37:35–44
Cowland JW, Wong SCK (1993) Performance of a road embankment on soft clay supported on a geocell mattress foundation. Geotext Geomembr 12:687–705
Dash SK, Krishnaswamy NR, Rajagopal K (2001a) Bearing capacity of strip footings supported on geocell-reinforced sand. Geotext Geomembr 19:235–256
Dash SK, Rajagopal K, Krishnaswamy NR (2001b) Strip footing on geocell reinforced sand beds with additional planar reinforcement. Geotext Geomembr 19:529–538
Dash SK, Sireesh S, Sitharam TG (2003) Model studies on circular footing supported on geocell reinforced sand underlain by soft clay. Geotext Geomembr 21:197–219
Davarifard S, Tafreshi SM (2015) Plate load tests of multi-layered geocell reinforced bed considering embedment depth of footing. Proc Earth Planet Sci 15:105–110
Duncan JM, Chang CY (1970) Non-linear analysis of stress and strain in soils. J Soil Mech Foundations Division 96:1629–1653
Emersleben A, Meyer N (2008) Bearing capacity improvement of gravel base layers in road constructions using geocells. In: Proceedings of 12th international conference of international association for computer methods and advances in geomechanics(IACMG), Goa, India, pp 3538–3545 1–6 Oct 2008
Guo J, Han J, Schrock SD, Parsons RL (2015) Field evaluation of vegetation growth in geocell-reinforced unpaved shoulders. Geotext Geomembr 43(5):403–411
Han J, Yang X, Leshchinsky D, Parsons RL (2008) Behaviour of geocell reinforced sand under a vertical load. J Transp Res Board 2045:95–101
Han J, Pokhrel SK, Yang X, Manandhar C, Leshchinsky D, Halahmi I, Parsons RL (2011) Performance of geocell reinforced RAP bases over weak subgrade under full scale moving wheel loads. J Mater Civil Eng 23(11):1525–1534
Hegde A (2015) Ground improvement using 3d-cellular confinement systems: experimental and numerical studies. Ph.D. thesis submitted to Indian Institute of Science Bangalore, India
Hegde A (2017) Geocell reinforced foundation beds-past findings, present trends and future prospects: a state-of-the-art review. Constr Build Mater 154:658–674
Hegde A, Sitharam TG (2013) Experimental and numerical studies on footings supported on geocell reinforced sand and clay beds. Int J Geotech Eng 7(4):346–354
Hegde A, Sitharam TG (2015a) Use of bamboo in soft ground engineering and its performance comparison with geosynthetics: experimental studies. J Mater Civ Eng ASCE 27(9):04014256
Hegde A, Sitharam TG (2015b) Joint strength and wall deformation characteristics of a single cell geocell subjected to uniaxial compression. Int J Geomech (ASCE) 15(5):04014080
Hegde A, Sitharam TG (2015c) Effect of infill materials on the performance of geocell reinforced soft clay beds. Geomech Geoeng Int J 10(3):163–173
Hegde A, Sitharam TG (2015d) 3-dimensional numerical modelling of geocell reinforced sand beds. Geotext Geomembr 43:171–181

Hegde AM, Sitharam TG (2015e) 3-Dimensional numerical analysis of geocell reinforced soft clay beds by considering the actual geometry of geocell pockets. Can Geotech J 52(9):1396–1407
Hegde A, Sitharam TG (2016) Behaviour of geocell reinforced soft clay bed subjected to incremental cyclic loading. Geomech Eng 10(4):405–422
Hegde A, Sitharam TG (2017) Experiment and 3D-numerical studies on soft clay bed reinforced with different types of cellular confinement systems. Transp Geotech 10:73–84
Henkel DJ, Gilbert GD (1952) The effect of the rubber membrane on the measured triaxial compression strength of clay samples. Geotechnique 3(1):20–29
Huang CC, Tatsuoka E (1988) Prediction of bearing capacity in level sandy ground reinforced with strip reinforcement. In: Proceedings international geotechnical symposium on theory and practice of earth reinforcement, Balkema, Fukuoka, Kyushu, Japan, pp 191–196
Huang CC, Tatsuoka F (1990) Bearing capacity of reinforced horizontal sandy ground. Geotext Geomembr 9(1):51–82
Indraratna B, Biabani MM, Nimbalkar S (2015) Behaviour of geocell-reinforced subballast subjected to cyclic loading in plane-strain condition. J Geotech Geoenviron Eng 141(1):04014081
ISO 11359-2 (1999) Determination of coefficient of linear thermal expansion and glass transition temperature. Geneva
ISO 11357 (2006) Determination of oxidation induction time of a polyolefin. Geneva
Janbu N (1963) Soil compressibility as determined by odometer and triaxial tests. European Conf Soil Mech Foundation Eng 1:19–25 (Wiesbaden, Germany)
Kief O, Rajagopal K, Veeraraghavan A, Chandramouli S (2011) Modulus improvement factor for geocell-reinforced bases. Geosynthetics India-11, Chennai, India
Koerner RM (1998) Designing with geosynthetics, 4th edn. Prentice Hall, Englewood Cliffs, New Jersey
Ling H, Leshchinsky D, Wang J, Mohri Y, Rosen A (2009) Seismic response of geocell retaining walls: experimental studies. J Geotech Geoenviron Eng 135:4(515), 515–524. https://doi.org/10.1061/(asce)1090-0241
Madhavi Latha G (2000) Investigations on the behaviour of Geocell supported embankments. Ph.D. thesis, Indian Institute of Technology, Madras, India
Madhavi Latha G, Somwanshi A (2009) Effect of reinforcement form on the bearing capacity of square footing on sand. Geotext Geomembr 27:409–422
Madhavi LG, Rajagopal K (2007) Parametric finite element analyses of geocell-supported embankment. Can Geotech J 44(8):917–927
Madhavi LG, Dask SK, Rajagopal K (2008) Equivalent continuum simulations of geocell reinforced sand beds supporting strip footings. Geotech Geol Eng 26:387–398
Madhavi LG, Dask SK, Rajagopal K (2009) Numerical simulation of the behaviour of geocell reinforced sand foundations. Int J Geomech 9(4):143–152
Mhaiskar SY, Mandal JN (1996) Investigations on soft clay subgrade strengthening using geocells. Constr Build Mater 10(4):281–286
Moghaddas Tafreshi SN, Dawson AR (2010) Behaviour of footings on reinforced sand subjected to repeated loading comparing use of 3D and planar geotextile. Geotext Geomembr 28:434–447
Moghaddas Tafreshi SN, Khalaj O, Dawson AR (2014) Repeated loading of soil containing granulated rubber and multiple geocell layers. Geotext Geomembr 42:25–38
Pokharel SK, Han J, Leshchinsky D, Parsons RL, Halahmi I (2010) Investigation of factors influencing behaviour of single geocell reinforced bases under static loading. Geotext Geomembr 28(6):570–578
Presto (2008) Geoweb load support system—technical overview. Presto Products Company, Appleton, WI, USA
Rai R, Khandelwal M, Jaiswal A (2012) Application of geogrids in waste dump stability: a numerical modeling approach. Environ Earth Sci 66(5):1459–1465
Rajagopal K, Krishnaswamy NR, Madhavi Latha G (1999) Behaviour of sand confined with single and multiple geocells. Geotext Geomembr 17:171–181

Rajagopal K, Chandramouli S, Parayil A, Iniyan K (2014) Studies on geosynthetic-reinforced road pavement structures. Int J Geotech Eng 8(3):287–298
Saride S, Gowrisetti S, Sitharam TG, Puppala AJ (2009) Numerical simulations of sand and clay. Ground Improvement 162(GI4):185–198
Schlosser E, Jacobsen HM, Juran I (1983) Soil reinforcement: General Report. In: 8th European conference on soil mechanics and foundation engineering, Balkema, Helsinki, pp 83–103
Sitharam TG, Hegde A (2013) Design and construction of geocell foundation to support embankment on soft settled red mud. Geotext Geomembr 41:55–63
Sitharam TG, Sireesh S (2004) Model studies of embedded circular footing on geogrid reinforced sand beds. Ground Improvement 8(2):69–75
Sitharam TG, Sireesh S (2005) Behaviour of embedded footings supported on geocell reinforced foundation beds. Geotech Test J ASTM 28(5):452–463
Takemura J, Okamura M, Suesmasa N, Kimura T (1992) Bearing capacity and deformations of sand reinforced with geogrids. In: Proceedings of earth reinforcement practice, Balkema, Fukuoka, Kyushu, Japan, pp 695–700
Tanyu BF, Aydilek AH, Lau AW, Edil TB, Benson CH (2013) Laboratory evaluation of geocell-reinforced gravel subbase over poor subgrades. Geosynth Int 20(2):47–61
Tavakoli Mehrjardi Gh, Moghaddas Tafreshi SN, Dawson AR (2013) Pipe response in a geocell-reinforced trench and compaction considerations. Geosynth Int 20(2):105–118
Yang X, Han J, Parsons RL, Leshchinsky D (2010) Three-dimensional numerical modelling of single geocell reinforced sand. Front Archit Civ Eng China 4(2):233–240
Yang X, Han J, Pokharel SK, Manandhar C, Parsons RL, Leshchinsky D, Halahmi I (2012) Accelerated pavement testing of unpaved roads with geocell reinforced sand bases. Geotext Geomembr 32:95–103
Zhang MX, Javadi AA, Min X (2006) Triaxial tests of sand reinforced with 3D inclusions. Geotext Geomembr 24:201–209
Zhang L, Zhao M, Shi C, Zhao H (2010) Bearing capacity of geocell reinforcement in embankment engineering. Geotext Geomembr 28:475–482
Zhao MH, Zhang L, Zou XJ, Zhao H (2009) Research progress in two direction composite foundation formed by geocell reinforced mattress and gravel piles. Chinese J Highway Transp 22(1):1–10
Zhou H, Wen X (2008) Model studies on geogrid-or geocell-reinforced sand cushion on soft soil. Geotext Geomembr 26(3):231–238

Chapter 3
Neoloy—Developing a Novel Polymeric Alloy for Geocells

Yitzchak Schary

Abstract While a range of geosynthetics is routinely used in civil infrastructure projects, the use of geocells is more modest. This chapter offers assumptions as to why and describes how advances in geocell technology can change the situation. The evolution of geocell technology is traced from a "sand-grid" for temporary roads to a promising reinforcement geosynthetics for large infrastructure projects. Geocells remained a niche geosynthetic for decades despite their proven effectiveness, due in part to their origin as a temporary solution, and in part to their success as a soil erosion solution. Geocells were seldom a topic in published literature, little known by most engineers and infrequently used in infrastructure. Some two decades ago a collaborative R&D effort of private industry and academia began to research the geocell reinforcement mechanisms and influencing factors. Research established that tensile strength, elastic stiffness, and creep resistance are key properties to maintain geocell geometry in low-deformation applications and to retain confinement and reinforcement. Recognizing the limitations of commonly used HDPE material, a novel polymeric alloy (NPA), called Neoloy® was developed for geocells. This provided geocells the requisite stiffness, strength, and durability to prevent volumetric change under dynamic loading, making them well suited for the service life of critical infrastructure. This serves as an example for the geosynthetic industry of how to develop a new product, advance technology, enhance standards, and expand widespread adoption.

Keywords Geocell research · Geocell technology · HDPE · Creep · Deformation · NPA · Novel polymeric alloy

Y. Schary (✉)
PRS Geo-Technologies, 4 Kaufman St, Tel Aviv, Israel
e-mail: yitzchak@prs-med.com

T. G. Sitharam et al. (eds.), *Geocells*, Springer Transactions in Civil and Environmental Engineering,
https://doi.org/10.1007/978-981-15-6095-8_3

3.1 Evolutionary Development of Geocells

3.1.1 Creation and Divergent Evolution

The evolution of geocells and geocell technology was early impacted by unique market and "environmental" factors that caused them to diverge from the mainstream geosynthetics branch. The creation of geocells by the US Army Corps of Engineers (USACE) half a century ago is well known. Called "sand-grids", their goal was to stabilize soft subgrades to construct temporary roads for heavy military vehicles. Commercial production of geocells began in the civilian market began in the 1980s under license from the USACE. However, several unique developments were to alter the perception of geocells and their use.

Despite their creation as solution for roads, geocells were found to be quite effective for earth stabilization on slopes too steep for conventional methods: slope protection, trenches, and retention walls. The success of these solutions contributed to a perception of geocells as an erosion control or landscape product, rather than for pavements (Richardson 2004a, b). When implemented for soil stabilization solutions in roadways, geocells were typically used per their original intent for short-term or low volume roads.

Compounding this perception was the fact that some geocells were manufactured by geogrid-geosynthetic manufacturers, as part of their product portfolio. These manufacturers did not want to position geocells as a solution for road reinforcement, thereby competing directly with their own geogrid products, preferring to market their geocells as erosion control solutions (Rimoldi 2018).

3.1.2 Market and Engineering Perception

Despite their effectiveness in lowering stresses, reducing settlements, and increase load-bearing capacity, the perception of geocells as a landscape product limited their appeal to engineers. Geocells were not part of the terminology of pavement design, barely mentioned in engineering school curricula, and largely absent from critical infrastructure projects. In fact, little research was invested on geocells in the two decades after their invention (Richardson 2004a). The geocell reinforcement mechanism and influencing factors were not widely understood and there was a lack of recognized methods, standards, and design methodologies for geocells (Yuu et al. 2008).

The above contributed to the lack of awareness, prevalent until today by both industry and engineering professionals, of geocells as a suitable reinforcement solution for heavy-duty pavements and transportation infrastructure. It is interesting to note that this period from the early 1980s to the early 2000s was characterized by advances in materials, standards, and testing of other sectors of the geosynthetic industries, as well as by the widespread acceptance of geogrids as a soil stabilization

and pavement reinforcement solution (Koerner et al. 2012). Geocells appeared to lag far behind.

3.2 HDPE Geocells

3.2.1 HDPE Polymer

Although HDPE—High-Density Polyethylene—is the commonly used polymer to manufacture geocells, this may have impeded the use of geocells for infrastructure projects. Geocells were manufactured from HDPE due to its relative strength, low cost, and ease of manufacturing. It was the best available material at the time.

HDPE is an inert, thermoplastic polyolefin material made from ethylene. The mechanical and chemical properties of the end product, for example, density, stiffness, tensile strength, flexibility, elongation and creep characteristics are largely determined by the number, size, and type of the crystalline chains in Polyethylene (PE). The chains in HDPE are highly ordered with little side branching, creating a polymer of densely packed molecular chains, very high molecular weight and high density (greater than 0.940 g/cm^3) (Gabriel 2018).

HDPE has a theoretically moderate tensile strength (to 15 MPa), but this is a short-term value, while actual perforated HDPE geocells have lower tensile strength (insufficient for paved roads, railroads, and platform applications). HDPE is flexible and lightweight, has excellent chemical and corrosion resistance, but poor resistance to UV light and to oxidizing agents. However, HDPE is known to have high creep, while questions arise if HDPE geocell stiffness and strength are sufficient for load support applications, such as roads and railways (Leshchinsky 2009).

3.2.2 HDPE Geocells—High Creep and Low Strength

HDPE geocells are unsuitable for heavy pavement reinforcement due to their tendency to creep under load—plastic deformation over time. Even small deformations in the range of 2–3% can be decisive in road and rail applications. HDPE creep strain increases with an increase in the magnitude of applied loads, number of cycles, and temperature over time. HPDE quickly reaches secondary creep (unpredictable) and deformation from ratcheting under thermal cycling and applied loading (Kanthabhabha et al. 2018).

Geocell behavior can be verified by standard test methods that predict the long-term behavior of geocells: stepped isothermal method—SIM (ASTM 6992) to evaluate creep; dynamic mechanical analysis–DMA (ASTM E2254) to evaluate dynamic stiffness; and wide-width tensile method (ISO 10319) to evaluate tensile strength, particularly of perforated geocells. These methods are described in detail in Sect. 5.2.

For example, the high permanent deformation of geocells is clearly demonstrated by the SIM accelerated test method, which shows that HDPE geocells reach their plastic limit under heavy loading (6.1 kN/m) within a year and exceed allowable stresses in load support applications within two months (see Fig. 3.1) (Unpublished raw data derived from internal testing, PRS Geo-Technologies 2017).

Although HDPE was the polymer of choice used for geocells since their inception, researchers such as Leshchinsky (2009) questioned the suitability of HDPE-based geocells for long-term infrastructure: "*Clearly, while the HDPE geocell used was adequate to test a design-oriented analysis, it lacks long-term strength to serve as reinforcement….However, without improvement, HDPE are not suitable for long-term applications….Low stiffness and strength may lead to significant creep having poor long-term dimensional stability.*"

Recent guidelines for reinforcement geosynthetics published in the Netherlands (Vega et al. 2018) highlight the reservations about HPDE that: "*HPDE polymers are less suitable for reinforcement and stabilization in view of the higher elongation at*

Fig. 3.1 SIM test showing creep of HDPE Geocell (left side) versus Neoloy Geocell (left side)

break and lower stiffness….because the behavior of small deformations is decisive for application in road bases."

In addition, experimental and analytical concerns about HDPE may be backed up by facts on the ground, in which the number of projects that utilize HDPE geocells in the base layer of paved highways, railways, and airports—which are subject to long-term, heavy-duty, dynamic loading, and strict low-deformation levels—is relatively small.

3.2.3 HDPE Geocell Limitations

Improvement of HDPE geocell is constrained by the prevailing conventions in the industry, the lack of an engineering design approach, and the inherent limitations of HDPE material.

For example, the type of parameters used by HPDE geocell manufacturers today to evaluate geocells includes physical properties (e.g., dimensions, density) of the cells; properties of virgin materials (e.g., carbon content, ESCR); and seam peel performance, one which involves hanging samples material on a rack for 416 days (ASTM Standard 1159). However, laboratory tests of individual strips and virgin materials do not reflect 3D geocell geometry and material performance in the field.

Aside from the fact that such parameters lack relevant value for engineering design; attempts to improve the existing parameters may be misleading. For example, increasing the percentage of carbon black additive does not directly indicate the level of UV protection. Increasing density can be achieved with quality or inferior additives; density indicates virgin material strength but not geocell strength or stiffness. Thicker cell wall strips do not necessarily provide stronger performance—examples abound of thinner, lighter polymer composites (e.g., Kevlar® fiber material) that well exceed the performance of thicker traditional materials (steel).

Not only do these parameters not reflect the behavior of 3D geocells in soil; they do not relate to the functionality of the geocell versus the relevant forces in the field. A new conceptual basis was needed that took into account geocell reinforcement mechanisms, the relevant properties required for long-term geocell performance and suitable test methods to evaluate these parameters (Kief et al. 2014).

3.3 Key Factors in Geocell Reinforcement

3.3.1 Basic Geocell Reinforcement Mechanism

Geocells are a 3D mechanical soil stabilization and road reinforcement method. The system is formed by bonded polymeric strips, which are opened on site to form

(a) Vertical stresses (b) Lateral stresses (c) Hoop tensile stresses

Fig. 3.2 Vertical **a** lateral **b** and hoop **c** stresses on cell

a honeycombed structure. A new composite entity is created when filled with soil materials due to the unique interaction of geometry, soil, and the cell-wall material.

Geocells act as a mattress (or slab) that distributes a portion of applied vertical forces (e.g., vehicle wheel) laterally. The confinement restrains the lateral movement of soil particles via hoop stress on the geocell walls. This maximizes the distribution of lateral and vertical stresses, resulting in stabilized soil, basal layer reinforcement and reduced surface degradation, among other benefits (Kief et al. 2014). The typical stresses exerted on a cell are shown in Fig. 3.2 below:

Polymers tend to lose elastic modulus (stiffness) over time, particularly under dynamic loading. Whereas load support applications, especially roads and railways, are generally subjected to millions of cyclic loads, geocells need to retain their dimensional stability with very low plastic deformation. Dynamic loading on a geocell may result in a reduction in strength, or fatigue. Tolerances for volumetric change must be strict in order to maintain the cell geometry and confinement for the project service life.

Therefore, performance requirements for a geocell should have the following parameters: sufficient resistance to accept high stress without plastic deformation; elastic stiffness under repeated and continuous loading and/or long service periods; and tensile strength that can sustain hoop forces on the cell wall without deformation (ASTM Standard WK61159).

3.3.2 From Durability to Resistance to Permanent Deformation

While durability in geosynthetics is a central premise in the industry, it typically refers to resistance to deformation (aging) from environmental factors (e.g., leaching, oxidation, UV radiation) (Kay et al. 2004). Durability in geocells should also refer to resistance to deformation from heavy, long-term dynamic, mechanical stress. This is the key to maintain confinement in cyclical low-deformation applications, such as road and rail pavements. A geometric change or loss of dimensional stability of 2–3% deformation in a geocell in a load support application may have critical

consequences: loss of confinement, compaction, and result in settlement; this in turn may invalidate the design parameters and cause fatigue or failure (Vega et al. 2018).

Of the three basic components of a geocell system—geometry, infill, and cell wall (or strip) material—it is the **material** that is the variable under manufacturer control. It is the geosynthetic polymeric material and its specific formulation, as well as on in situ loading conditions and environment that determine durability (Koerner 2007).

Whereas tensile stiffness determines the magnitude of lateral confinement for geogrids, in three-dimensional geocell systems, the tensile stiffness is dependent on the elastic modulus of the material as well as the geometry (Vega et al. 2018).

An additional factor to be considered is the current trend toward sustainability, for example, where locally available but marginal quality soils are used for structural infill. The weaker the soil is, the larger are applied loads to geocell walls. Therefore, the strength and stiffness of the geocell become more critical (Yang 2012).

3.4 Comprehensive International R&D Effort

At the turn of the twenty-first century, industry professionals and geotechnical experts in academia initiated a comprehensive, international R&D effort to advance geocell technology and apply it to road pavements. The R&D effort was an international collaborative effort with leading geotechnical engineers, universities, and road research institutions (Kief et al. 2014).

The research goals were to understand the mechanisms and influencing factors of geocell reinforcement, develop a new polymeric material for geocells, evaluate the geocell effectiveness in improving roadway performance, and calibrate design methods for roadway applications. Experimental, numerical, analytical, and field testing were carried out at the University of Kansas (*Han, Pokharel,* et al.), Indian Institute of Technology at Madras *(Rajagopal, Kief,* et al.*)* and Patna (*Hedge,* et al.*),* Indian Institute of Science, Bangalore (*Sitharam,* et al.), Columbia University (*Ling, B. Leshchinsky*), University of Delaware (*Zarembski, D. Leshchinsky,* et al.), Clausthal University, Germany (*Emersleben, Meyer*), and Kiwa KOAC Institute, Netherlands (*van Gurp,* et al.), while other individual studies were performed around the globe, such as the US Strategic Highway Research Program 2 (*White,* et al.) (Kief et al. 2014; Hegde 2017; Swaraj 2014; Han et al. 2011, 2013).

The researchers concluded that dimensional stability was a key factor to retain geocell geometry and prevent volumetric change (Hegde 2017). This necessitated a stronger polymeric material to increase the tensile stiffness of a geocell. However, in terms of long-term performance additional factors were deemed necessary: the viscoelastic properties of a polymer under dynamic loading and the resistance to polymeric material to creep (Han et al. 2011; Greenwood et al. 2012). At the same time, environmental durability was still a concern, as geocells are still used in a variety of earth stabilization applications.

Table 3.1 summarizes the key factors in geocell performance, along with the applicable test standards for evaluating the level of performance.

Table 3.1 Geocell key performance parameters

Key factor in geocell performance	Test method standard
Elastic behavior defines the elastic behavior and the ability of a geocell to store and release dynamic loading, while maintaining geometry over time	Net elastic modulus—DMA (Dynamic Mechanical Analysis) ISO 6721-1, ASTM E2254 DMA
Resistance to creep defines the geocell plastic behavior and effective service life under static loading	Resistance to permanent deformation—SIM (Stepped Isothermal Method) ASTM D-6992
Cell tensile strength defines the strength to withstand vertical load transferred to hoop (cell wall and weld) tensile forces	Strip tensile strength (Wide-Width) ISO 10319:2015; Seam weld tensile strength (SPLIT) ISO 13426-1 (Part 1, Method C)
Photochemical (UV) and oxidation resistance long-term resistance to aging and environmental influence	Environmental Durability—HPOIT (High-Pressure Oxidation Inductive Time) ASTM D5885

Source Geosynthetics for Geocell Reinforcement, Guideline Standard (Vega et al. 2018)

To evaluate the performance parameters of a geocell as in Table 3.1, ISO and ASTM standards were applied to geocells. These methods are commonly used to test polymer plastics in the automobile, aeronautic, military, and other industries, including other geosynthetic sectors. These methods are suitable to predict long-term behavior in a geocell under loading under different mechanical stresses, frequencies, and temperatures.

This close cooperation and iterative research and development process between private industry and academia was cited by the editor of *Geosynthetics* magazine, as: "***an example of how product development for the geosynthetics industry can be done effectively… and can further advance the geosynthetics industry into the twenty-first century with much success***."(Leshchinsky 2009).

3.5 Neoloy Novel Polymeric Alloy

An integral part of the R&D program was to develop a new geocell material with performance properties aligned to the engineering needs of infrastructure projects. The goal was to create a geocell that would maintain its dimensional stability under heavy-duty, cyclical, and long-term loading.

The result of intensive cooperation between polymer chemists and civil engineers was the creation of a novel polymeric alloy (NPA) called Neoloy®. Neoloy is a composite polymer alloy comprised of a high-performance engineering thermoplastic with a polyolefin blend (PP, PE). The blend is immiscible with high-performance nano-polymer compound (copolymers, block copolymers, blends, and/or other combinations) which is dispersed in a polyolefin matrix.

The Neoloy strip is coextruded in multiple layers with a high-strength inner core layer for optimal performance. The core layer is formed from a high-performance polyamide polymer blend for high strength and stiffness, while the outer polyolefin layers provide resistance to chemicals, stress cracking, and tear. These layers create a composite material balancing brittle polypropylene that is stiff enough for robust engineering applications, with softer polyethylene to retain flexibility for handling and installation (PRS Geo-Technologies).

3.5.1 Geocell Categories to Optimize Designs

An additional aspect of the development of Neoloy was to manufacture geocells in several strength-performance category types. This enables an optimized geocell solution that best fits the specific application profiles/project requirements, similar to other geosynthetics, such as geogrids. The types include moderate strength (B)—for erosion control, channels, walls, and subgrade stabilization; high strength (C)—for road base reinforcement, and heavy-duty (D)—for use in airports, railways, ports, platforms. The category of geocell strength can be selected after calculating the typical use, loads, soils, environmental conditions of a project/design. Matching the geocell category type with the requirements of the project optimizes cost versus performance.

3.5.2 Neoloy Geocell Performance Data

The following is the performance specifications for Neoloy geocells:

The ability of Neoloy-based geocells to maintain their engineering properties without permanent deformation over time has been confirmed by numerous plate load tests, numerical modeling, and full-scale trafficking tests and validated in extensively published papers (Kief et al. 2014; Hegde 2017).

Plate loading tests on geocells in the above laboratories verified that the performance of geocell-reinforced bases depends on the **elastic modulus** of the geocell. The geocell with a higher elastic modulus had a higher bearing capacity and stiffness in a reinforced base. Laboratory studies, numerical studies, full-scale moving wheel tests, and field demonstrations showed that Neoloy-based geocell reinforcement increased stiffness and bearing capacity, distributed stress widely, reduced permanent deformation, and prolonged road life (Han et al. 2011).

Results of these studies validated that geocells made from Neoloy were found significantly better in ultimate bearing capacity, stiffness, and reinforcement relative to geocells made from HDPE. Neoloy geocells showed better creep resistance and better retention of stiffness and creep resistance particularly at elevated temperatures, verified by plate load testing, numerical modeling, and full-scale trafficking tests (Pokharel et al. 2010; Yang 2010; ISO Standard WD TR 18228-5).

3.5.3 Facts in the Field–Project Implementation

The effectiveness and benefits of geocells can be ascertained from their successful implementation in large-scale infrastructure projects. Each project dealt with challenging soil, environmental, and loading conditions. The Neoloy-based geocells were chosen as the best possible solution to optimize performance versus costs. Established design methodologies integrating the Neoloy geocell contribution factors were used for unpaved (revised Giroud-Han) and paved roads (Mechanistic-Empirical Method for Flexible Pavements). Sample projects are listed below.

3.5.4 International Standards for Geocells

Considering geocells' evolutionary rise as a player on the field with other geosynthetics, and cognizant of the fact that guidelines and standards for geocells did not exist, the international (ISO, ASTM) and national (e.g., CROW, Netherlands) standards organizations are making significant strides to close the gap and create. Each of these new standards incorporates performance-based parameters, such as those cited in Table 3.2.

Widely recognized standards organizations, such as SBRCURnet (CROW), Netherlands have recently published guideline standards for the use geocells in road

Table 3.2 Performance parameters for neoloy geocells

Essential characteristics	Performance categories			Unit	Harmonized technical specifications
	B	C	D		
Net elastic modulus (DMA) +30 °C +45 °C +60 °C	>750 >650 >450	>775 >675 >525	>800 >700 >600	MPa	ISO 6721-1:2011 ASTM E2254 (DMA—Dynamic Mechanical Analysis)
Plastic permanent deformation (creep resistance)—SIM: 3 Steps: 44 °C, 51 °C, 58 °C	≤3.0 cumulative			%	ASTM D6992-16 (SIM—Simulated Incremental Method)
Tensile strength@ Yield (non-perforated) @ Yield (perforated) Seam Weld Strength—Weld Splitting	>21 >16 >16	>23 >19 >19	>25 >22 >22	kN/m	ISO 10319:2015 (wide-width) ISO-13426-1, Part 1, Method C
UV & Oxidation resistance (HPOIT @150 °C)	≥1600			min	ASTM D5885 (HPOIT—High Pressure Oxidation Inductive Time)

Source PRS Geo-Technologies
Note: these test methods are briefly described in Table 3.1

building. These guidelines emphasize that: (1) the extent of the reinforcing or stabilizing effect is determined by the material from which the product is made and the geometry; and (2) the most important material properties are the **elastic stiffness** and the **resistance to permanent deformation (creep)** (Vega et al. 2018).

ISO is currently compiling a comprehensive standard (working draft status) for the use of reinforcement geosynthetics (geogrids and geocells) with a chapter dedicated to road stabilization (ISO Standard WD TR 1822-5). The ASTM is currently working on guidelines (working draft status) for the use and design of geocells ASTM Standard WK61159. These documents include the elastic behavior and resistance to creep as key performance parameters for geocells as well (Table 3.3).

3.6 Conclusion

The evolution of geocells progressed slowly. Although the soil stabilization benefits of geocells were acknowledged, geocells were not widely used for reinforcement for infrastructure-scale projects. The development of geocells and geocell technology lagged behind other geosynthetics. This is due in part to the successful use of geocells in erosion control, and part due to HPDE—the conventional material used to manufacture geocells. HDPE-based geocells exhibit high creep and low elastic modulus (stiffness) over time, particularly under heavy dynamic loading, and these factors did not help build confidence in the technology as a ground reinforcement solution for infrastructure.

About 15 years ago, comprehensive international research between private industry and academia initiated a surge in basic research in geocells. The first result of these studies was a broader understanding of the reinforcement mechanisms and performance factors required for heavy-duty pavement applications. It was established that geocells required a high elastic modulus and resistance to creep to maintain long-term cell geometry and confinement under dynamic loading.

The second result was the development of a novel polymeric alloy (NPA) for geocells, called Neoloy®, to meet these engineering requirements. This material with performance-based parameters that are relevant to design engineers: high elastic stiffness, low permanent deformation, and high tensile strength, aligned them with the critical loads and service life of infrastructure projects.

The third result was increasing awareness of Neoloy-based geocell performance for pavement applications. This was accompanied by a significant knowledge base of published literature, testing methods, design methodologies, and new standard and guidelines created new confidence in geocell solutions.

The last result was a construction industry eager for more sustainable, durable and cost-saving innovation, such as Neoloy geocells. These have been implemented in critical infrastructure projects to resolve a variety engineering, economic and environmental challenges—in airports, railways, rural roads, and port construction.

The widespread adoption of Neoloy-based geocells would benefit the geosynthetics industry as well as the civil and transportation engineering community.

Table 3.3 Examples of large infrastructure projects using Neoloy-based geocells

	**Ground Reinforcement for New International Airport Roadways, Mexico**—Soil stabilization for heavily trafficked asphalt roads constructed over extreme soil conditions (muddy clay with CBR<0.6%) for huge new airport facility. Solution reduced pavement weight by 60% and reduced construction time and costs significantly
	**Stabilization of Feeder Roads, UN, South Sudan**—used low quality, but locally available sandy soil to build "permanent" road infrastructure to provide security, aid, and opportunity in very remote regions. Solution was sustainable, validated for long-term use, and lowered construction costs
	**Neoloy Geocell Soil Stabilization for High-Speed Passenger Rail Operations, Amtrak, USA**—Soil stabilization of high-speed track suffering mud pumping and track geometry degradation from poor subgrade. Solution reduced subgrade pressure by 50% and reduced track surface maintenance cycles by a factor of 6.7x
	**Load Transfer Platforms for Vertical Columns, Manzanillo Port, Mexico**— reinforced load transfer platform (LTP) on saturated silty sand for new wharves in Manzanillo Port, Mexico, reducing pavement thickness by 49%, as well as the number of pile columns and construction costs

Source PRS Geo-Technologies

The comprehensive R&D program to advance geocell technology was a successful synthesis of academia with private industry and cited as a positive example of product development for the geosynthetics industry.

References

ASTM Standard WK61159. New Guide for Use of Geocells in Geotechnical and Roadway Projects. ASTM International, West Conshocken, PA. Unpublished work item

Gabriel LH (2018) Chapter 1: history and physical chemistry of HDPE. http://www.parsethylene-kish.com/UserFiles/Uploads/HDPE%20Corrugated%20pipe-chapter-1-history-physical-chemistry-hdpe.pdf. Last accessed 8 Sep 2018. (n.d.)

Geoweb System Material Specification: https://www.prestogeo.com/wp-content/uploads/2016/10/GW-geoweb-material-specification.pdf. Last accessed 10 Aug 2018

Greenwood JH, Schroeder HF, Voskamp W (2012) Durability of geosynthetics, stichting CURNET, Gouda, The Netherlands. CUR report 243

Han J, Pokharel SK, Yang X, Thakur J (2011) Tough cell: geosynthetic reinforcement shows promise, roads and bridges. 40–43

Han J, Thakur JK, Parsons RL, Pokharel SK, Leshchinsky D, Yang X (2013) A summary of research on geocell-reinforced base courses. In: Ling H, Gottardi G, Cazzuffi D, Han J, Tatsuoka F (eds) Proceedings of design and practice of geosynthetic-reinforced soil structures, Bologna, Italy, pp 351–358, 14–16 Oct

Hegde A (2017) Geocell reinforced foundation beds-past findings, present trends and future prospects: a state-of-the-art review. Construct Build Mater 154:658–674. https://doi.org/10.1016/j.conbuildmat.2017.07.230

ISO Standard WD TR 18228-5. Design Using Geosynthetics—Part 5: Stabilization. International Organization for Standardization, Geneva, Switzerland. Unpublished document under development

Kanthabhabha Jeya RP, Bouzid AH (2018) Compression creep and thermal ratcheting behavior of high density polyethylene (HDPE). Polymers 10(2):156. https://doi.org/10.3390/polym10020156

Kay D, Blond E, Milynarek J (2004) Geosynthetics durability: a polymer chemistry issue. In: 57th Canadian Geotech Conf

Kief O, Schary Y, Pokharel SK (2014) High-modulus geocells for sustainable highway infrastructure. Indian Geotech J 45(4): 389–400. https://doi.org/10.1007/s40098-014-0129-z

Koerner RM (2012) Designing with Geosynthetics, 6th Edn, Xlibris Publishing Co.

Koerner GR, Hsuan YG, Koerner RM (2007) The durability of geosynthetics. In: Sarsby RW (ed) Woodhead Publishing Series in Textiles, Geosynthetics in Civil Engineering, Woodhead Publishing, pp 36–65. https://doi.org/10.1533/9781845692490.1.36

Leshchinsky D (2009) Research and innovation: seismic performance of various geocell earth-retention systems. Geosynthetics 27 (4):46–54. http://www.scopus.com/inward/record.url?eid=2-s2.0–76749117091&partnerID=40&md5=43741bffcff3f32dcad36ffaef71427c

Pokharel SK (2010) Experimental study on geocell-rein- forced bases under static and dynamic loading. PhD dissertation, Civil, Environmental, and Architectural Engineering Department, University of Kansas

Richardson GN (2004) Geocells: a 25-year perspective, part 1: roadway applications. GFR Magazine 22(6)

Richardson GN (2004) Geocells: a 25-year perspective, part 2: channel erosion control and retaining walls. GFR magazine 22(8)

Rimoldi P (2018) Personal Interview, 22 Aug 2018

Source derived from internal documentation (not publicly available) of PRS Geo-Technologies

Swaraj C, Shaktii S (2014) A review of studies on geocell-reinforced foundations. Res J Rec Sci 4:24–30

Unpublished raw data derived from internal testing (2017) PRS Geo-Technologies

Vega E, Van Gurp C, Kwast E (2008) Geokunststoffen als Funderingswapening in Ongebonden Funderingslagen (Geosynthetics for Reinforcement of Unbound Base and Subbase Pavement Layers), SBRCURnet (CROW), Netherlands. CRW C1001 (in Dutch)

Yang X (2010) Numerical analyses of geocell-reinforced granular soils under static and repeated loads. PhD dissertation, Civil, Environmental, and Architectural Engineering Department, University of Kansas

Yang X (2012) An assessment of the geometry effect of geosynthetics for base course reinforcements. Int J Transp Sci Tech 1(3):247–257

Yuu J, Han J, Rosen A, Parsons RL,Leshchinsky D (2008) Technical review of geocell-reinforced base courses over weak subgrade. In: The First Pan American geosynthetics conference & exhibition proceedings (GeoAmericas), Appendix VII, Cancun, Mexico

Chapter 4
Geocell-Reinforced Foundations

Gholamhosein Tavakoli Mehrjardi and Seyed Naser Moghaddas Tafreshi

Keywords Geocell-reinforced foundations · Bearing capacity · Failure mechanism · Scale effect

4.1 Introduction

Constructing over soft soils is a challenge for geotechnical engineers because of the low shear strength of the foundation, which causes excessive consolidation settlements and, sometimes, bearing capacity failure. A variety of ground improvement techniques, including vertical drains, grouting, complete soil replacement, geosynthetic reinforcement, and piling, have been developed to solve the problems (e.g. Liu et al. 2008; Rowe and Taechakumthorn 2008). Among these techniques, geosynthetic reinforcement has been increasingly used as basal reinforcement since it facilitates rapid construction at low costs (Rowe and Li 2005) although care is required when dealing with rate-sensitive soft soils (Li and Rowe 2008). Geocells account geosynthetic products with a three-dimensional cellular network constructed from thin polymeric strips. Many investigators have reported the beneficial use of geocell layer at the base of the embankment. To sum up: as an immediate working platform for the construction, more uniform settlements, reduced construction time and eliminated excavation and replacement costs, increased bearing capacity, and decreased settlements.

G. Tavakoli Mehrjardi
Department of Civil Engineering, Faculty of Engineering, Kharazmi University, Tehran, Iran
e-mail: ghtavakoli@khu.ac.ir

S. N. Moghaddas Tafreshi (✉)
Faculty of Civil Engineering, K.N. Toosi University of Technology, Tehran, Iran
e-mail: nas_moghaddas@kntu.ac.ir

T. G. Sitharam et al. (eds.), *Geocells*, Springer Transactions in Civil and Environmental Engineering,
https://doi.org/10.1007/978-981-15-6095-8_4

Many researchers investigated the beneficial ability of cellular geosynthetic mattress constructions, called "geocells-reinforced beds", to improve the bearing capacity and settlement of footings (Yang et al. 2012; Moghaddas Tafreshi et al. 2015; Tavakoli Mehrjardi et al. 2012, 2013, 2015; Avesani Neto et al. 2015; Hegde and Sitharam 2015; Aboobacker et al. 2015; Biabani et al. 2016; Kumar and Saride 2016; Sireesh et al. 2016). Rajagopal et al. (1999) investigated the influence of geocell confinement on the strength and stiffness behavior of granular soils through a number of triaxial compression tests. Latha et al. (2006) and Latha and Murthy (2007) conducted a series of compression tests to study the relative efficiency of three forms (i.e. planar, discrete fiber and cellular forms) of reinforcement in improving the shear strength of sand. They investigated that the cellular reinforcement, which improved the strength of soil by friction and all-round confinement, was found to be more effective in improving the soil strength than the planar reinforcement. Zhou and Wen (2008) also observed that geocell was a superior form of reinforcement than the planar reinforcement through triaxial compression tests. The results from their study also indicated that with the provision of a geocell-reinforced sand cushion, the subgrade reaction coefficient was improved by three times, and the deformation was reduced by 44%. Dash et al. (2001, 2003, 2007) investigated the reinforced performance of geocell foundation mattress with varying cell sizes, infill material properties, and loading conditions. They found that the effectiveness of the reinforcement depended not only on the adequate load transmission to the fill material (via friction and interlocking) but also on the stiffness of the reinforcement.

4.2 Failure Mechanisms

Based on experiments of various researchers, four types of failure mechanisms are observed in planar reinforcement according to Figs. 4.1, 4.2, 4.3, and 4.4:

(a) Failure above the upper reinforced layer according to Fig. 4.1 (Binquet and Lee 1975),
(b) Failure between reinforced layers according to Fig. 4.2 (Wayne et al. 1998),

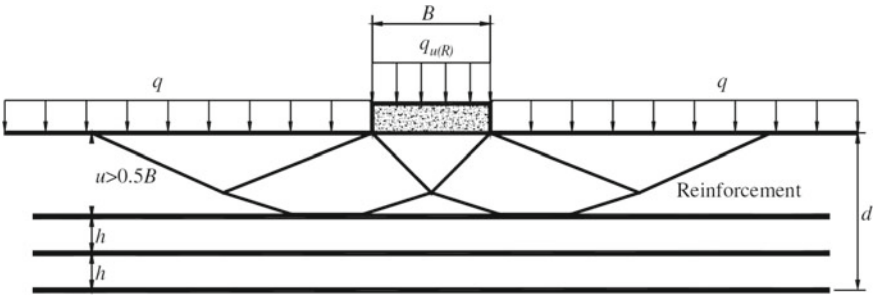

Fig. 4.1 Failure above the upper reinforced layer (Binquet and Lee 1975)

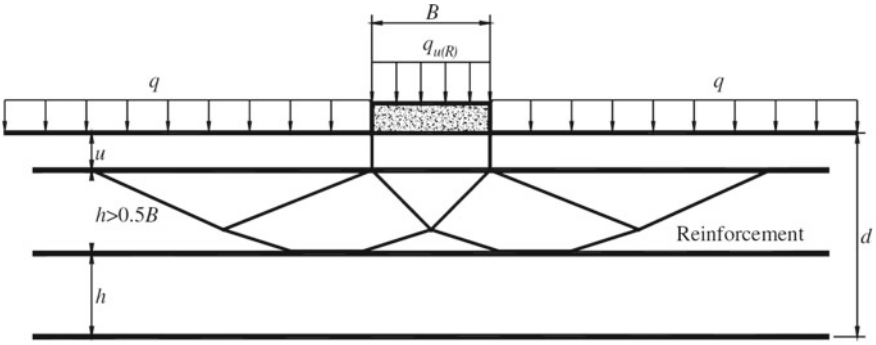

Fig. 4.2 Failure between reinforced layers (Wayne et al. 1998)

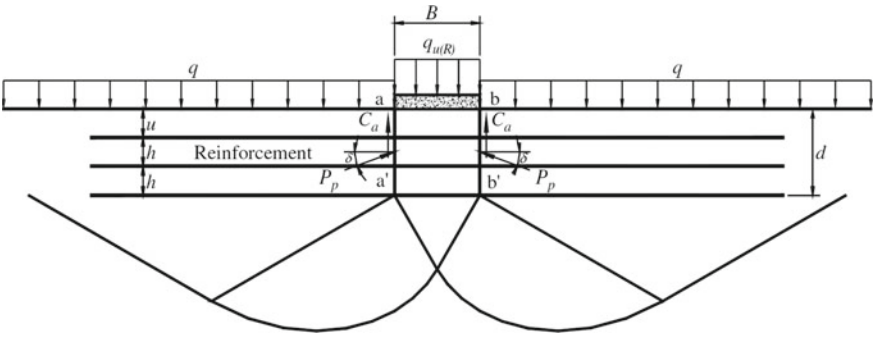

Fig. 4.3 Failure similar to footings on a two-layered soil (Wayne et al. 1998)

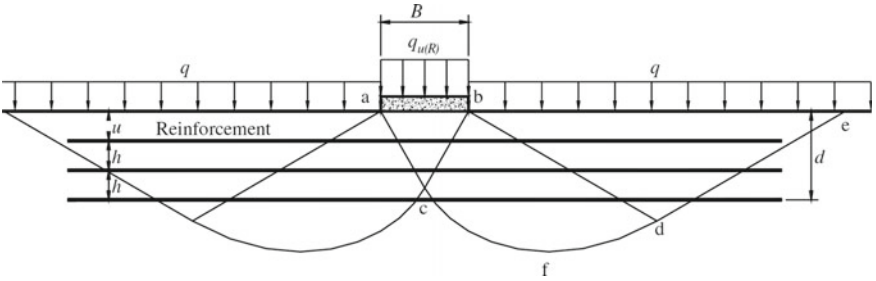

Fig. 4.4 Failure inside the reinforced zone (Sharma et al. 2009)

(c) Failure similar to footings on a two-layered soil (strong layer placed on weak layer) according to Fig. 4.3 (Wayne et al. 1998),
(d) Failure inside the reinforced layer according to Fig. 4.4 (Sharma et al. 2009).

According to Figs. 4.1 and 4.2, failures of type (a) and type (b) are most likely to happen when there is excessive distance between the foundation base to the upper

reinforcement layer (u) or the distance between reinforcement layers (h), presumably when $u > 0.5B$ or $h > 0.5B$. Laboratory studies by Chen et al. (2007) and Abu-Farsakh et al. (2008) shows that to prevent these types of failures, the distance between the bottom of the footing and the upper reinforcement layer (u) and the distance between reinforcement layers (h) should be less than half of the footing width ($0.5B$), where B is the width the foundation.

According to Fig. 4.3, if the strength of the reinforced zone is much greater than the strength of the underlying unreinforced layer and the depth ratio of reinforcement layers (d/B) is relatively low, shear punching failure occurs in the reinforced zone, followed by total shear failure in the unreinforced zone. Such a failure mechanism was first suggested by Meyerhof and Hanna (1978) for a strong soil layer placed on a weak soil layer. Wayne et al. (1998) expressed that with minor modifications to the solution by Meyerhof and Hanna (1978), it could be used for calculating the bearing capacity of foundations on reinforced beds.

According to Fig. 4.4, in regular reinforcement status, when the strength of the reinforced zone is slightly larger compared to the underlying unreinforced layer and the values of u and h are smaller than $0.5B$, the failure occurs inside the reinforcement zone. According to studies by Sharma et al. (2009), the proper type of failure mechanism for clayey and sandy soil are type (c) and type (d), respectively. Separate research experiments by Harikumar et al. (2016) and others on the square footing of a 150 mm dimension on multi-directional reinforcing elements reported the optimum embedment depth of $0.5B$. 1.3% increase in bearing capacity and 0.72% reduction in the settlement were obtained by embedding the reinforcement layer at depth of $0.5B$ compared to unreinforced beds. Based on the height of geocell, the distance between geocell layers and stiffness of soil layers, these failure mechanisms can be extended to geocell-reinforced systems, which need further investigation to obtain the exact limits for the influencing factors.

Zhao et al. (2009) reviewed the response of geocell-reinforced layers under embankments and suggested the three aspects of main geocell layer functions, including (a) vertical stress dispersion effect, (b) membrane effect, and (c) lateral resistance effect, which are explained briefly as the follows:

(a) ***Vertical stress dispersion effect***

The horizontal geocell-reinforced cushion behaves as an immediate working platform that redistributes the footing load per unit area over a wider area, as shown in Fig. 4.5. This refers to herein as "stress dispersion effect". As a result, the soil pressure onto the soft subgrade soil surface is smaller than that onto the subgrade soil in the absence of geocell.

As far as the applied surface stress can be distributed based on the 2:1 method in the unreinforced foundation, Tavakoli Mehrjardi et al. (2015) proposed that, in geocell-reinforced foundation, the stress can be considered to be longitudinally distributed on an equivalent circle with diameter "D" as per Eq. (4.1).

$$D = B + nH \tag{4.1}$$

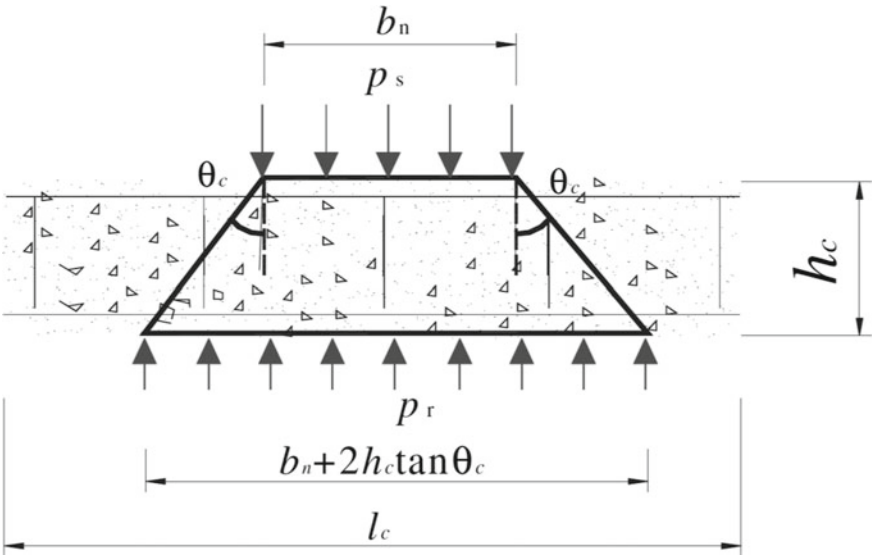

Fig. 4.5 Vertical stress dispersion effect of geocell reinforcement (Zhang et al. 2010a, b)

where

B Footing width
H considered depth of the foundation
n load spreading factor which ≈1.5.

(b) ***Membrane effect***

The loads from the embankment deflect the geocell reinforcement generating a further tension force, as shown in Fig. 4.6. The vertical component of the tension force in the reinforcement is helpful to reduce the pressure on the subgrade soil. Then, the vertical deformation of the soft subgrade is reduced and the bearing capacity of the subgrade soil is enhanced as well. In tandem with increasing the surface settlement, the geocell layer deformed more, bringing about a further tension force due to this membrane effect.

(c) **Lateral resistance effect**

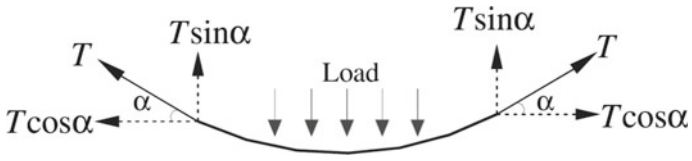

Fig. 4.6 Membrane effect of geocell reinforcement (Zhang et al. 2010a, b)

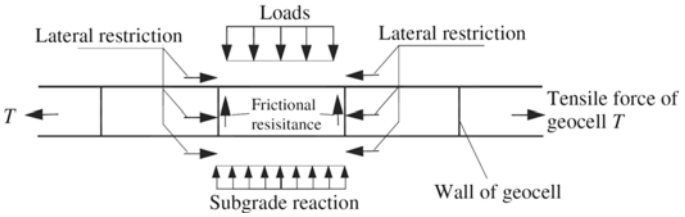

Fig. 4.7 Lateral resistance effect of geocell reinforcement (Zhang et al. 2010a, b)

Geocells consist of three-dimensional cells containing the filled materials, causing lateral spreading which, in turn, results in improving the shear strength of filled materials. Moreover, interfacial resistances, which result from the interaction between the geocell reinforcement and the soils below and above the reinforcement, as shown in Fig. 4.7, increase the lateral confinement and lower lateral strain, that results in an increase in the modulus of the cushion layer and improving vertical stress distribution on the subgrade which is called "vertical stress dispersion effect" reducing the vertical pressure on the top of the subgrade, correspondingly.

Since anchorage and/or tensioned membrane effects of geocells are predominantly influenced by the mobilized shear strength at the geocells–soil interface, therefore in the load support applications, the interfacial properties of geocell-reinforced soil should be determined. In this regard, Tavakoli Mehrjardi and Motarjemi (2018) carried out a series of large direct shear test to investigate the interactive parameters of geocell-soil composite on the interface's shear strength with respect to the backfill aggregate size. In this study, geocells made of a tape of Heat-Bonded Nonwoven geotextile (HBNW) had the pocket size and height of 55 mm × 55 mm and 50 mm, respectively. Moreover, two relative densities of fill materials (50 and 70% which represent medium dense and dense backfill, respectively), three aggregate sizes of fill materials (3, 6 and 12 mm–selected based on the scaling criteria on size of shear box and geocell pockets), and three normal stresses (100, 200 and 300 kPa—these values cover rather low to high vertical stress in a soil element of common geotechnical projects) have been examined.

To have a shortcut to the results observed in the study, Table 4.1 is presented. This table summarizes the influences of all studied parameters on the interfacial characteristics of grains-grains (unreinforced status) and grains-geocell (reinforced status) interactions. In way of illustration, Table 4.1 states that an upward trend of *medium grain size of fill materials improved both friction angle and cohesion mobilized at the interface, regardless of the reinforcement* statuses *(Tavakoli Mehrjardi and Motarjemi 2018). Further results can be summarized as follows*:

– Unlike the positive effect of geocell, the normal stress had a negative influence on the advancement of dilation angle, tending to reduction in the beneficial effect of the grains size increment on the improving interface's shear strength. Therefore, using geocells in low normal stress and large main particle size is more recommended.

Table 4.1 Properties of all three soils used in the tests

Parameters	Reinforcement Status	τ_{max}	τ_{cv}	ϕ	c	ψ
Relative density	Unreinforced	↑	↑	↑	← in $D_{50} = 3$ and 6 mm cte. in $D_{50} =$ 12 mm	↑
	Reinforced	← in $D_{50} = 3$ and 6 mm → in $D_{50} =$ 12 mm	↓	← in $D_{50} =$ 3 mm cte. in $D_{50} = 6$ and 12 mm	← in $D_{50} = 3$ and 6 mm → in $D_{50} =$ 12 mm	↑
Normal Stress	Unreinforced	↑	↑	↓	↑	↓
	Reinforced	↑	↑	↓	↑	↓
medium Grain Size	Unreinforced	↑	↑	↑	↑	↑
	Reinforced	↑	↑	↑	↑	↑
Geocell reinforcement	Reinforced	↑	↑	Cte. (excepted from large grains at low relative density)	↑	↑

Tavakoli Mehrjardi and Motarjemi (2018)
↑← mean increase and ↓→ mean decrease

- For medium dense fill materials, increasing soil particle size strengthens the beneficial role of the geocell and improved stability of the materials after reaching the shear strength at peak. On the contrary, the advancement of relative density and normal stress, to some extent, reduced the geocell efforts in increasing the shear strength of the interface.
- For coarse aggregates (cell aspect ratio smaller than 8.5), the geocell reinforcement was more efficient, in the order of two times, at least, more than compaction effort in the enhancement of shear characteristics mobilized at the interface.
- *geocell reinforcement had no significant effect on interface's friction angle at high relative density.*
- geocells mobilize an apparent cohesion on the shear interface owing to the provision of some confinement for the aggregates located in the neighbor of the shear plane. For geocell-reinforced samples with $D_r = 50\%$, the apparent cohesion has substantially increased by about 1.9–23 kPa.
- The results clarify that among the studied variables, geocell with cell aspect ratio [the ratio of the geocell's cells size (b) to the medium grains size (D_{50})] 4 has the best performance in the improvement of interface's shear strength.

Moreover, to observe the effective parameters on the shear characteristics of geocell–grains interface, Fig. 4.8 is illustrated. From this figure, during shearing, interlocking effect which mobilizes apparent cohesion and friction at the interface,

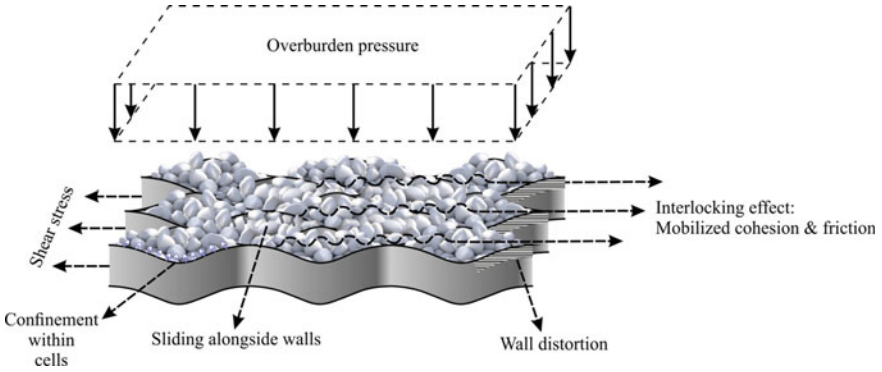

Fig. 4.8 Sketch of effective parameters on the shear characteristics of geocell–grains interface (Tavakoli Mehrjardi and Motarjemi 2018)

besides the confinement effect on grains within the geocell's cells, producing interface's shear strength. Based on the acquired results, it was found out that shear strength of the interface encountered weakness in the aftermath of grain sliding alongside the geocell's walls and also, geocell's walls distortion.

If the mentioned failure mechanisms of the geocell-reinforced bed include the layers of geocell, then the geocell has ruptured. The ruptured geocells can exhibit failure modes related to the junction welds between geocell strips. A series of tests were performed by Liu et al. (2019) on HPDE geocell to recognize possible failure modes of the junctions. According to the tensile tests, two failure modes were identified for geocell junctions under tensile loading, which can be observed in Fig. 4.9b, c. All specimens experienced identical behavior in their initial stage of failure, with the elongation initiating from approximately the middle of the welds, as shown in Fig. 4.9a. The initial stage was then followed by two different failure modes. Some specimens continued elongating in a vertical manner until rupture occurred (Fig. 4.9d). Whereas, for others, the fracture was initiated from the left-hand side after reaching its peak tensile strength and followed by rupture which propagated towards the right-hand edge. Similar failure modes were observed on the cell-wall which was attributed to the stress concentration caused by inconsistent indentation depths.

Regarding shearing, all specimens experienced similar failure modes, where the rupture occurred adjacent to the junction, as shown in Fig. 4.10. This indicates that the junction is unlikely to fail during shearing and the shear strength of the junction is significantly higher than the peak shear stresses obtained from the present experimental program, yet it is more vulnerable to tensile stress. This observation is confirmed by the elongation mode in Fig. 4.10b, where the specimen deformed only in the cell-wall strip, while the junction remained intact.

Under the action of peeling, two failure modes were observed, as are shown in Fig. 4.11. Only one of the five tested specimens experienced weld fracture (Fig. 4.11c), while the other specimens failed in the cell-wall adjacent to the

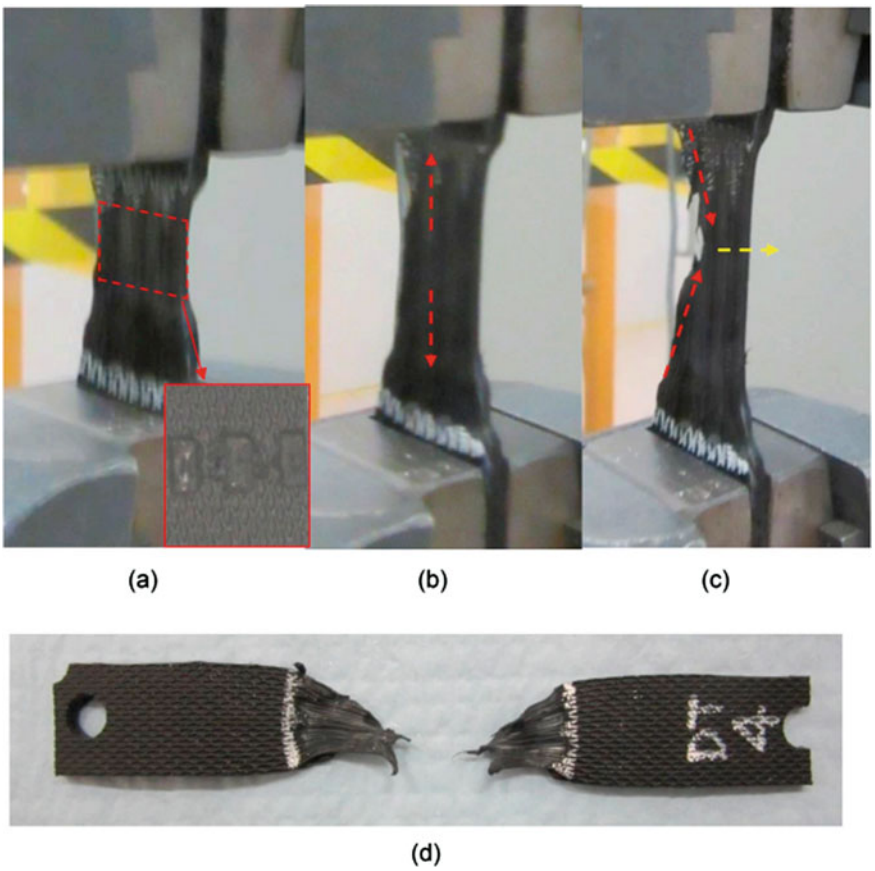

Fig. 4.9 Failure modes of the geocell junction subjected to uniaxial tension: **a** initial stage (pre-peak), **b** failure mode 1 (post-peak), **c** failure mode 2 (post-peak), and **d** ruptured specimen (Liu et al. 2019)

weld junction (weld failure). This specimen also experienced the most fluctuations throughout the loading process. Due to the low possibility of occurrence of this failure mode, it is considered that this is likely the result of faulty/unsatisfactory welding during manufacturing.

Unlike other loads, which occur less frequently when the geocell is placed in the field, such as in the case of pavement or slopes, the junctions are constantly subjected to a splitting force. Two types of failure mechanisms were observed, as shown in Fig. 4.12. The failure mode is shown in Fig. 4.12b can be described as occurring when the two welded, cell-wall strips completely separated from each other due to the rupture of the weld. The failure mode being shown in Fig. 4.12c is defined as cell-wall failure, as the junction did not fail under the influence of the splitting force. The latter mode is similar to the failure condition under shearing and peeling.

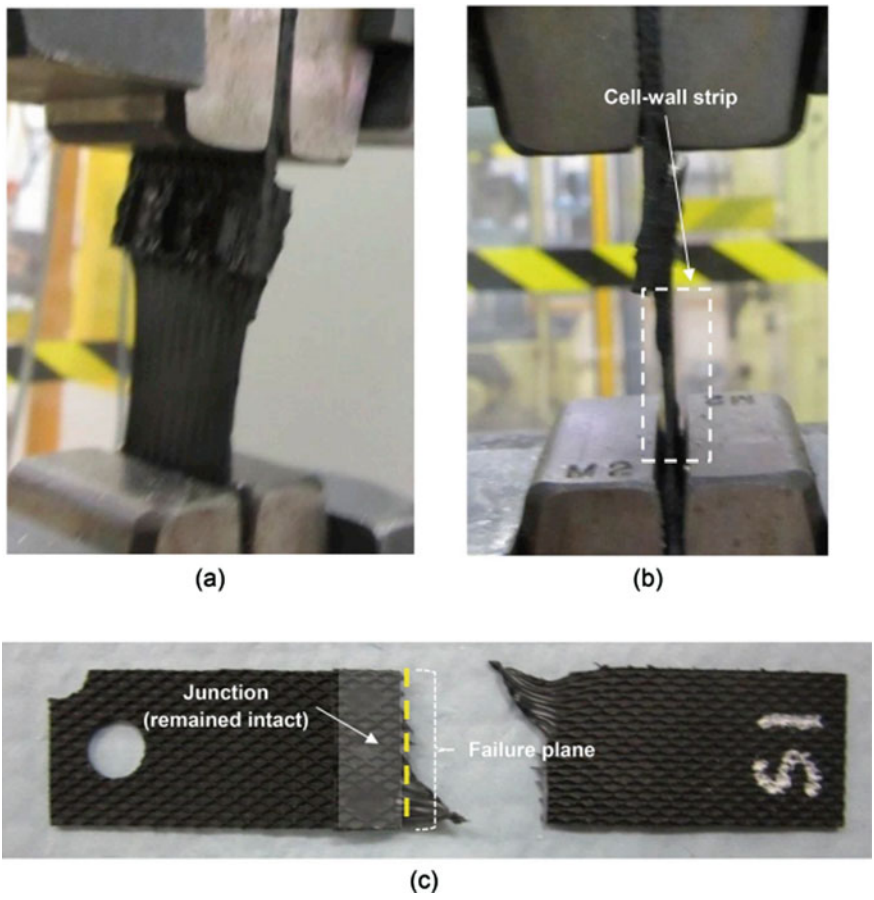

Fig. 4.10 Failure modes of geocell junctions subjected to shear force: **a** oblique view and **b** side view during testing, and **c** failed specimen (Liu et al. 2019)

It should be noted that geocell junctions exhibit a higher splitting strength when the junctions experience the failure mode of complete separation. As the stress–displacement relationship was obtained from the seam strength tests, the geocell junctions reached their peak strength under the splitting load, significantly slower than in other loading scenarios. This phenomenon suggests that when geocells are used in the field (such as in slope protection), it is possible that the soil structure will experience a gradual down-slope movement prior to failure if the gravitational load exceeds that specified by the manufacturer. The post-peak behavior suggests that, once the junction reaches its splitting strength, failure occurs faster when compared with other loading conditions.

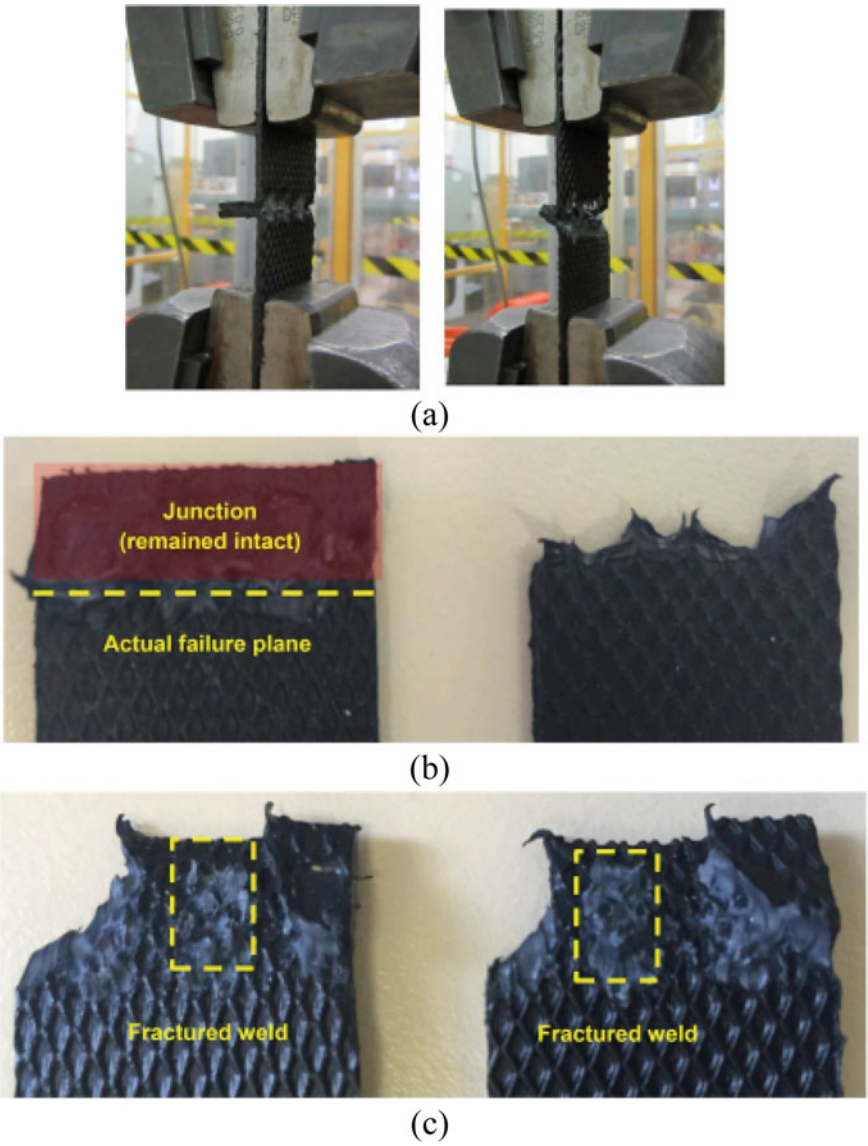

Fig. 4.11 Failure modes of geocell junctions subjected to peeling force: **a** during testing, **b** strip failure, **c** weld failure (Liu et al. 2019)

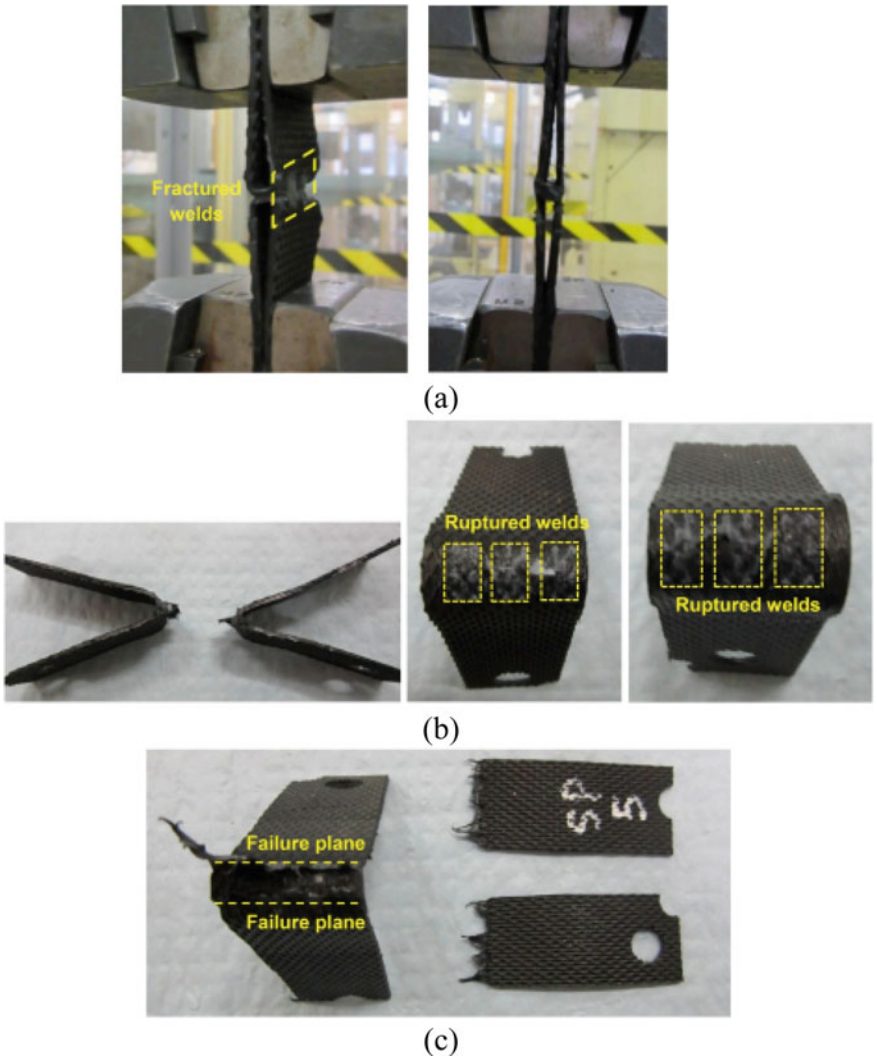

Fig. 4.12 Failure modes of geocell junctions subjected to a splitting force: **a** during testing; **b** junction failure; **c** cell-wall strip failure (Liu et al. 2019)

4.3 Equating the Response of Geocell-Reinforced Foundations

Limited works have been done on the design of road embankment supported by geocell-reinforced cushion. Jenner et al. (1988) used a slip line theory to calculate the increase in the bearing capacity of soft soil due to the provision of geocell cushion at the base of the embankment. In their method, plastic bearing failure of the soil was

assumed and the additional resistance due to geocell layer was calculated using a non-symmetric slip line field in the soft subgrade soil. This method was very complicated as it needed to construct a slip line field for every embankment problem. Koerner (1998) presented a bearing capacity calculation method by adapting the conventional plastic limit equilibrium mechanism as used in statically loaded shallow foundation bearing capacity. In his method, the shear strength between geocell wall and soil contained within it was considered as a bearing capacity increment on the foundation soil due to the presence of the geocell reinforcement at the base of the embankment. Latha et al. (2006) proposed a method to design the geocell-supported embankments based on the study of laboratory model tests. The method was based on the slope-stability analysis, and the critical slip surfaces of embankments should be checked by the slope-stability program for every design. In their analysis, the geocell layer was treated as a foundation soil layer with additional cohesive strength caused by confinement.

In this section, relevant equations for the response of geocell-reinforced foundations including bearing capacity and the corresponding settlements are presented.

4.3.1 Single-Layered Geocell-Reinforced Foundation

Zhang et al. (2010a, b) propose a simple bearing capacity calculation method for the geocell-supported embankment over soft soil, with consideration of the main reinforcement functions of geocell layer studied above. In this study, the bearing capacity of geocell-reinforced foundation "p_{rs}" is estimated by putting the bearing capacity of the untreated foundation soil "p_s" and the bearing capacity increment "Δp" on the foundation soil due to the presence of the geocell-reinforced cushion together. The methods to determine "p_s" have been developed or proposed correspondingly in the literature (Lambe and Whitman 1969). It can be determined by empirical values or equations, or site load testings.

As discussed beforehand, the main reinforcement mechanisms of the geocell in embankment engineering are "lateral resistance effect", "vertical stress dispersion effect" and "membrane effect". Generally, the effect of lateral resistance of geocell reinforcement is mostly related to the resistance against the lateral deformations of embankments. So, the lateral resistance effect of geocell reinforcement has no direct effect on increasing the bearing capacity of the subgrade soil. The bearing capacity increment "Δp" on the foundation soil can be made up of two aspects, notably the bearing capacity increment "Δp_1" due to the "vertical stress dispersion effect", and the bearing capacity increment "Δp_2" due to the "membrane effect" of the geocell reinforcement.

According to Fig. 4.6, the geocell-reinforced cushion widens the spreading of vertical stress so that, in turn, the subgrade soil can support more upper loads than that without geocell-reinforced cushion. The footing load per unit area increases from "p_s" to "p_r", according to Eq. (4.2).

$$\mathrm{p}_r = \frac{(b_n + 2h_c \tan\theta_c)}{b_n} p_s \tag{4.2}$$

where "p_r" is the footing load due to the vertical stress dispersion effect; "b_n" is the width of the uniform load "p_s", as shown in Fig. 4.6; "h_c" and "θ_c" are the height and the dispersion angle of geocell reinforcement, respectively. Thus, the bearing capacity increment "Δp_1" by the "vertical stress dispersion effect" can be calculated as Eq. (4.3).

$$\Delta p_1 = p_r - p_s = \frac{2h_c \tan\theta_c}{b_n} p_s \tag{4.3}$$

As shown in Fig. 4.7, the bearing capacity increment "Δp_2" on the foundation soil due to the tensile force of the geocell reinforcement can be estimated as Eq. (4.4).

$$\Delta p_2 = \frac{2T \sin\alpha}{b_n} \tag{4.4}$$

where "T" is the tensile force of the reinforcement and can be calculated from Eq. (4.5).

$$T = E_c \varepsilon h_g \tag{4.5}$$

where "E_c" is the tensile modulus of the geocell material and can be estimated by an indoor tensile test (ASTM D638-14); "ε" is the tensile strain of the geocell material; "h_g" is the height of the geocell wall; "a" is the horizontal angle of the tensional force "T".

Before calculating "ε", the deformation shape of the reinforcement should be determined. Sophisticated numerical analyses have shown that the shape of the deflected geocell is a catenary (BS8006 1995; Yin 2000). However, at relatively small deflections the catenary may be approximated by a parabola which simplifies the analysis procedure for determining the tensile force in the geocell. As shown in Fig. 4.13, the deformation on the road surface is in the form of Eq. (4.6).

$$y_0 = -\frac{\Delta_0}{r_0^2} x^2 + h_0 + \Delta s_0 \tag{4.6}$$

where "y_0" is the deformation on the road surface; "Δs_0" is the maximum differential settlement at the surface; "h_0" is the vertical distance from the origin of coordinates shown in Fig. 4.13 to the embankment surface. By differentiating Eqs. (4.5) and (4.7) is obtained.

$$\frac{\mathrm{d}y_0}{\mathrm{d}x} = -\frac{2\Delta s_0}{r_0^2} x \tag{4.7}$$

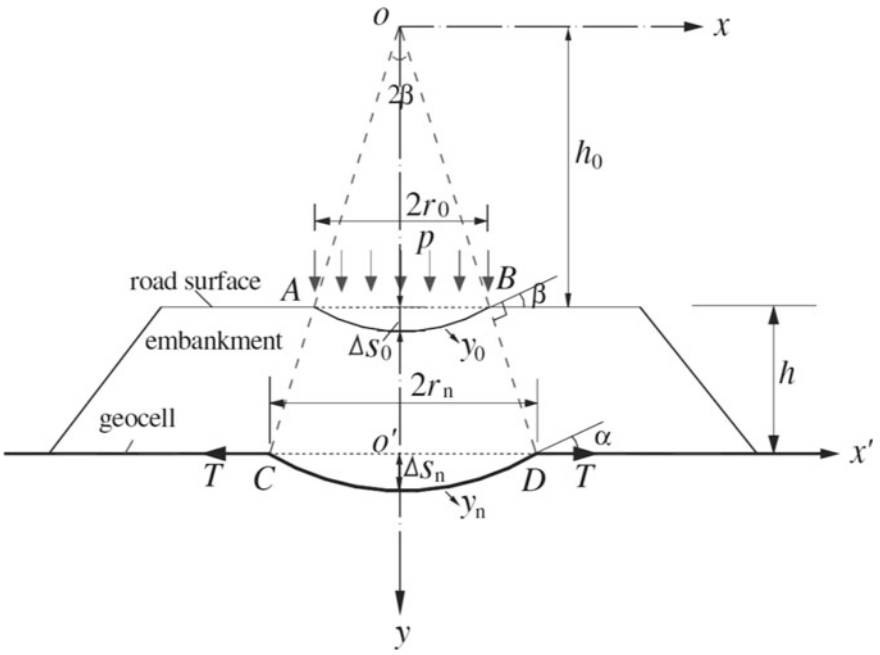

Fig. 4.13 Calculation model of the geocell-reinforced embankment (Zhang et al. 2010a, b)

When $x = r_0$, $\mathrm{d}y_0/\mathrm{d}x = -2\Delta s_0/r_0$. Supposing that the normal directions of points A and B on the deformation parabola are the same as the diffusion directions of embankment fill under the external load "p", then, Eq. (4.8) can be presented.

$$\tan\beta = \frac{2\Delta s_0}{r_0} = \frac{r_0}{h_0} = \frac{r_n}{h_0 + h} \tag{4.8}$$

where "b" is the angle depicted in Fig. 4.13; "r_n" is the half of the chord length of parabola depicted in Fig. 4.13 and calculated by Eq. (4.9); "h" is the height of the embankment.

$$r_n = \frac{r_0^2 + 2\Delta s_0 h}{r_0} \tag{4.9}$$

The relative deformation equation of the geocell reinforcement shown in Fig. 4.13 is in the form of Eq. (4.10).

$$y_n = -\frac{\Delta s_n}{r_n^2}x^2 + h_0 + h + \Delta s_n \tag{4.10}$$

where "y_n" is the deformation of the geocell reinforcement; "Δs_n" is the maximum vertical deformation of the reinforcement. Be similar to Eqs. (4.6) and (4.11) is

obtained.

$$\sin\alpha = \left[1 + \left(\frac{r_n}{2\Delta s_n}\right)^2\right]^{-\frac{1}{2}} \tag{4.11}$$

Then, the tensile strain of the geocell (ε) is determined as Eq. (4.12).

$$\varepsilon = \frac{1}{2}\delta + \frac{r_n}{4\Delta s_n}\ln\left[\frac{2\Delta s_n}{r_n} + \delta\right] - 1 \tag{4.12}$$

where δ is defined as Eq. (4.13).

$$\delta = \left[1 + \left(\frac{2\Delta s_n}{r_n}\right)^2\right]^{\frac{1}{2}} \tag{4.13}$$

By the way, the acceptance limit of the tensile strain (ε) is controlled by the ultimate tension strain of the geocell material and the maximum permissible differential settlement of embankment [Δs_0]. Δs_n and Δs_0 follow a relationship as Eq. (4.14).

$$\Delta s_0 = \Delta s_n + \Delta c \tag{4.14}$$

in which, "Δc" is the compression of the embankment material under the load "p". "Δc" can be determined by layer-wise summation method. If the embankment is not very high, "Δc" is nearly zero, and "Δs_n" is close to the differential settlement "Δs_0" on the embankment surface.

As mentioned earlier, the bearing capacity of the geocell-reinforced embankment foundation (p_{rs}) can be evaluated by putting the bearing capacity of the untreated foundation soil (p_s) and the bearing capacity increment (Δp) on the foundation soil due to the placement of the geocell-reinforced cushion at the base of the embankment together, leading to Eq. (4.15).

$$p_{rs} = p_s + \Delta p = p_s + \Delta p_1 + \Delta p_2 = p_s + \frac{2h_c \tan\theta_c}{b_n} p_s + \frac{2T\sin\alpha}{b_n} \tag{4.15}$$

Depending on what aspects of failure mechanisms for geocell-reinforced foundation had been considered, other researchers have presented relationships for other forms of bearing capacity, summerized in Table 4.2. In all equations:

p_r bearing capacity of geocell-reinforced foundation (kPa),
δ interface shear angle between the cell-wall and the filling soil (°),
k_0 coefficient earth pressure at rest,
p_u bearing capacity of unreinforced soil (kPa),
h/d geocell aspect ratio,
p applied pressure on the geocell mattress (kPa),

B width of the applied pressure system (m).

4.3.2 Multi-layered Geocell-Reinforced Foundation

For a semi-infinite soil medium of the elastic modulus E_n and Poisson's ratio ν_n, subjected to uniform pressure q on a circular footing with radius a, the immediate settlement at the depth z below the center of flexible footing is written as Eq. (4.16) (Harr 1966). Equation (4.16) is valid for a flexible footing and should be multiplied by $\pi/4$ for a rigid footing.

$$w(z) = \frac{2aq\left(1-\nu_n^2\right)}{E_n}\left(\sqrt{1+\frac{z^2}{a^2}}-\frac{z}{a}\right)\left\{1+\frac{z/a}{2(1-\nu_n)\sqrt{1+\frac{z^2}{a^2}}}\right\} \tag{4.16}$$

Hirai (2008) developed the elastic relationships of multi-layer soil stiffness modulus. Figure 4.14 shows a multi-layered soil system composed of n-layers of soil subjected to vertical loads q. As shown in Fig. 4.14, the present procedure uses the elastic moduli, i.e., Young's modulus of E_m, Poisson's ratio of ν_m and thickness of H_m for mth layer in n-layers of multi-layered soil system. Parameters D and D_f are the diameter and embedment depth of a footing, respectively. The n-layered soil system shown in Fig. 4.14 was transformed into an equivalent two-layered soil system illustrated in Fig. 4.15a. The equivalent elastic modulus of E_H (Hirai and Kamei 2003, 2004) for $(n-1)$ layers in Fig. 4.15a (where $H = H_1 + H_2 + H_3 + \cdots + H_{n-1}$) was represented by Eq. (4.17).

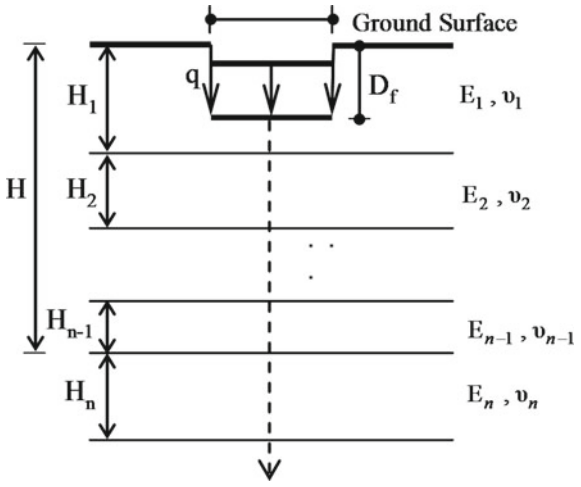

Fig. 4.14 Multi-layered soil systems (Hirai 2008)

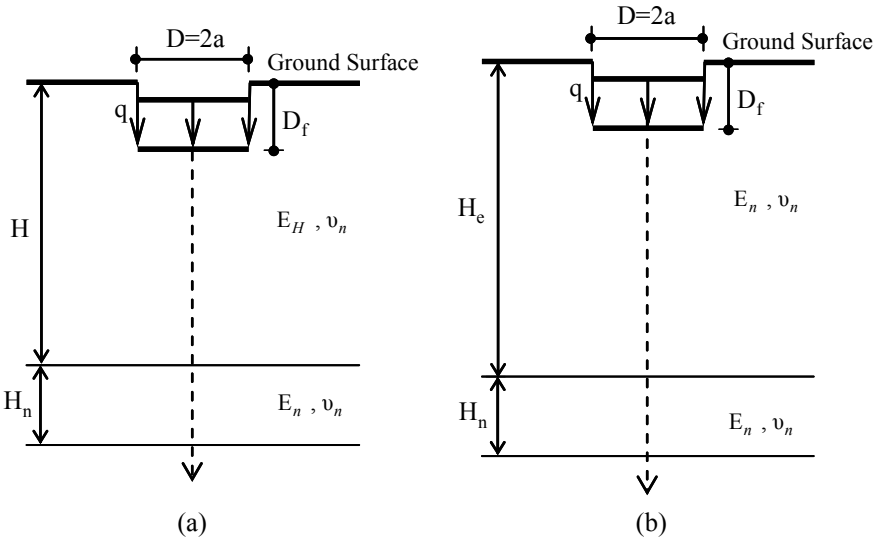

Fig. 4.15 **a** Equivalent two-layered soil system for Fig. 4.14, and **b** Equivalent single-layer soil system with the same E_n and ν_n for Fig. 4.15a (Hirai 2008)

$$E_H = \left[\left\{ E_1 \frac{(1-\nu_n^2)}{(1-\nu_1^2)} \right\}^{\frac{1}{3}} \frac{H_1 - D_f}{H - D_f} + \sum_{j=2}^{n-1} \left\{ E_j \frac{(1-\nu_n^2)}{\left(1-\nu_j^2\right)} \right\}^{\frac{1}{3}} \frac{H_j}{H - D_f} \right]^3 \tag{4.17}$$

Next, the two-layered soil system in Fig. 4.15a was transformed into an equivalent single soil layer with an elastic modulus of E_n and Poisson's ratio of ν_n, (the thickness of an equivalent single layer is $H = H_e + H_n$) as shown in Fig. 4.15b, using the equivalent thickness relations (4.18) and (4.19) (Hirai and Kamei 2003, 2004; Hirai 2008). For the case where $E_H \geq E_n$:

$$H_e - D_f = \left(\frac{E_H}{E_n} \right)^{1/3} (H - D_f) \quad \text{for } E_H \geq E_n \tag{4.18}$$

$$H_e - D_f = \left[0.75 + 0.25 \left(\frac{E_H}{E_n} \right)^{1/3} \right] (H - D_f) \quad \text{for } E_H \leq E_n \tag{4.19}$$

Likewise, Fig. 4.16 shows an equivalent system of soil layers to that previously illustrated in Fig. 4.14, but now each soil layer has an equivalent thickness of H_{ie} and uniform E and ν values for every layer (=E_n and ν_n). Thus, the system is reduced to a single-layer system of thickness $H_{1e} + H_{2e} + H_{3e} + \cdots + H_{(n-1)e} + H_n$ and stiffness properties E_n and ν_n. The equivalent thickness of each individual layer is required so as to obtain the thinning and strain of each layer of the multi-layered system as it is described later in the current section. According to the Palmer and Barber method

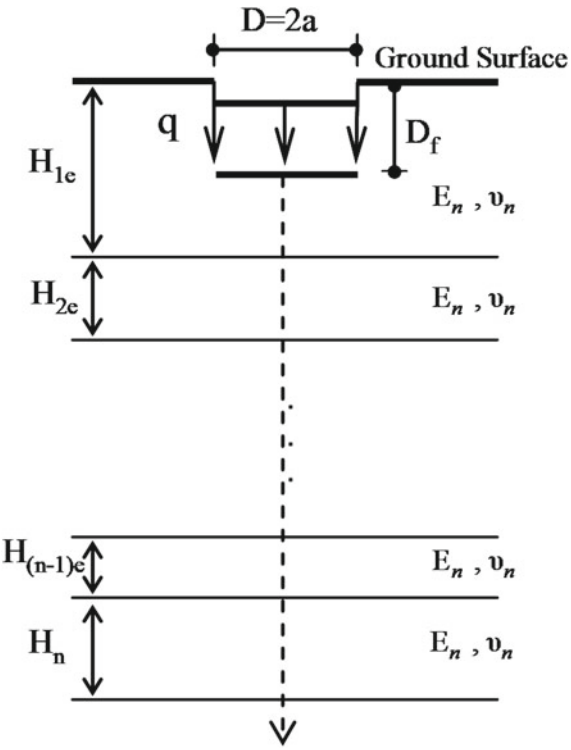

Fig. 4.16 Equivalent single soil layer with equivalent thickness of "$H_{1e} + H_{2e} + H_{3e} + \cdots + H_{(n-1)e} + H_n$" and E_n and ν_n for Fig. 4.14 (Hirai 2008)

(1940) for a two-layer system and to Odemark's method (1949) for a multi-layered soil system, Eqs. (4.20) and (4.21), respectively, were derived by Hirai (2008) for estimating the equivalent thickness of each layer for the case where $E_m \geq E_n$.

$$H_{1e} - D_f = \left\{ \frac{E_1\left(1-\nu_n^2\right)}{E_n\left(1-\nu_1^2\right)} \right\}^{1/3} (H_1 - D_f) \tag{4.20}$$

$$H_{me} = \left\{ \frac{E_m\left(1-\nu_n^2\right)}{E_n\left(1-\nu_m^2\right)} \right\}^{1/3} H_m (m = 2 \sim n) \tag{4.21}$$

For the case where $E_m \leq E_n$, by considering Terzaghi's approximate formula (1943), the equivalent thickness is given by Eqs. (4.22) and (4.23).

$$H_{1e} - D_f = \left[0.75 + 0.25 \left\{ \frac{E_1\left(1-\nu_n^2\right)}{E_n\left(1-\nu_1^2\right)} \right\}^{1/3} \right] (H_1 - D_f) \tag{4.22}$$

$$H_{me} = \left[0.75 + 0.25\left\{\frac{E_m\left(1-\upsilon_n^2\right)}{E_n\left(1-\upsilon_m^2\right)}\right\}^{1/3}\right] H_m (m = 2 \sim n) \tag{4.23}$$

where H_{1e} and H_{me} are the values of H_e for the first and subsequent layers ($m = 2$ to n), respectively, and E_1, υ_1, E_n, υ_n and E_m, υ_m are values of E_H and υ for layers 1, n and $m = 2$ to n, respectively.

$$w_1 = \frac{2aq\left(1-\upsilon_n^2\right)}{E_n}\left(\sqrt{1+\left(\frac{H_e}{a}\right)^2} - \frac{H_e}{a}\right)\left(1 + \frac{H_e}{2a(1-\upsilon_n)\sqrt{1+\left(\frac{H_e}{a}\right)^2}}\right) \tag{4.24}$$

Vakili (2008) developed the method of Foster and Ahlvin (1959) to evaluate the surface settlement of the equivalent system shown in Fig. 4.16. According to this method, the actual vertical surface deflection of a footing (w) was obtained by adding the amount of thinning, w_2, of the equivalent layer (with thickness of H_e) between the surface ($z = 0$) and a depth of $z = H_e$ to the vertical deflection at a depth of $z = H_e$ of a semi-infinite mass below that depth (i.e. deflection of w_1 at bottom of the equivalent layer). In the case of uniform pressure "q" on a flexible circular footing with radius "a" (Fig. 4.14), supported by a semi-infinite mass, w_1 is obtained by substituting the value of $z = H_e$ from Eq. (4.18)/ or Eq. (4.19) into Eq. (4.16) to obtain Eq. (4.24).

Similarly, the vertical deflection at the center of loading on the surface (i.e. w_0 at depth of $z = 0$) of uniform equivalent layer (i.e. for the footing on the equivalent layer), substituting the value of $z = 0$ into Eq. (4.16) results in Eq. (4.25).

$$w_0 = \frac{2a\left(1-\upsilon_n^2\right)q}{E_n} \tag{4.25}$$

Equations (4.24) and (4.25) are valid for a flexible footing and should be multiplied by $\pi/4$ for a rigid footing. The vertical thinning of the equivalent layer [with thickness of H_e as in Fig. 4.15b) between the loading surface ($z = 0$) and a depth of $z = H_e$ (i.e. $(w_0 - w_1)$], can be converted to the thinning, w_2, of the original layer (thickness H as in Figs. 4.14 and 4.15a), using Eq. (4.26).

$$w_2 = \frac{E_n}{E_H}(w_0 - w_1) \tag{4.26}$$

Hence, Eqs. (4.24) and (4.26) may be summed to obtain the actual total surface settlement of the circular footing ($w = w_1 + w_2$).

Moghaddas Tafreshi et al. (2015) presented a new analytical solution, based on the theory of multi-layered soil system to estimate the pressure-settlement response of a circular footing resting on multi-layered geocell-reinforced foundation comprising non-cohesive soil.

The "n"-layered soil system theory (Hirai 2008) and surface settlement of equivalent system (Vakili 2008) were employed to evaluate the pressure-settlement of footings supported by a multi-layer geocell-reinforced bed as shown in Fig. 4.17. This figure shows a schematic model of a shallow circular footing with diameter, $D = 2a$, located on a typical n-layer foundation bed composed of "m" geocell layers and "$n - m$" soil layers, under the application of a uniformly distributed surface load, q. The thicknesses of geocell and soil layers are h_g and h_s, respectively. The first geocell layer is placed at a depth of u beneath the footing and the remaining geocell layers are located after an unreinforced soil thickness of h_s. The effective depth, H_{eff}, is assumed as the depth to a point below the footing at which only 10% of the applied stress on footing surface acts. The elastic modulus, E_i, and Poisson's ratio, ν_i ($i = 1, 2, 3, \ldots, n$) of each layer is as given in Fig. 4.17. H_{n-1} is the thickness of the $(n - 1)$th layer which can be calculated using Eq. (4.27).

$$H_{n-1} = H_{\text{eff}} - u - mh_g - (m-1)h_s \tag{4.27}$$

Beforehand, it should be mentioned that the following simplifying assumptions are made in this analysis, as follows:

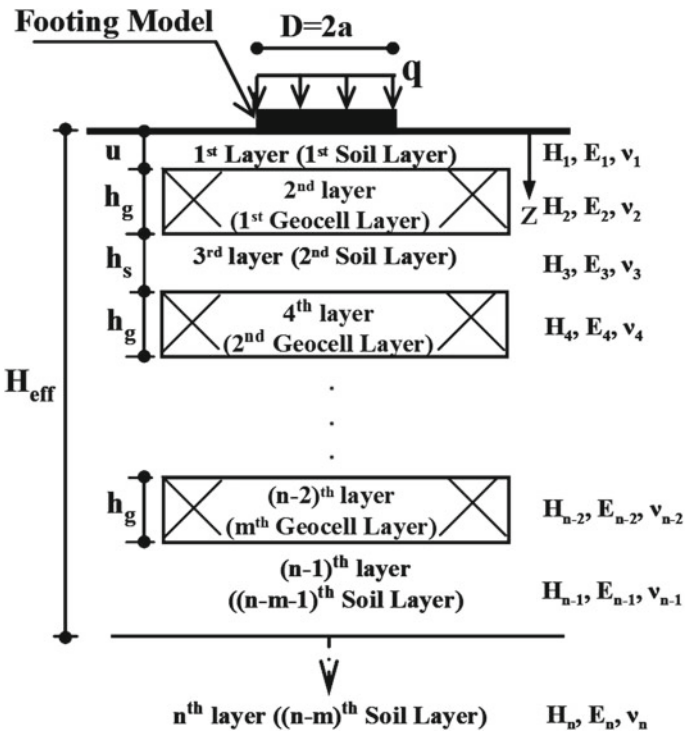

Fig. 4.17 "n" layer geocell-reinforced soil system containing "m" layers of geocell (Moghaddas Tafreshi et al. 2015)

- The soil layers are homogeneous, isotropic and non-cohesive;
- The unreinforced and reinforced layers deform only in the vertical direction;
- The footing is circular with no embedment depth, $D_f = 0$;
- The behavior of unreinforced and reinforced layers is assumed to be nonlinear elastic;
- Poisson's ratio is assumed to be in the range 0.2–0.3 (see below).

It is known that geocell layers don't expand much horizontally once properly filled with granular soil and compacted (Dash et al. 2007; Pokharel 2010). Thus, the proposed analytical model does not directly consider lateral deformation but, instead, allows for some, indirectly, by using:

(1) Elasticity moduli of the soil and geocell-reinforced layers that were obtained from calibration of the proposed equations (presented later in this section) to the data obtained in the triaxial test that included some lateral deformation, and
(2) Poisson's ratio values of 0.2–0.3, for the unreinforced and geocell-reinforced layers of the foundation bed to compute the equivalent thickness of the multi-layered system, being in line with typical values as used by Mhaiskar and Mandal (1996) and Zhang et al. (2010a, b), as described later.

To reach an equivalent single layer, first, the upper "$n-1$" layers of thicknesses $H_1, H_2, H_3, \ldots$ and H_{n-1} (Fig. 4.17) should be replaced by a single layer of thickness ($H_{\text{eff}} = H_1 + H_2 + H_3 + \cdots + H_{n-1}$) having an equivalent modulus of E_H in Fig. 4.18a

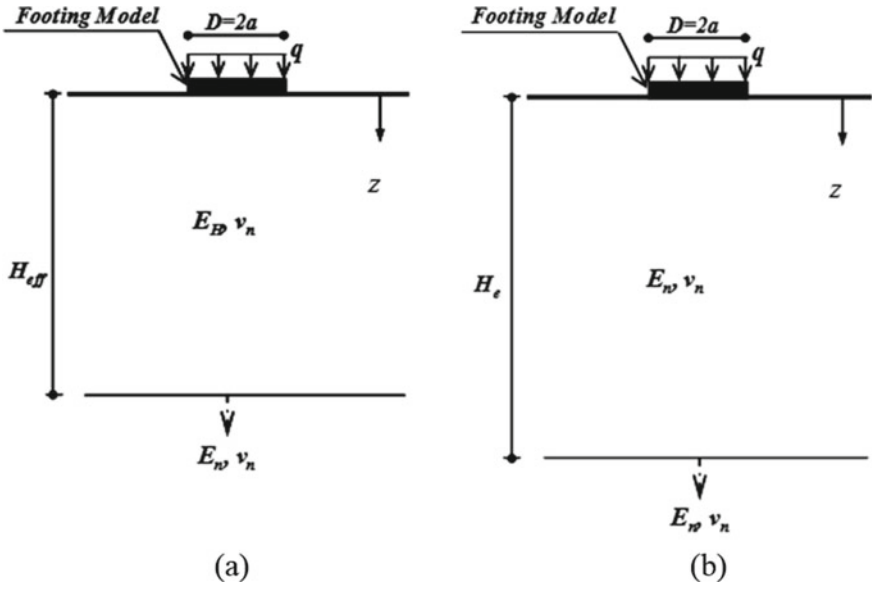

Fig. 4.18 Substituting n-layer system sequentially with **a** Equivalent two-layered system for n-layer system in Fig. 4.17, **b** equivalent single-layer system with the same E_n and ν_n for two-layered system in Fig. 4.18a

(Hirai 2008). The equivalent elastic modulus (E_H) of layers 1 to $n-1$, is calculated by using Eq. (4.17) for the footing with no embedment depth ($D_f = 0$) as Eq. (4.28).

$$E_H = \left[\sum_{j=1}^{n-1} \left\{ E_i \frac{(1-\nu_n^2)}{\left(1-\nu_j^2\right)} \right\}^{\frac{1}{3}} \frac{H_j}{H_{\text{eff.}}} \right]^3 \tag{4.28}$$

where, H_i and E_i are the thickness and elastic modulus of ith layer, respectively. The n-layer system in Fig. 4.17 is thus reduced to a two layers system as shown in Fig. 4.18a.

The two-layered system (Fig. 4.18a) can be reduced to an equivalent single-layer system (Fig. 4.18b) with elastic modulus of E_n and an equivalent thickness of H_e. The equivalent thickness (H_e) with the elastic modulus of E_n and Poisson's ratio of ν_n is then defined by Eq. (4.29) for the case where $E_H \geq E_n$ and by Eq. (4.30) for the case where $E_H \leq E_n$. Equations (4.29) and (4.30) provided for the same Poisson's ratio of the two layers in Fig. 4.18a where E_n is the elastic modulus of the nth layer.

$$H_e = \left(\frac{E_H}{E_n}\right)^{1/3} H_{eff} \tag{4.29}$$

$$H_e = \left[0.75 + 0.25\left(\frac{E_H}{E_n}\right)^{1/3}\right] H_{eff} \tag{4.30}$$

Consequently, the use of Eqs. (4.28)–(4.30) deliver an equivalent single homogeneous semi-infinite mass of material that can be substituted for the n-layer system as shown in Fig. 4.18b. Generally, the footing settlement (i.e., soil surface settlement), w should be calculated using Eqs. (4.24)–(4.27). Since the nature of footing pressure-settlement variation is nonlinear, the behavior of unreinforced layers and reinforced layers (Geocell and soil inside of its pockets) are considered to act as MLE (Multiple Linear Elastic) layers. The MLE model provides an ability to calculate the elastic modulus of each layer, for each load step, using the confining pressure of the current and previous stages as described in Eqs. (4.31)–(4.42).

To calculate the elastic modulus of the ith layer requires knowledge of the strain of layers 1 to $n-1$. To compute these, the deformation and equivalent thickness of the ith layer (Fig. 4.17) are required. Using Eqs. (4.20)–(4.23) for the footing with no embedment depth ($D_f = 0$), supported on a multi-layer system, the equivalent thickness of each soil layer, H_{ie} with the same E_n and ν_n was determined by Eq. (4.31) for the case where $E_i \geq E_n$ and by Eq. (4.32) for the case where $E_i \leq E_n$, respectively.

$$H_{ie} = \left\{ \frac{E_i\left(1-\nu_n^2\right)}{E_n\left(1-\nu_i^2\right)} \right\}^{1/3} H_i \tag{4.31}$$

$$H_{ie} = \left[0.75 + 0.25\left\{\frac{E_i\left(1-\upsilon_n^2\right)}{E_n\left(1-\upsilon_i^2\right)}\right\}^{1/3}\right] H_i \tag{4.32}$$

Then, from Eqs. (4.24) and (4.26), for a rigid circular footing with radius "a" subjected to uniform pressure "q", the thinning and strain of the ith layer are defined as Eqs. (4.33)–(4.35).

$$w_i = \frac{2\pi a q\left(1-\upsilon_n^2\right)}{4E_n}\left(\sqrt{1+\left(\frac{\sum_{l=1}^{l=i} H_{le}}{a}\right)^2} - \frac{\sum_{l=1}^{l=i} H_{le}}{a}\right)$$
$$\left(1 + \frac{\sum_{l=1}^{l=i} H_{le}}{2a(1-\upsilon_n)\sqrt{1+\left(\frac{\sum_{l=1}^{l=i} H_{le}}{a}\right)^2}}\right) \tag{4.33}$$

$$w_{p_i} = \frac{E_n}{E_i}(w_i - w_{i-1}) \tag{4.34}$$

$$\varepsilon_i = \frac{w_{p_i}}{H_i} \tag{4.35}$$

where

H_{ie} equivalent thickness of the ith layer based on the elastic parameters of the nth layer
w_i displacement at a depth of $\sum_{l=1}^{l=i} H_{le}$
w_{pi} the vertical deformation within the ith layer of thickness H_{ie}, (due to actual thinning of the ith layer)
ε_i the strain across the thickness of the ith layer.

In the jth loading step, the displacement increment of soil surface due to loading increment of $q_j - q_{j-1}$ can be calculated by Eqs. (4.36)–(4.39).

$$\Delta w_1^j = \frac{2\pi a(q_j - q_{j-1})\left(1-\upsilon_n^2\right)}{4E_n}\left(\sqrt{1+\left(\frac{H_e}{a}\right)^2} - \frac{H_e}{a}\right)$$
$$\left(1 + \frac{H_e}{2a(1-\upsilon_n)\sqrt{1+\left(\frac{H_e}{a}\right)^2}}\right) \tag{4.36}$$

$$\Delta w_0^j = \frac{2\pi a\left(1-\upsilon_n^2\right)(q_j - q_{j-1})}{4E_n} \tag{4.37}$$

$$\Delta w_2^j = \frac{\mathrm{E}_n}{\mathrm{E}_\mathrm{H}}\left(\Delta w_0^j - \Delta w_1^j\right) \tag{4.38}$$

$$w^j = \mathrm{w}^{j-1} + \Delta w_1^j + \Delta w_2^j \tag{4.39}$$

where:

Δw_1^j vertical displacement increment on loading centerline at a depth of H_e for loading increment of $q_j - q_{j-1}$, (i.e. at the bottom of the equivalenced layer),

Δw_0^j vertical displacement increment at surface (of equivalent layer) beneath centre of load for loading increment of $q_j - q_{j-1}$,

Δw_2^j vertical deformation (thinning) increment of the original layer of thickness of H,

w^j vertical displacement at surface of the system for loading of q_j.

Similarly, the strain increment for the ith layer at the jth loading step can be calculated using Eqs. (4.40)–(4.42) using the adjustments already employed to formulate Eqs. (4.14) and (4.16).

$$\Delta w_i^j = \frac{2\pi a(q_j - q_{j-1})\left(1-\upsilon_n^2\right)}{4E_n}\left(\sqrt{1+\left(\frac{\sum_{l=1}^{l=i} H_{le}}{a}\right)^2} - \frac{\sum_{l=1}^{l=i} H_{le}}{a}\right)$$
$$\left(1 + \frac{\sum_{l=1}^{l=i} H_{le}}{2a(1-\upsilon_n)\sqrt{1+\left(\frac{\sum_{l=1}^{l=i} H_{le}}{a}\right)^2}}\right) \tag{4.40}$$

$$(\Delta w_p)_i^j = \frac{E_n}{E_i}\left(\Delta w_i^j - \Delta w_{i-1}^j\right) \tag{4.41}$$

$$\varepsilon_i^j = \varepsilon_i^{j-1} + \frac{(\Delta w_p)_i^j}{H_i} \tag{4.42}$$

where:

H_{ie} equivalent thickness of the ith layer based on the elastic parameters and thickness of the nth layer as defined by Eqs. (4.31 and 4.32),

Δw_i^j displacement increment of equivalent layer for layers 1 to i based on the elastic parameters of nth layer in depth of $\sum_{l=1}^{l=i} H_{le}$ for loading increment of $q_j - q_{j-1}$,

$(\Delta \mathrm{w_p})_i^j$ deformation increment (thinning) of layer with thickness of H_i for loading increment $q_j - q_{j-1}$,

ε_i^j strain of layer with thickness of H_i subjected to loading q_j.

4.3.2.1 Results and Discussion

As can be seen, one of the contributing factors in settlement equations is elastic modulus of both geocell-reinforced and unreinforced soil layers. Since one of the

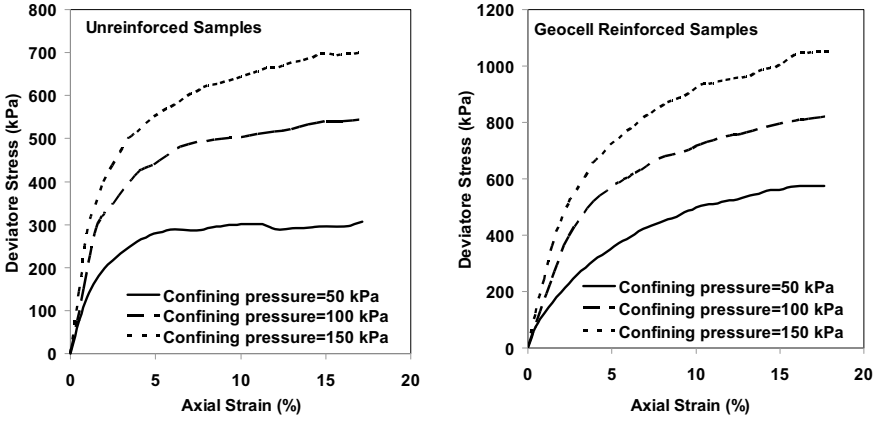

Fig. 4.19 Stress-axial strain curves for unreinforced and geocell-reinforced samples under confining pressure of 50, 100 and 150 kPa **a** unreinforced samples, **b** geocell-reinforced samples (Noori 2012)

most useful tests in determination of soils' elastic modulus is triaxial compression tests, herein the process of obtaining the elastic modulus of unreinforced and geocell-reinforced soil layers in terms of strain and confining pressure, $E = f(\sigma_3, \varepsilon)$ for each loading step, is presented.

(a) ***Elastic modulus of unreinforced layers***

Based on the data extracted from Fig. 4.19a, the vertical stress ($\sigma_1 = \sigma_3 + \sigma_d$) of triaxial samples was found to be a function of the confining pressure (σ_3) and axial strain (ε). Therefore, according to Eq. (4.43) a nonlinear regression model was developed to estimate the vertical stress (σ_1) for different values of σ_3 and ε.

$$\sigma_1 = 61.47\,\sigma_3^{0.73}\,\varepsilon^{0.34}\,\mathrm{e}^{-3.17\varepsilon} \tag{4.43}$$

The tangential modulus of elasticity can be derived as the derivative of stress with respect to strain (from Eq. 4.43) as presented in Eq. (4.44). The function of $f(\varepsilon)$ is defined in Eq. (4.45).

$$E = 61.47\,\sigma_3^{0.73} * f(\varepsilon) \tag{4.44}$$

$$f(\varepsilon) = \left(-3.17\,\mathrm{e}^{-3.17\varepsilon}\varepsilon^{0.34} + \frac{0.34\,\varepsilon^{0.34}}{\varepsilon}\mathrm{e}^{-3.17\varepsilon}\right) \tag{4.45}$$

(b) ***Elastic modulus of geocell-reinforced layers***

Madhavi Latha (2000), based on the results of triaxial compression tests on geocell-encased sand, proposed an empirical equation in the form of Eq. (4.46) to express

the elastic modulus of the geocell-reinforced sand (E_g).

$$E_g = 4\,\sigma_3^{0.7}(K_u + 200M^{0.16}) \tag{4.46}$$

where

K_u the dimensionless modulus number of the unreinforced sand in the hyperbolic model proposed by Duncan and Chang (1970),
M the secant tensile modulus of the geocell material (e.g., geotextile and geogrid) in *kN/m,* assessed at an average strain of 2.5% in load-elongation, and
σ_3 the confining pressure in kPa.

In fact, the geocell layers are modeled as equivalent composite layers with enhanced stiffness and shear strength properties. The term in parentheses of Eq. (4.46) expresses Young's modulus parameter of geocell-reinforced soil in terms of the secant modulus of the geocell material (M) and the dimensionless modulus number of the unreinforced soil (K_u).

However, due to the fact that the suggested relationship by Madhavi Latha (2000), Eq. (4.46), is not a function of axial strain level, it is modified to Eq. (4.47) as a function of both confining pressure (σ_3) and axial strain (ε).

$$E_g = a_1\,\sigma_3^{b_1}\,(K_u + a_2 M^{b_2}) * f(\varepsilon) \tag{4.47}$$

The function of $f(\varepsilon)$ is assumed as Eq. (4.45) and then the parameters of a_1, a_2, b_1, and b_2 are obtained from the triaxial test results of geocell-reinforced soil (Fig. 4.19b). The constants parameters in Eq. (4.47) depend on the type of infill soil and strength of geocell material, which must be calibrated according to the results of triaxial tests on soil and geocell, with the same properties that would be used in the foundation bed. Fitting Eq. (4.47) to the data of Noori (2012) yields the elastic modulus as a function of σ_3, ε, K_u and M as Eq. (4.48).

$$E_g = 0.12\,\sigma_3^{0.73}\,(K_u + 100M^{0.1}) * f(\varepsilon) \tag{4.48}$$

At each loading step, the elastic modulus of unreinforced and reinforced layers was estimated using the confining pressure (at mid-height of the layer) and the strain computed at the end of the previous loading step. The confining pressure in the middle of each reinforced layer was obtained by multiplying the distributed vertical stress by the coefficient of lateral pressure (k_r) calculated in Eq. (4.49). The value of lateral pressure coefficient for unreinforced soil $k_{un} = 0.5$ has been suggested by Madhavi Latha (2000). For $M = 0$, Eq. (4.49) results in the lateral pressure coefficient of unreinforced soil (k_{un}).

$$k_r = k_{un}\,(K_u + 100M^{0.1})/K_u \tag{4.49}$$

Overall, Eqs. (4.44)–(4.49) reveal that the proposed formulations would be able to consider the variation of geocell performance in regard to the strain level and confinement stress variations across the depth of the foundation bed, provided the elastic modulus of the different layers (soil layers and the geocell-reinforced layers) are allotted appropriate values that differ from layer-to-layer and from one loading step to the next. Based on the results of triaxial compression tests, the value of the hyperbolic parameter of Duncan and Chang (1970), K_u, is found as 483.3 (the authors' evaluation not reported here). Also, the secant modulus of the geocell material at 2.5% strain, M, is given by the manufacturer as 114 kN/m ($M = 114$ kN/m). Due to the confinement of the soil by the geocell wall, the Poisson's ratio of geocell-reinforced layers may be less than that in unreinforced layers. The range of Poisson's ratio for granular soil (i.e. sand in the present paper) is about 0.3–0.35 and for geocell filled with sand from 0.17 (Mhaiskar and Mandal 1996) to 0.25 (Zhang et al., 2010a, b). Thus, a Poisson's ratio of 0.3 is used for unreinforced layers, and a Poisson's ratio of 0.25, 0.2, and 0.2, is used, respectively for reinforced layers with one, two, and three layers of geocell.

4.3.2.2 Validation of Proposed Analytical Method

The presented analytical method was validated by comparing the results of model analyses with plate load test results (Moghaddas Tafreshi et al. 2013) for an unreinforced bed and for beds reinforced by three layers of geocell. Figure 4.20 compares the results of the analytical method and tests in the form of footing pressure-settlement responses, for different values of geocell mass. These comparisons are done for parameters of $K_u = 483.3$, $M = 114$ kN/m, $h_g = 100$ mm and $D = 300$ mm. Since

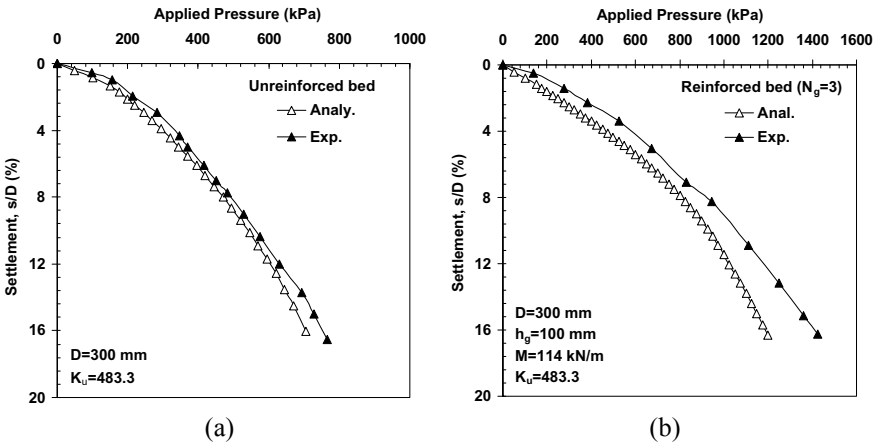

Fig. 4.20 Comparison of analytical and experimental results for **a** unreinforced bed, **b** reinforced bed with three layers of geocell (Moghaddas Tafreshi et al. 2015)

the analytical method has not considered any variation in the geocells' width; it is assumed that the width of the geocell-reinforced layers being sufficient to ensure the anchorage derived from the adjacent stable soil mass.

The predicted responses show a better match with the experimental ones at lower footing settlement levels (i.e., $s/D < 8\%$). For larger footing settlements (e.g., $s/D > 8\%$), the analytical predictions underestimate the experimentally determined settlements, implying strain softening in the geocell-soil layers in situ relative to the performance in the triaxial or that the assumption of no lateral strain is non-conservative. The difference between the predicted responses and experimental ones might more generally be attributed to the selected value of lateral pressure coefficient, the selected values of Poisson's ratio, the simplifying assumptions used in the analytical method, the discrepancies between the experimental and analytical systems and the differences in simulating the field and the experimental conditions of multiple layers.

Since the practical design of shallow footings is mostly governed by footing settlement, footing settlement must be limited to specific values, depending on the super-structure. Thus, the close comparison of analytical and experimental results in the lower range of settlement (i.e., less than 6% of the footing diameter) is encouraging. This implies that the analytical method presented is capable of estimating the behavior of footings supported by geocell layers and maybe conveniently applied as a tool to estimate the pressure-settlement response of footings over most practical ranges of geotechnical use.

4.4 Contributing Factors

Moghaddas Tafreshi et al. (2015) carried out a parametric study using the analytical model presented to understand how the considered parameters affect the response of the geocell-reinforced foundations. The investigated parameters comprised variation in the secant modulus of geocell (M), the dimensionless modulus number of the soil (K_u), the thickness of geocell layers (h_g), and the number of geocell layers (N_g).

Figure 4.21a shows the effect of the secant modulus of the geocell (M) on the pressure-settlement response of a foundation reinforced with three layers of geocell. The results reveal the beneficial effect of the reinforcement's rigidity (see Eq. 4.48) in decreasing the footing settlements so that at a given bearing pressure, the value of the settlement decreases as the secant modulus of geocell (M) increases. The similar results reported by Madhavi Latha et al. (2006) for geocell-supported embankments showed that higher surcharge capacity and lower deformations are associated with an increase in the value of the M parameter. This performance could be attributed to the internal confinement provided by geocell reinforcement with an increase in M. The confinement effect is dependent on the secant modulus of the reinforcement, the friction at the soil-reinforcement interface and the confining stress developed on the infilling soil inside the geocell pocket due to the passive resistance provided by the 3D structure of geocell (Sireesh et al. 2009; Moghaddas Tafreshi and Dawson

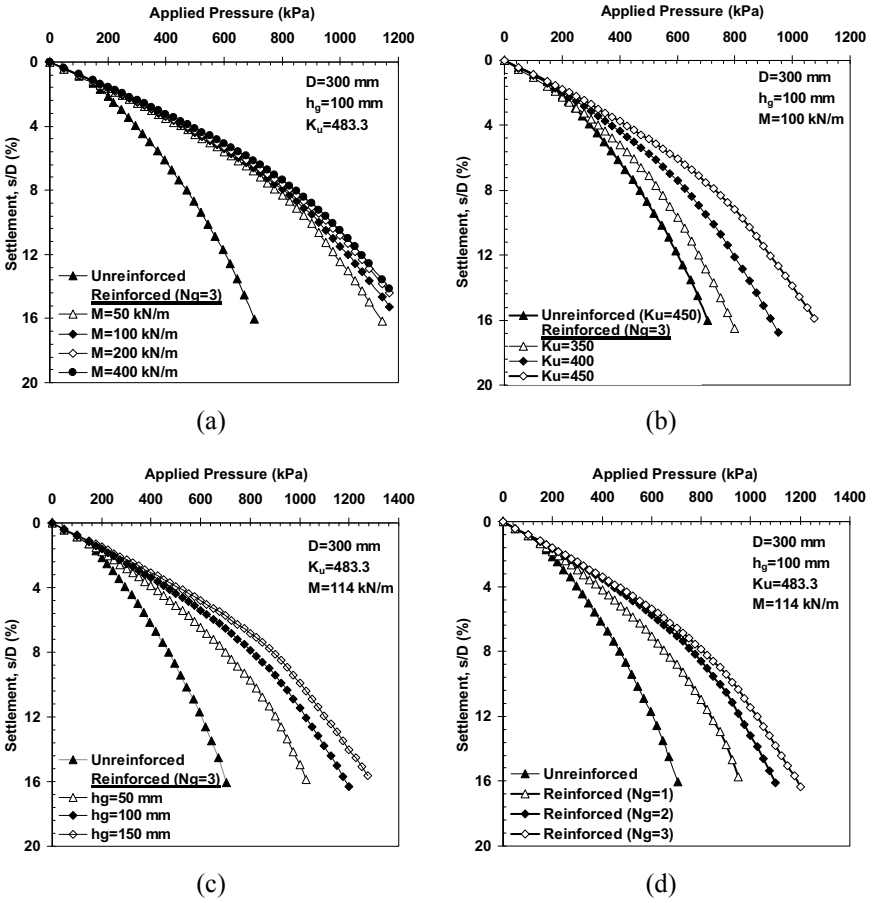

Fig. 4.21 Variation of pressure-settlement response of geocell-reinforced bed for different **a** secant modulus of geocell (M), **b** soil dimensionless modulus (K_u), **c** thickness of geocell layers (h_g), and **d** number of geocell layers (N_g) (Moghaddas Tafreshi et al. 2015)

2010a). In addition, as seen in Fig. 4.21a, there is a limiting value of M (=100 kN/m) beyond which no further load-settlement benefit is achieved. Almost certainly this is because the behavior of the unreinforced soil between the reinforced layers is now limiting the response of the overall system.

To see what the effect of K_u is, the variation of pressure-settlement of the reinforced bed with three layers of geocell is presented in Fig. 4.21b. The results show that the bearing capacity of a footing at a given settlement is significantly increased due to an increase in the K_u value. Thus, the role of the soil type and the soil compaction in the performance of geocell-reinforced beds, which the composite model suggested in the present study, can take into account this effect. However, a dense sand matrix tends to dilate under footing penetration, thereby mobilizing higher strength in the

geocell reinforcement, leading to greater performance improvement (Madhavi Latha et al. 2009).

The rigidity of the geocell layer is predominantly influenced by the thickness of geocell. To have a better assessment of the effect of a geocell's thickness in a geocell-reinforced foundation, the variation of the pressure-settlement relationship of the unreinforced bed and of the reinforced bed with three layers of geocell is presented in Fig. 4.21c. The benefit of a thicker geocell mat is evident, so that a thicker geocell decreases the footing settlements, tending to improve its bearing capacity. This appears to be a consequence of greater opportunity of geocell-soil interaction (in the form of wall-friction and confining pressure imposed by the pocket walls) and the increased stiffness of the effective zone beneath the footing consequent upon an increase in the thickness of geocell. This is in line with the findings of Dash et al. (2007), Madhavi Latha et al. (2006) Moghaddas Tafreshi and Dawson (2010a) who reported that the settlement of a trench's soil surface was decreased due to the provision of a thicker geocell in the backfill. Furthermore, the rate of reduction in footing settlement and the rate of enhancement in load-carrying capacity of the footing can also be seen to reduce with an increase in the value of h_g. The reason is that, as multiple, thicker reinforcement layers are used, then the reinforced zone extends deeper beyond the zone most significantly strained by the applied load, so that little further benefit accrues. From a practical point of view, as the thickness of a geocell layer is increased; the problem of lower achieved compaction in the geocell packets would be encountered, so that higher compactive effort is necessary as the thickness of vertical webs of the geocell is increased, owing to hindering of vertical densification (Thakur et al. 2012; Tavakoli Mehrjardi et al. 2013). For this reason, multiple thin geocell layers may, in practice, be preferred to fewer, thicker layers.

Figure 4.21d presents the bearing pressure-settlement response of the unreinforced and reinforced foundation beds with one, two, three layers of geocell. From this figure, it may be clearly observed that, as the number of geocell layers increases (i.e., the increase in the depth of the reinforced zone), both stiffness and bearing pressure at a specified settlement increase substantially. Likewise, at a given bearing pressure, the value of the settlement decreases as the number of geocell layers increases. However, the rate of reduction in footing settlement is seen to reduce with an increase in the number of geocell layers. It is likely that the additional layers are interacting with soil that is strained less and less by the applied load, therefore delivering diminishing increments of additional reinforcement effect. Yoon et al. (2008) and Moghaddas Tafreshi et al. (2013) in their studies on the effect of multi-layered geocell reported a similar effect with increase in the number of 3D reinforcement layers.

The reinforcing effects of multiple layers of geocell in sand were also measured using plate loading at a diameter of 300 mm (Moghaddas Tafreshi et al. 2013). Granular soil passing through the 38 mm sieve with a specific gravity of 2.68 (G_s = 2.68) was used as backfill soil in the testing program which is classified as well-graded sand. The maximum dry density was about 20.62 kN/m^3, which corresponds to an optimum moisture content of 5.7%. The average measured dry densities of unreinforced soil and the soil filled in geocell pockets after compaction of each layer were 18.56 and 18.25 kN/m^3. Figure 4.22a presents the bearing pressure-settlement

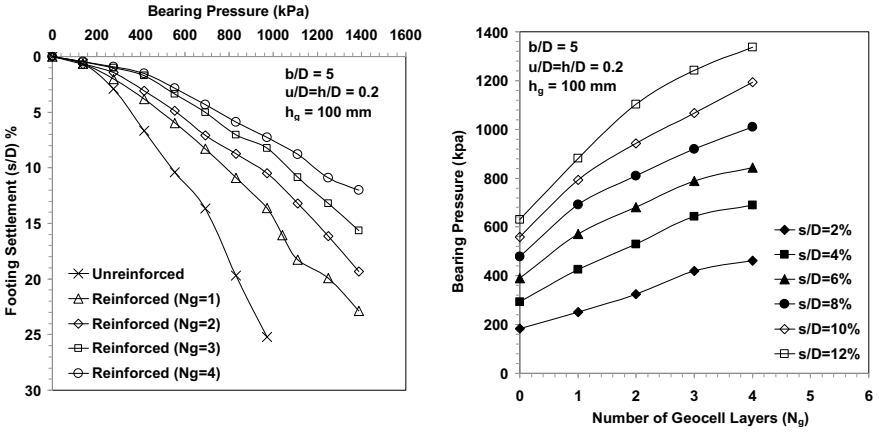

Fig. 4.22 Variation of bearing pressure with **a** the footing settlement for the unreinforced and geocell-reinforced foundation beds with one, two, three, and four layers of geocell, and **b** the number of geocell layers at different levels of settlement (Moghaddas Tafreshi et al. 2013)

behavior of the unreinforced and reinforced foundation beds with one, two, three and four layers of geocell ($N = 1, 2, 3, 4$) when the layers of geocell were placed at the optimum values of u/D and h/D ($u/D = h/D = 0.2$).

From Fig. 4.22, it may be clearly observed that as the number of geocell layers increased (i.e. with the increase in the depth of the reinforced zone), both stiffness and bearing pressure at a specified settlement increase substantially. This figure shows that no clear bearing capacity failure point was evident, even at a settlement level of 20–25%, regardless of the mass of geocell in the foundation bed. Beyond a certain footing settlement level—that is, at s/D around 2–4%, depending on the mass of reinforcement beneath the footing base—there was an increase in the slope of the settlement–pressure curves. This may be attributed to local foundation breakage in the region under and around the footing, because of high deformation induced by the large settlement under the footing. This would lead to a reduction in the load-carrying capacity of the footing as indicated by the softening in the slope of the pressure-settlement responses. Beyond this stage, the slope of the curves remained almost constant with the footing bearing pressure continuously increasing, suggesting that this mode of damage developed progressively. In order to have a direct comparison of the results for the unreinforced and multi-layered geocell-reinforced beds, the bearing pressure values corresponding to settlement ratios of 2, 4, 6, 8, 10, and 12% were extracted from Fig. 4.23a for different numbers of geocell layers. Figure 4.22b plots these data against the number of geocell layers (N_g). This range of settlement levels (less than 12%) was selected to reflect a range of practical interest. It can be seen that as the number of geocell layers increased, the bearing pressure increased steadily, regardless of the settlement ratio. For example, at the settlement ratio of $s/B = 4\%$, the bearing capacity values were about 292, 427, 530, 642, and 688 kPa

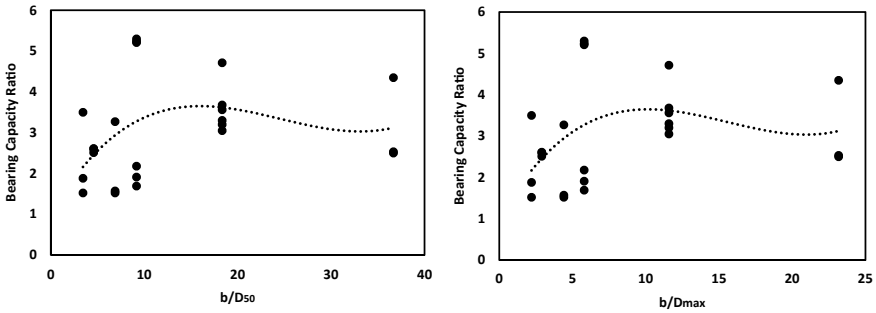

Fig. 4.23 Variation of bearing capacity ratio versus the ratio of the geocell's cells size to **a** the medium grains size (D_{50}), **b** the maximum grains size (D_{max}) (Tavakoli Mehrjardi et al. 2019)

for unreinforced bed, and reinforced bed with one, two, three and four layers of geocell, respectively. Thus the increases in bearing pressure were about 46, 82, 120, and 135% for one, two, three, and four layers of geocell reinforcement, respectively. A comparison with Fig. 4.22a shows that this increased bearing pressure was a consequence of the increased stiffness consequent upon geocell reinforcement. At low settlement ratios, $s/D < 4\%$, the benefit of three reinforcing layers is evidenced by the higher gradient of the lines in the figure. For practical applications, small settlements are almost always needed and three reinforcing layers are associated with the greatest bearing pressure increase for the same settlement.

Fig. 4.22b also indicates that the benefits of reinforcement increase as the footing settlement increases. This performance could be attributed to the internal confinement provided by geocell reinforcement. The concept of confinement reinforcement, which may be called internal confinement, was explained by Yang (1974). The confinement effect is dependent on the tensile strength of the reinforcement, the friction at the soil-reinforcement interface and the confining stress developed on the infilling soil inside the geocell pocket due to the passive resistance provided by the 3D structure of geocell (Sitharam and Sireesh 2005). Obviously, the reinforced system must exhibit some settlement, and consequently, strain (elongation) must develop in the reinforcement layers to affect the geocell modulus, tensile and frictional strength, and the passive resistance offered by the geocell layers. Additionally, this comparison indicates that it is necessary to consider the footing settlement level while investigating the effects of reinforcement on the bearing pressure of reinforced sand.

Among the effective parameters on the performance of geocell-reinforced foundations, the situation of geoccell embedment and also, the width of geocell layers expanded beneath the footings have been discussed by previous researchers. Table 4.3 presents the optimum values for the burial depth of the first geocell layer (u), the vertical spacing of geocell layers, in multi-layered systems, (h) and width of geocell (b).

Table 4.2 Relationships for bearing capacity of geocell-reinforced foundations

Researcher	Mechanism considered	Bearing capacity equation	Parameters
Koerner (1998)	Lateral resistance effect	$p_r = 2p\tan^2(45 - \emptyset/2)\tan\delta + cN_cS_c + qN_qS_q + 0.5\gamma BN_\gamma S_\gamma$	p = applied pressure on geocell matress (kPa) $\emptyset$ = friction angle of the soil used to fill the geocell pocket (degrees) c = cohesion of the soil (kPa) q = surcharge load (kPa) γ = unit weight of the soil (kN/m^3) $N_c, N_q, N\,\gamma$ = bearing capacity factors $S_c, S_q, S\,\gamma$ = shape factors
Presto (2008)	N/A	$p_r = 2\frac{h}{d}k_a\sigma_{vm}\tan\delta + c_uN_c$	k_a = coefficient of active earth pressure σ_{vm} = average vertical stress (kPa) c_u = subgrade shear strength (kPa) N_c = bearing capacity coefficient
Avesani Neto et al. (2013)	Confinement effect, stress dispersion effect and the membrane effect	$p_r = p_u + 4\frac{h}{d}k_0pe\tan\delta + (1-e)p$	e = stress redistribution effect
Sitharam and Hegde (2013)	Lteral resistance effect, vertical stress dispersion and membrane mechanisms	$p_r = p_u + 2p\tan^2(45 - \emptyset/2)\tan\delta + p_r\left(1 - \frac{B}{B+2D_r\tan\beta}\right) + \frac{4TS}{B_gB}$	$\emptyset$ = friction angle of the soil used to fill the geocell pockets (degrees) D_r = depth of the reinforcement (m) βn = load dispersion angle (degrees) T = tensile strength of the basal geogrid material (kN/m) B_g = width of the basal geogrid (m) S = footing settlement measured at the surface (m)

It should not lose sight of the fact that the beneficial performance of geocell is absolutely dependent on its installation in the backfill. Tavakoli Mehrjardi et al. (2013) observed the importance of compaction both below and above the level of the geocell installation. On the other hand, if the geocell is situated on low-density backfill layer, it gives rise to poorer performance of the geocell even compared with the unreinforced status. In effect, the vertical webs of the geocell hindered vertical densification. Necessarily, they must also stop inter-meshing of stones in adjacent pockets of the web structure. Consequently, the effective reinforcement and improvement of the backfill system are achievable if the geocell is installed in the backfill with an appropriate compaction process.

4.5 Scale Effects

Performance of a system in the context of physical modeling is directly dependent on geometrical matters and considered aspect ratio. In other words, a study about the scale effect is absolutely timely and crucial in the interpretation of the obtained results, especially when it applies to prototype and practical models. Many experimental studies in the field of reinforced embankments have been carried out with small or large-scale physical modeling at which the scale effects are rarely fully considered. However, one of the most challengeable matters in this area is how the reduced-scale model and prototype model tests can be bridged. Recently, some experimental and numerical studies have been carried out to understand the parametric sensitivity of geogrid-reinforced soil (Góngora and Palmeira 2016; Brown et al. 2007; Cuelho et al. 2014; Tavakoli Mehrjardi and Khazaei 2017; McDowell et al. 2006). Table 4.4 summarizes the optimum values for a different studied parameter. In this table, "a_{eq}" is equal aperture size of geogrids; "B" is loading plate's diameter; "D_{50}" is the medium aggregates size, and "D_{max}" is maximum aggregates size.

Although many investigations have been carried out on geogrid-soil interactions, there is a serious lack of studies on the response of geocells in soil medium with regard to the geometrical variations. Tavakoli Mehrjardi et al. (2019) carried out a series

Table 4.3 The optimum values for the burial depth of first geocell layer (u), the vertical spacing of geocell layers, in multi-layered systems, (h) and width of geocell (b)

Researcher	u	h	b
Sireesh et al. (2009)	NE[a]	NE[b]	4.9D
Dash et al. (2001)	0.1B	NE[b]	4B
Sitharam and Sireesh (2005)	0.05B	NE[b]	5B
Moghaddas Tafreshi and Dawson (2010a)	0.1B	NE[b]	3.2B
Moghaddas Tafreshi et al. (2013)	0.2B	0.2B	NE[a]

[a]*NE* Not evaluated
[b]*NE* Not evaluated due to use the single geocell layer

Table 4.4 The optimum values for proposed aspect ratio in geogrid-reinforced foundations

Researchers	a_{eq}/D_{50}	a_{eq}/D_{max}	B/D_{50}	a_{eq}/B
McDowell et al. (2006)	NE[a]	1.4	NE	NE
Brown et al. (2007)	NE	1.2–1.6	NE	NE
Cuelho et al. (2014)[b]	3.9	1.2	NE	NE
Góngora and Palmeira (2016)	NE	0.7–1.35	NE	NE
Tavakoli Mehrjardi and Khazaei (2017)	4	2.1–2.6	13–25	0.2

[a]*NE* not investigated
[b]referred by Palmeira and Góngora (2016)

of plate load tests to investigate the sensitivity of reduced-scale geocell-reinforced soil to variation of deciding key factors, notably loading plate size, soil grain size, and geocell's opening size. Four types of uniformly graded soils as backfill materials with the medium grain size (D_{50}) of 3, 6, 12, and 16 mm were considered. The utilized geocells made of heat-bonded nonwoven geotextile had the cell equivalent diameter/height of 55/50 and 110/50 mm, respectively (Table 4.4).

The major physical parameters influencing the response of geocell-reinforced backfill systems can be summarized as B, u, L, D_{50}, γ, E_{soil}, E_{GC}, and b; where "γ" and "E_{soil}" are unit weight and secant elastic modulus of the backfill, respectively, "E_{GC}" is the elastic modulus of geocells, "u" is the burial depth of geocell, "B" is loading plate's diameter, and "L" is the width of geocells expanded beneath the loading plate. The function (f) that governs the geocell-reinforced backfill systems can be written as Eq. (4.50).

$$q_u = f(B, u, L, D_{50}, \gamma, E_{soil}, E_{GC}, b) \tag{4.50}$$

The equation comprises eight parameters containing two fundamental dimensions (i.e., length and force). Therefore, Eq. (4.50) can be reduced to six independent parameters ($\pi_1, \pi_2, \pi_3, \ldots, \pi_6$) and substituted with Eq. (4.51). As can be seen, the obtained non-dimensional parameters could predominantly affect the response of geocell-reinforced systems. The similarity in response is achievable if the π terms, both for model and prototype are equal.

$$\frac{q_u}{\gamma B} = f\left(\frac{u}{B}, \frac{h}{B}, \frac{D_{50}}{B}, \frac{\gamma D_{50}}{E_{soil}}, \frac{E_{soil}}{E_{GC}}, \frac{b}{D_{50}}\right) \tag{4.51}$$

As an example, assuming that the soils used in the model and prototype do have the same unit weight and footing diameter of a prototype model (B_p) is n times as many as that of the test model (B_m), Eq. (4.52) can be satisfied to obtain the bearing capacity of prototype system.

$$\left(\frac{q_u}{\gamma B}\right)_m = \left(\frac{q_u}{\gamma B}\right)_p \xrightarrow{\text{yields}} (q_u)_p = n(q_u)_m \tag{4.52}$$

Herein, some questions have arisen in this study: what is the effect of aggregates size? What is enough loading plate size to minimize the scale effect? Is there any optimum cells size for a geocell to provide maximum reinforcement efficiency?

One of the major issues in approaching the optimal design of geocell-reinforced backfill is to understand the fundamental mechanics of aggregate/geocell interactions. In particular, it should be possible to optimize the mechanical and geometric properties of the geocell, gaining maximum reinforcement efficiency. In this respect, according to Fig. 4.23a, studying the variation of bearing capacity ratio versus the ratio of the geocell's cells size (b) to the medium grains size (D_{50}) can be predominant. It is clearly seen that the highest values of BCR, irrespective of the loading plate size, are attainable when the ratio b/D_{50} is in the range of 12–18. Reasonably, it is certified that the optimum nominal cell size of geocells is about 15 times of medium grain size of soil. In other words, in the case of larger backfill's particles (left side of the mentioned range), geocell/backfill interactions get deteriorated, resulted in reduction in bearing capacity ratio. On the other side, for the smaller backfill's particles or larger geocell's cells ($b/D_{50} > 15$), less stone–stone interactions are provided and therefore, lateral buckling of particles columns in the geocell's plane is encountered and eventually, bearing capacity ratio is reduced, dramatically. Much as there is no available data on the effectiveness of b/D_{50} for geocell-reinforced system, Tavakoli Mehrjardi and Khazaei (2017) and Cuelho et al. (2014), reported that restricting the ratio of the geogrid's apertures size to the medium grains size to the value of about 4, had the highest beneficial circumstances on geogrid-reinforced backfill behavior. Also, Tavakoli Mehrjardi et al. (2016), by conducting plate load tests on poor-graded fine and coarse sands and reinforced by geogrids, found out that the ratio of the geogrid apertures sizes to the medium soil grains sizes is a deciding factor in the interaction between soil's grains and geogrid.

Moreover, to see variations of bearing capacity ratio versus the ratio of the geocell's cells size to the maximum grains size (b/D_{max}), Fig. 4.23b is illustrated. Accordingly, there is an optimum range of 7–11 for (b/D_{max}) ratio which affords the maximum bearing capacity ratio.

Although practically, footing width is much greater than soil's medium grains size, in geotechnical test methods (plate load test; in particular), special attention should be given to the ratio of the loading plate size (B) to the medium grains size (D_{50}). With this respect, Fig. 4.24 presents the variation of bearing capacity ratio versus the ratio of the loading plate size to the medium grains size (B/D_{50}). According to the observed variations, the best efficiency of geocell reinforcement has been achieved for the optimal amount of B/D_{50} in the range of 13–27 (approximately 20; in average). In the outer of the mentioned optimum range, BCR decreased drastically. In the line with this conclusion, Tavakoli Mehrjardi and Khazaei (2017) observed that in order to obtain the highest benefits from geogrid reinforcement in geogrid-reinforced backfill, the footing's width should be in the range of 13–25 times of medium grain size. Moreover, Hsieh and Mao (2005) reported when the loading plate's diameter was larger than 15 times the D_{50} of the soil test, no marked influence of plate size on surface settlement would be expected.

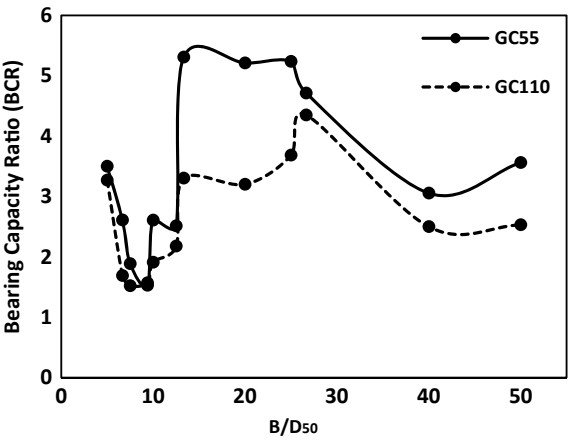

Fig. 4.24 Variation of bearing capacity ratio versus the ratio of the loading plate's diameter (B) to the medium grains size (D_{50}) (Tavakoli Mehrjardi et al. 2019)

According to Eq. (4.50) and based on dimensional analysis rules (see Eq. 4.51), the studied length-dimensional parameters including B, $D_{50,}$ and b can at most be converted to two independent non-dimensional parameters. Previously, the importance of non-dimensional parameters, namely B/D_{50} and b/D_{50} was explained. This means that the r*atio of the loading plate size to the geocell cells sizes (B/b)* does not seem to be a contributory parameter in the bearing capacity ratio. This is the exact reason for placement of B/D_{50} and b/D_{50} as independent parameters in Eq. (4.51). From this point of view, by taking right precautions, it can be concluded that the B/b ratio should be selected larger than 1.5 which could provide a more stable and reliable geocell-reinforced backfill. This statement is more likely to be useful if the surface stress would be applied over a small area such as tire print, railway sleeper, or footprint. In fact, geocells possessing large cells in comparison with footing size (small values of B/b) ruin the beneficial role of reinforcement in that each cell does likely behave as an unreinforced soil element (Tavakoli Mehrjardi et al. 2019).

4.6 Comparing the Performances of Geocell and Planar Reinforcements

Geocell is an advantageous soil-reinforcement method that can provide stiffer and stronger foundations compared to planar reinforcement methods. Due to the three-dimensional honeycomb nature of geocell, it is capable of generating several mechanisms for improving the performance of foundations. A higher stiffness, bearing capacity and better pressure distributing characteristic could be achieved by incorporating single and multiple layers of geocell or planar reinforcement. Using such methods, the performance of a foundation bed is also much improved under cyclic loading of machines or vehicles. In this chapter, the advantages of geocell reinforcement compared to planar geotextile reinforcement are described under static

and repeated loading conditions. Then the usage of geocell and planar geotextile reinforcements are extended to multiple layers of geocell reinforcement. The results presented in this chapter are fully obtained from scaled models or full-scale experiments and thus, could provide a solid understanding for designing and construction of geocell-reinforced foundations.

4.6.1 Performance of Single Geocell Reinforcement Compared to Multiple Geotextile Reinforcement

Comprehensive results from laboratory model tests on strip footings with width of 75 mm supported on the geocell- and geotextile-reinforced sand beds with the same characteristics of geotextile are reported by Moghaddas Tafreshi and Dawson (2010a). The soil used is relatively uniform silica sand with grain sizes between 0.85 and 2.18 mm and with a specific gravity (G_s) of 2.68. It has a Coefficient of uniformity (C_u) of 1.35, Coefficient of curvature (C_c) of 0.95, an effective grain size (D_{10}) of 1.2 mm and mean grain size (D_{50}) of 1.53, which means that almost all the grains are between 1 and 2 mm in size. The maximum and minimum void ratios (e_{max} and e_{min}) of the sand were 0.82 and 0.54, respectively. According to the Unified Soil Classification System, the sand is classified as poorly graded sand with letter symbol SP (see Fig. 4.25a). The angle of internal friction of sand obtained through drained triaxial compression tests on dry sand samples at a relative density of 72% was 37.5 (all tests being run on dry sand at this relative density).

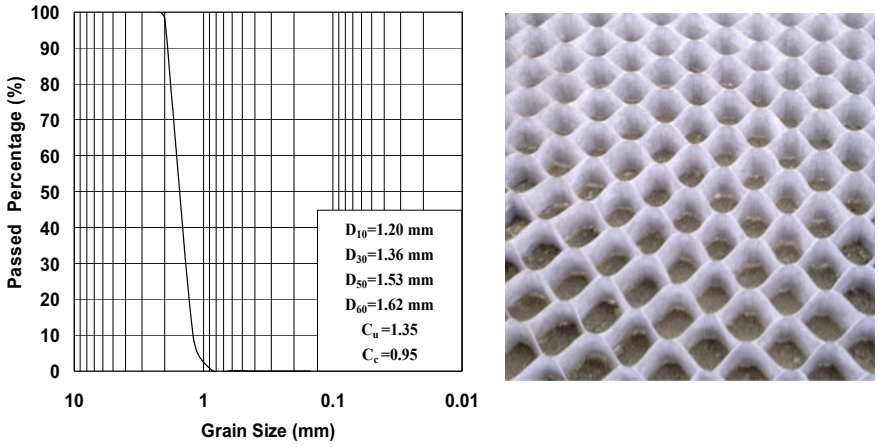

Fig. 4.25 **a** Particle size distribution curve **b** Isometric view of the geocell (Moghaddas Tafreshi and Dawson 2010a)

The geocell and geotextile layers used were both made and supplied by the same company. The geocell was fabricated from the same geotextile material that forms the planar geotextile. Geocells consist of a cellular structure manufactured from flexible, semi-flexible, or strong geosynthetics such as geotextile (see Fig. 4.25b). It comprises a polymeric, honeycomb-like structure with open top and bottom manufactured from strips of geotextile that are thermo-welded into a cellular system. The type of geotextile is nonwoven. The area weight (g/m^2), tensile strength (kN/m) and thickness under 200 kN/m^2 (mm) are 190, 13.1 and 0.47, respectively. When filled with soil or other mineral material, it provides an ideal surface for construction projects such as foundations, slopes, driveways, etc. The high tensile strength of both the weld and geotextile provide an ideal structure with high capacity that prevents infill from spreading thus hindering settlement. The pocket size (d) of the geocell used was kept constant (at $d = 50$ mm). It was used at heights (H) of 25, 50, and 100 mm in the testing program. The geocell and geotextile properties are the same throughout this chapter.

In order to provide a meaningful comparative assessment between the geotextile and geocell reinforcement, the quantity of material used must be matched. The quantity of material used in each test relative to that used in the least reinforced test is termed as 'a', which is equivalent to the mass of a single sheet of geotextile reinforcement of the smallest width used in the tests. Assessment of performance was undertaken for arrangements with geotextile sheet and geocell reinforcement of the same mass of geotextile being paired together. For example, the experiment reinforced by two layers of short geotextile reinforcement has exactly the same mass of geotextile as that reinforced by the short geocell reinforcement at $H/B = 0.66$ (see Fig. 4.26 for the definition of H and B). This pair both have two units 'a' of reinforcement the same as the long pair of one layer for geotextile or $H/B = 0.33$ for geocell reinforcement. It should be noted that the amount of material used in each test is a function of reinforcement width and of the number of layers of geotextile or height of geocell reinforcement.

Geocell benefits are assessed in terms of increased bearing capacity of a strip footing subjected to a monotonically increasing load. Provision of the geocell reinforcement in reinforcing the sand layer significantly increases the load-carrying

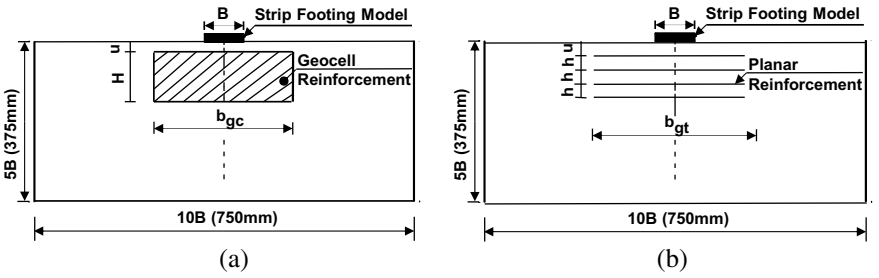

Fig. 4.26 Geometry of the **a** geocell-reinforced foundation bed **b** geotextile-reinforced foundation bed (Moghaddas Tafreshi and Dawson 2010a)

capacity, reduces the footing settlement, and decreases the surface heave of the footing bed more than the geotextile reinforcement with the same characteristics and the same mass used. Overall, with an increase in the number of geotextile reinforcement layers, the height of geocell reinforcement, and the reinforcement width, the bearing pressure of the foundation bed increases and the footing settlement decreases. Thus, the efficiency of reinforcement decreases by increasing the above parameters. A detailed discussion on the effect of different parameters (as shown in Fig. 4.26) will be presented hereafter.

An important factor for obtaining the best performance in soil reinforcement is the embedment depth (u) and width of reinforced layer (b_{gc} for geocell and b_{gt} for geotextile layer- see Fig. 4.26). The optimum depth of the topmost layer of geocell reinforcement is approximately 0.35 times the footing width ($u/B = 0.35$), while the depth to the top of the geocell should be approximately 0.1 times of the footing width ($u/B = 0.1$). The vertical spacing of the geotextile layers was selected to be equal to u/B and held constant in all the tests at $h/B = 0.35$. The tests performed with different reinforcement widths (short, medium and long reinforcement width) indicate that increasing the reinforcement width more than 4.2 and 5.5 (i.e., long width) times the footing width for the geocell and geotextile reinforcement, respectively, would not provide much additional improvement in bearing pressure.

Figure 4.27 shows the bearing pressure with footing settlement (s/B) for the geocell-reinforced, planar-reinforced, and unreinforced beds. From this figure, it may be clearly observed that with increasing the mass of reinforcement (increase in the height of the geocell reinforcement; H/B or in the number of layers of geotextile reinforcement; N); both stiffness and bearing pressure (bearing pressure at a specified settlement) considerably increase. In the case of the unreinforced sand bed, it is apparent that the bearing capacity failure has taken place at a settlement equal to 12% of footing width while in case of both the geocell- and geotextile-reinforced

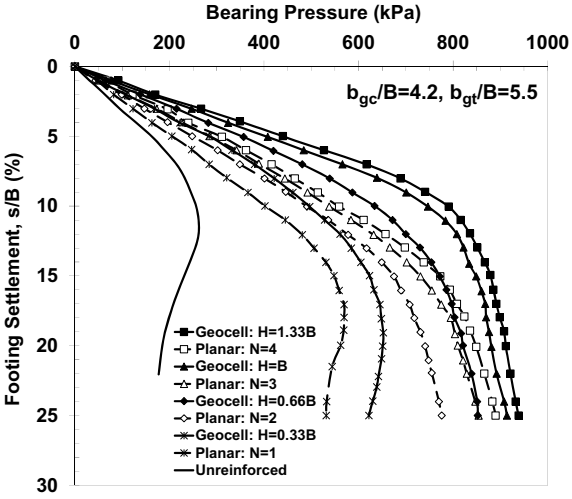

Fig. 4.27 Variation of bearing pressure with settlement for the geocell and geotextile reinforcement with Long width ($b_{gc}/B = 4.2$ and $b_{gt}/B = 5.5$, see Fig. 4.26 for the definition of b_{gc} and b_{gt}), (Moghaddas Tafreshi and Dawson 2010a)

sand beds; no clear failure point is evident for the larger masses of reinforcement ($N \geq 2$ or $H/B \geq 0.66$). Beyond a settlement of 10–16% there is a reduction in the slope of the pressure-settlement curve. However, when lightly reinforced ($N = 1$ and $H/B = 0.33$, respectively, for geotextile reinforcement and geocell reinforcement) failure is observed at settlements of 16–18% with clear post-failure reductions in bearing capacity.

The performance improvement due to the provision of reinforcement is represented using non-dimensional improvement factor of *IF* which compares the bearing pressure of the geotextile or geocell reinforcement bed to that of the unreinforced bed at a given settlement, s_i.

$$\mathrm{IF_{gt}} = \frac{q_{\mathrm{geotextile}}}{q_{\mathrm{unrein.}}} \text{ OR } \mathrm{IF_{gc}} = \frac{q_{\mathrm{geocell}}}{q_{\mathrm{unrein.}}} \quad s_i / B = 2, 4, 6, 8, 10 \text{ and } 12\% \tag{4.53}$$

where q_{unrein}, $q_{\mathrm{geotextile,}}$ and q_{geocell} are, respectively, the values of bearing pressure of the unreinforced bed, the geotextile-reinforced bed, and the geocell-reinforced bed.

The variation of these two parameters, $\mathrm{IF_{gt}}$ and $\mathrm{IF_{gc}}$ with footing settlement for long, medium, and short reinforcement width are shown in Fig. 4.28. According to this figure, it is evident that for the same mass of geotextile material used in the tests at the settlement level of 4%, the maximum improvement in bearing capacity (IF) was obtained as 2.73 and 1.88 with the provision of geocell and the equivalent geotextile reinforcement, respectively. Therefore, improvement of foundation performance is proved and it can be concluded that geocell provides more benefits compared to geotextile forms of reinforcement. For amounts of settlement that are tolerated in practical applications, improvements in bearing capacity greater than 200% can be achieved with the application of geocell reinforcement, whereas geotextile reinforcement arrangements can only deliver 150% for these two quantities, respectively.

In many applications, the foundation is subjected to a number of load repetitions and hence, it is also essential to figure out the reinforced foundation performance under repeated loading. Moghaddas Tafreshi and Dawson (2010b) performed a series of laboratory model tests on strip footings supported on geocell and geotextile-reinforced sand beds under a combination of static and repeated loads. Footing settlement due to initial static applied load and up to 20,000 subsequent load repetitions was recorded until its value becomes stable or failure occurred due to excessive settlement. The typical scheme of repeated loading with the definition of static and dynamic loads is presented in Fig. 4.29. The properties of the material used in these tests are similar to the static tests describe previously (see the beginning of Sect. 4.1).

The variation of the footing settlement, *s/B*, at the peak of each load pulse with the number of load cycles as a consequence of the repeated loading pattern (as illustrated in Fig. 4.29), is plotted in Fig. 4.30 for unreinforced, geotextile-reinforced, and geocell-reinforced sand beds. The reinforced cases had the same mass of geotextile ($N = 2$ and $H/B = 0.66$). Based on Fig. 4.30, using the geocell reinforcement, or the planar geotextile reinforcement with the number of layers greater than 1, leads

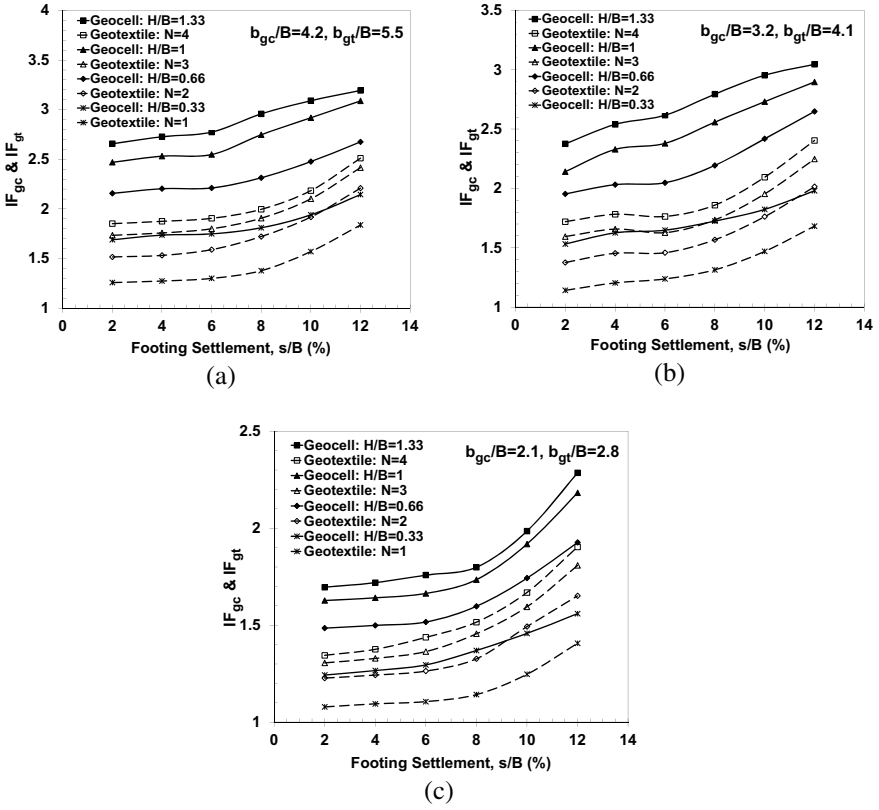

Fig. 4.28 Variation of the bearing capacity improvement factor (IF) with footing settlement for the geocell and geotextile reinforcement, **a** Long width ($b_g/B = 4.2$ and $b_p/B = 5.5$), **b** medium width ($b_g/B = 3.2$ and $b_p/B = 4.1$) and **c** short width ($b_g/B = 2.1$ and $b_p/B = 2.8$), (Moghaddas Tafreshi and Dawson 2010a)

to stabilizing behavior, irrespective of the repeated load level, q_{dyn}/q_{stat}, whereas no-reinforcement ($q_{dyn}/q_{stat} = 30$ and 50%) or under reinforcement ($N = 1$ for geotextile at $q_{dyn}/q_{stat} = 50\%$) allows excessive settlement and unstable behavior to develop. The only unreinforced bed to show a stabilizing response was that loaded at $q_{dyn}/q_{stat} = 20\%$ which became stable at a maximum (shakedown) settlement, s/B, equal to 9.11% at approximately 15,400 load cycles. In the case of the unreinforced sand beds under repeated loading, it is apparent that the excessive settlement commenced at about 3700 cycles (e.g., point X on Fig. 4.30) and 170 cycles, respectively, for repeated load amplitudes that were 30 and 50% of static load (q_{dyn}/q_{stat}). For the experiment containing one layer of geotextile reinforcement ($N = 1$) and subjected to a repeated loading amplitude that was 50% of the static load ($q_{dyn}/q_{stat} = 50\%$), the excessive settlement commenced at about 2220 cycles. This point of inflexion in the number of cycles versus the settlement curve appears to evidence a change in the internal behavior of the sand. After this number of cycles, unstable behavior

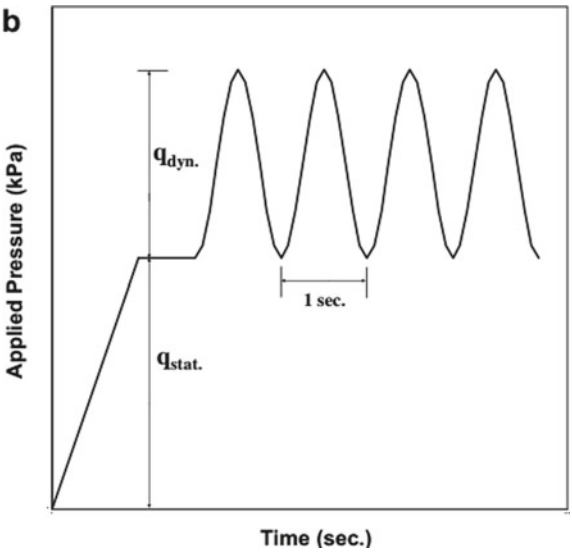

Fig. 4.29 Typical time history of initial static and repeated load on footing (Moghaddas Tafreshi and Dawson 2010b)

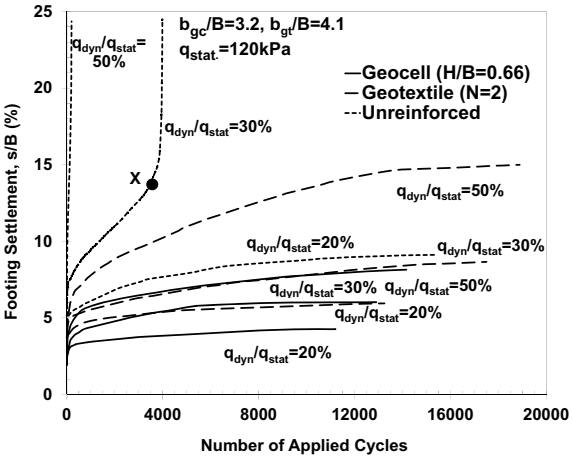

Fig. 4.30 Variation of the footing settlement (s/B) with number of applied load repetitions for the unreinforced, geocell ($H/B = 0.66$), and geotextile ($N = 2$) reinforced beds. Loading amplitude of repeated loads (q_{dyn}/q_{stat}) was 20, 30 and 50%, (Moghaddas Tafreshi and Dawson 2010b)

develops and the value of s/B accelerates with further load applications. When a non-stabilizing response is observed, due to excessive footing settlement, a significant heave of the fill surface starts. This response indicates that the unreinforced soil, or soil-reinforcement composite material with a small mass of reinforcement, when subjected to strong repeated loads, ruptures locally in the region under and around the footing, permitting large settlements. In the case of the geocell reinforcement and the geotextile reinforcement (with $N > 1$), an initial, rapid settlement during the first load applications is followed by a secondary settlement at a slower rate. Finally, the settlement rate of the footing is very small or insignificant.

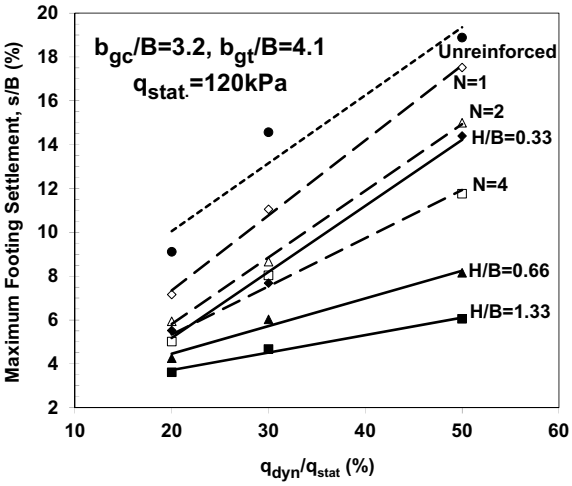

Fig. 4.31 Variation of the maximum footing settlement (*s/B*) with amplitude of repeated loads for unreinforced and both the geocell and the geotextile-reinforced bed (Moghaddas Tafreshi and Dawson 2010b)

Figure 4.31 shows the variation of the maximum footing settlement (*s*/*B*) with an amplitude of repeated loads for the geocell-reinforced, geotextile-reinforced, and unreinforced beds. From this figure, it can be observed that, although there is some scatter, the footing settlement varies linearly with q_{dyn}/q_{stat}, irrespective of reinforcement type (geocell or geotextile) and amount. With an increase in the height of the geocell reinforcement or in the number of geotextile reinforcement layers the rigidity of the reinforced system increases or, to state this another way, the maximum value of footing settlement (*s*/*B*) decreases at any given q_{dyn}/q_{stat}. This implies that increasing the amount of reinforcement mass in the sand can control (lessen) the footing settlement and provide greater stability to a footing even under strong dynamic loads. Also, Fig. 4.31 makes plain that, even when comprising half the mass of geotextile material ($H/B = 0.66$ compared with $N = 4$), the geocell-reinforced sand can deliver a greater improvement (decrease) in the maximum settlement of the footing compared with the geotextile-reinforced one at any given q_{dyn}/q_{stat}.

Figure 4.32 summarizes the variation in the maximum footing settlement (non-dimensionalized as *s*/*B*) with number of applied load repetitions for the three geotextile-reinforced cases ($N = 1, 2, 4$) for the experiments with the three different heights of geocell reinforcement ($H/B = 0.33, 0.66, 1.33$) and for the unreinforced sand bed. The figure shows the results for the repeated loading case having an amplitude of 20% of applied static load ($q_{dyn}/q_{stat} = 20\%$). The lines show the cumulative plastic and resilient settlement measured at the peak of each load pulse. It can be noted that the variation rate of peak footing settlement reduces as the number of cycles increase, and finally becomes stable after a certain number cycles, irrespective of the height of the geocell reinforcement (*H*/*B*) or the number of layers of geotextile reinforcement (*N*). This indicates that, where the total loading is insufficient to cause rupture within the soil system, reorientation of particles in the soil adjacent to the geotextile ceases relative rapidly, the system becomes stable and can be said to have

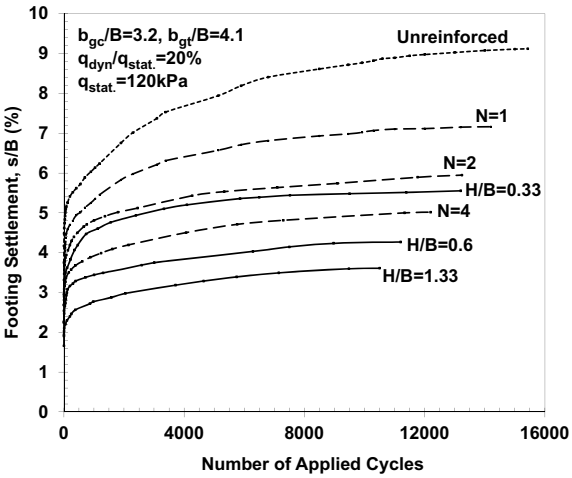

Fig. 4.32 Variation of the footing settlement (s/B) with number of applied load repetitions at $q_{dyn}/q_{stat} = 20\%$ for the unreinforced, geocell-reinforced and geotextile-reinforced beds (Moghaddas Tafreshi and Dawson 2010b)

reached a state of plastic shakedown (Werkmeister et al. 2005). On the other hand, the magnitude of footing settlement increases with the number of cycles and reaches a sensibly constant maximum value at the number of load cycles. The maximum footing settlement, s/B, is considerably decreased relative to the unreinforced one as a consequence of either increase in the height of the geocell reinforcement (H/B) or in the number of layers of geotextile reinforcement (N).

The performance of the geocell is much improved over that of the geotextile for the same mass of geotextile material used. The performance of reinforcement in decreasing the settlement of a sand bed subjected to dynamic loads of various amplitudes [either by adding geocell of increasing height (H/B) or by adding layers of the geotextile (N)], is the subject of Fig. 4.33. The variation of the maximum value of footing settlement (in terms of s/B) as a function of the number of layers of geotextile (N) and the height of geocell (H/B) is shown for the three repeated load amplitudes ($q_{dyn}/q_{stat} = 20$, 30 and 50%).

To summarize, it can be concluded that, the rate of footing settlement decreases significantly as the number of loading cycles increases. Consequently, a resilient response condition, known as plastic shakedown, is achieved after 10,000–20,000 cycles dependent on the type and the mass of reinforcement and the magnitude of the repeated load applied to the footing. The largest portion of the footing settlement occurs after the first ten cycles. The ratio of footing settlement during the first ten to that achieved by the last cycle varies between 0.35 and 0.6. The magnitude of the maximum footing settlement and the number of cycles required to develop plastic shakedown of the footing are a function of the initial applied static load (q_{stat}), the amplitude of the repeated load (q_{dyn}) and the mass of reinforcement below the footing base (N and H/B). For a given value of amplitude of repeated load, with increase in the number of geotextile reinforcement layers and in the height of geocell reinforcement, the footing settlement decreases. The efficiency (expressed in relation to the mass of reinforcement) was decreased by increasing the above parameters. With an increase

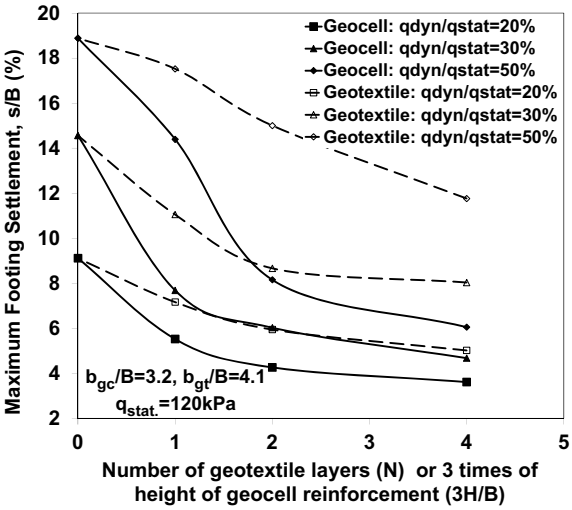

Fig. 4.33 Variation of the maximum footing settlement (*s/B*) with number of layers of geotextile, or height of 3D, reinforcements under repeated loading of amplitude $q_{dyn}/q_{stat} = 20$, 30 and 50% (Moghaddas Tafreshi and Dawson 2010b)

in the amplitude of repeated load, the value of footing settlement increases in a broadly linear manner, irrespective of the number of geotextile reinforcement layers or of the height of geocell reinforcement.

4.6.2 Performance of Multiple Geocell and Geotextile Reinforcement Layers

The previous section showed that geocell reinforcement can be significantly more effective than a geotextile, in improving the behavior of foundation beds under static and repeated loads. The evident benefit of using multiple geotextile or geogrid layers (e.g., Sitharam et al. 2005; Sitharam and Sireesh 2005) suggests that the use of multiple geocell layers could be beneficial. Geosynthetic inclusions will be most effective if used in the zone significantly stressed by the footing—which may be over a depth of 1 or 2 diameters beneath the footing—i.e., over a depth of approximately 0.6–2 m for typical strip/rectangular footing widths. Since the heights of commercially produced geocells are usually standard and most manufacturers of geocell produce them only at heights less than 200 mm, the use of a 0.6–2 m thick layer of geocell beneath the footing is impossible. Even if it were, such a thick geocell layer would likely make compaction of cell-fill extremely difficult, probably negating any reinforcement benefit. Hence, the use of several layers of geocell (say, three or four) each with a thickness $\leq$200 mm and with vertical spacing between successive layers of geocell is a practical alternative and could be a beneficial means of reinforcing the soil beneath a footing.

Moghaddas Tafreshi et al. (2016) performed a series of laboratory model tests on a model circular footing with 112.8 mm diameter (*D*), supported on multi-layered

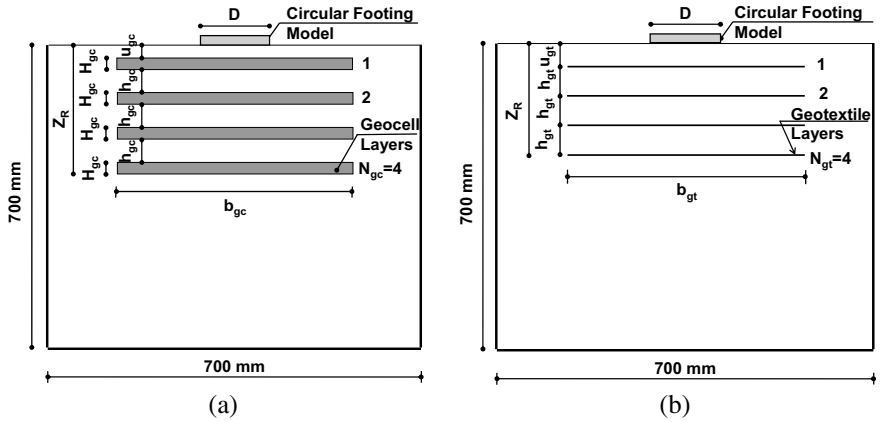

Fig. 4.34 **a** Layout of the multi-layered geocell-reinforced installation, **b** Layout of the multi-layered geotextile-reinforced installation (Moghaddas Tafreshi et al. 2016)

of geocell and geotextile-reinforced sand beds. Figure 4.34 shows the test setup and parameters used for the evaluation of such pavement systems, according to studies by Moghaddas Tafreshi et al. (2016).

The width of the geocell and geotextile layers (b_{gc} for geocell and b_{gt} for geotextile) and the depth to the top of the first geocell and geotextile layer below the footing (u_{gc} for geocell and u_{gt} for geotextile) are expressed in non-dimensional form with respect to footing diameter (D). In a previous study by Moghaddas Tafreshi and Dawson (2010a) optimum values of these parameters were $b_{gc}/D = 3.2$, $b_{gt}/D = 4.1$, $u_{gc}/D = 0.1$ and $u_{gt}/D = 0.32$. The same values were used and kept constant in the tests described here. The pocket size (d) of the geocell used was kept constant (d = 50 mm), while the geocell was used at a thickness (H_g) of 25 mm. The optimum vertical spacing of geocell reinforcement layers and geotextile reinforcement layers are approximately 0.36 and 0.4 times footing diameter (h_{gc}/D = 0.36 and h_{gt}/D = 0.4), respectively, which not reported here as detailed. The properties and classification of soil and geocell are identical to the previous section.

Figure 4.35 presents the bearing pressure-settlement behavior of geocell- and geotextile-reinforced foundations when the layers of geocell and geotextile were placed at (u_{gc}/D = 0.1 and h_{gc}/D = 0.36) and (u_{gt}/D = 0.32 and h_{gt}/D = 0.4), respectively. For any matching pair of geocell and geotextile reinforcement (N_{gc} = N_{pt} = 1; etc.), the width of geocell and geotextile reinforcement are kept constant (as before, at $b_{gc}/D = 3.2$, $b_{gt}/D = 4.1$, respectively) and the mass of geosynthetic material in the geocell will be 1.28 times less than that in its 'twinned' geotextile installation. It may be observed that as the layers of reinforcement are increased (increased mass of the geocell and geotextile reinforcement and consequent increase in the depth of the reinforced zone; Z_R), both the stiffness and bearing pressure (bearing pressure at a specified settlement) increase considerably. In the case of the unreinforced soil, it is apparent from Fig. 4.35 that the peak bearing pressure takes

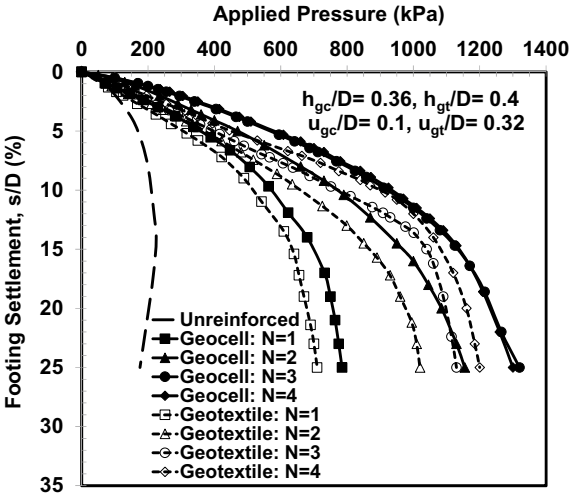

Fig. 4.35 Variation of bearing pressure with settlement for the geocell and geotextile reinforcement ($h_{gc}/D = 0.36$, $h_{gt}/D = 0.4$), (Moghaddas Tafreshi et al. 2016)

place at a footing settlement equal to approximately 13% of footing diameter. In the case of both the geocell- and geotextile-reinforced soil, however, no clear failure point is evident.

The performance of the geocell reinforcement and geotextile reinforcement in increasing the subgrade modulus of a reinforced bed due to the increase in the number of the geocell layers (N_{gc}), or in the number of layers of the geotextile reinforcement (N_{gt}), is shown in Fig. 4.36. In this figure, a comparison can be drawn between an unreinforced bed, and the effect of the variation of the subgrade modulus improvement factor (Ik_{gc} and Ik_{gt}) with a number of reinforcement layers is indicated. The

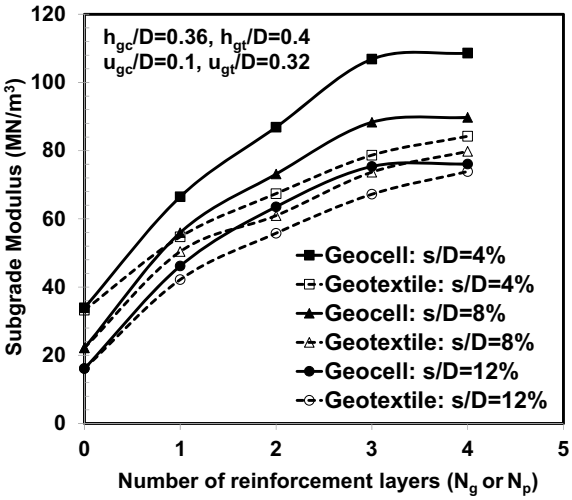

Fig. 4.36 Variation of IF_{gc} and IF_{gt} with the number of geocell layers and geotextile layers (N_{gc} and N_{gt}) at different levels of settlement ($s/D = 4$, 8 and 12%) for $h_{gc}/D = 0.36$ and $h_{gt}/D = 0.4$ (Moghaddas Tafreshi et al. 2016)

subgrade modulus improvement factor (Ik) at different footing settlements is defined as $Ik_p = k_p/k_{un}$ *for the geotextile reinforcement* and as $Ik_g = k_g/k_{un}$ for the geocell reinforcement (where $k_{un.}$, $k_{p,}$ and k_g are the subgrade modulus values of the unreinforced bed, the geotextile-reinforced bed and the geocell-reinforced bed at a given settlement, respectively). The subgrade modulus k, is the secant modulus (i.e. the slope of the line joining the point on the stress-settlement curve, at a given settlement, to the origin) calculated at different footing settlements.

In all situations, the values of Ik_{gc} and Ik_{gt} are larger at greater footing settlement for both geotextile and geocell cases, with greater reinforcement as the footing penetrates further. This is attributable to the greater mobilization of tensile strain in the reinforcement layers and to the confinement provided between layers by the reinforcement. For the multi-layered geocell, no significant improvement in performance is achieved when more than three ($N_{gc} = 3$) geocell layers are used. Therefore, when three layers of geocell are located at $h_{gc}/D = 0.36$, the maximum zone of soil that can usefully be reinforced extends to a depth of approximately $1.48D$ ($Z_R = 1.48D$). In contrast, Fig. 4.36 shows that the performance improvement due to the provision of geotextile reinforcement may continue beyond four layers ($N_{gt} = 4$ with a reinforcement zone of $Z_R = 1.52D$). Figure 4.36 also shows that improvement in subgrade modulus is greater for geocell reinforcement than for geotextile reinforcement, irrespective of the settlement ratio of the footing. For example, for $N_{gc} = N_{gt} = 3$ and a settlement ratio of $s/D = 4\%$, the geocell installation improves the subgrade modulus by as much as 84% more than the geotextile installation.

For most practical purposes, performance of reinforced systems at low footing settlement ratios, s/D (say, less than 2%) is critical, hence footing performance (in terms of subgrade modulus improvement factor, Ik_{gc} and Ik_{gt}) at such low settlements is made the subject of Fig. 4.37. Again, comparing the "twinned" geocell and geotex-

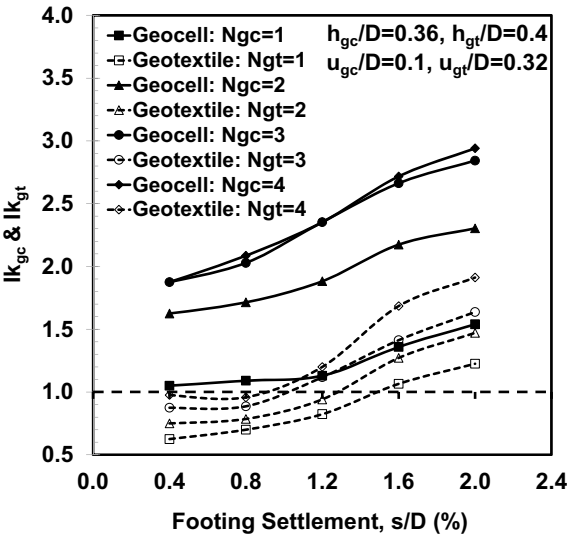

Fig. 4.37 Variation of IF_{gc} and IF_{gt} with the number of geocell layers and geotextile layers (N_{gc} and N_{gt}) at different levels of settlement ($s/D = 4$, 8 and 12%) for $h_{gc}/D = 0.36$ and $h_{gt}/D = 0.4$ (Moghaddas Tafreshi et al. 2016)

tile installations, the multi-layered geocell reinforcement system is both stiffer and more effective than the system with multi-layered geotextile reinforcement system. Furthermore, benefit of the geocell reinforcement is gained at very low settlement ratios ($s/D = 0.4\%$) whereas, in the case of geotextile reinforcement, the benefit only appears at footing settlement ratios of around 1–1.5%. At low settlements, apparently, before the geotextile has attracted loading to itself, geotextile installations may actually lead to a softer response than when unreinforced. The cause of this is uncertain but is probably indicative of lower geotextile-soil interface friction than soil–soil friction at a point in the loading sequence before the geotextile has been tensioned and is able to deliver benefit. Similar results were observed in the pressure-settlement of geotextile and geogrid reinforcement (Madhavi Latha and Somwanshi 2009) and of geocell reinforcement (Dash et al. 2001, 2003).

It is likely that the better performance at low settlement levels of the multi-layered geocell, compared with that of the multi-layered geotextile, is due to the geocell system gaining its resistance from the soil confinement that occurs when localized hoop stresses are developed in the walls of cells close (vertically and horizontally) to the footing. In a planar system, reinforcing action requires outward shear stress to be developed in the horizontal plane between the geotextile and soil throughout a zone whose size is controlled by the load spreading achieved in the soil between the footing and the uppermost geotextile layer. Such shear strains are not thought to be necessary for the geocell system, as localized compression alone will be sufficient to generate the hoop strain.

References

Aboobacker FMP, Saride S, Madhira MR (2015) Numerical modelling of strip footing on geocell-reinforced beds. Proc Inst Civ Eng Gr Improv 168(3):194–205

Abu-Farsakh M, Chen Q, Sharma R, Zhang X (2008) Large-scale model footing tests on geogrid-reinforced foundation and marginal embankment soils. Geotech Test J 31(5):413–423

American Society for Testing and Materials (ASTM) (2014) Standard test method for tensile properties of plastics. ASTM D638-14

Avesani Neto JO, Bueno BS, Futai MM (2013) A bearing capacity calculation method for soil reinforced with a geocell. Geosynthetics Int 20(3):129–142

Avesani Neto JO, Bueno BS, Futai MM (2015) Evaluation of a calculation method for embankments reinforced with geocells over soft soils using finite-element analysis. Geosynthetics Int 22(6):439–451

Biabani M, Indraratna B, Ngo NT (2016) Modelling of geocell-reinforced subballast subjected to cyclic loading. Geotext Geomembr 44(4):489–503

Binquet J, Lee KL (1975) Bearing capacity tests on reinforced earth slabs. J Geotech Eng ASCE 101(12):1241–1255

Brown SF, Kwan J, Thom NH (2007) Identifying the key parameters that influence geogrid reinforcement of railway ballast. Geotext Geomembr 25(6):326–335

BS8006 (1995) British standard: code of practice for strengthened/reinforced soils and other fills

Chen Q, Abu-Farsakh M, Sharma R, Zhang X (2007) Laboratory investigation of behavior of foundations on geosynthetic-reinforced clayey soil. Transp Res Rec: J Transp Res Board 2004:28–38

Cuelho E, Perkins S, Morris Z (2014) Relative operational performance of geosynthetic used as subgrade stabilization, Final Project Report, FHWA/MT-14-002/7712-251, Research Programs, State of Montana Department of Transportation, Montana, USA

Dash SK, Krishnaswamy NR, Rajagopal K (2001) Bearing capacity of strip footings supported on geocell-reinforced sand. Geotext Geomembr 19(4):235–256

Dash SK, Rajagopal K, Krishnaswamy NR (2007) Behavior of geocell reinforced sand beds under strip loading. Can Geotech J 44:905–916

Dash SK, Sireesh S, Sitharam TG (2003) Model studies on circular footing supported on geocell reinforced sand underlain by soft clay. Geotext Geomembr 21(4):197–219

Duncan JM, Chang CY (1970) Nonlinear analysis of stress and strain in soils. J Soil Mech Found Div 96(5):1629–1653

Foster CR, Ahlvin RG (1959) Stresses and deflections induced by a uniform circular load. Proc Highw Res Board 33:467–470

Góngora IAMG, Palmeira EM (2016) Assessing the influence of some soil-reinforcement interaction parameters on the performance of a low fill on compressible subgrade. Part II: Influence of surface maintenance. Int J Geosynthetics Gr Eng 2(1):18–29

Harikumar M, Sankar N, Chandrakaran S (2016) Behaviour of model footing resting on sand bed reinforced with multi-directional reinforcing elements. Geotext Geomembr 44(4):568–578

Harr ME (1966) Foundations of theoretical soil mechanics. McGraw-Hill, New York

Hegde AM, Sitharam TG (2015) Three-dimensional numerical analysis of geocell-reinforced soft clay beds by considering the actual geometry of geocell pockets. Can Geotech J 52(9):1396–1407

Hirai H (2008) Settlements and stresses of multi-layered grounds and improved grounds by equivalent elastic method. Int J Numer Anal Meth Geomech 32(5):523–557

Hirai H, Kamei T (2004) A method to calculate settlement, stress, failure and allowable stress of multi-layered ground by equivalent thickness theory. J Struct Constr Eng 581:79–86

Hirai H, Kamei TA (2003) A method to calculate settlement, stress and allowable stress of multi-layered ground. J Struct Constr Eng 573:81–88

Hsieh C, Mao HL (2005) A bench-scale performance test for evaluation of the geosynthetic reinforcement effects on granular base courses. In: ASCE, Geosynthetics research and development in progress, geo-frontiers, pp 1–11

Jenner CG, Basset RH, Bush DI (1988) The use of slip line fields to assess the improvement in bearing capacity of soft ground given by cellular foundation cushion installed at the base of an embankment. In: Proceedings of international geotechnical symposium on theory and practice of Earth reinforcement. Fukuoka, Japan, pp 209–214

Koerner RM (1998) Designing with geosynthetics. Prentice Hall, New Jersey

Kumar VV, Saride S (2016) Rutting behavior of geocell reinforced base layer overlying weak sand subgrades. Procedia Eng 143:1409–1416

Lambe TW, Whitman RV (1969) Soil mechanics. Wiley, New York

Latha GM, Murthy VS (2007) Effects of reinforcement from on the behavior of geosynthetic reinforced sand. Geotext Geomembr 25:23–32

Latha GM, Rajagopal K, Krishnaswamy NR (2006) Experimental and theoretical investigations on geocell-supported embankments. Int J Geomech 6(1):30–35

Li AL, Rowe RK (2008) Effects of viscous behaviour of geosynthetic reinforcement and foundation soils on embankment performance. Geotext Geomembr 26(4):317–334

Liu SY, Han J, Zhang DW, Hong ZS (2008) A combined DJM-PVD method for soft ground improvement. Geosynthetics Int 15(1):43–54

Liu Y, Deng A, Jaksa M (2019) Failure mechanisms of geocell walls and junctions. Geotext Geomembr 47(2):104–120

Madhavi Latha GM (2000) Investigation on the behavior of geocell supported embankments, Ph.D. thesis, Department of Civil Engineering, Indian Institute of Technology Madras, Chennai

Madhavi Latha GM, Dash SK, Rajagopal K (2009) Numerical simulation of the behavior of geocell reinforced. Int J Geomech ASCE 9(4):143–152

Madhavi Latha GM, Rajagopal K, Krishnaswamy NR (2006) Experimental and theoretical investigations on geocell-supported embankments. Int J Geomech ASCE 6(1):30–35
Madhavi Latha GM, Somwanshi A (2009) Bearing capacity of square footings on geosynthetic reinforced sand. Geotext Geomembr 27(4):281–294
McDowell GR, Harireche O, Konietzky H, Brown SF, Thom NH (2006) Discrete element modelling of geogrid-reinforced aggregates. Proc Inst Civ Eng—Geotech Eng 159(1):35–48
Meyerhof G, Hanna A (1978) Ultimate bearing capacity of foundations on layered soils under inclined load. Can Geotech J 15(4):565–572
Mhaiskar SY, Mandal JN (1996) Investigations on soft clay subgrade strengthening using geocells. Constr Build Mater 10(4):281–286
Moghaddas Tafreshi SN, Dawson AR (2010a) Comparison of bearing capacity of a strip footing on sand with geocell and with planar forms of geotextile reinforcement. Geotext Geomembr 28(1):72–84
Moghaddas Tafreshi SN, Dawson AR (2010b) Behaviour of footings on reinforced sand subjected to repeated loading–comparing use of 3D and planar geotextile. Geotext Geomembr 28(5):434–447
Moghaddas Tafreshi SN, Khalaj O, Dawson AR (2013) Pilot-scale load tests of a combined multilayered geocell and rubber-reinforced foundation. Geosynthetics Int 20(3):143–161
Moghaddas Tafreshi SN, Shaghaghi T, Tavakoli Mehrjardi Gh, Dawson AR, Ghadrdan M (2015) A simplified method for predicting the settlement of circular footings on multi-layered geocell-reinforced non-cohesive soils. Geotext Geomembr 43(4):332–344
Moghaddas Tafreshi SN, Sharifi P, Dawson AR (2016) Performance of circular footings on sand by use of multiple-geocell or-planar geotextile reinforcing layers. Soils Found 56(6):984–997
Noori B (2012) Experimental investigation of the behavior of geocell reinforced rubber soil mixture. M.Sc. thesis, Faculty of Civil Engineering, K.N. Toosi University of Technology, Tehran, Iran
Odemark N (1949) Investigations as to the elastic properties of soils and design of pavements according to the theory of elasticity, vol 77. Statens Vaginstitute, Meddelande, Stockholm, Sweden
Palmeira EM, Gongora IAMG (2016) Assessing the influence of soil reinforcement interaction parameters on the performance of a low fill on compressible subgrade. Part I: Fill performance and relevance of interaction parameters. Int J Geosynth Ground Eng 2(1):1–17
Palmer LA, Barber ES (1940) Soil displacement under a circular loaded area. Proc Highway Res Board 20:279–286
Pokharel SK (2010) Experimental Study on geocell-reinforced bases under static and dynamic loading. Ph.D. thesis. University of Kansas, USA
Presto (2008) Geoweb Load Support System—Technical Overview, Presto Products Company. Appleton, WI, USA
Rajagopal K, Krishnaswamy NR, Latha Madhavi (1999) Behavior of sand confined with single and multiple geocells. Geotext Geomembr 17(3):171–184
Rowe RK, Li AL (2005) Geosynthetic-reinforced embankments over soft foundations. Geosynthetics Int 12(1):50–85
Rowe RK, Taechakumthorn C (2008) Combined effect of PVDs and reinforcement on embankments over rate-sensitive soils. Geotext Geomembr 26(3):239–249
Sharma R, Chen Q, Abu-Farsakh M, Yoon S (2009) Analytical modeling of geogrid reinforced soil foundation. Geotext Geomembr 27(1):63–72
Sireesh S, Faby Mole PA, Madhav MR, Vijay Kumar R (2016) Non-linear response of geocell reinforced dense granular layer over weak soil under circular loading. Int J Geotech Eng 10(1):23–30
Sireesh S, Sitharam TG, Dash SK (2009) Bearing capacity of circular footing on geocellesand mattress overlying clay bed with void. Geotext Geomembr 27(2):89–98
Sitharam TG, Hegde A (2013) Design and construction of geocell foundation to support embankment on soft settled red mud. Geotext Geomembr 41:55–63
Sitharam TG, Sireesh S (2005) Behaviour of embedded footings supported on geocell reinforced foundation beds, geotech. Test J ASTM 28(5):452–463
Sitharam TG, Sireesh S, Dash SK (2005) Model studies of a circular footing supported on geocell-reinforced clay. Can Geotech J 42(2):693–703

Tavakoli Mehrjardi Gh, Behrad R, Moghaddas Tafreshi SN (2019) Scale effect on the behavior of geocell-reinforced soil. Geotext Geomembr 47(2):154–163
Tavakoli Mehrjardi Gh, Ghanbari A, Mehdizadeh H (2016) Experimental study on the behavior of geogrid-reinforced slopes with respect to aggregate size. Geotext Geomembr 44(6):862–871
Tavakoli Mehrjardi Gh, Khazaei M (2017) Scale effect on the behavior of geogrid-reinforced soil under repeated loads. Geotext Geomembr 45(6):603–615
Tavakoli Mehrjardi Gh, Moghaddas Tafreshi SN, Dawson AR (2012) Combined use of geocell reinforcement and rubberesoil mixtures to improve performance of buried pipes. Geotext Geomemb 34(October):116–130
Tavakoli Mehrjardi Gh, Moghaddas Tafreshi SN, Dawson AR (2013) Pipe response in a geocell reinforced trench and compaction considerations. Geosynthetics Int 20(2):105–118
Tavakoli Mehrjardi Gh, Moghadas Tafreshi SN, Dawson AR (2015) Numerical analysis on buried pipes protected by combination of geocell reinforcement and rubber-soil mixture. Int J Civ Eng 13(2B):90–104
Tavakoli Mehrjardi Gh, Motarjemi F (2018) Interfacial properties of geocell-reinforced granular soils. Geotext Geomembr 46(4):384–395
Terzaghi K (1943) Theoretical soil mechanics. Wiley, New York
Thakur JK, Han J, Pokharel SK, Parsons RL (2012) Performance of geocell-reinforced recycled asphalt pavement (RAP) bases over weak subgrade under cyclic plate loading. Geotext Geomembr 35(December):14–24
Vakili J (2008) A simplified method for evaluation of pavement layers moduli using surface deflection data. In: The 12th international conference of international association for computer methods and advances in geomechanics (IACMAG), Goa, India, 1–6
Wayne MH, Han J, Akins K (1998) The design of geosynthetic reinforced foundations. Paper presented at the Geosynthetics in foundation reinforcement and erosion control systems
Werkmeister S, Dawson AR, Wellner F (2005) Permanent deformation behavior of granular materials: the shakedown theory. Transp Res Board 6(1):31–57
Yang X, Han J, Pokharel SK, Manandhar C, Parsons RL, Leshchinsky D, Halahmi I (2012) Accelerated pavement testing of unpaved roads with geocell-reinforced sand bases. Geotext Geomembr 32(June):95–103
Yang Z (1974) Strength and deformation characteristics of reinforced sand. Ph.D. thesis, University of California, Los Angeles, CA, USA
Yin JH (2000) Comparative modeling study of reinforced beam on elastic foundation. J Geotech Geoenviron Eng 126(3):265–271
Yoon YW, Heo SB, Kim SK (2008) Geotechnical performance of waste tires for soil reinforcement from chamber tests. Geotext Geomembr 26(1):100–107
Zhang L, Qiangkang G, Guoping C (2010a) Effect of geo-cell reinforced soil structure used in flexible airfield pavement. In: ICLEM logistics for sustained economic development. ASCE, pp 1629–1635
Zhang L, Zhao M, Shi C, Zhao H (2010b) Bearing capacity of geocell reinforcement in embankment engineering. Geotext Geomembr 28:475–482
Zhao MH, Zhang L, Zou XJ, Zhao H (2009) Research progress in two direction composite foundation formed by geocell reinforced mattress and gravel piles. Chin J Highw Transp 22(1):1–10
Zhou HB, Wen XJ (2008) Model studies on geogrid- or geocell-reinforced sand mattress on soft soil. Geotext Geomembr 26:231–238

Chapter 5
Effect of Geocells Geometry on the Performance of the Foundations

Sujit Kumar Dash

Abstract In the present study, a series of tests has been carried out to develop an understanding of the influence of geocell reinforcement in improving performance of foundation beds under strip loading. It is observed that with the provision of geocell reinforcement, the bearing capacity of sand bed can be increased as high as 8 times compared to the unreinforced case. Improvement in bearing capacity increases with decrease in pocket size of geocells. The performance improvement is significant up to a geocell height of about 2 times the width of the footing. The optimum width of the geocell layer is around 4 times the footing width (B) at which stage, the geocell would intercept all the potential rupture planes formed in the foundation soil. To obtain maximum benefit, the top of geocell mattress should be at a depth of about $0.1B$ from the bottom of the footing. The findings of this study will be of use in efficient utilization of geocell reinforcement in increasing the performance of foundation beds.

Keywords Reinforced soil · Geocell reinforcement · Strip footing

5.1 Introduction

Owing to rapid urbanization and industrialization in the present days, the requirement for in situ treatment of foundation soil to improve its bearing capacity has risen markedly. Among the various ground improvement techniques used, geosynthetic reinforcement is probably the most popular one. This is primarily due to its simplicity, ease of construction and overall economy that find favor with the practicing engineers. The more recent advancement in this field is to provide three-dimensional confinement to the soil by using geocells. The geocell reinforcement consists of a series of interlocking cells constructed from polymer grid reinforcement (Fig. 5.1), which contains and confines the soil within its pockets.

S. K. Dash (✉)
Indian Institute of Technology Kharagpur, Kharagpur 721302, India
e-mail: sujit@civil.iitkgp.ac.in

T. G. Sitharam et al. (eds.), *Geocells*, Springer Transactions in Civil and Environmental Engineering,
https://doi.org/10.1007/978-981-15-6095-8_5

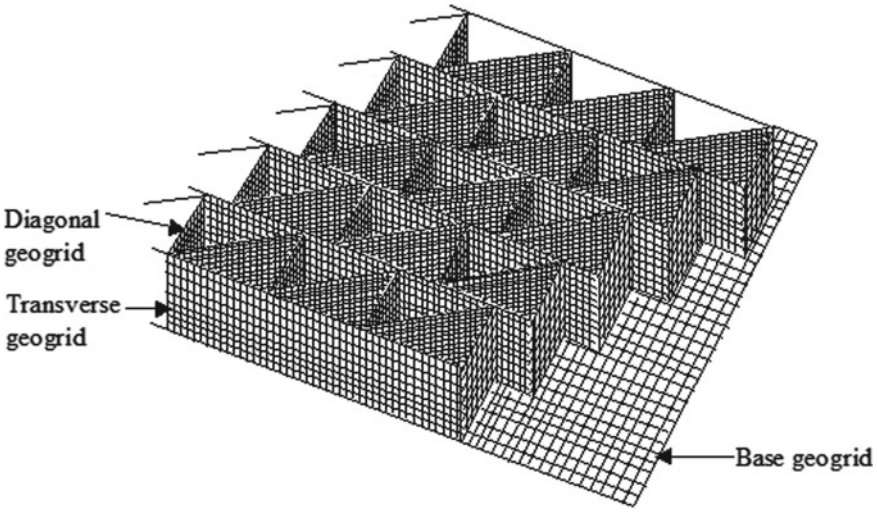

Fig. 5.1 Geocell reinforcement with base geogrid

Several studies have been reported highlighting the beneficial use of geocells. Rea and Mitchell (1978) and Mitchell et al. (1979) conducted a series of model plate load tests on circular footings supported over sand-filled square-shaped paper grid cells. Based on which the modes of failure are identified as: cell penetration, cell bursting, cell wall buckling, bearing capacity failure, bending failure, and excessive rutting. Webster and Watkins (1977), Alford and Webster (1978) through full-scale traffic load tests have observed that the geocell-reinforced sand can provide significantly greater load-carrying capacity than the soil alone. Bathurst and Jarrett (1989) have reported the application of geocell reinforcement for construction of pavements over weak peat subgrades. Studies have been carried out by Krishnaswamy et al. (2000) to evaluate the beneficial effects of geocell mattress placed at the interface of earth embankment and soft clay bed by conducting model tests. Cowland and Wong (1993) reported a case study of the performance of a geocell supported embankment on soft clay. The findings suggest that the geocell mattress has behaved as a raft foundation. Based on slip line theory, Bush et al. (1990) have proposed a design methodology which calculates the increase in bearing capacity due to basal geocell mattress in embankments over soft soil. The laboratory model studies by Dash et al. (2001) on a strip footing supported by geocell-reinforced sand beds have shown significant performance improvement. Hegde and Sitharam (2015) have studied the influence of different parameters on performance of single and multiple geocells in foundation beds. It is observed that with increase in frictional resistance of the infill material, the deformations in the geocells tend to reduce. The geocells with textured surface yield better performance than the smooth ones. Increase in strength of geocells leads to increase in load-carrying capacity of the system. Presented herein, an experimental study on geocell-reinforced sand foundations under strip loading. Influence of various

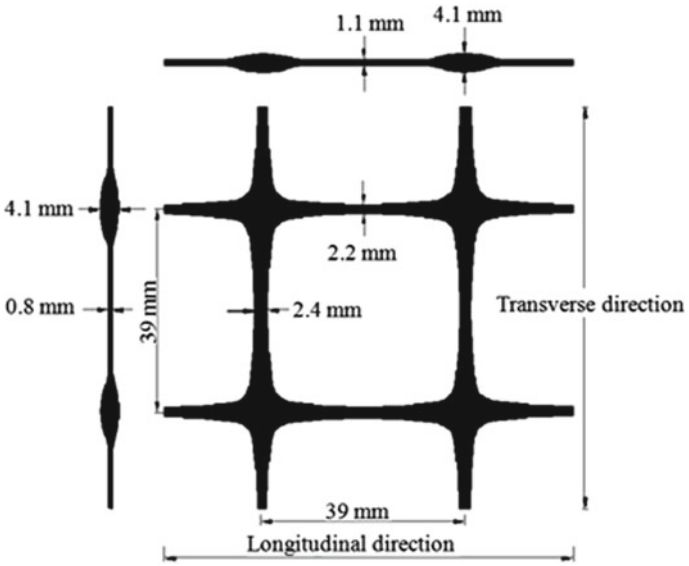

Fig. 5.2 Details of the geogrid used to make geocells

parameters such as the pocket size of geocells, height of geocell layer, the width of the geocell mattress, and depth placement of the geocell layer has been studied.

5.2 Experimental Details

The model tests were conducted in a steel tank measuring 1200 mm length × 332 mm width × 700 mm height. The long sides of the tank were made of 15 mm thick Perspex sheet and were braced with steel angles to avoid lateral yielding during the tests. The footing used was made of steel and measured 330 mm long × 100 mm wide × 25 mm thick. Since the inside width of the tank was chosen to be almost equal to the length of the footing, a plane strain condition was generally maintained.

The soil used was uniformly graded river sand (SP) with uniformity coefficient of 2.3 and curvature coefficient of 1.03. Its maximum and minimum densities are found to be 17.4 and 14.3 kN/m^3, respectively. The tests were carried out at 70% relative density of sand. The average peak angle of internal friction of sand as determined from direct shear tests is 46°. To achieve uniform density in the test tank, sand raining technique was used.

The geocell reinforcements used were fabricated from a biaxial geogrid made of oriented polymer. It has square-shaped apertures with opening size of 35 mm × 35 mm. Geometrical details of the geogrid are shown in Fig. 5.2. The properties of the geogrid determined from standard wide width tension tests (ASTM D-4595) are: ultimate tensile strength = 20 kN/m, elongation at yield = 23%, Secant modulus at

5% strain = 160 kN/m and Secant modulus at 10% strain = 125 kN/m. The geocell mattresses were prepared by cutting the geogrids to required length and height from full rolls and placing them in transverse and diagonal directions as shown in Fig. 5.1, with bodkin joints at the intersections (Simac 1990; Bush et al. 1990)). The bodkins in the present tests are 6 mm wide and 3 mm thick plastic strips made of low-density polypropylene. The joint strength of geocells, obtained through tensile tests, was found to be 4.75 kN/m. Such low strength of joints was adopted to scale down the overall strength of the geocell reinforcement, making it suitable for the model tests.

Figure 5.3 depicts the test geometry considered in the present investigation. In total, five different series tests were carried out the details of which are presented in Table 5.1. Within each series, only one parameter was varied, while the others were kept constant. Tests in series A were conducted on unreinforced soil bed with 70% relative density. Under series B, C, D, and E, tests were conducted by varying the pocket size of geocells (d), height of geocell layer (h), width of the geocell mattress (b), and depth to top of geocell layer below footing (u), respectively. The pocket size (d) of geocells is taken as the diameter of an equivalent circular area of the geocell pocket opening.

The model tests were conducted in a test bed-cum-loading frame assembly in the laboratory (Fig. 5.4). The soil beds were prepared in a steel tank with inside

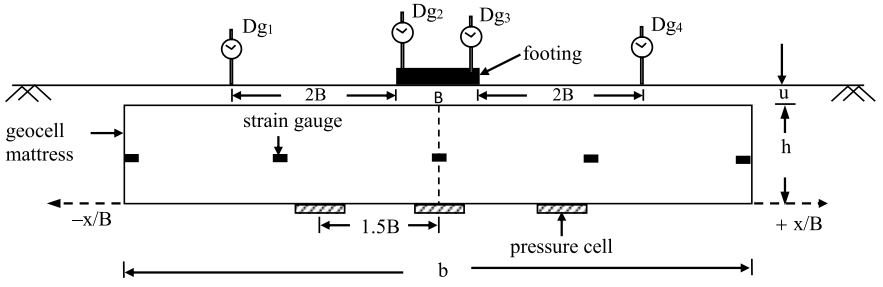

Fig. 5.3 Test geometry and instrumentation details

Table 5.1 Details of model tests

Test series	Details	
A	Tests on unreinforced sand with relative density (ID) of 70%	
B	Variable parameter Constant parameters	d/B = 1.2, 1.5, 2.7 h/B = 0.8, b/B = 12, u/B = 0.1
C	Variable parameter Constant parameters	h/B = 0.8, 1.2, 1.6, 2.0, 2.75, 3.14 d/B = 1.2, b/B = 12, u/B = 0.1
D	Variable parameter Constant parameters	b/B = 1,2,4,6,8,10,12 d/B = 1.2, h/B = 2.75, u/B = 0.1
E	Variable parameter Constant parameters	u/B = 0.0, 0.1, 0.25, 0.5, 0.75, 1.0, 1.5 d/B = 1.2, h/B = 2.75, b/B = 8

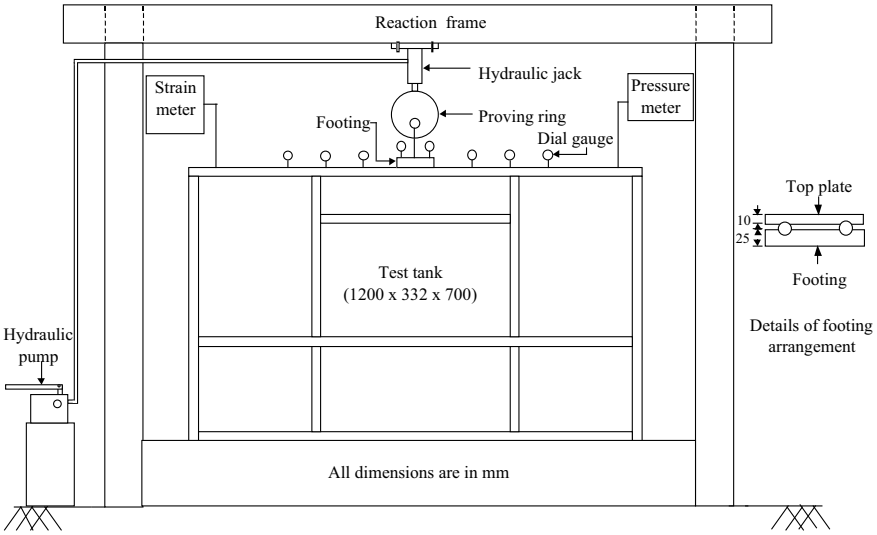

Fig. 5.4 Schematic diagram of test setup

dimensions of 1200 mm length, 332 mm width, and 700 mm height. The two long sides of the tank were made of 15 mm thick perspex sheet and were braced on the outer surface with steel angles to avoid yielding during tests. The perspex wall apart from minimizing the friction between the soil and the tank permitted observation of pattern of deformations of the sand during test. The model foundation used was made of a rigid steel plate and measured 330 mm length × 100 mm width × 25 mm thickness. A rough-base condition was achieved by cementing a thin layer of sand on to the base of the model foundation with epoxy glue. The footing was centered in the tank with the length of the footing parallel to the width of the tank. In order to create plane strain conditions within the test setup, the length of the footing was made almost equal to the width of the tank. On each side of the tank, a 1 mm gap was given to prevent contact between the footing and the side walls. The side wall friction effects on the model test results were reduced by coating the inside of the perspex walls with petroleum jelly. The two ends of the footing plate were polished to have smooth surface and also coated with petroleum jelly to minimize the end friction effects. To ensure uniform distribution of applied load on the model footing, two rollers of 10 mm diameter and 330 mm length made of high strength steel were placed on the two parallel grooves made at the top of the footing. These grooves were made along the length of the footing, each at a distance of 32.5 mm from the center line of the footing on either side. A 10 mm thick steel plate having the same plan dimensions and grooves as the model footing was mounted on the rollers. Grooves at the bottom of this steel plate ensured the perfect seating of it over the rollers. The footing was loaded with a hand-operated hydraulic jack (250 kN capacity) supported against the upper cross head of a reaction frame. The reaction frame is anchored to the concrete floor by means of base plates and anchor bolts, independent of the test

container. Upon filling the whole tank, the top surface was leveled and the footing was placed on a predefined alignment such that the loads from the jack and loading frame would be transferred concentrically to the footing. The hydraulic jack was connected to the footing through a proving ring to measure the load applied on the footing. The load was transmitted to the footing through a rigid spacer (made of steel) of 60 mm diameter and 60 mm height, centered on the top plate below the proving ring. A ball bearing was positioned between the proving ring and the spacer to ensure that no extraneous moment was applied to the footing.

The depth of the soil in the test tank was 7 times the footing width and the distance between the center of the footing to the edges of the tank (parallel to the footing length) was 6 times the footing width. Terzaghi (1943) proposed the failure wedge below strip footing on cohesion less soil to be of a length of around 5*B* from the edge of the footing and a depth of 1.6*B* below the base of the footing. Selig and Mckee (1961) and Chummar (1972) observed the failure wedge below strip footing on a sand bed to be extended around 2–2.5*B* on either side of the footing and a depth of around 1.1*B* from the bottom of the footing. From the above observations, it could be concluded that the tank used in the current investigation is considerably large enough and is not likely to interfere with the failure zones and hence the experimental results.

The footing was loaded through a hand-operated hydraulic jack supported against a reaction frame. The loads transferred to the footing were recorded by a proving ring installed between the hydraulic jack and the test footing. A ball bearing was positioned between the proving ring and the footing to ensure that no extraneous moment was applied to the footing. The load was applied in small increments. Each load increment was maintained constant until the footing settlements under that load increment became constant. Settlements of the footing were measured by two dial gauges situated on diagonally opposite sides of the footing. The deformations (heave/settlement) of the fill surface were also measured by dial gauges on both sides of the footing (Fig. 5.4).

The strains in the geocell reinforcement were measured through electrical resistance-type strain gauges fixed horizontally at various locations on the geocell walls (Fig. 5.3). They had a gauge length of 10 mm, gauge factor of 2.1 ± 2%, and resistance of 120 ± 0.2 ohms. At each gauge location, the geogrid surface was cleaned by emery paper to remove dust and oily matter if any and then wiped clean with a clean cloth. Subsequently, the strain gauge was pasted with a quick setting adhesive. Lead wires were soldered with strain gauge leads and were connected to a strain meter. The measured strains in micro-strain units (μstrains) were converted to percentage as μstrains × $100/10^6$. The strain measurements are reported at various normalized footing load levels (BPR). The bearing pressure ratio (BPR) is defined as the ratio between the footing pressure with geocell (q) and the ultimate footing pressure (q_{ult}) in tests on unreinforced soil. The compressive strains are reported with negative sign and the tensile strains with positive sign.

The vertical pressure transmitted to the subgrade soil below the geocell mattress (σ) was measured by placing strain gauge-type earth pressure cells below the geocell layer (Fig. 5.3). The overall diameter and thickness of the pressure cells were 60 mm and 10 mm, respectively. In total, three pressure cells were used. One of the pressure

cells was kept at the center of the footing and the other two at a distance of 1.5B from the footing centerline on either side of the footing. In the case of unreinforced earth beds, the earth pressures were measured at various depths (corresponding to the base levels of geocells) in different tests for direct comparison with those measured below the geocells. The pressure cells were 60 mm in diameter with a rated capacity of 1000 kPa. In geocell-reinforced test beds, the earth pressure cells were placed below the pocket openings of the geocells rather than below its walls so as to avoid any abnormal pressure readings due to stress concentration effects. At required depth, raining of the sand was temporarily stopped; the earth pressure cells were set on the fill surface after which the sand raining was continued. The pressures were recorded through a digital display unit. The measured pressures were normalized with respect to the applied footing pressure (q). The normalized pressures (σ/q) that represent the percentage of the footing pressures transmitted to the base of the geocell mattress are plotted at different footing loads expressed in terms of the bearing pressure ratio (BPR). The results obtained are presented and discussed in the following section.

5.3 Results and Discussion

Typical-bearing pressure–displacement responses of the foundation bed, with and without geocell reinforcement, are shown in Fig. 5.5. It can be seen that the geocell reinforcement has significantly enhanced the load-carrying capacity and has induced a stable behavior until very large settlement. This is because the geocells provide all-round confinement to the encapsulated soil mass, and the interconnected cells form a panel-like structure that redistributes the footing load over a wider area leading to reduced stress in the foundation bed. The openings in the geocell walls facilitate continuity of the soil mass across the cells that an interlocking system is formed which mobilizes increased shear resistance leading to enhanced performance improvement. Besides, the rough texture of the geocell walls mobilizes higher shear resistance at the interface which continues to increase with increase in size of the geocell mattress leading to large performance improvement. Even at a settlement equal to about 50% of the footing width, clear signs of failure were not evident in many cases with geocell reinforcement. At this stage, the load on the footing was as high as 8 times the ultimate capacity of the unreinforced sand. In many of these tests, the failure was not apparent in the geocell-reinforced sand beds even at settlements as high as 5 times the failure settlement of the unreinforced footings. Hence, a five-fold increase in permissible settlement may be allowed for the geocell-reinforced sand beds without much serious consequence in the superstructure.

Figure 5.6 shows strain variations along width of geocell mattress at its mid-height, for a typical case with $d/B = 1.2$, $h/B = 0.8$, $b/B = 12$, $u/B = 0.1$. Similar pattern of strain variation was observed in other cases as well. It can be seen that the strain in the geocell mattress is maximum in the central region underneath the footing. This is because in the region underneath the footing, the geocell reinforcement actively restrains the stress concentration induced yield in the soil mass and thereby

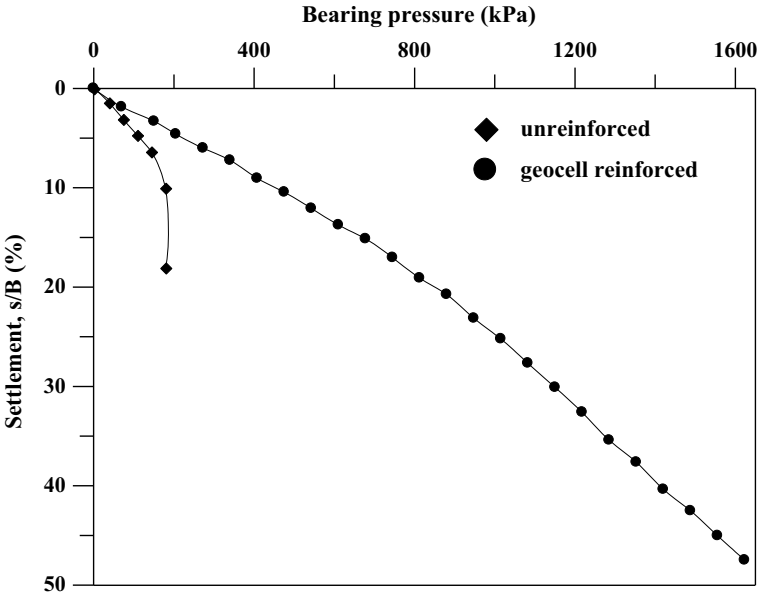

Fig. 5.5 Bearing pressure-settlement responses depicting the influence of geocell reinforcement ($b/B = 12$)—Test series A, D

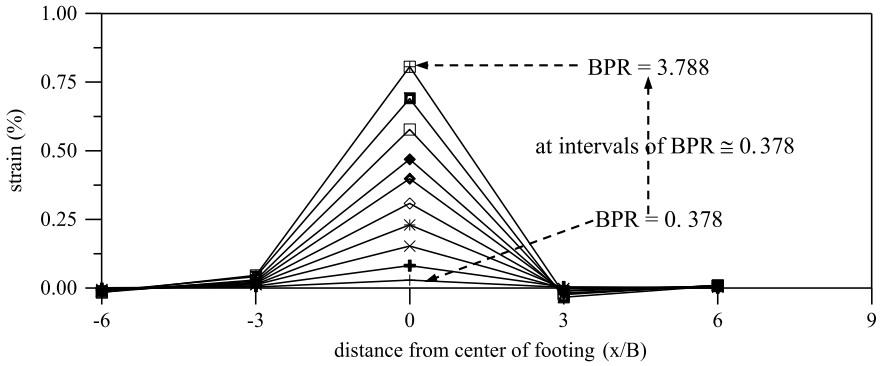

Fig. 5.6 Strain variation at mid-height of geocell mattress ($d/B = 1.2$)—Test series B

its strength is significantly mobilized leading to enhanced load-carrying capacity. The adjacent portions of the geocell mattress only contribute in a secondary manner through frictional and passive resistance developed at the soil–geocell interfaces.

Figure 5.7 shows a typical variation of the contact normal pressure (σ/q) on the subgrade soil below the geocell mattress. It may be seen that the contact pressure, on the subgrade soil, is maximum at the center of the footing and relatively low in the region beyond the loaded area. This is to be expected due to the load dispersion

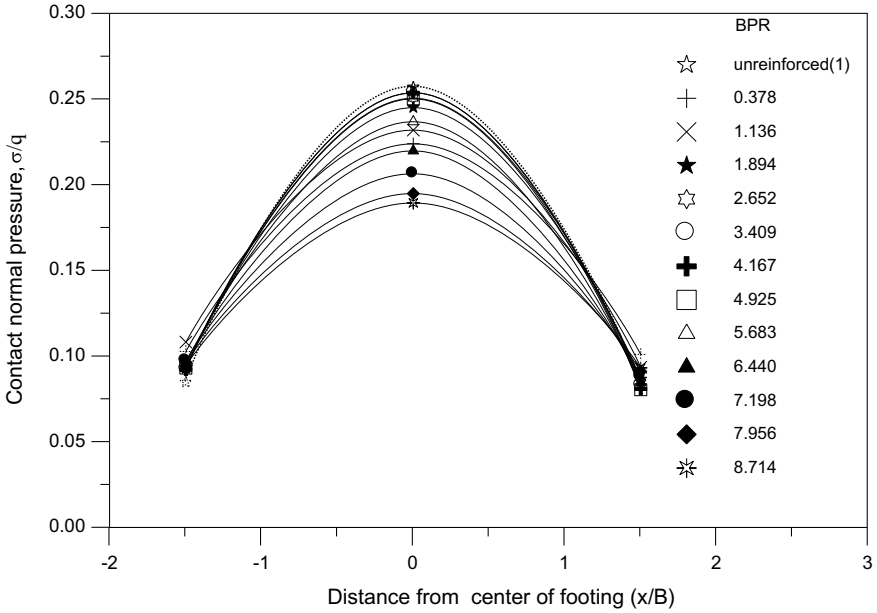

Fig. 5.7 Vertical pressure at base of geocell mattress (b/B = 12)—Test series D

from the footing edges. The geocell-reinforced foundation bed tends to exhibit elastic behavior as the contact pressure responses are found to be almost falling within a narrow range (i.e., with nearly same percentage of pressure transferred to the base) in the initial stages and beyond that tend to be varying proportionately with the applied loading. It is observed that the contact pressure initially increases with increase in footing pressure, to reach a peak value, beyond which it continues to decrease. This is because, initially, the geocell mattress behaves as a coherent mass that deflects as a centrally loaded, subgrade supported, beam under footing loading. With increase in loading, there develops local shearing of sand immediately below the footing due to which the geocell reinforcement starts sharing higher proportion of the applied load thereby bringing forth a reduction in the pressure transmitted to the subgrade soil below. Influence of various parameters on the performance of the geocell-reinforced foundation beds are discussed in the following paragraphs.

5.3.1 Influence of Pocket Size of Geocell

Figure 5.8 shows the variation of improvement factor with footing settlement for different pocket sizes (d/B) of geocell (Test series B). The increase in load-carrying capacity with decrease in pocket size is due to the overall increase in rigidity of the mattress. At the same time, the confinement offered by cells per unit volume

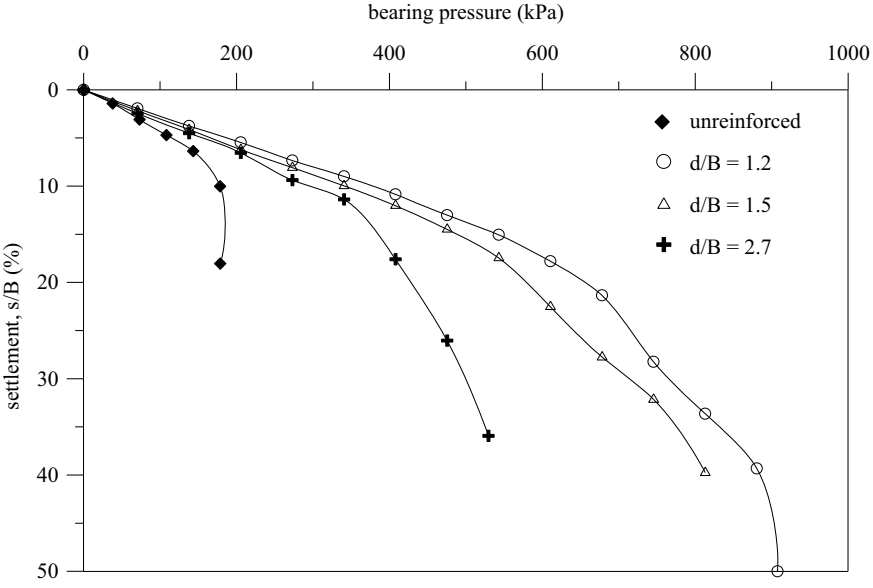

Fig. 5.8 Bearing pressure versus footing settlement for different pocket sizes of geocell—Test series B

of soil also increases with decrease in pocket size. Both these factors contribute to the overall improvement of performance. The effect of the pocket size on the soil behavior is more clearly evident from the data in Fig. 5.9. The solid and dotted lines indicate the surface deformation (heave/settlement) measurements at points 250 mm ($x = 2.5B$) to the left and right of the footing centerline. It can be seen that the heave of soil is higher for larger pocket sizes. As the pocket size increases, confinement reduces and hence the soil freely moves out of the pockets leading to larger surface heave. Rajagopal et al. (1999) have also observed similar trends from triaxial tests on sand confined with multiple geocells that, the apparent cohesion, which is a function of confinement increases with decrease in pocket size, which adds more validity to the present findings.

From the numerical values of strains [strain measured at (0, h/2)] presented in Table 5.2, it is found that the strain in the geocell wall increased with the increase in pocket size. This is because, with increase in pocket size, the surface area of geocells available for distribution of footing pressure decreases that brings forth a decrease in stiffness of the geocell mattress thereby an increase in strain in the geocell wall. The increase in strain from $d/B = 1.5$ to $d/B = 2.7$ is found to be marginal. This may have happened due to the local folding of geocell walls under the action of footing loads instead of being stretched due to the smaller stiffness of the geocell wall with larger d/B ratio. Indeed, the post-test observations have clearly indicated that the geocell had folded below the footing which supports the above proposition.

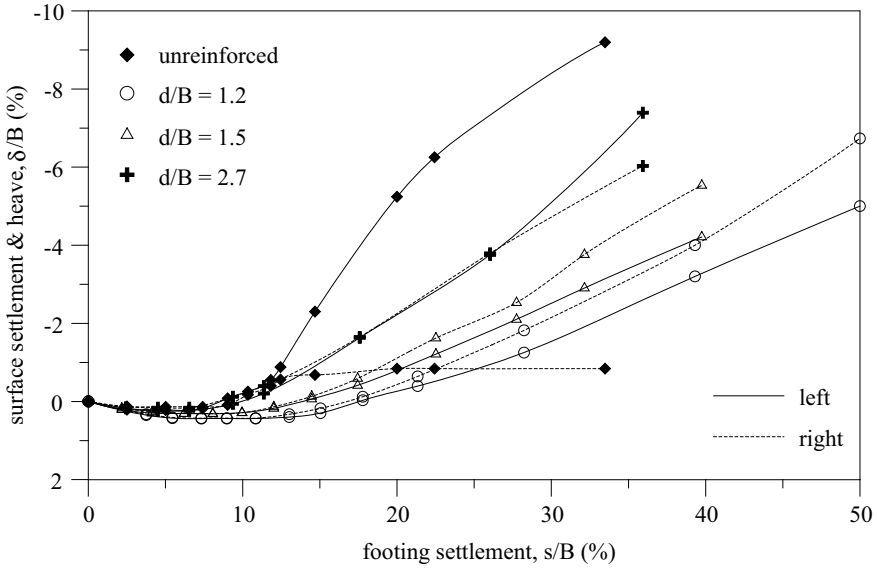

Fig. 5.9 Surface deformation versus footing settlement for different pocket sizes of geocell—Test series B

Table 5.2 Strain ε_h (%) at center of geocell mattress (0, $h/2$)—test series B

BPR	Pocket size of geocell (d/B)		
	$d/B = 1.2$	$d/B = 1.5$	$d/B = 2.7$
0.378	0.028	0.070	0.080
0.757	0.081	0.175	0.191
1.136	0.153	0.285	0.301
1.515	0.230	0.418	0.455
1.894	0.308	0.536	0.582
2.273	0.398	0.669	0.713

The vertical pressures measured on the subgrade soil at center of footing ($x/B = 0$) are given in Table 5.3. It is found that for all the pocket sizes, there is an increase in normalized pressure with increase in footing pressure. It could also be observed that the pressure recorded at the center of geocell mattress ($x/B = 0$) is higher for geocells with larger pocket size. This is because as the pocket size increases, the rigidity of the geocell mattress decreases, which gives rise to higher deflections under the same footing pressure thereby inducing higher pressures on the underlying soil layer. In the case of geocell with pocket size equal to 2.7B, the normalized pressure below the geocell did not increase appreciably with increase in footing pressure and had suddenly dropped when the footing pressure reached the ultimate value. This could have happened due to the large shear deformations of the soil inside the geocell pockets due to general shear failure. With shearing of soil, a larger portion of footing

Table 5.3 Pressure (σ/q) below geocell mattress ($x/B = 0$)—Test series B

BPR	Pocket size of geocell (d/B)		
	$d/B = 1.2$	$d/B = 1.5$	$d/B = 2.7$
0.378	0.329	0.391	0.610
1.136	0.467	0.476	0.622
1.894	0.528	0.559	0.639
2.652	0.551	0.680	0.387
3.409	0.606	0.731	–
4.167	0.662	–	–

pressure is directly transmitted to the geocell cage thereby bringing about a reduction in the pressure transmitted to the base of the mattress. The tests with smaller pocket sizes had to be terminated at early stages as the pressure cell directly below the footing has neared its capacity. Hence, the decreasing trend in normalized pressure could not be observed in these two cases.

5.3.2 Influence of Height of Geocell Mattress

Influence of height of geocell mattress on performance improvement of the footing (Test series C) is shown in Fig. 5.10. As the height of geocell layer is increased, the footing load is dispersed over a larger area that reduces the pressure transmitted to the soil and hence the footing settlement. Apart from this, the moment of inertia of the reinforcement cage increases with increase in height, which enhances its flexural rigidity and thereby, the load-carrying capacity. However, beyond a h/B ratio of 2, the pressure-settlement responses have not shown significant further improvement. The reason for this is that at higher load stage the geocell walls buckle locally just under the footing leading to higher settlements. This has been confirmed from the post test observations that the geocell walls just below the footing were found to be vividly deformed. Hence, the bearing capacity has not increased directly in proportion to the height of geocell layer. Based on these results, it can be said that beyond a certain h/B ratio, the increased flexural rigidity of the geocell layer remains immobilized because of its local buckling below the footing. The results are further analyzed in terms of surface deformation on both sides of the footing as presented in Fig. 5.11. It shows that with increase in height of geocell, the surface heave decreases and for $h/B \geq 2$, the surface undergoes settlements only, instead of heave. This is believed to be due to the fact that, at smaller cell heights, the sand below the footing overcomes the frictional resistance on the vertical cell surface and moves out through its bottom leading to surface heave. However, with increase in height, the sand remains confined within the cell and the mattress deflects as a composite body thereby, increasing the load-carrying capacity. This may be the cause of the little improvement noticed beyond $h/B \geq 2$.

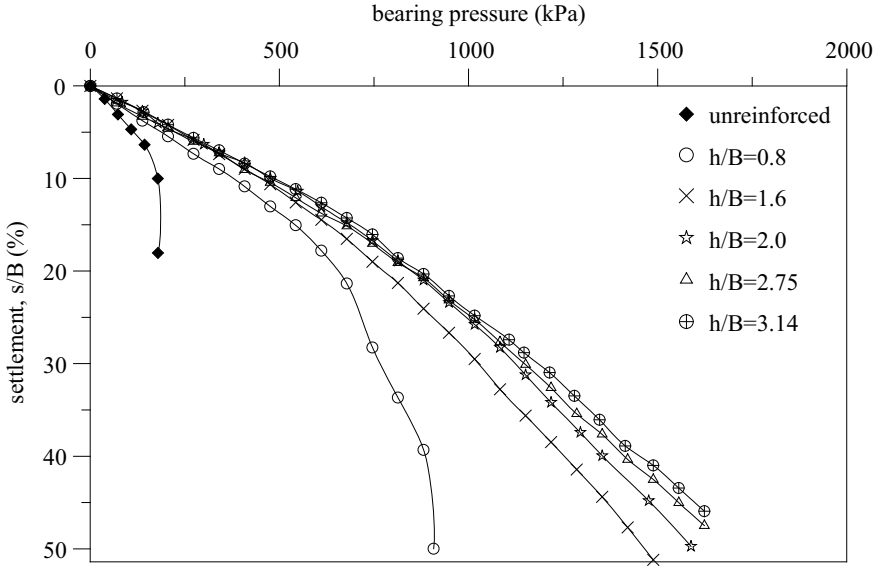

Fig. 5.10 Bearing pressure versus footing settlement for different heights of geocell mattress—Test series C

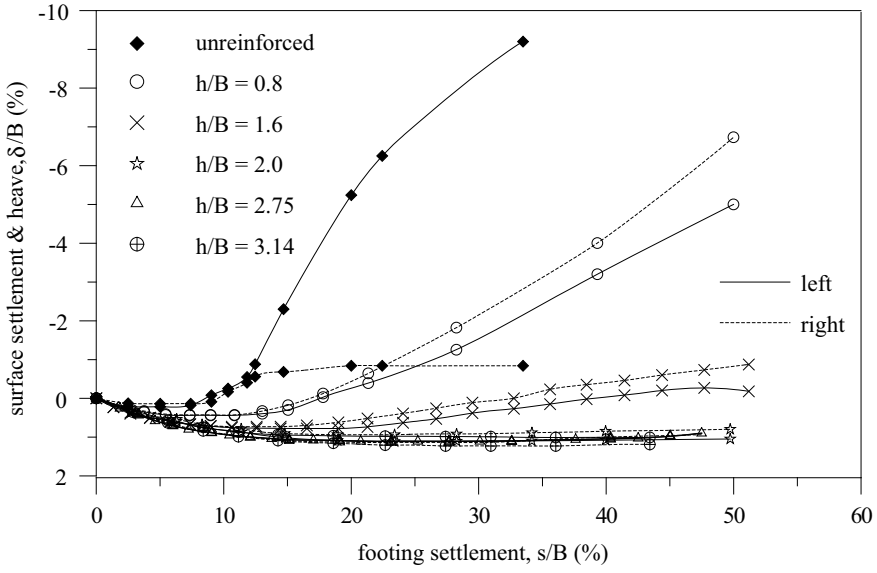

Fig. 5.11 Surface deformation versus footing settlement for different heights of geocell mattress—Test series C

Table 5.4 Strain ε_h (%) at center of geocell mattress (0, h/2)—Test series C

BPR	Height of geocell mattress (h/B)				
	h/B = 0.8	*h/B = 1.6*	*h/B = 2.0*	*h/B = 2.75*	*h/B = 3.14*
0.378	0.029	0.029	0.008	0.053	0.020
0.757	0.082	0.081	0.033	0.127	0.063
1.136	0.154	0.153	0.148	0.211	0.152
1.515	0.230	0.213	0.211	0.296	0.220
1.894	0.308	0.275	0.270	0.426	0.321
2.273	0.398	0.344	0.328	0.536	0.435
2.652	0.469	0.421	0.388	0.644	0.532
3.031	0.578	0.476	0.445	0.680	0.632
3.409	0.690	0.526	0.500	0.768	0.750
3.788	0.807	0.588	0.553	0.884	0.880

Strains measured at the center of the geocell mattress (0, h/2) for this series of tests are summarized in Table 5.4. From the results presented in this table, it is observed that the strain decreases with increase in height of geocell up to $h/B = 2$. This is because with increase in height, the geocell mattress redistributes the footing pressure over a larger area thereby reducing the intensity of pressure within the mattress and hence the strain in the geocell wall. It could also be attributed due to the increase in section modulus with the increase in height that reduces the deflection of the geocell mattress, thereby reducing the strain in the geocell wall. For $h/B = 2.75$, the strain is higher than with $h/B \leq 2$. It is believed that at this stage, the increase in rigidity of the geocell layer due to increase in its height remains unmobilized due to local buckling below the footing, that does not help in further reducing the strain in the geocell wall. However, due to the increase in surface area, the frictional resistance on the geocell wall completely arrests downward punching of the sand column due to footing pressure. In such a context, the volumetric expansion of the sand would exert additional pressure on the geocell wall, thereby giving rise to higher strain. But for the case with $h/B = 3.14$, though the strain is much higher than the case with $h/B = 2$, there is a slight reduction in strain in comparison to the case with $h/B = 2.75$. This is because at a deeper depth, there could have been a reduction in dilation due to decrease in the shear strains (intensity of footing pressure). This might have brought about a reduction in volume expansion thereby reducing the strains in geocell wall.

The values of pressure (σ/q) recorded at the center of the geocell mattress (i.e., $x/B = 0$) with different heights are presented in Table 5.5. For relatively smaller heights of geocell mattress (i.e., $h/B \leq 1.6$), there is a gradual increase in the normalized pressure with increase in footing pressure (BPR). However, at larger height of the mattress ($h/B \geq 2$), it is found to decrease with increase in the footing pressure. In other words, the percentage of footing pressure transmitted to the underlying sand layer below geocell mattress increases with increase in footing pressure for lower height of geocell mattress but decreases with increase in footing pressure for higher

Table 5.5 Pressure (σ/q) below geocell mattress ($x/B = 0$)—Test series C

BPR	Height of geocell mattress (h/B)				
	$h/B = 0.8$	$h/B = 1.6$	$h/B = 2.0$	$h/B = 2.75$	$h/B = 3.14$
0.378	0.329	0.327	0.318	0.224	0.218
1.136	0.467	0.394	0.392	0.232	0.191
1.894	0.528	0.433	0.391	0.245	0.177
2.652	0.551	0.481	0.391	0.251	0.176
3.409	0.606	0.518	0.391	0.254	0.176
4.167	0.662	0.525	0.348	0.254	0.175
4.925	–	0.510	0.300	0.251	0.170
5.683	–	0.500	0.279	0.237	0.158
6.440	–	–	0.276	0.220	0.146
7.198	–	–	0.272	0.207	0.139
7.956	–	–	0.270	0.195	0.132

height of geocell mattress. This may be because the geocell mattress of smaller height bends like a centrally loaded shallow beam that deflects more with increased footing pressure and hence exerts more pressure on the underlying soil layer. In the case of higher heights of geocell mattress, the end anchorage that develops due to frictional and passive resistance of the soil is quite high to hold the geocell mattress against downward deflection due to footing pressure thereby reducing the percentage of vertical pressure transmitted to its base. Besides, the deep beam behavior of the mattress, which manifests at higher height, might have further reduced the deflection in the geocell mattress thereby reducing the normal pressure at its base.

5.3.3 Influence of Width of Geocell Mattress

The effect of the width of the geocell mattress on the performance of footing (Test series D) is shown in Fig. 5.12. It may be seen that even with a geocell mattress of width equal to the width of the footing ($b/B = 1$), significant performance improvement is obtained. As the footing is supported by relatively rigid geocell mattress, the loads are transferred to the foundation soil at the base of the geocell. For this test configuration, the geocell base is at a depth of 285 mm (i.e., $2.85B$). Because of the depth effect and overburden pressure effects, the surface footing behaves like a footing placed at some depth below the surface. These factors would have contributed to the improvement in the overall performance even when the geocell layer does not extend beyond the footing edges. As the width of geocell mattress increases, the performance improves up to a b/B ratio of 4. Beyond that width of the geocell mattress, increase in performance improvement decreases and becomes marginal for $b/B \geq 8$.

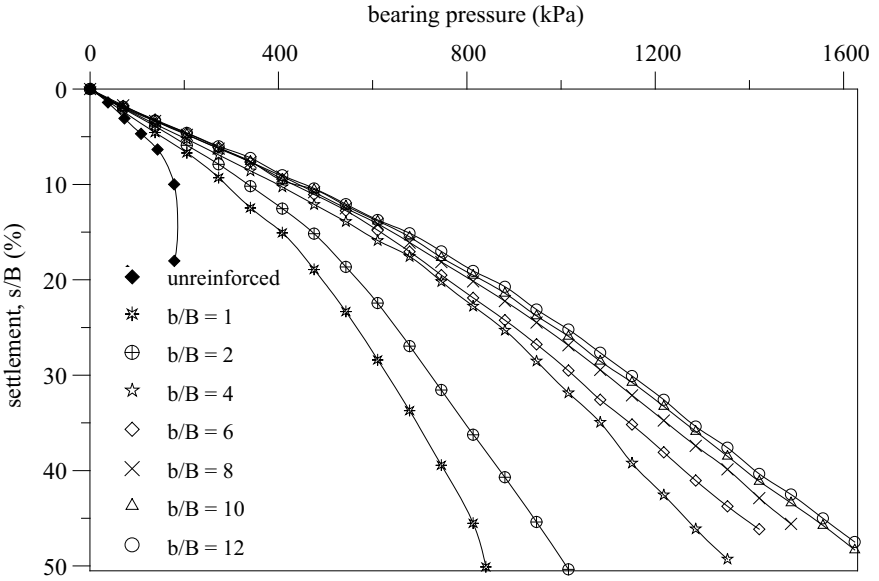

Fig. 5.12 Bearing pressure versus footing settlement for different widths of geocell mattress—Test series *D*

This trend can be explained with the help of the observed surface deformation measurements as presented in Fig. 5.13. The soil surface has heaved up to a geocell width of $b/B = 2$. At b/B ratio of 4, there was slight heaving tendency at relatively large settlements ($s/B > 40\%$). At higher b/B ratios, the surface has not undergone heaving even at large settlements. This can be explained from the fact that as the width of the geocell layer is increased beyond a certain limit, it intercepts all the potential rupture planes thus preventing the soil to heave. From the observed heave patterns in this investigation, it may be said that the farthest rupture plane would be at a distance of around 2B from the center line of the footing on both sides. Similar observations were made by Selig and Mckee (1961) and Chummar (1972) on the extent of the rupture planes in a homogeneous sand bed below strip footing. As the geocell layer of width about 4B completely encapsulates the failure zone of the soil, any increase in its width would only contribute in a secondary manner (as illustrated in Fig. 4.15) by deriving anchorage from the side soil. Beyond $b/B = 8$, the increase in performance improvement is practically negligible which may be due to the local buckling of geocells below the footing.

From Table 5.6, it is observed that the strain measured at (0, $h/2$) decreases with the decrease in the width of the geocell mattress. This is due to the reduction in anchorage for shorter widths of geocells. However, the strains in geocell with $b/B = 1$ are comparable to those with $b/B = 12$. In this case, the entire geocell is directly resting under the footing leading to lateral expansion at mid-height under the vertical compression due to footing loads. This may have caused large strains in this case.

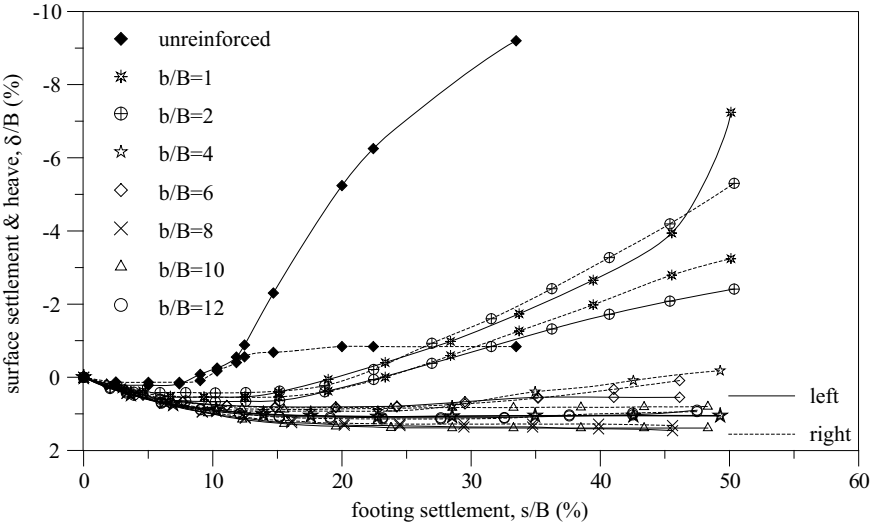

Fig. 5.13 Surface deformation versus footing settlement for different widths of geocell mattress—Test series D

Table 5.6 Strain, ε_h (%) at center of geocell mattress (0, h/2)—Test series D

BPR	Width of geocell mattress (b/B)				
	$b/B = 12$	$b/B = 10$	$b/B = 8$	$b/B = 4$	$b/B = 1$
0.378	0.053	0.037	0.010	0.006	0.013
0.757	0.127	0.075	0.027	0.014	0.076
1.136	0.211	0.126	0.054	0.022	0.155
1.515	0.296	0.147	0.101	0.052	0.268
1.894	0.426	0.210	0.171	0.116	0.385
2.273	0.536	0.302	0.269	0.219	0.479
2.652	0.644	0.412	0.379	0.321	0.560
3.031	0.680	0.543	0.482	0.406	0.634
3.409	0.734	0.556	0.535	0.411	0.704
3.788	0.784	0.625	0.601	–	–

An analogy for this can be the lateral expansion of samples in triaxial compression tests. This higher strain may also have been caused by local rotation leading to higher strains on one side than on other side.

Values of the normal pressure on subgrade soil recorded at the mid-section of the footing are given in Table 5.7. It is observed that for $b/B = 12$, there is a decrease in normalized pressure with increase in footing pressure. But for $b/B \leq 10$, it increases with increase in footing pressure. This is because with decrease in geocell area, the end anchorage reduces. As this anchorage was holding the mattress against bending

Table 5.7 Pressure (σ/q) below geocell mattress ($x/B = 0$)—Test series D

BPR	Width of geocell mattress (b/B)						
	$b/B = 12$	$b/B = 10$	$b/B = 8$	$b/B = 6$	$b/B = 4$	$b/B = 2$	$b/B = 1$
0.378	0.224	0.227	0.253	0.268	0.295	0.326	0.336
1.136	0.232	0.235	0.257	0.280	0.301	0.343	0.352
1.894	0.245	0.247	0.276	0.299	0.319	0.350	0.360
2.652	0.251	0.263	0.298	0.323	0.329	0.352	0.371
3.409	0.254	0.279	0.320	0.346	0.363	0.367	0.385
4.167	0.254	0.290	0.344	0.372	0.376	0.387	0.390
4.925	0.251	0.292	0.360	0.378	0.385	0.386	–
5.683	0.237	0.286	0.362	0.368	0.381	0.383	–
6.440	0.220	0.277	0.346	0.352	0.358	–	–
7.198	0.207	0.267	0.319	0.334	0.343	–	–
7.956	0.195	0.257	0.308	0.326	0.334	–	–
8.714	0.189	0.253	–	–	–	–	–

under footing pressure with its reduction, it deflects more; thereby, bringing forth an increase in pressure at the base of the mattress. From the Table 5.7, it is observed that, the percentage pressure transmitted to the base of the geocell mattress increases with decrease in width of the mattress. The possible reason for this may be that with decrease in its width, the geocell mattress behavior tends to shift from deep beam to pedestal. As a result of which the footing pressure instead of getting redistributed over a wider area gets concentrated more in and around the footing center line and hence causes an increase in pressure on the underlying sand layer. For the cases with $b/B \leq 10$, the decrease in normalized pressure in the later stages of loading is attributed to the local shearing of sand below footing as has been discussed earlier.

5.3.4 Influence of Depth of Placement of Geocell Mattress

The influence of depth of placement of geocell layer (defined by u/B ratio) on the bearing capacity of the foundation (Test series E) is shown in Fig. 5.14. It is seen that, there is a slight improvement in load-carrying capacity when u/B was increased from 0 to 0.1 and thereafter, the load-carrying capacity continued to decrease with increase in the depth of placement. This slight increase in load-carrying capacity with u/B of 0.10 may be due to the effect of soil cushion spreading the load over larger area of geocell and preventing the geocell wall from direct contact with the footing that would bring an early buckling. With further increase of the depth of placement, the soil between the footing and the geocell layer would squeeze out leading to larger settlements. This is reflected in the reduction in bearing capacity improvement for higher u/B ratios. These results suggest that to get maximum benefit, the top of the

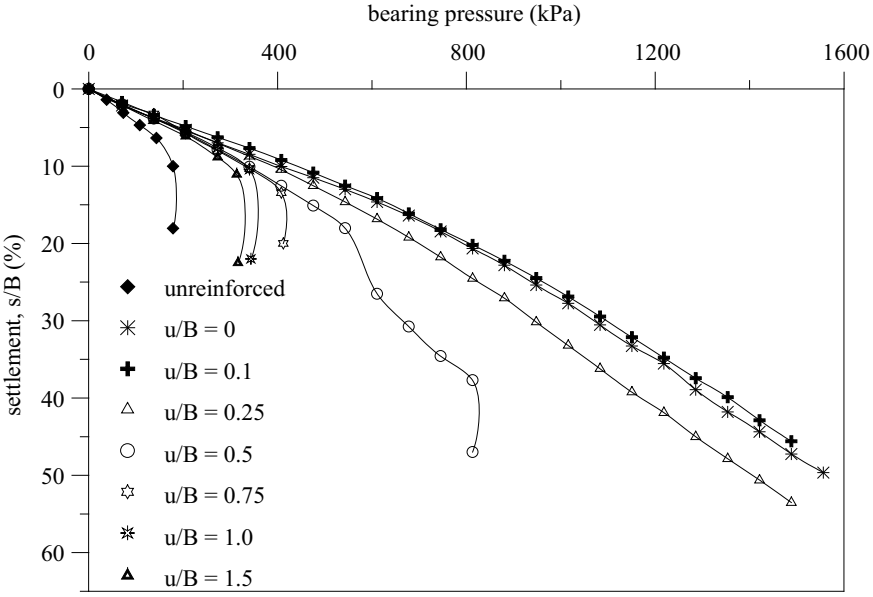

Fig. 5.14 Bearing pressure versus footing settlement for different depths of placement of geocell mattress—Test series E

geocell mattress should be at a depth of about 0.1*B* from the bottom of the footing. Up to *u*/*B* ratio of 0.25, the footings have not shown evidence of failure even at large settlements. When *u*/*B* was 0.50, the footing had an initial failure at a settlement of about 0.2*B* and later started taking higher loads and finally reached its ultimate capacity at settlement of about 0.4*B*. When *u*/*B* ratio was increased beyond 0.5, the footings have reached ultimate pressures at much smaller settlements of about 0.15*B*. When the geocell layer was placed at larger depths, the surface heave significantly increased indicating that the sand has squeezed out laterally between the footing and the relatively rigid geocell layer. From these results, it may be said that when geocell layer is placed at depths greater than 0.5*B*, its contribution to the improvement is only marginal. When placed at such depths, its role would be similar to that of a rough, rigid base at shallow depths below the footings.

The values of the central (0, *h*/2) strain gauge readings for different *u*/*B* ratios are tabulated in Table 5.8. It can be seen that there is decrease in strain magnitude with the increase in u/B ratio, except for the case with $u/B = 0.1$. At $u/B = 0.1$, the magnitude of strain is maximum, indicating that the geocell mattress has a better reinforcing efficacy when placed at this depth. This is in consonance with the observation presented in Fig. 5.14, which shows that maximum performance improvement is obtained for the geocell reinforcement at $u/B = 0.1$. The decrease in strain with increase in depth of placement is believed to be due to the decrease in intensity of stress inside the geocell mattress because of dispersion of footing pressure.

Table 5.8 Strain, ε_h (%) at center of geocell mattress (0, h/2)—Test series E

BPR	Depth of placement of geocell mattress (u/B)				
	$u/B = 0$	$u/B = 0.1$	$u/B = 0.25$	$u/B = 0.75$	$u/B = 1.0$
0.378	0.007	0.010	0.004	0.001	0.000
0.757	0.012	0.027	0.005	0.003	0.001
1.136	0.045	0.054	0.020	0.008	0.003
1.515	0.125	0.135	0.073	0.050	0.025
1.894	0.195	0.209	0.134	0.099	0.074
2.273	0.274	0.280	0.211	0.178	–
2.652	0.353	0.379	0.335	–	–
3.409	0.523	0.606	0.503	–	–
4.167	0.661	0.840	0.654	–	–
4.925	0.811	1.086	0.801	–	–
5.683	0.942	1.353	0.931	–	–
6.440	1.091	1.651	1.051	–	–

The contact pressure on subgrade soil below geocell mattress measured at $x/B = 0$ is presented in Table 5.9. As noted in the earlier section (Sect. 5.3.3), for a geocell mattress width of 8B, the percentage of pressure transmitted to the base should increase with increase in footing pressure. The same trend was observed up to u/B values of 0.75 while at higher depths of placement, the normalized pressure decreased with increase in footing pressure. This is believed to be due to the fact that at shallow depth of placement, the geocell mattress intersects the shear zone formed within the sand bed below the footing and therefore effectively transmits the footing pressure to the underlying soil layer. Whereas for higher depths of placement ($u/B > 0.75$), the shear zone mostly remains above the top of the geocell mattress. With increase in footing pressure, the soil on the top of geocell mattress starts slipping and hence its continuity with the underlying soil layer through the body of the geocell mattress

Table 5.9 Pressure (σ/q) below geocell mattress ($x/B = 0$)—Test series E

BPR	Depth of placement of geocell mattress (u/B)						
	$u/B = 0$	$u/B = 0.1$	$u/B = 0.25$	u/B = 0.5	u/B = 0.75	u/B = 1	u/B = 1.5
0.378	0.249	0.253	0.248	0.212	0.208	0.201	0.199
1.136	0.251	0.257	0.254	0.222	0.211	0.192	0.167
1.894	0.255	0.276	0.266	0.242	0.238	0.169	–
2.652	0.262	0.298	0.287	0.269	–	–	–
3.409	0.282	0.320	0.311	0.294	–	–	–
4.925	0.335	0.360	0.334	–	–	–	–
6.440	0.319	0.346	0.310	–	–	–	–
7.956	0.303	0.308	0.237	–	–	–	–

starts diminishing, thereby reducing the percentage of footing pressure transmitted to the base of the mattress. It can further be observed that relatively lower contact pressures are recorded in case of $u/B = 0$ than in case of $u/B = 0.1$ contrary to the general trend where pressure transmitted to the subgrade soil decreases with increase in depth of placement of geocell mattress. This is because some part of the footing load is directly transferred to the walls of the geocell that is in contact with it and only the remaining part is transferred to the soil.

5.4 Conclusions

Influence of geocell reinforcement on performance improvement of foundation beds has been studied herein through model tests. These test data though have scale effects, provide insight into the basic reinforcing mechanism that establishes the load deformation behavior geocell-reinforced foundation beds. Large-scale tests by Milligan et al. (1986) have shown that the general mechanisms and behavior observed in the model tests are mostly reproduced in large-scale tests. Consequently, the findings from the present study will provide general guidelines for construction as well as large-scale field tests and would lead to the developments of a rational design methodology. However, the extrapolation of the results from these model tests to field cases can be done making use of a suitable scaling law with careful consideration of different parameters as discussed by Butterfield (1999). Based on the findings from the present investigation, the following conclusions can be made on the behavior geocell-reinforced foundation beds under strip footing.

The bearing pressure of geocell-reinforced foundation bed continues to increase even up to a settlement of about 50% of the footing width and a load as high as 8 times the ultimate capacity of the unreinforced foundation. Very good improvement in the footing performance can be obtained even with geocell mattress of width equal to the width of the footing, because of the transfer of footing loads to deeper depths through the geocell layer. The surface footing in this case behaves like a deeply embedded footing thus improving the overall performance. Improvement in bearing capacity increases with decrease in pocket size of geocells. The performance improvement is significant up to a geocell height of about 2 times the width of the footing. Beyond that height, the improvement is only marginal. The optimum width of the geocell layer is around 4 times the footing width at which stage, the geocell would intercept all the potential rupture planes formed in the foundation soil. To obtain maximum benefit, the top of geocell mattress should be at a depth of about $0.1B$ from the bottom of the footing.

The surface heave and footing rotation can be reduced substantially by providing geocell of sufficient width to restrict the formation of the rupture plane within the foundation soil. The strain in geocell wall is found to be maximum under the footing and much smaller in the extended portions outside the footing width. This suggests that the reinforcing efficacy of the geocell layer is maximum below the footing and the end portions contribute only in a secondary manner by deriving anchorage from

the soil through mobilization of soil passive resistance and geogrid–soil interfacial frictional resistance. The provision of geocell layer is observed to transmit the footing pressures to deeper depths. It is governed by factors such as pocket size of geocells, height, width, and placement depth of geocell mattress.

References

Alford SJ, Webster SL (1978) Investigation of construction concepts for pavements across soft ground. Technical Report No. S-78-6, U.S. Army Engineer Waterways Experiment Station, March

Bathurst RJ, Jarrett PM (1989) Large scale model tests of geocomposite mattresses over peat subgrades. Transp Res Rec 1188:28–36

Bush DI, Jenner CG, Bassett RH (1990) The design and construction of geocell foundation mattress supporting embankments over soft ground. Geotext Geomembr 9:83–98

Butterfield R (1999) Dimensional analysis for geotechnical engineers. Geotechnique, Lond, UK 49(3):357–366

Chummar AV (1972) Bearing capacity theory from experimental results. J Soil Mech Found Div, ASCE 98:1311–1324

Cowland JW, Wong SCK (1993) Performance of a road embankment on soft clay supported on a geocell mattress foundation. Geotext Geomembr 12:687–705

Dash SK, Krishnaswamy NR, Rajagopal K (2001) Bearing capacity of strip footings supported on geocell-reinforced sand. Geotext Geomembr 19:235–256

Hegde A, Sitharam TG (2015) 3-Dimensional numerical modelling of geocell reinforced sand beds. Geotext Geomembr 43:171–181

Krishnaswamy NR, Rajagopal K, Madhavi Latha G (2000) Model studies on geocell supported embankments constructed over soft clay foundation. Geotech Test J, ASTM, 23:45–54

Milligan GWE, Fannin RJ, Farrar DM (1986) Model and full-scale tests of granular layers reinforced with a geogrid. In: Proceedings of third international conference on geotextiles, vol 1, pp 61–66 Vienna

Mitchell JK, Kao TC, Kavazanjiam E Jr (1979) Analysis of grid cell reinforced pavement bases. Technical Report No. GL-79-8, U.S. Army Waterways Experiment Station, July

Rajagopal K, Krishnaswamy NR, Madhavi Latha G (1999) Behaviour of sand confined with single and multiple geocells. Geotext Geomembr 17:171–181

Rea C, Mitchell JK (1978) Sand reinforcement using paper grid cells. ASCE Spring Convention and Exhibit, Preprint 3130, Pittsburgh, PA, 24–28 April

Selig ET, McKee KE (1961) Static and dynamic behaviour of small footings. J Soil Mech Found Div, ASCE 87:29–47

Simac MR (1990) Connections for geogrid systems. Geotext Geomembr 9:537–546

Terzaghi K (1943) Theoretical soil mechanics. Wiley, New York, p 118

Webster SL, Watkins JE (1977) Investigation of construction techniques for tactical bridge approach roads across soft ground. Technical Report No. S-77-1, U.S. Army Engineer Waterways Experiment Station, February

Chapter 6
Performance of Geocell-Reinforced Sand Foundations with Clay Subgrades of Varying Strength

A. Murali Krishna, Arghadeep Biswas, S. B. Prasath, and Sujit Kumar Dash

Abstract This chapter provides an understanding of the performance of the geocell-reinforced sand foundations having clay subgrades of varying strengths. Model tests were conducted on a rigid circular model footing of 150 mm diameter (D) resting on foundation beds of different configurations prepared in a steel tank having dimensions of 1 m × 1 m × 1 m. Different foundation configurations were considered by varying thickness of reinforced and unreinforced sand layers overlying a wide range of subsoil strengths, from very soft to stiff clay, varying the undrained shear strengths (c_u) from 7 to 60 kPa. The results are presented in terms of bearing pressure and surface deformations responses at different loading stages. The results are further analyzed in terms of foundation reaction modulus, improvement factors, and percentage reduction in settlement. The outcomes of the study indicate that the geocell-induced improvement in the foundation performance is significantly influenced by the subgrade strength. For lower subgrade strength soil, the degree of improvement is highest, and it is decreased nonlinearly with increase in subgrade strength.

Keywords Clay subgrade · Sand · Geocell-reinforcement · Bearing capacity improvement · Settlement reduction

A. Murali Krishna (✉)
Department of Civil and Environmental Engineering, Indian Institute of Technology Tirupati, Tirupati, India
e-mail: amk@iittp.ac.in

A. Biswas
Department of Civil Engineering, Jalpaiguri Government Engineering College, Jalpaiguri, India
e-mail: arghadeep.biswas@gmail.com

S. B. Prasath
Department of Civil Engineering, Indian Institute of Technology Guwahati, Guwahati, India
e-mail: prasathcbt@gmail.com

S. K. Dash
Department of Civil Engineering, Indian Institute of Technology Kharagpur, Kharagpur, India
e-mail: sujit@civil.iitkgp.ac.in

T. G. Sitharam et al. (eds.), *Geocells*, Springer Transactions in Civil and Environmental Engineering,
https://doi.org/10.1007/978-981-15-6095-8_6

6.1 Introduction

Soil reinforcement, in various forms, has been rigorously applied in several civil engineering applications, such as foundations, pavements, slopes, retaining walls, and embankments. In past few decades, soil-reinforcements are evolved through several modifications, in terms of material (metallic to geosynthetics) and type (two-dimensional planar strip, and sheet to three-dimensional geocell). Geocell is a three-dimensional honeycombing confining system of interconnected cells, made of thermally welded or mechanically bonded polypropylene and polyethylene materials. Readymade geocells are available commercially, which are easy to handle and transport in collapsed form and can be expanded as mattress at site (Fig. 6.1). They can also be made in field using planar geotextiles or geogrids as per required dimensions.

The benefits of planar reinforcements are demonstrated by Binquet and Lee (1975), Akinmusuru and Akinbolade (1981), Fragaszy and Lawton (1984), Khing et al. (1994), Mandal and Sah (1992), Sitharam and Sireesh (2004), and Biswas et al. (2015). As compared to planar form, geocell is a comparatively new invention in soil reinforcement, devised by Webster and Watkins (1977). Different studies have revealed its superiority over the planar reinforcements and/or various traditional ground improvement techniques, such as heavy compaction, soil replacement, and chemical stabilization. The advantage of using geocells is established through several applications, such as foundations, embankments, bridge abutments, gravity walls and steepened slopes, roadways, and railways. (Rajagopal et al. 1999).

Schematic configuration of a typical geocell-reinforced foundation system is shown in Fig. 6.2. To improve the bearing capacity of foundation soil, geocells are placed directly over the native soft ground, and then, the pockets of geocell are filled, preferably, with granular materials like sand which have better drainage properties and reinforcement interaction behavior. Two types of soils can be noticed in the figure: The Soil Type-2 is the native soil underneath the reinforced-soil, and the Soil Type-1 is geocell-reinforced/unreinforced fill soil. D is the diameter of the footing. H is the thickness of geocell-reinforced sand layer overlying the clay subgrade, d is the geocell opening size, u is the depth of placement of geocell-mattress below the

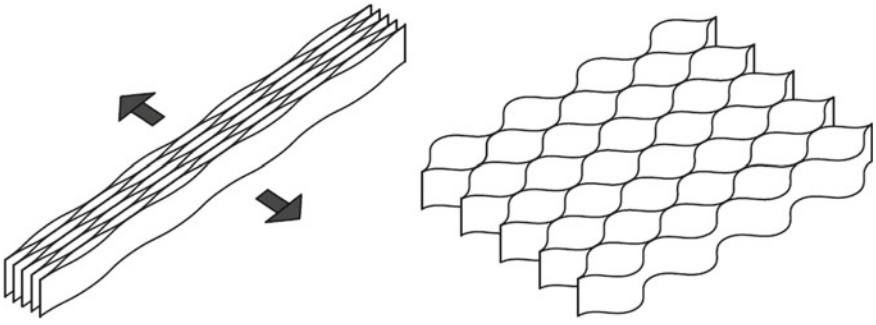

Fig. 6.1 Typical geometry of geocell (Yang et al. 2010)

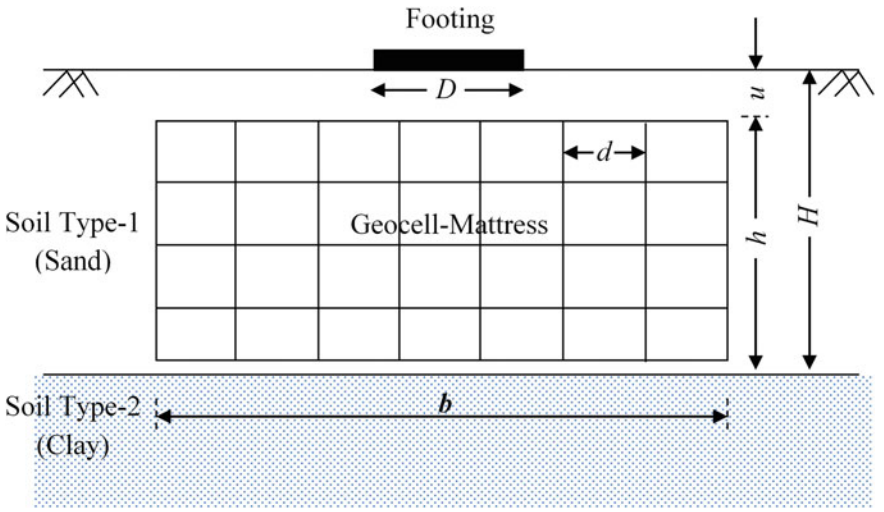

Fig. 6.2 Schematic configuration of geocell-reinforced foundation systems (after Biswas et al. 2016)

base of footing, b is the width of geocell-mattress, and h is the height of geocell-mattress. In practice, natural ground (subgrade) may exist at different strength levels, and situations may arise where reasonably strong soils also fail to meet the design requirements which need to be improved. In such situations, performance of reinforced foundations with different subgrade strengths should be considered. As can be seen in Fig. 6.1, the entire geocell-mattress is supported by the underlying subgrade. Hence, the behavior of geocell-reinforced foundation system is largely dependent on the underlying subgrade.

In view of this, the main objective of this chapter is to provide insight into the performance of geocell-reinforced sand beds resting on clay subgrades of various strengths. Biswas et al. (2013, 2015, 2016), Biswas (2016), performed various physical model tests with soil subgrades of varied strengths, from very soft to stiff clay, varying the undrained shear strengths (c_u) from 7 to 60 kPa overlain by geocell-reinforced sand mattresses of different heights. This chapter briefly describes the physical model tests conducted and presents the outcomes of model studies in terms of foundation reaction modulus, improvement factor, and percentage reduction in settlement.

6.2 Physical Model Tests

Model tests were carried out on a circular footing of 150 mm diameter (D) resting on 1 m × 1 m × 1 m foundation bed (test bed-cum loading frame assembly in the laboratory) having clay subgrades of different undrained shear strengths (c_u), ranging

Table 6.1 Material properties (Biswas 2016)

Material	Property		Value
Clay (*CL*)	Specific gravity		2.65
	Liquid limit (%)		42
	Plastic limit (%)		21
Sand (*SP*)	Specific gravity		2.68
	Coefficient of uniformity		3.06
	Coefficient of curvature		0.62
	γ_d (kN/m^3)	Maximum	16.4
		Minimum	13.8
	Friction angle ($\phi°$)	Direct shear	43
		Triaxial compression	40
Geocell (made of geogrid)	Geogrid aperture size (mm)		38 × 38
	Tensile strength (kN/m) (at failure strain, %)	Geogrid	20 (at 11%)
		Bodkin joint	3.3 (at 9%)

from 7 to 60 kPa. Different series of laboratory model tests were performed on homogeneous and layered foundation systems. The layered systems were comprised of unreinforced and reinforced sand of varying layer thicknesses ($H = 0.63D$ to $2.19D$) overlying the clay subgrades. Two types of soils were used: a locally available clay soil for the subgrades and a river sand for the overlying layer. The geocell-reinforcements were formed using a biaxial geogrid through bodkin joints (with plastic dowel strips). A brief summary of the materials used and their properties are presented in Table 6.1.

6.2.1 Preparation of Clay Bed/Subgrade

A calibration curve (Fig. 6.3a) depicting the variation of shear strength with water content of clay, for a uniform compaction effort, was developed through a series of trial tests (details were presented in Biswas et al. 2015). The clay soil was pulverized, air dried, and mixed with the required water (as per the calibration curve) to achieve the desired shear strength. The wet soil was kept in sealed containers for about a week to get moisture equilibrium. The prepared clay was placed in the test tank and compacted in layers of 50 mm thickness, until the desired height was reached. In order to verify the uniformity, clay samples from different locations and layers were collected by pressing mold into the clay beds. The shear strength values of the samples were determined through vane shear apparatus and found to be with ± 2% variation from the targeted shear strength values.

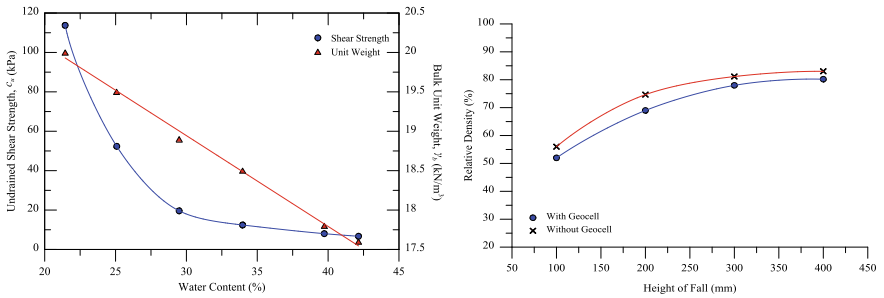

Fig. 6.3 Calibration curves: **a** for clay and **b** for sand (after Biswas 2016)

6.2.2 Preparation of Sand Bed

Sand beds were prepared through raining technique. The raining device consisted of a large container and a long hollow pipe having a 60° inverted cone connected at its bottom. By trial, the height of fall was adjusted to attain the required density in both reinforced and unreinforced cases, as shown in Fig. 6.3b. It may be noticed that to attain a desired density, the raining heights for geocell-beds were more compared to unreinforced case as higher energy was required to compensate the geocell-wall-interruption. Relative density (D_r) of sand was maintained as 80% ($\gamma_d = 15.83$ kN/m^3) throughout the experimental program.

6.2.3 Geocell

The geocell-mattresses were prepared with geogrid strips, cut from a full roll into required dimensions, and assembled in chevron pattern using 'bodkin' joints (Simac 1990; Caroll and Curtis 1990; Biswas et al. 2015). The HDPE geogrid, with 38 × 38 mm aperture size, was having tensile strength of 20 kN/m at 11% of axial strain. The bodkin-dowels were 3 mm thick and 6 mm wide plastic strips, made of low-density polypropylene. Maximum tensile strength of the bodkin joints used was found to be 3.3 kN/m at axial strain of 9%. To prepare the geocell-mattress, the transverse and longitudinal geogrid members were cut from a long roll and assembled in 'chevron' pattern using 'bodkin' joints (Fig. 6.4).

6.2.4 Test Setup

The test setup for the experimental program is shown in Fig. 6.5. Foundation beds were prepared in a steel tank of 1 m × 1 m × 1 m in dimension. The tank walls were

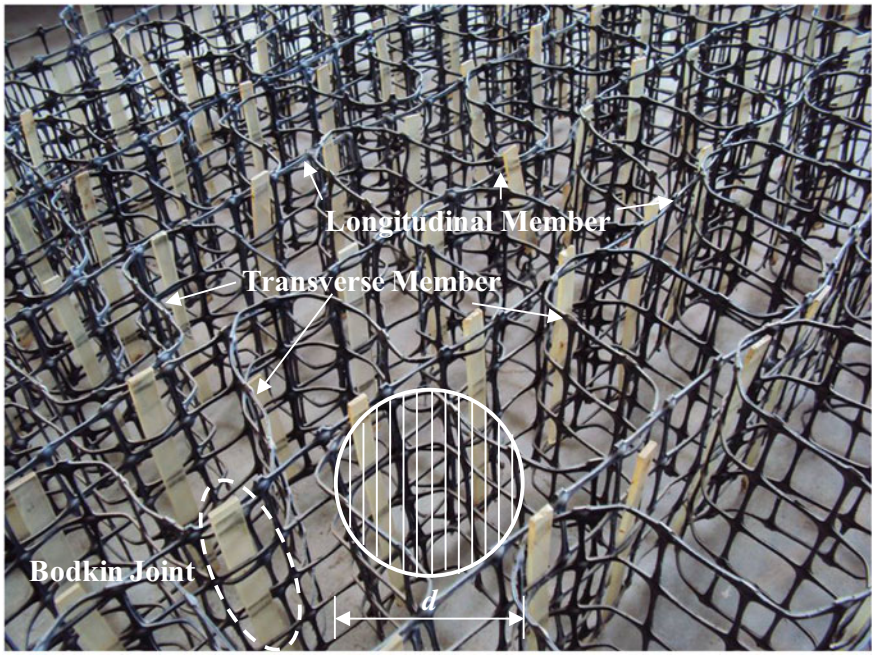

Fig. 6.4 Photograph of typical geocell-mattress in chevron pattern

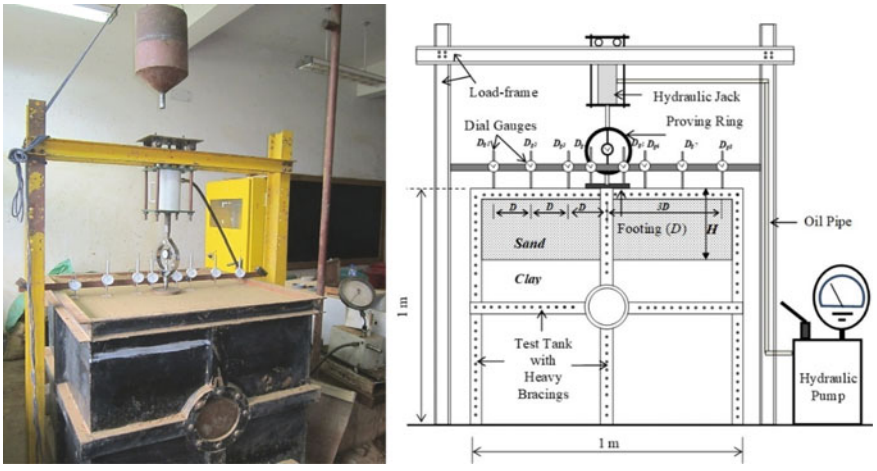

Fig. 6.5 Experimental setup (after Biswas et al. 2013)

well braced with heavy steel-sections (horizontally and vertically) to avoid lateral deformation, if any during testing. The test tank was provided with a loading frame for load application. The load was applied, by pushing the footing into the soil (at approximately 3 mm/min), through a hydraulic jack. The load applied was measured through a pre-calibrated proving ring, placed between hydraulic jack and footing. In order to ensure verticality of loading, a ball-bearing was positioned between proving ring and the footing. Responses of the model foundations were monitored at different loading stages by recording the deformations (heave or settlement) at different locations on the foundation surface through eight dial gauges (D_{g1} to D_{g8} shown in Fig. 6.5) of 0.01 mm accuracy. Two dial gauges (D_{g4} and D_{g5}) were placed diagonally opposite on the footing, while the other six were placed on the soil surface, at distances of D, $2D$, and $3D$. The spindles of these dial gauges were rested over small plates of perspex sheet placed on the foundation surfaces. Observations were recorded at regular intervals of footing settlement (s) and continued till the failure of foundation or up to $s/D = 24\%$.

6.2.5 *Experimental Program*

Tests were conducted on different homogeneous and layered configurations (unreinforced and reinforced) of foundations having varying clay subgrades under circular footing, as listed in Table 6.2. Pressure-settlement behavior of homogeneous sand and clay of varying strength was studied in series A. Unreinforced layered foundations with different thickness of sand layer ($H/D = 0.63$, 1.15, 1.67 and 2.19) over the clay subgrades of varying strength ($c_u = 7$, 15, 30 and 60 kPa) were studied in series B. The response of geocell-reinforced foundations with different subgrades was examined in series C. In total, 37 model tests were performed under three different test series (Table 6.2). In the layered configurations, the subgrade strength (c_u) and layer thicknesses (H) were varied keeping other parameters constant at their optimum (Biswas and Krishna 2017a).

Table 6.2 Details of model tests

Test series	Foundation system	Test parameters	
		Constant	Variable
A	Homogeneous clay and sand bed	–	c_u: 7, 15, 30, 60 kPa (clay) D_r: 80% (sand)
B	Unreinforced sand over clay subgrade	D_r: 80%	c_u: 7, 15, 30, 60 kPa H/D: 0.63, 1.15,1.67, 2.19
C	Geocell-reinforced sand over clay subgrade	d/D: 0.8 u/D: 0.1 b/D: 6.67	c_u: 7, 15, 30, 60 kPa H/D: 0.63, 1.15,1.67, 2.19 (h/D: 0.53, 1.05, 1.57, 2.09)

6.3 Test Results

The results obtained are presented as bearing pressure-settlement responses and footing settlement vs surface deformation graphs. Parameters such as sand layer thickness (H), height (h), and width (b) of geocell-mattress, depth of sand cushion on top of geocell-mattress (u), and footing settlement (s) are normalized with respect to the footing diameter (D) and expressed as H/D, h/D, b/D, u/D, and s/D, respectively.

6.3.1 Bearing Pressure—Settlement Behavior

A typical comparison of pressure-settlement responses of unreinforced and geocell-reinforced foundation systems, for $c_u = 7$ kPa, is presented in Fig. 6.6. Higher bearing pressures at larger footing settlements can be noticed. The geocell-reinforced bearing pressure is increased from 77 to 119 kPa, for the footing settlement (s/D) variation from 12 to 24% (at $H = 0.63D$). In similar foundation configurations, the variation of bearing pressures for unreinforced foundations was from 45 to 56 kPa. This indicates considerably high improvement in pressure values, for geocell-reinforced foundation systems as compared to unreinforced cases. Besides, it is seen that this improvement was increased with increasing settlement levels.

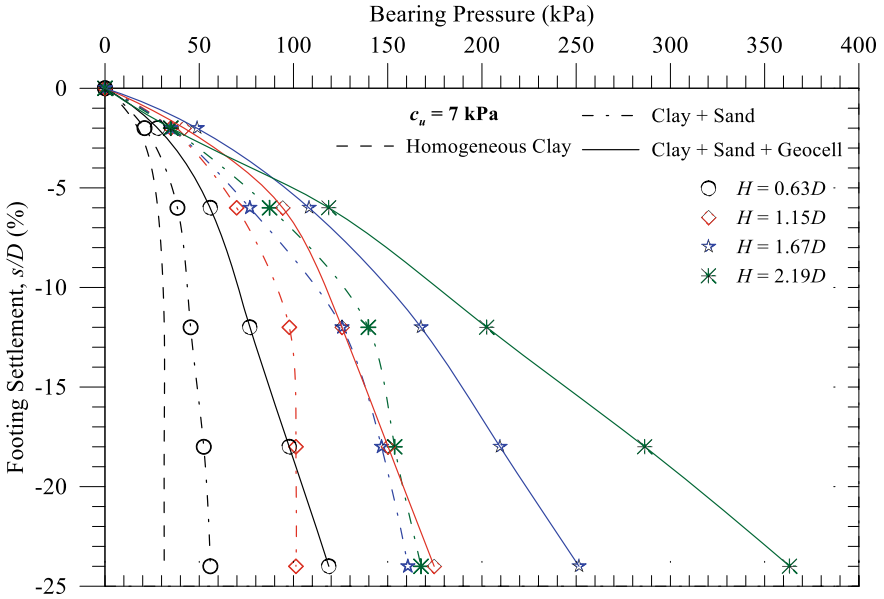

Fig. 6.6 Typical pressure-settlement responses for unreinforced and geocell-reinforced foundations (different H/D) with $c_u = 7$ kPa

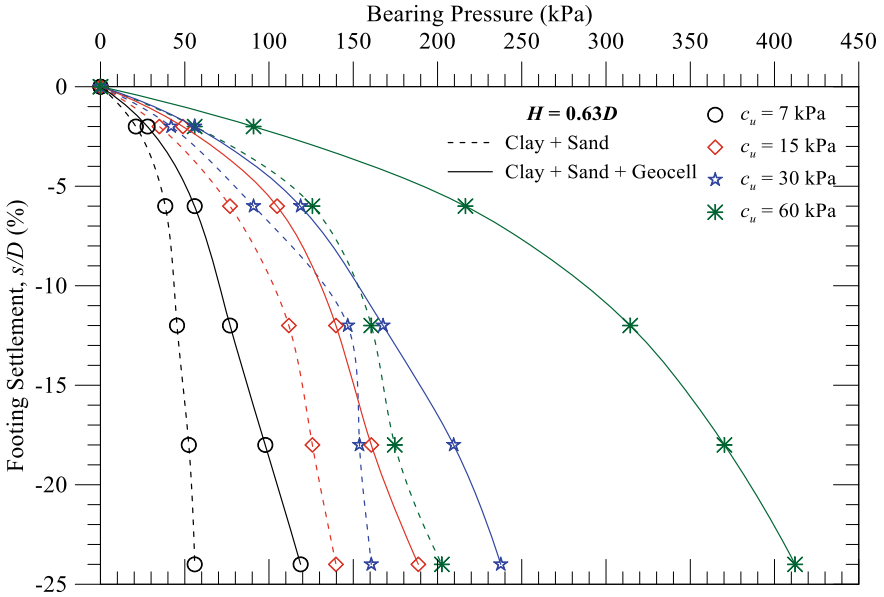

Fig. 6.7 Typical pressure-settlement responses for different clay subgrades with unreinforced and reinforced sand layer foundations with $H = 0.63D$ (after Biswas 2016)

The pressure-settlement responses showing the influence of subgrade strength on the performance of geocell-reinforced foundations (at $H = 0.63D$) are presented in Fig. 6.7. Substantial improvements, with higher bearing pressures for stiffer subgrades, can be noticed in the figure. The bearing pressures at $s/D = 24\%$ are 56, 140, 161, and 203 kPa for unreinforced layered systems having $c_u = 7$, 15, 30, and 60 kPa, while bearing pressures were increased to about 119, 189, 238, and 413 kPa, respectively, with geocell-reinforcement.

6.3.2 *Surface Deformation—Settlement Behavior*

A typical surface deformation profiles of homogeneous bed ($c_u = 15$ kPa) at different levels of footing settlements (s/D) are presented in Fig. 6.8. The distance from the footing center 'x' is expressed in non-dimensional form as x/D. The surface settlement and heave are differentiated with '−' and '+' signs, respectively. It can be noticed that the surface deformations were mostly pronounced around the footing center (at $x = D$); while it was reduced as the distances increased (at $x = 2D$ and $3D$).

A typical variation of surface deformation (δ/D) with footing settlement (s/D) is shown in Fig. 6.9, for different foundation systems overlying clay subgrade of 7 kPa (c_u) at $H = 0.63D$. It can be noticed that as compared to the unreinforced foundations, the geocell-reinforced system has shown higher settlement at $x = D$

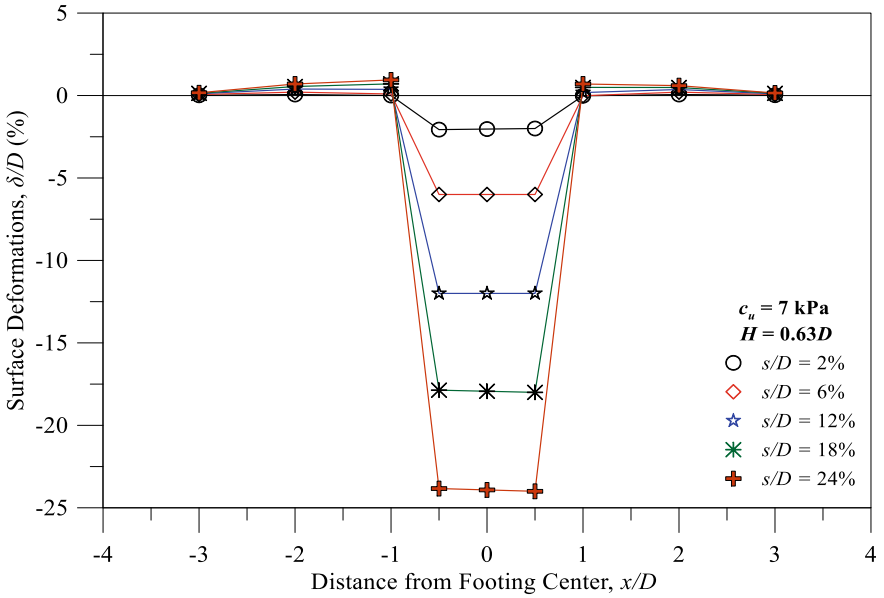

Fig. 6.8 Surface deformation profile at different *s/D* for $c_u = 15$ kPa

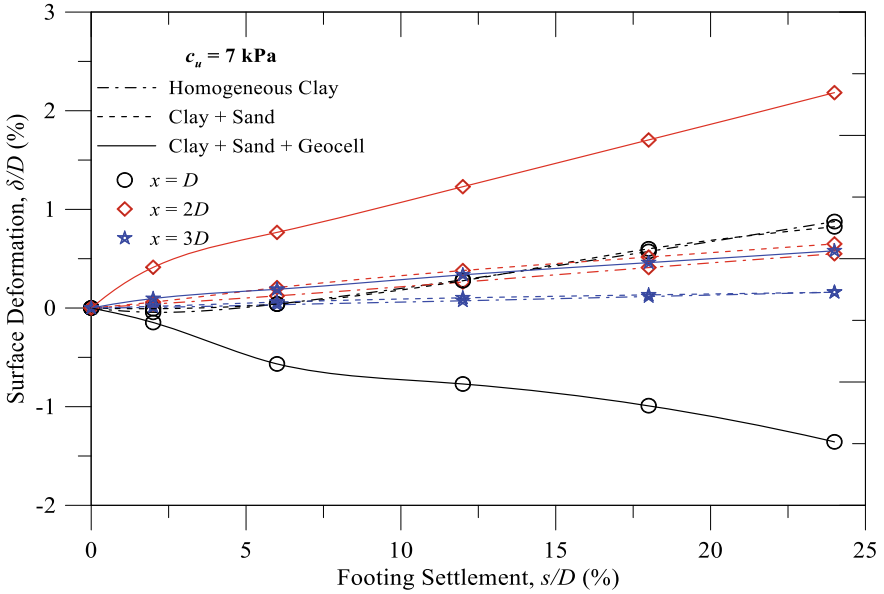

Fig. 6.9 Variation of δ/D with s/D at $x = D$, $2D$, and $3D$ for $c_u = 7$ kPa ($H = 0.63D$)

and more heaving at $x = 2D$ and $3D$. Such deformation profile is attributed to the deep beam action of geocell-mattress (Dash et al. 2003) which undergone sagging (causing settlement) around the footing center and hogging (causing heaving) away from the loading. However, the magnitude of deformations is dependent on thickness of geocell-mattress (h) and the strengths of the underlying subgrades (c_u).

Biswas et al. (2016) concluded that the sand layer thickness, $H = 1.15D$ has better performance among the performed four different sand layer thickness of $H/D = 0.63$, 1.15, 1.67, and 2.19. The geocell-reinforced layered foundation has higher bearing capacity with reduced settlement compared to the unreinforced layered foundation. The beneficial effect was attributed to reinforcing action namely pocket all round confinement provided by geocell due to its cellular structure (Dash et al. 2003) and the interface frictional resistance from adjacent cells (Pokharel et al. 2010; Biswas et al. 2016). Besides, stiffness of geocell plays vital role in providing the degree of improvement of reinforced layer (Bathurst and Rajagopal 1993).

6.4 Interpretations of the Test Results

The test results obtained are analyzed and discussed in terms of the interpreted values, as foundation reaction modulus, improvement factor, and percentage reduction in settlement values for different foundation configurations.

6.4.1 Foundation Reaction Modulus, $\mathbf{k}_f$

The foundation reaction modulus (k_f) is the secant modulus of the foundation system corresponding to a given settlement (slope of the line joining the origin to any point on pressure-settlement curve at the given settlement level). k_f values for model foundations with different configurations at different settlement levels were evaluated and presented herein.

Figure 6.10 presents the variation of k_f values with footing settlement (s/D) for different subgrades (c_u) and different foundation configurations (for $H = 1.15D$). In general, the figure indicates that k_f values decrease nonlinearly with increase in settlement levels for unreinforced foundations. A steep decrease of k_f in between 2 and 6% of s/D is followed by gradual reduction till the maximum level of settlements ($s/D = 24\%$). This behavior can be related to the surface deformation behavior of the foundation system. Biswas and Krishna (2017b) reported negligible surface deformation at initial settlement levels ($s/D < 6\%$) and from thereon the surface deformations increased with footing load till the end of test. However, in the case of reinforced foundations, the introduction of geocell-reinforcement enhanced the reaction modulus values significantly in comparison with the corresponding values for unreinforced (homogeneous and layered) foundations as shown in Fig. 6.10. For geocell-reinforced systems, the reduction in k_f with s/D is fairly linear. In this case,

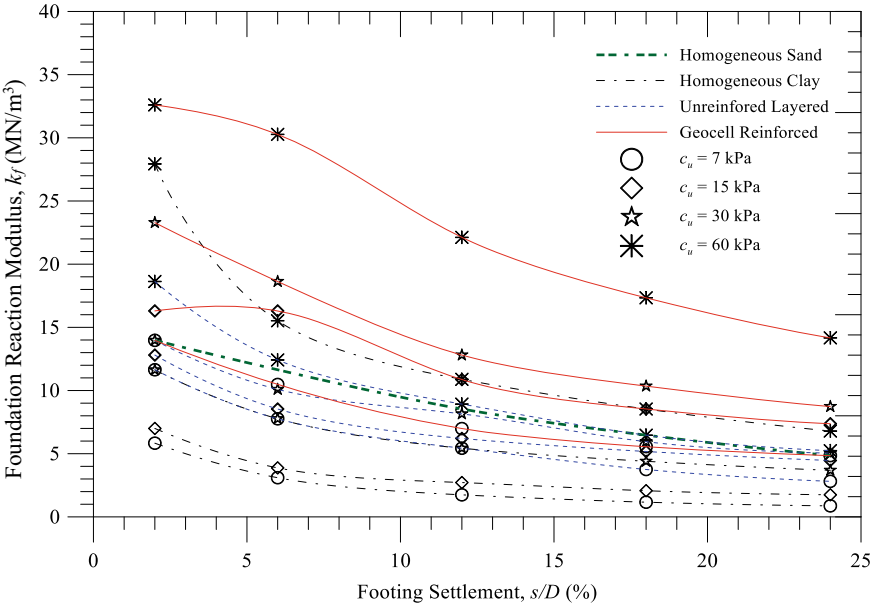

Fig. 6.10 Variation of k_f values with footing settlement (s/D) for different subgrades (c_u) and foundation configurations (with $H = 1.15D$)

geocell-pockets completely arrest the shearing of sand from footing bottom and cut the potential failure planes to force it deeper into the foundation beds making the geocell-sand bed as an elastic coherent layer. Besides, as reported by Biswas et al. (2013), the deformations at foundation surfaces also satisfy the confinement effect indicating significant reduction in surface heaving. Figure 6.11 shows the variation of k_f values with subgrade strengths (c_u) for different foundation configurations at different settlement levels ($s/D = 2$, 6 and 12%). It is to be noticed that the foundation reaction modulus increases for subgrade strength for any settlement level (s/D). In general, higher k_f values are found for superior foundation configurations, i.e., geocell-reinforced > unreinforced layered > homogeneous clay.

6.4.2 *Improvement Factor,* $\mathbf{I}_f$

The ratio of bearing pressure of layered foundation to that of homogeneous clay bed foundation, at similar level of footing settlement, is defined as improvement factor (I_f). Three improvement factors, I_{fs} (Eq. 6.1), I_{fsgc} (Eq. 6.2), and I_{fgs} (Eq. 6.3), to represent the improvement of the geocell-reinforced foundation with respect to homogeneous clay and unreinforced layered foundation, are evaluated (refer Fig. 6.12) for different foundations at different settlement levels. The improvement factors evaluated for different foundation configurations are summarized in Table 6.3.

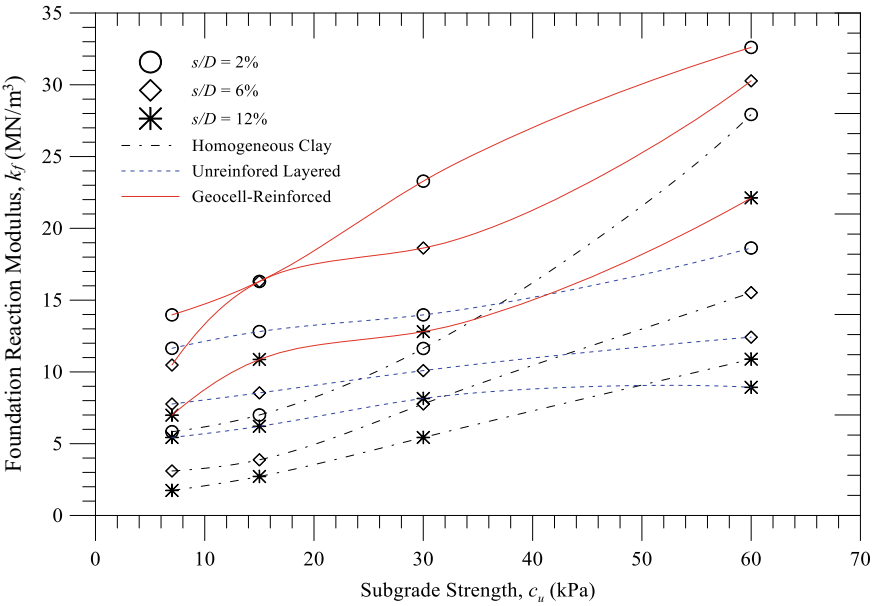

Fig. 6.11 Variation of k_f values with subgrade strength at s/D = 2, 6 and 12% for different foundation configurations (with $H = 1.15D$)

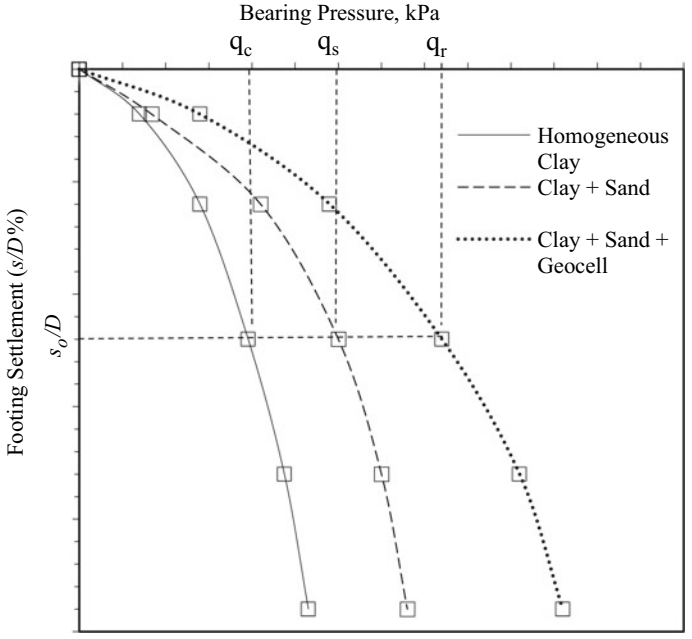

Fig. 6.12 Definition sketch of calculation of improvement factors

Table 6.3 Summary of bearing pressure improvement factors

s/D (%)	H/D	Bearing pressure improvement factor							
		$c_u = 7$ kPa		$c_u = 15$ kPa		$c_u = 30$ kPa		$c_u = 60$ kPa	
		I_{fsgc}	I_{fgc}	I_{fsgc}	I_{fgc}	I_{fsgc}	I_{fgc}	I_{fsgc}	I_{fgc}
2	0.63	1.60	1.33	2.33	1.40	1.60	1.33	1.08	1.63
	1.15	2.40	1.20	2.33	1.27	2.00	1.67	1.17	1.75
	1.17	2.79	1.40	2.66	1.45	2.20	1.22	1.00	1.71
	2.19	2.00	1.00	2.33	1.75	1.40	1.00	1.00	1.71
6	0.63	2.00	1.45	3.00	1.36	1.70	1.31	1.55	1.72
	1.15	3.38	1.35	4.20	1.91	2.40	1.85	1.95	2.44
	1.17	3.88	1.41	4.00	1.54	2.20	1.00	1.10	1.38
	2.19	4.26	1.36	3.60	1.64	1.90	1.00	1.45	1.81
12	0.63	2.45	1.69	2.86	1.25	1.71	1.14	1.60	1.96
	1.15	4.00	1.29	4.00	1.75	2.36	1.57	2.03	2.48
	1.17	5.34	1.33	4.29	1.50	2.36	1.03	1.35	1.65
	2.19	6.45	1.45	4.29	1.76	2.14	1.11	1.78	2.17
18	0.63	3.11	1.87	2.87	1.28	1.76	1.36	1.61	2.12
	1.15	4.78	1.48	4.12	1.65	2.35	1.74	2.03	2.68
	1.17	6.67	1.43	4.87	1.70	2.47	1.24	1.70	2.24
	2.19	9.12	1.86	5.50	2.00	2.47	1.40	2.00	2.64
24	0.63	3.78	2.13	3.00	1.35	1.79	1.48	1.69	2.03
	1.15	5.56	1.72	4.22	1.65	2.37	1.73	2.09	2.70
	1.17	8.01	1.57	5.33	1.92	2.68	1.65	2.20	2.85
	2.19	11.57	2.17	6.00	2.25	3.00	1.84	2.29	2.96

$$I_{fs} = \frac{\text{Bearing pressure of unreinforced layered foundations at } \frac{s_o}{D} (= q_s)}{\text{Bearing pressure of homogeneous clay beds at } \frac{s_o}{D} (= q_c)}. \quad (6.1)$$

$$I_{fsgc} = \frac{\text{Bearing pressure of geocell} - \text{reinforced foundations at } \frac{s_o}{D} (= q_r)}{\text{Bearing pressure of homogeneous clay beds at } \frac{s_o}{D} (= q_c)} \quad (6.2)$$

$$I_{fgc} = \frac{\text{Bearing pressure of geocell} - \text{reinforced foundations at } \frac{s_o}{D} (= q_r)}{\text{Bearing pressure of unreinforced layered foundations at } \frac{s_o}{D} (= q_s)} \quad (6.3)$$

Variations of improvement factors, I_{fsgc}, with footing settlement, for different layered configurations on very soft clay subgrade ($c_u = 7$ kPa), are presented in Fig. 6.13. The figure also shows the improvement factors, I_{fs}, obtained for the unreinforced layered configurations. It can be observed that the improvement factors, I_{fsgc} and I_{fs}, are increased with increasing footing settlement. Variation of I_{fsgc} as 3.38–5.56 can be noted with footing settlement (*s/D*) in the range of 6–24%, for $c_u = 7$ kPa at $H = 1.15D$, while the corresponding variation in I_{fs} is 1.35–1.72. A

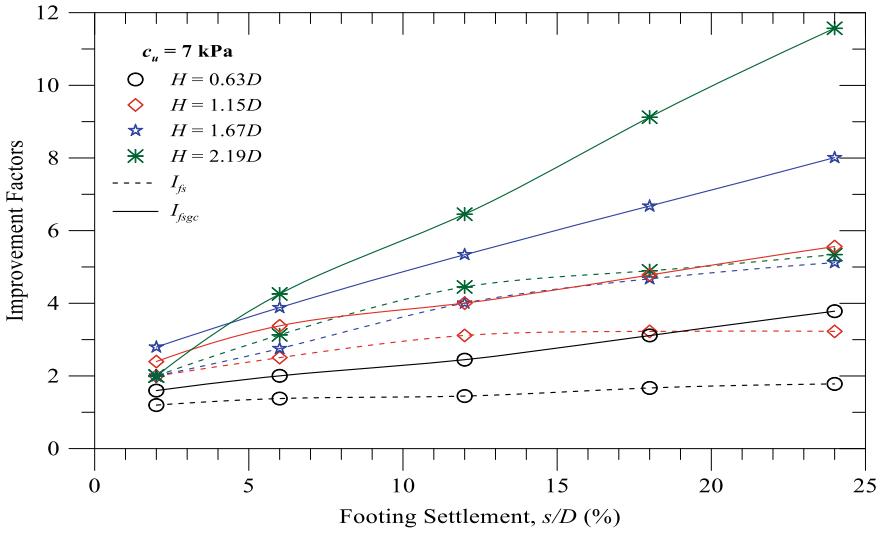

Fig. 6.13 Variation of I_{fs} and I_{fsgc} with s/D for $c_u = 7$ kPa

very high improvement factor of 11.6 is observed for $c_u = 7$ kPa, for the thickest geocell-mattress of $h = 2.09D$ ($H = 2.19D$), at the largest settlement level tested ($s/D = 24\%$). This higher improvement in bearing pressure responses is contributed by the geocell-reinforcement.

Variations of I_{fgc} with footing settlement for different subgrades ($c_u = 7$, 15, 30, and 60 kPa) are presented in Fig. 6.14, for two different layer thicknesses, such as $H = 0.63D$ and $1.15D$. It can be noticed that the variation of I_{fgc}, in Fig. 6.14, is not very consistent for all subgrades and for the layer thickness variations. However, in most of the cases, it was found increasing with settlement, showing more geocell contribution at higher strain.

Variations in improvement factors (I_{fs} and I_{fsgc}) for different subgrades (c_u) with varying layer thicknesses (H/D) are presented in Fig. 6.15 (at 12% of s/D). It is observed that the improvement factors are decreased with the increase in subgrade strength. At $H = 2.19D$, the improvement factor I_{fs} (dotted lines) is varied from 4.45 to 0.82 as the subgrade strength (c_u) increased from 7 to 60 kPa, while with geocell-reinforcement in similar condition, the I_{fsgc} variation is 6.45–1.78. However, at $H = 0.63D$, for both the foundation systems, the improvement factors (I_{fs} and I_{fsgc}) were greater for the subgrade having $c_u = 15$ kPa. The improvement factor, I_{fs}, was found as 2.29 compared to 1.45 (for $c_u = 7$ kPa), 1.5 (for $c_u = 30$ kPa), and 0.82 (for $c_u = 60$ kPa). Similarly, for 15 kPa, the I_{fsgc} was 2.86 compared to 2.45, 1.71, and 1.60, for $c_u = 7$, 30, and 60 kPa, respectively. Due to the inclusion of geocell-reinforcements, the shearing of sand layer was arrested, and geocell-sand layer behaved like semi-rigid slab to increase the overall bearing capacity higher than the unreinforced layer configuration (even higher that the corresponding homogenous clay responses).

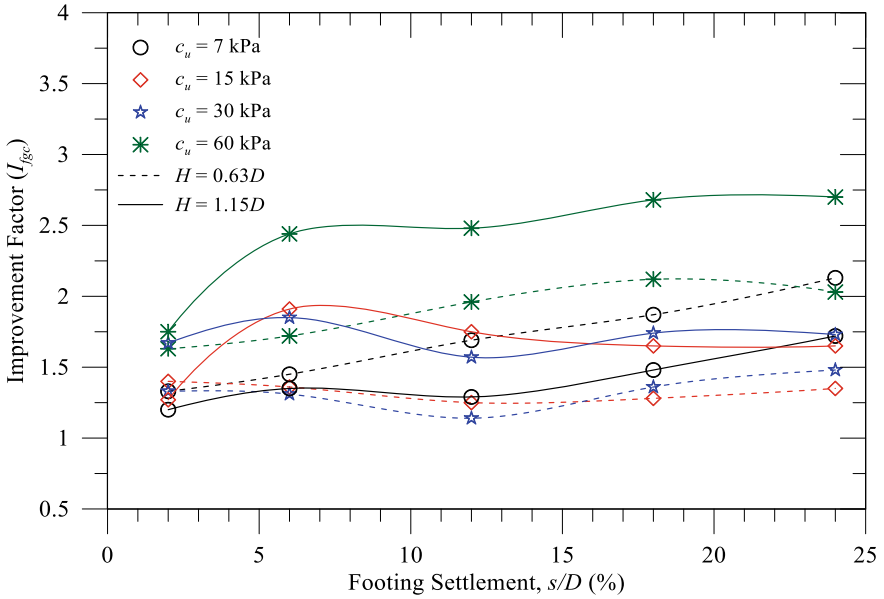

Fig. 6.14 Variation of I_{fgc} with s/D for different c_{u} at $H = 0.63$ and $1.15D$

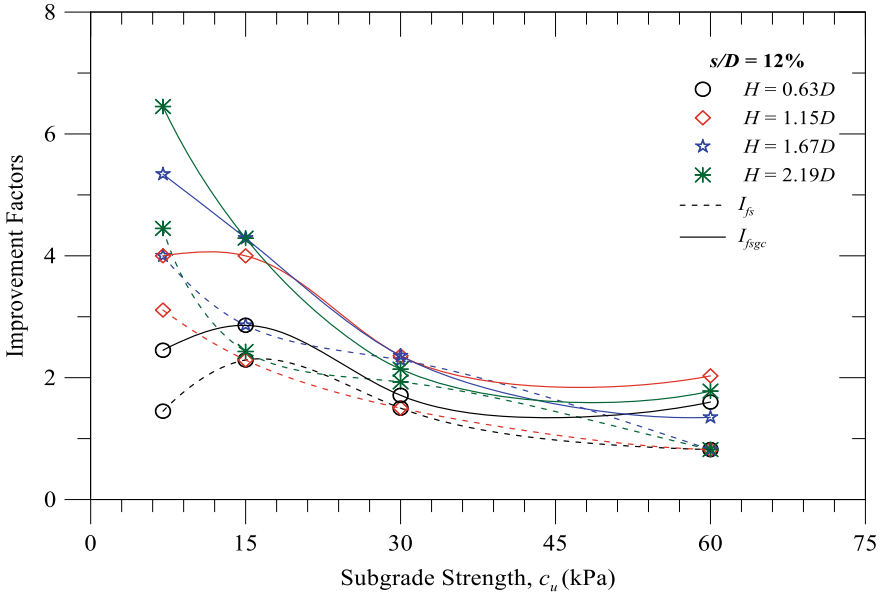

Fig. 6.15 Variation of I_{fs} and I_{fsgc} with c_{u} for different H/D at $s/D = 12\%$

6.4.3 Percentage Reduction in Settlement, PRS

The performance of geocell-reinforced foundations over clay beds of varying subgrade strength is also quantified with respect to reduction in footing settlements using a non-dimensional parameter described as "percentage reduction in settlement" (Sitharam et al. 2007). Referring Fig. 6.16, if s_o be the settlement of homogeneous beds and s_r be the settlement of geocell-reinforced foundation at a given pressure value q_o (corresponding to $s_o = 2, 6, 12, 18$, and 24% of D), the percentage reduction in settlements (*PRS)* can be expressed as Eq. 6.4.

$$\text{PRS} = \frac{s_o - s_r}{s_o} \times 100\% \tag{6.4}$$

Figure 6.17 shows the variation in *PRS* with respect to subgrade clay strength (c_u) for different settlement levels (*s/D*%). In general, the figure shows a trend of increase in *PRS* value with increase in *s/D* (%). The behavior indicates that the beneficial effect of geocell-reinforcements (confinement, interfacial resistance, and acting as semi-rigid slab) increases with increase in footing settlement. However, the trend for variation in *PRS* with respect to subgrade strength (c_u) is opposite as seen

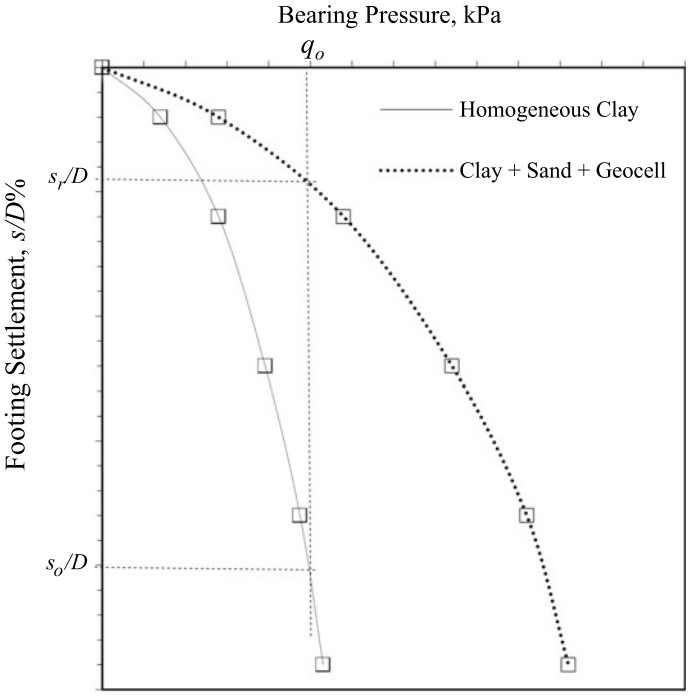

Fig. 6.16 Definition sketch for calculation of *PRS*

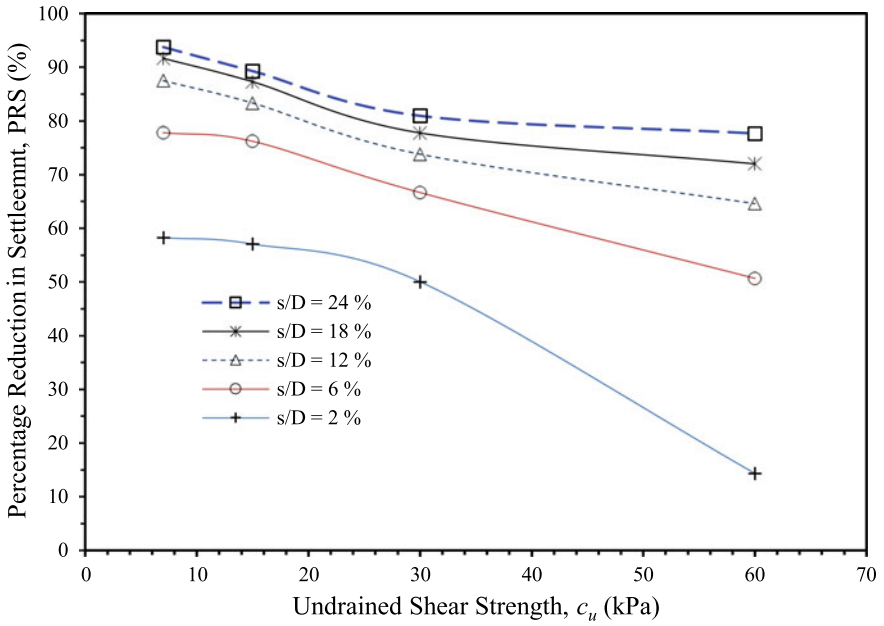

Fig. 6.17 Variation of *PRS* for different c_u at $H = 1.15D$

in case of *s/D* (%). The variation in *PRS* is decreased nonlinearly with increase in c_u. Though the settlements are significantly reduced even for higher subgrade strength soils, for lower subgrade strength soils, the reduction is more. For example, PRS values for c_u of 7 kPa ranged in between 60 and 95% for different settlement levels. The corresponding PRS values for c_u of 60 kPa are in the range of 15–80%.

6.5 Conclusion

This article reported observations from physical model tests carried out on model circular footing resting on foundation beds of different configurations having clay subgrades of varying strengths underneath. The responses obtained clearly indicated that the subgrade strength, irrespective of presence of reinforcement, largely influences the foundation behavior. The unreinforced sand layer favors softer clay subgrades ($c_u \leq 30$ kPa), while it affected negatively on stiff clay of 60 kPa. In the case of reinforced foundations, the introduction of geocell-reinforcement enhanced the reaction modulus (k_f) values significantly in comparison with corresponding values for unreinforced (homogeneous and layered) foundations. k_f values decrease with increase in settlement levels. For a given settlement level, k_f increased with increase in subgrade strength, indicating higher performance for clay subgrade with higher strength.

The reinforcements have positive impact on all clay subgrades; however, the degree of improvement, with reference to native subgrade soil capacity, reduced with increase in undrained strength of clay. The degree of improvement, both in terms of strength (I_{fsgc} or I_{fgc}) and settlement (*PRS*), with respect to homogeneous clay is considerably high in case of foundation with soft clay ($c_u = 7$ kPa), while it was reduced with increase in subgrade strength. Though the settlements are significantly reduced even for higher subgrade strength soils, for lower subgrade strength soils, the reduction is more. Thus, depending on the observations, it is concluded that the use of geocell and/or layers of compacted unreinforced soil (sand) must be in accordance to native subgrade strength. The degree of improvement expected to be achieved (both in terms of increase in bearing pressure and reduction in settlement) from reinforcement shall be evaluated according to the subgrade shear strength.

References

Akinmusuru JO, Akinbolade JA (1981) Stability of loaded footings on reinforced soil. J Geotech Eng Div, ASCE 107(6):819–827

Bathurst RJ, Rajagopal K (1993) Large scale triaxial compression testing of geocell reinforced granular soil. Geotech Test J, GTJODJ 16(3):296–303

Binquet J, Lee KL (1975) Bearing capacity tests on reinforced earth slabs. J Geotech Eng Div, ASCE 101(12):1241–1255

Biswas A, Krishna AM, Dash SK (2016) Behavior of geosynthetic reinforced soil foundation systems of different configurations over a stiff clay subgrade. Int J Geomech ASCE. https://doi.org/10.1061/(ASCE)GM.1943-5622.0000559

Biswas A (2016) Influence of subsoil strength on performance of geosynthetic-reinforced foundations. Ph.D. Thesis, IIT Guwahati, India

Biswas A, Krishna AM (2017a) Behaviour of circular footing resting on layered foundation: sand overlying clay of varying strengths. Int J Geotech Eng. https://doi.org/10.1080/19386362.2017.1314242

Biswas A, Krishna AM (2017b) Geocell-reinforced foundation systems: a critical review. Int J Geosynthetics Gr Eng, Springer. https://doi.org/10.1007/s40891-017-0093-7

Biswas A, Dash SK, Krishna AM (2013) Parameters influencing the performance of geocell-reinforced foundation system: a brief review. In: Proceedings of Indian geotechnical conference, IIT Delhi, vol 1, pp 365–368

Biswas A, Ansari MA, Dash SK, Krishna AM (2015) Behavior of geogrid reinforced foundation systems supported on clay subgrades of different strengths. Int J Geosynthetics Gr Eng, Springer 1(3):1–10

Caroll RG, Curtis VC (1990) Geogrid connections. Geotext Geomembr 9(4–6):515–530

Dash SK, Sireesh S, Sitharam TG (2003) Behaviour of geocell reinforced sand beds under circular footing. Gr Improv 7(3):111–115

Fragaszy RJ, Lawton E (1984) Bearing capacity of reinforced sand subgrades. J Geotech Eng Div, ASCE 110(10):1500–1507

Khing KH, Das BM, Puri VK, Yen SC, Cook EE (1994) Foundation on strong sand underlain by weak clay with geogrid at the interface. Geotext Geomembr 13(3):199–206

Mandal JN, Sah HS (1992) Bearing capacity tests on geogrid-reinforced clay. Geotext Geomembr 11(3):327–333

Pokharel SK, Han J, Leshchinsky D, Parsons RL, Halahmi I (2010) Investigation of factors influencing behaviour of single geocell-reinforced bases under static loading. Geotext Geomembr 28(6):570–578

Rajagopal K, Krishnaswamy NR, Madhavi Latha G (1999) Behaviour of sand confined with single and multiple geocells. Geotext Geomembr 17(3):171–184

Simac MR (1990) Connections for geogrid systems. Geotext Geomembr 9(4):537–546

Sitharam GT, Sireesh S, Dash SK (2007) Performance of surface footing on geocell-reinforced soft clay beds. Geotech Geol Eng 25:509–524

Sitharam TG, Sireesh S (2004) Model studies of embedded circular footing on geogrid reinforced sand beds. Gr Improv 8(2):69–75

Webster SL, Watkins JE (1977) Investigation of construction techniques for tactical bridge approach roads across soft ground. Technical Report S-77-1, United State Army Corps of Engineers, Waterway Experiment Station, Mississippi, USA

Yang X, Han J, Parsons RL, Leshchinsky D (2010) Three-dimensional numerical modelling of single geocell-reinforced sand. Front Archit Civ Eng China 4(2):233–240

Chapter 7
Interference Effect of Footings on Geocell and Geogrid-Reinforced Clay Beds

Prof. T. G. Sitharam and Akash Gupta

Abstract When two footings are placed close enough to each other, they interfere with each other and the soil beneath the footings behaves differently than it would when the footing was isolated. Interference effect causes the soil region between the interfering footings to undergo some sort of confinement due to which the bearing capacity of the soil increases. In this paper, the authors have illustrated how the soil would behave due to interference in clay bed and compared that with clay bed reinforced with geocell confinement. For this, model test experiments were conducted on geocell reinforced clay bed. Three-dimensional numerical simulations using FLAC 3D were run to study parametric study after validating with experimental results. Modified Cam Clay model was used to simulate the behavior of clay bed. Mohr–Coulomb model was used to simulate the behavior of the infill material (i.e., coarse sand). To model the actual shape of the geocell used, the unique and actual curvature of geocell pockets is considered and a realistic approach of modeling is proposed. The optimum spacing (S) between the footings was found to be 0.5 times the width of footing (B) for both unreinforced and geocell reinforced clay beds where bearing capacity is maximum. The maximum interference factor of 1.15 is observed in unreinforced clay. Interference effect is more in geocell reinforced clay than in geogrid-reinforced clay. Maximum interference factor of 1.33 is observed in the case of geocell + geogrid-reinforced clay beds. When the clay was reinforced with geocell and basal geogrid, there was dramatic reduction in the depth of stress distribution, and major stress was accumulated in the geocell membrane preventing the stress distribution to the deeper level.

Keywords Geocells · Geogrid · Footing · Interference effect · Clay bed · FLAC

A. Gupta
Department of Civil Engineering, Indian Institute of Science, Bangalore 560012, India
e-mail: gakash@iisc.ac.in

Prof. T. G. Sitharam (✉)
Department of Civil Engineering, Indian Institute of Technology Guwahati (IITG), Surjyamukhi Road, North, Amingaon, Guwahati, Assam 781039, India
e-mail: sitharam@iisc.ac.in

T. G. Sitharam et al. (eds.), *Geocells*, Springer Transactions in Civil and Environmental Engineering,
https://doi.org/10.1007/978-981-15-6095-8_7

7.1 Introduction

Due to the lack of suitable construction sites, we are forced to place the footings at close spacing, and interference of footings is inevitable in many construction sites which results in changing the ultimate bearing capacity, the settlement behavior, and the tilt based on the considered spacing. Study of interference could be traced back to the early 1960s were Stuart (1962) firstly started to study the effect of interference of strip footings theoretically. Graham et al. (1984) reported that during interference, pre-failure settlements become larger and ductile behavior is observed at post-failure. In their study, Graham et al. had used the method of characteristics and calculated bearing capacity of parallel strip footings. They also conducted experiments on three parallel strip footings with various spacing on two kinds of sands. Kumar and Ghosh (2007) studied interference on two closely spaced strip footings with the help of upper bound limit analysis and calculated bearing capacities and found that their values were generally lower than that of Stuart's theoretical study. Saran and Agarwal (1974) with laboratory tests illustrated interference effect of two closely placed strip footings on sand. Das and Larbi-Cherif (1983) also conducted laboratory tests to study the effect of interference on two adjacent strip footings on sand. Their results found that practical efficiencies were lower than those found by theoretical analysis of Stuart (1962).

Hazell (2004) studied interference effect on adjacent strip footings on loose and dense sand. Kumar and Bhoi (2009) conducted a series of small scale laboratory model tests to study interference on multiple strip footings on sand. Kumar and Saran (2003) conducted a series of laboratory model tests to illustrate the effect of interference on geogrid-reinforced sand beds. Mabrouki et al. (2010) showed interference on closely spaced strip footings through numerical simulations using a finite difference code. Ghazavi and Lavasan (2008) illustrated in detail with finite-element modeling, the interference effect of square and strip footings on geogrid-reinforced sand and found higher efficiency of reinforcement on bearing capacity for interfering reinforced footings than that on an isolated reinforced.

Although considerable advancements in the study of interference effect on unreinforced sand and geogrid-reinforced sand have been made, a closure study that concerns the evaluation of interference effect of footings on geocell reinforced clay bed hasn't received any attention.

With an increase in demand for land for construction projects and recent advancements in research and application on geocell, this paper is important for the structures which deal with both closely spaced foundations and/or application of geogrid and geocell. The aim of this paper is to provide laboratory model tank test results on interfering effect of closely spaced square footings laid on (1) unreinforced clay bed (2) geogrid-reinforced clay bed (3) geocell reinforced clay bed and (4) geocell + geogrid-reinforced clay bed.

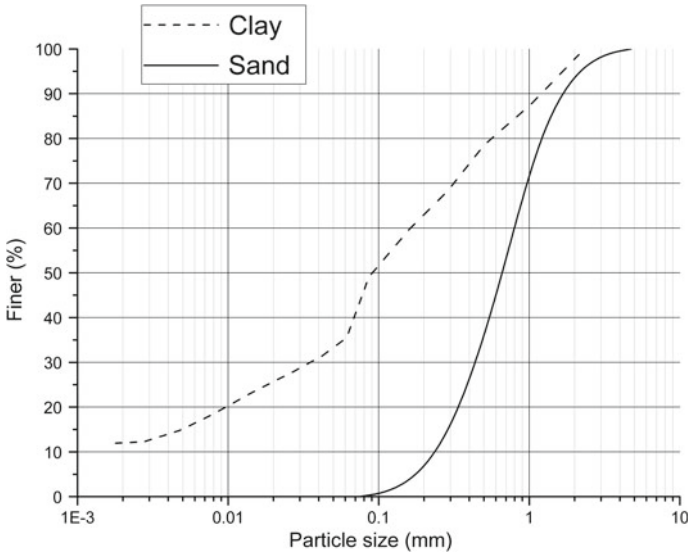

Fig. 7.1 Grain size distribution of the clay and sand (used as an infill in geocell)

7.2 Materials Used

7.2.1 Clay

Clay used in the study was collected from the north Bangalore region, Bangalore city. Figure 7.1 shows grain size distribution of the clay. As per Unified Classification system (ASTM D2487-11) the clay was classified as fine-grained soil. The properties of the clay are shown in Table 7.1.

7.2.2 Sand

Dry river sand was used as an infill material to fill geocell pockets. The properties of the sand used in summarized in Table 7.1 and the grain size distribution of the sand is presented in Fig. 7.1. The properties of sand used to fill geocell pockets are tabulated in Table 7.1.

Table 7.1 Properties of the clay and sand (used as an infill in geocell)

Clay		Sand	
Specific gravity, G	2.65	Specific gravity, G	2.65
Liquid limit (%)	41	Maximum void ratio, e_{max}	0.8
Plastic limit (%)	16	Minimum void ratio, e_{min}	0.5
Shrinkage limit (%)	14	Effective particle size D_{10} (mm)	0.27
Plastic index	25	D_{30} (mm)	0.46
Activity	1.53	D_{60} (mm)	0.8
Unified soil classification	Cl	C_u	2.96
Maximum dry density (kN/m^3)	18.4	C_c	0.98
Optimum moisture content (%)	13.5	IS classification	SP
Clay mineral	Kaolinite		
Coefficient of consolidation, C_v (m^2/year)	8.1		
	100		
Pre-consolidation pressure, p'_c (kPa)	0.5		
Compression index, C_c	0.2		
Swelling index, C_s	3.24×10^{-7}		
Coefficient of permeability, k (m/s)			

Table 7.2 Properties of the geocell and geogrid

Geocell		Geogrid	
Aspect ratio	0.6	Polymer	Polypropylene
Equivalent cell dia (mm)	220	Aperture size (MD × XMD)	35 × 35
No. of cells/m^2	40	(mm)	210
Cell depth (mm)	150	Secant modulus at 2% strain	20
Strip thickness (mm)	1.53	(kN/m)	220
Tensile strength (kN/m)	20	Ultimate tensile stress (kN/m)	Square
Cell seam strength (N)	2100(±)5%	Mass per unit area (g/m^2)	
Density (g/cm^3)	0.95(±)1.5%	Shape of aperture opening	

7.2.3 Geocell

In the study, clay bed is reinforced with Neoweb geocell. It is composed of polyolefin and thermoplastic engineering polymer which have high strength and durability. Some properties of the geocell material used in the investigation are shown in Table 7.2. The tensile strength of the geocell sample was 20 kN/m. Tensile stress-strain behavior of the Neoweb geocell used in the test is shown in Fig. 7.2. Photograph of the geocell used in the experiments is shown in Fig. 7.3.

7.2.4 Geogrid

A biaxial geogrid with commercial name SS-20 was used at the base of the geocell mattress for experimental investigation. Sample of geogrid used is shown in Fig. 7.3b.

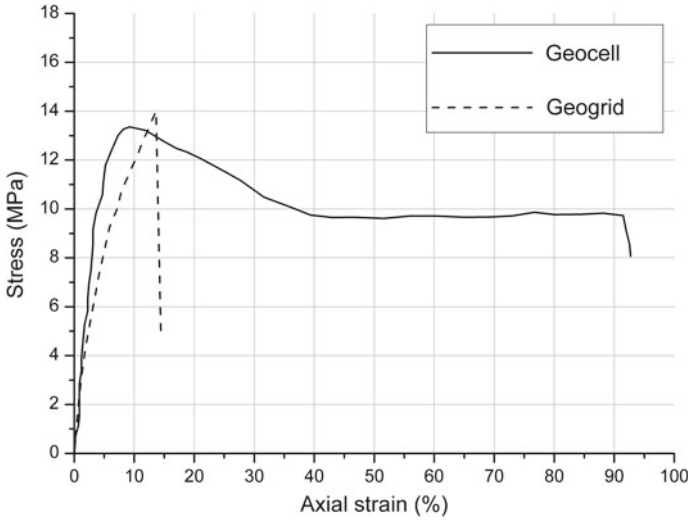

Fig. 7.2 Tensile stress-strain behavior of geocell and geogrid

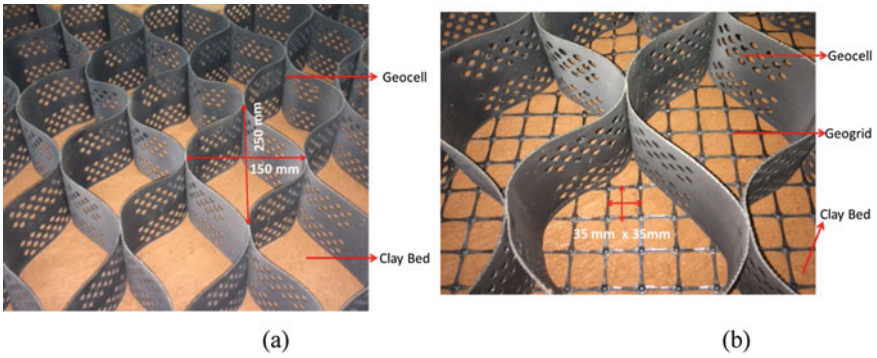

Fig. 7.3 Photograph of the reinforcements used in the experiments **a** geocell on the clay bed; **b** geocell + geogrid on the clay bed

The base material of the geogrid was made up of Polypropylene. Tensile load—axial strain characteristic behavior of a sample geogrid is plotted in Fig. 7.2. ASTM D-6637 was followed for multiple rib tensile tests on the geogrid sample and ultimate strength of the sample was found to be 20 kN/m^3 which corresponds to 13.33 MPa ultimate tensile stress. Table 7.2 represents the properties of the geogrid used in the experimental investigations.

7.3 Test Procedure

Four series of 1 g plate load tests in the model tank (A, B, C, and D) were conducted, where series A represents unreinforced clay bed; series B represents geocell reinforced clay bed; series C represents geogrid-reinforced clay bed and series D represents both geocell + geogrid-reinforced clay bed. In each series four experiments were conducted with varying spacing between the interfering footings of 0.5*B*, 1*B,* and 2*B* and one isolated footing, where *B* is width of the footing used in the experiments. Schematic diagram and photograph of the problem definition are shown in Fig. 7.4. The load is applied on the footing using a hydraulic jack supported against the loading frame as shown in Fig. 7.4b; reinforcement details are shown in Fig. 7.6. The loading frame was designed in such a way that there were no undesirable deflections on any element of the frame. The size of the tank was 0.9 m × 0.9 m × 0.6 m and footing size was 100 mm × 100 mm × 20 mm; to simulate the rough footings bottom of the footings are glued with coarse sand. In order to avoid the boundary effects due to wall of the tank, the size of the tank and the footings were in accordance with Selig and Mckee (1961) and Chunmar (1972). They found that failure wedge extends maximum to the distance 2–2.5*B* from an edge the footing and up to depth of 1.1*B*. For larger spacing between the footings, the distance between center of the footing and tank's edge was about 2.5*B*, width of the footing and the tank's height was 6*B*. Loads were applied simultaneously on both the footings. The loading was carried out through manually operated hydraulic jack until ultimate vertical displacement was achieved. The plate load test was in accordance with ASTM-D1196M (2012), for each increase in load, rate of settlement of the footing was maintained less than 0.03 mm/minute for three consecutive minutes. Linear Variable Differential Transducers (LVDTs) of 0.01% accuracy of 100 mm full range were used to measure the settlement of the footings. To measure the applied loads on the footings two load cells ±0.02% accuracy of 2 tonne capacity were used which were placed between the hydraulic jack and footing with ball bearing arrangement. Each plate load test took 30 man-hours on average.

7.3.1 Clay Bed Preparation

The clay was pulverized and then mixed with a predetermined quantity of water. The mixture was then placed in an airtight container for 72 h for uniform distribution of moisture and then the mixture was thoroughly kneaded. The soil was then uniformly compacted in layers of 25 mm to obtain the required height of the clay bed. Each and every step while making the clay bed was controlled carefully. In both test series B and D, coarse sand was used to fill geocell pockets as infill material and undrained shear strength of the clay bed was maintained equal to 10 kPa in test series C and D. In order to determine undrained shear strength of the clay bed, Swedish fall (Zreik et al. 1995) apparatus was used. The calibration chart was first prepared using the

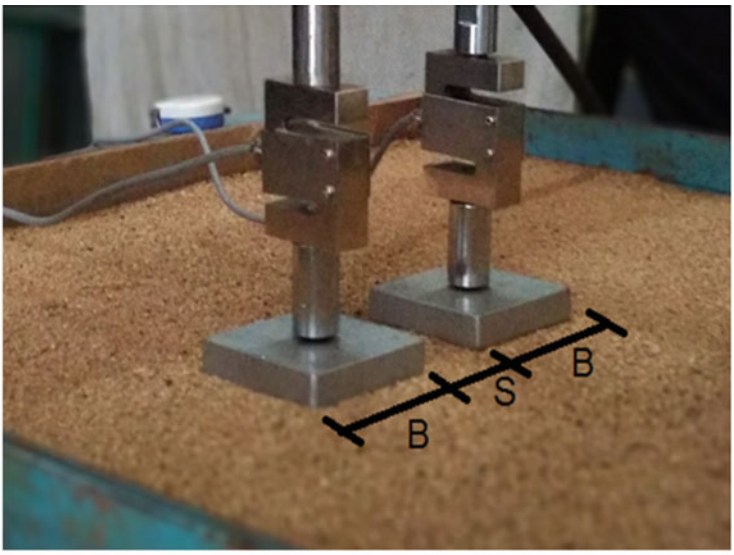

(a)

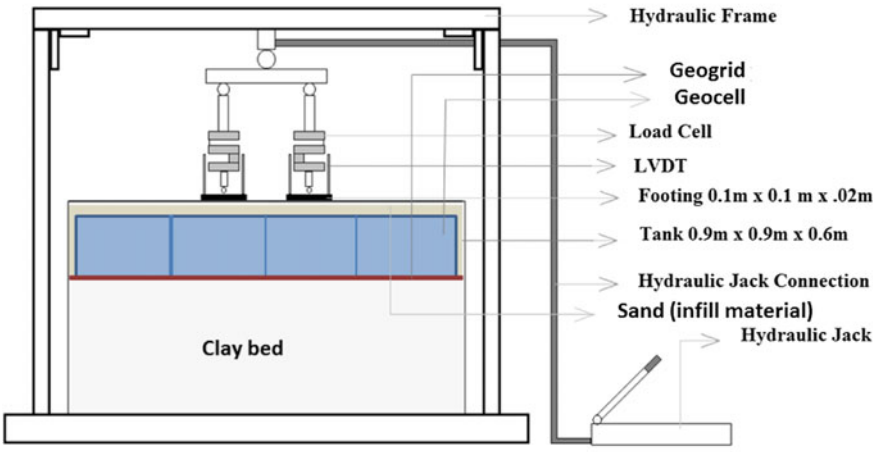

(b)

Fig. 7.4 Test setup and footing geometry **a** photograph; **b** schematic diagram

Swedish fall cone apparatus with undrained shear strength varying with moisture content along with bulk unit weight in the secondary *y*-axis. Required moisture content and bulk density of the clay bed were then traced back from the calibration chart corresponding to 10 kPa undrained shear strength as shown in Fig. 7.5. The clay was difficult to work with, however, with great precision and carefully controlling

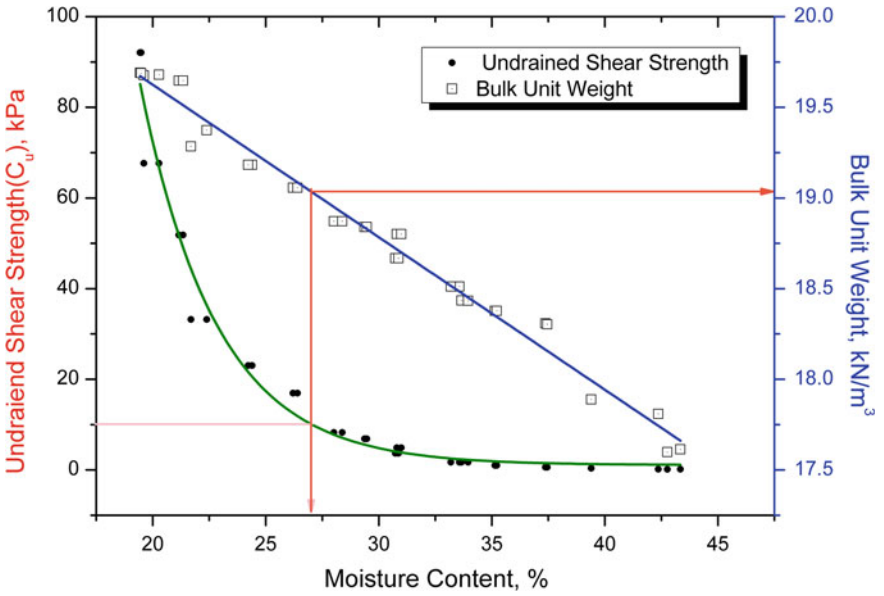

Fig. 7.5 Calibration curve: undrained shear strength versus moisture content

Table 7.3 Properties of the clay bed

Properties of clay bed	
Moisture content (%)	26
Bulk unit weight (kN/m^3)	19.05
Dry unit weight (kN/m^3)	15.12
Undrained shear strength (kPa)	10

compaction effort and meticulously maintaining water content of the test clay beds, a uniform test condition was maintained throughout the experimental investigations. Unit weight, degree of saturation, moisture content and undrained shear strength of the sample was determined from the undisturbed samples collected at various locations in the testbed. Each clay bed took approximately 24 man-hours to complete. Table 7.3 represents properties of clay bed maintained throughout the experimental investigation.

7.3.2 Details of Reinforcement

Clay bed was reinforced in three cases, (1) Geogrid, (2) Geocell, and (3) Geocell + geogrid. The geogrid was laid on the clay bed covering entire model tank area, geogrid was placed meticulously to ensure its placement was flat and horizontal;

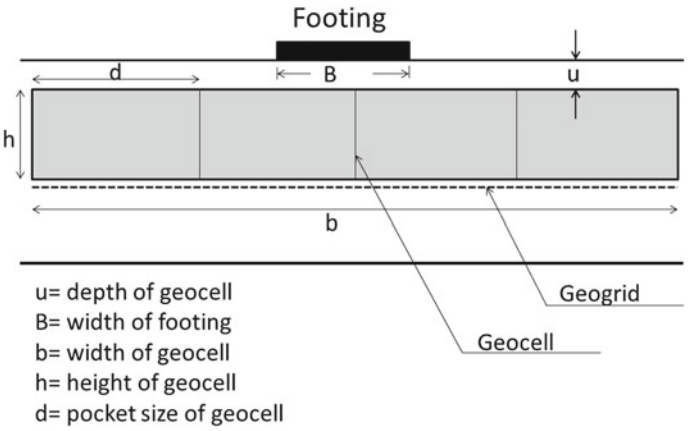

Fig. 7.6 Geometry of placement of reinforcement

many studies found that optimum depth of the placement of planar geogrid ranging from 0.3 to 0.37B (B = width of the footing) (Huang and Tatsuoka 1990; Omar et al. 1993); after the placement of geogrid, coarse sand was laid using sand raining technique ensuring desired unit relative density of 70%. To ensure uniformity in the sand layer, trial sand raining was done on an empty tank keeping density cups in three different regions in the tank. The preparation of geogrid-reinforced clay bed and the sand layer was highly controlled and maintained meticulously throughout the testing program.

Geocell reinforcement was placed for the full-width tank avoiding sides of the tank to avert the boundary condition by leaving small gaps between the tank wall and the reinforcement. Many researchers example (Dash et al. 2001) have concluded that the optimum depth of placement of geocell is 0.1B (u) hence in the present study geocell was placed at 0.1B. Coarse sand was used as infill material maintaining relative density as 70% in all the tests.

For reinforcing clay bed with both geogrid and geocell, geogrid was placed just beneath the geocell as shown in Fig. 7.6.

7.4 Numerical Studies

For the numerical investigation, FLAC 3D, finite difference code was used to simulate the interference of footings. FLAC 3D is explicit finite difference software used for soil and rock engineering problems and computations. FLAC 3D has is used to simulate soil material that undergoes plastic deformation, when soil yield after application of load. In the current study, three-dimensional simulations for clay model and footings in the test tanks were run to investigate the influence on interference and geometric variation of footings. Full-scale model with the size of model was 0.9 m

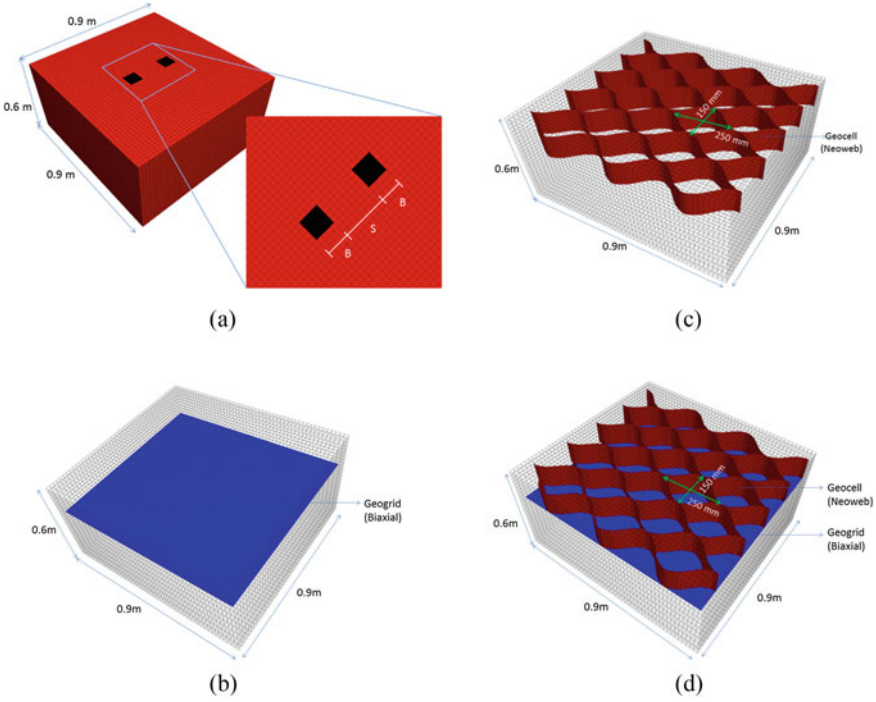

Fig. 7.7 Full-scale FLAC 3D numerical model showing **a** geometry of footings and spacing ($S/B = 1$); **b** geogrid-reinforced claybed; **c** geocell reinforced claybed; **d** geocell + geogrid-reinforced claybed

$\times$ 0.9 m $\times$ 0.6 m which was discretized into 56,400 zones. Each grid was 0.025 m in size. To create the zone, polyhedral '*brick*' an in-built element is chosen. Numerical model and geometry of footings are shown in Fig. 7.7. Dimension of square footing in the model is identical to that used in the experimental study, i.e. 100 mm. Sides of the model are constrained in horizontal direction and the bottom is constrained in all three directions. To simulate the rough footings, bottom nodes of the footings are constrained in horizontal direction. Modified Cam Clay model to simulate behavior of the clay bed, modified Cam Clay model was selected whereas; Mohr–Coulomb model was used to simulate the behavior of the infill material (i.e. coarse sand). To model the actual shape of the geocell used, an attempt was made considering actual curvature using FALC 3D. FLAC 3D uses various geomaterials and the support system. The geocell was modeled using structural element, *geogrid* in FLAC 3D, which exhibits a linear elastic model and uses joints and interface properties to accurately predict the behavior of the geocell and infill system. Interface properties between the wall of the geocell and the infill material (coarse sand) are presented in Table 7.4. Applied controlled velocity was in the current study is 2×10^{-7} m/step. The applied velocity progressively induces an increase in stress in the soil mass, at a

Table 7.4 Material model parameters for numerical modeling

Properties of clay	
Slope of NCL, λ	0.22
Slope of swelling line, k	0.09
Pre-consolidation pressure, p'_c	100
Friction constant, M Shear modulus, G (MPa) Specific volume at reference pressure, v_λ Unit weight, γ (kN/m^3)	0.68 1.38 1.78 20
Properties of geogrid	
Young's modulus, E (MPa) Poisson's ratio, μ Interface shear modulus, k_i (MPa/m) Interface cohesion, c_i (kPa) Interface friction, ϕ_i (°) Thickness, t_i (mm)	210 0.33 2.36 0 18 1.5
Properties of geocell	
Young's modulus, E (MPa) Poisson's ratio, μ Interface shear modulus, k_i (MPa/m) Interface cohesion, c_i (kPa) Interface friction, ϕ_i (°) Thickness, t_i (mm)	275 0.45 2.36 0 30 1.52

specific point large settlement is caused by no increase in stress; this stress is taken as ultimate bearing capacity. Each simulation took 48 h to complete on an average.

The Mohr–Coulomb criterion, characterized by two parameters (cohesion, c, and friction angle, φ). Modified Cam Clay yield function corresponding to a particular value of p_c of the consolidation pressure has the form

$$f(q, p) = q^2 + M^2 p(p - p_c)$$

where M is a material constant.

7.4.1 Selection of Model Parameters

Shear strength parameters ($\boldsymbol{c}$ and $\boldsymbol{\phi}$) were determined from undrained triaxial compression tests. Properties of the materials used for the numerical investigations are tabulated in Table 7.4. The stress levels in model tests are much smaller than the prototype footings. Since it is difficult to perform these laboratory triaxial tests under such low confining pressure, elastic moduli of soils adopted in the present numerical study were directly taken from the pressure-settlement response of plate load tests; this method was adopted by few researchers in the past working in similar areas

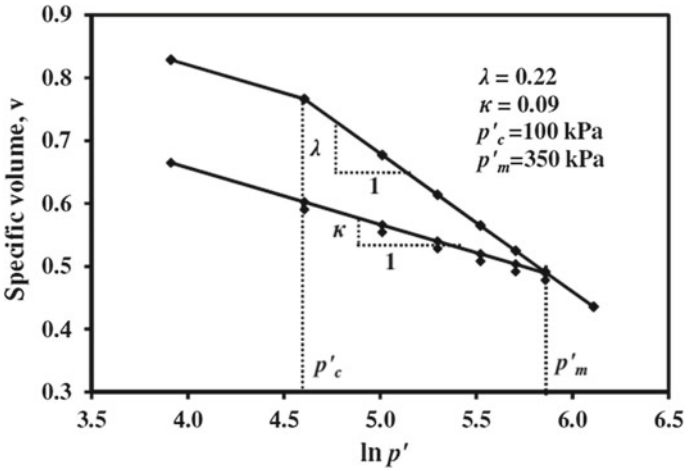

Fig. 7.8 Cam clay: v versus ln p'

(Gupta and Sitharam 2018; Latha and Somwanshi 2009). Assuming Poisson's ratio of sand to be 0.3, bulk modulus and shear modulus values were determined. Same clay as used by Hegde (2014) was used in the current study. Therefore, the Cam Clay parameters, viz. slope of the normal consolidation (λ), slope of the swelling line (k), and pre-consolidation pressure (p'_c), were taken from his study. Hegde (2014) conducted isotropic triaxial compression test that was conducted as shown in Fig. 7.8 to obtain the above values. The shear modulus of the clay bed was determined from the elastic modulus assuming the Poison's ratio as 0.5.

7.4.2 Three-Dimensional Modeling of Geocell Reinforcement

Many researchers attempted to attain actual shape of the geocell for example, (Han et al. 2008) ran series of simulations on FLAC 3D using single-cell geocell which actually was modeled as the square box as he faced modeling challenges in creating the actual shape of geocell. A similar square box technique was adopted by few researchers (Sireesh, 2005; Leshchinsky and Ling, 2013) in the following years until single-cell geocell was modeled by Yang et al. (2010). However, full-scale geocell considering its actual shape has not been reported by any researchers or the authors are not aware of such studies.

In the current study, geocell and geogrid reinforcement were modeled using '*Geogrid structural elements*' an in-built structure in FLAC 3D, that are three-nodded, flat finite elements that are assigned a finite-element type that resists membrane but does not resist bending loading. '*Geogrid structural elements*' behaves as an isotropic or orthotropic, linearly elastic materials with no failure limit (Itasca, 2008). In this study, firstly actual geometry and coordinates of the geocell curvature

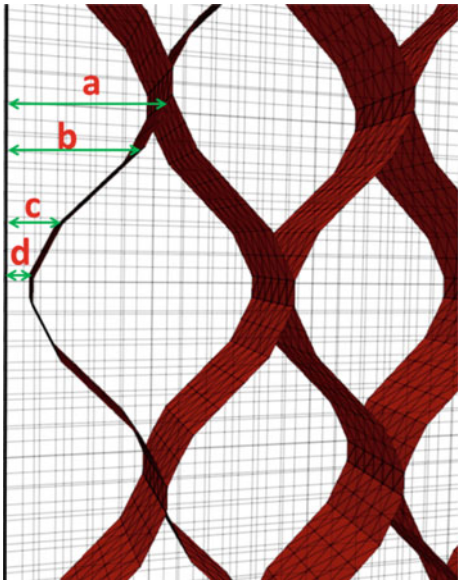

Fig. 7.9 Making of geocell in FLAC 3D

were noted and then virtually superimposed over the pre-existing zone (soil) and then, geocell of required depth was constructed on the edge of the zone. After that, each node of the geocell was pushed to the required coordinates (example: the virtual coordinates a, b, c, and d distance apart from the edge) as shown in Fig. 7.9 to create geocell curvature. This step was repeated until full-scale geocell is created into the zone. Joints of the geocell were created by superimposing the elements of geocell of two adjacent geocell curvature of the same strength. The making of geocell in FLAC 3D is quite tedious and requires a great level of precision to create joints. Modeling of basal geogrid was much easier and took very less time. Basal geogrid was first constructed on the surface of the pre-existing zone and pushed further to desired location. The interface properties are provided in detail in Table 7.4.

7.4.3 Validation of Numerical Model

Fineness of the mesh plays an important role to determine bearing capacity in numerical models. Sensitivity analysis with varying mesh size was run and smaller and optimum mesh size depending on accuracy and simulation time period was selected. Frydman and Burd (1997) in their study demonstrated importance of small velocity which gave better and reasonable results during bearing capacity calculation for rough footing. In this numerical study, preliminary analysis was carried out to avoid boundary effects. It was concluded that stress and deformations were contained within selected boundaries. Sensitivity analysis was done to select the optimum mesh

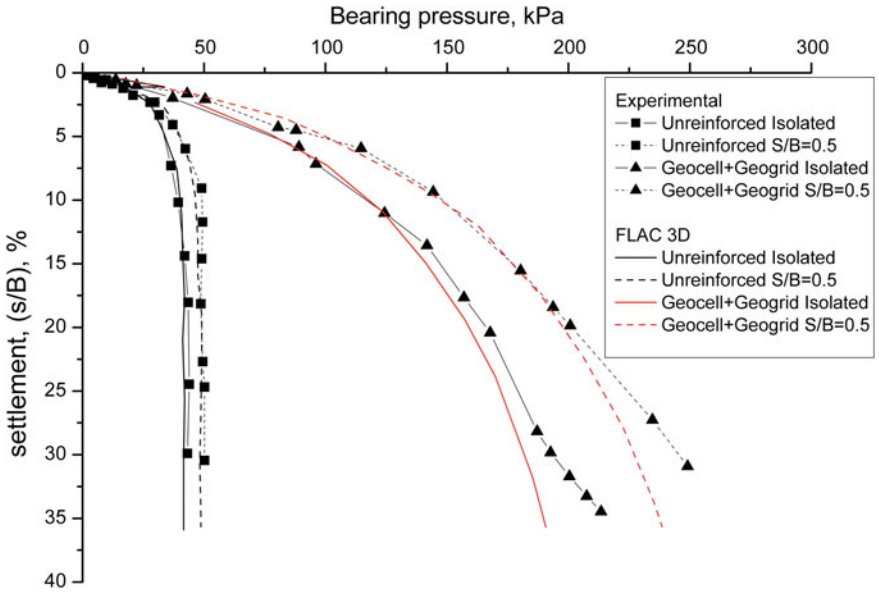

Fig. 7.10 Comparison between experimental and numerical results

size of the model. Before carrying out the simulations onto the reinforced bed, unreinforced model was validated with Boussinesq's theory. To this end, uniform pressure was applied at the center of the model and corresponding stress was measured on vertical and horizontal planes, these values were compared with that of Boussinesq's theory. Values from FLAC 3D and Boussinesq's theory were in good agreement. First numerical analysis on unreinforced isolated footing was run and compared and then numerical results from unreinforced interfering footing with spacing/width ratio 0.5 were compared with respective experimental data. Second, both were repeated for geocell and geogrid-reinforced clay bed. A good agreement between experimental and numerical investigation was observed, as shown in as illustrated in Fig. 7.10.

For numerical investigation, as discussed in Sect. 7.4.1, properties used are tabulated in Table 7.4. Properties of Cam Clay model were determined from isotropic triaxial compression test. However, elastic modulus of soil is determined directly from the pressure-settlement response of plate load test; the reason is mentioned in Sect. 7.4.1.

7.5 Results and Discussion

To analyze experimental data in an effective way, the footing settlement (s) and clear spacing (S) are normalized with width of the footing (B) to express them in non-dimensional form as s/B and S/B respectively. In the case of reinforced clay bed,

no distinct failure point was observed in the load versus settlement curve; therefore, tangent intersection method was adopted to determine the ultimate bearing capacity (q_u), as shown in Fig. 7.13. However, in case of unreinforced clay bed, definite failure point was observed in load versus settlement curve, which was used to determine ultimate bearing capacity.

Interference factor has been defined as

$$IF = \frac{\text{ultimate load carrying capacity of interfering footing}}{\text{ultimate load carrying capacity of isolated footing}}$$

7.5.1 Experimental Results

Load versus settlement curve of the interfering footing for spacing ranging from 0.5, 1, 2 for unreinforced, geogrid-reinforced, geocell reinforced and both geocell + geogrid-reinforced clay bed is presented in Fig. 7.11. Irrespective of the type of reinforcement provided, maximum interference effect was observed when the spacing between the footings was 0.5*B*. Figure 7.12 represents an increase in bearing pressure for various types of reinforcement for $S/B = 0.5$. When spacing between the footings was 2*B* there was minimal interference, the footings almost behaved as isolated footings; because of which the curve for $S/B = 2$ tends towards an isolated footing curve.

7.5.2 Numerical Results

Load versus settlement curve from the numerical analysis for isolated and $S/B = 0.5$ is presented in Fig. 7.13. Findings from numerical investigations are in good accordance with the experimental data and fairly good agreement between experimental and numerical results is observed which is presented in Fig. 7.10. Interference factor (for $S/B = 0.5$) for various reinforcement systems are tabulated in Table 7.5. Figure 7.14 represents interference factor for various reinforcement and spacing between the footings.

Figure 7.15a–d represents pressure bulb corresponding to 0.1 q_u for isolated unreinforced, unreinforced interfering footing with 0.5*B* spacing, geocell with basal geogrid-reinforced isolated footing and geocell with basal geogrid-reinforced interfering footing with 0.5*B* spacing. Pressure bulb was created using '*iso-surface*' in-built tool in the FLAC3D. *Iso-surface* creates 3D images of desired parameter; here we used 0.1 of maximum vertical stress. When the soil was unreinforced, pressure bulb was circular and dispersed deeper into the soil. In case of interfering footing, pressure bulb spread on to the lateral sides as shown in Fig. 7.15b. This could explain

the confinement effect due to the interaction of adjacent failure surfaces from corresponding footings. When soil was reinforced with geocell and geogrid, there was a significant reduction in the size of the pressure bulb which was locally confined; this is because of blocking effect of geocell pocket and accumulation of stress on the geocell membrane. Figure 7.16a–d represents vertical pressure distribution for isolated unreinforced, unreinforced interfering footing with 0.5*B* spacing and geocell with basal

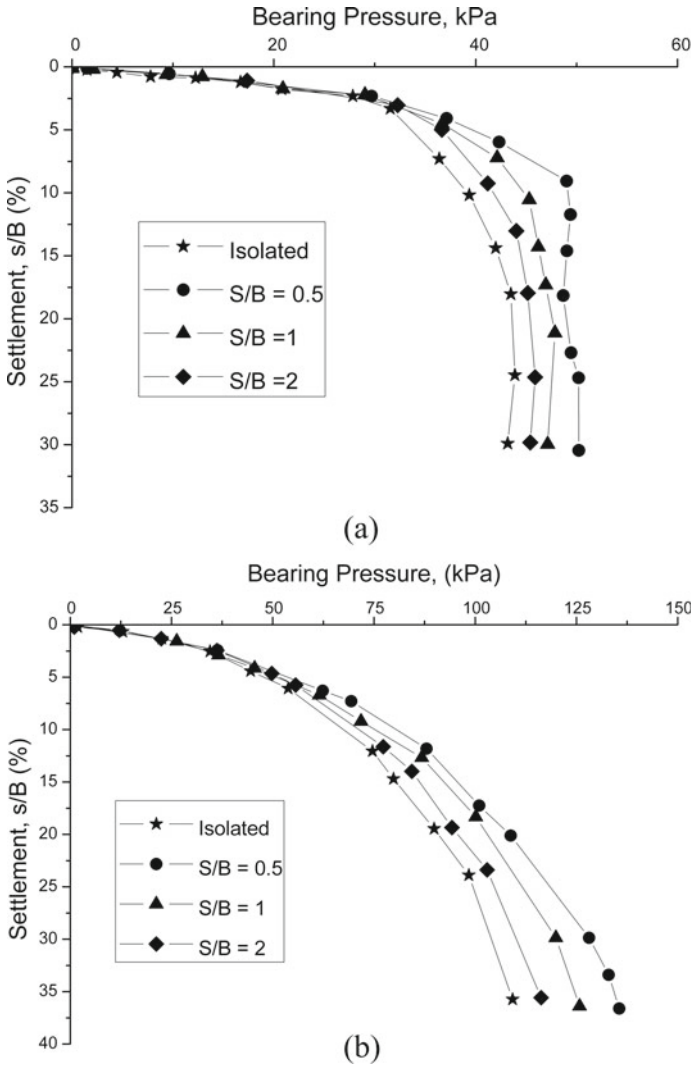

Fig. 7.11 Load versus settlement curve for different spacing between the footings for **a** Unreinforced; **b** geogrid-reinforced; **c** geocell reinforced; **d** geocell + geogrid-reinforced

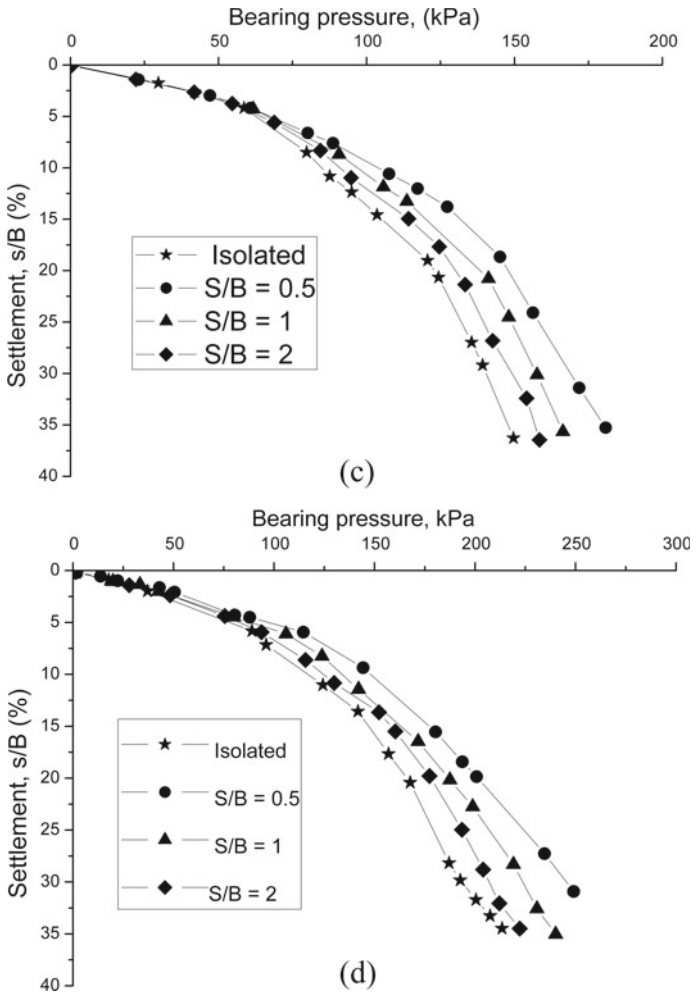

Fig. 7.11 (continued)

geogrid-reinforced isolated footing and geocell with basal geogrid-reinforced interfering footing with 0.5*B* spacing. From all the figures, it was clear that there were no effects due to tank boundaries. In case of unreinforced and isolated footings, uniform distribution of stress up to larger depth was observed compared to that of unreinforced interfering footings, indicating there is confinement effect between the footings that cause lateral confinement of the stress preventing the stress to propagate in the deeper levels. When the clay was reinforced with geocell and basal geogrid, there was a dramatic reduction in the depth of stress distribution and major stress was accumulated in the lateral direction, the reason is same as explained above,

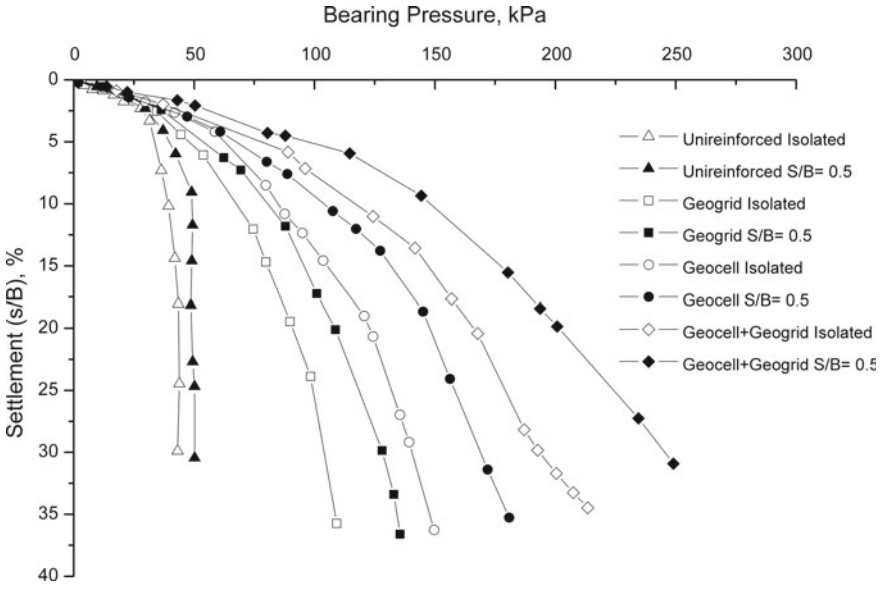

Fig. 7.12 Load versus settlement curve for isolated and $S/B = 0.5$ for various reinforcement

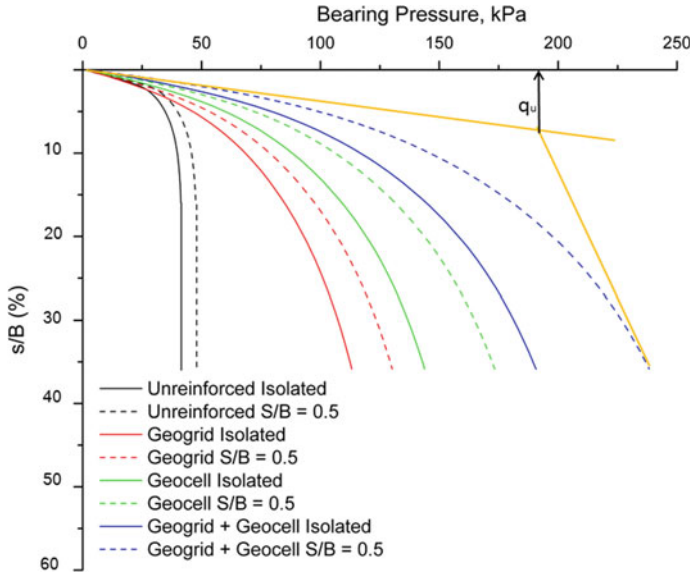

Fig. 7.13 Load settlement curve, FLAC 3D results

Table 7.5 Interference factor (for $S/B = 0.5$) for various reinforcement systems

Reinforcement type	Interference factor	
	Experimental	Numerical
Isolated	1.15	1.18
Geogrid	1.18	1.21
Geocell	1.25	1.28
Geocell + geogrid	1.29	1.33

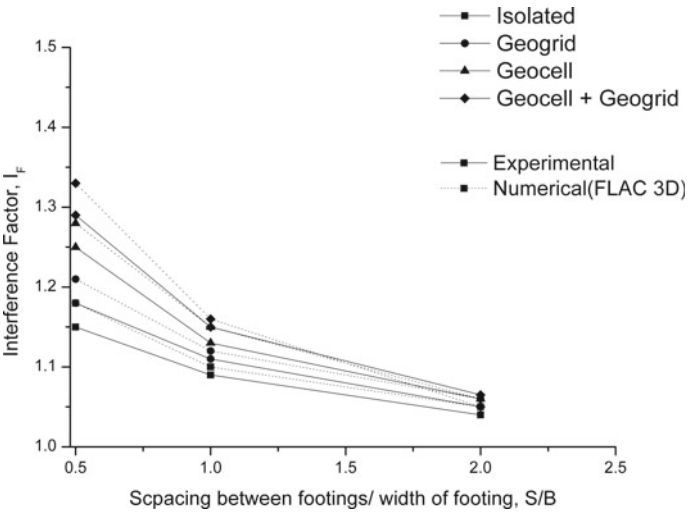

Fig. 7.14 Interference factor for various reinforcement system and spacing between the footings

i.e. geocell membrane accumulates major proportion of stress preventing the stress distribution in the deeper level.

7.6 Effect of Footing Size

To study the scale effect of the size footings, the size of the footings were doubled from 100 to 200 mm and series of numerical analyses were conducted with various spacing. The stress distribution is similar to that when footing size was 100 mm confirming the applicability of the current findings. Figure 7.17a–d represents vertical pressure distribution for isolated unreinforced, unreinforced interfering footing with $0.5B$ spacing and geocell with basal geogrid-reinforced isolated footing and geocell with basal geogrid-reinforced interfering footing with $0.5B$ spacing. From all the figures, it was clear that there were no effects due to tank boundaries. In case of unreinforced and isolated footings, uniform distribution of stress up to larger depth was observed compared to that of unreinforced interfering footings, indicating there

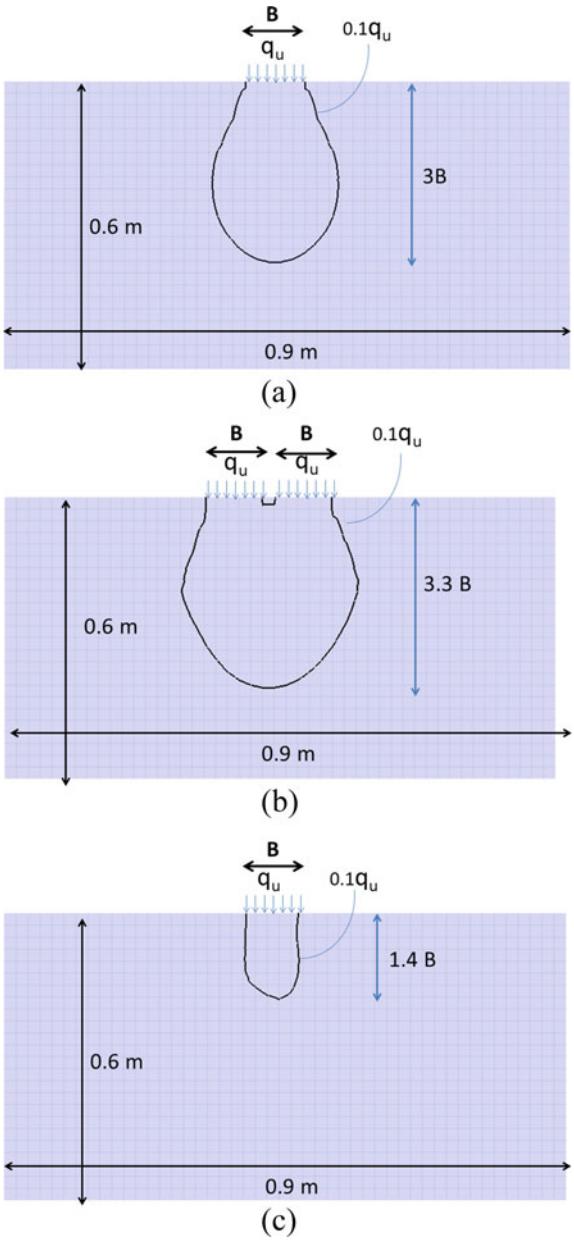

Fig. 7.15 Pressure bulb of 0.1 q_u: **a** unreinforced isolated; **b** unreinforced with spacing 0.5*B*; **c** reinforced with both geocell + geogrid isolated footing; **d** reinforced with both geocell + geogrid with spacing 0.5*B*

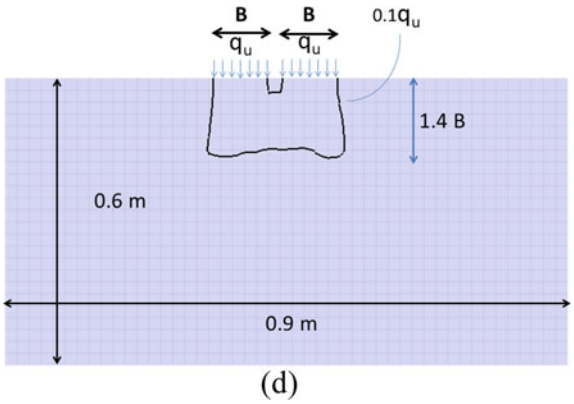

Fig. 7.15 (continued)

is confinement effect between the footings that cause lateral confinement of the stress preventing the stress to propagate in the deeper levels.

7.7 Conclusion

A series of laboratory model plate tests were performed on interfering footings with various spacing (0.5*B*, 1*B* and 2*B*). The tests were performed on unreinforced clay bed and three types of reinforcement systems namely, (i) geogrid-reinforced (ii) geocell reinforced and (iii) geocell + geogrid-reinforced clay bed. FLAC 3D was used for numerical investigations. Full-scale 3D models were adopted for rigorous numerical simulations. Numerical model was verified with four plate load conditions viz. isolated and interfering footing with spacing/width ratio 0.5 for both unreinforced and geocell + geogrid-reinforced clay beds and very good agreement between numerical and experimental data for all was observed.

Geocell was modeled capturing its actual curvature and honeycomb structure; entire numerical simulation series was run on full-scale 3D models. Modified Cam Clay model was used to simulate the behavior of the soft clay and Mohr–Coulomb model was used to simulate the behavior of the infill soil (sand). From the experimental and numerical investigations, the following conclusions were drawn.

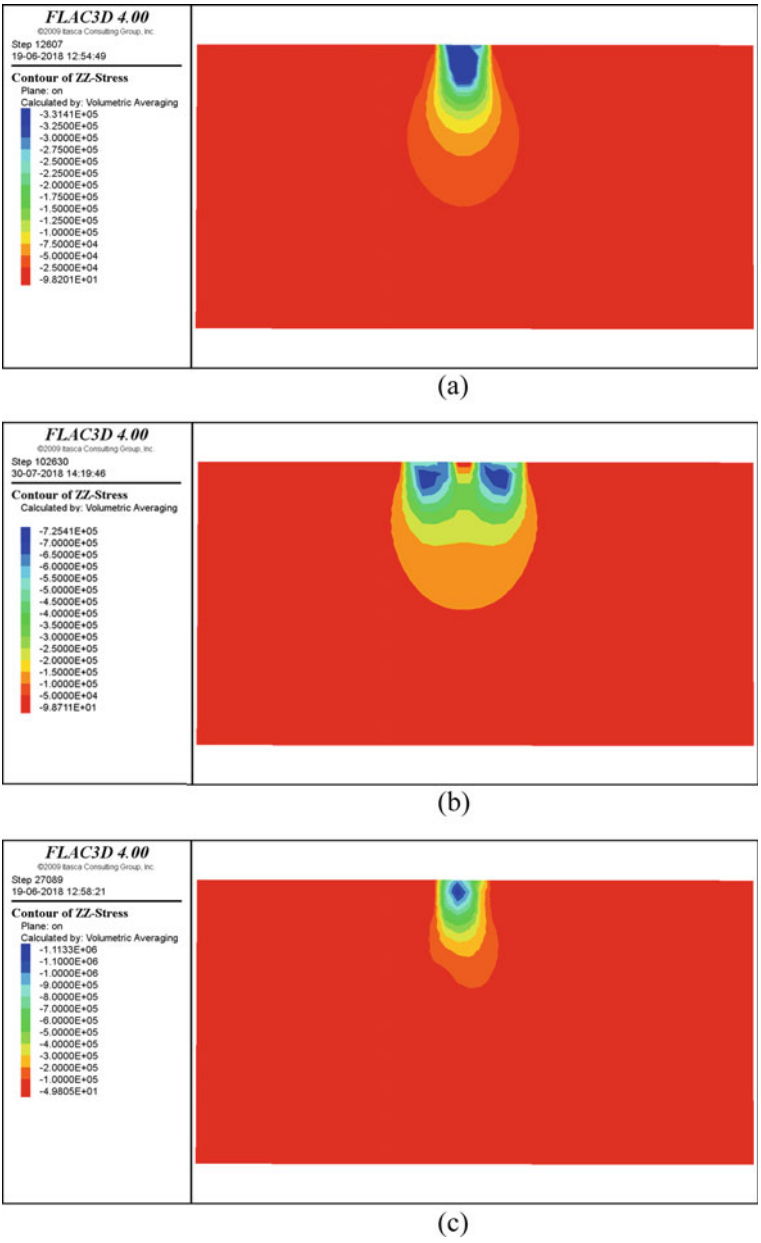

Fig. 7.16 vertical stress distribution: **a** unreinforced isolated; **b** unreinforced with spacing 0.5*B*; **c** reinforced with both geocell + geogrid isolated footing; **d** reinforced with both geocell + geogrid with spacing 0.5*B*

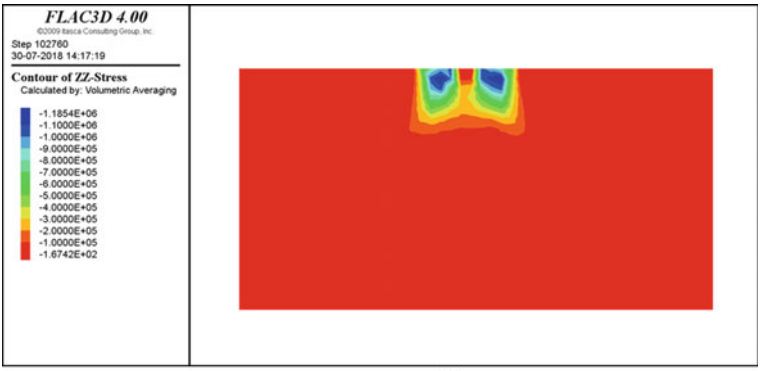

Fig. 7.16 (continued)

(1) The optimum spacing between the footings for maximum ultimate bearing capacity, irrespective of type of reinforcement systems used was found to be 0.5*B*.
(2) Interference factor (I_F) was maximum in case of geocell + geogrid reinforcement system. Effect of interference was significantly high when reinforcement was provided. Compared to unreinforced clay bed, I_F increased up to 14% for geocell + geogrid-reinforced clay bed.
(3) interference factor reduces as the spacing between footings increases, when the spacing between footings was 2*B*, there was minimal interference this is because the footings tend to act independently unaffected by each other.
(4) Applying reinforcement (geocell and or geocell) on clay bed significantly improves the bearing capacity and curbs the propagation of shear strain into the soil.

Generally, due to interference effect, there is an increase in bearing capacity by 15% in unreinforced clay; this becomes higher (18–33%) in reinforced clay; the interference effect becomes highest and the bearing capacity increases up to 33% when the clay is reinforced with both geocell and geogrid.

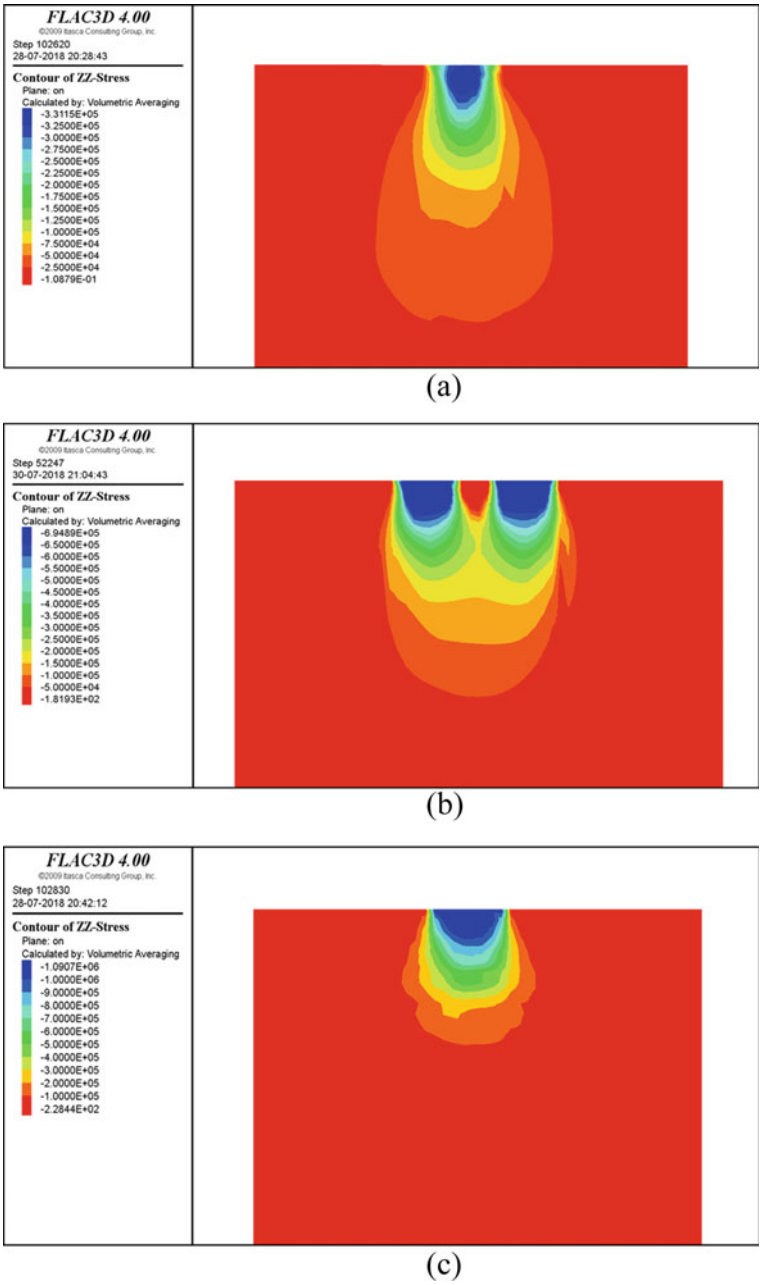

Fig. 7.17 Vertical stress contour for footing of size 200 mm **a** unreinforced isolated; **b** unreinforced with spacing 0.5*B*; **c** reinforced with both geocell + geogrid isolated footing; **d** reinforced with both geocell + geogrid with spacing 0.5*B*

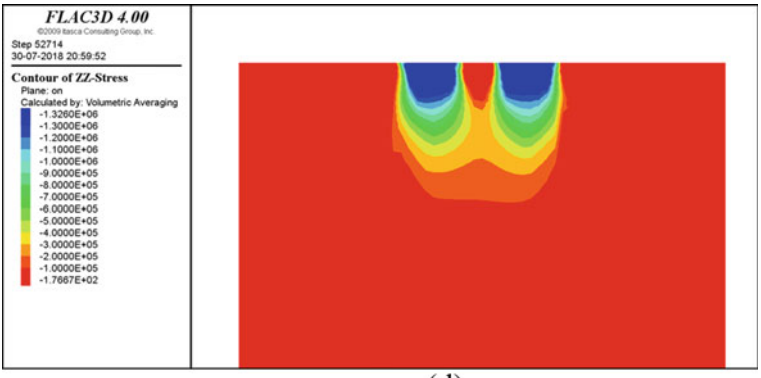

Fig. 7.17 (continued)

References

ASTM D1196 (2012) Standard test method for nonrepetitive static plate load tests of soils and flexible pavement components, for use in evaluation and design of Airport and highway pavements. ASTM International, West Conshohocken, PA, USA

ASTM D6637-11 (2011) Standard test method for determining the tensile properties of geogrid by the single or multi-rib tensile method. ASTM International, West Conshohocken, PA, USA

Das BM, Larbi-Cherif S (1983) Bearing capacity of two closely spaced shallow foundations on sand. Soils Found 23(1):1–7

Chunmar AV (1972) Bearing capacity theory from experimental results. J Geotech Eng Div, ASCE 98(12):1311–1324

Dash SK, Krishnaswamy NR, Rajagopal K (2001) Bearing capacity of strip footings supported on geocell-reinforced sand. Geotext Geomembr 19:235–256

Frydman S, Burd HJ (1997) Numerical studies of bearing capacity factor Nc. J Geotech Geoenviron Eng ASCE 123(1):20–29

Latha GM, Somwanshi A (2009) Bearing capacity of square footings on geosynthetic reinforced sand Geotext. Geomembr 27(4):281–294

Ghazavi M, Lavasan AA (2008). Interference effect of shallow foundations constructed on sand reinforced with geosynthetics. Geotext Geomembranes 26(5):404–415

Graham J, Raymond GP, Suppiah A (1984) Bearing capacity of three closely- spaced footings on sand. Geotechnique 34(2):173–182

Gupta A, Sitharam TG (2018) Experimental and numerical investigations on interference of closely spaced square footings on sand. Int J Geotech Eng 1–7

Han J, Yang X, Leshchinsky D, Parsons RL (2008) Behaviour of geocell reinforced sand under a vertical load. J Transp Res Board 2045:95–101

Hazell ECJ (2004) Interaction of closely spaced strip footings. Final year project report, Department of Engineering Science, University of Oxford

Hegde A (2014) Ground improvement using 3D-cellular confinement systems: experimental and numerical studies. Ph.D. thesis, Department of Civil Engineering, Indian Institute of Science

Huang CC, Tatsuoka F (1990) Bearing capacity of reinforced horizontal sandy ground. Geotext Geomembr 9:51–82

Itasca (2008) Fast Lagrangian analysis of Continua (FLAC3D 4.00). Itasca Consulting Group Inc., Minneapolis, USA

Kumar A, Saran S (2003) Closely spaced footings on geogrid-reinforced sand. J Geotech Geoenviron Eng 129(7):660–664
Kumar J, Bhoi MK (2009) Interference of two closely spaced strip footings on sand using model tests. J Geotech Geoenviron Eng, ASCE 135(4):595–604
Kumar J, Ghosh P (2007) Upper bound limit analysis for finding interference effect of two nearby strip footings on sand. Geotech Geol Eng 25(5):499–507
Leshchinsky B, Ling H (2013) Effects of geocell confinement on strength and deformation behaviour of gravel. J Geotech Geoenviron Eng 139(2):340–352
Mabrouki A, Benmeddour D, Frank R, Mellas M (2010) Numerical study of the bearing capacity for two interfering strip footings on sands. Comput Geotech 2010(37):431–439
Omar MT, Das BM, Puri VK, Yen SC (1993) Ultimate bearing capacity of shallow foundations on sand with geogrid reinforcement. Can Geotech J 30:545–549
Sireesh S (2005) Behaviour of geocell reinforced foundation beds. Ph.D. thesis, Department of Civil Engineering, Indian Institute of Science Bangalore, India
Saran S, Agarwal VC (1974) Interference of surface footings on sand. Indian Geotech J 4(2):129–139
Selig ET, McKee KE (1961) Static and dynamic behaviour of small footings. J Solid Mech Found, Div, ASCE 87:29–47
Stuart JG (1962) Interference between foundations with special reference to surface footings in sand. Geotechnique 12(1):15–23
Yang X, Han J, Parsons RL, Leshchinsky D (2010) Three-dimensional numerical modelling of single geocell reinforced sand. Front Archit Civ Eng China 4(2):233–240
Zreik DA, Ladd CC, Germaine JT (1995) A new fall cone device for measuring the undrained strength of very weak cohesive soils. Geotech Test J 18(4):472–482

Chapter 8
Performance Evaluation of Geocell Reinforced Machine Foundation Beds

Hasthi Venkateswarlu and Amarnath M. Hegde

Abstract The present chapter describes the results of large-scale field vibration tests and cyclic plate load tests conducted on geosynthetics reinforced soil beds. A series of vertical mode block resonance tests are conducted over a rigid concrete footing resting on different reinforced soil conditions. The tests are performed in a test pit of size 2 m × 2 m × 0.5 m using a concrete footing of size 0.6 m × 0.6 m × 0.5 m. Four different conditions, namely unreinforced, single-layer geogrid reinforced, two-layer geogrid reinforced and geocell reinforced conditions were considered. The tests are performed under six different dynamic force levels using a Lazen-type mechanical oscillator. In total, 38 number of field tests are conducted. The dynamic response is studied in terms of reduction in resonant amplitude, peak particle velocity (*PPV*) and improvement in dynamic properties of the soil. Experimental results revealed that the displacement amplitude of vibration significantly reduced in the presence of geosynthetics. The maximum reduction is observed in the presence of geocell reinforcement as compared to other conditions. In the presence of geocell reinforcement, the resonant amplitude is decreased by 61% and the natural frequency of the soil system is increased by 1.38 times as compared to the unreinforced condition. In addition, the geocell reinforcement found to reduce the PPV by 48% at a distance of 0.5 m from the footing face. The elastic uniform compression of the foundation bed is improved by 91% in the presence of geocell reinforcement. From the cyclic plate load test results, four times improvement in natural frequency of the foundation soil system and 92% reduction in amplitude of the vibration were observed by the combined utilization of geocell and geogrid.

Keywords Geosynthetics · Dynamic response · Machine vibrations · Geocell · Geogrid

H. Venkateswarlu · A. M. Hegde (✉)
Department of Civil and Environmental Engineering, Indian Institute of Technology Patna, Patna 801106, India
e-mail: ahegde@iitp.ac.in

H. Venkateswarlu
e-mail: hasthi.pce16@iitp.ac.in

T. G. Sitharam et al. (eds.), *Geocells*, Springer Transactions in Civil and Environmental Engineering,
https://doi.org/10.1007/978-981-15-6095-8_8

Nomenclature

A	Contact area of the footing with the soil mass (m^2)
A_r	Displacement amplitude of reinforced condition (mm)
A_{un}	Displacement amplitude of unreinforced condition (mm)
b	Width of the reinforcement (m)
B	Width of the footing (m)
C	Cohesion (kPa)
C_u	Coefficient of elastic uniform compression (kN/m^3)
C_τ	Coefficient of elastic uniform shear (kN/m^3)
C_ϕ	Coefficient of elastic non-uniform compression (kN/m^3)
C_Ψ	Coefficient of elastic non-uniform shear (kN/m^3)
D	Diameter of the footing (m)
d_o	Equivalent pocket diameter of the geocell material (m)
e	Eccentric distance between center of mass and the center of rotation (m)
E	Young's modulus (MPa)
E_c	Modulus of elasticity of concrete (MPa)
f_{nz}	Natural frequency of the foundation soil system (Hz)
F	The dynamic force excited over the footing in a vertical mode (N)
F_o	Total dynamic force (N)
F_{if}	Frequency improvement factor (dimensionless)
F_r	Resonant frequency of the reinforced soil system (Hz)
F_u	Resonant frequency of the unreinforced soil system (Hz)
g	Acceleration due to gravity (m/sec^2)
G	Shear modulus (MPa)
h	Distance between two geogrid layers (m)
H	Height of the geocell layer (m)
K	Stiffness of the soil (kN/m)
M	Mass of the vibrating block, oscillator and motor (kg)
m	Center of gravity of the rotating mass
m_e	Eccentric mass weight (kg)
N	Geocell seam strength (N)
o	Center of rotation
PPV	Peak particle velocity (mm/s)
$PRDA$	Percentage reduction in displacement amplitude (dimensionless)
t	Dynamic time (s)
t_i	Thickness of reinforcement (geogrid and geocell) material (mm)
u	Depth of placement of the geogrid (m)
u_c	Depth of placement of the geocell (m)
U_x, U_y and U_z	Displacements in X-, Y- and Z-directions under dynamic excitation (mm)
ω	Circular natural frequency in cycles (rotations) per minute
γ	Unit weight of concrete (kN/m^3)

γ_d	Dry density of the foundation soil (kN/m^3)
φ	Angle of shearing resistance (°)
φ_i	Interface friction angle (°)
ν	Poisson's ratio (dimensionless)
θ	Eccentricity angle (°)

8.1 Introduction

The foundation beds are often subjected to cyclic loads due to many circumstances, such as earthquakes, traffic loads and the machine vibrations in the case of the machine foundations. These cyclic loads are generally smaller as compared to the static loads; but are repetitive. As a result of these cyclic forces, the soil bed may undergo large settlements and subsequently may fail to support the superstructure above. In such cases, the performance can be enhanced in two ways. One way is to increase the stiffness of the soil to resist the cyclic stresses. The other approach is to increase the elasticity of the soil. With the increase in the elasticity of the soil, the soil will regain its original position before the next cycle of cyclic stress is applied. This will lead to the lesser permanent deformation of the foundation bed.

At present, the rapid growth in urbanization and the scarcity of land have increased the construction of various industrial projects (nuclear and power plants) closer to the residential areas and civil engineering structures. These industrial setups majorly consist of high-frequency machines, namely rotary compressors, turbogenerators, gas or diesel generators, high-speed generators and turbines, etc. These vibratory sources are supported on the heavy foundations. Due to the vibration caused by these machines, the adjacent structures may be subjected to severe damage or settlements. The induced ground vibrations not only create problems for the structures but also are problematic for inhabitants and sensitive parts of the machines. Thus, it is obligatory to control such unfavorable vibrations at their source of generation. The understanding about the key parameters, namely resonance and the nature of the foundation bed, is essential to avoid excessive vibrations generated from the machines and to control settlement of the structures. At resonance, the operating frequency of the machine matches with the natural frequency of the foundation soil system (f_{nz}) and leads to higher amplitude of the vibration. To encounter excessive vibration, f_{nz} should be increased or machine can be operated at lower frequencies. The settlement of the machine foundation under cyclic stresses induced by the machine parts can be controlled by enhancing the elasticity of the foundation bed. Generally, rubber pads, cork sheets and the spring coils are used below the foundations to increase the elastic properties of the soil (Srinivasalu and Vaidyanathan 1976; Bhatia 2008; Hegde and Sitharam 2016).

From the past few decades, geosynthetics have found a widespread application in various geotechnical engineering projects. Some of those include foundations (Tafreshi and Dawson 2012; Hegde 2017; Mehrjardi and Khazaei 2017; Saha Roy

and Deb 2017; Shahin et al. 2017), pavements (Nejad et al. 2016; Chen et al. 2017; Correia and Zornberg 2018; Mousavi et al. 2017; Saride and Kumar 2017; Suku et al. 2017; Sun et al. 2017), railway lines (Biabani and Indraratna 2015; Biabani et al. 2016; Esmaeili et al. 2017; Nimbalkar and Indraratna 2016; Wan 2018), buried lifelines (Hegde et al. 2014; Hegde and Sitharam 2015), embankments (Cao et al. 2016; Chen et al. 2016; Rowe and Taechakumthorn 2011; Sitharam and Hegde 2013; Girout et al. 2018; King et al. 2017; Mohapatra and Rajagopal 2017), retaining walls (Costa et al. 2016; Plácido et al. 2018; Song et al. 2018; Yoo 2018; Yu et al. 2016) and slope stability (Ferreira et al. 2016; Gao et al. 2016; Javankhoshdel and Bathurst 2016; Mehrjardi et al. 2016; Abd and Utili 2017; Luo et al. 2018). Also, the use of the geosynthetics is found to increase the stiffness of the soil. However, the application of these reinforcement materials is not very well explored to support the machine foundation beds. Very limited literature is available to understand the behavior of geosynthetics reinforced soil under machine foundations. Boominathan et al. (1991) have conducted the block resonance tests to understand the dynamic response of reinforced earth under vertical mode of vibrations. Geotextile and geogrid made up of high tensile wire grid have been used as a reinforcement material in this investigation. Results revealed that the maximum improvement in shear modulus and reduction in displacement amplitude were observed in the presence of tensile wire grid. In addition, the slight improvement in resonant frequency was also observed in the presence of reinforcement material. Clement (2015) has studied the dynamic behavior of reinforced soil under machine vibrations through laboratory studies. Model test results revealed the improvement in stiffness and damping ratio of the soil, when it was reinforced with geogrid reinforcement. Similarly, the model studies conducted by Sreedhar and Abhishek (2016) highlighted the reduction in resonant amplitude and improvement in resonant frequency in the presence of geogrid reinforcement. Hegde and Sitharam (2016) studied the performance of geocell reinforced soil under machine foundation with the help of the cyclic plate load test. Figure 8.1 represents the schematic view of the machine foundation resting on the geocell and geogrid reinforced clay bed.

It is observed from the literature that the elastic properties of the foundation bed can be evaluated using cyclic plate load test and block vibration test. The present study is aimed to quantify the improvement in elastic response of the foundation bed in the presence of geosynthetics using both the tests. Firstly, the results of laboratory cyclic plate load tests have been described. The results of block resonance tests have been discussed in the second part of the chapter.

8.2 Cyclic Plate Load Test

A cast iron test tank of 900 mm long, 900 mm wide and 600 mm in height was used in the experimental investigation. The natural silty clay with specific gravity 2.66 was used to prepare the foundation bed. The commercially available Neoloy geocells were used in the study. Below the geocell, a layer of biaxial geogrid made

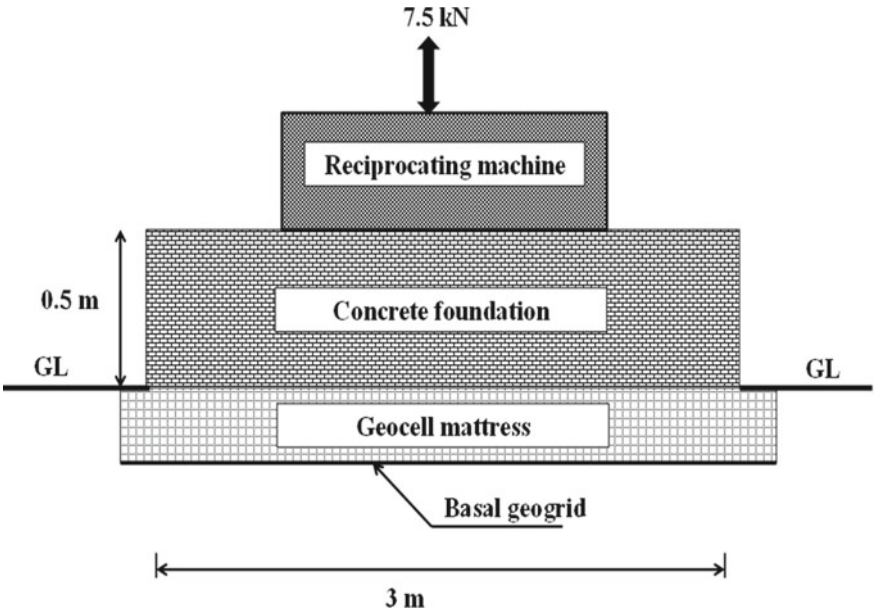

Fig. 8.1 Schematic view of the geocell supported machine foundation. *Source* from Hegde and Sitharam (2016)

of polypropylene was used. The aperture opening of the geogrid was square in shape with size 35 mm × 35 mm. The tank was connected to the loading frame which was internally connected to manually operated hydraulic jack. A 20-mm-thick square steel plate with width 150 mm was used as the loading plate. The loading plate was selected in such a way that its width was equal to 1/6th of the width of the tank in order to avert the boundary effects. The bottom of the plate was made rough by coating a thin layer of sand with epoxy glue. The load was applied to the plate through the hydraulic jack. A pre-calibrated proving ring was placed between the plate and hydraulic jack to measure the applied load. A ball bearing arrangement was used to prevent the eccentric application of the load. Figure 8.2 represents the schematic and the photographic view of the test setup.

The bearing pressure-settlement response for the three different cases, namely unreinforced, geocell reinforced and geocell, with additional basal geogrid reinforced cases is shown in Fig. 8.3. In case of the unreinforced bed, the failure occurred in the third load increment itself. The failure of the bed was indicted by the large settlement of the plate. The maximum bearing capacity of 28 kPa was observed. In case of the geocell reinforced case and the geocell with additional basal geogrid case, the test was stopped after seventh load increments as there was no failure of the bed. In all the three cases, every loading cycle was followed by a gradual unloading of the entire load. The elastic rebound of the plate was recorded for every loading and unloading cycle. After the tests, the infill soil was scooped out and geocell was removed.

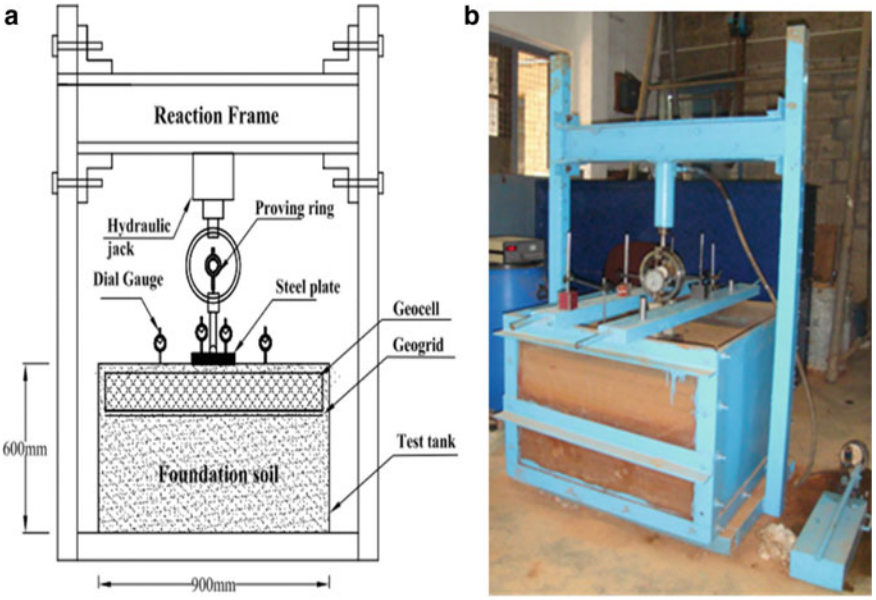

Fig. 8.2 Test setup: **a** Schematic view; **b** Photographic view. *Source* from Hegde and Sitharam (2016)

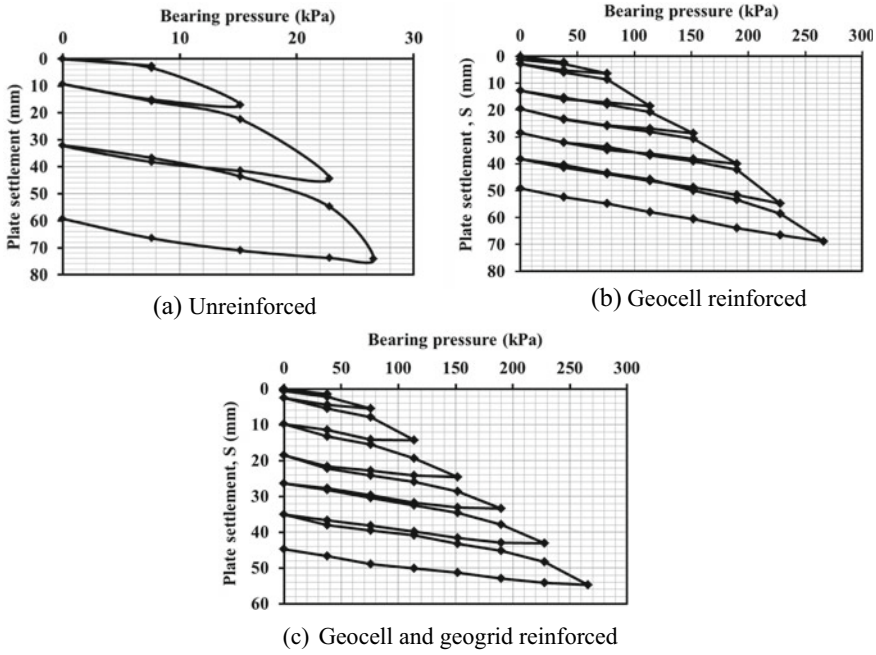

Fig. 8.3 Bearing pressure-settlement responses. *Source* from Hegde and Sitharam (2016)

The advantage of the cyclic plate load test is that it not only provides the information about the elastic properties of the soil, but also provides information about bearing capacity and the settlement of the bed. From the cyclic bearing pressure-settlement response, the increase in elastic response of the foundation bed in the presence of geosynthetics was evaluated. Basically, the coefficient of elastic uniform compression (C_u) is the measure of the elastic modulus of the soil. It is defined as the ratio of the compressive stress (P) applied to the soil to the elastic part of the settlement (S_e) induced. Generally, it is determined from the cyclic plate load tests.

$$C_u = P/S_e \tag{1}$$

Higher value of C_u indicates the high elastic modulus of the soil. Based on the laboratory results, two hypothetical cases of machine foundation are compared. In the first case, the foundation was assumed to be resting on the unreinforced clay bed, and in the second case, it was assumed to be resting on the geocell and geogrid reinforced clay beds. Further, a low-frequency reciprocating machine was assumed to be placed on the foundation in both the cases. The step-by-step calculations for the determination of the amplitude of vibration for the two different cases are listed in Table 8.1.

It should be noted that the hypothetical case considered has nothing to do with the model size and the loading conditions adopted in the laboratory tests. Here, the emphasis is only on the coefficient of elastic uniform compression. For the sake of convenience, the C_u values obtained from the model tests were used. The amplitude of the vibration (A_z) decreases in the presence of geocell reinforcement. About 87% reduction in the A_z value was observed in case of geocells, and about 92% reduction in A_z was observed in the case of geocell with basal geogrid.

8.3 Block Resonance Test

8.3.1 Test Setup

The block vibration test setup majorly consists of three essential components, namely mechanical oscillator, DC motor and data acquisition system. The data acquisition system comprises the speed control unit and vibration meter. The mechanical oscillator used in this study was a Lazen-type to represent high-speed rotary machine. The oscillator was mounted on top of the concrete block through the bolting arrangement. The M20 grade concrete block was placed over the prepared foundation bed. The mechanical oscillator was connected with the DC motor through flexible shaft. The rotating speed of the oscillator depends upon the speed of the DC motor. The capacity of the DC motor used in this study was 6 HP and can run up to the maximum speed of 3000 rpm (50 Hz). The rotating speed of the motor was monitored by using the speed control unit. A non-contact-type speed sensor was used to sense the rpm

Table 8.1 Calculation of the amplitude of vibration for different cases

S No.	Parameter	Unreinforced	Geocell reinforced	Geocell and geogrid reinforced
1	Coefficient of elastic uniform compression, Cu (kN/m^3)	1850	14,600	24,260
2	Natural frequency of the foundation soil system, ω_n (rad/s) $\omega_n = \sqrt{\frac{C_u A}{m}}$	33	92	119
3	Natural frequency of the foundation soil system, ω_n (RPM)	314	881	1135
4	Limiting operating frequency of the machine, ω (rad/s), $\omega = 0.5 \times \omega_n$	16.5	46	60
5	Limiting operating frequency of the machine, ω (RPM)	157	440	568
6	Amplitude of vibration neglecting damping, (m) $A_z = \frac{Q_o}{m(\omega_n^2 - \omega^2)}$	6E−4	7.6E−5	4.58E−5
7	Reduction in the amplitude of vibration (%)	–	87	92

of the rotating shaft of the motor. It can sense the speed of the rotating shaft from a distance of 2 mm. In this study, the sensor was set at a distance of 1.5 mm between the sensing probe and the rotating shaft of the motor. The resolution of the sensor is 1 rpm. The speed of the motor is controlled through the speed control unit. The motor and speed control units are connected through wiring arrangement. In addition, the amplitude of the vibration induced from the machine was monitored with the help of digital vibration meter. It can display the velocity and displacement amplitude of vibration generated from the machine with the help of piezoelectric accelerometer (sensing element). The accelerometer used in this study can measure the amplitude up to 20 mm with a least count of 0.01 mm. Similarly, the velocity can be monitored up to the range of 200 mm/s with a resolution of 0.1 mm/s. The accelerometer was placed on the concrete block, and it was connected to vibration meter. The schematic representation of the block vibration test setup is shown in Fig. 8.4a. The oscillator consists of rotating element (eccentric mass) with a total eccentric mass of m_e. It can generate a rotating mass-type excitation with a maximum dynamic force of 2400 kgf. The dynamic force level can be varied by changing the eccentric setting value (θ). It is the angle maintained by the eccentric distance (e) with the axis of rotation. The eccentric distance is the distance between center of rotation (o) to the center of

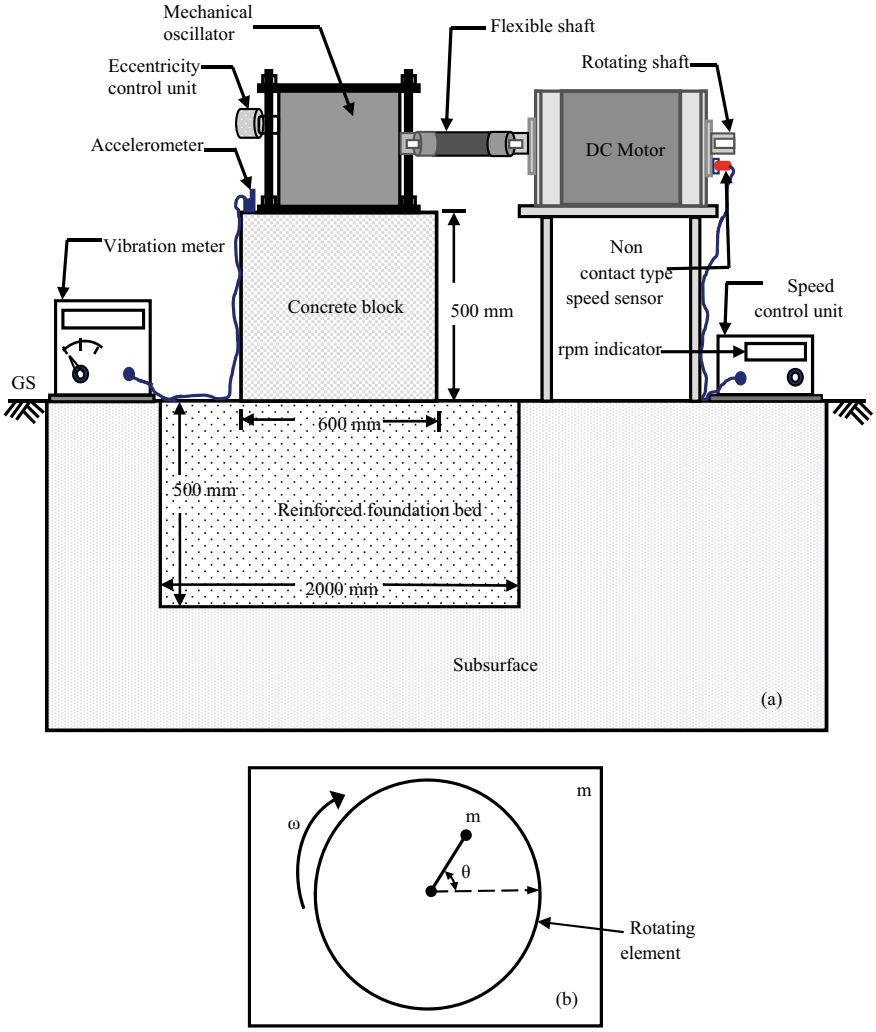

Fig. 8.4 Block vibration test setup: **a** Schematic representation; **b** Rotating mechanism of mechanical oscillator. *Source* from Venkateswarlu et al. (2018)

gravity of rotating mass (m) (Richart et al. 1970). The eccentricity angle can be varied from 0° to 180° with the help of eccentricity control unit. The maximum dynamic force is obtained when the eccentric angle becomes 180°. The rotating mechanism of mechanical oscillator is presented in Fig. 8.4b.

8.3.2 Materials Used

In the present investigation, the foundation bed was prepared with the help of locally available soil. It was classified as silty sand (SM) as per Unified Soil Classification System. The specific gravity of sand was 2.64. It consists of 16% fines content passing through the 75 μm sieve. The compaction characteristics of the foundation soil were determined from the standard proctor test. The optimum moisture content and maximum dry density of the foundation soil were 12.6% and 17.9 kN/m^3, respectively. The angle of shearing resistance and cohesion of the foundation soil were 32° and 1 kPa, respectively. The grain size distribution of the foundation soil is presented in Fig. 8.5.

Two types of geosynthetics, namely geogrid and geocell were used as reinforcement materials. The biaxial geogrid used in this study consists of square shape aperture with the dimensions of 35 mm × 35 mm. The geogrid was made up of with high tenacity polyester yarn and coated with highly refined and solvent extracted crystalline form of bitumen. The coated bitumen enables rough texturing and provides high frictional characteristics than other coating systems. The geocell made up of novel polymeric alloy (NPA or Neoloy) was used in this study. The novel polymeric alloy is majorly composed of polyolefin and thermoplastic engineering polymer. The NPA geocells are specifically manufactured for commercial applications and known for its high strength and durability. The tensile strength characteristics of geogrid and geocell were determined from tensile strength test as per the guidelines of ASTM D-6637 (2011) and ASTM D-4885 (2011), respectively. The tensile behavior of the reinforcement materials used in this study is presented in Fig. 8.6. The geometrical properties of the reinforcement materials used in this study were summarized in Table 8.2.

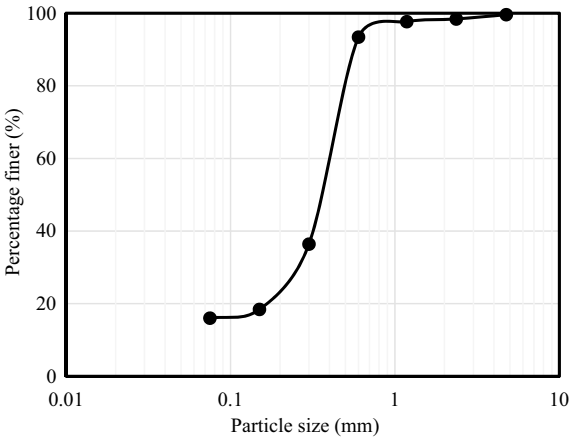

Fig. 8.5 Particle size distribution of the foundation soil. *Source* from Venkateswarlu et al. (2018)

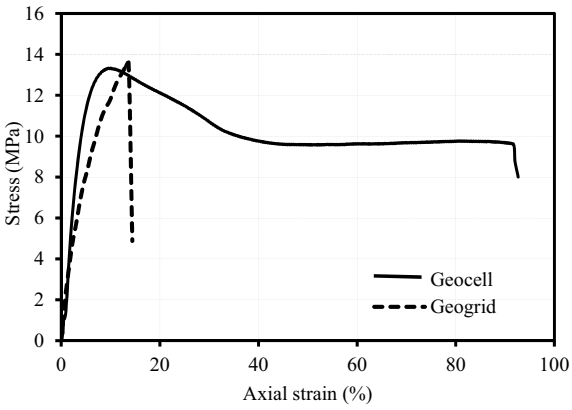

Fig. 8.6 Stress–strain behavior of reinforcement materials *Source* from Venkateswarlu et al. (2018)

Table 8.2 Properties of the reinforcement materials

Property	Quantity
Geocell	
Polymer type	Neoloy
Cell depth (mm)	120
Cell length (mm)	245
Cell width (mm)	210
Number of cells/m^2	39
Strip thickness (mm)	1.53
Cell wall surface	Perforated
Density (g/cm^3)	0.95 (±1.5%)
Cell seam strength (N)	2150 (±5%)
Geogrid	
Polymer	Polyester
Aperture size (MD × XMD) (mm)	35 × 35
Shape of the aperture	Square
Mass per unit area (g/m^2)	250

Source from Venkateswarlu et al. (2018)
Note MD—machine direction; XMD—cross machine direction

8.3.3 Preparation of the Foundation Bed

The foundation bed was prepared in the excavated test pit having the dimensions of 2 m × 2 m × 0.5 m in the field. Raman (1975) has investigated the effect of test pit size on the dynamic response of the system. The test pits of lengths 3.3*D* and 4.6*D* (where *D* is the diameter of the footing) were considered. The identical nature of the dynamic response was observed from both the pits. Hence, in the present study, the width of the foundation bed was considered equal to the 3.3 times the width

of machine foundation. The depth of the foundation depends upon the choice of the designer (IS 5249 1992). Hence, the depth of the foundation bed was selected as 0.5 m. Initially, the foundation soil (silty sand) was collected from the depth of 0.25 m from the ground surface. The method of disturbed sampling technique was used to collect the soil sample. The collected soil sample was air dried for 36 h in order to make air-dried sample. Initially, the predetermined amount of water was added to the air-dried sample to get the achievable dry density of the soil. The optimum amount of water content was determined through the standard proctor test. The foundation bed was prepared by layerwise with the moist soil, in order to maintain uniform density throughout the foundation bed. The foundation bed was prepared in ten numbers of layers having thickness of 50 mm each. The manual compaction mode was adopted to compact the each layer of the foundation bed. The each layer was compacted with the compaction effort equal to the standard proctor test. A steel hammer of 11 kg weight was used for the purpose. The height of fall was maintained as similar to the standard proctor test. It has a provision of cylindrical plate with the dimensions of 140 mm diameter and 75 mm thick at its bottom. The number of blows required to achieve the maximum dry density of each layer was determined by equating the compaction effort of rammer with the compaction effort of standard proctor. Primarily, trail tests were performed to study the density and moisture content distribution in the foundation bed. During the trail tests, the preparation of the foundation bed was divided into two layers, namely top and bottom layers with a thickness of 0.25 m each. Each layer was prepared with five sub-layers having each layer thickness of 0.05 m. Total nine numbers of samples were collected from the top and bottom layers to check the moisture content and density variation throughout the layers. The samples were collected using the core cutter method as per the recommendations of IS: 2720-29 (1975). The average density and water content of nine samples were considered as density and moisture content of the respective layer. The similar properties were maintained in all the test conditions. The foundation bed was prepared freshly for every new test condition. The properties of the prepared foundation bed were presented in Table 8.3.

In addition to the unreinforced condition, other conditions, namely geogrid and geocell reinforced foundation beds were prepared. In this study, the width of the reinforcement (geogrid and geocell) was provided similar to the width of the foundation bed. The approach similar to the unreinforced condition was adopted for the

Table 8.3 Properties of the prepared foundation bed

Parameter	Bottom layer	Top layer
	Average of nine samples	Average of nine samples
Water content, w (%)	12.3	12.5
Dry density, γ_d (kN/m^3)	17.2	17.7

Source from Venkateswarlu et al. (2018)

preparation of geogrid reinforced foundation bed. However, it was reinforced with geogrid layers at the specified locations. The procedure for the preparation of geocell reinforced case was slightly different. Primarily, the foundation bed was prepared up to the required height from the bottom. The expanded geocell layer was placed over the compacted soil surface. The geocell pockets were filled with the same soil used in the preparation of unreinforced foundation bed. The proper sequence was followed to fill the geocell pockets to avoid the distortion of cell material. Initially, first two rows of the geocell layer were filled to half height before filling the first layer to its full height. The similar sequence was continued to fill the complete portion of the geocell layer. In this study, each geocell pocket was filled in three numbers of layers. Each layer was compacted at similar compaction effort to obtain the required density of the infill material. Upon filling of all the pockets, the top layer with a thickness of 60 mm was provided. Figure 8.7 shows the photographic representation of the different steps involved in the preparation of foundation beds.

Fig. 8.7 Preparation of foundation bed: **a** Excavated test pit; **b** Partially filled geogrid; **c** Partially filled geocell pockets; **d** Levelled foundation bed. *Source* from Venkateswarlu et al. (2018)

8.3.4 Test Procedure

A rigid concrete footing of size 0.6 m × 0.6 m × 0.5 m was used in the experimental investigation. The concrete footing was placed centrally over the prepared foundation bed at predetermined location. The square mild steel plate having the dimensions of 480 mm wide with 20 mm thickness was fixed to the block. The mechanical oscillator was properly placed over the steel plate. Another steel plate was placed over the oscillator to provide sufficient static weight. It was fixed tightly with the help of steel ingots, such that entire system behaves like a single unit. In addition, proper measure was taken such that the center of gravity of the footing and assembly must lie in a same vertical line. In this study, total static weight of 5.6 kN (combined weight of footing and the machine) was used. The eccentric moment and the dynamic force induced by the oscillator can be determined based on the recommendations of Bhatia (2009) by using the following equations:

$$F_0 = m_0 e \omega^2 \tag{8.2}$$

The maximum dynamic force induced over the footing in a vertical mode is obtained by

$$F = F_0 \sin\left(\frac{\theta}{2}\right) \tag{8.3}$$

where m_0 is the total eccentric mass weight in kg, e is the eccentric distance between center of mass and the center of rotation in m, θ is the eccentricity angle, F_0 is the total unbalanced dynamic force excited over the footing in N, F is the vertical component of the total dynamic force in N, and ω is the circular natural frequency in cycles (rotations) per minute. With an increase in eccentricity angle, the vertical dynamic force excited over the footing is increased. The variation in dynamic force with the change in frequency and eccentricity angle is shown in Fig. 8.8.

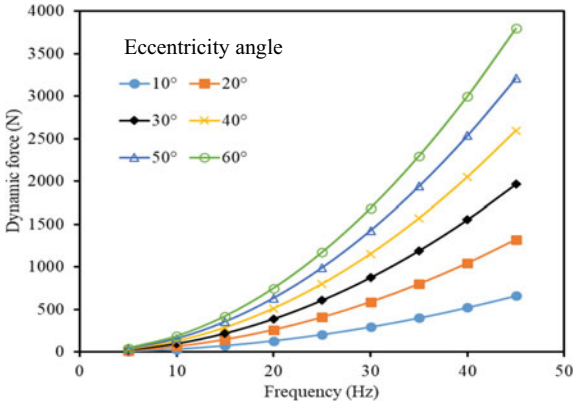

Fig. 8.8 Variation of dynamic force with increase in eccentricity angle and frequency of the excitation. *Source* from Venkateswarlu et al. (2018)

The detailed description about the abovementioned formulae can be found in Richart et al. (1970) and Das (1992). The mechanical oscillator was connected with DC motor through flexible shaft. The piezoelectric accelerometer was placed over the footing to measure the amplitude of the vibration with the help of vibration meter. Before starting the experiment, the required eccentricity angle was set through the eccentricity control unit to produce the desired dynamic force level. The mechanical oscillator was run slowly through the motor with the help of the speed control unit. The rotating speed of the oscillator was increased slowly, in order to avoid the sudden application of dynamic load over the footing. Therefore, the foundation bed was subjected to the vertical mode of harmonic excitation. The test was continued by measuring the amplitude of the vibration with increase in frequency of the dynamic excitation. To measure the actual resonant frequency of the system, the frequency was increased with an interval of 60–120 rpm (2 Hz). At a particular frequency, the displacement amplitude was found to stabilize approximately after 10 s. The readings were recorded once it was stabilized. It provides the exact measurement of displacement amplitude corresponding to its frequency. The similar procedure was adopted to study the dynamic behavior of all the conditions considered in the present study. Finally, the displacement amplitude versus frequency response was plotted for the unreinforced and reinforced conditions.

8.3.5 Experimental Program

Total four different series of block resonance tests were conducted: (i) series A: vibration tests on unreinforced foundation bed, (ii) series B: vibration tests on single-layer geogrid reinforced bed, (iii) series C: vibration tests on two-layer geogrid reinforced bed and (iv) series D: vibration tests on geocell reinforced foundation bed. The tests were conducted with six different eccentricity angles. The increase in eccentricity angle simulates the different dynamic loading conditions over the footing. The schematic representation of different test conditions prepared in the field for the present investigation is shown in Fig. 8.9.

In each case, the frequency of the excitation was varied from 5 to 45 Hz with an increment of 5 Hz. Similarly, the eccentricity angle was varied from 10° to 60° with an increment of 10°. In series B, the optimum depth of placement of geogrid was determined by varying the location of geogrid from the ground surface. The optimum depth of geogrid was determined based on the rate of reduction in displacement amplitude induced from the machine foundation. In addition, the effect of the second geogrid layer on reduction in amplitude was studied in the series C. The depth of placement of first geogrid layer (u) and vertical spacing between two geogrid layers (h) were maintained as $0.3B$ and $0.25B$, respectively (shown in Fig. 8.9c). In series D, the geocell was placed at a depth of $0.1B$ (where B is the width of the concrete footing) from the ground surface. The width of the geogrid and geocell was used as $3.3B$ in all the conditions. The fresh reinforced foundation bed was prepared for every new test condition. Total 38 numbers of field tests were conducted to understand the

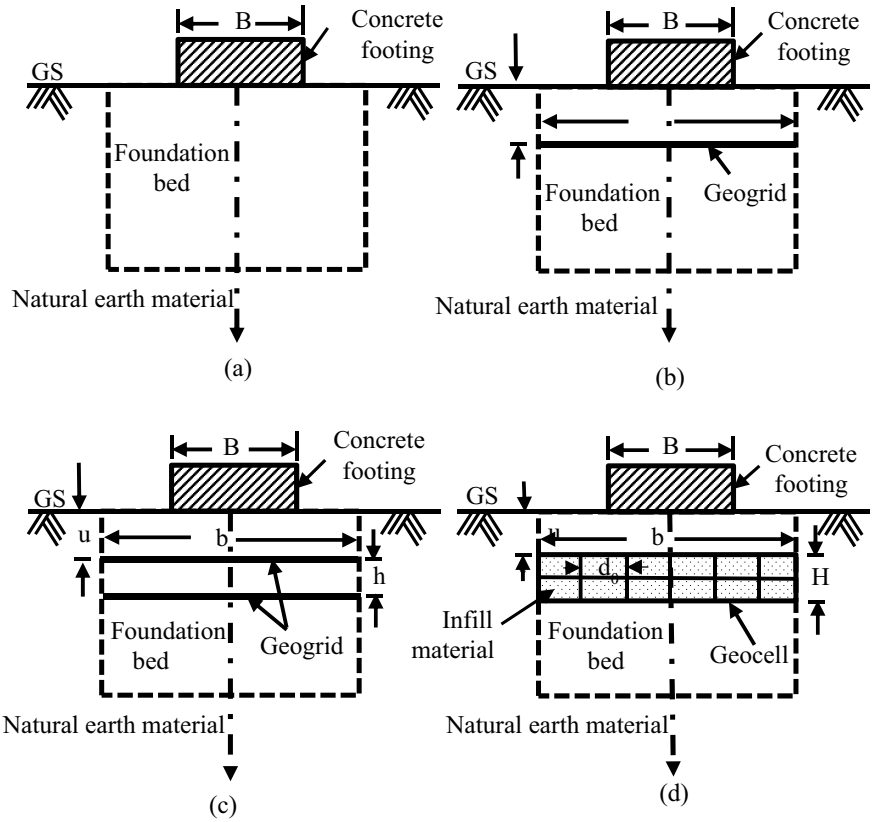

Fig. 8.9 Experimental program: **a** Unreinforced; **b** Geogrid reinforced; **c** Two-layer geogrid reinforced; **d** Geocell reinforced conditions. *Source* from Venkateswarlu et al. (2018)

dynamic response of geosynthetics reinforced soil under machine foundations. The details of the experimental investigation adopted for this study were presented in Table 8.4.

8.4 Results and Discussion

The variation in displacement amplitude with increase in frequency of the excitation and eccentricity angle (°) for unreinforced condition is presented in Fig. 8.10. From the figure, it is observed that the displacement amplitude was increased and resonant frequency was decreased with increase in eccentricity setting value. Several researchers (Baidya and Murali Krishna 2001; Baidya and Mandal 2006; Kumar and Reddy 2006; Mandal et al. 2012) have also reported the similar response. In addition, the maximum displacement amplitude was observed as compared to the remaining

Table 8.4 Details of the experimental investigation

Series number	Condition	u/B or u_c/B	Eccentricity angle (°)	Frequency (Hz)	Number of field tests
A	Unreinforced condition	…	10, 20, 30, 40, 50 and 60	5–45	6 + 2[a]
B	Single-layer geogrid reinforced condition	0.15,0.3, and 0.45	10, 20, 30, 40, 50 and 60	5–45	18
C	Reinforced with two layers of geogrid	0.3	10, 20, 30, 40, 50 and 60	5–45	6
D	Geocell reinforced condition	0.1	10, 20, 30, 40, 50 and 60	5–45	6
			Total number of tests		38

Source from Venkateswarlu et al. (2018)
[a]Represents the trail tests

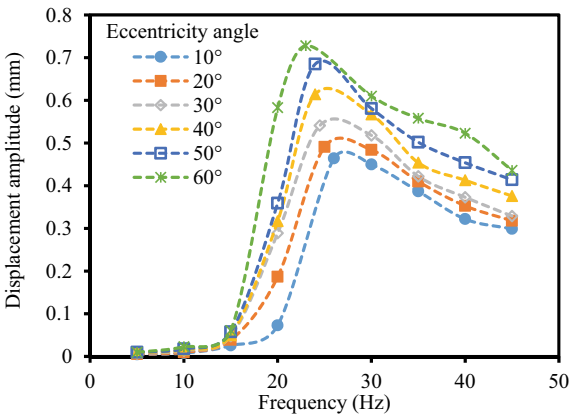

Fig. 8.10 Displacement amplitude versus frequency response for unreinforced condition. *Source* from Venkateswarlu et al. (2018)

conditions. The resonant frequency was found to vary between 26 and 23 Hz with the change in eccentricity angle from 10° to 60°.

The variation in displacement amplitude with the change in depth of placement of geogrid is presented in Fig. 8.11a–c. From the figure, it is observed that the amplitude of vibration was slightly reduced in the presence of geogrid as compared to the unreinforced condition. The maximum reduction in displacement amplitude was observed, when the geogrid was placed at a depth of 0.3B from the ground surface under the machine foundation. With the increase in depth of geogrid beyond 0.3B, i.e., at 0.45B, the increment in resonant amplitude was observed. Hence, 0.3B was considered as optimum depth of placement of geogrid for controlling the machine-induced

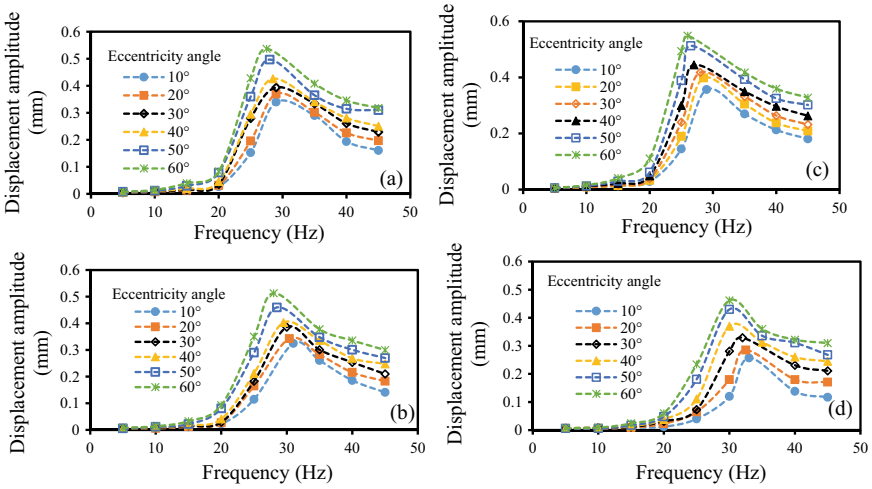

Fig. 8.11 Displacement amplitude versus frequency response for geogrid reinforced condition: **a** Geogrid @ 0.15*B*; **b** Geogrid @ 0.3*B*; **c** Geogrid @ 0.45*B*; **d** Reinforced with two layers of geogrid. *Source* from Venkateswarlu et al. (2018)

vibrations. The improvement in soil strength due to the lateral resistance mechanism provided by the geogrid reinforcement might be the reason for the reduction in displacement amplitude. In addition, the provision of geogrid reinforcement slightly improved the natural frequency of the foundation soil system.

Boominathan et al. (1991) and Sreedhar and Abhishek (2016) have reported the improvement in natural frequency of the system in the presence of reinforcement. Figure 8.11d shows the dynamic response of a two-layer geogrid reinforced soil system. From the figure, it is observed that the rate of reduction in displacement amplitude is high as compared to the single geogrid reinforced condition. Provision of the second layer has also enhanced the natural frequency of the system significantly.

The dynamic response of the geocell reinforced soil system is presented in Fig. 8.12. From the figure, the maximum reduction in resonant amplitude and improvement in resonant frequency were observed. It was found that the provision of geocell reinforcement exhibited better performance in controlling the amplitude of vibrations as compared to other conditions considered in the present study. It was majorly attributed due to the densification of the foundation bed through the all-round confinement provided by the geocell reinforcement. Further, the densification of foundation bed leads to the maximum improvement in natural frequency of the system.

In addition, from the displacement amplitude versus frequency response, the frequency improvement factor (F_{if}) and percentage reduction in displacement amplitude were calculated. The frequency improvement factor represents the improvement in resonant frequency of the foundation soil system in the presence of reinforcement. The F_{if} can be defined as

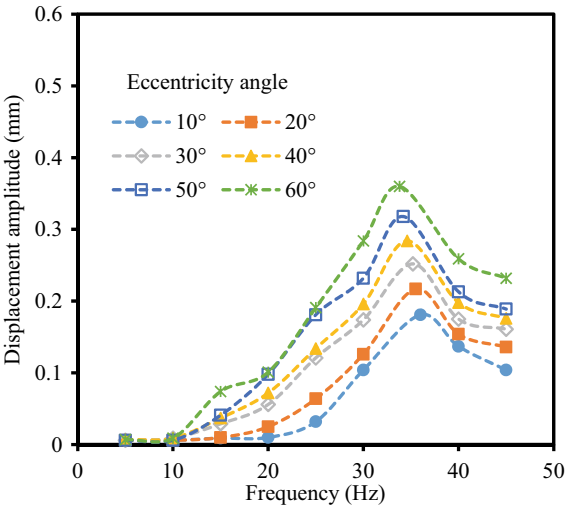

Fig. 8.12 Displacement amplitude versus frequency response for geocell reinforced condition. Sourced from Venkateswarlu et al. (2018)

$$F_{if} = \frac{F_r}{F_u} \tag{8.4}$$

where F_r is the resonant frequency of the reinforced soil system, and F_u is the resonant frequency of the unreinforced soil system at resonance. Figure 8.13 shows the variation of frequency improvement factor with increase in eccentricity angle for different reinforced conditions. From the figure, it was observed that the improvement in F_{if} with increase in eccentricity angle for the different conditions. However, the maximum F_{if} value i.e., 1.38 was observed in the presence of geocell reinforcement at an eccentricity angle of 60°. It means the resonant frequency of the foundation bed increased by 1.38 times due to the provision of geocell reinforcement. The improvement in resonant frequency helps to avoid the resonance. Similarly, the efficacy of reinforcement in reducing the displacement amplitude of unreinforced condition was

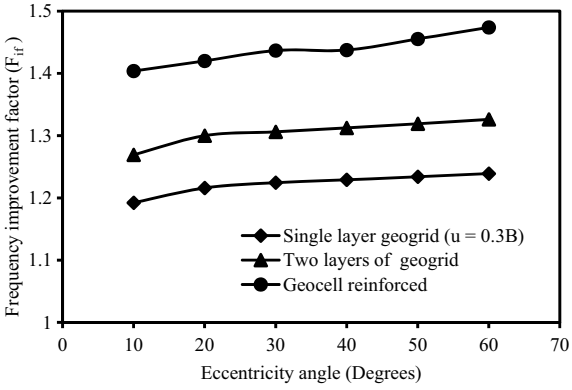

Fig. 8.13 Variation of frequency improvement factor with the increase in eccentricity angle for different conditions. *Source* from Venkateswarlu et al. (2018)

quantified in terms of percentage reduction in displacement amplitude (PRDA). The PRDA is defined as

$$\text{PRDA} = \left(\frac{A_{\text{un}} - A_{\text{r}}}{A_{\text{un}}}\right) \times 100 \tag{8.5}$$

where A_{un} is the displacement amplitude of unreinforced foundation bed corresponding to the resonant frequency, and A_{r} is the displacement amplitude of reinforced foundation bed at its resonant frequency. The reduction in displacement amplitude of the foundation bed was observed by 61%, 44% and 29%, respectively, in the presence of geocell, two-layer and single-layer geogrid cases.

The foundation beds supporting the machine foundations are recurrently subjected to the cyclic stresses due to rotating parts of the machine. These stresses are repetitive in nature and lead to increase in the permanent deformation of the foundation bed. It can be controlled by improving the elastic response of the soil. In the present study, the improvement in elasticity of the soil was studied in terms of coefficient of elastic uniform compression (C_{u}). It is the parameter, which represents the coefficient of subgrade reaction of the soil in vertical deformation mode. It is defined as the ratio between the pressure causing compression in the vertical direction to the corresponding vertical deformation. It can be determined by

$$C_{\text{u}} = 4\pi^2 f_{\text{nz}}^2 \frac{M}{A} \tag{8.6}$$

where M is the total mass of the concrete block and oscillator assembly, A is the contact area of the block with the soil, and f_{nz} is the natural frequency of the foundation soil system. The variation in coefficient of elastic uniform compression (C_{u}) with increase in eccentric setting value was shown in Fig. 8.14. From the figure, it was observed that the C_{u} of unreinforced bed was significantly improved in the presence of geosynthetics. The elastic response (C_{u}) was decreased with increase in

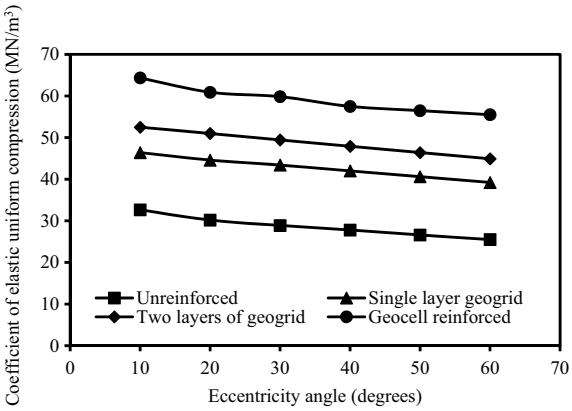

Fig. 8.14 Variation in coefficient of elastic uniform compression with increase in eccentricity value for different reinforced conditions. *Source* from Venkateswarlu et al. (2018)

eccentricity value. It was attributed due to the reduction in natural frequency of the system with increase in eccentricity value. Whereas, the percentage improvement in elastic response of unreinforced bed was increased. In the presence of geocell reinforcement, the improvement in C_u was observed in between 91 and 118% when the eccentricity value increased from 10° to 60°.

Based on the parameter C_u, the remaining coefficients, namely coefficient of elastic uniform shear (C_τ), coefficient of elastic non-uniform compression (C_ϕ) and coefficient of elastic non-uniform shear (C_Ψ) were determined. These parameters represent the deformation modes in uniform shear, non-uniform compression and non-uniform shear directions. These parameters were determined by using the relationships suggested by Barken (1962) as shown in Table 8.5. The reported results in the Table are corresponding to the eccentricity angle of 10° for different conditions.

The vibrations originated from the machine source may damage the adjacent structure or sensitive equipment of the machine. The amount of damage depends upon the ground motion behavior of the foundation bed. Hence, it is important to monitor the ground vibration levels caused by machine source, to take necessary measures to control their unfavorable effects. The ground motion behavior due to machine-induced vibrations was estimated in terms of peak particle velocity (*PPV*). It can be defined as the maximum velocity at which an individual soil particle vibrates or moves when the induced wave passes through the soil medium. In this study, the *PPV* was

Table 8.5 Variation of dynamic properties for different reinforced conditions

	Reinforced condition			
Dynamic property	Unreinforced	Single-layer geogrid reinforce (at 0.3*B*)	Two layers of geogrid reinforced	Geocell reinforced
Coefficient of elastic uniform compression, (C_u) (MN/m^3)	33.8	46.4	52.6	64.4
Coefficient of elastic uniform shear, ($C_\tau = 0.5\ C_u$) (MN/m^3)	16.9	23.2	26.3	32.2
Coefficient of elastic non-uniform compression, ($C_\phi = 2\ C_u$) (MN/m^3)	67.6	92.8	105.2	128.8
Coefficient of elastic non-uniform shear, ($C_\Psi = 0.75\ C_u$) (MN/m^3)	25.35	34.8	39.45	48.3

Source from Venkateswarlu et al. (2018)

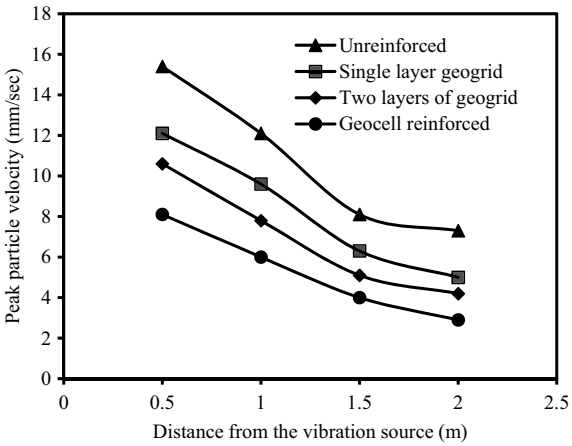

Fig. 8.15 Variation of peak particle velocity along the centerline of the footing for different conditions. *Source* from Venkateswarlu et al. (2018)

monitored at predetermined locations over the ground surface along the longitudinal direction of the foundation bed. The soil particle velocity was monitored through vibration meter by placing the accelerometer at required locations. These distances were varied from 0.5 to 2 m with an interval of 0.5 m. Figure 8.15 shows the variation of *PPV* for different conditions at an eccentricity angle of 100 at different distances away from the block. From the figure, it was observed that the *PPV* decreased with increase in distance from the footing in all the conditions. The maximum *PPV* was reported in the case of unreinforced condition. In addition, the reduction in *PPV* was observed in the presence of geogrid and geocell reinforcements. However, the maximum reduction in *PPV* was observed in the presence of geocell reinforcement. About 33, 24 and 48% reductions in *PPV* were observed in the presence of geocell at 0.5 m distance from the footing face as compared to the single, two-layer geogrid and unreinforced conditions, respectively. It is evident from the figure that the role of geocell was significant in controlling the ground vibration levels induced from the vibration (machine) source. It was attributed due to the absorption of the vibration in the presence of geocell reinforcement.

8.5 Conclusions

The efficacy of geosynthetics in improving the performance of machine foundation bed has been evaluated through the laboratory cyclic plate load tests and vertical mode block resonance tests. The cyclic plate load test results revealed the four times improvement in the natural frequency of the foundation bed in the presence of geocell and geogrid. During block resonance tests, four different conditions, namely unreinforced, single-layer geogrid reinforced, two layers of geogrid reinforced and geocell reinforced conditions were considered. The effectiveness of geosynthetics reinforced soil mass was evaluated based on the reduction in amplitude of the vibration and soil

particle velocity. From the experimental results, the performance of geosynthetics reinforced soil was found to be effective in controlling the machine vibrations. The optimum depth of placement of geogrid was found at $0.3B$ in the case of geogrid reinforced condition. The performance of geocell was found more effective than other conditions considered in the present study. In the presence of geocell, the displacement amplitude was reduced by 61, 44 and 29% as compared to the unreinforced, single and double-layer geogrid reinforced conditions. The peak particle velocity of unreinforced soil was reduced by 48% with the provision of geocell reinforcement. In addition, 91% improvement in the elastic properties of the foundation bed was observed in the presence of geocell as compared to the unreinforced condition. In this way, the present study demonstrates the efficacy of geosynthetics in supporting machine foundations.

References

Abd AH, Utili S (2017) Design of geosynthetic-reinforced slopes in cohesive backfills. Geotext Geomembr 45(6):627–641

ASTM D-4885 (2011) Standard test method for determining performance strength of geomembranes by wide strip tensile method. ASTM International, West Conshohocken, PA, USA

ASTM D-6637 (2011) Standard test method for determining the tensile properties of geogrid by the single or multi-rib tensile method. ASTM International, West Conshohocken, PA, USA

Baidya DK, Mandal A (2006) Dynamic response of footing resting on a layered soil system. West Indian J Eng 28(2):65–79

Baidya D, Murali Krishna G (2001) Investigation of resonant frequency and amplitude of vibrating footing resting on a layered soil system. ASTM Geotech Test J 24(4):409–417

Barkan DD (1962) Dynamics of bases and foundations. McGraw Hill Book Co., Inc., New York, NY, USA

Bhatia KG (2008) Foundations for industrial machines and earthquake effects. ISET J Earthq Technol 45:13–29

Bhatia KG (2009) Foundations for industrial machines: handbook for practising engineers. CRC

Biabani MM, Indraratna B (2015) An evaluation of the interface behaviour of rail subballast stabilised with geogrids and geomembranes. Geotext Geomembr 43(3):240–249

Biabani MM, Indraratna B, Ngo NT (2016) Modelling of geocell-reinforced subballast subjected to cyclic loading. Geotext Geomembr 44(4):489–503

Boominathan S, Senathipathi K, Jayaprakasam V (1991) Field studies on dynamic properties of reinforced earth. Soil Dyn Earthq Eng 10(8):402–406

Cao WZ, Zheng JJ, Zhang J, Zhang RJ (2016) Field test of a geogrid-reinforced and floating pile-supported embankment. Geosynthetics Int 23(5):348–361

Chen RP, Wang YW, Ye XW, Bian XC, Dong XP (2016) Tensile force of geogrids embedded in pile-supported reinforced embankment: a full-scale experimental study. Geotext Geomembr 44(2):157–169

Chen Q, Hanandeh S, Abu-Farsakh M, Mohammad L (2017) Performance evaluation of full-scale geosynthetic reinforced flexible pavement. Geosynthetics Int 25(1):26–36

Clement S (2015) Experimental studies on dynamic response of a block foundation on sand reinforced with geogrid. In: Geosynthetics 2015, 15–18 Feb Portland, Oregon, pp 479–488

Correia NS, Zornberg JG (2018) Strain distribution along geogrid-reinforced asphalt overlays under traffic loading. Geotext Geomembr 46(1):111–120

Costa CML, Zornberg JG, de Souza Bueno B, Costa YDJ (2016) Centrifuge evaluation of the time-dependent behavior of geotextile-reinforced soil walls. Geotext Geomembr 44(2):188–200
Das BM (1992) Principles of soil dynamics. PWS-KENT Publishing Company, Boston
Esmaeili M, Zakeri JA, Babaei M (2017) Laboratory and field investigation of the effect of geogrid-reinforced ballast on railway track lateral resistance. Geotext Geomembr 45(2):23–33
Ferreira FB, Topa Gomes A, Vieira CS, Lopes ML (2016) Reliability analysis of geosynthetic-reinforced steep slopes. Geosynthetics Int 23(4):301–315
Gao Y, Yang S, Zhang F, Leshchinsky B (2016) Three-dimensional reinforced slopes: evaluation of required reinforcement strength and embedment length using limit analysis. Geotext Geomembr 44(2):133–142
Girout R, Blanc M, Thorel L, Dias D (2018) Geosynthetic reinforcement of pile-supported embankments. Geosynthetics Int 1–13
Hegde A (2017) Geocell reinforced foundation beds-past findings, present trends and future prospects: a state-of-the-art review. Constr Build Mater 154:658–674
Hegde AM, Sitharam TG (2015) Experimental and numerical studies on protection of buried pipelines and underground utilities using geocells. Geotext Geomembr 43(5):372–381
Hegde A, Sitharam TG (2016) Behaviour of geocell reinforced soft clay bed subjected to incremental cyclic loading. Geomech Eng 10(4):405–422
Hegde, A., Kadabinakatti, S., & Sitharam, T. G. (2014). Protection of buried pipelines using a combination of geocell and geogrid reinforcement: experimental studies. In: Ground improvement and geosynthetics, pp 289–298
IS 5249 (1992) Determination of dynamic properties of soil-method of test. Indian standard, New Delhi, India, 110002
IS: 2720-29 (1975) Methods of test for soil—part XXIX: determination of dry density of soils in-place. Prabhat Offset Press, Delhi, India, 4–8
Javankhoshdel S, Bathurst RJ (2016) Deterministic and probabilistic failure analysis of simple geosynthetic reinforced soil slopes. Geosynthetics Int 24(1):14–29
King DJ, Bouazza A, Gniel J, Rowe K, Bui H (2017) Geosynthetic reinforced column supported embankments and the role of ground improvement installation effects. Can Geotech J 1–18
Kumar J, Reddy CO (2006) Dynamic response of footing and machine with spring mounting base. Geotech Geol Eng 24(1):15–27
Luo F, Zhang G, Liu Y, Ma C (2018) Centrifuge modeling of the geotextile reinforced slope subject to drawdown. Geotext Geomembr 46(1):11–21
Mandal A, Baidya DK, Roy D (2012) Dynamic response of the foundations resting on a two-layered soil underlain by a rigid layer. Geotech Geol Eng 30(4):775–786
Mehrjardi GT, Khazaei M (2017) Scale effect on the behaviour of geogrid-reinforced soil under repeated loads. Geotext Geomembr 45(6):603–615
Mehrjardi GT, Ghanbari A, Mehdizadeh H (2016) Experimental study on the behaviour of geogrid-reinforced slopes with respect to aggregate size. Geotext Geomembr 44(6):862–871
Mohapatra SR, Rajagopal K (2017) Undrained stability analysis of embankments supported on geosynthetic encased granular columns. Geosynthetics International 24(5):465–479
Mousavi SH, Gabr MA, Borden RH (2017) Optimum location of geogrid reinforcement in unpaved road. Can Geotech J 54(7):1047–1054
Nejad FM, Asadi S, Fallah S, Vadood M (2016) Statistical-experimental study of geosynthetics performance on reflection cracking phenomenon. Geotext Geomembr 44:178–187
Nimbalkar S, Indraratna B (2016) Improved performance of ballasted rail track using geosynthetics and rubber shockmat. J Geotech Geoenviron Eng 142(8):1–13
Plácido R, Portelinha FHM, Futai MM (2018) Field and laboratory time-dependent behaviors of geotextiles in reinforced soil walls. Geosynthetics Int 1–15
Raman J (1975) Dynamic response of footing soil system to vertical vibration. Ph.D. thesis, Indian Institute of Science, Bangalore, India
Richart FE Jr, Hall JR, Woods RD (1970) Vibrations of soils and foundations. Prentice-Hall, Inc., Englewood Cliffs

Rowe RK, Taechakumthorn C (2011) Design of reinforced embankments on soft clay deposits considering the viscosity of both foundation and reinforcement. Geotext Geomembr 29:448–461
Saha Roy S, Deb K (2017) Effects of aspect ratio of footings on bearing capacity for geogrid-reinforced sand over soft soil. Geosynthetics Int 24(4):362–382
Saride S, Kumar VV (2017) Influence of geosynthetic-interlayers on the performance of asphalt overlays on pre-cracked pavements. Geotext Geomembr 45(3):184–196
Shahin HM, Nakai T, Morikawa Y, Masuda S, Mio S (2017) Effective use of geosynthetics to increase bearing capacity of shallow foundations. Can Geotech J 54(12):1647–1658
Sitharam TG, Hegde A (2013) Design and construction of geocell foundation to support the embankment on settled red mud. Geotext Geomembr 41:55–63
Song F, Liu H, Hu H, Xie Y (2018) Centrifuge tests of geocell-reinforced retaining walls at limit equilibrium. J Geotech Geoenviron Eng 144(3):1–13
Sreedhar MVS, Abhishek J (2016) Effect of geosynthetic reinforcement on dynamic characteristics through model block resonance tests. In: Indian Geotechnical conference IGC 2016, pp 1–4
Srinivasalu P, Vaidyanathan CV (1976) Handbook of machine foundations. Tata Mcgraw Hill Publishing Company Limited, New Delhi, India
Suku L, Prabhu SS, Babu GS (2017) Effect of geogrid-reinforcement in granular bases under repeated loading. Geotext Geomembr 45(4):377–389
Sun X, Han J, Corey R (2017) Equivalent modulus of geogrid-stabilized granular base back-calculated using permanent deformation. J Geotech Geoenviron Eng 143(9):1–8
Tafreshi SM, Dawson AR (2012) A comparison of static and cyclic loading responses of foundations on geocell-reinforced sand. Geotext Geomembr 32:55–68
Venkateswarlu H, Ujjawal KN, Hegde A (2018) Laboratory and numerical investigation of machine foundations reinforced with geogrids and geocells. Geotext Geomembr 46(6):882–896
Wan, HL, Chen RP, Cheng W, Qi S, Cui YJ (2018) Full-scale model study on variations of soil stress in geosynthetic-reinforced pile-supported track-bed with water level change and loading cycles. Can Geotech J 1–44
Yoo C (2018) Serviceability state deformation behaviour of two-tiered geosynthetic reinforced soil walls. Geosynthetics Int 1–14
Yu Y, Bathurst RJ, Allen TM, Nelson R (2016) Physical and numerical modelling of a geogrid-reinforced incremental concrete panel retaining wall. Can Geotech J 53(12):1883–1901

Chapter 9
Design of Geocell-Reinforced Pavement Bases

Sireesh Saride and Vijay Kumar Rayabharapu

Abstract This chapter deals with the design of geocell-reinforced pavement bases which includes the evaluation of the influence of geocell reinforcement on granular aggregate base courses overlying weak clayey soil subgrades. A series of large-scale model tests under static and repeated loading was performed to obtain the influence of geocell-reinforcement, with and without basal geogrid, on the structural capacity of the base layer. An improved stiffness and resilient behavior of the granular base layer was obtained with the geocell-reinforcement in lieu of an additional lateral confinement provided to the granular material. The normalized contact pressure at the interface of the granular base and weak subgrade layers was observed to be well minimal. From the pilot field studies, it was also observed that about 62% of the applied pressure has been absorbed by the reinforced granular base layer and transmitted about 38% to the underlying weak subgrade layer. Finally, two design methodologies, viz traffic benefit ratio (TBR) approach and layer coefficient ratio (LCR) approach, are discussed in this chapter along with the examples from the inputs of the large-scale testing.

Keywords Base course · Geocell reinforcement · Contact pressure · Settlements · Traffic benefit ratio · Layer coefficient ratio

9.1 Introduction and Background

A variety of soil subgrades ranging from dense to very loose and stiff to very weak are encountered around the world. Stabilizing such weak subgrades is inevitable as availability of good construction sites is limited and at times, they are unavoidable. For the past few decades, the use of geosynthetics has been gaining advantages

S. Saride (✉)
Indian Institute of Technology, Hyderabad, Telangana, India
e-mail: sireesh@ce.iith.ac.in

V. K. Rayabharapu
BV Raju Institute of Technology, Narsapur, Telangana, India
e-mail: vkraya@gmail.com

T. G. Sitharam et al. (eds.), *Geocells*, Springer Transactions in Civil and Environmental Engineering,
https://doi.org/10.1007/978-981-15-6095-8_9

over the other improvement methods, especially in the pavement industry. Recently, the application of geocells in pavement layers has been showing high-performance improvement as it can provide additional lateral confinement to the infill material over and above the stabilization functions provided by conventional geosynthetics. Several research studies have shown in the past that the geocell reinforcement is effective when a granular infill is used over weak subgrades (Dash et al. 2003; Rajagopal et al. 2012; Pokharel et al. 2011; Perkins and Ismeik 1997; Latha et al. 2010) under monotonic loading conditions. Studies were performed on varieties of geosynthetics such as geotextiles and grids under cyclic loading under a moving single wheel system in an outdoor test track (Barker 1987; Haas et al. 1988; Barksdale et al. 1989; Collin et al. 1996). These studies reported a traffic benefit ratio (TBR) of 2.8 and 2.3 when a moving single wheel applying a pressure of 500 kPa. Pokharel (2010) demonstrated the behavior of geocell-reinforced granular bases over clay subgrades under cyclic loading. However, not much information is reported in the literature on repeated load tests on pavement sections reinforced with geocells with extensive instrumentation.

Besides, field performance studies on geocell-reinforced pavements are very few. Field tests on full-scale road sections have been conducted by Perkins and Ismeik (1997) and compared the results from nine test track sections including indoor and outdoor using a two-axle, dual-wheel truck to load the pavement which resulted in significant improvement with the geosynthetic reinforcement. Latha et al. (2010) performed field studies on unpaved roads reinforced with a variety of geosynthetics including geocells and reported an increase in load-carrying capacity with a reduction in rut depth. However, the behavior of geocells in the actual field conditions under cyclic/repeated loading is not understood completely to derive the design parameters.

The reinforcing effect of geosynthetics in pavements is usually assessed through two parameters, i.e., traffic benefit ratio (TBR) (AASHTO 2009) and layer coefficient ratio (LCR). The LCR is defined as the ratio of the layer coefficient of a reinforced section to reach a given rutting depth to the ratio of layer coefficient of an unreinforced section with the same geometry and material constituents that reaches the same rutting depth. The LCR value can be determined in the laboratory on a large-scale test through modulus improvement factor, MIF (Giroud and Han 2013) as follows.

$$\mathrm{LCR} = \frac{0.249 \log 10\left(\mathrm{MIF} * \frac{\mathrm{Mrbc}}{0.0069}\right) - 0.977}{0.249 \log 10\left(\frac{\mathrm{Mrbc}}{0.0069}\right) - 0.977} \tag{9.1}$$

where

MIF = Modulus improvement factor

M_{rbc} = Resilient modulus of base course in MPa.

The American Association of State Highways and Transportation Officials (AASHTO) proposed a flexible pavement design based on overall structural number (SN) (AASHTO 1993) as follows.

$$\mathrm{SN} = a_1 D_1 + a_2 D_2 m_2 + a_3 D_3 m_3 \tag{9.2}$$

where SN = Structural number depends on the pavement layer thicknesses (D), layer coefficients (a), and drainage coefficients (m).

In order to design the reinforced pavement section, the traffic benefit ratio (TBR) can be used. The effect of geocell reinforcement is quantified in terms of equivalent structural number by considering traffic to be catered by the pavement and TBR that can be obtained with selected geocell. The equivalent structural number of geocell is then used to reduce the unreinforced pavement layer thicknesses to the extent of the reinforcement effect.

In this chapter, the behaviors of geocell, with/without basal layers overlying weak clay subgrades subjected to static and repeated loading, are discussed through extensive experimental studies and field studies. At this point, the guidelines available to design pavements incorporating geosynthetics are in the nascent stage. The design methodologies presented in IRC SP 59 (2019) are discussed.

9.2 Experimental Studies

Before conducting actual field studies on geocell-reinforced granular bases, extensive laboratory studies were performed to ascertain the efficacy of the geocell reinforcement in pavements. For the laboratory experimental program, clayey soil was selected to replicate a very weak subgrade. It was envisioned that the effect of geocells can be visualized over weak subgrades. Conventional granular aggregate material (wet mix macadam, WMM) was adopted to use as an infill material, and a geocell mattress made of high-density polypropylene (HDPE) material was selected.

9.2.1 Material Properties

Clayey Soil

The material used for the preparation of subgrade is a natural lateritic sandy clay obtained from an open excavation on the campus of the Indian Institute of Technology, Hyderabad. Wet sieve analysis was performed to determine the particle size distribution of the soil. Figure 9.1 shows the particle size distribution curve of clayey soil, which had a 40% fines fraction smaller than 75 μ sieve size. The specific gravity of the soil is 2.68.

The maximum unit weight of 20.5 kN/m^3 and 14% optimum moisture content are obtained for the soil. Liquid limit and plastic limits are found to be 46% and 21%, respectively. As per the USCS, the soil can be classified as clayey sand (SC). To know the shear strength parameters of the soil, compacted at wet unit weight, standard triaxial compression tests were conducted. A friction angle of 14° and a cohesion of 14 kPa were observed from the triaxial tests.

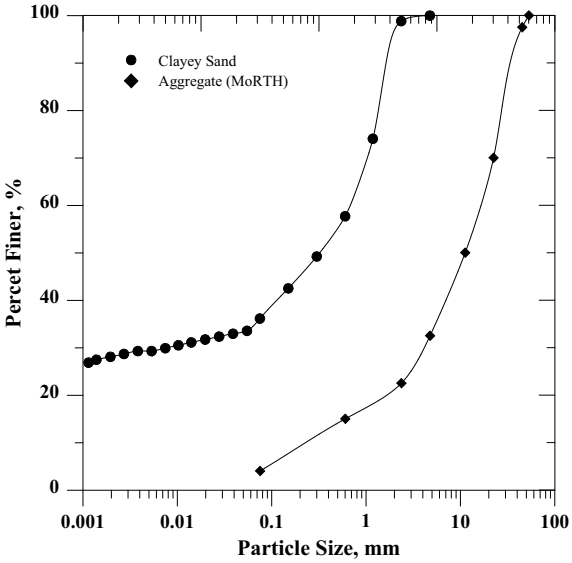

Fig. 9.1 Grain size distribution of clayey soil and granular base material

Granular Aggregate

The granular base infill material was obtained from a local suburban quarry site near the campus. The aggregate material has been chosen according to the Ministry of Road transport and Highways (MORTH) specification for the pavement base layers. The particle size distribution of aggregates is obtained by performing dry sieve analysis and the corresponding gradation curve of aggregates as shown in Fig. 9.1.

Geocell

A high-density polyethylene (HDPE) geocell material was selected for the study. Various properties of the geocells like the material composition, density, weld spacing, weld depth, and seam strength are given in Table 9.1.

Test Setup

Table 9.1 Properties of geocell material

Properties	Values
Density, g/cm^3	0.935–0.965
Weld spacing (mm)	356
Cell depth (mm)	200
Min. seam strength (N)	2800
Cell size (±10%) (mm)	259 × 224
Cell area (±4%)	290

Figure 9.2 shows the experimental facility consisting of a test tank of size 1.0 m × 1.0 m × 1.0 m, a double-acting linear actuator to apply traffic loads a reaction frame to support the actuator, and a controller and recording system used in the current study. The clayey soil subgrade was first prepared in a test tank. A fairly uniform average bulk unit weight of 20.5 kN/m^3 at 20% placement water content was consistently maintained throughout the test program. In order to verify the uniformity of the testbed, undisturbed core samples were collected from different locations to determine the in situ unit weight and moisture contents. The data shows that the bed properties are fairly maintained with an error margin of 2%. At this compacted condition, the subgrade has an undrained strength of 10 kPa determined from a series of unconfined compressive strength tests. Once the weak subgrade was prepared up to the required grade in the test tank, granular base layers were prepared on the weak subgrade with or without geocell reinforcement.

To prepare the unreinforced testbed, the granular base layer was placed in the test tank and compacted in 50 mm thick layers till the desired height was reached. For each layer, the required amount of aggregate to produce a desired bulk unit weight 23 kN/m^3 was weighed out and placed in the test box making use of a metal scoop. The granular base was then gently leveled and compacted using a 5.0 kg drop hammer to a pre-calibrated number of blows to achieve the required density. A similar procedure was used to compact the base material inside the geocell pockets as well. Once the

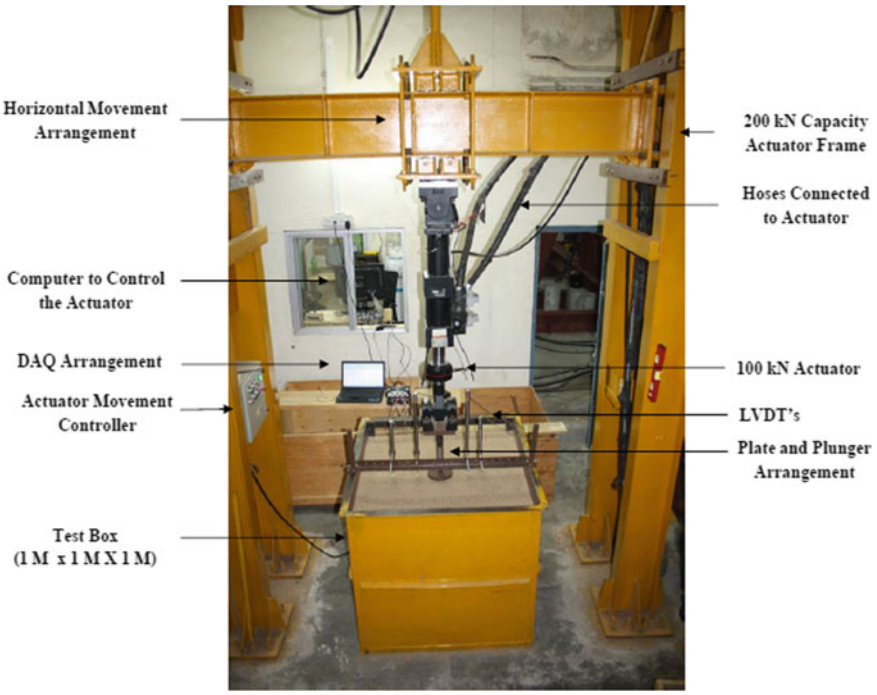

Fig. 9.2 Experimental facility used in the current study

final grade was reached, a rigid thin steel plate of 150 mm diameter (D) and 15 mm thickness was concentrically placed to apply an appropriate repeated traffic loading. Loading was given by graphical user interfaced MTS® multi-purpose test software with the help of hydraulic power unit (HPU), hydraulic service manifold (HSM), and sophisticated double-acting linear dynamic 100 kN capacity actuator which is attached to a 3.5 m high, 200 kN capacity reaction frame as shown in Fig. 9.2.

Normal contact pressure developed on the subgrade at various points was measured using strain gauge type earth pressure cells. Five numbers of total earth pressure cells (TPC) with one 1000 kPa, two of 500 kPa, and two of 200 kPa capacities were used. The 1000 kPa capacity pressure cell was placed at the centerline of the loading plate, and 500 and 200 kPa TPCs were kept at a distance of 1.0D, 1.5D, and 2D from the centerline of the loading plate on either side of the plate, respectively, as shown in test schematic Fig. 9.3. In the case of unreinforced sections, the TPCs were placed at the interface. The pressures were measured from a DAQ system, which directly shows the pressure through the computer display connected to it.

In addition, the vertical deformations (i.e., settlement of the loading plate and surface heave/settlement of the bed) were measured using linear variable differential transformers (LVDT's). The LVDT's were of 50 mm and 100 mm travel with 0.001 accuracy. Small plates of size 20 mm length × 20 mm width × 4 mm thickness made of perspex sheet were placed on the compacted granular surface at required locations to support the LVDTs, where the surface deformations are to be measured.

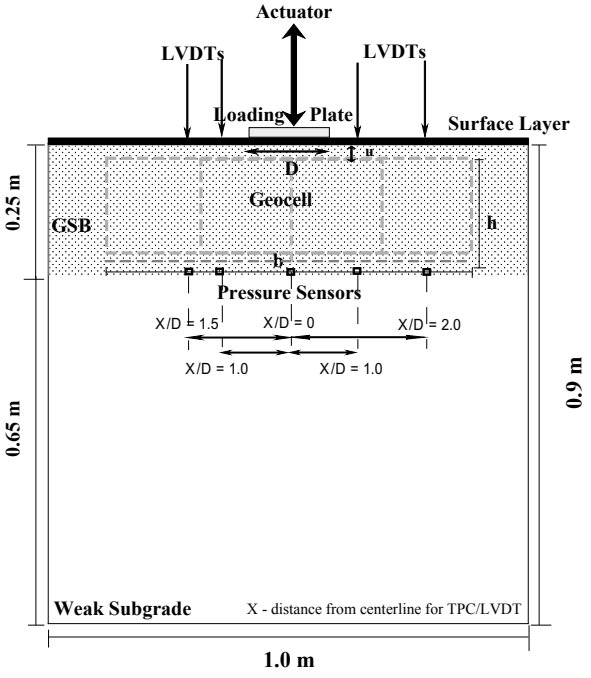

Fig. 9.3 Schematic test setup of geocell-reinforced clayey soil subgrade

The deformations (heave/settlement) of the soil surface on either side of the footing were measured by dial gauges placed at a distance of 1.0*D*, 1.5*D,* and 2.0*D* from the centerline on either side of the loading plate. The placement position of these LVDT's was decided based on the findings reported by Chummar (1972) that the heaving on soil surface extends up to a distance of about twice the width of the footing from the edge of the footing with a maximum heaving occurring at around 1.5D from the center of the footing. A close-up view of the LVDT's used in the test setup can also be seen in Figs. 9.2 and 9.3.

9.3 Experimental Program

Figure 9.3 shows the schematic of geocell-reinforced granular base over weak clayey subgrades used in the study. A series of monotonic and repeated load tests were conducted on geocell-reinforced granular base over weak clayey subgrades and along with the placement of additional basal geogrid as summarized in Table 9.2. All the other optimum geocell geometric parameters were maintained from Saride et al. (2015) while subgrade conditions are kept constant. The objective of the experimental program is to understand how much rut depth can be controlled by using geocells in the base layer as well as to quantify the benefit in terms of traffic.

In a static load test, the load was applied in displacement mode at a rate of 0.5 mm/min. In a repeated load test, the load was applied on to the plate using a

Table 9.2 Details of testing program

Test description/Nomenclature	Constant parameters
Unreinforced **g**ranular base over **c**layey soil subgrade (UGC)	$\Upsilon_d = 23.1$ kN/m^3 $C_u = 10$ kPa $H/D = 1.67$
Unreinforced **g**ranular base over **c**layey soil subgrade and **s**urface **l**ayer (U G C SL)	Surface layer $\Upsilon_d = 23.1$ kN/m^3, $C_u = 10$ kPa $H/D = 1.67$
Geocell-reinforced **g**ranular base over **c**layey soil subgrade (G G C)	$\Upsilon_d = 23.1$ kN/m^3, $C_u = 10$ kPa $H/D = 1.67$, $b/D = 4$, $h/D = 1.33$.
Geocell and **b**asal **g**eogrid-reinforced **g**ranular base over **c**layey soil subgrade (G BG G C)	$\Upsilon_d = 23.1$ kN/m^3, $C_u = 10$ kPa $H/D = 1.67$, $b/D = 4$, $h/D = 1.33$, $B/D = 4.33$.
Geocell-reinforced **g**ranular base over **c**layey soil subgrade and **s**urface **l**ayer (G G C SL)	Surface layer $\Upsilon_d = 23.1$ kN/m^3, $C_u = 10$ kPa $H/D = 1.67$, $b/D = 4$, $h/D = 1.33$.
Geocell and **b**asal **g**eogrid-reinforced **g**ranular base over **c**layey soil subgrade and **s**urface **l**ayer (G BG G C SL)	Surface layer $\Upsilon_d = 23.1$ kN/m^3, $C_u = 10$ kPa $H/D = 1.67$, $b/D = 4$, $h/D = 1.33$, $B/D = 4.33$

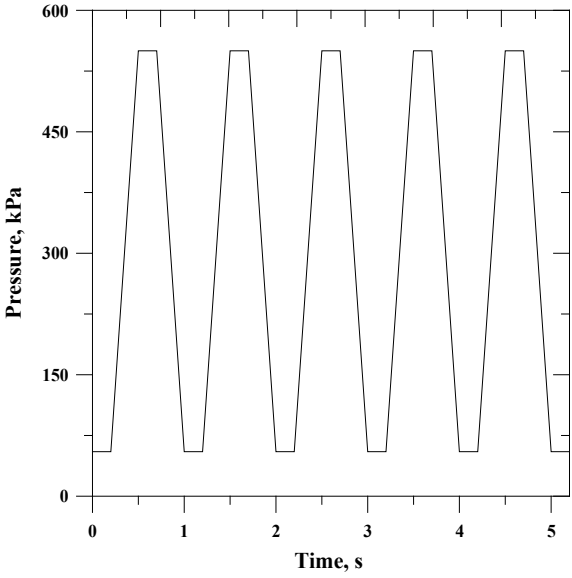

Fig. 9.4 Typical loading pattern used in the test

computer-controlled servo-hydraulic actuator, with a maximum load of 9.7 kN and a minimum of 0.97 kN (10% of the maximum load) using a continuous haversine loading pattern as shown in Fig. 9.4 at a frequency of 1.0 Hz as described in Saride et al. (2013) to maintain a single-axle wheel load corresponding to a contact pressure of 550 kPa.

The depth of the reinforcement layer from the bottom of the plate was maintained at 0.1 times the diameter of the plate ($u/D = 0.1$) according to Sitharam and Saride (2005) and Dash et al. (2003). The equivalent diameter of geocell pockets, d_c, was maintained at about $1.6D$ in all the tests. Tests were terminated while reaching a plate settlement of about 20%.

9.4 Test Results

The data obtained from static and repeated load tests along with the instrumentation data are presented in terms of performance indicators. Influence of geocell, geocell with additional basal geogrid, geocell, and basal geogrid with flexible surface layer reinforcements on the performance improvement of weak clayey soil subgrades are presented. The performance improvement is quantified using several relevant parameters including improvement factors (I_f), reduction in settlement (RS), especially from static load tests. The performance improvement due to repeated load tests is presented in terms of plastic deformations (PD), cumulative plastic deformations (CPD), which are also can be referred to as rut depth, and traffic benefit ratio (TBR), in addition to the elastic moduli viz apparent resilient modulus (M_r), and modulus

improvement factor (MIF). The definitions of performance indicators are presented in the discussions.

9.4.1 Static Tests

Pressure-settlement responses were monitored to verify the performance of reinforced granular base layer overlying weak subgrade soil. The pressure-settlement responses observed for unreinforced and geocell-reinforced granular base test series are shown in Fig. 9.5. The stiffness of the granular base layers reinforced with different reinforcement forms viz geocell, geocell with additional basal geogrid with and without surface layer, has increased with amount and form of reinforcement. The load-bearing pressure of weak subgrade can be improved by placing a dense granular layer. It is noted that the load-bearing pressure of the weak subgrade has been increased by about two times with granular bases.

The improvement factor (I_f), defined as the ratio of bearing pressure (q_c) with geocell reinforcement at a given settlement to the corresponding pressure on unreinforced soil (q_o) at the same settlement, is calculated for various reinforcement cases, and the variation of improvement factor for various test cases is presented in Fig. 9.6. The test configuration with geocell-reinforced granular base layer with basal geogrid and surface layer at 5% settlement ratio has obtained the maximum improvement factor of about 1.7. The geocell and basal geogrid provide lateral confinement and membrane support, respectively which is very important in any pavement section.

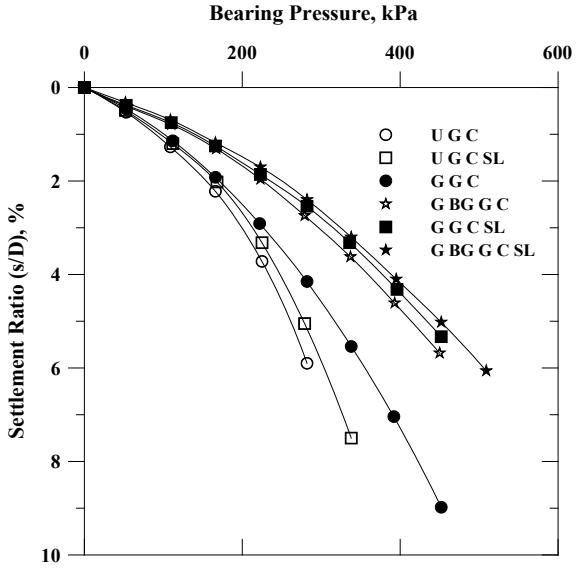

Fig. 9.5 Variation of bearing pressure with settlement ratio for unreinforced and reinforced bases under static loading

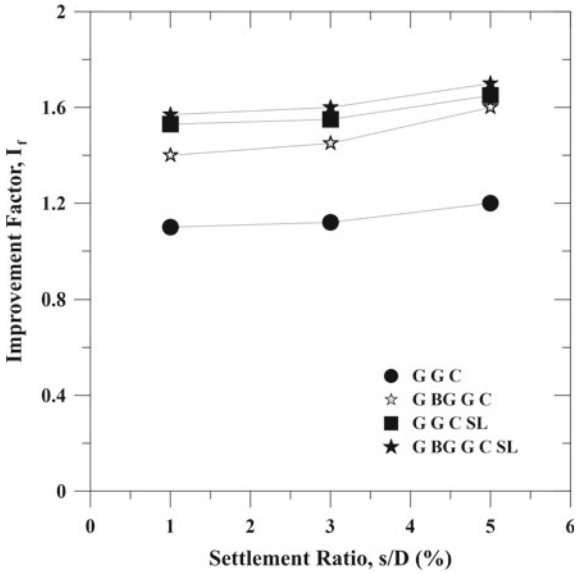

Fig. 9.6 Variation of improvement factors with settlement ratio for reinforced bases

The percentage reduction in settlements (RS) is calculated at the loading plate settlements (s_r) in the case of reinforced sand bed corresponding to the plate settlement (s_o) of the unreinforced bed. The percentage reduction in settlement for granular bases is calculated for geocell, geocell with additional basal geogrid layer and surface layers, and the RS values are ranging between 30 and 60%. The maximum RS is obtained for the geocell and basal geogrid with surface layer case and minimum in the case of only geocell which is attributed to the decreased settlements corresponding to the ultimate bearing pressure of the unreinforced bed. The variation of the percent reduction in settlements is shown in Fig. 9.7 for different test configurations.

It is important to obtain the elastic modulus of unreinforced and reinforced granular base layers to visualize the contribution from reinforced base layer alone in the load-carrying mechanism. This information is crucial in obtaining the base layer thicknesses with and without geocell reinforcement using available elastic solutions for two-layer systems. The elastic modulus of unreinforced and reinforced beds, independent of the base material, using three well-known methods is calculated. The details of these well-versed methods are not discussed here. The elastic modulus obtained from each method is presented in Table 9.3. It can be seen that the Ueshita and Meyerhof (1967) and Burmister (1943) theories yielded similar results; however, the KENPAVE approach predicted slightly higher elastic modulus. The highest modulus of about 125 MPa was obtained in the case of geocell with a basal geogrid-reinforced granular base layer.

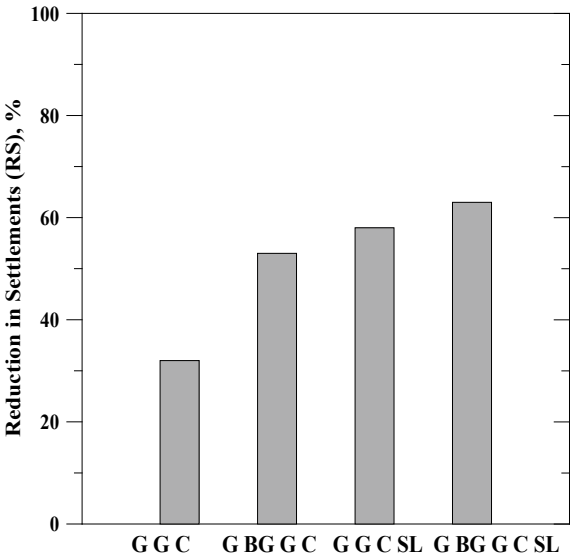

Fig. 9.7 Variation of percent reduction in settlements, RS

Table 9.3 Modulus of base layer using different methods for various test cases

Method	Ueshita and Meyerhof (1967)	Burmister (1943)	Modulus improvement factor
Test case	E_1 (MPa)	E_1 (MPa)	MIF $= E_{1r}/E_{1u}$
U G C	49.6	49.5	–
G G C	82	81.8	1.65
G BG G C	117.6	117.5	2.4

9.4.2 Repeated Load Tests

Repeated load tests, as discussed in Sect. 9.2, were performed on the test configurations presented in Table 9.2. The data obtained from the repeated load tests along with the instrumentation data are presented in terms of performance indicators.

The performance improvement due to repeated load tests are presented in terms of cumulative plastic deformations (CPD), which also can be referred as rut depth, and traffic benefit ratio (TBR). The plastic/permanent deformations are cumulatively added to obtain the cumulative permanent deformations (CPDs) expressed in percentage of the plate diameter. Extension of the life of a pavement is defined in terms of traffic benefit ratio (TBR). TBR is defined as the ratio of the number of cycles necessary to reach a given rut depth for a test section containing reinforcement, divided by the number of cycles necessary to reach the same rut depth for an unreinforced section with the same section thickness and subgrade properties.

The pressure-settlement response of geocell with and without basal layer reinforced granular base course overlying weak subgrade under repeated loading is shown in Fig. 9.8. The total settlement ratio, *s*/*D*, defined as the ratio of plate settlement and the diameter of the plate, is higher for the initial loading cycles, while their magnitude attenuates with the number of repetitions. The geocell with basal layer-reinforced aggregate base sustained for higher repeated cycles due to higher frictional resistance of the aggregate material, which will provide higher interlocking and confinement, by the geocells and membrane effect by the basal layer (Fig. 9.8).

The pressure-settlement data is further analyzed to evaluate the permanent deformations (rutting) on the surface and elastic nature of the beds by separating the elastic and plastic components of the total plate settlement for each repetitive load cycle. The variation of plastic/permanent deformations with the number of load cycles for various cases of reinforced granular base layers overlying weak clayey subgrade is shown in Fig. 9.9. The permanent deformations are predominant in the initial cycles as can be witnessed from corresponding pressure-settlement curves (Fig. 9.8) and become almost minimal with an increase in the number of load repetitions. The highest permanent deformation for aggregate base, is about 3.0 mm for geocell alone case, and it has been reduced to 1.5 mm with the inclusion of basal geogrid (Fig. 9.9). This is due to the structural support provided by the geocell and the membrane support by the geogrid layer to the encapsulated base material within the geocell pockets.

Further, the permanent deformations are cumulatively added to obtain the cumulative permanent deformations (CPDs) expressed in percentage of the plate diameter. The variation of CPD's with the number of cycles is seen in Fig. 9.10. It is observed that the granular bases have sustained lower CPDs for a given number of load repetitions. The reduction in CPD's for reinforced cases is attributed to the increase in elastic response of the bed due to the reinforcement.

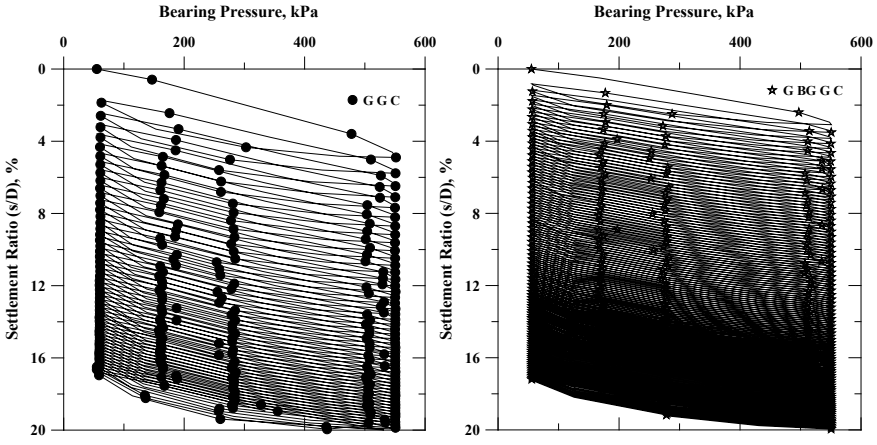

Fig. 9.8 Variation of bearing pressure with settlement ratio for geocell, geocell with basal geogrid-reinforced granular base layer

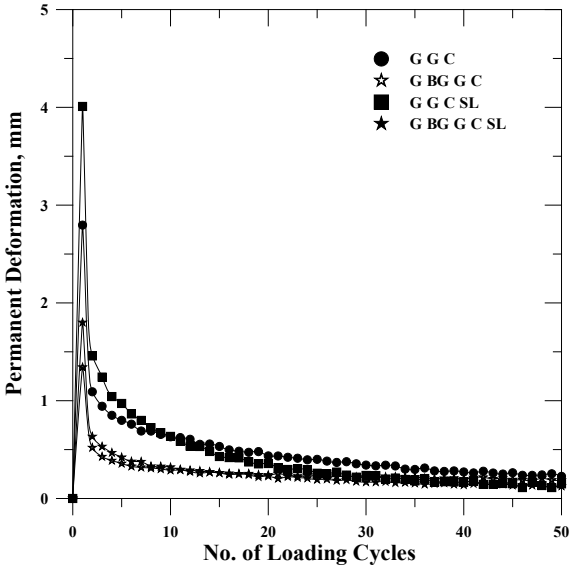

Fig. 9.9 Variation of permanent deformations with number of cycles for granular base layers

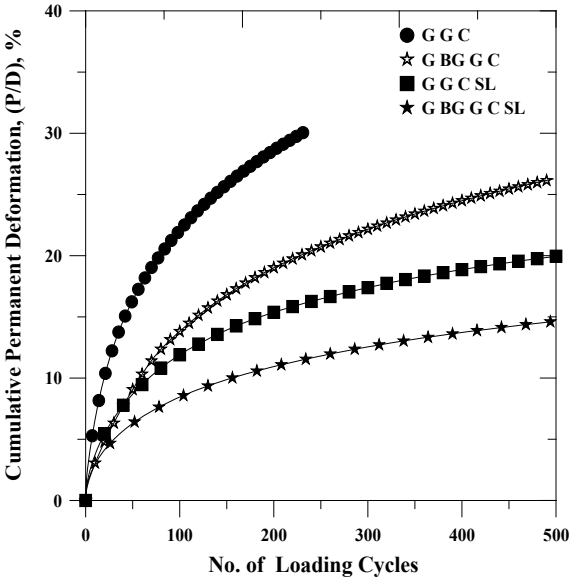

Fig. 9.10 Variation of cumulative plastic deformations with number of cycles for granular bases

Further, the variation of TBR with the number of load repetitions is shown in Fig. 9.11. The traffic benefit with geocell reinforcement gradually increased with an increase in load repetitions. The case with geocell and geocell with basal geogrid-reinforced granular base layers resulted in a TBR of 1.5 and 5, respectively, at a 5% settlement ratio. The TBR further increased to 4 and 8 with the surface layer. The

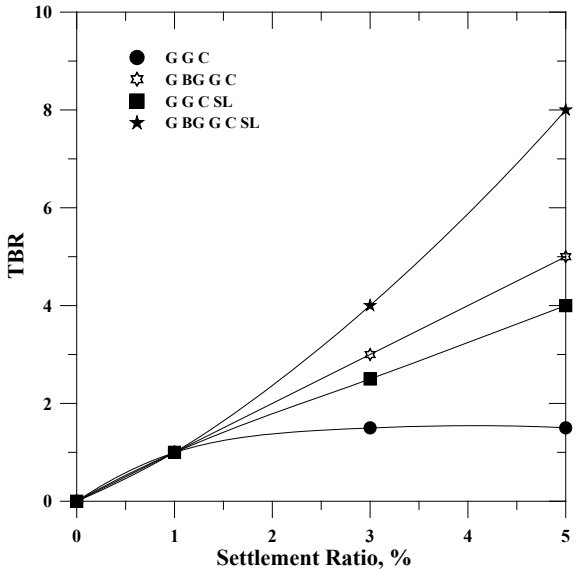

Fig. 9.11 Variation of TBR with settlement ratio for granular bases

higher TBRs are due to the combined membrane effect of the basal geogrid in addition to the confinement effect of the geocell and a stiff surface layer. Hence, for all practical purposes, the traffic benefit ratio shall be calculated when all the layers of flexible pavements are provided. The TBR values signify that the design life (or design traffic) of the pavement can be increased by about five times than its unreinforced section. In other words, the thickness of the pavement can be reduced with the optimal geocell configuration for a given design life of the pavement. Hence, base course thickness reduction can lead to economical pavement construction.

Contact Stress Distribution

The contact pressure on the weak subgrade was measured through several total earth pressure cells (TPC) placed at the interface as shown in Fig. 9.3. Figures 9.12, 9.13, and 9.14 present the surface deformations and contact stress distribution on the weak subgrade underlying unreinforced, geocell with/without basal geogrid-reinforced granular base layers with/without surface layer, respectively, under repeated single-axle traffic load conditions. The repeated load tests were conducted until the failure of the testbed. The contact pressure was recorded for each load cycle applied on the surface. The number of repetitive load cycles applied on the surface depends on the given configuration of the testbed. The contact pressure data is presented in terms of normalized contact pressure defined as a ratio of measured contact pressure on the weak subgrade to the applied contact tire pressure on the surface.

Figure 9.12 depicts the contact pressure distribution on the weak subgrade due to gradually increasing the cyclic load on the unreinforced granular base layer, as the unreinforced bed could not sustain at least a single repetitive load. Failure has occurred when the contact pressure reached about 400 kPa. At this pressure, the

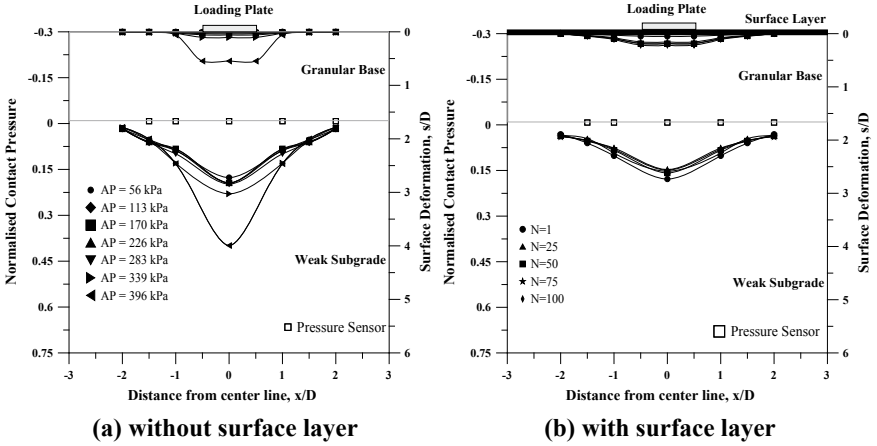

Fig. 9.12 Surface deformation and contact pressure distribution on weak subgrade due to repeated load on unreinforced granular base layer

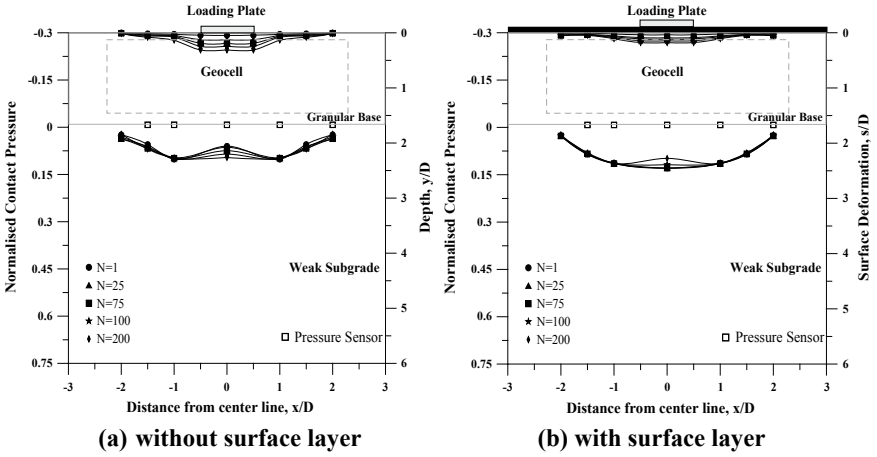

Fig. 9.13 Surface deformation and contact pressure distribution on weak subgrade due to repeated load on geocell-reinforced granular base layer

contact pressure on the weak subgrade right underneath the loading area for the granular base is observed to be 145 kPa representing about 38% of the applied pressure. In other words, about 62% of the applied pressure has been absorbed by the granular base layer. It can also be seen that the pressure transmitted to the weak subgrade soil diminishes away from the loading region in the lateral direction. The contact pressure as low as about 1% of maximum applied pressure is recorded at a distance of 2*D* and about 5% at 1.5*D* from the centerline of the loading plate. Hence, the majority of the applied pressure has been transferred to the weak subgrade soil right underneath the

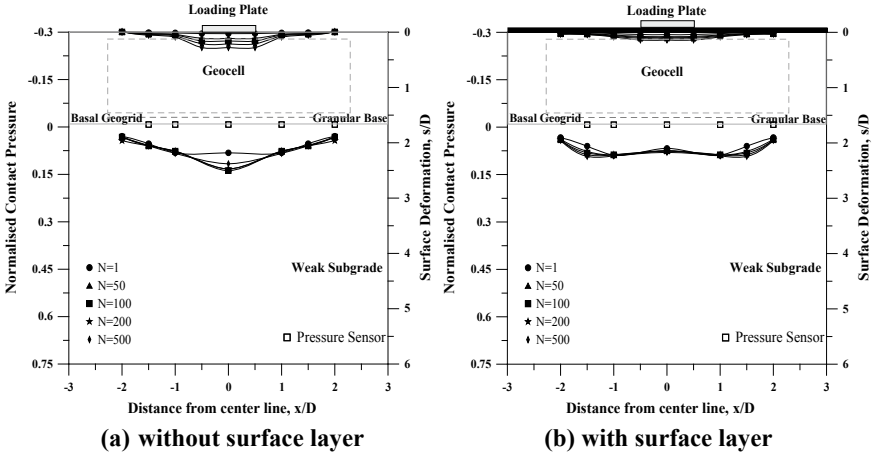

Fig. 9.14 Surface deformation and contact pressure distribution on weak subgrade due to repeated load on geocell with basal geogrid-reinforced granular base layer

loading region leading to a low bearing pressure. With the surface layer on top, the contact pressures at the interface have drastically reduced.

The surface deformation at a maximum applied pressure of 400 kPa is 70 mm at the center underneath the loading region; however, the surface deformation is only 7 mm at the contact pressure of 340 kPa. With the surface layer, the surface deformations have reduced by about 70% even in the unreinforced test case. No heave is noticed on the surface.

With the inclusion of the geocell mattress of a predetermined size in the granular base layer, it has improved the performance of the bed (Fig. 9.13). Geocell reinforcement owing to its lateral confinement effect has improved the stiffness of the dense granular base layer. However, the test configuration has not sustained higher a number of repetitive load cycles owing to the interaction between the geocell and the granular base layer. However, a uniform contact pressure distribution is observed in this case. The normalized contact pressure is well within the range of 0.15. With the additional surface layer, the contact pressures have become more uniform under the loading region.

Figure 9.14 demonstrates that the geocell and basal geogrid reinforcement could enhance the performance of the granular base layer over weak subgrade under repetitive loading. Compared to the geocell-reinforced bed, geocell with basal geogrid-reinforced granular base performed well over the weak subgrade in terms of load repetitions before it has shown the failure. Geocell reinforcement owing to its lateral confinement and membrane effect of geogrid has improved the stiffness of the dense base layer. The surface layer could further reduce the contact pressure on the weak subgrade which can also be ascertained from the minimal surface deformations observed on the surface.

Further to the extensive laboratory study on the geocell-reinforced granular base layers, to establish the efficacy of the geocells in real field conditions, field trials were conducted.

9.5 Field Study

The field study was conducted on the Karnataka State Highway No 46 (KA SH 46), which mostly traverses through Ghats sections of the Dandeli reserve forest. The state highway is a two-lane road mostly on rolling terrain. The pavement section in the Dandeli forest area experienced severe rutting from heavy trailer traffic and weather conditions. Karnataka public works department (PWD) has proposed to rehabilitate these distressed roads. A trial section was given to experiment with geocell technology. It was proposed to use the granular sub-base (GSB) material as an infill for geocell mattress in place of conventional GSB base layers over an area of 8600 m^2 (about 1.5 km).

9.5.1 Construction of Test Sections

Two test sections viz unreinforced and geocell-reinforced (referred to as reinforced) GSB layers were built on SH 46 at Chainages 75 + 100 km and 75 + 110 km, respectively. At both locations, the existing pavement layers were completely removed up to the natural subgrade level. It was noticed that the existing road was built on a soling layer with a boulder-sized (300 mm) stones. The unreinforced section was constructed using a conventional GSB material alone. This section was used as a control section to compare the test data. In the case of the reinforced section, geocell was first stretched and filled with the GSB material. A typical schematic of the test sections (plan and sectional views) is shown in Fig. 9.15. A glimpse of the construction of test sections can be visualized in Fig. 9.16 in a sequence of plates.

Construction and Testing Sequence

- The existing pavement was scarified and removed with an excavator up to the subgrade level (Fig. 9.16a).
- Soling layer with boulder-sized stones was encountered and removed to the possible extent to reach the subgrade layer (Fig. 9.16a).
- Then, the subgrade was leveled and compacted using an 11.7-ton roller.
- A plate load test (PLT-1) was conducted on the subgrade.
- TPCs (#1, #2) were placed at predefined locations with utmost care to protect the cables.

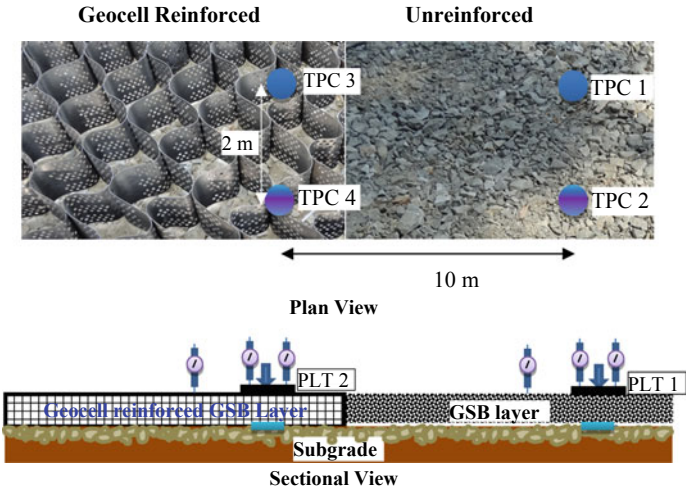

Fig. 9.15 Plan and sectional views of the reinforced/unreinforced test sections

- A 150 mm thick and 10 m length GSB layer was placed, leveled, and compacted with the roller. Alternate roller passes were applied with a vibrating drum (Fig. 9.16b).
- In the case of geocell-reinforced section, after installing the TPCs (#3, #4), geocell mattress was spread on the subgrade. Then, the GSB material was spread in the geocell pockets (Fig. 9.16b).
- Then geocell-reinforced GSB layer of 150 mm and 10 m long section was built very adjacent to the unreinforced GSB section.
- Similar TPCs were used underneath the geocell-reinforced section (Fig. 9.16b).
- Cyclic plate load tests (PLT) were conducted, concentrically above the TPC nos. 2 and 4, again on both unreinforced and geocell-reinforced sections, respectively (Fig. 9.16c).
- Data from the near and farther TPCs were collected at each load increment.

9.5.2 Plate Load Tests

Slow cyclic plate load tests were conducted on the subgrade, unreinforced, and geocell-reinforced sections as per the procedure laid down in IS 1888-1982. A circular plate of size 300 mm diameter was selected to mimic the contact area of the vehicle's tire pressure. Two dial gauges were placed on the circular plate which was supported independently from an angular support system placed away from the loading area. Two dial gauges were used to monitor the fill surface movements. Since, one way of the road was operational and could not divert the traffic during testing, arranging a conventional type loading platform was replaced with a loaded multi-axel trailer


a Excavation of existing pavement, preparation of site with instrumentation (TPCs)


b Instrumentation and construction of reinforced section


c Construction of geocell reinforced GSB layer and load test

Fig. 9.16 Construction sequence of unreinforced and reinforced pavement sections

weighing about 35 tons. Several other vehicles were tried prior such as a smooth drum roller of 11.7-ton capacity and a 20-ton capacity trailer. These relatively lighter vehicles were lifted off by the hydraulic jack system during the tests on subgrade soil itself, and hence, tests were repeated with a 35-ton multi-axel trailer with a full load. A typical arrangement of PLTs can be seen in Figs. 9.15 and 9.16. A hydraulic

jack of 30-ton with 150 mm travel was used to apply the load on to the plate against the reaction obtained from the trailer. The estimated ultimate load was applied in multiple increments, and the data from TPCs' dial gauges were collected at each load increment. The load on the circular plate was removed to zero levels at predetermined values. The settlement and elastic/plastic rebound of the plate were measured through dial gauges.

9.5.3 Instrumentation and Data Collection

The basic objective of instrumenting the test sections is to verify the total pressure distribution patterns beneath the unreinforced and geocell-reinforced layers. In each section, two total earth pressure cells (TPCs) were installed. These TPCs were spaced at a spacing of 2 m center to center [i.e., seven times the diameter of the plate approx. (7D)] and at a distance of 0.6 m from the edge of the pavement as shown in the schematic presented in Fig. 9.15. These locations are identified based on the estimation of the probable location of the wheel-base of most of the trailer traffic expected on the road. Four sensitive displacement dial gauges were used to measure the plate settlements and surface deformations. The TPC data was collected at every stage of the construction of test sections, roller compaction, etc., and during each load increment during the plate load tests.

9.5.4 Results and Discussion

Pressure-Settlement Analysis

The data from PLTs were analyzed, and load-settlement patterns were obtained for all the tests on the subgrade, unreinforced, and geocell-reinforced GSB sections. Figure 9.17 presents the monotonic load-settlement patterns of all the cases. It is imperative that the stiffness of the geocell-reinforced bed is higher than the unreinforced and subgrade alone sections. The subgrade section has shown an ultimate bearing pressure of about 800 kPa. The bearing pressure value is slightly higher for a silty clay type of soil subgrade. The higher bearing pressure of the subgrade may be attributed to the left-out portion of the soling layer in the subgrade. The unreinforced section has not shown a prominent failure due to the presence of the soling layer, however, the slope of the curve changed at about 17 mm of plate settlement. It is evident that the geocell-reinforced bed has not shown any clear marks of failure, but the bearing pressure has been linearly increasing with the plate settlement.

Figure 9.18 presents the cyclic behavior of unreinforced and geocell-reinforced GSB layers. The unreinforced sections did not sustain more than three cycles of the load against the geocell-reinforced section which was subjected to six cycles without a sign of failure even at 10% of the plate settlement. The initial elastic modulus calculated for each test case is presented in Table 9.4. It can be seen that the initial

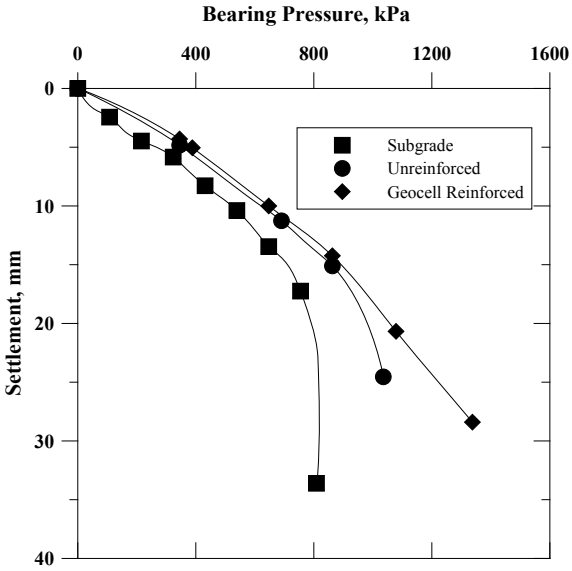

Fig. 9.17 Monotonic bearing pressure-settlement profiles

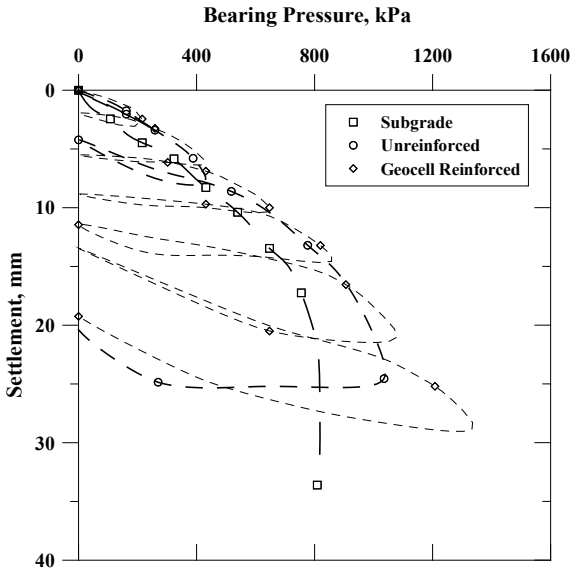

Fig. 9.18 Bearing pressure-settlement profiles under cyclic loading

Table 9.4 Properties of subgrade, GSB, and geocell-reinforced GSB materials

	E_s, MPa[a]	G, MPa[a]	k_s, kN/m^3	M_r MPa	MIF
Subgrade	9.7	3.9	44,236	–	–
Unreinforced bed	24	9.4	106,798	29	–
Reinforced bed	32	12.7	143,821	69	2.35

Note [a]Calculations are done based on $\mu = 0.25$; M_r = Resilient modulus, defined as the ratio of vertical stress to the elastic settlement

elastic modulus of the geocell-reinforced GSB is higher than the unreinforced bed owing to its higher confinement to the GSB materials which offers higher stiffness. The elastic modulus of subgrade, unreinforced, and reinforced beds are calculated by considering elastic rebound (settlement) from each cycle. It is apparent from Fig. 9.18 that the elastic component of the settlement of the unreinforced section is negligible in all the loading cycles. However, it can be seen that the elastic settlement of the geocell-reinforced section has increased with an increase in load due to the resilient response offered.

To quantify the efficacy of the geocell reinforcement further, deformation modulus values for each load cycle were calculated and presented in Fig. 9.20. The deformation modulus values were calculated from the initial tangent of each loading cycle. Besides, the deformation modulus was also calculated based on the German Institution of Standardization (DIN 18 2001) definition:

$$E_{\text{Def}} = 0.75 \times D \times \frac{\Delta\sigma}{\Delta s} \tag{9.3}$$

where D is the diameter of the plate and $\Delta\sigma$ and Δs are the incremental stress and settlement under a load cycle.

Figure 9.19 presents the deformation modulus calculated from both the methods. In general, the deformation modulus decreases with an increase in loading cycles for both unreinforced and reinforced beds. After three load cycles to reach a bearing pressure of 700 kPa, the deformation modulus decreased for the geocell-reinforced GSB layer. This observation also confirms that the influence of the geocell is more exercised when the pressures are higher on the plate. Overall, it is inferred from these results that the geocell reinforcement improves the load-bearing pressure of the pavement layers by increasing the stiffness of the base course, reducing the permanent deformations, and by improving the deformation modulus of the system. In addition, the effectiveness of the geocell reinforcement can be experienced with higher initial compaction stresses on the infill (GSB) material.

Table 9.4 shows the elastic properties of all the test sections. The initial elastic modulus (E_s), shear modulus (G), and modulus of subgrade reaction (k_s) have increased from subgrade case to geocell-reinforced GSB layer case. Besides, the geocell reinforcement has shown a higher resilient behavior than the unreinforced bed. However, at very high vertical stresses, the resilient modulus, defined as the ratio of vertical stress to the elastic settlement, of geocell-reinforced foundation bed

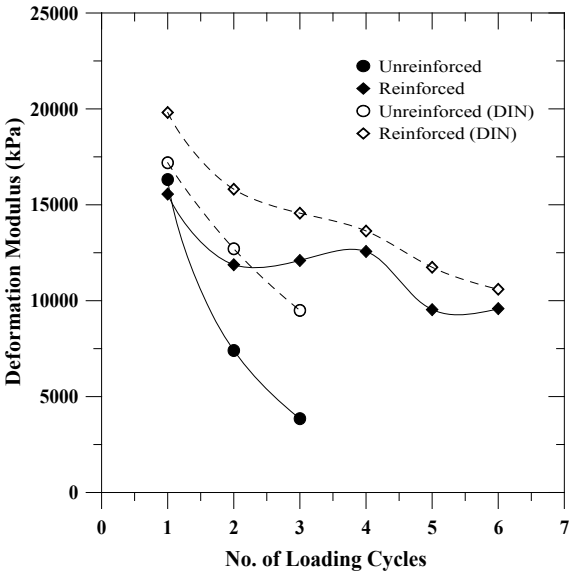

Fig. 9.19 Variation of deformation modulus with number of load cycles

has reduced due to higher elastic strain. Table 9.4 shows the resilient modulus of reinforced and unreinforced beds at vertical stress of 400 kPa.

9.5.5 Pressure Distribution Beneath the Unreinforced/Reinforced GSB Layers

Total earth pressure cells (TPCs) of 3500 kPa capacity were installed beneath the unreinforced and geocell-reinforced GSB layers. The location of these TPCs can be visualized in Fig. 9.15 (sectional view). The plate load tests were conducted approximately concentrically on the TPC nos. 2 and 4 as shown in Fig. 9.15. The objective of this arrangement is to directly measure how much pressure is being transmitted to the bottom layers (subgrade). The other two TPCs were placed at about seven times the diameter of the plate (300 mm) which comes to about 2 m. These TPCs were embedded at a depth of 150 mm from the bottom of the plate. The TPCs were monitored for each load increment on the plate, and the results are presented in Figs. 9.20 and 9.21. Figure 9.20 shows the pressure distribution beneath the unreinforced bed from TPCs 1 and 2. It is clearly seen that the TPC2 has experienced about 66% of the applied pressure on the plate. The pressures recorded at TPC1 is almost negligible in the pressure range applied to elucidate that the GSB layer is more discrete and distributed the pressure directly to the subgrade without spreading. On the contrary, the TPCs placed under the geocell-reinforced GSB layer have experienced much lesser pressure even at very high pressures on the plate. The applied pressure transmitted to the subgrade accounts to about only 16% of the total

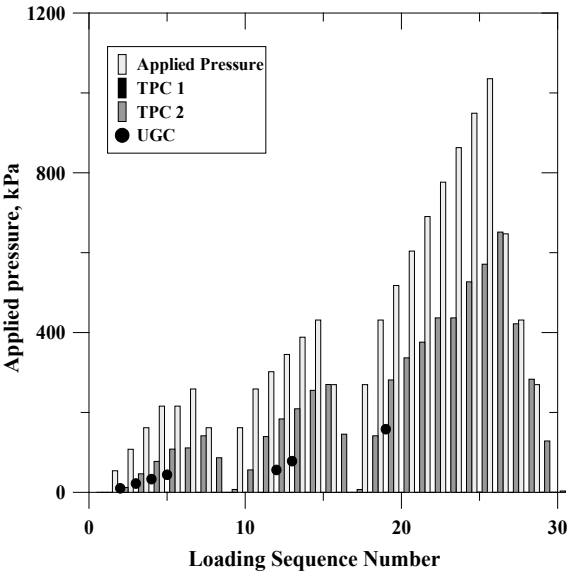

Fig. 9.20 Pressure distribution below the unreinforced GSB layer

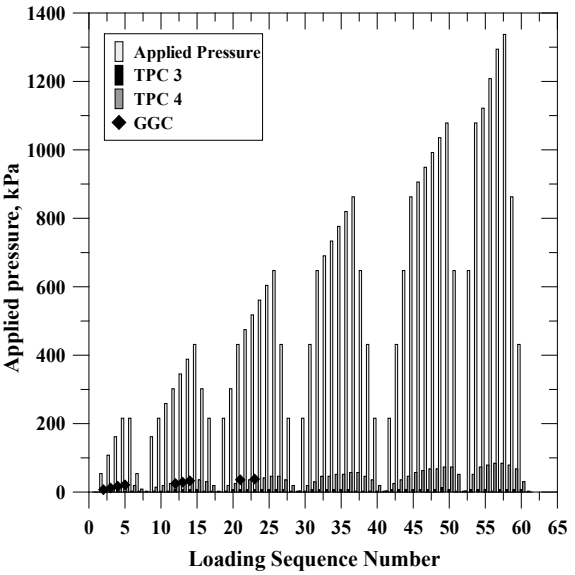

Fig. 9.21 Pressure distribution below the geocell-reinforced GSB layer

applied pressure on the plate. The reinforced bed has distributed the applied pressure to a larger area, where the TPC3 placed at a distance of 7D has experienced about 12% of the pressure transmitted under the area of loading (at TPC4). It is interesting to note that the influence of the geocell mattress is better drawn for higher load applications. This can be illustrated that the pressure transmitted to the subgrade is

only 5.8% at the maximum pressure (~1000 kPa) on the plate. This confirms that the geocell reinforcement is redistributing the applied pressure transmitting to a wider area around the loading region. This higher pressure re-distribution would have taken place up to a distance of about 5*D* from the centerline of the loading plate.

Figure 9.21 also depicts the contact pressure measured in the laboratory experiments for similar test cases (refer Figs. 9.12a and 9.13a) under similar loading conditions. It is interesting to see that the field and laboratory observations are closely matching. Small deviations observed can be attributed to the prevailing subgrade conditions. In the case of laboratory tests, the subgrade is softer than the field situation.

Overall, the performance of the granular base layers in terms of an increase in load-carrying capacity and reduction in rutting and contact pressure over the weak subgrades can be improved through geocell reinforcement. The resilient modulus and modulus improvement factors obtained from both laboratory and field studies are in concurrence, and these parameters will be very vital in designing the pavements with geocell reinforcement.

9.6 Design of Geocell-Reinforced Pavements

The Indian roads congress (IRC) and Ministry of Road Transport and Highways (MoRTH) approved the use of geosynthetics in highway construction. Guidelines for using geosynthetics in road pavements were issued by IRC (2019) and MoRTH (Section 700) (Ministry of Road Transport & Highways 2013). Currently, IRC (2019) has incorporated geogrids and geocells in road pavement construction. The IRC SP 59 (2019) uses the following design methodologies to incorporate geogrids and geocells in the pavement construction.

9.6.1 Traffic Benefit Ratio (TBR) Based Design

To design a pavement with geocell reinforcement, the TBR approach can be adopted either to reduce the thickness of the base course or to increase the service life of the pavement. In brief, to design an unreinforced pavement section, according to the American Association of State Highways and Transportation Officials (AASHTO), flexible pavement's overall structural number (SN) needs to be calculated (AASHTO 1993). In order to design the geocell-reinforced pavement, TBR is used. The effect of geocell reinforcement is quantified in terms of equivalent structural number by considering traffic to be catered by the pavement and TBR that can be obtained with selected geocell. The equivalent structural number of geocell is then used to reduce the unreinforced pavement base layer thickness to the extent of the reinforcement effect. A step by step procedure to design geocell-reinforced pavement using TBR approach is as follows:

Step 1. Design the unreinforced pavement by considering subgrade soil CBR or resilient modulus and the traffic to be catered as per the guidelines provided by IRC 37 (2012).

Step 2. Compute the total structural number (SN_{UR}) of the unreinforced pavement structure designed in Step 1 taking into account the appropriate layer coefficients and drainage coefficients and thickness of each layer per AASHTO (1993) using Eq. 9.4.

$$SN_{UR} = a_1 D_1 + a_2 D_2 m_2 + a_3 D_3 m_3 \tag{9.4}$$

Step 3 Compute the SN_{req} required over the subgrade of unreinforced pavement to cater the design traffic (number of standard axle load passes, W_{18UR}) using the following equation and substituting the appropriate values in Eq. 9.5.

$$\log(W_{18}) = Z_R S_0 + 9.36 \log_{10}(SN + 1) - 0.2 + \frac{\log_{10}\left[\frac{\Delta PSI}{4.2-1.5}\right]}{0.4 + \frac{1094}{(SN+1)^{5.19}}} + 2.32 \log_{10} M_R - 8.02 \tag{9.5}$$

Step 4. Select an appropriate traffic benefit ratio (TBR) based on full-scale field studies or large-scale laboratory studies that represent similar field conditions and failure criteria. TBR typically ranges from 2 to 6 depending on the stiffness of the geocell/geogrid, subgrade CBR, base/sub-base thickness, and asphalt concrete layer thickness.

Step 5. Compute the number of standard axle load passes, W_{18R}, that can be allowed on the reinforced pavement structure by multiplying TBR with W_{18UR}.

Step 6. Compute the structural number, SN_R, of pavement which can cater computed number of standard axle passes, W_{18R}, with reinforcement using Eq. 9.5.

Step 7. Find the equivalent structural number of geocell by subtracting SN_{UR} from SN_R.

Step 8. Reduce the base/sub-base layer thickness taking into account the equivalent structural number of geocell meeting the minimum base/sub-base layer thickness criteria and total structural number (*SN*) of unreinforced pavement.

Example: Design of reinforced flexible pavements using TBR approach

Consider designing a pavement section on a weak subgrade *CBR* of 3% and for design traffic of 50 msa.

Design Steps:

- Obtain the unreinforced pavement layer thicknesses as per IRC: 37 (2012):
  Combined bituminous layers = 190 mm
  Granular base and sub-base layers = 600 mm

- Compute the Structural Number (SN) $= a_1 * D_1 + a_2 * D_2 * m_2 + a_3 * D_3 * m_3$
  Compute resilient moduli of pavement layers:
  From IRC 37-2012, $M_{\text{RBitumen mix}} = 3000$ MPa $= 435{,}113$ psi
  $a_1 = 0.171$ (ln $(M_{\text{RBitumen mix}})) - 1.784 = 0.436$/in. $=$ **0.0172/mm**
  From IRC 37-2012, for base $M_{\text{R\_gb}} = 0.2 * M_{\text{R\_gsb}} * h^{0.45}$
  $M_{\text{R\_gb}} = 0.2 * 84 * 250^{0.45} = 200.95$ MPa $= 29{,}145$ psi
  $a_2 = 0.249(\log_{10}(M_{\text{R\_gb}})) - 0.977 = 0.135$/in. $=$ **0.0053/mm**
  Form IRC 37-2012 for sub-base $M_{\text{R\_gsb}} = 0.2 * M_{\text{R\_subgrade}} * h^{0.45}$
  $M_{\text{R\_subgrade}} = 10 * CBR$ MPa $= 30$ MPa
  $M_{\text{R\_gsb}} = 0.2 * 30 * 350^{0.45} = 84$ MPa $= 12{,}147$ psi
  $a_3 = 0.227(\log_{10}(M_{\text{R\_gsb}})) - 0.839 = 0.0918$/in, $=$ **0.0035/mm**
  Let drainage coefficients m_2 and m_3 be 1.00 and 1.00 for WMM and GSB
  $\text{SN} = 0.0172 * (190) + 0.0053 * 250 * 1.0 + 0.0035 * 350 * 1.0$
  $\text{SN}_{\text{UR}} = 5.803$
- Now, compute the required structural number:

$$\log(W_{18}) = Z_{\text{R}} S_0 + 9.36 \log_{10}(\text{SN} + 1) - 0.2 + \frac{\log_{10}\left[\frac{\Delta\text{PSI}}{4.2-1.5}\right]}{0.4 + \frac{1094}{(\text{SN}+1)^{5.19}}} + 2.32 \log_{10} M_{\text{R}} - 8.02$$

  $W_{18\ \text{Unreinforced}} = 50$ MSA
  $Z_{\text{R}} = -1.282$ (for 90% reliability)
  $S_0 = 0.4$ (overall standard deviation for flexible pavement)
  Change in pavement serviceability index (PSI) = Initial PSI—terminal PSI
  $\Delta\text{PSI} = p_0 - p_t = 4.3 - 2.0 = 2.3$
  $M_{\text{R}} = 4351$ PSI $= 30$ MPa (3 * 10 for 3% *CBR* subgrade soil)
  $\text{SN}_{\text{Req}} = 6.521$
- **Computation of SN_{R}**
  Let *TBR* be 3.0
  $\text{W}_{18\text{Reinforced}} = 50 * 3 = 150$ msa

$$150\ \text{msa} = Z_{\text{R}} S_0 + 9.36 \log_{10}(\text{SN} + 1) - 0.2 + \frac{\log_{10}\left[\frac{\Delta\text{PSI}}{4.2-1.5}\right]}{0.4 + \frac{1094}{(\text{SN}+1)^{5.19}}} + 2.32 \log_{10} M_{\text{R}} - 8.02.$$

  $\therefore$ **$\text{SN}_{\text{R}} = 7.469$**
- Equivalent structural number of geocell $= \text{SN}_{\text{R}} - \text{SN}_{\text{Req}} = 7.469 - 6.521 = 0.948$
- Reduce base layer thicknesses of geocell-reinforced pavement after considering the equivalent structural number of geocell:
  Adjust the thicknesses of pavement layers to yield an SN ≥ 4.855 $(5.803 - 0.948)$.
  Maintain a minimum base thickness of 150 mm (IRC 37 2012).
  Trial 1: Let the reduced thickness of GSB be 210 mm
  $\text{SN} = a_1 * D_1 + a_2 * D_2 * m_2 + a_3 * D_3 * m_3$
  $\text{SN} = 0.0172 * 190 + 0.0047 * 250 * 1.0 + 0.0032 * 210 * 1.00 =$ **4.947 > 4.855**
  (a_2, a_3 are computed based on the reduced thickness).

The reduced thickness of the GSB layer satisfies the structural number required. Hence, the pavement is safe against the fatigue and rutting strains (which can be verified by the IITPAVE program) for the reduced pavement thickness. In this analysis, the geocell reinforcement could reduce a combined base/sub-base course thickness from 600 to 360 mm, which is about a 40% reduction in granular layers.

9.6.2 Layer Coefficient Ratio (LCR) Based Design

The layer coefficient represents the improvement in the strength of the pavement layer. It can be estimated based on the modulus improvement factor (MIF) (Giroud and Han 2013) as shown below.

$$\mathrm{LCR} = \frac{0.249 \log 10\left(\mathrm{MIF} * \frac{\mathrm{Mrbc}}{0.0069}\right) - 0.977}{0.249 \log 10\left(\frac{\mathrm{Mrbc}}{0.0069}\right) - 0.977} \tag{9.6}$$

where

M_{rbc} = Resilient modulus of base course

MIF = Modulus improvement factor.

The resilient modulus of the base layer (M_{rbc}) can be obtained from Eq. 9.7 presented in IRC-37 (2012). The modulus may also be obtained from the resilient modulus test obtained using a cyclic triaxial test on the material. Eq. 9.7 may be used to calculate the MR_{bc}.

$$M_{\mathrm{rbc}}(\mathrm{MPa}) = 29.4(\mathrm{CBR})_{\mathrm{bc}}^{0.4358} \tag{9.7}$$

where $\mathrm{CBR}_{\mathrm{bc}}$ = CBR value of the base course in percentage.

Modulus improvement factor (MIF) is a ratio of elastic modulus of the upper reinforced base layer ($E_{1\mathrm{R}}$) to the elastic modulus of the unreinforced bed ($E_{1\mathrm{U}}$) with the same test configuration.

$$\mathrm{MIF} = \frac{E_{1\mathrm{R}}}{E_{1\mathrm{U}}} \tag{9.8}$$

where

E_1 = Elastic modulus of the base layer with and without geocell reinforcement.

These values under laboratory and field test conditions can be seen in Tables 9.3 and 9.4, respectively. Based on the MIF values, the layer coefficient ratio (LCR) of the geocell-reinforced base layers may vary between 1.2 and 1.7. Beyond this range, the pavements may become unsafe either in fatigue or rutting, or uneconomical.

9.7 Conclusions

1. Geocell can be effectively used as a reinforcement system in pavement base/subbase layers to increase the stiffness and resilient behavior.
2. The provision of additional basal geogrid to the geocell reinforcement resulted in a reduction of 75% in permanent settlements.
3. The elastic modulus of the geocell-reinforced aggregate base with an additional basal layer is found to be 125 MPa against a modulus of 4.4 MPa for unreinforced bed.
4. The apparent resilient modulus from the cyclic load tests on geocell-reinforced aggregate base with additional basal layer is found to be 65 MPa against 20 MPa for unreinforced bed.
5. As high as 86% reduction of contact pressure on the clayey soil subgrade is obtained. It has been noticed that the distribution of pressures is uniform over a wider area in the case of geocell and geogrid-reinforced dense granular base layers with a surface layer in cyclic load tests.
6. Geocell and basal geogrid with surface layer reinforcement reduce the plastic settlements by about eight and elastic settlements by twofolds, referred to as rutting and resilient behavior on the pavement surface by providing lateral confinement from the geocell and membrane support from geogrid and surface layer to the infill soil.
7. A CPD reduction of almost five and sevenfold against geocell-reinforced alone is observed. The reduction in CPD's for reinforced cases is attributed to the increase in elastic response of the bed.
8. Traffic benefit ratio (TBR) calculated at 5% of the loading plate settlement has increased with reinforced test cases. A TBR of as high as eight is observed in the case of geocell with basal geogrid-reinforced granular bases with a surface layer. The modulus improvement factors are observed to be about 2.5 based on both laboratory and field studies.
9. Geocell reinforcement owing to its lateral confinement has improved the stiffness of the dense granular base layer. A fairly uniform contact pressure distribution is observed. The normalized contact pressure at the interface of the granular base and weak subgrade layers is observed to be well within the range of 0.15.
10. It can be observed that about 62% of the applied pressure has been absorbed by the granular base layer and transmitted about 38% to the underlying weak subgrade layer.
11. The deformation modulus seems to reduce with an increase in reinforcement form in the base layer.
12. Two design methodologies viz traffic benefit ratio approach, and layer coefficient ratio approach are discussed.

References

AASHTO (1993) Guide for design of pavement structures. American Association of State Highway and Transportation Officials, Washington, DC

AASHTO (2009) Standard practice for geosynthetic reinforcement of the aggregate base course of flexible pavement structures. American Association of State Highway and Transportation Officials (AASHTO), R 50-09, Washington, DC

Barke WR (1987) Open-graded bases for airfield pavements, Technical Report GL-87-16, USAE Waterways Experiment Station, Vicksburg, MS, USA, 76 p

Barksdale RD, Brown SF, Chan F (1989) Potential benefits of geosynthetics in flexible pavement systems, National Cooperative Highway Research Program Report No. 315, Transportation Research Board, National Research Council, Washington, DC

Burmister DM (1943) The theory of stresses and displacements in layered systems and applications to the design of airport runways. In: Proceedings of the 23rd Annual Meeting of the Highway Research Board, pp 126–148

Chummar AV (1972) Bearing capacity theory from experimental results. J of the Geotech Engg, ASCE 98(12):1311–1324

Collin JG, Kinney TC, Fu X (1996) Full scale highway load test of flexible pavement systems with geogrid reinforced base courses. In: Geosynthetics Intentional, Industrial Fabrics Association International, Roseville, MN, 3(4):537–549

Dash SK, Saride S, Sitharam TG (2003) Model studies on circular footing supported on geocell reinforced sand underlain by soft clay. Geotext Geomembr 21(4):197–219

DIN 18 134 (2001) Determining the deformation and strength characteristics of soil by the plate loading test. German Standards

Giroud JP, Han J (2013) Design of geosynthetic-reinforced unpaved and paved roads. Short course, Geosynthetics 2013, Long Beach, CA, April 4

Haas R, Wall J, Carroll RG (1988) Geogrid reinforcement of granular bases in flexible pavements. In: Transportation Research Record 1188, TRB, National Research Council, Washington, DC, USA, pp 19–27

IRC SP 59 (2019) Guidelines for use of geotextiles in road pavements and associated works, First revision, Indian Roads Congress, New Delhi

IRC: 37-(2012) Guidelines for the design of flexible pavements (3rd Revision)

Latha GM, Nair AM, Hemalatha MS (2010) Performance of geosynthetics in unpaved roads. Int J Geotech Eng 4(2):151–164

Ministry of Road Transport & Highways (2013) Specifications for road and bridge works, Section 700, 5th revision

Perkins SW, Ismeik MA (1997) Synthesis and evaluation of geosynthetic-reinforced base course layers in flexible pavements: part i experimental work. Geosynthetics Int 4(6):549–604

Pokharel SK (2010) Experimental study on geocell-reinforced bases under static and dynamic loading. D Phil Thesis, University of Kansas, USA

Pokharel SK, Han J, Manandhar C, Yang X, Leshchinsky D, Halahmi I, Parsons RL (2011) Accelerated pavement testing of geocell-reinforced unpaved roads over weak subgrade. Transp Res Rec 2204:67–75

Rajagopal K, Veeraragavan A, Chandramouli S (2012) Studies on geocell reinforced road pavement structures. Geosynthetics Asia 2012, Thailand

Saride S, Rayabarapu VK, Suraj V, Anand JP (2013) Repeated load tests on geocell reinforced sand subgrades. In: Proceedings of the geosynthetics international conference, Long Beach, CA, 3(4):537–549

Saride S, Rayabarapu VK, Suraj V (2015) Evaluation of rutting behavior of geocell reinforced sand subgrades under cyclic loading. Indian Geotech J 45(4):378–388

Sitharam TG, Saride S (2005) Behaviour of embedded footings supported on geocell reinforced foundation beds. ASTM Geotech Test J 28(5):452–463

Ueshita K, Meyerhof GG (1967) Deflection of multilayer soil systems. J Soil Mech Found Div ASCE SM5:257–282

Chapter 10
Geocell Applications in Stabilizing Waste Materials for Sustainable Pavement Constructions

M. N. Asha and V. Divya

Abstract Utilization of waste materials for infrastructure development has become a sustainable solution for waste management. However, assessment of the suitability of these materials for construction has become a challenge. The present paper explores the potential of using four different waste materials in unreinforced and reinforced conditions for highway construction. The different waste materials considered are demolition waste, pond ash, quarry dust and tyre shreds. For reinforcing the waste materials, geocell reinforcement is used. The experimental studies were conducted in a steel tank 750 mm × 750 mm in plan, using plate load test set up. The test arrangement consists of geocell reinforced sections of 100 mm height prepared over a cohesionless fill of 400 mm height at 85% relative density. Since tyre shreds are compressible in nature, they are used along with quarry dust in three different volume proportions. The pressure versus settlement responses for both reinforced and unreinforced sections are studied. Among the various waste materials tested, it is observed that pond ash proves to be a suitable material for pavements as they sustain higher bearing pressure and reduce the surface heave extensively.

Keywords Demolition waste · Pond ash · Tyre shreds · Quarry dust · Geocell

10.1 Introduction

Infrastructure development is reflective of the growth of a country, but to support such a growth availability of construction materials is very important. Strong and stable in situ soil is also one of the requirements for this rapid development. However, the foundation soil may not be strong to support this hasty growth which has led to the development of innovative materials, methods and technologies for stabilizing the

M. N. Asha (✉) · V. Divya
CMR Institute of Technology, Bengaluru, Karnataka, India
e-mail: asha.n@cmrit.ac.in

V. Divya
e-mail: divya.v@cmrit.ac.in

T. G. Sitharam et al. (eds.), *Geocells*, Springer Transactions in Civil and Environmental Engineering,
https://doi.org/10.1007/978-981-15-6095-8_10

in situ ground. Development of technology is always associated with the generation of tonnes of waste materials and managing the same has become a major challenge. Hence, the development of sustainable and cost-effective solutions for waste management is essential to maintain the overall balance of the eco-system. Extensive research studies are happening to find suitable alternative construction materials which impact the ecosystem in a positive way. As a result, reliable substitutes have found its way for various construction-related activities. Leverage of waste materials as backfill material in retaining walls, stabilizers in embankment construction or as admixtures in concrete are different examples of this.

The different waste materials that are getting accumulated in the landfills by virtue of infrastructure development or rapid increase in population or imbalance in ecosystem include plastic wastes, construction waste, e-waste, domestic and commercial wastes, animal wastes, biomedical wastes, industrial solid wastes, biodegradable wastes and so on. The last two decades have witnessed an enormous growth in the number of vehicles plying on the road. As a by-product of this growth, disposal of scrap tyres has also become an alarming concern in waste management. Recent years have witnessed extensive research towards deploying the different waste materials for different sustainable constructions.

Fly ash and bottom ash are the by-products of thermal power plants. The pond ash is a waste product obtained from the wet disposal of the fly ash, which when gets mixed with bottom ash is disposed off in large pond or dykes as slurry. Over the last two decades, research studies have been carried out to investigate the properties of the ashes generated. The suitability of fly/bottom ash mixtures as fill materials in highway embankments was investigated by Kim et al. (2005). According to Pandian (2013), fly ash by virtue of its low specific gravity, free-draining properties and high frictional angle (greater than 30°) makes it suitable for geotechnical applications when used in combination with other additives. Saride and Dutta (2016) have reported that fly ash can be used for stabilization of expansive soils and it is used as an admixture in such soils increases its shear modulus and decreases the damping ratio irrespective of curing. Jakka et al. (2010) have studied the shear behaviour of pond ash to assess its liquefaction resistance. Ghosh (2009) has studied the possibility of stabilizing pond ash using lime and phosphogypsum which extends its application for road base and subbase construction. Kumar and Gupta (2016) have studied the effect of addition of pond ash, rice husk ash, cement and fibres on strength characteristics of clay. The studies revealed the potential of using pond ash as a lightweight fill material in the construction of various structures.

The suitability of recycled construction and demolition materials as alternative pipe backfilling materials for storm water and sewer pipes was studied by Rahman et al. (2014). Cardoso et al. (2016) have carried out a comprehensive review on the use of recycled aggregates derived from construction and demolition waste. From their review, it was observed that pavements constructed using recycled aggregate exhibit high CBR and resilient moduli over time; however, the permeability characteristics of the matrix containing recycled aggregate need to be further investigated.

Use of waste rubber tyre shreds for civil engineering application has several advantages. Some of its advantages are its lightweight, cost-effectiveness, easiness

to compact, free-draining property and incompressibility. Additionally, this use is beneficial to the environment since a waste material is recycled and reused. Stiffness and strength properties of tyre shreds and rubber sand were studied by Lee et al. (1999) through laboratory tests. The analysis indicated that the performance of rubber sand was satisfactory when compared with that of sandy gravel and make it suitable as a backfill material. Hazarika et al. (2012) have reported that the tyre shreds should be used in combination with sand and can decrease the shear strain which makes it a potential material of earthquake-resistant constructions. The low specific gravity of tyre shreds decreases the lateral earth pressure and hence lower design requirements (Reddy and Krishna 2017).

Geocells are strong three-dimensional systems fabricated from high-density polymers. These expandable panels open up more avenues of applications in the field of geotechnical engineering ranging from providing strength to geo-systems to protection against erosion. The concept of lateral confinement of geocells was developed by the Army Corps of Engineers in the late 1970s for rapid roadway/runway construction (Webster 1979). The strength properties of geocell–soil composite systems and the frictional resistance of the infill were studied by Bathurst and Karpurapu (1993). Since then many researchers have been studying the effectiveness of geocell. Rajagopal et al. (1999), Saride (2005), Tafreshi and Dawson (2012) are a few who have investigated the potential of using geocells for a wide variety of engineering applications. However, majority of the literature has reported the beneficial effect of geocell with the use of sand as infill in it.

The choice of infill for geocell or performance of geocell bed for different infill itself has been a topic of research. Hedge and Sitharam (2015) have studied the performance of three different infills, viz. aggregate, sand and red mud within the geocell. From the experimental and simulation studies carried out by them, it was reported the performance of geocells is immaterial of the type of infill because of marginal variations. Nair and Latha (2016) have investigated the performance of geocell beds with granular sub-bases. Pokharel et al. (2010) have studied the performance of single geocell for two different bases, viz. Kansas River sand and quarry dust to investigate the effect of fines in the geocell performance. Thakur et al. (2012) have reported that the use of recycled asphalt pavement along with geocell offers a stable base course over weak subgrade, and the infill density is critical as far as the performance of geocell is concerned. Dutta and Mandal (2017) have reported the effectiveness of a composite system comprising of geocell encased flyash column along with a geocell mattress in stabilizing foundation beds. In their study, the sustainable use of two different waste materials, viz. plastic bottles and flyash, has been explored. Arulrajah et al. (2013) have studied the viability of using three different types of construction and demolition waste, viz. recycled concrete aggregate, crushed brick and reclaimed asphalt pavement, when used in combination with geogrid. Han and Thakur (2015) have reported that use of waste materials like recycled asphalt pavement, recycled aggregate and recycled ballast when used in combination with geosynethtics can reduce horizontal and vertical settlements with reduced creep and permanent deformations. Xiao et al. (2012) have reported the uses of tyre derived aggregates in combination with geogrids as backfill has higher

seismic resistance against conventional granular backfill. Latha et al. (2010) have reported that performance of tyre shred embedded road section is in par with that of geotextile reinforced sections.

From the literature review, it can be summarized that geocells are quite effective in stabilizing subgrade soil. At the same time, over the years researchers have been using different waste materials for sustainable constructions. In this paper, the viability of using waste materials in combination with geocell reinforcement has been studied. The various waste materials considered for the present study are quarry dust, demolition waste and tyre shreds. Since tyre shreds are compressible in nature, they are used along with quarry dust in three different volume proportions. Model plate load tests have been carried out on the unreinforced and reinforced beds to investigate the performance improvement of the geocell reinforced beds.

10.2 Methodology

The methodology adopted in the present experimental study can be sequenced as follows:

1. Characterization of raw materials
2. Design of dimensions of the testing facility
3. Development of test set-up
4. Design of test sections
5. Performance evaluation of geocell reinforced beds over unreinforced ones
6. Discussions and conclusions

10.3 Characterization of Materials

The different materials used in the present study are

1. White sand
2. Quarry dust
3. Demolition waste
4. Pond ash
5. Tyre shreds
6. Geocell reinforcement

The properties of the different materials used in the experimental studies are given below.

10.3.1 White Sand

While preparing model sections, the white sand was used as the foundation material. All the unreinforced and reinforced beds were prepared over this bed. The maximum and minimum dry unit weights of white sand were determined as per IS 2720 (Part 14) 1983 and were recorded as 1760 kg/m^3 and 1400 kg/m^3, respectively. The material had a specific gravity of 2.58 with an angle of internal friction of 24.22° as determined from direct shear tests at a density of 1600 kg/m^3.

10.3.2 Quarry Dust

Quarry dust used for the experiments was collected from a nearby quarry. The quarry dust (QD) used for the study was uniformly graded and had an effective size of 0.42 mm with a specific gravity of 2.55. The maximum and minimum dry unit weights of quarry dust were recorded as 1940 kg/m^3 and 1460 kg/m^3, respectively. The material had an angle of internal friction of 32.33° and cohesion of 7.83 kPa as determined from direct shear tests at a unit weight of 1850 kg/m^3.

10.3.3 Demolition Waste

Demolition waste used for the studies was collected from a nearby site. The construction used for the experimental studies mainly comprised of plaster waste. The waste was crushed in the laboratory such that it had an average size of 2 mm. The maximum and minimum dry unit weights of quarry dust were recorded as 1829 kg/m^3 and 1293 kg/m^3, respectively, with a specific gravity of 2.67. The material had an angle of internal friction of 45.4° and cohesion of 1.84 kPa as determined from direct shear test.

10.3.4 Pond Ash

Pond ash used for the experiments was uniform graded and had a specific gravity of 1.86. It was mixed with 16% of water content and compacted at dry density of 1375 kg/m^3 (85% relative compaction). The material possessed an angle of internal friction of 27.47° and cohesion of 2.81 kPa as determined from direct shear test.

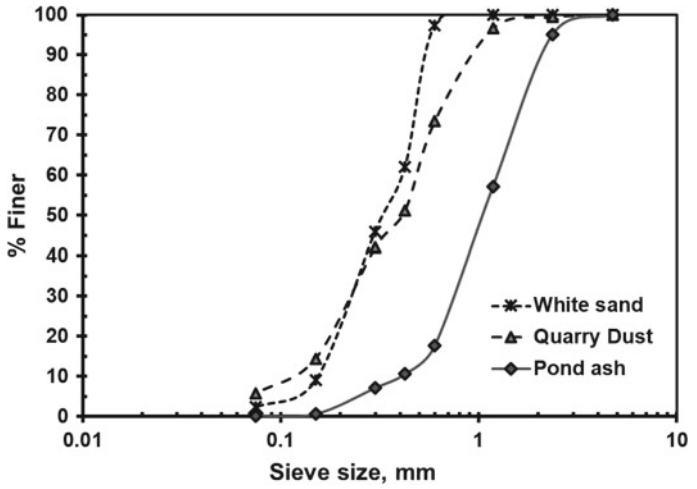

Fig. 10.1 Gradation curve for white sand, quarry dust and pond ash

10.3.5 Tyre Shreds

Tyre shreds used for the experiments had an average size of 2 mm × 5 mm with a specific gravity of 1.18. Since tyre shreds have high compressibility, in the experimental studies they were used in combination with quarry dust. Tyre shreds were mixed with quarry dust in three different volume proportions, viz. 2.5, 5 and 7.5%, such that the mixture had a density of 1850 kg/m^3. The grain size distribution curve of the different materials used in the experimental studies is presented in Fig. 10.1. Photograph of the different material used for the experimental study is shown in Fig. 10.2. Summary of the different properties is presented in Table 10.1.

10.3.6 Geocells

A geocell is an array of lightweight containment cells resembling a honeycomb structure which is usually filled with granular infill. When subjected to vertical pressure, the confined cohesionless infill within a geocell induces lateral stresses and thereby causing it to deform laterally. But this lateral deformation is restricted, the adjacent cells are also full with infill material. The generation of high hoop strength of the geocell wall along with frictional resistance developed along the wall constrains the lateral movement of the infills and offers a higher stability to the bed. This process increases the shear strength of the confined soil, hence creating a stiff mattress, which helps in distributing load over a wider area. This horizontal stress acting normal to the cell wall increases the vertical frictional

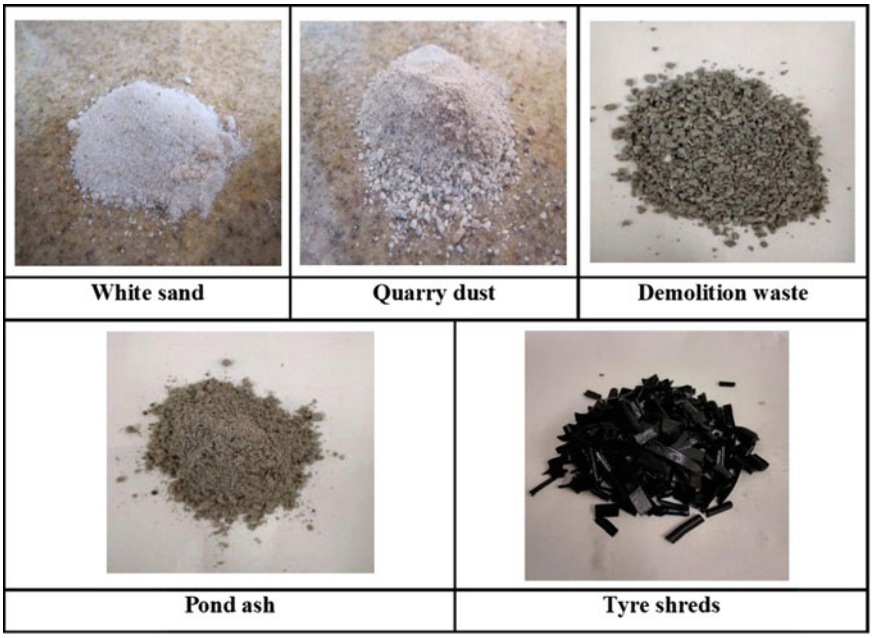

Fig. 10.2 Photograph of the different materials used for the experimental studies

Table 10.1 Properties of the different materials used in the study

Property	Material			
	White sand	Quarry dust	Construction waste	Pond ash
Specific gravity	2.58	2.55	2.67	1.86
Maximum density (kg/m^3)	1760	1940	1829	1375[a]
Minimum density (kg/m^3)	1400	1460	1293	–
Shear parameter, c, in kPa	0	7.83	1.84	2.81
Shear parameter, φ in degrees	24.22	32.33	45.43	27.47

[a]Due to the presence of fines, compaction test was carried out on pond ash and a maximum dry density of 1375 kg/m^3 was obtained at an optimum moisture content of 16%

resistance between the infill and the geocell wall, which in turn diminishes the stress applied to the ground below geocell.

Commercially available geocells were used in the experimental studies. The geocells used were perforated on the sides and had a pocket size of 330 mm × 170 mm (when expanded) with a weld thickness of 30 mm. The geocell specimen had target seam strength of 14.2 kN/m (as provided by the supplier).

10.4 Design of Dimensions of the Testing Facility

The dimensions of the testing facility have been decided on the basis of an extensive literature review. In the model tests on road sections carried out by earlier researchers (Palmeria and Antunes 2010; Hedge and Sitharam 2015), the length/width of the tank was at least equal to 5 times the size of the loading plate, whereas height of the fill inside the tank was 2.7–5 times the size of the loading plate. In the present study, the dimensions of the tank and the loading plate were decided such that it conforms with the literature and there exists no interference with the boundary, i.e. width of tank is 5 times the size of the plate and height of fill is 4 times the size of loading plate. The thickness of the different model sections has also been designed in accordance with the literature.

10.5 Development of Test Setup

Experimental studies were carried out in a steel tank of 750 mm × 750 mm in plan and 620 mm height. White sand was used as the bottom fill in all the experiments for a total thickness of 400 mm. Bottom fill was filled in the test tank in 4 layers, each of 100 mm thickness at 85% relative density. Over white sand, the overlying fill was filled in three layers comprising of two bottom lifts of 50 mm thickness and one top lift of 20 mm thickness (total 120 mm thickness). Compaction of the fills was done using rammer, and the number of blows and height of fall was adjusted such that prescribed density will be achieved. After preparing each layer, the surface was checked for its horizontality using a levelling head. Figure 10.3 presents the schematic of the model section.

The reinforced sections were prepared by placing the geocell at the interface and then stretching in position with the help of weights or blocks. The geocell was filled with different waste materials to one-third height initially as shown in Fig. 10.4. Progressively, it was filled to two-third height and then finally after removing the weights or blocks, the pockets were filled to the full height. For preparing infills within geocell, the rammer was used.

Static loading was applied to the model sections using a loading plate of 150 mm diameter and 12 mm thickness. Vertical settlements of the plate were measured using 50 mm dial gauge, and to measure surface heave, two dial gauges were placed at a distance of 190 mm from the centre. Figure 10.5 presents the instrumented model section in which construction waste is used as infill.

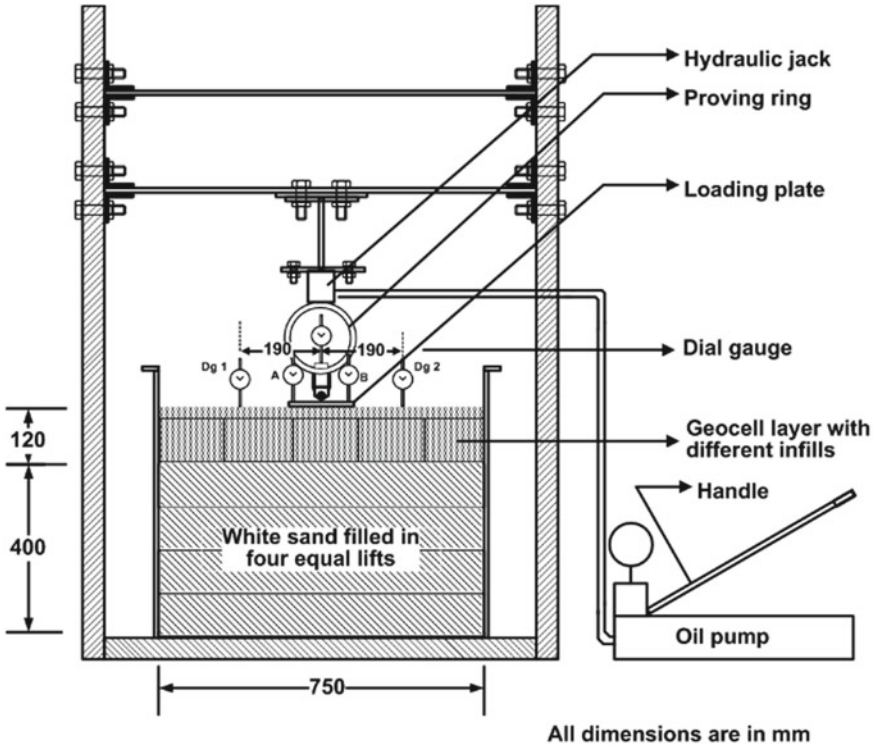

Fig. 10.3 Schematic of the test set-up

10.6 Design of Test Sections

In all the model tests carried out, the underlying foundation remained the same, viz. 400 mm thick bed of white sand. Different tests were planned by varying the infills in the geocell layer. The test plan adopted for the present study, and the abbreviations used are presented in Table 10.2.

The performance of different test sections is analysed by comparing the bearing pressures sustained with respect to settlement. Surface heave and improvement factors developed in the different sections are also studied to compare the effectiveness of geocell. From the experimental studies, an optimum percentage of tyre shreds are also arrived at. Efforts are made to understand the mobilization of tensile strength of these sections over higher deformations.

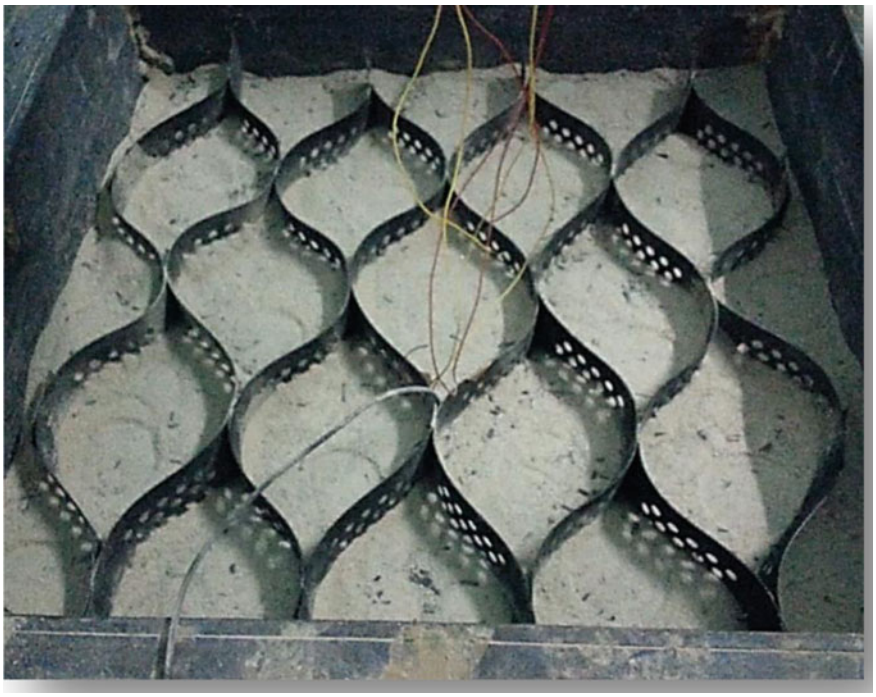

Fig. 10.4 Expanded form of geocells used in the experimental studies

10.7 Results and Comparisons

10.7.1 Optimum Percentage of Tyre Shreds

The proportion of tyre shreds added to the quarry dust was decided on the basis of the literature review. From the literature, it is observed that in most of the cyclic/repeated tests carried out on tyre shred embedded sections, the percentage of tyre shreds added range from 10% to 50 (Hataf and Rahimi 2006; Reddy and Krishna (2017), whereas in most of the static tests carried out on tyre shred embedded beds the percentage of tyre shreds was maintained less than 10% (Özkul and Baykal 2007; Cabalar et al. 2014).

Figure 10.6 presents the pressure versus settlement relationships for quarry dust (QD) mixed with different percentages of tyre shreds (TS). From the figure, it is observed that the pressure–settlement relationship is almost the same for a settlement up to 5 mm. However, beyond 5 mm there is a slight difference in the settlements of the different sections. On increasing the percentage of tyre shreds, it is observed that the pressure sustained by the model section increases and the settlement of the sections also increases. High settlements are not desirable as far as any construction is concerned because allowable bearing capacity is dependent on both shear and

Fig. 10.5 Instrumented model section with construction waste as overlying fill

Table 10.2 Test plan and the abbreviations used

S. No.	Details of tests carried out with respect to different base courses or infills	Abbreviations
1	Quarry dust with 0% Tyre shreds	QD + 0% TS
2	Quarry dust with 2.5% Tyre shreds	QD + 2.5% TS
3	Quarry dust with 5% Tyre shreds	QD + 5% TS
4	Quarry dust with 7.5% Tyre shreds	QD + 7.5% TS
5	Demolition waste	DW
6	Pond Ash	PA

settlement criterion. For any settlement, the pressure sustained by 5% tyre shreds is the highest. Hence, the optimum percentage of tyre shreds was decided as 5% in the later tests with geocell confinement.

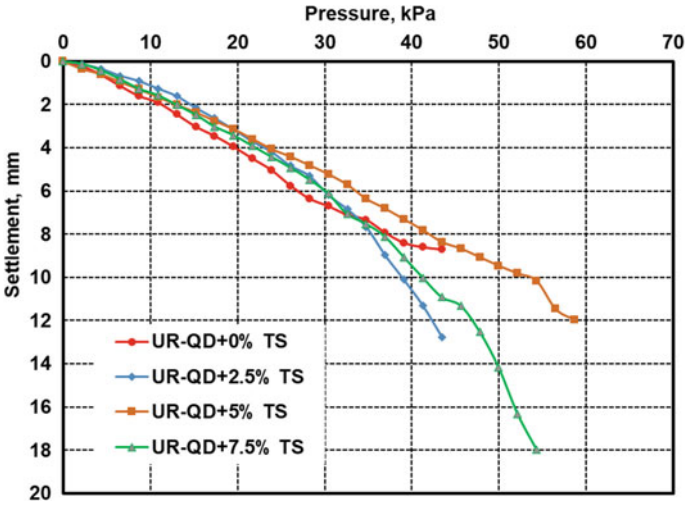

Fig. 10.6 Pressure–settlement relationship for quarry dust mixed with different percentages of tyre shreds

10.7.2 Effect of Geocell Confinement on Different Waste Materials

For comparing the effectiveness in stabilizing waste materials, four different waste materials are considered as infills, viz. geocell with quarry dust (R-QD), geocell with quarry dust and 5% tyre shreds (R-QD + 2.5% TS), geocell with demolition waste (R-DW), geocell with pond ash (R-PA). Figure 10.7 compares pressure versus settlement response for geocell reinforced model sections. From the figure, it is observed that demolition waste had higher bearing resistance compared to pond ash. However, the beneficial effect of geocell is more for pond ash.

To quantify the effectiveness of geocell in reducing surface heave and settlement, the different model sections have been compared, viz. UR-PA, R-PA, UR-QD + 5%TS and R-QD + 5% TS, and the result is presented in Fig. 10.8. In the figure, D represents the width of the footing. This graphical representation helps us to compare the surface heave induced for unreinforced and reinforced sections with respect to settlements. Here, comparisons are made with reference to normalized surface heave and normalized surface settlement (Saride 2005).

As expected the geocell was quite effective in reducing the vertical settlement and surface heave. However, the extent of this improvement is dependent upon the properties of infill. From Fig. 10.8, it is observed that the heave and settlements are more in tyre shreds when compared to pond ash. The geocell is effective in arresting heave completely in the case of pond ash. In the case of tyre shreds, also the effectiveness of geocell is there but the heave induced is more than pond ash.

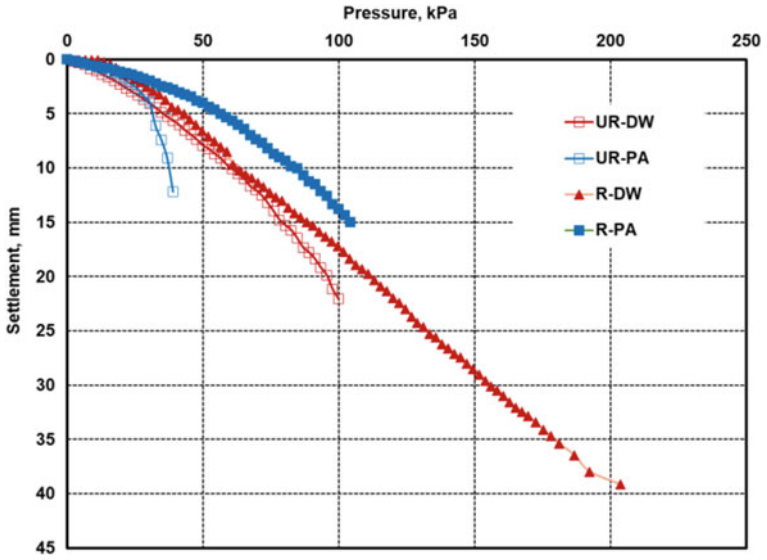

Fig. 10.7 Pressure versus settlement graph for unreinforced and geocell embedded model sections for two different infills

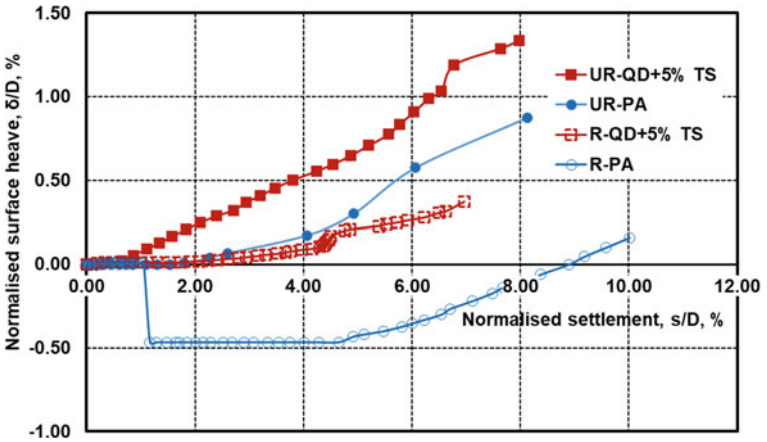

Fig. 10.8 Normalized surface heave versus normalized settlement curves for unreinforced and geocell embedded model sections of quarry dust with 5% tyre shreds and pond ash as infill

This is because pond ash has low specific gravity and the addition of moisture (@ 16% optimum moisture content) makes it more compressible.

10.7.3 Variation in Improvement Factor of Geocell Reinforced Sections

A dimensionless factor, I_f has been used extensively by researchers (Hedge and Sitharam 2015) to quantify the beneficial effect of geocell in arresting settlement and increasing the bearing resistance. It is defined as follows:

$$I_{\mathrm{f}} = \frac{q_{\mathrm{r}}}{q_{\mathrm{u}}} \tag{10.1}$$

where q_r is the bearing resistance of reinforced model section and q_u is the bearing resistance of unreinforced model section at the same settlement. Mobilization of geocell reinforcement can happen at high levels of displacement. Hence, it is important to know the settlement range at which geocells are effective for different infills. A comparison of the improvement factors over settlements has been made for different infills and is presented in Fig. 10.9. Geocell reinforcement increased the bearing resistance of all the sections seen in Fig. 10.9. The least improvement was exhibited by demolition waste (I_{f} in the range 1.5–1.2). The highest improvement was exhibited by pond ash (I_{f} in the range 1.4–2) but those sections exhibited high range of settlements. The inclusion of tyre shreds makes the quarry dust ductile. A comparison of the different materials concludes that geocell reinforced pond ash helps the system sustain more bearing pressure, and hence, serviceability criteria can be ensured by such systems even under high displacements.

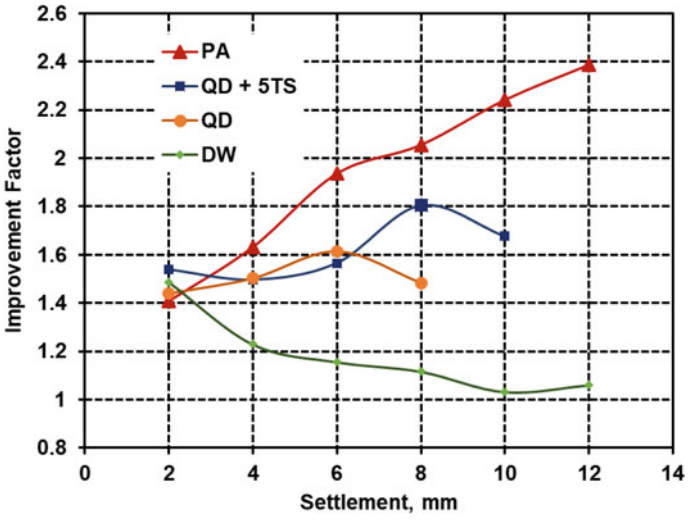

Fig. 10.9 Settlement versus improvement factor for geocell confined waste materials

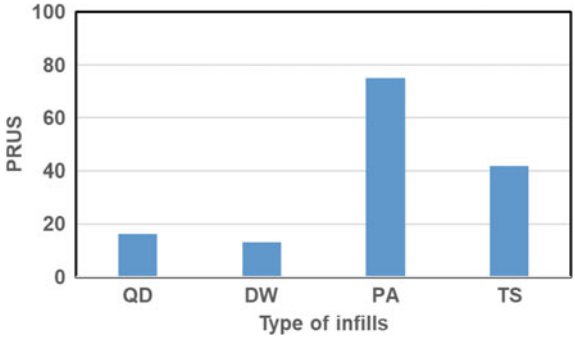

Fig. 10.10 Percentage reduction in ultimate settlement for different infills

10.7.4 Effect on Percentage Reduction in Ultimate Settlement (PRUS)

Many researchers have used the concept of percentage reduction in ultimate settlement for quantifying the benefit of geosynthetics. The percentage reduction in settlement can be estimated as follows:

$$\text{PRUS} = \frac{S_u - S_r}{S_u} \times 100 \tag{10.2}$$

where S_u is the settlement of unreinforced bed corresponding to ultimate bearing resistance and S_r is the settlement of reinforced bed corresponding to ultimate bearing resistance of unreinforced model section. The ultimate bearing resistance of the unreinforced bed is taken as the minimum of the following:

1. The bearing resistance corresponding to 10% of the foundation width (D) (Hegde and Sitharam 2015) or
2. The maximum bearing resistance sustained by the infill (wherein the infill could sustain a settlement less than 10% of the foundation width (D))

From Fig. 10.10, it is clear that the beneficial effect of geocell is high is for pond ash and this highlights the fact that for other waste materials especially for demolition waste and quarry dust, the beneficial effect of geocell is evident only at very large settlements. This is because of the large strains required for mobilizing the strength of the geocell.

10.7.5 Effect on Modulus of Sub-Grade Reaction (K)

Though there are different applications where these waste materials can be used, highway construction is one area where bulk utilization of these waste materials can be made. Modulus of subgrade reaction is a measure of the stiffness of subgrade, and

Table 10.3 Summary of modulus of subgrade reaction different sections

Material specification	Corrected value of modulus of subgrade reaction, k (KPa/m)		
	Unreinforced section (kPa/m)	Reinforced section (kPa/m)	$\frac{k_r}{k_u}$
Quarry dust	5600	8294	1.48
Quarry dust + 5% tyre shreds	6400	10,189	1.59
Pond ash	14,400	17,578	1.22
Demolition waste	8000	17,122	2.14

this property is used for the design of rigid or airfield pavements (Miura et al. 1990; Hedge and Sitharam 2015). Modulus of subgrade reaction is defined as follows

$$k(\text{kPa/m}) = \frac{q_{1.25}(\text{kPa})}{0.00125} \tag{10.3}$$

Table 10.3 compares the modulus of subgrade reaction of the different sections in unreinforced and reinforced condition. A comparison of the values reveals that all the waste materials considered are good substitutes for pavement construction. The modulus of subgrade reaction has increased with the embedment of geocell reinforcement. However, the increase in stiffness offered by geocell layer range from 1.2 to 2.2. The modulus of subgrade reaction of reinforced sections has not exhibited an enormous increase at a deformation of 1.25 mm.

10.8 Analysis and Discussions

Since the inception of the technology of using cellular confinement or geocell for soil stabilization, researchers have been carrying out parametric studies with reference to type of the material used for making geocell, types of infills, its shape, its configuration, its position in the foundation bed, field application and so on. This paper offers the advantage of comparing the performance of geocells with respect to two different parameters as listed below:

1. Effectiveness of geocell as a reinforcing material.
2. Effectiveness of different waste materials.

10.8.1 Effectiveness of Geocell as a Reinforcing Material

Geocells have been found to be effective for most of the infills. However, the effectiveness of geocells is dependent upon the infills. For instance, Bathurst and Karpurapu

(1993) have reported that the peak friction angle of the infill decides the performance of the geocell. Similarly, the effectiveness of geocell is dependent upon the shear strength of the foundation bed. For weak foundations like the one made of soft clay, the performance of geocell reinforced beds is more effective when compared to that of strong foundations. For example, in the studies reported by Hedge and Sitharam (2015), the subgrade modulus increased by 8 times when the foundation bed is of soft clay. However, in the present study, the increase in stiffness ranges from 1.2 to 2.2 (similar to Pokharel et al. 2010) because the foundation bed is comparatively strong (made of white sand). Performance of such reinforced beds is dependent upon the relative stiffness of the stabilized bed and the underlying foundation soil.

10.8.2 Suitability of Different Waste Materials

Majority of the literature work discusses the application of geocells with sand as the infill. However, in the last decade few literatures have been reported, that emphasize on the use of geocells for stabilizing waste materials. However, the reinforcing action of geocells is dependent mainly upon the infills. Vieira and Pereira (2015) have reported that the recycled aggregates have very high frictional resistance. But such materials undergo large amount of crushing on repeated loading. This crushing can cause an increase in the fines to present and tend to reduce friction angle. This could be the reason for decrease in the improvement factor of the geocell reinforcement with demolition waste as infill in the present study.

Similarly, pond ash used for different studies can vary in size. Jakka et al. (2010) have investigated the liquefaction resistance of ash collected at different points of ash pond. From the experimental studies, it has been reported that the ash collected at the inflow point is coarser and the shear behaviour of such materials is almost in par or better than that of sand. On the contrary, the ash collected at the outflow point is finer and their performance is inferior to that of the sand itself. In the present study, the pond ash selected in the study is coarser, and probably, this could be the reason for the better performance of pond ash.

According to the literature, the presence of moisture can impair the performance of reinforced bed which is indirectly related to the fines present. The presence of fines increases the apparent cohesion of the infill (Pokharel et al. 2010). Similarly, Hedge and Sitharam (2015) have reported that the use of coarser infill like aggregates ensures a better performance of geocell reinforced bed when compared to sand or clay. In the present study, for all the waste materials the fine percentage was less than 7% and except pond ash all infills were placed in dry condition. Owing to the dust generated in pond ash, it was placed at 85% relative compaction. However, the performance of geocell bed is at the maximum for pond ash. This ensures that more than the presence of moisture, it is the grain size of the material that ensures its performance as an infill. However, further investigations are required on pond ash (microstructure and leachate studies) to study its potential in pavement bases which can be a promising solution to the waste generation from thermal plants.

Rao and Dutta [36] have reported that the inclusion of tyre chips in sand beyond 20% may cause a drastic increase in compressibility (owed to direct contact) and the vertical strains induced also decrease with decrease in the size of the chips. Also, they have reported that initial tangent modulus and secant modulus decreases with increase in the percentage of tyre shreds with the decrease being drastic at a percentage replacement greater than 5%. In the present studies, with the inclusion of tyre shreds there is an increase in the improvement factor and stiffness. However, a detailed study on the same is required for varying sizes and aspect ratios of tyre shreds for developing design guidelines on the same.

10.9 Conclusions

From the present experimental study, the following conclusions can be drawn:

- Use of quarry dust blended with tyre shreds in foundation beds sustains greater bearing resistance at less settlements (Fig. 10.6).
- Geocells are effective in reinforcing foundation beds and pavement bases (Fig. 10.7).
- Geocell reinforced beds are effective in reducing surface heave and settlements (Fig. 10.8).
- Among the different geocell infills, pond ash was considered to be the best with reference to improvement factor and percentage reduction in ultimate settlement, i.e. 75% (Fig. 10.10).
- Use of geocell as a reinforcing material in the foundation bed increases the stiffness of the foundation in the range of 1.2–2.2 (Table 10.3).
- The beneficial effect of geocell was evident in demolition waste at initial levels of plate settlement (Table 10.3). With the increase in plate settlement, this beneficial effect decreased (Fig. 10.9).

10.10 Scope for Future Study

A comparison of the present work with the literature reveals that there exist no design standards for construction with waste materials. However, further studies are required in this area before it can be applied to field. A review of the literature reveals that crushing of particles under static and cyclic loading needs further investigation. This is highly important as far as the use of demolition waste is concerned. Similarly, the presence of moisture in the infill also needs to be studied. These parametric studies along with detailed investigations of the frictional characteristics of infill can help the practicing engineer to make the right choice of infill and provide a sustainable solution for waste management.

Acknowledgements The authors would like to express their sincere thanks to Dr. G. Madhavi Latha for giving permission to utilize the facilities at the Indian Institute of Science, Bengaluru, to carry out the experimental studies. The authors are also thankful to the undergraduate students Mr. Fateh, Ms. Priya, Mr. Sashi and Mr. Khaja for providing support in conducting the experimental studies. Authors also appreciate the help extended by Mr. Anthony in performing the experiments.

References

Arulrajah A, Rahman MA, Piratheepan J, Bo MW, Imteaz MA (2013) Interface shear strength testing of geogrid-reinforced construction and demolition materials. Adv Civil Eng Mater 2(1):189–200

Bathurst RJ, Karpurapu R (1993) Large-scale triaxial compression testing of geocell-reinforced granular soils. Geotech Test J 16(3):296–303

Cabalar AF, Karabash Z, Mustafa WS (2014) Stabilising a clay using tyrebuffings and lime. Road Mater Pavement Des 15(4):872–891

Cardoso R, Silva RV, de Brito J, Dhir R (2016) Use of recycled aggregates from construction and demolition waste in geotechnical applications. A Lit Rev Waste Manage 49:131–145

Dutta S, Mandal JN (2017) Model studies on encased fly ash column–geocell composite systems in soft clay. J Hazard Toxic Radioact Waste 21(3):04017001

Ghosh A (2009) Compaction characteristics and bearing ratio of pond ash stabilized with lime and phosphogypsum. J Mater Civ Eng 22(4):343–351

Han J, Thakur JK (2015) Sustainable roadway construction using recycled aggregates with geosynthetics. Sustain Cities Soc 14:342–350

Hataf N, Rahimi MM (2006) Experimental investigation of bearing capacity of sand reinforced with randomly distributed tire shreds. Constr Build Mater 20(10):910–916

Hazarika H, Otani J, Kikuchi Y (2012) Evaluation of tyre products as ground improving geomaterials. Proc Inst Civil Eng Ground Improv 165(4):267–282

Hegde AM, Sitharam TG (2015a) Effect of infill materials on the performance of geocell reinforced soft clay beds. Geomech Geoengineering 10(3):163–173

Hegde A, Sitharam TG (2015b) Experimental and analytical studies on soft clay beds reinforced with bamboo cells and geocells. Int J Geosynthetics Ground Eng 1(2):13

Jakka RS, Datta M, Ramana GV (2010) Liquefaction behavior of loose and compacted pond ash. Soil Dyn Earthq Eng 30(7):580–590

Kim B, Prezzi M, Salgado R (2005) Geotechnical properties of fly and bottom ash mixtures for use in highway embankments. J Geotech Geoenviron Eng 131(7):914–924

Kumar A, Gupta D (2016) Behavior of cement-stabilized fiber-reinforced pond ash, rice husk ash–soil mixtures. Geotext Geomembr 44(3):466–474

Latha G, Nair A, Hemalatha M (2010) Performance of geosynthetics in unpaved roads. Int J Geotech Eng 4(3):337–349

Lee JH, Salgado R, Bernal A, Lovell CW (1999) Shredded tires and rubber-sand as lightweight backfill. J Geotech Geoenviron Eng 125(2):132–141

Miura N, Sakai A, Taesiri Y, Yamanouchi T, Yasuhara K (1990) Polymer grid reinforced pavement on soft clay grounds. Geotext Geomembr 9(1):99–123

Nair AM, Latha GM (2016) Repeated load tests on geosynthetic reinforced unpaved road sections. Geomech Geoengineering 11(2):95–103

Özkul ZH, Baykal G (2007) Shear behavior of compacted rubber fiber-clay composite in drained and undrained loading. J Geotech Geoenviron Eng 133(7):767–781

Palmeira EM, Antunes LG (2010) Large scale tests on geosynthetic reinforced unpaved roads subjected to surface maintenance. Geotext Geomembr 28(6):547–558

Pandian NS (2013) Fly ash characterization with reference to geotechnical applications. J Indian Inst Sci 84(6):189

Pokharel SK, Han J, Leshchinsky D, Parsons RL, Halahmi I (2010) Investigation of factors influencing behavior of single geocell-reinforced bases under static loading. Geotext Geomembr 28(6):570–578

Rahman MA, Imteaz M, Arulrajah A, Disfani MM (2014) Suitability of recycled construction and demolition aggregates as alternative pipe backfilling materials. J Clean Prod 66:75–84

Rajagopal K, Krishnaswamy NR, Latha GM (1999) Behaviour of sand confined with single and multiple geocells. Geotext Geomembr 17(3):171–184

Rao GV, Dutta RK (2006) Compressibility and strength behaviour of sand–tyre chip mixtures. Geotech Geol Eng 24(3):711–724

Reddy SB, Krishna AM (2017) Tyre chips as compressible inclusions in earth-retaining walls. Proc Inst Civil Eng Ground Improv 170(3):137–148

Saride S (2005) Behaviour of geocell reinforced foundation beds. PhD thesis submitted to Department of Civil Engineering, Indian Institute of Science, 306

Saride S, Dutta TT (2016) Effect of fly-ash stabilization on stiffness modulus degradation of expansive clays. J Mater Civ Eng 28(12):04016166

Tafreshi SNM, Dawson AR (2012) A comparison of static and cyclic loading responses of foundations on geocell-reinforced sand. Geotext Geomembr 32:55–68

Thakur JK, Han J, Parsons RL (2012) Creep behavior of geocell-reinforced recycled asphalt pavement bases. J Mater Civ Eng 25(10):1533–1542

Vieira CS, Pereira PM (2015) Use of recycled construction and demolition materials in geotechnical applications: a review. Resour Conserv Recycl 103:192–204

Webster SL (1979) Investigation of beach sand trafficability enhancement using sand-grid confinement and membrane reinforcement concepts. U.S. Army Engineer Waterways Experiment Station, Vicksburg, MS, 79–20

Xiao M, Bowen J, Graham M, Larralde J (2012) Comparison of seismic responses of geosynthetically reinforced walls with tire-derived aggregates and granular backfills. J Mater Civ Eng 24(11):1368–1377

Chapter 11
Performance Improvement of Ballasted Railway Tracks Using Geocells: Present State of the Art

Sanjay Nimbalkar, Piyush Punetha, and Sakdirat Kaewunruen

Abstract The dramatic increase in the axle load and speed of the rolling stock over recent years has posed several challenges in terms of maintaining the stability and performance of the railway tracks. Consequently, the rail track engineers are exploring suitable measures to improve the performance of the tracks. The geocells can offer a cost-effective and technically viable alternative for enhancing the track performance. Although the performance of geocells in numerous geotechnical applications such as reinforced retaining walls, slopes, embankments, pavements, etc. is well-proven, their application to the railway tracks is still in the nascent stage. This chapter examines the potential benefits of using geocells in the railway tracks. The results of the numerous experimental, numerical, and field studies are critically reviewed. The influence of geocell reinforcement on the parameters (or material properties) essential for the track stability has been discussed. The past studies indicate that the geocells can be effectively used to improve the performance of the railway tracks. The geocells provide confinement which increases the strength and stiffness of the infill materials. Moreover, the geocell reinforcement significantly reduces the irrecoverable deformations of the track granular media, both vertically and laterally. However, the effectiveness of their use is influenced by several parameters such as the properties of the geocell, infill soil, subgrade, and the location of the geocell reinforced layer. This chapter elucidates the role of these influencing parameters in track stability. Furthermore, the satisfactory performance of geocells in the field substantiates their enormous applications in the railway tracks.

Keywords Geocell · Railways · Resilient modulus · Permanent deformation · Confinement · Analytical model

S. Nimbalkar (✉) · P. Punetha
University of Technology Sydney, Sydney, NSW 2007, Australia
e-mail: Sanjay.Nimbalkar@uts.edu.au

S. Kaewunruen
The University of Birmingham, Edgbaston, Birmingham B152TT, UK

T. G. Sitharam et al. (eds.), *Geocells*, Springer Transactions in Civil and Environmental Engineering,
https://doi.org/10.1007/978-981-15-6095-8_11

Notations

a^*, b^*, b'	Empirical coefficients
a', m^*, b	Material parameters
A_d	Maximum normal operating cant deficiency angle
A_y	Angle of lateral ramp discontinuity
A_z	Total angle of vertical ramp discontinuity
b_t	Track width
C	Coefficient in Japanese standard
C_z	Effective vertical rail damping rate per wheel
D	Diameter of soil sample
d	Diameter of soil specimen in triaxial test
D_g	Diameter of geocell opening
D_w	Diameter of wheel
E_i	Initial Young's modulus
E_{sec}	Secant Young's modulus
g	Acceleration due to gravity
H	Lateral load
h	Vertical distance from rail top to center of gravity of train
H_{mean}	Mean lateral load
h_s	Super-elevation
H_w	Crosswind force
k	Foundation coefficient or track modulus
k'	Ratio of circumferential strain to the radial strain in the geocell
k^*, k_1, k_2, k_3	Model parameters
K_1, K_2, K_3, K_4	Fitting parameters that depend on the type and physical state of the soil
K_j	Track stiffness at joint
K_y	Effective lateral rail stiffness per wheel
K_z	Effective vertical rail stiffness per wheel
l_c	Distance between rail top and center of gravity of train
l_g	Gauge width
l_w	Distance between center of rails and the resultant wind force
M	Modulus of the membrane (or geocell)
m, n	Model parameters
M_m	Mobilized modulus of geocell
M_r	Resilient modulus
M_t	Tensile stiffness of the geocell
M_u	Effective lateral unsprung mass per axle
M_v	Effective vertical unsprung mass per wheel
M_y	Effective lateral rail mass per wheel
M_z	Effective vertical rail mass per wheel
N_l	Number of load cycles
N_{lim}	Number of load cycles required to reach stable zone

N_{limit}	Number of load repetitions required to reach the resilient state
P	Static axle load
P_0	Static wheel load
P_{a}	Atmospheric pressure
P_{d}	Design wheel load
P_{dynamic}	Dynamic component of load
$P_{\text{quasi-static}}$	Quasi-static wheel load
P_{total}	Total vertical wheel load
Q	Wheel load
R_{c}	Radius of curvature of track
t	Factor that depends on the upper confidence limit (UCL)
V	Train speed
V_{m}	Maximum normal operating speed
W_{u}	Unsprung weight at one wheel
α'	Coefficient relating track irregularities, train suspension, and speed
β'	Coefficient accounting for the movement of train along a curve
γ'	Coefficient relating the train speed and configuration, track condition
δ	Factor that depends on the track condition
$\Delta\sigma_3$	Additional confining stress due to geocell
$\varepsilon_0/\varepsilon_{\text{r}}$, ρ, β	Fitting parameters for the permanent deformation of UGM
$\varepsilon_{1,1}^{p}$	Plastic axial strain after the first load cycle
ε_1^{p}	Plastic axial strain
ε_1^{e}	Vertical resilient strain
ε_{a}	Axial strain in soil specimen
ε_{c}	Circumferential strain
ε_{p}	Cumulative plastic strain
η	Factor that depends on the speed of vehicle
θ	Bulk stress
$\theta_1 + \theta_2$	Total dip angle of the rail joint
μ_{g}	Poisson's ratio of geocell
σ_1, σ_2, σ_3	Major, intermediate and minor principal stresses
σ_3'	Effective confining stress
σ_{cyc}	Cyclic deviator stress
σ_{d}	Deviator stress
σ_{oct}	Octahedral normal stress
σ_{s}	Static strength of the soil
τ_{oct}	Octahedral shear stress
φ	Dynamic amplification factor
ψ	Dilation angle
ψ_{m}	Mobilized dilation angle

11.1 Introduction

The rapid growth in population has substantially increased the transportation of passengers, resources, and goods throughout the world (Ngamkhanong and Kaewunruen 2018). Therefore, the demand for transportation facilities is escalating tremendously (Connolly et al. 2015). To cater to such huge demands, the existing modes of transportation are undergoing a rapid expansion in their infrastructure (Indraratna et al. 2016). Consequently, the number of road vehicles, trains, and aircrafts have significantly increased. However, the increase in the number of vehicles has resulted in a tremendous amount of congestion and air pollution (Indraratna et al. 2015; Powrie 2014; Krylov 2001).

The rail transport, on the other hand, is considered as an environment-friendly mode of transportation for the conveyance of a large volume of freight and a large number of passengers over long distances (Krylov 2001). Similar to its counterparts, the railway transport has adopted modern technologies to increase the speed of passenger trains and to improve the capacity of the freight trains in order to meet the ever-growing demands (Connolly et al. 2015). Consequently, the frequency and magnitude of the load on existing railway tracks have dramatically increased (Indraratna et al. 2011). However, most of the existing tracks have not been designed to meet these additional load requirements. Therefore, the stability of the track may get compromised in most of the conventional tracks (Indraratna et al. 2016).

The stability of a railway track is inevitable for the smooth and safe operation of the railway traffic, whether it be a passenger train, a freight train, or other rolling stock. The track deterioration poses severe consequences on the safety of the trains (Selig and Waters 1994). Moreover, track instability reduces the comfort of the passengers and may even endanger their lives.

The stability of a railway track depends on the hydraulic and mechanical behavior of the constituent materials [such as ballast, subballast (popularly known as capping in Australia), structural fill and general fill] and the soil subgrade (prepared and natural subgrade) under the train-induced quasi-static and dynamic loading. Throughout the service life, the track is subjected to repetitive loads due to the movement of the trains. With an increase in the frequency and magnitude of the load, the subgrade and the constituent materials undergo a substantial amount of deformation and deterioration (Nimbalkar et al. 2012). This degradation leads to unacceptable differential settlements, lateral instability, and a loss of track geometry (Sun et al. 2014). Consequently, the track loses its efficiency resulting in reduced train speed or costly maintenance and upgrade (Nimbalkar et al. 2012).

The maintenance work usually involves the replacement of the deteriorated constituent materials. However, the disposal of a massive quantity of the degraded material poses a serious challenge to the rail authorities due to the strict regulations imposed by the environment protection agency (Indraratna and Salim 2003). An alternative is to recycle the degraded material and re-use it for the construction of the tracks. The locally available materials could also be used to reduce the overall

maintenance costs (Indraratna et al. 2015). However, the recycled and locally available materials often possess inadequate strength and stiffness. Therefore, the use of these inferior quality materials may be detrimental for the track performance and may lead to extensive lateral spreading and differential settlements.

The geosynthetics can offer an economical and feasible solution for improving the performance of the railway tracks (Indraratna et al. 2015; Indraratna et al. 2010; Indraratna and Nimbalkar 2013; Indraratna et al. 2014; Nimbalkar and Indraratna 2016). Geosynthetics are the polymeric materials that are used for numerous applications such as soil reinforcement, slope stabilization, filtration, drainage, etc. (Koerner 2012). They have become an indispensable component in most of the geotechnical engineering projects. Moreover, the geosynthetics such as geogrids, geotextiles, and geocomposites have been used successfully for a long period in the railways for improving the stability of the tracks on soft subgrade (Li and Selig 1998).

The railway tracks often exhibit a significant amount of lateral spreading due to lack of sufficient confinement, especially when the subgrade is stiff (Indraratna et al. 2015). The geosynthetics, such as geocells can reduce this lateral deformation by confining the constituent materials. Geocells are the three-dimensional honey-comb shaped polymeric materials that are used to improve the strength and stiffness of the granular materials by providing additional confinement (Satyal et al. 2018). The geocells have been used for the construction of slopes, embankments, retaining walls, pavements, etc., however, their application to the field of railways is still minimal (e.g., Raymond 2001; Zarembski et al. 2017). This is probably due to the lack of proper design guidelines or due to the conservative approach adopted by the railroad track designers (Leshchinsky and Ling 2013a). Several studies have reported the beneficial role of geocell (Indraratna et al. 2015; Satyal et al. 2018; Leshchinsky and Ling 2013a, b; Bathurst and Karpurapu 1993; Pokharel et al. 2010, 2011, 2018; Tanyu et al. 2013; Giroud and Han 2004; Yang and Han 2013). However, most of these studies primarily focus on the pavements with only a few dealing with the railways.

The present chapter aims to explore the beneficial role of geocells in enhancing the stability of the railway tracks. The chapter is presented in the following sequence: the first section discusses the basic concepts for track design. This section helps the readers to develop a basic understanding of the track structure and the different types of loads that are exerted on the tracks. This knowledge is inevitable before the application of geocells in the railway tracks. The subsequent sections describe the potential benefits of using geocells in railways such as improvement in resilient modulus, reduction in plastic deformation, additional confinement, etc. and the mathematical models that can be used for their quantification. Finally, the case studies on the use of geocells in the railway tracks are discussed.

11.2 Railway Track—Basic Concepts

The railway track is the structure on which the trains and other rolling stocks move. The primary function of a railway track is to provide a stable and robust bed for the movement of the trains. The track must be able to transfer the traffic-induced loads safely to the subgrade soil. Safety implies that the stresses transferred to the soil must be within the permissible limits, enabling a sufficient safety margin for various risks and uncertainties (Esveld 2001). The settlement of the track must also be within the acceptable limits.

11.2.1 Structure of the Ballasted Railway Track

The ballasted railway tracks employ multiple layers of unbound granular material to transfer the train-induced loads safely to the subgrade. These tracks consist of two essential components: superstructure and substructure. The superstructure comprises rails, rail pads, sleepers (or ties), and the fasteners. Moreover, the substructure constitutes ballast, subballast (capping), structural fill, general fill, and soil subgrade (prepared and natural subgrade or formation). Figure 11.1 shows a typical cross-section of the ballasted track.

The rail is a longitudinal steel member which is supported by sleepers at regular intervals. It provides a firm base for the movement of trains. It must possess adequate

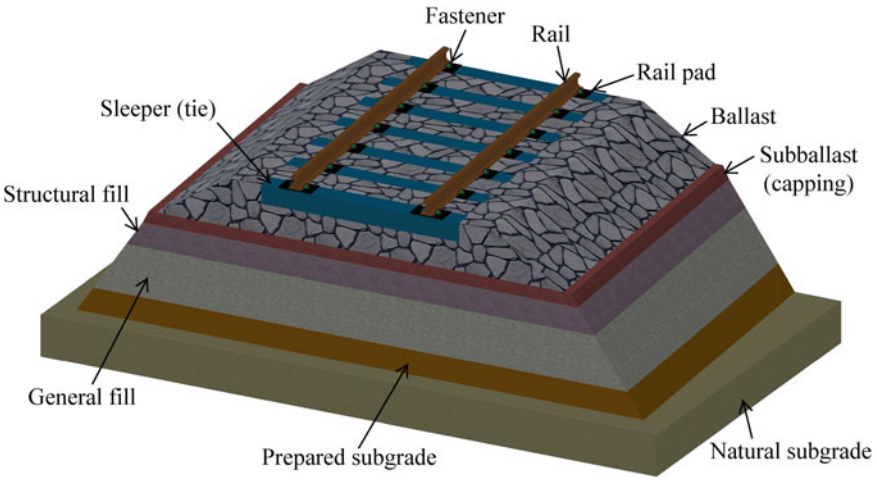

Fig. 11.1 Ballasted track structure

strength and stiffness to resist the forces exerted by the rolling stock without undergoing significant deformation. The rail primarily accommodates the wheel and transfers the load from the train to the sleepers. Moreover, it may also serve as an electric signal conductor in an electrified line (Indraratna et al. 2011; Remennikov and Kaewunruen 2008).

The rail pads are often provided below the rail to filter out or dampen the dynamic forces generated from the movement of the high-speed rolling stock (Indraratna et al. 2011). Therefore, they reduce the amount of vibration transmitted to the sleeper and the substructure.

The sleepers (or ties) are the transverse beams that support the rails and transfer the traffic-induced vertical, lateral, and longitudinal forces to the substructure (Doyle 1980). The sleepers can be manufactured using steel, concrete, or timber. However, the pre-stressed concrete sleepers are the most commonly used sleepers due to their high strength and durability (Remennikov and Kaewunruen 2008).

The fasteners are used to maintain the position of the rail on the sleepers. They resist a combination of train-induced vertical, lateral, and longitudinal forces in addition to the overturning moments (Remennikov and Kaewunruen 2008).

The ballast bed is a layer of coarse-aggregates that provides support to the sleepers. It comprises crushed stones and gravel with a typical particle size ranging between 20 and 60 mm (Esveld 2001). The primary functions of the ballast bed are to provide a stiff bearing surface for the sleepers and to transfer the imposed superstructure loads safely to the underlying layers and the subgrade (Doyle 1980). Moreover, the ballast bed facilitates the drainage of water away from the track, reduces vibrations, and absorbs the noise (Selig and Waters 1994).

The subballast bed (capping) is a layer of granular material that acts as a filter to prevent the movement of fines from the underlying layers to the ballast. Moreover, it arrests the penetration of the ballast into the bottom layers and drains water away from the subgrade into the ditches. The subballast layer also distributes the traffic-induced stresses uniformly over a wide area of the subgrade or the embankment fill (Indraratna et al. 2011).

The railway tracks are laid on embankments to maintain the vertical alignment either in the case of low-lying areas or areas where deposits of soft/weak subgrade are encountered. The embankments usually comprise structural fill and general fill. The structural fill is a layer of compacted material lying below the subballast bed whose thickness depends on the strength of the underlying layers (Asset Standards Authority 2018). The general fill is a layer of compacted material that is provided between the structural fill and the subgrade. The general fill material usually possesses lower strength than the structural fill material (Asset Standards Authority 2018).

The subgrade is the lowermost part of the railway track that ultimately bears the weight of the track and the traffic-induced loads. The safety and long-term performance of a track primarily depend on the mechanical and hydraulic behavior of the subgrade. Therefore, it must possess adequate strength (bearing capacity), stiffness, and drainage ability. However, some natural subgrades such as soft compressible clays possess poor engineering properties and require engineering treatment

before the construction of the overlying track layers. The treated layer with enhanced engineering properties is known as the prepared subgrade.

11.2.2 Loads on a Track

A railway track withstands a combination of loads in vertical, lateral, and longitudinal directions resulting from the traffic, track condition, and temperature. The vertical load is primarily due to the weight of the rolling stock. In addition to the weight, the vertical forces also emerge due to the movement of the vehicle on the track with geometrical irregularities. These forces are known as the dynamic forces, and their magnitude and frequency depend on the amount of rail/wheel irregularities (Remennikov and Kaewunruen 2008). The lateral loading arises from the wind, train's reaction to geometric deviations in the track, centrifugal force in curves, buckling reaction force on the rail (at high rail temperatures), etc. (Indraratna et al. 2011). Moreover, the longitudinal loading originates from the traction and braking forces from the trains, thermal effects, and wave action of rail (Selig and Waters 1994).

Vertical Load. The vertical load is a combination of moving static and dynamic loads (Esveld 2001). The total vertical load on a railway track is given as:

$$P_{\text{total}} = P_{\text{quasi - static}} + P_{\text{dynamic}} \tag{11.1}$$

where P_{total} is the total vertical wheel load; $P_{\text{quasi-static}}$ is the quasi-static wheel load, which is the sum of the static wheel load, wind load and non-compensated centrifugal force on the outer rail (in a curve); P_{dynamic} is the dynamic component of load that depends on the speed of the train, quality of the track and the wheel, vehicle parameters (such as wheel diameter and unsprung mass), etc.

$$P_{\text{quasi-static}} = \left(\frac{P}{2}\right) + H_{\text{w}}\frac{l_{\text{w}}}{b_{\text{t}}} + P\frac{l_c}{b_t^2}\left(\frac{b_{\text{t}}V^2}{gR_{\text{c}}} - h_{\text{s}}\right) \tag{11.2}$$

where P is the static axle load; H_{w} is the crosswind force; l_{w} is the distance between center of rails and the resultant wind force; l_{c} is the distance between rail top and center of gravity of the train; b_{t} is the track width; V is the train speed; g is the acceleration due to gravity; R_{c} is the radius of curvature of track; h_{s} is the super-elevation.

The dynamic component of the load is very complex as it depends on a large number of parameters such as track geometry, train configuration, and speed, among others. Consequently, the dynamic effect is represented in the form of a factor which is a multiplier to the static wheel load (Eq. 11.3) (Remennikov and Kaewunruen 2008; Doyle 1980). This factor is known as the dynamic amplification factor (DAF) or the impact factor. It depends on the parameters such as the train speed, quality (or condition) of the rail and wheel as well as the stiffness of subgrade (Sayeed and

Shahin 2016). The total design wheel load is calculated using the following equation.

$$P_{\mathrm{d}} = \varphi P_0 \tag{11.3}$$

where P_{d} is the design wheel load; φ is the DAF (always greater than 1); P_0 is the static wheel load. Table 11.1 shows the different empirical equations to evaluate the DAF. More details of these methods can be found elsewhere (Indraratna et al. 2011; Doyle 1980; Prause et al. 1974).

Lateral Loads. The loads acting on the railhead in the lateral direction depend on the parameters such as the radius of curvature of the track, speed, and configuration of the train, etc. (Doyle 1980). Several empirical expressions have been developed based on the field investigations to evaluate the magnitude of the lateral load exerted by the wheel flange on the railhead while negotiating the curves. Some of these empirical expressions are discussed by Doyle (1980).

ORE Formula. The ORE conducted field investigations to evaluate the magnitude of the lateral load exerted by the wheel flange on the railhead for different train configurations, speed (up to 200 km/h), and curve radii. The results showed that the lateral force depends only on the radius of curvature of the track. Moreover, the following equation was developed to calculate the magnitude of the lateral load:

$$H = 35 + \frac{7400}{R_{\mathrm{c}}} \tag{11.4}$$

where H is the lateral load (kN).

Swedish Railways Formula. The Swedish Railways conducted similar field investigations to evaluate the magnitude of the lateral load exerted by the wheel flange on the railhead for different train configurations, speed, and a curve radius of 600 m. The following empirical expression was developed:

$$H_{\mathrm{mean}} = 17 + \frac{V}{27.6} \tag{11.5}$$

where H_{mean} is the mean lateral load (kN).

British Railways Formula. The British Railways recommend the evaluation of the lateral load using the following relationship (British Railways Board 1993).

$$H = P A_{\mathrm{d}} + A_{\mathrm{y}} V_{\mathrm{m}} \sqrt{\frac{M_{\mathrm{u}}}{M_{\mathrm{u}} + M_{\mathrm{y}}}} \left(K_{\mathrm{y}} M_{\mathrm{u}}\right)^{0.5} \tag{11.6}$$

where A_{d} is the maximum normal operating cant deficiency angle (rad); V_{m} is the maximum normal operating speed (m/s); M_{u} is the effective lateral unsprung mass per axle (kg); A_{y} is the angle of lateral ramp discontinuity (0.0039 rad); M_{y} is the effective lateral rail mass per wheel (170 kg); K_{y} is the effective lateral rail stiffness per wheel

Table 11.1 Empirical equations to calculate the impact factor or DAF

Method	Equation	Remarks
AREA (1978)[a]	$\varphi = 1 + \frac{0.00521\ V}{D_w}$	V is the speed of the train (km/h); D_w is the diameter of wheel (m)
Eisenmann (1972)	$\varphi = 1 + \delta\eta t$ $\eta = 1$ for $V < 60$ km/h $\eta = \left(1 + \frac{V-60}{140}\right)$ for $60 \leq V \leq 200$ km/h	δ is a factor that depends on the track condition; η is a factor that depends on the speed of the vehicle; t is a factor that depends on the upper confidence limit
ORE (1980, 1968)[b]	$\varphi = 1 + \alpha' + \beta' + \gamma'$ $\alpha' = 0.04\left(\frac{V}{100}\right)^3$ $\beta' = \frac{V^2(2h+h_s)}{127\ R_c l_g} - \frac{2h_s h}{l_g^2}$ $\gamma' = \gamma_0 a_0 b_0 \gamma_0 =$ $0.1 + 0.017\left(\frac{V}{100}\right)^3$	α' is a coefficient that depends on the track irregularities, train suspension, and speed; β' is a coefficient that accounts for the movement of train along a curve, γ' is a coefficient that depends on the train speed and configuration, and track condition; V is the speed of train (km/h), l_g is the gauge width (m), h is the vertical distance from rail top to center of gravity of train (m), h_s is the super-elevation (m), R_c is the radius of curvature (m), a_0 and b_0 are the locomotive and track maintenance factors.
Japanese Standard (Atalar et al. 2018)	$\varphi = \left(1 + 0.3\frac{V}{100}\right)(1 + C)$	C is a coefficient (value ≈ 0.3); V is the speed of the train (km/h).
British Railways (Doyle 1980)	$\varphi =$ $1 + \frac{8.784(\theta_1+\theta_2)V}{P_0}\left(\frac{K_j W_u}{g}\right)^{0.5}$	$(\theta_1 + \theta_2)$ is the total dip angle of the rail joint (radians); V is the train speed (km/h); P_0 is the static wheel load (kN); K_j is the track stiffness at joint (kN/mm); W_u is the unsprung weight at one wheel (kN); g is the acceleration due to gravity (m/s^2)
Indian Railways (Doyle 1980)	$\varphi = 1 + \frac{V}{58.14(k)^{0.5}}$	V is the speed of the train (km/h); k is the track modulus (MPa)
German formula (Doyle 1980)	$\varphi = 1 + \frac{V^2}{3\times10^4}$ for $V \leq 100$ km/h $\varphi = 1 + \frac{4.5V^2}{10^5} - \frac{1.5V^3}{10^7}$ for $V > 100$ km/h	V is the speed of train (km/h)
South African formula (Doyle 1980)	$\varphi = 1 + \frac{4.92\ V}{D_w}$	D_w is the diameter of wheel (mm)
WMATA (Prause et al. 1974)[c]	$\varphi = \left(1 + 0.0001V^2\right)^{0.67}$	V is the speed of train (miles/h)

[a] American Railway Engineering Association
[b] Office for Research and Experiments
[c] Washington Metropolitan Area Transit Authority

(25×10^6 N/m). As per the British standards (British Railways Board 1993), the total lateral load per axle on the track must not exceed 71 kN when a rolling stock negotiates a curve with a lateral ramp discontinuity at maximum permissible speed and cant deficiency. The maximum permissible value of 71 kN corresponds to the lateral force theoretically induced by a Class 86/2 electric locomotive traveling at a speed of 180 km/h over a curve with a lateral ramp in outer rail and a cant deficiency of 5.8° (British Railways Board 1995). Moreover, the lateral load on the track per axle (sustained over a length ≥2 m) must never be greater than ($P/3 + 10$) kN.

Longitudinal Loads. The longitudinal loads develop from the thermal expansion and contraction of the rails, wheel action, and the traction and braking forces from the wheel. The thermal effects can lead to the buckling of the rail and are much more pronounced in the continuously welded rails. Moreover, the traction and braking result in excessive wear and tear on both rails and wheels (Prause et al. 1974).

Impact Loads. In addition to the quasi-static forces, the railway track is often subjected to impact loads due to inevitable track and train abnormalities. The impact loads are characterized by a high magnitude and short duration. Worn wheel/rail surface profile, wheel flats, bad welds, switches, dipped rails, joints, rail corrugation, turnouts, unsupported sleepers, an abrupt change in track stiffness are some of the inevitable causative factors of the impact loads in a railway track (Nimbalkar et al. 2012; Remennikov and Kaewunruen 2008).

The impact loads generate two distinct force peaks. The first peak is characterized by a large magnitude and a small duration (known as P_1). Whereas, the second peak is characterized by a small magnitude and large duration (known as P_2) (Indraratna et al. 2011). The peak P_1 occurs due to the inertia of the rail and sleepers, and it doesn't affect the track substructure. However, the peak P_2 occurs due to the mechanical resistance offered by the track substructure (Indraratna et al. 2011) and is responsible for the deterioration of the constituent materials of the track (Indraratna et al. 2016).

The P_2 force can be evaluated using the following formula (British Railways Board 1993):

$$P_2 = Q + \left(A_z V_m M C' K\right) \tag{11.7}$$

where Q is the maximum static wheel load (N); V_m is the maximum normal operating speed of the train (m/s); A_z is the total angle of vertical ramp discontinuity (0.02 rad).

$$M = \left(\frac{M_v}{M_v + M_z}\right)^{0.5} \tag{11.8}$$

$$C' = 1 - \left[\frac{\pi C_z}{4\{K_z(M_v + M_z)\}^{0.5}}\right] \tag{11.9}$$

$$K = (K_z M_v)^{0.5} \tag{11.10}$$

where M_v is effective vertical unsprung mass per wheel (kg); M_z is effective vertical rail mass per wheel (245 kg); C_z is effective vertical rail damping rate per wheel (55.4×10^3 Ns/m); K_z is the effective vertical rail stiffness per wheel (62×10^6 N/m).

The British standards restrict the maximum value of P_2 force to 322 kN per wheel (British Railways Board 1993). The maximum permissible value of 322 kN corresponds to the P_2 force theoretically induced by the Class 55 Deltic locomotive while traveling over a dipped rail joint (total dip angle of 0.02 rad) with a speed of 161 km/h (British Railways Board 1995).

The impact loads induce vibrations and oscillations in the train body and the various track components. Additionally, they generate a considerable amount of noise. The vibrations affect the performance of the track as well as passenger comfort. The magnitude and nature of the vibration depend on the characteristics of the geometric irregularity of the track and the wheel. A geometric irregularity with a large wavelength (e.g., due to differential settlement of the track) primarily causes train body vibrations that reduce the comfort of the passengers. However, the irregularity with a small wavelength (wheel or rail corrugations) primarily generates the wheel vibration. The wheel vibration leads to the fluctuation in axle weight and results in the vibration in the track (Miura et al. 1998). Moreover, the vibrations produced due to the impact loads accelerate the deterioration of the ballast and subballast bed (especially for stiff subgrade) and consequently, endanger the stability and efficiency of a track (Nimbalkar et al. 2012). The impact loads may also lead to the differential track settlement due to the localized compaction of the subgrade at the impact location (Sadri and Steenbergen 2018).

Figure 11.2 shows an example of the impact loads generated near the bridge approach. A railroad vehicle experiences an abrupt change in the track stiffness while approaching a bridge. This change leads to an amplification of the dynamic forces induced by the train-track interaction. These amplified dynamic forces are known as the impact forces.

The track substructure undergoes a considerable amount of deterioration due to these impact loads and ultimately results in undesirable differential settlements. The

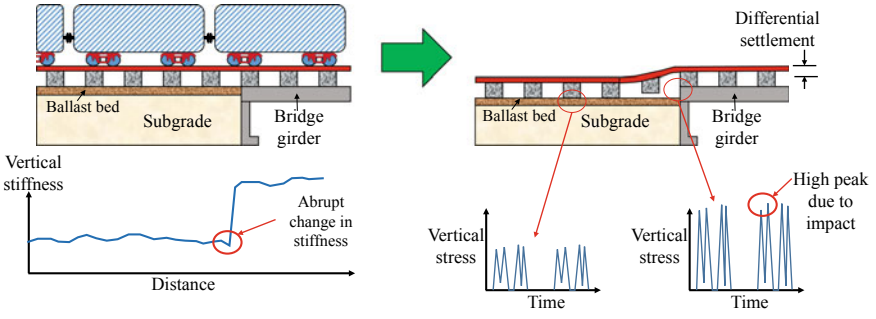

Fig. 11.2 Impact loads generated near the bridge approach. Modified from Wang and Markine (2018)

differential settlement further exacerbates the track stability and undermines the safety of the passengers (Kaewunruen et al. 2016). Therefore, frequent maintenance is required near the bridge approaches to keep the track in an operating condition.

A possible solution to this problem is to gradually increase the vertical track stiffness in the transition zone between the open track and the bridge. The gradual increase in the track stiffness reduces the magnitude of impact forces and preserves the track geometry over an extended period. The geocells can be used to increase the vertical track stiffness in the transition zones near the bridge ends. A case study regarding the use of geocells in the transition zones has been discussed later in the present chapter.

11.2.3 Track Design

The design of a ballasted railway track involves the determination of the stresses and settlements at critical locations within the track such as the sleeper-ballast, ballast-subballast, subballast-embankment fill, and fill-subgrade interface. Subsequently, the magnitude of the induced stresses and settlements are compared with the permissible values to arrive at a suitable factor of safety (Doyle 1980). The dimensions of the sleepers and the thickness of the granular layers (viz. ballast, subballast, structural fill, and general fill) are then adjusted to control the magnitude of the stresses and settlements (Doyle 1980; Li and Selig 1998). Figure 11.3 shows the flowchart for the design of a ballasted railway track.

The design technique uses semi-empirical equations to evaluate the load and deformations in the track. This is primarily due to the complexity in the accurate prediction of the train-induced loads and the corresponding track response. The loads are complex combinations of moving static and dynamic components (as discussed in the previous sections). Moreover, the track structure increases this complexity manifolds since it comprises different layers with distinct properties. Consequently, the present track design techniques are still very conservative and require further development (Indraratna et al. 2010).

11.3 Beneficial Role of Geocell in Railways

11.3.1 General

The conventional ballasted tracks require frequent maintenance due to the deterioration/degradation of the granular layers under repeated traffic loading (Esveld 2001). The degradation primarily involves the crushing or churning up of the ballast particles which produces fines. The fines clog the voids and decrease the permeability of the ballast bed. Moreover, the track loses its geometry under repetitive loads due

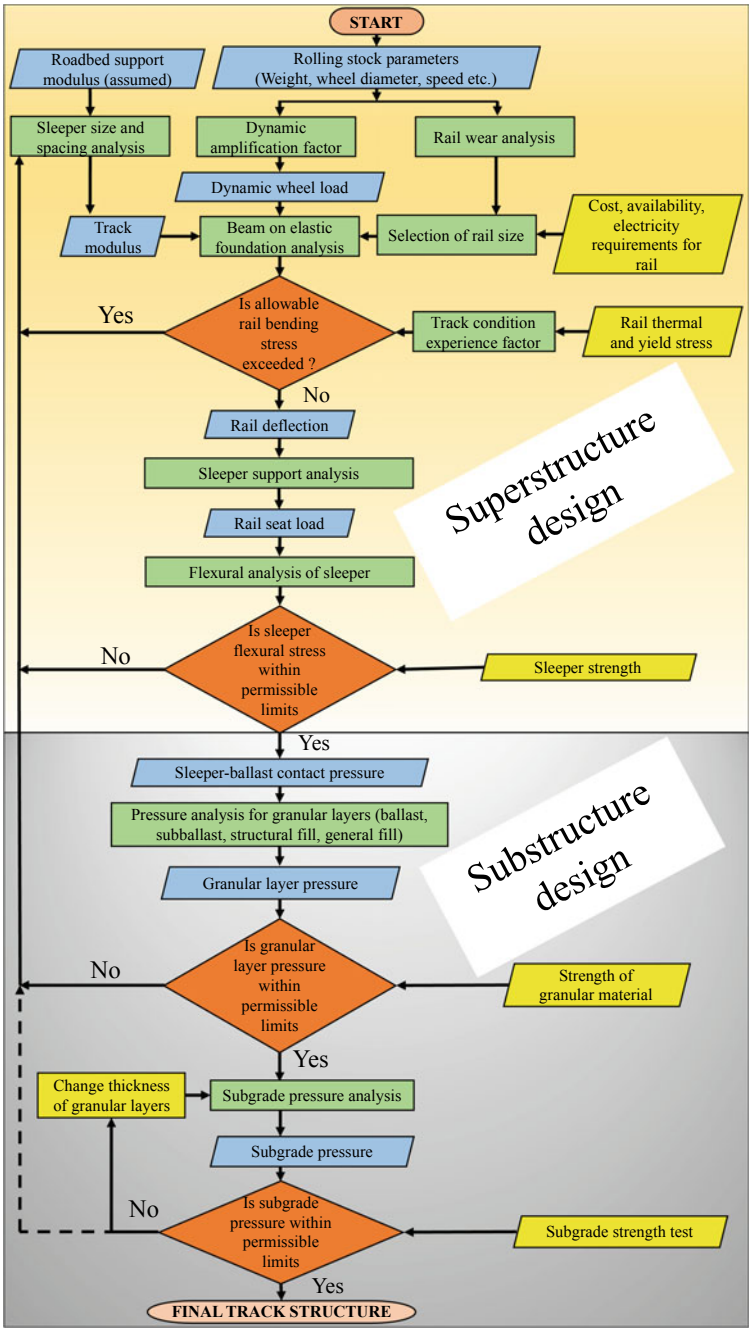

Fig. 11.3 Flowchart for the design of conventional ballasted track. Modified from Doyle (1980)

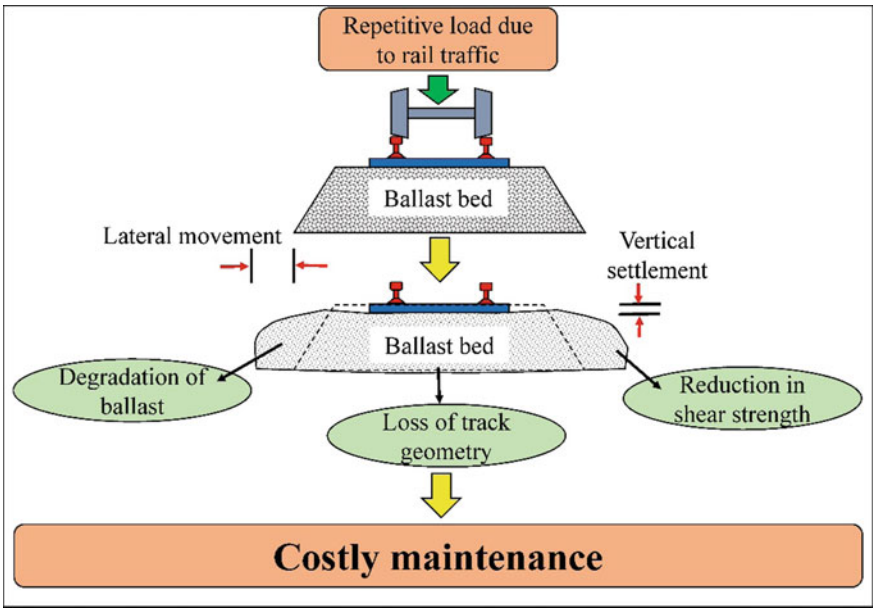

Fig. 11.4 Key problems governing the instability of ballasted railway tracks

to inadequate confinement of the ballast/subballast bed. Additionally, the problems may arise due to mud pumping or the intrusion of clay and silt size particles from the subgrade (saturated, soft subgrade) into the ballast bed, lateral buckling of rails due to insufficient track confinement, etc. (Indraratna et al. 2011). In Fig. 11.4, a schematic diagram is shown which illustrates the associated key issues governing the track instability during the normal track operations.

The maintenance work is not only expensive but also disrupts the traffic and reduces the availability and efficiency of the track. Therefore, the rail track designers are exploring suitable measures to improve the performance of the tracks and reduce the frequency of maintenance cycles. The geocells can provide a cost-effective solution in this aspect.

11.3.2 Potential Benefits of Using Geocells

The use of geocell can be highly beneficial for the long-term stability of the railway tracks. As discussed above, the traffic-induced load (moving static and dynamic) leads to the degradation of the constituent materials. Consequently, the track loses its geometry and efficiency and demands costly maintenance. The geocells provide confinement to the infill materials and may protect the track geometry for a long period and ultimately, reduce the frequency of the maintenance cycles.

Numerous experimental, numerical, and analytical studies have indicated that the geocells can be used to improve the performance of a ballasted track (Leshchinsky and Ling 2013a, b). The results of the studies show that:

- The geocell confines the infill material, which increases its strength and stiffness. Consequently, the traffic-induced stress gets uniformly distributed to a wide area (Chrismer 1997; Zhou and Wen 2008).
- The geocell confinement may reduce (redistribute) the shear stresses at the ballast (or subballast)-subgrade interface (Giroud and Han 2004).
- The use of geocell preserves the track geometry by reducing the permanent deformation in the subgrade. Moreover, it increases the strength and resilience of the infill material under cyclic loading (Indraratna et al. 2010; Raymond 2001; Chrismer 1997).
- The confinement provided by the geocell reduces the lateral deformations in the track and thus, maintains the track shape (Satyal et al. 2018).

11.3.3 Factors Affecting Geocell Applications in Railways

The past studies indicate that the geocells can be effectively used to improve the stability of the railway tracks. However, the degree of improvement depends on a large number of parameters. Some of the crucial parameters are discussed below.

Geocell Properties. The stiffness, size, shape, seam strength are some of the properties that may influence the performance of the geocell. The stiffness of geocell is crucial for the long-term stability and the overall cost of the reinforced track. The use of stiffer materials usually improves the confinement. However, the stiffer materials may be more expensive as compared to the soft materials. Moreover, large strains are generated in the soft material as compared to the rigid material for the same amount of vertical load (Leshchinsky and Ling 2013a). In soft material, the strains may even exceed the elastic limit and prevent the geocell from performing its intended function.

The shape of the geocell significantly influences the response of the geocell reinforced layer. The layers with elliptical geocells are less stiff as compared to the layers with circular geocells (Pokharel et al. 2010). Furthermore, the performance of the geocell reinforced layer decreases with an increase in the geocell pocket size (Yang and Han 2013).

Subgrade Properties. The subgrade strength and stiffness play a crucial role in the load-deformation behavior of the geocell reinforced track. The total deformation in a railway track comprises ballast deformation (or subballast deformation) and the subgrade deformation. For soft subgrades, the contribution of subgrade deformation is much higher as compared to the ballast deformation. However, for the stiff subgrades, the contribution of ballast deformation is significant (Doyle 1980). For stiff subgrade soils, the ballast (or subballast) layer tends to deform laterally which leads to the vertical deformation of the track. The geocells can significantly improve the performance of the track in this case by providing additional confinement to the

ballast and reducing the lateral deformation. Moreover, for soft soils, the geocells distribute the loads over a wider area and reduce the subgrade stress (Zhou and Wen 2008). Consequently, the settlement of subgrade decreases.

Furthermore, the subgrade stiffness influences the magnitude of the strain developed in the geocell. A large amount of strain is developed in the geocell for very soft subgrades as compared to the soft subgrades (Leshchinsky and Ling 2013a).

Properties of Infill Materials. The performance of a geocell reinforced layer also depends on the properties of the infill soil. Pokharel et al. (2010) observed that the geocell confinement provides an apparent cohesion to the infill material. They reported that the benefit of using geocell reduces if the infill material contains a significant amount of cohesion. Conversely, repeated plate load tests by Pokharel et al. (2018) showed that the geocell reinforcement also reduces the cumulative deformation in infill with fines as compared to the unreinforced case. Moreover, the use of low strength materials as infill increases the effectiveness of geocell (Leshchinsky and Ling 2013a). Thus, the geocells may prove beneficial in the construction of tracks using inferior quality recycled and locally available materials.

The Position of Geocells Within the Rail Track. The amount of improvement in the track stability depends on the placement position of the geocell. Several researchers have studied the performance of geocell reinforced infill layer at different locations within a track, such as, in the ballast bed, the subballast bed, or in the soil subgrade (Indraratna et al. 2015; Satyal et al. 2018; Leshchinsky and Ling 2013b). The ideal location of the geocell layer is in the ballast bed immediately below the sleepers. However, a minimum gap of 15–25 cm has to be maintained below the sleeper for the regular maintenance operations (Satyal et al. 2018; Leshchinsky and Ling 2013a). Furthermore, the service life of the geocell may reduce when it is placed near the top of the ballast bed due to a large amount of bending incurred from a high magnitude of vertical stress (Liu et al. 2018).

The presence of geocell reinforced layer in the track substructure reduces the vertical stress which minimizes the settlement and lateral spreading of the bottom layers (Liu et al. 2018). The effectiveness of using geocell in reducing the settlement may decrease with an increase in depth of the geocell layer from the top (or base of sleepers). Figure 11.5 shows the variation of subgrade stress below a railway track with (a) unreinforced ballast bed; (b) ballast bed reinforced with geocell near the sleeper base; (c) ballast bed reinforced with geocell at the bottom.

It is apparent that the load is distributed uniformly over a wide area of the subgrade for geocell reinforced ballast. Moreover, the load spread area is higher when the geocell is placed near the sleeper as compared to the case when it is situated near the subballast. This is because the geocell reinforced ballast is subjected to a high magnitude of vertical stress when it is placed near the top. Consequently, more confinement is mobilized and the load is spread over a wider area. Conversely, the high magnitude of vertical stress induces a large amount of bending in the geocell. Due to bending, high tensile stresses are generated near the bottom portion of the geocell layer (Leshchinsky and Ling 2013b). These stresses may exceed the seam

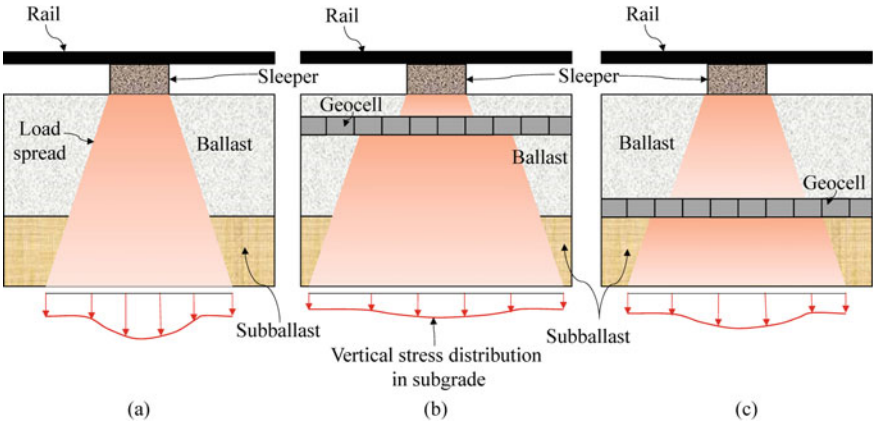

Fig. 11.5 The vertical stress distribution in the subgrade for the ballasted track **a** without geocell layer; **b** geocell layer near the top of ballast bed; **c** geocell layer near the bottom of ballast bed

strength (which is usually smaller than the tensile strength) and lead to wear and tear in the geocell. This wear and tear ultimately reduce the service life of geocell.

However, the geocell reinforced layer is subjected to low vertical stress when it is positioned near the base. Therefore, less confinement is mobilized, and the load is distributed over a small area. Nevertheless, the amount of load spread also depends on the relative stiffness between the subgrade and the geocell reinforced layer (Leshchinsky and Ling 2013a). The stiffness ratio between the geocell reinforced layer and subgrade must be large. However, there is an upper limit to the stiffness ratio because Leshchinsky and Ling (2013a) observed a non-uniform stress distribution at the subgrade due to the use of rigid (steel) geocell.

Therefore, it is very challenging to decide the most suitable position of the geocell layer within the rail track. Factors such as the nature of subgrade, intended function of geocell (i.e., to reduce the subgrade stress or the lateral deformation of granular layers or both), geocell material, etc. may govern the selection of the most appropriate location.

It is clear that the geocells can improve the performance of the railway tracks. However, it is essential to critically evaluate the improvement in terms of the parameters (or material properties) that are crucial for the track stability before their installation in the track. Therefore, the subsequent sections discuss the influence of geocells on the key parameters pertaining to track stability.

11.4 Resilient Modulus

11.4.1 Definition

The resilient modulus is defined as the ratio of the cyclic deviator stress (σ_{cyc}) to the elastic vertical strain (resilient strain) during unloading (ε_1^e) (Elliott and Thornton 1998). It is expressed as:

$$M_r = \frac{\sigma_{cyc}}{\varepsilon_1^e} \tag{11.11}$$

The resilient modulus (M_r) is most commonly determined using the cyclic triaxial tests with a constant value of confining pressure and a cyclic variation of the deviator stress (Li and Selig 1994). However, it is often very challenging to conduct laboratory testing on geomaterials prior to their use in rail or road applications. Therefore, several models (based on the experimental investigations) have been developed that can be used to directly evaluate the value of resilient modulus at specific physical states, loading conditions, and stress states (Li and Selig 1994).

11.4.2 Resilient Modulus Versus Young's Modulus

The resilient modulus of the granular material is often confused with Young's modulus. Although, both the terms measure the resistance against the elastic deformation, they distinctly differ in terms of evaluation and application. The resilient modulus is most commonly used to describe the behavior of granular materials under repeated (cyclic) loading. It is an essential parameter for the design of the pavements and the railway tracks (Christopher et al. 2006).

The Young's modulus of a material is the ratio of the stress to the strain under loading, within the elastic limits. It is generally employed to describe the behavior of a material under monotonic loading conditions, and its value is constant for an isotropic linear-elastic material. The Young's modulus is the slope of the linear (elastic) portion of the stress-strain curve of the material, usually obtained from axial compression or tension tests. However, the soil (or granular material) often exhibits nonlinear elastic behavior. Therefore, two Young's moduli are used to describe its response: initial Young's modulus (E_i) and secant Young's modulus (E_{sec}). The initial Young's modulus is the slope of the initial portion of the stress-strain curve, whereas, the secant modulus is the slope of the line joining the origin to a particular level of stress (or strain) in the stress-strain curve (Budhu 2015).

The behavior of the granular material (or soil) may change significantly under the cyclic load. When a granular material is subjected to cyclic loading, the amount of deformation in each cycle includes a resilient component (recoverable) and a plastic component (irrecoverable) (refer Fig. 11.6). The resilient (elastic) component for

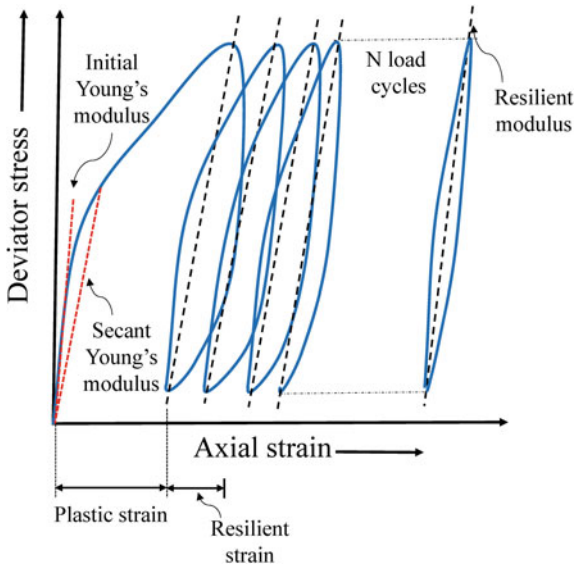

Fig. 11.6 Young's modulus and resilient modulus for soil

each cycle is calculated by subtracting the maximum strain under the peak load with the permanent strain after unloading.

Initially, the amount of plastic strain increment is much higher than the resilient strain. However, with an increase in the number of cycles, the magnitude of plastic strain increment decreases. Subsequently, a stage is reached (known as shakedown) when the plastic strain increment diminishes, and the elastic strain becomes virtually constant (Selig and Waters 1994). The corresponding ratio of the deviator stress to the recoverable (elastic) strain at this stage is termed as the resilient modulus of the material. It must be noted that the variation of plastic strain with the number of cycles also depends on the stress levels. The plastic strain may increase continuously with an increase in the number of cycles at high deviator stress and low confining pressure (Lekarp et al. 2000).

The resilient modulus is usually determined after the completion of a certain number of cycles (Selig and Waters 1994; Christopher et al. 2006). However, it may also be calculated for each load cycle for the accurate (or more realistic) prediction of the material behavior under repeated loading. The magnitude of the resilient modulus (if calculated for each cycle) increases with an increase in the number of load cycles and becomes almost constant after a particular value. Moreover, the material becomes progressively stiffer with an increase in the number of load cycles (Lekarp et al. 2000). Consequently, the magnitude of the resilient modulus of a material may even exceed Young's modulus.

11.4.3 Resilient Modulus Versus Track Modulus

The track modulus is defined as the force per unit deflection per unit length of the track (Doyle 1980). It is a measure of the resistance against deflection, produced by the track when a static wheel load is applied on the rail. In other words, track modulus is the static wheel load per unit length of the rail that is required to produce unit deflection in the track. The magnitude of the track modulus primarily depends on the properties of both the substructure and the superstructure, such as rail size, quality, dimensions and spacing of sleepers, quality, and degree of compaction of ballast, subballast, structural fill, general fill and the subgrade (Doyle 1980). Moreover, the train parameters such as speed and axle load also influence the magnitude of the track modulus (Nimbalkar and Indraratna 2016).

The track modulus is a measure of the overall response of the railway track to a static wheel load whereas the resilient modulus is a measure of the response of a particular material layer (ballast, subballast, or subgrade) to repeated loading. In other words, track modulus is the property on a global level, whereas, the resilient modulus is the property of individual components.

11.4.4 Young's Modulus Versus Stiffness

The Young's modulus of a material is the ratio of the stress to the strain within the elastic limit. It is a measure of the resistance offered by a material to the elastic deformation under loading. It is a material property and doesn't depend on the shape and size of the material under loading. The unit of Young's modulus is identical to the unit of stress, i.e., N/m^2.

The stiffness of the material is a measure of the resistance offered by the material against deformation under loading. It depends on the shape and size of the material. The unit of stiffness is N/m.

11.4.5 Empirical Models for Resilient Modulus

Several empirical models have been developed for the prediction of resilient modulus for soil (Li and Selig 1994). Table 11.2 lists the various models.

Here, σ_{di} is the deviator stress at which slope of the resilient modulus (M_r) versus deviator stress (σ_d) curve changes; $\dot{\sigma}_3$ is the effective confining stress; σ_{oct} and τ_{oct} are the octahedral normal and shear stresses, respectively; P_a is the atmospheric pressure; θ is the bulk stress.

The stress-dependent model given by Uzan (1985) (Table 11.2) is the most commonly used method to evaluate the resilient modulus. The bulk and octahedral shear stresses in this model can be evaluated by using the following equations:

Table 11.2 Empirical models for the prediction of resilient modulus

Type	Model	References	Fitting parameters
Bilinear	$M_r = K_1 + K_2\sigma_d$, for $\sigma_d < \sigma_{di}$	Thompson and Robnett (1976)	K_1, K_2
	$M_r = K_3 + K_4\sigma_d$, for $\sigma_d > \sigma_{di}$		K_3, K_4
Power	$M_r = k^*\sigma_d^n$	Moossazadeh and Witczak (1981)	k^*, n
Power	$M_r = k^*\left(\frac{\sigma_d}{\sigma_3}\right)^n$, for saturated over-consolidated soils	Brown et al. (1975)	k^*, n
Semi-log	$M_r = 10^{(k^* - n\sigma_d)}$	Fredlund et al. (1975)	k^*, n
Semi-log	$\log(M_r) = \left(k^* - n\frac{\sigma_d}{\sigma_{d(failure)}}\right)$	Raymond et al. (1979)	k^*, n
Hyperbolic	$M_r = \frac{k^* + n\sigma_d}{\sigma_d}$	Drumm et al. (1990)	k^*, n
Octahedral	$M_r = k^*\left(\frac{\sigma_{oct}^n}{\tau_{oct}^m}\right)$	Shackel (1973)	k^*, m, n
Stress-dependent	$M_r = k_1 P_a\left(\frac{\theta}{P_a}\right)^{k_2}\left(\frac{\tau_{oct}}{P_a} + 1\right)^{k_3}$	Uzan (1985)	k_1, k_2, k_3 ($k_1 > 0$, $k_2 \geq 0$ and $k_3 \leq 0$)

$$\tau_{oct} = \frac{1}{3}\sqrt{(\sigma_1 - \sigma_2)^2 + (\sigma_1 - \sigma_3)^2 + (\sigma_2 - \sigma_3)^2} \tag{11.12}$$

$$\theta = \sigma_1 + \sigma_2 + \sigma_3 \tag{11.13}$$

where σ_1, σ_2, and σ_3 are the major, intermediate, and minor principal stresses, respectively. It is interesting to note that the stress-dependent model by Uzan (1985) applies to both coarse-grained and fine-grained soils (Christopher et al. 2006). The model includes both the increment of resilient modulus with bulk stress and the reduction with an increase in the deviator stress for the coarse-grained and fine-grained soils, respectively (Thompson and Robnett 1976; Mengelt et al. 2006).

The resilient modulus is a measure of the elastic stiffness of the geomaterials used for the construction of the track substructure (Li and Selig 1994). Therefore, it can be used to predict the track performance (in terms of settlement) under repeated loads due to the rail traffic. Consequently, its study is essential for the design of the railway tracks. The resilient modulus of the soil depends on: (i) the properties of the material such as type, gradation, degree of compaction, moisture content; (ii) state of stress such as confining stress; and (iii) the loading parameters such as magnitude,

frequency, duration and the number of load cycles (Li and Selig 1994; Janaidhanam and Desai 1983).

11.4.6 *Influence of Geocell Reinforcement on Resilient Modulus*

Several researchers have conducted experimental and numerical investigations to understand the effect of geocell reinforcement on the resilient modulus of geomaterials. Some of the investigations are briefly discussed below.

Experimental and Field Investigations. The geocell reinforcement generally improves the resilient modulus of the soil. However, the magnitude of improvement depends on the conditions, such as the type of soil (fine-grained or coarse-grained), moisture content, confining pressure, deviator stress, frequency, number of load cycles, etc. (Indraratna et al. 2015; Mengelt et al. 2006). The experimental investigations by Edil and Bosscher (1994) revealed that the resilient modulus of sand increases with confinement. Moreover, the field investigations by Al-Qadi and Hughes (2000) on a pavement in Pennsylvania showed that the combination of geocell, geotextile, and geogrid can improve the resilient modulus of the aggregates.

Mengelt et al. (2006) conducted cyclic triaxial tests to study the influence of geocell reinforcement on the resilient modulus and plastic deformation behavior of the soil. The use of geocell increased the resilient modulus by 1.4–3.2% and 16.5–17.9% for the coarse-grained and fine-grained soils, respectively. Thus, the results indicated that the improvement is highly dependent on the soil type.

Tanyu et al. (2013) conducted large-scale repeated load tests (in a 3 m × 3 m × 3.5 m reinforced concrete pit) on geocell reinforced gravel (which represents granular sub-base layer for pavements). They observed a 40–50% increase in the resilient modulus on reinforcing the gravel with the geocell. Moreover, the increment was dependent on the thickness of the geocell reinforced layer. They stated that a higher degree of improvement might be observed in thin layers as compared to thick layers.

Indraratna et al. (2015) conducted repeated load tests on unreinforced and geocell reinforced subballast under plane-strain conditions. The use of plane-strain conditions gave a realistic approach to investigate the behavior of the subballast. The use of geocell increased the resilient modulus of the unreinforced subballast by 10–18%. Moreover, the resilient modulus for both the reinforced and unreinforced specimens increased (about 20%) with an increase in the confining pressure and the loading frequency. Furthermore, the effect of frequency was more pronounced in the geocell reinforced specimens.

Numerical and Analytical Investigations. Yang and Han (2013) observed that the use of geocell increases the resilient modulus of Unbound Granular Material (UGM). The amount of improvement in resilient modulus increased non-linearly with an

increase in the tensile stiffness and the cyclic deviator stress. Moreover, the improvement also increased with a reduction in geocell pocket size and an increment in dilation angle of the infill material. However, the improvement decreased with an increase in the resilient modulus of the infill material and the confining pressure.

Liu et al. (2018) studied the mechanical response of straight and curved geocell reinforced ballast embankment under monotonic and cyclic loading conditions using discrete element method (DEM). The results showed an increase in stiffness of the ballast bed under monotonic loading conditions and an increase in resilience under cyclic loading conditions.

Thus, the results from previous studies show that the geocells improve the resilient modulus of the granular materials. However, the degree of improvement depends on the parameters such as properties of the geocell, infill soil, subgrade, stress state, and the loading conditions.

11.5 Additional Confinement

11.5.1 General

The geocells provide an additional horizontal and vertical confinement to the infill material and restrain the upward movement of the underlying material (material below the geocell layer) outside the loaded area (mattress effect) (Pokharel et al. 2009, 2011). The horizontal confinement reduces the lateral deformation of the infill material. Moreover, the mattress effect results in a wider distribution of vehicle load which prevents excessive deformation (or failure) in soft subgrades (Pokharel et al. 2011).

However, the magnitude of additional confinement depends on the properties of the geocell, infill soil, and the loading conditions. Yang and Han (2013) observed that the additional confining pressure provided by the geocell reinforcement decreases with an increase in the geocell pocket size. This reduction is because the quantity of geocell material that reinforces the infill decreases with an increase in pocket size.

Moreover, the plane-strain cyclic loading tests by Indraratna et al. (2015) revealed that the loading frequency and external confining pressure significantly affect the extra confinement offered by the geocell. The additional confinement increased with an increase in loading frequency. However, it decreased with an increase in the external confining pressure at a particular loading frequency.

11.5.2 Models to Quantify Additional Confinement

The confinement provided by the geocells to the infill soil is identical to the confinement provided by the membrane to the soil sample in a triaxial test. Therefore,

the magnitude of additional confinement can be evaluated using the classical work of Henkel and Gilbert (1952). Henkel and Gilbert (1952) quantified the additional confinement provided by the membrane (in a triaxial test) and its influence on the shear strength of the soil (Mengelt et al. 2006).

Tanyu et al. (2013) used the theory developed by Henkel and Gilbert (1952) to evaluate the additional confining stress produced by the geocells on the soil (Eq. 11.14). The geocell strain data collected from the experiments were used in Eq. 11.14 to determine the additional confining stress ($\Delta\sigma_3$).

$$\Delta\sigma_3 = \frac{2M\varepsilon_c}{d(1-\varepsilon_a)} \tag{11.14}$$

where M is the modulus of the membrane (or geocell); ε_a is the axial strain of the specimen (soil); d is the diameter of the specimen; ε_c is the circumferential strain which can be calculated using Eq. 11.15.

$$\varepsilon_c = \frac{1-\sqrt{1-\varepsilon_a}}{\sqrt{1-\varepsilon_a}} \tag{11.15}$$

Yang and Han (2013) developed an analytical model to predict the additional confinement provided by the geocell in the repeated load triaxial tests. They suggested that the hoop stress developed in the geocell generates additional confining pressure within the infill material. Moreover, they assumed a uniform distribution of hoop stress along the height of the geocell. The additional confining pressure due to the incorporation of geocell was mathematically represented as:

$$\Delta\sigma_3 = \frac{M_t}{D}\left[\frac{-\Delta\sigma_3}{M_{r,1}} + \frac{\sigma_1 - (\sigma_3 + \Delta\sigma_3)}{M_{r,2}}\right]\left\{\frac{\varepsilon_0}{\varepsilon_r}\right\} e^{-\left(\frac{\rho}{N_{limit}}\right)^{\beta}}\left(\frac{1+\sin\psi}{1-\sin\psi}\right) \tag{11.16}$$

where $\Delta\sigma_3$ is the additional confining pressure; M_t is the tensile stiffness of the geocell; D is the diameter of the sample; ψ is the dilation angle; $\varepsilon_0/\varepsilon_r$, ρ and β are the fitting parameters that can be determined by using the permanent deformation test curve of UGM; N_{limit} is the number of load repetitions required to reach the resilient state; $M_{r,1}$ and $M_{r,2}$ are the resilient modulus of the granular material corresponding to the first and second stages of repeated load triaxial tests, respectively. The first stage corresponds to the condition when the axial stress increases from σ_3 to $\sigma_3 + \Delta\sigma_3$. The second stage corresponds to the increase of axial stress from $\sigma_3 + \Delta\sigma_3$ to σ_1.

However, Yang and Han (2013) ignored the influence of loading frequency on the additional confining pressure. Furthermore, the resilient modulus and mobilized dilation angle vary with the number of loading cycles (Indraratna et al. 2015). Therefore, using a constant value of resilient modulus and dilation angle can limit the accuracy of the proposed model.

Indraratna et al. (2015) derived a semi-empirical model using hoop tension theory, to determine the additional confinement provided by the geocell to an infill soil under

the plane-strain loading condition. They also incorporated the influence of loading frequency and load cycles on the mobilized modulus of geocell and the mobilized dilation angle for the infill material. This was done by varying the mobilized geocell modulus and mobilized dilation angle in accordance with the strain reached during a particular loading cycle. The additional confinement was calculated as

$$\Delta\sigma_3' = \int_1^{N_{\lim}} \left[\frac{2M_m}{D_g} \left\{ \frac{(1-\mu_g)k' + \mu_g}{(1+\mu_g)(1-2\mu_g)} \right\} \left\{ \frac{-\mu_g \sigma_{cyc}}{dM_r} + \varepsilon_{1,1}^{p} \left(\frac{a^*}{N_l} + \frac{b'}{N_l} \right) \left(\frac{1+\sin\psi_m}{1-\sin\psi_m} \right) \right\} \right] dN_l \tag{11.17}$$

where $\Delta\dot{\sigma}_3$ is the additional confining pressure; N_l is the number of load cycles; N_{lim} is the number of cycles required to reach a stable zone; M_m and μ_g are the mobilized modulus and the Poisson's ratio of the geocell, respectively; k' is the ratio of circumferential strain to the radial strain in geocell; D_g is the diameter of the geocell opening (the geocell opening is assumed circular); σ_{cyc} is the cyclic deviator stress; M_r is the resilient modulus of infill soil; $\varepsilon_{1,1}{}^{p}$ is the permanent axial strain after the first load cycle; a^* and b' are the empirical coefficients; ψ_m is the mobilized dilation angle.

11.6 Irrecoverable Deformations

11.6.1 General

The long-term performance of a railway track depends on the plastic deformations of its constituent materials. The excessive plastic deformation of the soil subgrade or the granular layers (ballast, subballast, structural fill, and general fill) under repeated traffic loads is detrimental for the stability of a rail track. It demands frequent maintenance cycles and also leads to poor riding quality which decreases the passenger comfort (Li and Selig 1996).

The granular materials usually tend to densify under the application of cyclic or repeated loading (Indraratna et al. 2010; Indraratna and Nimbalkar 2013). This densification is due to the reorientation and rearrangement of the particles, and also due to the particle breakage in response to the repeated loading. This response leads to permanent deformation in the track, and consequently, the track efficiency decreases. Nevertheless, the plastic response of the granular materials depends on a large number of factors such as (Lekarp et al. 2000; Sun et al. 2017; Li et al. 2018):

- Stress levels—plastic deformation is directly proportional to the deviator stress and inversely proportional to the confining pressure.
- Principal stress rotation—leads to larger permanent strain than those predicted by cyclic triaxial tests.
- Number of load cycles.

- Moisture content—plastic deformation may increase due to excessive positive pore water pressure or lubrication.
- Density—deformation decreases with an increase in density.
- Stress history.
- Grading, type of aggregate and fine content.

11.6.2 Influence of Geocell Reinforcement on Irrecoverable Deformations

Pokharel et al. (2009) conducted monotonic and repeated plate load tests on sand and reported that the geocell reinforcement reduces the permanent deformation, and increases the stiffness and bearing capacity. Moreover, the moving wheel test conducted by Pokharel et al. (2011) revealed that the geocell reinforcement increases the confinement in infill and distributes the load over a wide area, which results in a reduction in subgrade stress and deformation.

The studies by Yang and Han (2013) revealed that the geocell reinforcement reduces the permanent deformation of the UGM. Moreover, they observed that the reduction in permanent deformation due to geocell reinforcement depends on the external confining pressure, tensile stiffness, and the opening size of the geocell. The reduction in permanent deformation:

- Increased non-linearly with an increase in the tensile stiffness of geocell.
- Increased with a reduction in geocell size.
- Increased with an increase in the dilation angle of the infill material.
- Decreased with an increase in the resilient modulus of the infill soil.
- Decreased with an increase in confining pressure and cyclic deviator stress.

Leshchinsky and Ling (2013b) conducted a series of model tests to investigate the influence of the number and location of the geocell layers on the strength and stiffness of an embankment of poorly graded gravel. The poorly graded gravel embankment was assumed representative of the ballast bed in railways. The gravel embankment was loaded both monotonically and cyclically, and results of the tests with and without geocell reinforcement were compared. The experimental results showed that the reinforcement of gravel with geocell significantly reduces the vertical settlement and lateral deformation in both monotonic and repeated loading tests. Interestingly, the results showed that the maximum amount of lateral spreading occurred just above the geocell layer. Subsequently, a parametric study was conducted using finite element analysis to investigate the influence of geocell stiffness, type of subgrade, and strength of gravel on the behavior of geocell reinforced gravel embankment. The results showed that the settlement and subgrade stress reduced significantly with an increase in the geocell stiffness. However, the magnitude of stress reduction was dependent on the stiffness of the subgrade. No significant stress reduction was observed for a stiff subgrade. Nevertheless, the settlement reduced considerably for

the stiff subgrade. Thus, the authors stated that the geocell might have a beneficial effect on both the soft and stiff subgrade.

Leshchinsky and Ling (2013a) used 3D finite element analyses to investigate the behavior of ballasted railway track with and without geocell reinforcement under monotonic loading. The results showed that the reinforcement of ballast by geocell significantly reduces the vertical settlement of the track. However, the amount of reduction depends on the stiffness of geocell and subgrade in addition to the ballast strength. The decrease in the vertical settlement was more effective in case of soft or stiff subgrade, however, in a very soft subgrade, there was a little benefit. This effect was probably due to the tendency of the ballast to undergo a significant amount of lateral deformation when a stiff subgrade underlies it. The geocell prevents this lateral deformation and hence, reduces the vertical settlement of the track. Moreover, the geocell stiffness had little influence on the vertical settlement and lateral deformation of the ballasted track. Furthermore, the decrease in settlement and lateral deformation was more significant for low strength ballast as compared to high strength ballast on soft subgrades.

The experimental investigation by Indraratna et al. (2015) showed that the addition of geocells in the subballast layer decreases the permanent axial strain. Moreover, this beneficial role of geocell was more pronounced at low confining pressures (5–10 kPa). Furthermore, the reduction in permanent axial strain increased with an increase in the loading frequency.

Satyal et al. (2018) conducted cyclic plate load tests, and 3D finite element analyses on geocell reinforced ballast over soft subgrade to assess the beneficial role of geocell in the railway tracks. They observed that the geocell reinforced ballast layer distributes the traffic-induced load uniformly to a wide area in the soil subgrade and consequently, reduces the plastic deformation. Moreover, the strain in the geocell was within the elastic range, and no significant damage was observed in geocells. Subsequently, they validated the numerical results with the experimental plate load tests and then conducted a parametric study. The parametric studies showed an overall 30% reduction in track settlement on reinforcing the ballast by geocell. Moreover, the amount of settlement reduction was dependent on the position and number of geocell layers. The use of two geocell layers one above the other produced the least settlement. Further, the effectiveness of geocell reinforcement decreased with an increase in the strength of subgrades.

The DEM analyses of geocell reinforced straight, and curved embankments by Liu et al. (2018) showed that the application of geocell significantly reduces the vertical deformation of ballasted embankment under both monotonic and cyclic loading. This effect was more pronounced if the layer was placed at some distance above the subgrade. Moreover, it was observed that at the initial stages of monotonic loading, the geocell confinement was not mobilized and both the unreinforced and reinforced embankments showed similar stiffness. However, after a particular value of the load, the stiffness of geocell reinforced embankment increased. Furthermore, the ballast inside the geocell tends to move downwards, however, the ballast for unreinforced case tends to move sideways in addition to the vertical movement.

The repeated plate loading tests by Pokharel et al. (2018) showed that the use of geocell reduces the permanent deformation of a layer as compared to the unreinforced case.

Therefore, the results from the aforementioned studies indicate that the geocell reinforcement significantly decreases the lateral and vertical deformation of the infill materials. However, the amount of reduction depends on the properties of the geocell, infill soil, subgrade, and loading conditions.

11.6.3 Empirical Models for Irrecoverable Deformations

Several mathematical models are available to predict the plastic deformations of the soil subgrade and the granular layers under repeated loading (Lekarp et al. 2000). Some of the models are discussed below.

Li and Selig (1996) gave a power model to predict the cumulative plastic deformation in fine-grained subgrade soils under repeated loading. The model considered the influence of the number of load cycles, and the type, stress state (deviator stress) and physical state (dry density and moisture content) of the soil on the cumulative plastic strain (Eq. 11.18).

$$\varepsilon_{\mathrm{p}} = a'\left(\frac{\sigma_{\mathrm{d}}}{\sigma_{\mathrm{s}}}\right)^{m^*} N_1^{\mathrm{b}} \tag{11.18}$$

where a', m^* and b are the material parameters; N_1 is the number of load cycles; σ_{s} and σ_{d} are the static strength of the soil and deviator stress, respectively; ε_{p} is the cumulative plastic strain. The static strength of the soil represents the influence of the physical state on the cumulative plastic strain (and to some extent on the structure of the soil). The parameters a', m^* and b depend on the type of soil, and their average values vary between 0.64–1.2, 1.7–2.4 and 0.1–0.18, respectively for the fine-grained soils [ML, MH, CL and CH as per Unified soil classification system (USCS)] (Li and Selig 1996).

Yang and Han (2013) proposed an analytical model to evaluate the permanent deformation of geocell reinforced UGM under repeated load triaxial tests when it reaches the resilient state.

$$\varepsilon_1^{\mathrm{p}} = \left[-\frac{\Delta\sigma_3}{M_{\mathrm{r},1}} + \frac{\sigma_1 - (\sigma_3 + \Delta\sigma_3)}{M_{\mathrm{r},2}}\right]\left(\frac{\varepsilon_0}{\varepsilon_{\mathrm{r}}}\right)\mathrm{e}^{-(\rho/N_{\mathrm{limit}})^{\beta}} \tag{11.19}$$

where $\varepsilon_1^{\mathrm{p}}$ is the permanent axial strain. The other parameters have the same meaning as in Eq. 11.16. Thus, to evaluate the permanent axial deformation, the additional confining pressure due to geocell need to be evaluated. Moreover, the parameters $M_{\mathrm{r},1}$ and $M_{\mathrm{r},2}$ can be calculated using the equations in Table 11.2.

Indraratna and Nimbalkar (2013) proposed a model to evaluate the variation of permanent axial strain in the ballast with the number of load cycles (Eq. 11.20).

$$\varepsilon_1^{\mathrm{p}} = \varepsilon_{1,1}^{\mathrm{p}}\left[1 + a^* \ln N_l + 0.5b^* (\ln N_1)^2\right] \tag{11.20}$$

An attempt has been made to predict the variation of permanent deformation with the number of load cycles for different types of infill (for both unreinforced and geocell reinforced cases). The experimental data from the cyclic plate load tests conducted by different researchers were used to derive the empirical coefficients a^* and b^*. The permanent deformation was then predicted using the Eq. 11.20. Subsequently, the accuracy of the coefficients was investigated by comparing the back-fitted data with the experimental data. Table 11.3 gives the values of empirical coefficients (or model parameters) obtained for the unreinforced and geocell reinforced cases.

Figure 11.7 shows the experimental versus predicted results for the tests conducted by Pokharel et al. (2018), Tanyu et al. (2013), Leshchinsky and Ling (2013b), and Thakur et al. (2012). The permanent deformation has been normalized with the

Table 11.3 Model parameters to predict permanent deformation

S. No.	References	Infill	Condition	Model parameters	
				a^*	b^*
1	Thakur et al. (2012)	Recycled asphalt pavement (RAP)	Unreinforced	0.148	1.820
2	Thakur et al. (2012)	RAP	Geocell reinforced	0.155	0.591
3	Leshchinsky and Ling (2013b)	Gravel	Unreinforced embankment	32.89	6.459
4	Leshchinsky and Ling (2013b)	Gravel	Geocell reinforced embankment (single layer)	0.1	122.5
5	Tanyu et al. (2013)	Grade-2 gravel	Unreinforced	0.05	0.68
6	Tanyu et al. (2013)	Grade-2 gravel	Reinforced (geocell with 200 mm diameter and 200 mm height)	1.386	0.461
7	Pokharel et al. (2018)	Aggregate base type 3 (AB-3)	Unreinforced (Maximum applied pressure—552 kPa)	0.217	0.026
8	Pokharel et al. (2018)	AB-3	Geocell reinforced (single cell, maximum applied pressure—552 kPa)	0.146	0.079
9	Pokharel et al. (2018)	AB-3	Geocell reinforced (multiple cells, maximum applied pressure—552 kPa)	0.415	0.050

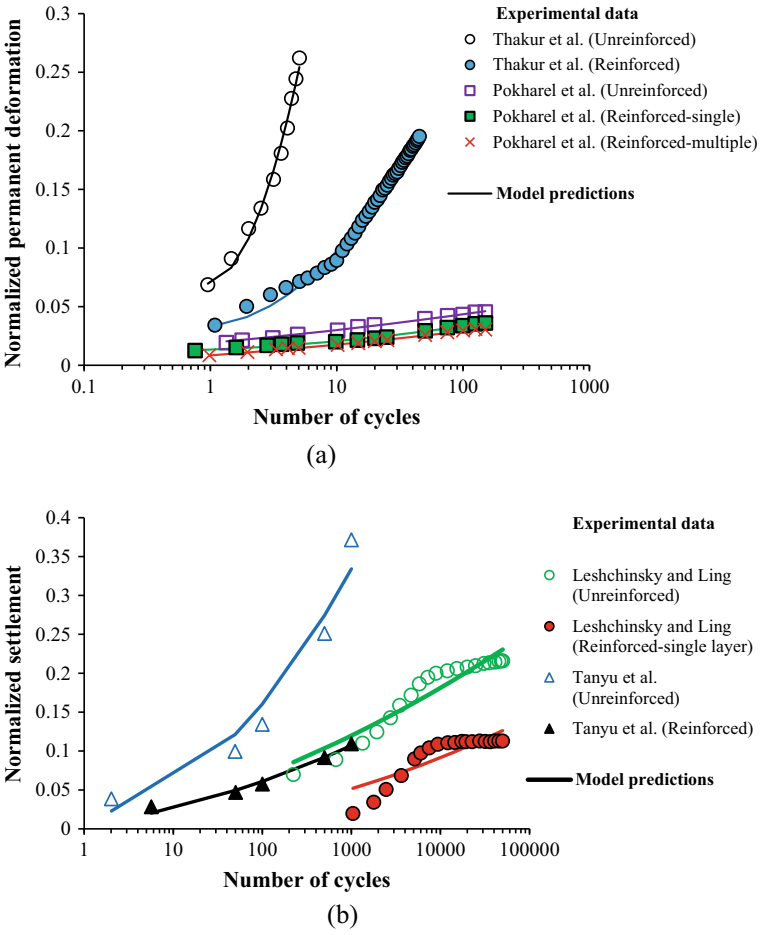

Fig. 11.7 Comparison of predicted and experimental results from previous studies

layer/specimen thickness to allow the comparison of results from the different studies. The figure shows that for all the cases, the geocell reinforcement significantly reduces the permanent deformation or settlement of the infill. Moreover, the results from model predictions are in close agreement with the experimental results.

11.7 Field Performance of Geocells

This section discusses a few case studies where geocells have been used for the stabilization of the railway tracks.

11.7.1 Reconstruction of Ballasted Track for Gantry Crane Using Geocells

Raymond (2001) reported the reconstruction of a ballasted track for a gantry crane in Canada. A 200 mm thick geocell reinforced subballast layer was provided below the sleepers (with a gap of 200 mm between the sleeper and geocell layer) during the reconstruction. The use of geocell reduced the settlement and lateral deformation of the track significantly.

11.7.2 Retrofitting of a Portion of Amtrak's North-East Corridor Railway Line Using Geocells

Zarembski et al. (2017) discussed the reconstruction of a portion of Amtrak's north-east corridor railway line using geocells. The presence of soft subgrade in the site and extensive ballast fouling resulted in significant loss in track geometry which demanded frequent maintenance. Consequently, a layer of geocell was provided in the subballast to reduce the subgrade stress and the track geometry degradation. Furthermore, a part of the track was reconstructed without geocell to compare the results. The field investigations revealed that the geocell stabilized section showed a minimal amount of settlement and subgrade stress as compared to the non-reinforced section. Moreover, the rate of track geometry degradation reduced for the geocell reinforced track.

11.7.3 Construction of a Transition Zone Near a Railway Bridge on the South Coast of New South Wales, Australia

Kaewunruen et al. (2016) investigated the performance of a transition zone near a railway bridge on the south coast of New South Wales, Australia. The transition zone comprised geocells along with track superstructure elements such as resilient baseplates and sleepers to mitigate the traffic-induced vibrations and increase the stiffness of the track. Figure 11.8 shows the placement of the geocells below the ballast bed near the bridge end.

Additionally, stiffness transfer sleepers with rail pads were provided after the geocell reinforced section. The rail pads were employed to dampen the traffic-induced vibrations. Accelerometers were used to monitor the vibrations generated in the rail, sleepers, and the ballast at the bridge, the bridge ends, the transition zone, the section with stiffness transfer sleepers, and the region with ordinary sleepers. Figure 11.9 shows the placement positions of the geocells and superstructure elements (pads, sleepers) along the track.

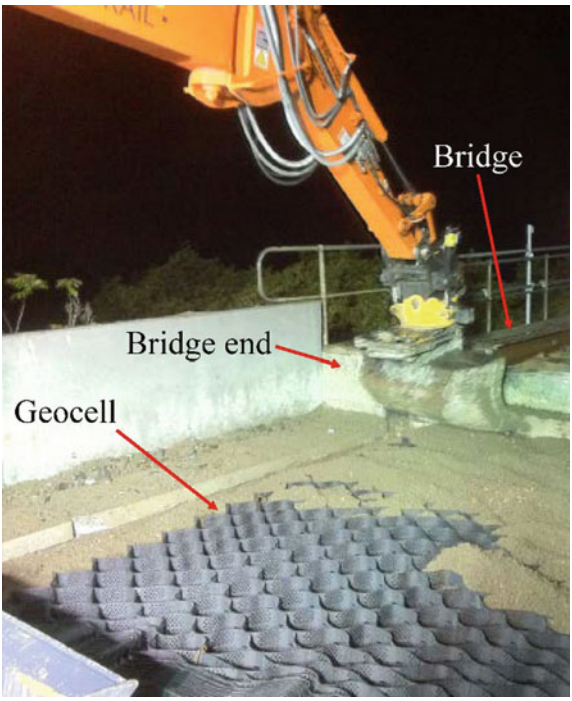

Fig. 11.8 Installation of geocells at the railway bridge ends on the south coast line of New South Wales, Australia. Modified from Kaewunruen et al. (2016)

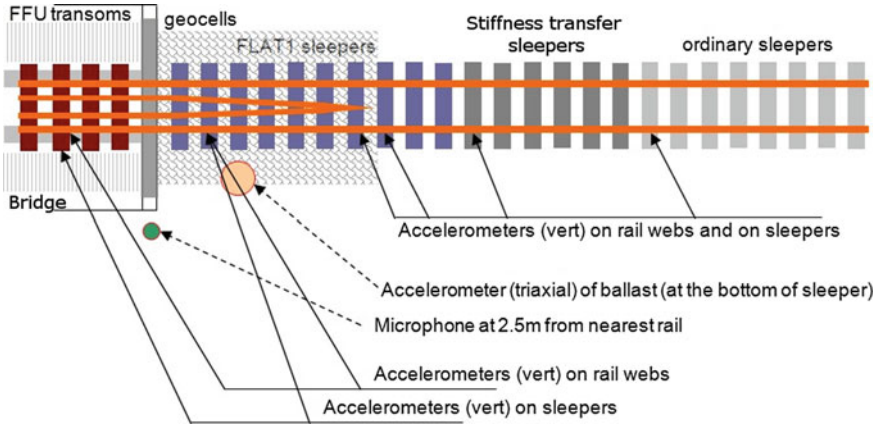

Fig. 11.9 Track longitudinal profile showing the location of the geocells and superstructure elements (pads, sleepers). Modified from Kaewunruen et al. (2016)

Figures 11.10, 11.11 and 11.12 show the typical Fourier amplitude spectra of the acceleration recorded in different components of a railway track at different sections (for the passage of three different trains) (Kaewunruen et al. 2016). It is apparent from the figures that as the trains move from the region with ordinary sleepers towards the bridge, the vibration in the sleepers increases. However, the magnitude of rail

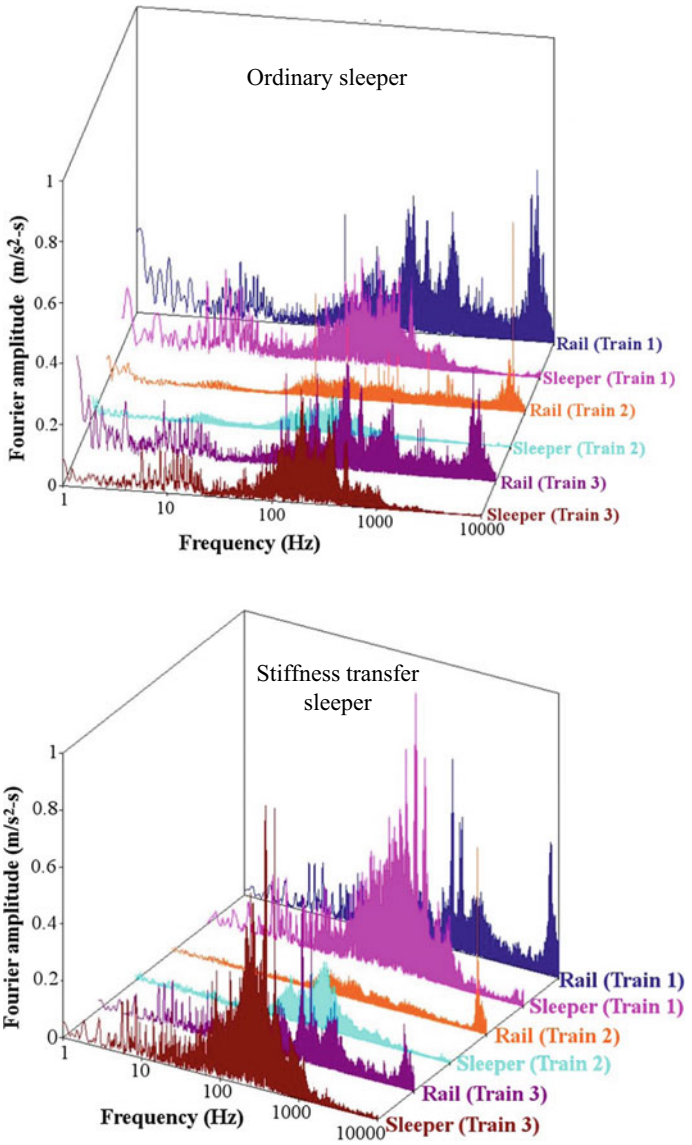

Fig. 11.10 Typical Fourier amplitude spectrum for field accelerometer data recorded at the region with ordinary sleeper and stiffness transfer sleeper. Adapted from Kaewunruen et al. (2016)

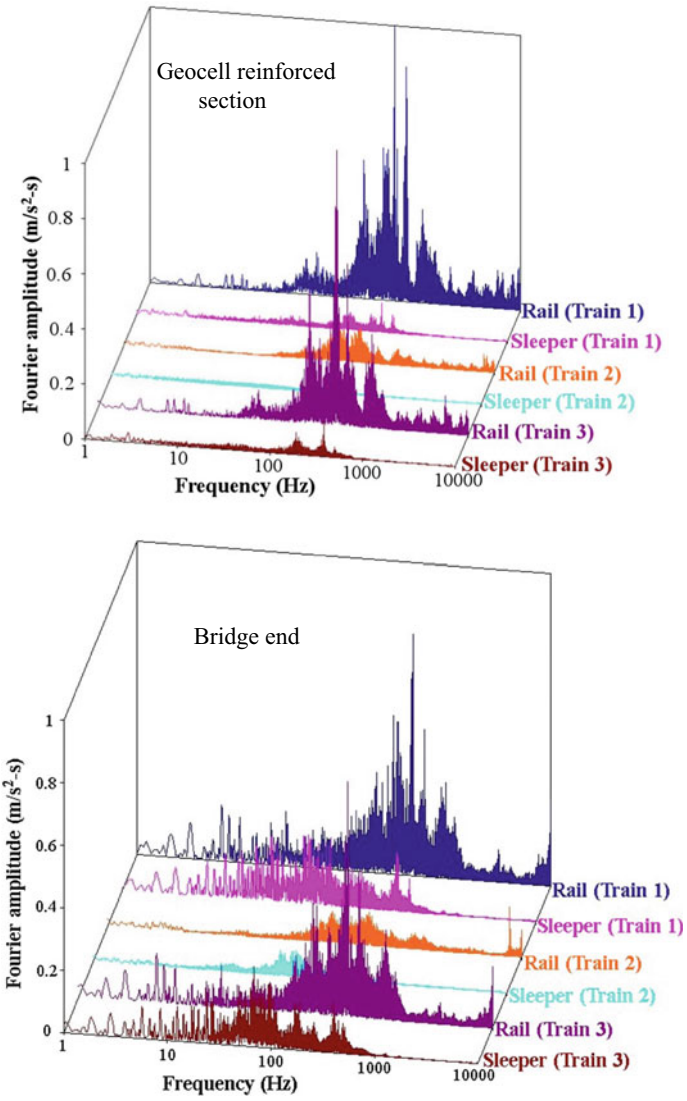

Fig. 11.11 Fourier amplitude spectrum for field accelerometer data recorded in the geocell reinforced section and at the bridge end. Adapted from Kaewunruen et al. (2016)

vibration is almost identical at the bridge end and the geocell reinforced zone. This behavior may be attributed to the increased stiffness of the track by the use of geocells in the transition zone which mitigated the impact loads on the track. As explained in the previous section (Sect. 11.2.2), an abrupt change in track stiffness generates the impact loads near the bridge ends which produce excessive vibrations and endangers the track stability (Nimbalkar et al. 2018). However, the geocells reduced the stiffness

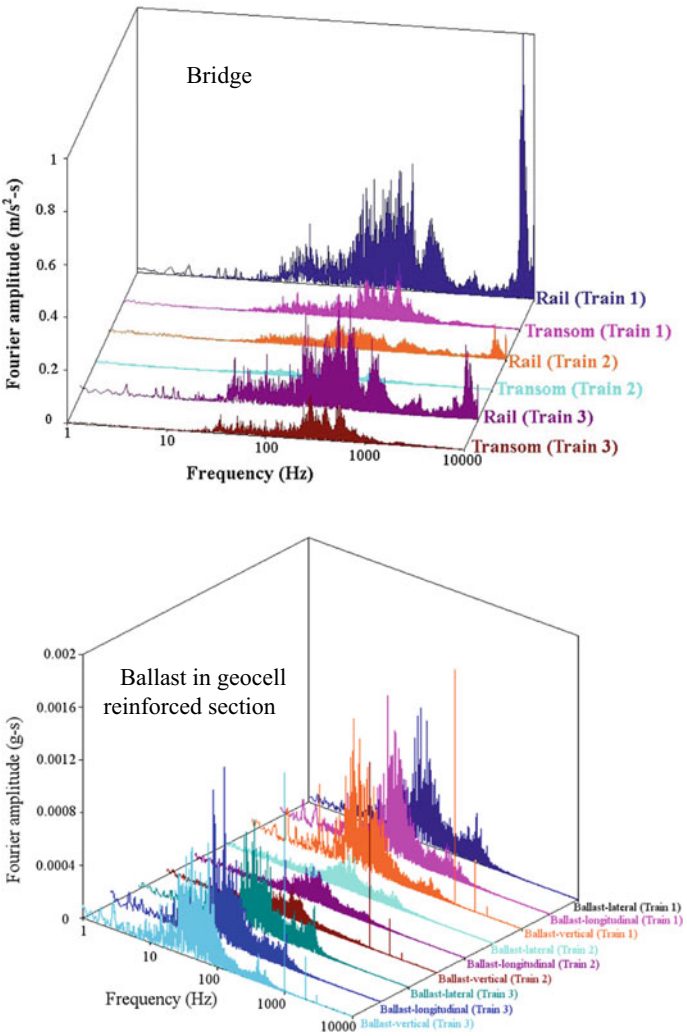

Fig. 11.12 Fourier amplitude spectrum for field accelerometer data recorded at the bridge and the ballast in geocell reinforced section. Adapted from Kaewunruen et al. (2016)

difference near the bridge end and consequently, abated the magnitude of the impact loads.

Moreover, Fig. 11.12 shows that the magnitude of vibration in the ballast is very small as compared to the sleepers. The higher rate of vibration attenuation with depth could be attributed to the use of vibration isolation fastening systems such as resilient baseplates.

Figure 11.13 shows the deviations in track geometry along the bridge after the construction of the transition zone. The data has been obtained from the axle-box

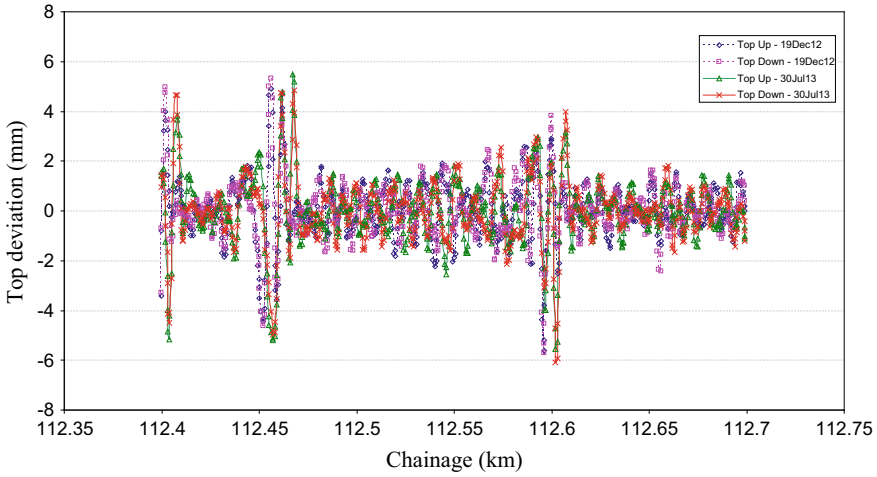

Fig. 11.13 Variation in track geometry data along the rail bridge after the construction of the transition zone. Adapted from Kaewunruen et al. (2016)

accelerometers installed in an inspection vehicle (Kaewunruen et al. 2016). The transition zone was constructed in late November 2012. The figure shows the track geometry measurements taken immediately after the construction, i.e., in December 2012 and after seven months of construction, i.e., in July 2013. The track was bi-directional, therefore, the data was taken in both up and down directions. The up and down directions correspond to the cases when the bridge end act as the exit end and the entrance end, respectively.

The figure shows that the deviation in the track is almost identical for both the measurements conducted in December 2012 and July 2013. This observation indicates that the rate of track geometry deterioration is very slow. This slow rate of deterioration is probably due to the mitigation of impact forces by the installation of the geocell layer in the transition zone.

11.8 Summary

This chapter examined the potential for the use of geocells in the railway tracks. The following concluding remarks may be drawn from the present chapter:

- The geocell confinement significantly improves the strength and stiffness of the granular infill materials in the track. The confinement reduces the track deformations in both lateral and vertical directions. Moreover, the geocell reinforced granular layer behaves as a rigid slab and distribute the train-induced loads uniformly over a wide area of the subgrade. Consequently, the settlement in the subgrade reduces and the track geometry is retained over an extended period.

- The performance of a geocell reinforced layer depends on the properties of the geocell, infill soil, subgrade, location of the layer within the track, and the loading conditions. A thorough analysis of these parameters is essential for the selection of a suitable type of geocell.
- The geocells increase the strength and resilience of the geomaterials under cyclic loading. However, the amount of improvement depends on the properties of geocell, infill soil, and the loading conditions such as frequency and magnitude of the vertical load.
- The geocell reinforcement decreases the magnitude and rate of plastic deformations in the track. This effect is beneficial for maintaining the track geometry over an extended period and reducing the frequency of maintenance cycles. However, the reduction in permanent deformation depends on several parameters such as the magnitude and frequency of load, and the properties of the geocell, infill, and subgrade.
- Several analytical models have been developed to evaluate the increase in confining pressure due to geocell reinforcement. These models can be used effectively to predict the improvement in the performance of a track layer when it is reinforced with the geocells.
- The geocells are provided in the transition zones near the railway bridges to increase the stiffness of the track gradually. This increase in track stiffness reduces the magnitude of the impact loads near the bridge ends and prevents the track geometry degradation.

Thus, the geocell reinforcement possesses enormous applications in the railway tracks. Recently, the industry guidelines such as ARTC RTS 3430 (Australian Rail Track Corporation 2006) have recommended the use of geocell immediately below the ballast layer for the stabilization of the subgrade with a CBR value of 1 or less. While Australia's coastal zone holds tremendous national significance, it also suffers from thick deposits of soft compressible clays. In view of this, ARTC recommendation is a testimony of interest among railway industries for the dissemination of geocell technology in Australasian track practice.

Acknowledgements The authors wish to thank Sydney Trains for their support. The second author acknowledges the Australian Government Research Training Program Scholarship for funding support. The last author wishes to thank the European Commission for H2020-MSCA-RISE, Project No. 691135 "RISEN 2018. Rail Infrastructure Systems Engineering Network", which enables a global research network that tackles the grand challenge in railway infrastructure resilience and advanced sensing (www.risen2rail.eu).

References

Al-Qadi I, Hughes J (2000) Field evaluation of geocell use in flexible pavements. Transp Res Rec 1709:26–35. https://doi.org/10.3141/1709-04

AREA (1978) Manual of recommended practice. American Railway Engineering Association, Washington D.C., USA
Asset Standards Authority (2018) T HR CI 12110 ST -Earthworks and formation. Transport for NSW, New South Wales
Atalar C, Das BM, Shin EC, Kim DH (2018) Settlement of geogrid-reinforced railroad bed due to cyclic load. In: Proceedings of the 15th international conference on soil mechanics and geotechnical engineering
Australian Rail Track Corporation (2006) RTS 3430—track reconditioning guidelines. Eng Practices Manual—Civ Eng, NSW
Bathurst RJ, Karpurapu R (1993) Large-scale triaxial compression testing of geocell-reinforced granular soils. Geotech Test J 16(3):296–303. https://doi.org/10.1520/GTJ10050J
British Railways Board (1993) GM/TT0088-permissible track forces for railway vehicles. Group Standards, Railway Technical Centre, Derby
British Railways Board (1995) Commentary on permissible track forces for railway vehicles. Technical Commentary, Safety and Standards Directorate, Railtrack Railway Technical Centre, London
Brown S, Lashine A, Hyde A (1975) Repeated load triaxial testing of a silty clay. Géotechnique 25(1):95–114. https://doi.org/10.1680/geot.1975.25.1.95
Budhu M (2015) Soil mechanics fundamentals. Wiley (2015)
Chrismer S (1997) Test of Geoweb to improve track stability over soft subgrade. Assoc American Railroads, Washington DC
Christopher BR, Schwartz C, Boudreau R (2006) Geotechnical aspects of pavements. Federal Highway Administration, Washington DC
Connolly DP, Kouroussis G, Laghrouche O, Ho CL, Forde MC (2015) Benchmarking railway vibrations—track, vehicle, ground and building effects. Constr Build Mater 92:64–81. https://doi.org/10.1016/j.conbuildmat.2014.07.042
Doyle NF (1980) Railway track design a review of current practice. Australian government publishing service, Canberra
Drumm E, Boateng-Poku Y, Johnson Pierce T (1990) Estimation of subgrade resilient modulus from standard tests. J Geotech Eng 116(5):774–789. https://doi.org/10.1061/(ASCE)0733-9410(1990)116:5(774)
Edil TB, Bosscher PJ (1994) Engineering properties of tire chips and soil mixtures. Geotech Test J 17(4):453–464. https://doi.org/10.1520/GTJ10306J
Eisenmann J (1972) Germans gain a better understanding of track structure. Railway Gaz Int 128(8)
Elliott RP, Thornton SI (1998) Resilient modulus and AASHTO pavement design. Transp Res Rec 1196
Esveld C (2001) Modern railway track. MRT-Productions, Delft, The Netherlands
European Commission for H2020-MSCA-RISE Project No. 691135 RISEN (2018) rail infrastructure systems engineering network. http://www.risen2rail.eu. Last accessed 14 Sep 2018
Fredlund D, Bergan A, Sauer E (1975) Deformation characterization of subgrade soils for highways and runways in northern environments. Can Geotech J 12(2):213–223. https://doi.org/10.1139/t75-026
Giroud J, Han J (2004) Design method for geogrid-reinforced unpaved roads. II. Calibration and applications. J Geotech Geoenviron Eng 130(8), 787–797. https://doi.org/10.1061/(asce)1090-0241(2004)130:8(787)
Henkel D, Gilbert G (1952) The effect measured of the rubber membrane on the triaxial compression strength of clay samples. Géotechnique 3(1):20–29. https://doi.org/10.1680/geot.1952.3.1.20
Indraratna B, Nimbalkar S (2013) Stress-strain degradation response of railway ballast stabilized with geosynthetics. J Geotech Geoenviron Eng 139(5):684–700. https://doi.org/10.1061/(ASCE)GT.1943-5606.0000758
Indraratna B, Salim W (2003) Deformation and degradation mechanics of recycled ballast stabilised with geosynthetics. Soils Found 43(4):35–46. https://doi.org/10.3208/sandf.43.4_35

Indraratna B, Nimbalkar S, Christie D, Rujikiatkamjorn C, Vinod J (2010) Field assessment of the performance of a ballasted rail track with and without geosynthetics. J Geotechn Geoenviron Eng 136(7):907–917. https://doi.org/10.1061/(ASCE)GT.1943-5606.0000312

Indraratna B, Salim W, Rujikiatkamjorn C (2011) Advanced rail geotechnology—ballasted track. CRC Press, Balkema

Indraratna B, Nimbalkar S, Neville T (2014) Performance assessment of reinforced ballasted rail track. Proc ICE: Ground Improv 167(1):24–34. https://doi.org/10.1680/grim.13.00018

Indraratna B, Biabani MM, Nimbalkar S (2015) Behavior of geocell-reinforced subballast subjected to cyclic loading in plane-strain condition. J Geotech Geoenviron Eng 141(1). https://doi.org/10.1061/(asce)gt.1943-5606.0001199

Indraratna B, Sun Y, Nimbalkar S (2016) Laboratory assessment of the role of particle size distribution on the deformation and degradation of ballast under cyclic loading. J Geotech Geoenviron Eng 142(7). https://doi.org/10.1061/(asce)gt.1943-5606.0001463

Indraratna B, Nimbalkar S, Ngo NT, Neville T (2016) Performance improvement of rail track substructure using artificial inclusions—experimental and numerical studies. Transp Geotech 8:69–85. https://doi.org/10.1016/j.trgeo.2016.04.001

Janaidhanam R, Desai CS (1983) Three-dimensional testing and modeling of ballast. J Geotech Eng 109(6):783–796. https://doi.org/10.1061/(ASCE)0733-9410(1983)109:6(783)

Kaewunruen S, Remennikov AM, Nguyen P, Aikawa A (2016) Field performance to mitigate impact vibration at railway bridge ends using soft baseplates. In: 11th world congress on railway research, Milan, Italy

Koerner RM (2012) Designing with geosynthetics, vol 1. Xlibris Corporation

Krylov VV (2001) Noise and vibration from high-speed trains. Thomas Telford

Lekarp F, Isacsson U, Dawson A (2000) State of the art. II: permanent strain response of unbound aggregates. J Transp Eng 126(1):76–83. https://doi.org/10.1061/(asce)0733-947x(2000)126:1(76)

Leshchinsky B, Ling HI (2013a) Numerical modeling of behavior of railway ballasted structure with geocell confinement. Geotext Geomembr 36:33–43. https://doi.org/10.1016/j.geotexmem.2012.10.006

Leshchinsky B, Ling H (2013b) Effects of geocell confinement on strength and deformation behavior of gravel. J Geotech Geoenviron Eng 139(2):340–352. https://doi.org/10.1061/(ASCE)GT.1943-5606.0000757

Li D, Selig ET (1994) Resilient modulus for fine-grained subgrade soils. J Geotech Eng 120(6):939–957. https://doi.org/10.1061/(ASCE)0733-9410(1994)120:6(939)

Li D, Selig ET (1996) Cumulative plastic deformation for fine-grained subgrade soils. J Geotechn Eng 122(12):1006–1013. https://doi.org/10.1061/(ASCE)0733-9410(1996)122:12(1006)

Li D, Selig ET (1998a) Method for railroad track foundation design. II: applications. J Geotech Geoenviron Eng 124(4):323–329. https://doi.org/10.1061/(asce)1090-0241(1998)124:4(323)

Li D, Selig ET (1998b) Method for railroad track foundation design. I: development. J Geotech Eng 124(4):316–322. https://doi.org/10.1061/(asce)1090-0241(1998)124:4(316)

Li L, Nimbalkar S, Zhong R (2018) Finite element model of ballasted rail-way with infinite boundaries considering effects of moving train loads and Rayleigh waves. Soil Dynam Earthq Eng 114(11):147–153. https://doi.org/10.1016/j.soildyn.2018.06.033

Liu Y, Deng A, Jaksa M (2018) Three-dimensional modeling of geocell-reinforced straight and curved ballast embankments. Comput Geotech 102:53–65. https://doi.org/10.1016/j.compgeo.2018.05.011

Mengelt M, Edil TB, Benson CH (2006) Resilient modulus and plastic deformation of soil confined in a geocell. Geosynthetics Int 13(5):195–205. https://doi.org/10.1680/gein.2006.13.5.195

Miura S, Takai H, Uchida M, Fukada Y (1998) The mechanism of railway tracks. Jap Railway Trans Rev 3:38–45

Moossazadeh J, Witczak MW (1981) Prediction of subgrade moduli for soil that exhibits nonlinear behavior. Transp Res Rec 810 (1981)

Ngamkhanong C, Kaewunruen S (2018) The effect of ground borne vibrations from high speed train on overhead line equipment (OHLE) structure considering soil-structure interaction. Sci Total Environ 627:934–941. https://doi.org/10.1016/j.scitotenv.2018.01.298

Nimbalkar S, Indraratna B (2016) Improved performance of ballasted rail track using geosynthetics and rubber shockmat. J Geotech Geoenviron Eng 142(8).https://doi.org/10.1061/(asce)gt.1943-5606.0001491

Nimbalkar S, Indraratna B, Dash SK, Christie D (2012) Improved performance of railway ballast under impact loads using shock mats. J Geotech Geoenviron Eng 138(3):281–294. https://doi.org/10.1061/(ASCE)GT.1943-5606.0000598

Nimbalkar S, Dash SK, Indraratna B (2018) Performance of ballasted track under impact loading and applications of recycled rubber inclusion. Geotech Eng J 49(4):79–91

ORE (1968) Stresses in the rails. Report No. D 71/RP8/E, Office for Research and Experiments, Utrecht

Pokharel SK, Han J, Leshchinsky D, Parsons RL, Halahmi I (2009) Behavior of geocell-reinforced granular bases under static and repeated loads. In: Proceeding contemporary topics in ground modification, problem soils, and geo-support, pp 409–416

Pokharel SK, Han J, Leshchinsky D, Parsons RL, Halahmi I (2010) Investigation of factors influencing behavior of single geocell-reinforced bases under static loading. Geotext Geomembr 28(6):570–578. https://doi.org/10.1016/j.geotexmem.2010.06.002

Pokharel SK, Han J, Manandhar C, Yang X, Leshchinsky D, Halahmi I, Parsons RL (2011) Accelerated pavement testing of geocell-reinforced unpaved roads over weak subgrade. Transp Res Rec 2204(1):67–75. https://doi.org/10.3141/2204-09

Pokharel SK, Han J, Leshchinsky D, Parsons RL (2018) Experimental evaluation of geocell-reinforced bases under repeated loading. Int J Pavement Res Technol 11(2):114–127. https://doi.org/10.1016/j.ijprt.2017.03.007

Powrie W (2014) On track: the future for rail infrastructure systems. Proc Inst Civil Eng Civil Eng 167(4):177–185. https://doi.org/10.1680/cien.14.00014

Prause RH, Meacham HC, Harrison HD, Johns TG, Glaeser WA (1974) Assessment of design tools and criteria for urban rail track structures. Report No. UMTA-MA-06-0025-74-3, Urban Mass Transportation Administration, Washington DC

Raymond GP (2001) Failure and reconstruction of a gantry crane ballasted track. Can Geotech J 38(3):507–529. https://doi.org/10.1139/t00-121

Raymond G, Gaskin P, Addo-Abedi F (1979) Repeated compressive loading of Leda clay. Can Geotech J 16(1):1–10. https://doi.org/10.1139/t79-001

Remennikov AM, Kaewunruen S (2008) A review of loading conditions for railway track structures due to train and track vertical interaction. Struct Control Health Monit 15(2):207–234. https://doi.org/10.1002/stc.227

Sadri M, Steenbergen M (2018) Effects of railway track design on the expected degradation: parametric study on energy dissipation. J Sound Vib 419:281–301. https://doi.org/10.1016/j.jsv.2018.01.029

Satyal SR, Leshchinsky B, Han J, Neupane M (2018) Use of cellular confinement for improved railway performance on soft subgrades. Geotext Geomembr 46(2):190–205. https://doi.org/10.1016/j.geotexmem.2017.11.006

Sayeed MA, Shahin MA (2016) Three-dimensional numerical modelling of ballasted railway track foundations for high-speed trains with special reference to critical speed. Transp Geotech 6:55–65. https://doi.org/10.1016/j.trgeo.2016.01.003

Selig ET, Waters JM (1994) Track geotechnology and substructure management. Thomas Telford, London

Shackel B (1973) The derivation of complex stress–strain relations. In: 15th international conference on soil mechanics and geotechnical engineering

Sun QD, Indraratna B, Nimbalkar S (2014) Effect of cyclic loading frequency on the permanent deformation and degradation of railway ballast. Géotechnique 64(9):746–751. https://doi.org/10.1680/geot.14.T.015

Sun Y, Chen C, Nimbalkar S (2017) Identification of ballast grading for heavy-haul rail track. J Rock Mech Geotech Eng 9(5):945–954. https://doi.org/10.1016/j.jrmge.2017.04.006

Tanyu BF, Aydilek AH, Lau AW, Edil TB, Benson CH (2013) Laboratory evaluation of geocell-reinforced gravel subbase over poor subgrades. Geosynthetics Int 20(2):47–61. https://doi.org/10.1680/gein.13.00001

Thakur JK, Han J, Pokharel SK, Parsons RL (2012) Performance of geocell-reinforced recycled asphalt pavement (RAP) bases over weak subgrade under cyclic plate loading. Geotext Geomembr 35:14–24. https://doi.org/10.1016/j.geotexmem.2012.06.004

Thompson MR, Robnett QL (1976) Resilient properties of subgrade soils. Report No. FHWA-IL-UI-160, Federal Highway Administration, Washington DC (1976)

Uzan J (1985) Characterization of granular material. Transp Res Rec 1022(1):52–59

Wang H, Markine V (2018) Corrective countermeasure for track transition zones in railways: adjustable fastener. Eng Struct 169:1–14. https://doi.org/10.1016/j.engstruct.2018.05.004

Yang X, Han J (2013) Analytical model for resilient modulus and permanent deformation of geosynthetic-reinforced unbound granular material. J Geotech Geoenviron Eng 139(9):1443–1453. https://doi.org/10.1061/(ASCE)GT.1943-5606.0000879

Zarembski AM, Palese J, Hartsough CM, Ling HI, Thompson H (2017) Application of geocell track substructure support system to correct surface degradation problems under high-speed passenger railroad operations. Trans Infrastruct Geotechnol 4(4):106–125. https://doi.org/10.1007/s40515-017-0042-x

Zhou H, Wen X (2008) Model studies on geogrid-or geocell-reinforced sand cushion on soft soil. Geotext Geomembr 26(3):231–238. https://doi.org/10.1016/j.geotexmem.2007.10.002

Chapter 12
Geocells Applications in Enhancing Trafficability in Desert Soils

Kaustav Chatterjee, Akshay Pratap Singh, and Anand Kumar

Abstract Infrastructure development, which is highly demanding in present scenario, depends on the soil characteristics, a considerable parameter before any type of construction. The challenges for transportation infrastructure in desert terrain are more than budgetary due to the peculiar characteristics of desert soils. The shear strength of sandy soil present in desert terrain is very small; hence, there is a need of ground improvement. Use of geocells is one of the most economical methods of soil improvement that is used to increase strength. The present study describes the influence of geocells on sandy soil based on direct shear tests and plate load test as well as field test results, using various load class vehicles including heavy load military vehicles as actual conditions in desert areas of Rajasthan. The study comes out with the fact that this technique increases the strength and stiffness property of sandy soil considerably and provides solution for preventing settlement and subsidence. It provides all-round confinement to the material and thus prevents the lateral spreading of soil when load is applied. As a result of which higher loading is induced on the failure plane leading to enhanced load-carrying capacity. Ease of construction, overall economy and less time consumption are major advantages of geocells. A cost comparison shows that use of geocell as reinforcement method is nearly 25% cheaper as compared to the conventional methods for track construction in deserts.

Keywords Geocell · Soil reinforcement · Confinement · Trafficability

K. Chatterjee (✉) · A. Pratap Singh · A. Kumar
Indian Institute of Technology Roorkee, Roorkee 247667, India
e-mail: kchatfce@iitr.ac.in

A. Pratap Singh
e-mail: apcl4.dce2017@iitr.ac.in

A. Kumar
e-mail: anand_engrs@rediffmail.com

T. G. Sitharam et al. (eds.), *Geocells*, Springer Transactions in Civil and Environmental Engineering,
https://doi.org/10.1007/978-981-15-6095-8_12

12.1 Introduction

It is essential for a civil engineer to enhance the soil properties incorporating different techniques. Soil reinforcement is one of the ground improvement techniques which can be used to improve the soil behaviour. Ease in the construction, overall economy, less time consuming, etc., are some of the advantages because of which soil reinforcement is popular all over the world. Geogrid, geocell, geocomposite and geotextiles are some of the geosynthetics which are generally used for ground improvement. The geocell is tree-dimensional (3D), polymeric, honey-comb resembling arrangements of cells interconnected at joints as shown in Fig. 12.1. Geocell was used by the US Army Corps of Engineers for stabilization of sand beach. Use of geocells as means of soil reinforcement due to its economy and simplicity of construction in shortest time is one of the most efficient means to enhance trafficability in desert soil.

Thar Desert in western part of India particularly consists of granular sand. These offer major problem to mobility of military vehicles like:-

1. The areas with granular sand offer low bearing capacity making mobility difficult.
2. High sinkage rate of tyres in granular soils.
3. Formation of deep ruts in granular sand due to large number of passes.
4. Granular sand offers minimum frictional resistance.
5. Higher water table in low lying areas with large silt content leads to large consolidation and settlement on movement of heavy vehicles.

Presently, the Indian Army uses Assault Track Ways (ATW) made up of aluminium frame as shown in Fig. 12.2. These are highly bulky and require large amount of resources in terms of manpower, equipment and time. They also require heavy daily maintenance. In view of this, there is a requirement to evolve a new methodology to enhance trafficability in desert terrain which is economical both in terms of time and resources.

The primary constraint to soil stability is low strength of most cohesionless soils. By providing geocell encasement, the problem can be effectively addressed. Geocells

Fig. 12.1 Honey-comb structure geocells

Fig. 12.2 Present methodology of military moblity in deserts

are three-dimensional (3D), honey-comb-shaped soil reinforcing geosynthetics structures which is made up of polymeric materials and are mostly used for confinement of coarse material. Geocell technique for stabilization of sand beaches was initially used by the US Army Corps of Engineers (Webster 1979). The research took into account the confinement of poorly, graded river sand and the characteristics and shape of geocell. The results from the initial experiments showed that the geocell-reinforced sand surface could provide greater soil stability than the compacted soil. The subsequent research from 1980 to 1990 has widened the scopes of this research and determined a large number of influence factors.

12.2 Review of Literature

12.2.1 Mechanics of Geocell Reinforcement

Geocell strengthening provides apparent cohesive strength even in cohesionless soils which depends on tensile modulus of the geosynthetic material used in geocell (Rajagopal et al. 1999). The reinforcing mechanism in geocell used provides an all-round confinement to materials due to its interconnected cells and prevents the lateral spreading of soil when load is functional.

As a result, a better combined material is formed and the geocell layer acts as a stiffer mattress that redistributes the footing load over a broader area (Dash et al. 2003a, b). Due to the application of load, pressure on soil increases and this leads to lateral defomation on the geocell membrane (Saride et al. 2009) which in turn activates stresses in the membrane and leads to an increase in the confinement pressure

which enhances the resistance against deformation and hence soil can with stand more loads. Once the geocells are filled with soil and compacted considerably, it produces a mattress that redistributes the load over a wider area.

12.2.2 Strength Parameters in Geocell-Reinforced Soil

Latha et al. (2009) studied the influence of various forms of reinforcement and created a theoretical model in order to determine the cohesive strength of geocell-encased composite by presuming angle of internal friction of geocell layer identical to angle of internal friction in the filled soil and all-round confinement by the membrane stresses to the soil in the wall of geocell.

Wang et al. (2008) evaluated the shear strength parameters of unreinforced and geocell-reinforced soils using large-scale direct shear tests. Direct shear tests were performed on three different samples viz. silty gravel soil, geocell-encased silty gravel soil and geocell-encased cement stabilizing silty gravel soils. The results from both large-scale direct shear test and that of triaxial tests were compared in order to estimate the influence of test methodology on the shear strength parameters. The results indicated that both unreinforced and geocell-encased soil gave similar nonlinear response in their shear strain behaviour. It was also observed that the geocell reinforcement resulted in an increase of cohesion of sand by nearly 242%, whereas in cement-stabilized soil, the increase in value of cohesion was around ten-folds. However, the friction angle was observed to remain almost unchanged.

12.2.3 Field Tests

Webster and Alford (1978) reported field testing of geocell-reinforced layers, fabricated out of plastic tube assembly and soil, on access and exit routes on softer subgrade. Webster and Watkins (1977) performed further trials with geocells fabricated from aluminium and it was found that the geocell-encased mechanism was an adequately appropriate method for construction of moist base. Edil et al. (2009) conducted further field trials with material made of industrial by-products as in fill material in the geocell. It was concluded that the geotextile acts like a partition for geocell in fill and subgrade whereas the geocell acts as a reinforcing layer.

Pokharel et al. (2009) and Han et al. (2008) investigated the behaviour of geocell-reinforced base layer under repeated and static loading. Pokharel et al. (2009) evaluated the bearing capacity and stiffness enhancement provided by reinforcement of geocell and also determined and compared the permanent deformation and percentage of elastic deformation and compared with the unreinforced soil surface. Han et al. (2008) modelled the test process with the help of numerical software FLAC3D in order to examine the mechanics of geocell and sand interactions. It was

established that geocell improved the bearing capacity as well as the modulus of sand. Further, circular-shaped geocells induced the maximum apparent cohesion.

12.2.4 Trafficability Model

Rush and Stinson (1961) performed trafficability trials with two-wheel-drive industrial tractor in a heavy clayey soil. The vehicle cone index (VCI) of tractor was estimated experimentally and a comparison was made with the calculated results. It was found that the efficacy of any vehicle can be related to soil strength in terms of rating cone index (RCI).

Freitag (1965) conducted series of remolding tests in order to calculate any loss of soil strength expected after trafficability. Remolding index (RI) was found out for various types of soils and was a ready reference for use in calculation of vehicle cone index (VCI). The fine-grained soil cone index when multiplied by the remolding index produced the rating cone index RCI used to indicate soil strength corrected for remolding. VCI indicated whether the vehicle can negotiate the given soil condition for a particular number of passes. From the above-given definitions, the simple correlation between RCI and VCI has been established: -

1. $VCI_1 \geq RCI$ implies that the soil cannot take even one pass of a given type of vehicle.
2. $VCI_{50} \leq RCI$ implies that given type of soil can take 50 passes of a given type of vehicle.

Based on the VCI, military vehicles can be classified into seven different categories as tabulated in Table 12.1.

12.2.5 Experimental Tests

Rea and Mitchell (1978) carried out a number of laboratory tests to evaluate the effect of sand-filled paper cells as reinforcement base layer in low cost highways construction. These interconnected and joint cells were made of 0.2 mm thick paper and expanded into rhomboidal shape with constant width of 51 mm. A range of parameters studied during the experimental tests were width of paper cell, height of paper cell, radius of loaded area, subgrade stiffness and repetitions of loading. The test results showed various modes of failure such as cell penetration, cell wall buckling, cell bursting, bearing capacity failure, extreme rutting and bending failure.

Sireesh and Kumar (2016) conducted a number of large-scale model load tests on both unreinforced and geocell-encased base layers lying over a relatively weaker sand subgrade. Reduction in settlement ratio was noticed with number of repetitive loading and geocell encasement can be used efficiently to enhance the quality and efficacy of the unsurfaced pavements in the rural areas by limiting the rutting.

Table 12.1 VCI for different categories of vehicles (Franks and McPeak 1994)

Categories	Range		Vehicle type
	VCI_1	VCI_{50}	
a	≤12	≤29	Light-weight vehicles with low contact pressures (<2.0 psi)
b	12–21	30–49	Engineer and high speed tractors with reasonably wide tracks and lower contact pressures
c	21–26	50–59	Tractors with average contact pressures, tracks with reasonably low contact pressures and few towed vehicles having lower contact pressures
d	26–30	60–69	Mainly, medium tanks, tractors with high contact pressures and all-wheel-drive trucks and towed vehicles with low contact pressures
e	31–35	70–79	Mainly, all-wheel-drive trucks, most of the trailed vehicles and heavier tanks
f	35–44	80–99	A large number of all-wheel-drive and rear-wheel-drive trucks and trailed vehicles anticipated mostly for move on highways
g	≥45	100 or greater	Rear-wheel-drive vehicles and vehicles which generally do not manoeuvre off roads, particularly in moist soils

12.3 Laboratory Experimental Programme

To appreciate the soil geocell composite system, it is imperative to realize and quantify the mechanical properties and behaviour of constituent material, i.e. soil and geocell. The purpose of the experimental tests performed during the study is to explicate the interaction mechanism of the soil geocell system and the mechanical behaviour of reinforced soil surface when it is subjected to loading. The experimental tests are aimed to evaluate the effect of various parameters on the reinforced soil mass and compare it with unreinforced soil mass.

12.3.1 Soil

The material used for the tests is desert soil obtained from Thar deserts of India. The particle size distribution of the soil particles was carried out by dry sieve analysis as per ASTM D6913/D6913M (2017). The sand used for the test is classified as poorly graded sand (SP) as per ASTM D2487 (2017). The specific gravity is determined as per ASTM D854 (2014). The maximum and minimum dry unit weight of this sandy soil was determined according to ASTM D4253 (2016) and ASTM D 4254 (2000). The properties of sand used in the present study are tabulated in Table 12.2.

Table 12.2 Properties of sand used in the present study

Properties	Values
Specific gravity (G)	2.61
Maximum void ratio (e_{max})	0.79
Minimum void ratio (e_{min})	0.57
Maximum dry unit weight (γ_{dmax})	16.21 kN/m^3
Minimum dry unit weight (γ_{dmin})	14.23 kN/m^3
Coefficient of uniformity (C_u)	4.0
Coefficient of curvature (C_c)	1.06

12.3.2 Geocell

The geocell used in the present study is non-woven geotextiles with high density polyethelene (HDPE) material having density of 0.94 gm/cm^3 and black in colour. The thickness and height of geocell used are 5 mm and 150 mm, respectively. In plate load test, the depth of geocell used is 10 cm and each cell having size of 18 cm $\times$ 12 cm. The tensile strength of geocell was calculated using creep testing machine (Fig. 12.3) and was found out to be 590 t/m^2 as shown in Fig. 12.4.

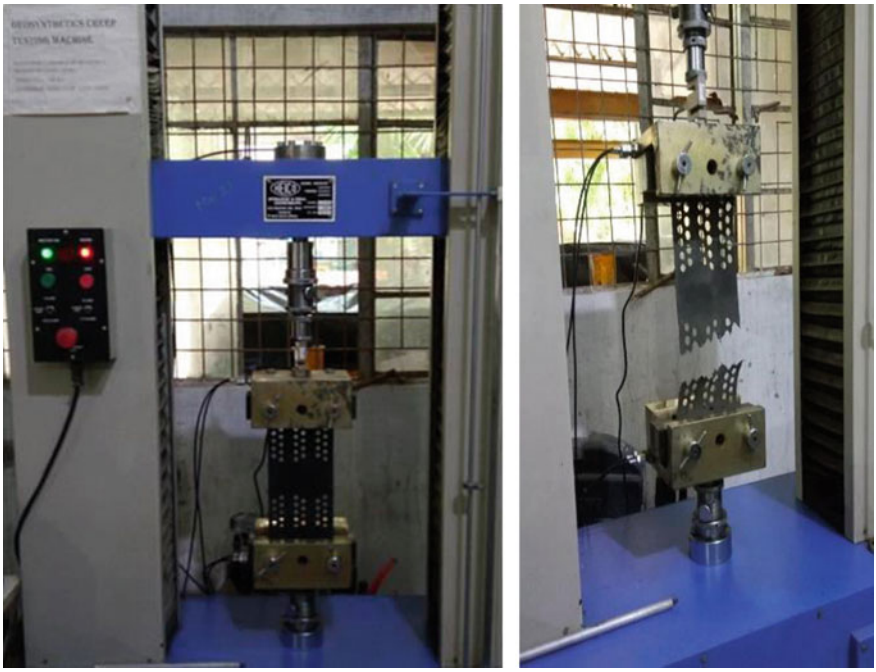

Fig. 12.3 Test set-up to determine tensile strength of geocell

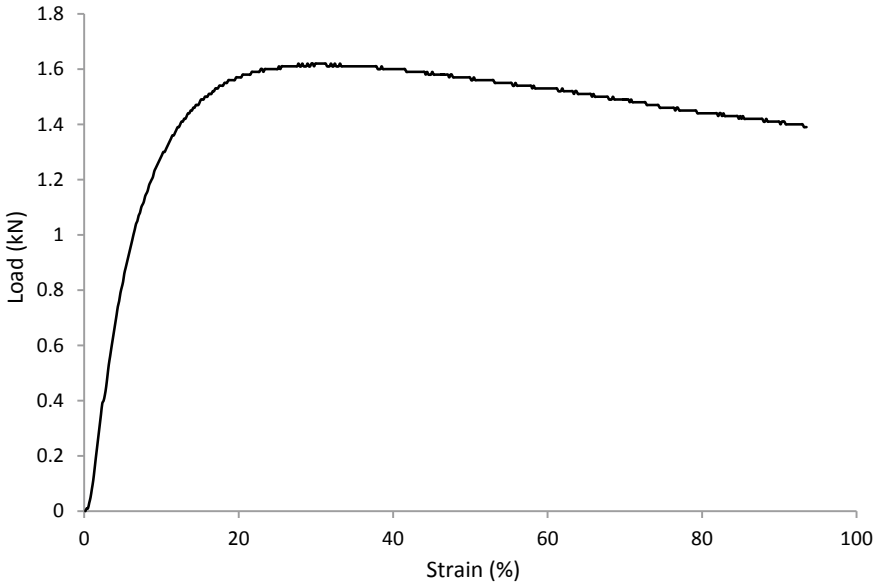

Fig. 12.4 Creep test carried out in present study

12.3.3 Plate Load Test

Plate load tests are performed to analyse the effect of geocell confinement on stiffness and load-carrying capacity of soil with a square wooden box of 53 cm × 53 cm and depth 40 cm. A plate square in dimension 10 cm × 10 cm is used for applying surcharge pressure. A total 16 plate load tests were conducted in the present study at 70% of maximum dry density of the sand. Pluviation technique (as shown in Fig. 12.5) is used to obtain the desired uniform density. However, in geocell-reinforced case, first a sand bed is levelled and then geocell was laid over it and again sand was poured. The loading plate was kept at the interlocking of gocell joints and also at the centre of geocell chambers to compare the results.

12.3.4 Large-Scale Direct Shear Test

The shear strength parameters of unreinforced and geocell-reinforced soil were determined by conducting large-scale direct shear test. For tests using geocells, the soil is enforced to slide along geocell over a uniform displacement rate, where as a uniform load is applied normal to the plane of relative movement. The test is conducted at different normal pressures. The large-scale test machine was setup in accordance to ASTM D5321/D5321M (2017) standard test methods with modifications. The apparatus consists of shear box having dimensions of 600 mm × 600 mm and height

Fig. 12.5 Pluviation technique carried out in present study

300 mm. Oven dried sand sample was used for all the tests. For geocell-reinforced soil, first 5 cm of lower box was filled thereafter geocells of cell size 8 cm × 6 cm and height 10 cm was laid and then it was filled with sand in layers after tamping. The test procedure similar to unreinforced case was followed. The full setup of large-scale direct shear test is shown in Fig. 12.6.

12.3.5 Results and Discussions

In this section, the results from laboratory tests conducted on geocell reinforced and unreinforced sand are presented and discussed. During every test, one particular parameter was varied, while the other parameters were kept uniform, to appreciate the effect of that parameter on the overall behaviour of the sand layer.

Plate Load Test Results. Plate load test was carried on both unreinforced and geocell encased sand bed. In the present study, the depth of reinforcement 'u' and location of loading plate is varied. Figure 12.7 shows the load–displacement curves obtained from the plate load tests. It is noticed that enforcement of geocell increased the

Fig. 12.6 Set-up for large-scale direct shear test used in present study

bearing capacity of the sand. The improvement factors for the geocell encased bases over the unreinforced bases in terms of stiffness and bearing capacity ranged from 1.35 to 2.0 and 1.4 to 2.6, respectively. Due to upliftment of geocell, the confined geocells failed while the unconfined geocells failed at the welds. The slopes of the load–displacement curves for both unreinforced and geocell-reinforced soil separated and moved apart once the displacement reached 2 mm. This is due to the fact that geocell reinforcement needs some displacement for it to take effect. Hoop stress from the geocell may be attributed for this behaviour which is proportional to the

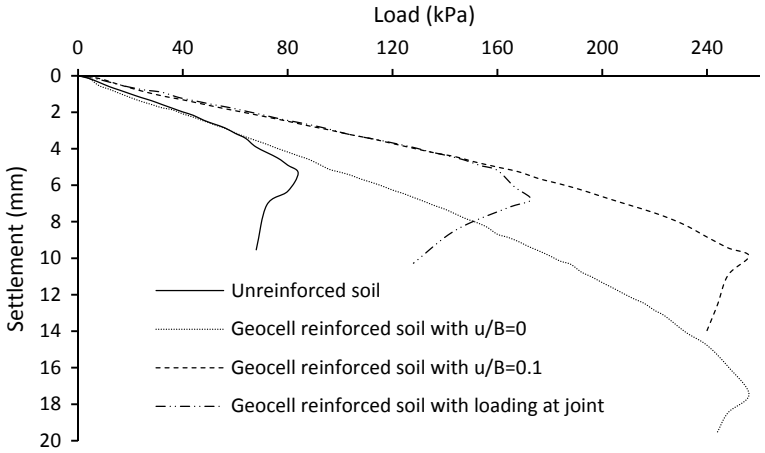

Fig. 12.7 Load versus settlement curve obtained from plate load test

tensile stress of geocell and thus due to the increase in tensile stress in the geocell, it provides significant confining stress to the sand.

It is also observed from Fig. 12.7 that $(u/B) = 0.1$ is the optimum depth of geocell reinforcement where B is the width of footing. These observations advocate that in order to obtain highest influence, the upper portion of the geocell mattress must be at a depth of 0.1 B from the base of the footing. The enhancement in ground improvement till $u/B = 0.1$ may be attributed to the surface soil layer, over the geocell encasement, which acts like cushion. It also avoids the direct contact of the geocell walls with the footing base. Hence, it distributes the footing pressure more uniformly over the geocell.

Direct Shear Test Results. Large-scale direct shear tests were carried out for unreinforced and geocell-reinforced soil. The variation of shear stress with horizontal displacement corresponding to normal stress 200 and 300 kPa is depicted in Fig. 12.8 for unreinforced sand as well as geocell-reinforced sand.

An increase in the maximum shear stress of geocell-reinforced soil is observed as compared to unreinforced soil as shown in Fig. 12.8, with the increase of shear stress being nearly 70 and 39% for normal stress of 200 kPa and 300 kPa, respectively. In case of unreinforced soil, the shear stress increases with increase in shear displacement. However, in case of geocell-reinforced soil, due to the better stiffness of the material, the curve shows visible strain softening and significant decline in post peak shear stresses. This is due to the additional friction on interface between the sand and geocell reinforcement and considerable degree of interlocking.

The shear strength parameters, cohesion and friction angle for unreinforced soil are 0.0 kPa and 37.4° while for geocell-reinforced soil are 76.8 kPa and 38.3°, respectively. The results indicate that the same soil with negligible cohesion if reinforced with geocell exhibited significant apparent cohesion while the friction angle increased slightly. This apparent cohesion may be due to the confinement provided

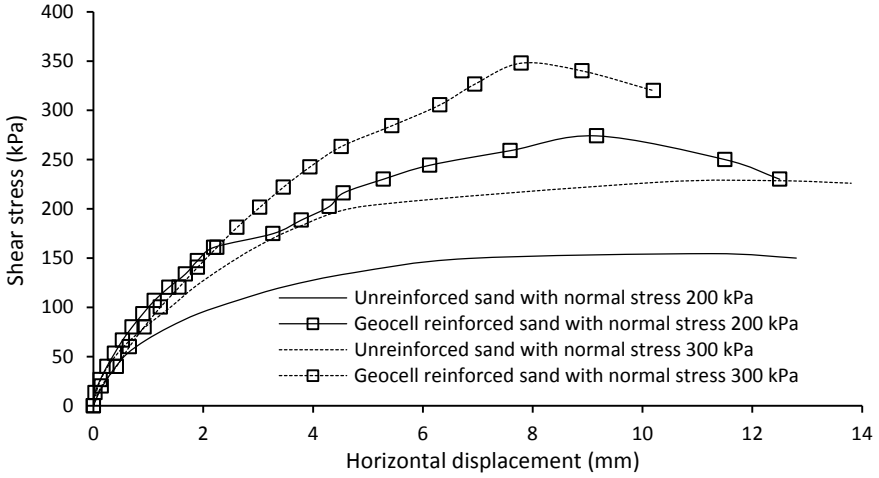

Fig. 12.8 Shear stress versus horizontal displacement of unreinforced and geocell-reinforced sand at different normal stresses

by geocell reinforcement (Bathurst and Rajagopal 1993). Thus, it can be attributed that geocell insertion in the soil imparts the cohesive strength.

12.4 Field Trials Incorporating Geocells

To understand the soil geocell composite system, a number of field trials using geocells on desert tracks were conducted at the test site location.

12.4.1 Test Sites

In order to get realistic data from field, four widely separated test sites located in different regions of Thar Desert in Rajasthan, in western part of India, were selected. Four border towns of Mahajan, Bhojusar, Devasar and Rajiysar were earmarked for carrying out the field tests. The digitised view of test areas along with details of latitude and longitude are shown in Fig. 12.9.

12.4.2 Soil Strength Measurement

There are two indices to measure the shearing resistance of tracks for traction and bearing capability of soil, i.e. rating cone index and vehicle cone index. Cone index

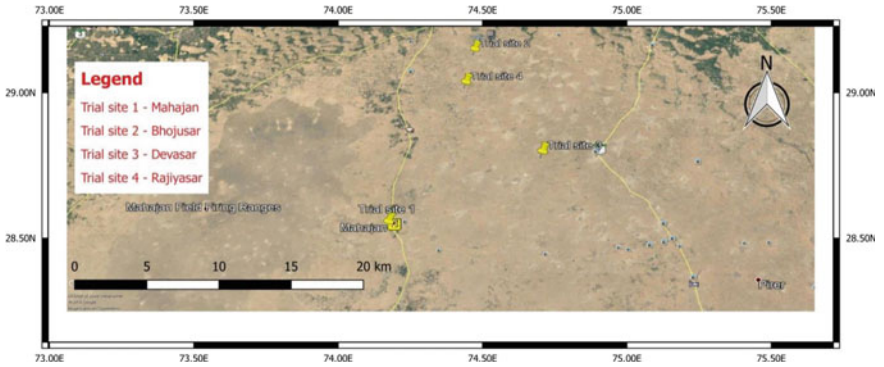

Fig. 12.9 Digitized image of trial sites

is used to estimate the shearing resistance with the help of cone penetrometer. The cone penetrometer is a field equipment which comprises of a 30-degree cone with a 0.5 sq.in. base area mounted on a 5/8 inch diameter shaft as illustrated in Fig. 12.10. The cone index of fine-grained soil when multiplied with rating index gives the rating cone index (RCI). In the present study, the value of RI is taken as 0.6 as suggested by Rush and Stinson (1961) for the various sandy soil sites. For predicting the surface to be a trafficable for a particular vehicle, RCI is compared with the vehicle cone index (VCI).

According to Freitag (1965), the values of VCI_1 and VCI_{50} for a 2.5 ton truck used for the trials are 30 and 69 and for a ALS truck are 35 and 80, respectively. The in situ results for trafficability of ALS truck are tabulated in Table 12.3. It is observed that soil is capable of taking a single pass for ALS truck while for 50 passess, soil improvement is necessary. A comparison of soil strength for number of passes for

Fig. 12.10 Cone penetrometer used in present study

Table 12.3 Determination of RCI and CBR for ALS truck at different test sites

Site	Vehicle pass 1 CI			Avg CI	RCI (CIx0.6)	VCI_1	Vehicle passes 50 CI			Avg CI	RCI CIx0.6)	VCI_{50}	CBR
Rajiyasar	95	90	85	90	54	35	75	80	70	75	45	80	1.4
Mahajan	120	115	125	120	72		95	100	105	100	60		1.5
Bhojusar	125	130	120	125	75		100	105	110	105	63		1.4
Devasar	140	135	145	140	84		105	110	120	112	67		1.6

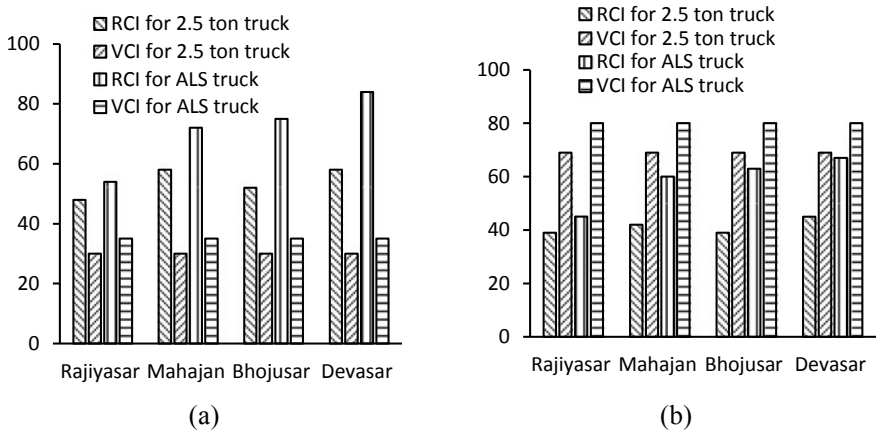

Fig. 12.11 Comparison between 2.5 ton truck and ALS truck for RCI and VCI corresponding to **a** 1 pass and **b** 50 passes

2.5 ton truck and ALS truck is shown in Fig. 12.11. It is seen that soil is capable enough to take one pass but for 50 passess, soil needs to be improved at the various test areas.

12.4.3 Rut Depth Measurement

Sinkage or rut depth, i.e. depression in road by the travel of wheels of vehicles plays a significant role in movement of vehicles in soft and sandy soil. A number of field tests were performed on different class of vehicles for sinkage over 50 passes. The variation in sinkage for various vehicles over 50 passes for unreinforced surface is given in Table 12.4. The rut depth corresponding to the number of passes in unreinforced soil for different vehicles is shown in Fig. 12.12.

Table 12.4 Variation of sinkage over 50 passes

Type of vehicle	Variation in sinkage over 50 passes (inches)	Weight (kg)
Gypsy	0.245–1.751	1470
2.5 ton truck	0.6083–4.81320	7650
ALS 9 ton truck	2.0810–7.1207	19,400

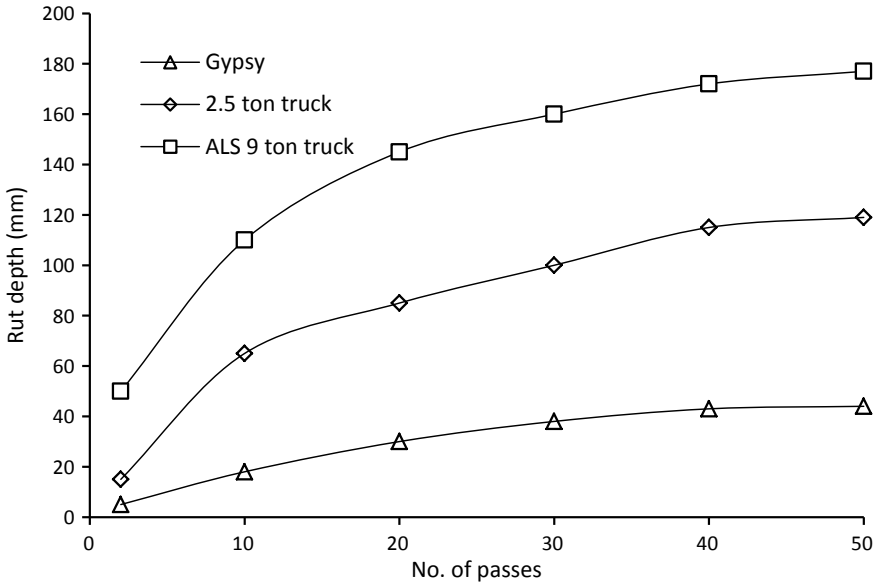

Fig. 12.12 Rut depth versus number of passes in unreinforced soil

12.4.4 Methodology Adopted for Field Tests

The geocell used for the field trials was of height 150 mm with plan dimensions of 2.8 m × 3 m taken as one pallet. For trial purpose, each pallet was unloaded and laid on preselected sites after unfolding them. These were stretched and laid over a stretch of 30 m at the trial site for the conduct of the trials as shown in Fig. 12.13. These pallets were extended by joining them at the edges.

The 3D honey-comb structure of geocell was filled with sand from the adjacent side of the track with the help of both manual as well as mechanical means as shown in Fig. 12.14.

The desired length was obtained by placing pallets next to each other. After filling the sand inside the geocell chamber, a cover of 10 cm of sand was put over the geocell surface as shown in Fig. 12.15. The geocell-reinforced track was ready for trials and three different types of vehicles, viz, Gypsy, 2.5 ton truck and ALS were made to pass 50–60 times. Figure 12.16 shows the movements of tank on geocell-reinforced track.

The geocells once laid were also recovered for future laying at different sites. The recovery was tried using both mechanical and manual means as shown in Figs. 12.17 and 12.18.

Fig. 12.13 Laying of geocell over 30 m stretch

Fig. 12.14 Mechanical and manual filling of geocells with sand

12.4.5 Results and Discussions

- **Laying time**. For a stretch of 100 m, the time taken to unload, lay and fill sand in the geocell was 25 min. It took an effort of one JCB and eight persons. When

Fig. 12.15 Finished track with sand cover

Fig. 12.16 Tank movements on geocell-reinforced track

this was compared with conventional method of track laying, it was found to be twice faster.

- **Requirement of vehicles for carriage**. For carrying 500 m of geocells, one ALS truck was required. However, for conventional track laying using ATW, one ALS truck was required per 100 m of track.
- **Manpower requirement**. Trial was conducted with the help of six persons which could attain an efficacy of 25 min for 100 m of geocell track.
- **Usage in marshy areas**. Trials were also conducted in marsh areas and were found to be equally effective.

Fig. 12.17 Recovery of geocell using mechanical means

Fig. 12.18 Recovery of geocells using manual means

- **Cost comparison**. Geocell was found to be much economical when compared to traditional method of track laying. A 25 m of geocell costs around Rs. 75,000 where as conventional ATW costs around Rs. 250,000.
- **Recovery of geocells**. During the trials, it was found that recovery of geocells once laid was difficult. During recovery, almost 30% of geocell got damaged.

Table 12.5 Comparison between geocell and ATW

Description	ATW	Geocell
Vehicle load	1 ALS per 100 m	1 ALS per 500 m
Weight	2800 kg per 100 m (350 kg per roll)	900 kg per 100 m[a]
Laying speed per sec	40 min per 100 m	25 min per 100 m[b]
Cost per 25 m	2.51 lakhs (per roll)	0.74 lakh
Maintenance	Regular	Minimal[c]
Recovery	100%	70% in boggy patches 80% in deserts[d]

[a]No fixed size
[b]3 × JCB required
[c]Only subsequent filling of soil required
[d]30–40% wastage after every use

A complete comparison of geocell versus ATW as track material is shown in Table 12.5.

- **Sinkage/Rut depth**. Based on the field observation, a plot of settlement over number of passes for all the three vehicles considered in the present study is shown in Fig. 12.19.

It is seen that there is a 3 times decrement observed in settlement on track with geocell reinforcement than unreinforced track as the geocell filled with sand and compacted formed a composite mattress which redistributes the surcharge over a wider area and increased the bearing capacity of soil substantially.

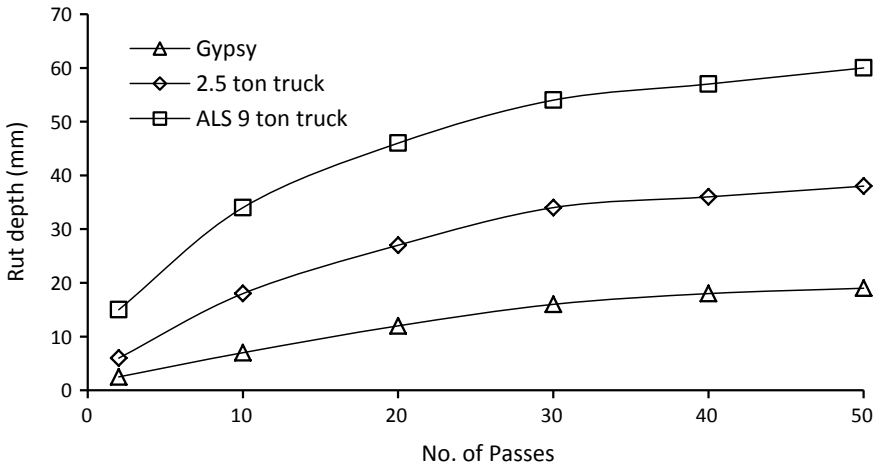

Fig. 12.19 Rut depth versus number of passes in geocell-reinforced soil

12.5 Conclusions

In the present study, various experiments and field trials were undertaken to investigate the influence of geocell in desert soil as a suitable ground improvement technique. The experiments included large-scale direct shear test to determine the shear strength parameter and plate load tests to analyse the characteristics of soil when subjected to vertical loading on both unreinforced and geocell-reinforced soil. The properties of soil and geocells have been tested in the geotechnical laboratory. Stiffness and bearing capacity of geocell-encased soil improved and the optimum depth of geocell reinforcement are about $u/B = 0.1$. Shear stress also increases with geocell-encased soil due to better stiffness of material and presence of geocell exhibits the apparent cohesion in the soil while keeping friction angle constant. Apart from these, extensive field trials were conducted in Thar deserts of Rajasthan. The rut depth reduced about 3 times when compared with unreinforced sand surface. The geocell-encased soil showed improvement in terms of laying time, requirement of vehicles for hauling material, cost and maintenance when compared with conventional method of track laying.

Acknowledgements The authors are thankful to 122 Engineer Regiment of Indian Army for providing their valuable support and resources during the conduct of field trials in Thar deserts of India for this research work.

References

ASTM D4254 (2000) Standard test methods for minimum index density and unit weight of soils and calculation of relative density. ASTM International, West Conshohocken, PA, USA

ASTM D854 (2014) Standard test methods for specific gravity of soil solids by water pycnometer. ASTM International, West Conshohocken, PA, USA

ASTM D4253 (2016) Standard test methods for maximum index density and unit weight of soils using a vibratory table. ASTM International, West Conshohocken, PA, USA

ASTM D2487 (2017) Standard practice for classification of soils for engineering purposes (unified soil classification system). ASTM International, West Conshohocken, PA, USA

Bathurst RJ, Rajagopal K (1993) Large scale triaxial compression testing of geocell reinforced granular soils. Geotech Test J 16(3):296–303

ASTM D5321/D5321M (2017) Standard test method for determining the shear strength of soil-geosynthetic and geosynthetic-geosynthetic interfaces by direct shear. ASTM International, West Conshohocken, PA, USA

ASTM D6913/D6913M (2017) Standard test methods for particle-size distribution (gradation) of soils using sieve analysis. ASTM International, West Conshohocken, PA, USA

Dash SK, Sireesh S, Sitharam TG (2003a) Behavior of geocell reinforced sand beds under circular footing. Proc Inst Civil Eng—Ground Improve 7(3):111–115

Dash SK, Sireesh S, Sitharam TG (2003b) Model studies on circular footing supported on geocell reinforced sand underlain by soft clay. Geotext Geomembr 21:197–219

Edil TB, Fratta D, Shuettpelz CC (2009) Development of testing methods to determine interaction of geogrid reinforced granular material for mechanistic pavement analysis, Wisconsin DOT and FHWA Project Report

Franks FM, McPeak MA (1994) Planning and design of roads, airfields and heliports in the theater of operations—road design. Department of the Army, Washington, DC, Field Manual No. 5-430-00-1

Freitag DR (1965) Wheels on soft soils: an analysis of existing data. United States Army Engineer Waterways Experiment Station, Corps of Engineers, Vicksburg, Mississippi, Technical Report No. 3-670, 1–168

Han J, Yang X, Leshchinsky D, Parsons RL (2008) Behavior of geocell reinforced sand under a vertical load. J Transp Res Board 2045:95–101

Latha GM, Dash SK, Rajagopal K (2009) Numerical simulation of the behavior of geocell reinforced sand in foundations. Int J Geomech ASCE 27(6):409–422

Pokharel SK, Han J, Leshchinsky D, Parsons RL, Halahmi I (2009) Behavior of geocellreinforced granular bases under static and repeated loads. International Foundation Congress and Equipment Expo, Orlando, Florida, United States

Rajagopal K, Krishnaswamy NR, Latha GM (1999) Behaviour of sand confined with single and multiple geocells. Geotext Geomembr 17:171–184

Rea C, Mitchell JK (1978) Sand reinforcement using paper grid cells. Reprint 3130, ASCE spring convention and exhibit, Pittsbutgh, PA, 24–28

Rush ES, Stinson BG (1961) Trafficability tests with a two-wheel-drive industrial tractor. United States Army Engineer Waterways Experiment Station, Corps of Engineers, Vicksburg, Mississippi, Miscellaneous Paper No. 4-917

Saride S, Gowrisetti S, Sithara TG, Puppala AJ (2009) Numerical simulation of geocell reinforced sand and clay. Proc Inst of Civil Eng—Ground Improv 162(4):185–198

Sireesh S, Kumar V (2016) Rutting behavior of geocell reinforced base layer overlying weak sand subgrades. In: 3rd International conference on transportation geotechnics (ICTG 2016), Portugal

Wang YM, Chen YK, Liu W (2008) Large scale direct shear testing of geocell reinforced soil. J Central South Univ Technol 15(6):895–900

Webster SL (1979) Investigation of beach sand trafficability enhancement using sand-grid confinement and membrane reinforcement concepts. United States Army Engineer Waterways Experiment Station, Corps of Engineers, Vicksburg, Mississippi, Technical Report No. 2, 1–109

Webster SL, Alford SJ (1978) Investigation of construction concepts for pavements across soft ground. United States Army Engineer Waterways Experiment Station, Corps of Engineers, Vicksburg, Mississippi, Technical Report No. S-78-6, 7–68

Webster SL, Watkins JE (1977) Investigation of construction techniques for tactical bridge approach roads across soft ground. United States Army Engineer Waterways Experiment Station, Corps of Engineers, Vicksburg, Mississippi, Technical Report No. S-77-1, 1–84

Chapter 13
Protection of Buried Pipelines and Underground Utilities Using Geocells

Amarnath M. Hegde and Prof. T. G. Sitharam

Abstract This chapter presents the results of the laboratory model tests and the numerical studies conducted on small diameter PVC pipes, buried in geocell reinforced sand beds. The aim of the study was to evaluate the suitability of the geocell reinforcement in protecting the underground utilities and buried pipelines. In addition to geocells, the efficacy of only geogrid and geocell with additional basal geogrid cases was also studied. A PVC (Poly Vinyl Chloride) pipe with external diameter 75 mm and thickness 1.4 mm was used in the experiments. The vehicle tire contact pressure was simulated by applying the pressure on the top of the bed with the help of a steel plate. Results suggest that the use of geocells with additional basal geogrid considerably reduces the deformation of the pipe as compared to other types of reinforcements. Further, the depth of placement of pipe was also varied between 1*B* and 2*B* (*B* is the width of loading plate) below the plate in the presence of geocell with additional basal geogrid. More than 50% reduction in the pressure and more than 40% reduction in the strain values were observed in the presence of reinforcements at different depths as compared to the unreinforced beds. Conversely, the performance of the subgrade soil was also found to be marginally influenced by the position of the pipe, even in the presence of the relatively stiff reinforcement system. Further, experimental results were validated with three-dimensional numerical studies using FLAC3D (Fast Lagrangian Analysis of Continua in 3D). A good agreement in the measured pipe stain values was observed between the experimental and numerical studies. Numerical studies revealed that the geocells distribute the stresses in the lateral direction and thus reduce the pressure on the pipe. In addition, the results of the 1-g model tests were scaled up to the prototype case of the shallow buried pipeline below the pavement using the appropriate scaling laws.

A. M. Hegde (✉)
Department of Civil and Environmental Engineering, Indian Institute of Technology Patna, Patna 801106, India
e-mail: ahegde@iitp.ac.in

Prof. T. G. Sitharam
Department of Civil Engineering, Indian Institute of Technology Guwahati (IITG), Surjyamukhi Road, North, Amingaon, Guwahati, Assam 781039, India

T. G. Sitharam et al. (eds.), *Geocells*, Springer Transactions in Civil and Environmental Engineering,
https://doi.org/10.1007/978-981-15-6095-8_13

Keywords Geosynthetics · Buried pipeline · Geocell · Geogrid · Pavement · Bearing pressure

List of notations

b	Width of the geocell mattress (m)
B	Width of the steel plate (m)
C	Cohesion (kPa)
C_c	Coefficient of curvature (dimensionless)
c_i	Interface cohesion (kPa)
C_u	Coefficient of uniformity (dimensionless)
d	Pocket size of geocell (m)
D	Diameter of the pipe (m)
D_{10}	Effective particle size (mm)
e_{max}	Maximum void ratio of sand (dimensionless)
e_{min}	Minimum void ratio sand (dimensionless)
G	Shear modulus of sand (MPa)
γ	Unit weight of sand (kN/m^3)
h	Height of the geocell mattress (m)
H	Depth of placement of pipe (m)
k_i	Interface shear modulus (MPa/m)
K_g	Stiffness of the geocell (kN/m)
K_p	Stiffness of the pipe (kN/m)
L	Length in general (m)
M	Mass in general (kg)
N	Scale factor (dimensionless)
T	Time in general (s)
F	Force in general (N)
P_u	Measured stresses on top of the pipe (kPa)
q_u	Applied pressure at the top of the bed (kPa)
q_r	Ultimate bearing capacity of the reinforced bed (kPa)
q_s	Ultimate bearing capacity of the unreinforced bed (kPa)
S	Settlement of the loading plate (mm)
u	Depth of placement of the geocell (m)
φ	Friction angle of the sand (°)
φ_i	Interface friction angle between geocell and sand (°)

13.1 Introduction

Underground conduits or utility pipelines form a complex network in the urban areas and are often laid below the pavements and the temporary structures. Often, these conduits or pipelines are buried at shallow depths in trenches with the help of flowable fills. These pipes tend to deform and damage due to the application of repeated traffic loads or heavy static loads from the vehicles. The damage leads to the discomfort of the consumers of the utility and also to the travelers on the road. In this research, it is proposed to design a shallow reinforcement system using geocells to bridge these utility lines. Many researchers in the past have studied the design and installation aspects of the buried pipes through small-and large-scale tests (Brachman et al. 2000; Mir Mohammad Hosseini and Moghaddas Tafreshi 2002; Arockiasamy et al. 2006; Srivastava et al. 2012).

Nowadays, reinforcing the soil in the form of geosynthetic reinforcement is gaining popularity in geotechnical engineering. These reinforcements increase the overall performance of the foundation bed by increasing the load-carrying capacity and reducing the settlement. Many researchers have studied the beneficial effect of the geosynthetic reinforcements in various geotechnical applications (Indraratna et al. 2010; Rowe and Taechakumthorn 2011; Demir et al. 2013; Bia et al. 2013; Almeida et al. 2014). However, the use of geosynthetic reinforcement to protect buried pipes and underground utilities is relatively a new concept. Moghaddas Tafreshi and Khalaj (2008) conducted laboratory studies on small diameter HDPE pipes buried in the geogrid reinforced sand subjected to repeated load. Researchers observed the significant reduction in the deformation of the pipe in the presence of geogrids. Palmeira and Andrade (2010) used the combination of geotextile and geogrid to protect the buried pipelines in their model studies. Researchers observed that the reinforcement offers significant resistance to sharp, penetrating object and helps to protect the buried pipes from the accidental damages.

In recent times, geocells are showing its efficacy in geotechnical engineering applications. Geocells are three-dimensional expandable panels made up of ultrasonically welded high strength polymers or the polymeric alloy such as Polyethylene, Polyolefin, etc. The interconnected cells in the geocell form a slab that behaves like a large pad that spreads the applied load over a wider area. Many researchers in the past have highlighted the advantages of using the geocells in geotechnical engineering applications (Moghaddas Tafreshi and Dawson 2010; Pokharel et al. 2010; Lambert et al. 2011; Yang et al. 2012; Thakur et al. 2012; Sitharam and Hegde 2013; Mehdipour et al. 2013; Hegde and Sitharam 2015a,b; Moghaddas Tafreshi et al. 2014; Hegde et al. 2014; Indraratna et al. 2014). Tavakoli et al. (2013) highlighted the beneficial use of geocells in protecting the buried pipelines in their studies. Researchers emphasized the importance of selection of suitable compaction technique to compact the backfill soil above and below the geocells. Tavakoli et al. (Tavakoli Mehrjardi et al. 2012) used the combination of geocell reinforcement and rubber soil mixture to protect buried pipes. It was observed that the combination of geocell reinforcement and 5% rubber mixed soil (irrespective of the size or type of the rubber) provides the

Table 13.1 Geosynthetics for protection of buried pipelines

Researchers	Type of soil	Pipe material	Pipe geometry	Reinforcement used
Moghaddas Tafreshi and Khalaj (2008)	Sand	HDPE	110 mm dia and 4 mm thick	geogrid
Palmeira and Andrade (2010)	Sand	Steel	75 mm dia and 1.5 mm thick	Combination of geotextile and geogrid
Tavakoli Mehrjardi et al. (2012)	Sand	PVC	160 mm dia and 4 mm thick	Geocell with rubber soil mixture
Tavakoli Mehrjardi et al. (2013)	Sand	PVC	160 mm dia and 4 mm thick	Geotextiles and geocells in separately
Hegde and Sitharam (2015c)	Sand	PVC	75 mm dia and 1.4 mm thick	Geogrid, geocell, and combination of both
Hegde et al. (2016)	Clay	PVC	75 mm dia and 1.4 mm thick	Combination of geocell and geogrid

best performance in terms of reduction in the pipe deformation and backfill settlement. The summary of the research in the subject area is presented in Table 13.1. In this chapter, the research works of Hegde and Sitharam (2015c) and Hegde et al. (2016) have been summarized. Contrary to the previous studies, the combination of geocell and geogrid was used in this study to protect the underground utilities and buried pipelines. The first part of the chapter deals with the 1-g model plate load tests while the second part of the manuscript demonstrates the three-dimensional numerical modeling of the problem.

13.2 Laboratory Tests

13.2.1 Experimental Setup

The experiments were conducted in the test tank of size 900 mm in length, 900 mm in width and 600 mm in height, made up of cast iron. The tank was fitted to the loading frame which was connected to manually operated hydraulic jack. The vehicle tire contact pressure was simulated by applying the pressure on the top of the bed with the help of a steel plate. A square-shaped steel plate with 20 mm thickness and 150 mm sides was used for the purpose. The load was applied through a hand-operated hydraulic jack. A pre-calibrated proving ring was used to measure the imposed load. To avoid the eccentric application of the load, the ball bearing arrangement was used. Two dial gauges (D_1 and D_2) were placed on either side of the centerline of the steel plate to record the settlement of the plate. Another set of dial gauges (S_1 and S_2) was placed at the distance of 1.5B (B is the width of the steel plate) from the centerline

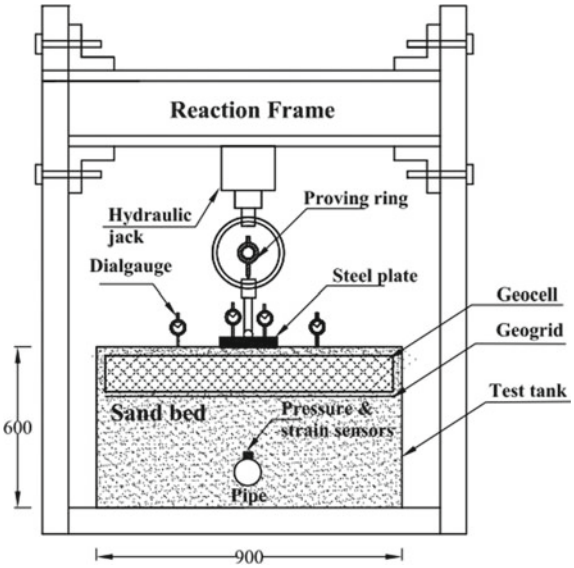

Fig. 13.1 Schematic view of the test setup. Sourced from Hegde and Sitharam (2015c)

of the plate to measure the deformation underwent by the fill surface. Schematic representation of test setup is shown in Fig. 13.1.

13.2.2 Materials Used

Sand used in the investigation was dry sand with specific gravity 2.64, effective particle size (D_{10}) 0.26 mm, coefficient of uniformity (C_u) 3.08, coefficient of curvature (C_c) 1.05, maximum void ratio (e_{max}) 0.81 and minimum void ratio (e_{min}) of 0.51. According Unified Soil Classification System (USCS) the sand was classified as poorly graded sand with symbol SP. Figure 13.2 represents the grain size distribution of sand. The geocell used in the study was made of Neoloy. Biaxial geogrid made up of Polypropylene with aperture size 35 mm × 35 mm was used. The properties of the geocell and the geogrid are summarized in Table 13.2. Pipe used in the study was made up of PVC (Polyvinyl Chloride) with external diameter 75 mm and thickness 1.4 mm. The tensile test was conducted on the pipe sample as per the guidelines of ASTM-D638 (ASTM 2010). From the tensile stress–strain response, the secant modulus of the pipe material corresponding to 2% axial strain was determined as 3.1 GPa. The ultimate tensile strength of the pipe was 42 kN/m. The tensile strength of the geocell strip and the geogrid were determined as per the guidelines of ASTM D-4885 (ASTM 2011) and ASTM D-6637 (ASTM 2011), respectively. Tensile load–strain behavior of geocell, geogrid, and pipe material are shown in Fig. 13.3.

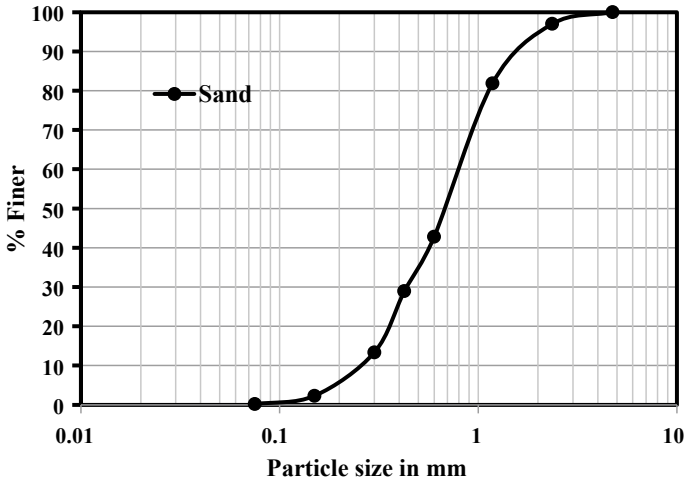

Fig. 13.2 Grain size distribution curve of sand. Sourced from Hegde and Sitharam (2015c)

Table 13.2 Properties of the geocell and geogrid. Courtesy Hegde and Sitharam (2015c)

Parameters	Quantity
Geocell	
Material	Neoloy
Cell size (mm)	250 × 210
No. of cells/m^2	40
Cell depth (mm)	150
Strip thickness (mm)	1.53
Cell seam strength (N)	2150(± 5%)
Density (g/cm^3)	0.95 (± 1.5%)
Short term yield strength (kN/m)	20
Geogrid	
Polymer	Polypropylene
Aperture size (mm)	35 × 35
Ultimate tensile strength (kN/m)	20
Mass per unit area (g/m^2)	220
Shape of aperture opening	Square

MD Machine direction; *XMD* Cross machine direction

13.2.3 Preparation of the Test Bed

First, the sides of the tank were coated with Polythene sheets to avoid the side friction. Pluviation technique was used to prepare the sand bed of 600 mm thick. Before the

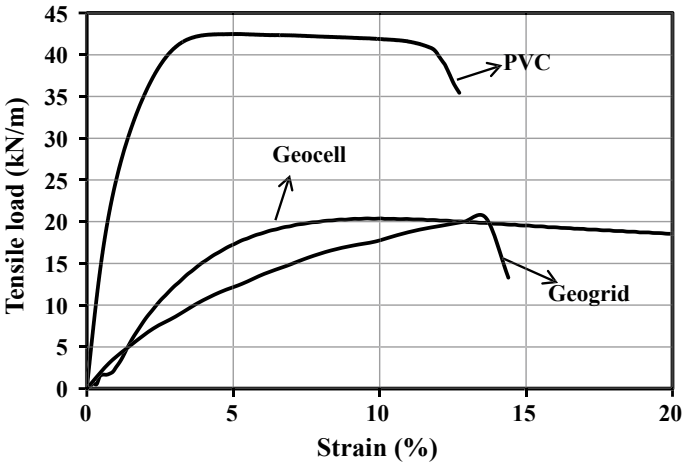

Fig. 13.3 Tensile load–strain behavior for different materials Sourced from Hegde and Sitharam (2015c)

start of the actual test, a series of trials were conducted to determine the height of fall required to achieve the desired relative density. In each trail, small aluminum cups with known volume were placed at the different locations of the tank. A calibration chart was prepared by knowing the maximum and minimum void ratios of the sand. All the tests were conducted at the constant relative density of 65%. The height of fall required to achieve 65% relative density was directly obtained from the chart. The pipe and the reinforcements were placed at the predetermined depth during the preparation of the sand bed. Geocell pockets were filled up with the sand using the pluviation technique. Figure 13.4a, b represents photographs showing the different stages of the bed preparation. After achieving the desired height of the bed, the fill was leveled using a trowel without disturbing the density of the bed.

13.2.4 Instrumentation

Strain gauges were mounted on the top surface of the pipe with a half-bridge circuit arrangement. Commercial adhesive was used to fix the strain gauges. At each gauge location, the pipe surface was rubbed with a sandpaper, before it wiped clean. Strain gauges had normal resistance of 120 Ω and maximum measuring capacity up to 1.5% strain (15,000 micro strains). Just above the strain gauges, exactly at the same locations, three earth pressure cells were placed in the sand bed to measure the vertical stress. Diameter and thickness of the pressure cells were 25 mm and 10 mm, respectively. These cells could measure the pressure in the range of 0–10 kg/cm^2 with a least count of 0.1 kg/cm^2. The strain gauges and pressure cells were connected to two separate display units through lead wires.

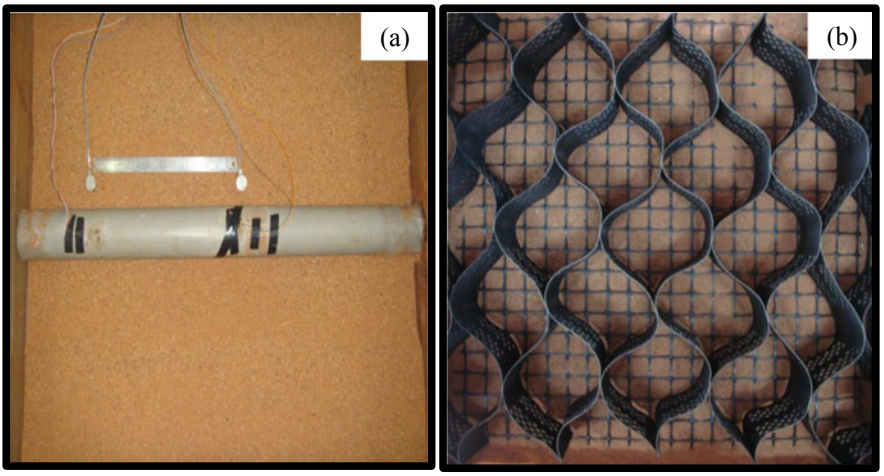

Fig. 13.4 **a** and **b** Photograph of the test: **a** placement of pipe; **b** expanded geocell Sourced from Hegde and Sitharam (2015c)

13.2.5 Testing Program

Three series of plate load tests were conducted. In the first series (A), the tests were conducted with three different types of reinforcements with fixed depth of placement of pipe, i.e., 1.5*B* below the steel plate. In the second series, the depth of the pipe was varied between 1*B* and 2*B* below the plate in the unreinforced condition. In the third series (C), the depth of the pipe was varied between 1*B* and 2*B* below the steel plate in the presence of geocell with additional basal geogrid. The details of the testing program are summarized in Table 13.3. The geocell mattress used was square in shape. The diameter of the pipe, size of plate, relative density of the sand bed, and the geocell geometry, i.e., height, width, and pocket size were kept constant in all the tests. The steel plate was placed on the surface of the sand bed. In reinforced

Table 13.3 Test details. Courtesy Hegde and Sitharam (2015c)

Test series	Details	
A	Variable parameters	Type of reinforcement: Unreinforced, only geogrid, only geocell, geocell with basal geogrid
	Constant parameters	$H/B = 1.5$, $b/B = 5.8$, $D/B = 0.5$, $ID = 65\%$
B	Variable parameters	Unreinforced condition $H/B = 1, 1.25, 1.5, 1.75, 2$
	Constant parameters	$D/B = 0.5$, $ID = 65\%$
C	Variable parameters	Geocell with basal geogrid reinforced $H/B = 1, 1.25, 1.5, 1.75, 2$
	Constant parameters	$D/B = 0.5$, $ID = 65\%$, $b/B = 5.8$, $h/B = 1$

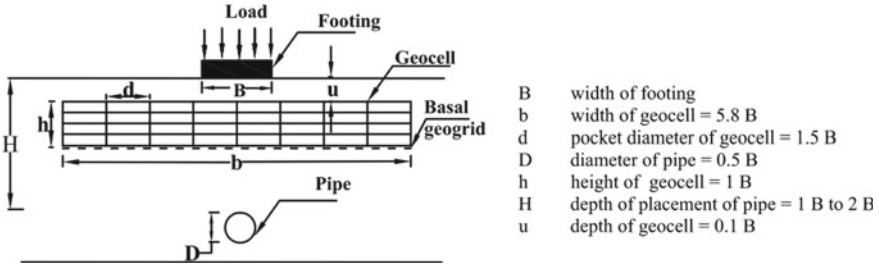

Fig. 13.5 Geometry of the test configuration. Sourced from Hegde and Sitharam (2015c)

tests, the geocell and geogrid reinforcements were placed to the full width of the tank leaving the small gap between the tank wall and the reinforcement to avert the boundary effects. In other words, the width of the reinforcement was about 5.8 times the width of the steel plate in all the tests. Dash et al. (Dash et al. 2001) reported the optimum depth of geocell placement as $0.1B$ from the bottom of the footing. Hence, in the present investigation, the geocell was placed at the depth of $0.1B$ below the steel plate. Figure 13.5 represents the geometry of the test configuration.

13.3 Results and Discussions

13.3.1 Effect of Reinforcement Types

The efficacy of geogrid, geocell, and geocell with additional basal geogrid reinforcements in protecting the buried pipelines are compared in this section. Throughout this test series, the pipe was placed at a depth of $1.5B$ below the loading plate. Figure 13.6 represents the bearing pressure-settlement response of the sand bed for the different test cases. For convenience, the settlement (S) of the loading plate was normalized with its width (B). Bearing capacity failure of the sand bed was observed in both unreinforced and geogrid reinforced cases at $S/B = 20\%$ and $S/B = 35\%$, respectively. The failure of the bed was indicated by the sudden reduction in the slope of the pressure-settlement curve, i.e., the curve becomes almost vertical. However, no failure was occurred in geocell reinforced case and geocell with additional basal geogrid reinforced case even up to the $S/B = 40\%$. The cell by virtue of its three-dimensional nature offers all-round confinement to the encapsulated soil. The interconnected cells form a slab that behaves like a large pad that spreads the applied load over a wider area and hence improves the performance of the sand bed. The maximum bearing pressure was observed when the bed was reinforced with the combination of geocell and geogrid. The planar geogrid contributes in improving the overall performance of the bed by resisting the downward movement of soil due to the loading by virtue of membrane mechanism (Hegde and Sitharam 2013). Hence, it is always beneficial to use the planar geogrid layer at the base of the geocell mattress.

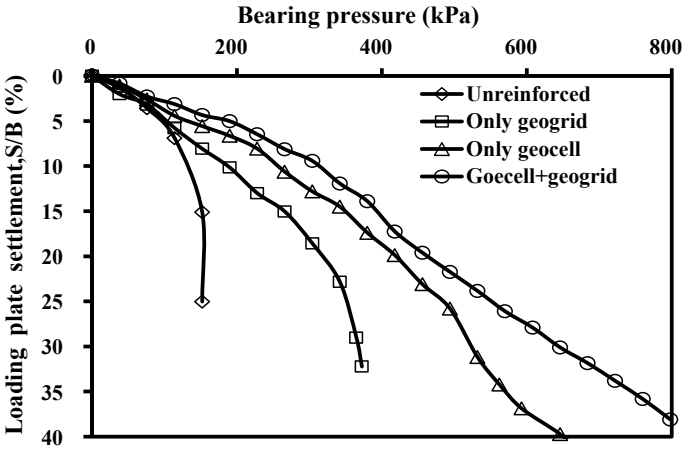

Fig. 13.6 Variation of bearing pressure with plate settlement for different types of reinforcements. Sourced from Hegde and Sitharam (2015c)

Figure 13.7 shows the variation of the vertical pressure on the top of the pipe for different reinforcement conditions. For convenience, the measured pressure value (P_u) was normalized with maximum applied pressure (q_u). The reported pressure values are corresponding to the q_u value equal to the ultimate bearing pressure of the unreinforced bed (i.e.,152 kPa). In the present case, the pressure values (P_u/q_u) observed in the unreinforced case was about 0.20. Similarly, the pressure values for different type of reinforcements were varied between 0.16 and 0.07. As compared

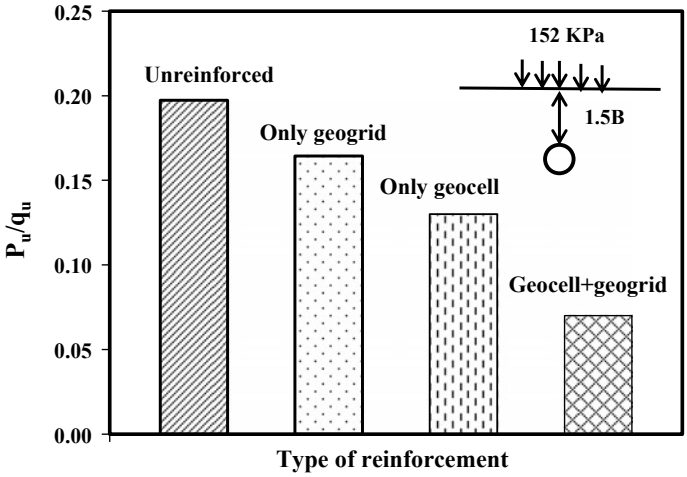

Fig. 13.7 Strain values at the top of the pipe for different types of reinforcement. Sourced from Hegde and Sitharam (2015c)

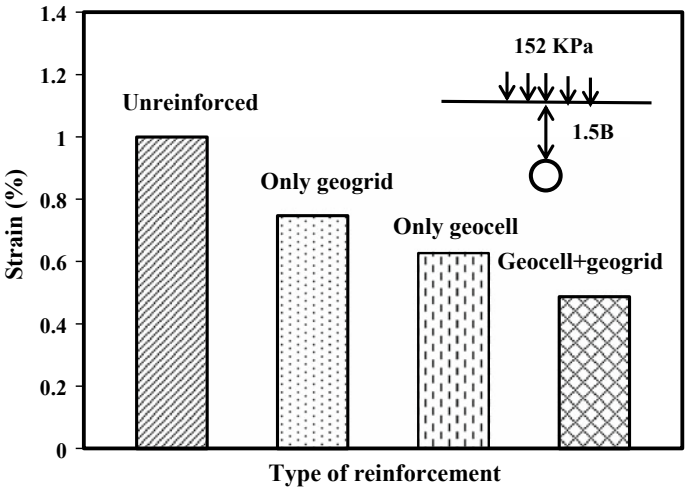

Fig. 13.8 Strain values at the top of the pipe for different types of reinforcement. Sourced from Hegde and Sitharam (2015c)

to unreinforced bed, about 65% reduction in the pressure value was observed at the top of the pipe when the combination of geocell and geogrid was used.

Similarly, Fig. 13.8 represents the measured strain values on the top of the pipe. The reported strain values are compressive in nature and measured at the center of the pipe, exactly below the loading plate. Brachman et al. (2008) observed that the measured vertical strain value in a pipe wall could vary a great deal, depending on the point on the periphery at which strain is measured. Another important factor that influences the accumulation of the strain is stiffness of the pipe. Stiffer the pipe lesser is the accumulated strain. In the present case, the strain value observed in unreinforced case was about 0.85%. The strain values were varied between 0.74 and 0.48% for different forms of reinforcements. Similar strain values were reported by Tavakoli et al. (2012) in their studies. The least strain on the pipe was observed when the geocell with additional basal geogrid was used as the reinforcement. Compared to unreinforced case, 43% reduction in the strain was observed when the combination of geocell and geogrid was used. It should be noted that the reported strain values were corresponding to pipe depth of 1.5*B* and applied pressure value of 152 kPa, which is nothing but the ultimate bearing capacity of the unreinforced bed.

13.3.2 Effect of Depth of Placement of Pipe

The geocell with additional basal geogrid found to provide better protection to buried pipelines as compared to other type of reinforcements. Hence, in this section, the depth of placement of the pipe was varied between 1*B* and 2*B* below the loading plate

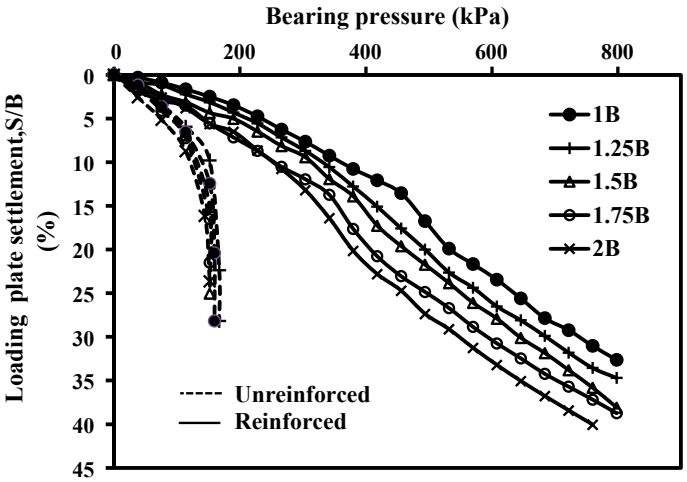

Fig. 13.9 Variation of bearing pressure with plate settlement for different depth of placement of pipe. Sourced from Hegde and Sitharam (2015c)

in the presence of geocell and geogrid reinforcement. The aim of the depth variation was to understand and compare the pressure and strain values experienced by the pipe at different depths. Figure 13.9 represents the variation of bearing pressure with plate settlement at different depth of placement of the pipe. The performance of the sand bed was found to be marginally influenced by the position of the pipe, even in the presence of relatively stiff reinforcement system. As the depth of the pipe increase, the settlement increases, and the bearing pressure decreases in all the cases. As the pipe stiffness is 2–3 times higher than the reinforcement system, the pipe itself acts as reinforcement along with the geocells.

Figures 13.10 and 13.11 represent the measured pressure and strain values on the pipe at different depth of placement. The reported pressure and strain values are corresponding to the applied pressure value of 152 kPa, which is nothing but the ultimate bearing capacity of the unreinforced bed. The measured pressure values (P_u/q_u) found to vary between 0.35 and 0.06 for different depths for the unreinforced case. For the same depths, the P_u/q_u values found to vary between 0.16 and 0.003 for the reinforced case. More than 50% reduction in the pressure was observed in the presence of reinforcement as compared to the unreinforced case at all the depths. In the presence of reinforcement, at a depth below 1.5*B*, the pressure value on the pipe reduced below 0.10, which is almost negligible. Similarly, the strain value found to vary between 1.15 and 0.65% for different depths for the unreinforced case. For the same depths, the strain values found to vary between 0.7 and 0.29% for the reinforced case. More than 40% reduction in the strain value was observed in the presence of reinforcement as compared to the unreinforced case at all the depths. The observed pressure and strain values indicate that the provision of the geocell with additional basal geogrid significantly reduces the depth of placement of the pipe. In a broader

perspective, these findings will have huge implications in reducing the installation costs of the buried pipelines in large projects, where pipelines are laid along several hundreds of kilometers.

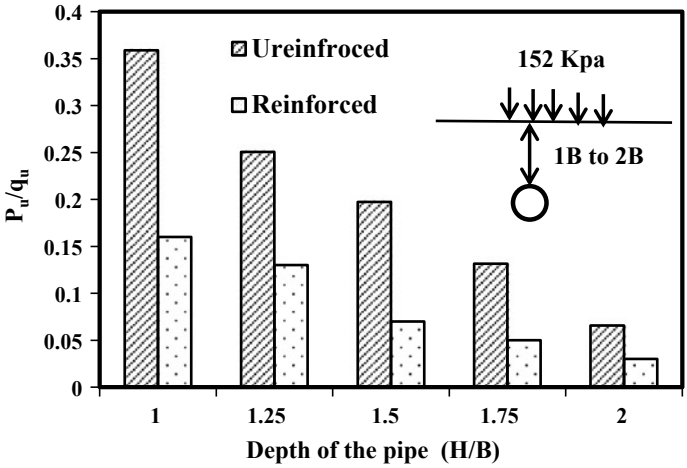

Fig. 13.10 Vertical pressure values at the top of the pipe for different depth of placement. Sourced from Hegde and Sitharam (2015c)

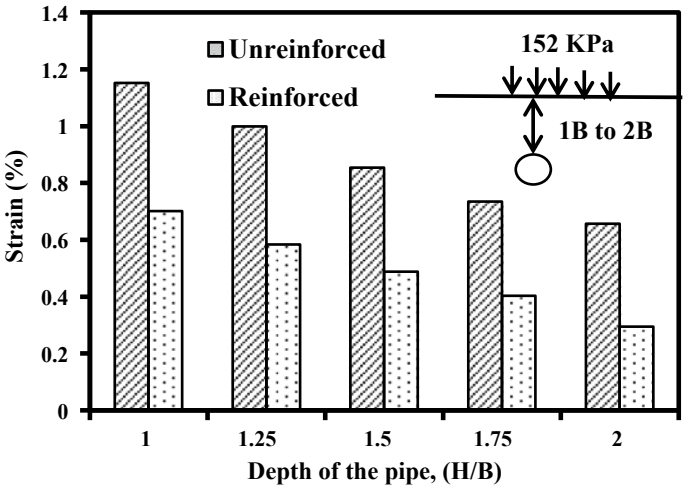

Fig. 13.11 Strain values at the top of the pipe for different depth of placement of pipe. Sourced from Hegde and Sitharam (2015c)

13.4 Numerical Modeling

Numerical modeling was carried out using FLAC3D considering its ability to model a wide range of geotechnical problems. FLAC3D uses an explicit finite difference solution scheme to solve the initial and boundary value problems. It has several built-in material models and structural elements to model the variety of geo-materials and the reinforcements. It provides the option to use the interface elements to accurately model the joints and the interfaces between two materials. The simulation was carried out for unreinforced case and the geocell with additional basal geogrid reinforced cases, when the pipe was placed at a depth of 1.5*B* below the loading plate. The dimension of the model was kept same as that of the dimension of test bed used in the experiments. The elastic-perfectly plastic Mohr–Coulomb model was used to simulate the behavior of the subgrade soil and the infill soil. The geocell was modeled using the geogrid structural element while the pipe was modeled using the shell structural element available in FLAC3D. Linear elastic model was used to simulate the behavior of the geocell and the pipe. The rigid nature of the geocell joint was simulated by fixing the nodes representing the joints. The interface between the geocell and the soil was linearly modeled with Mohr–Coulomb yield criterion. Figure 13.12a, b shows the skeleton view of the FLAC3D model for the unreinforced and reinforced cases.

Analyses were carried out under controlled velocity loading of 2.5 × E-5 m/step. Only a quarter portion of the test bed was modeled making use of the symmetry to reduce the computational effort. The quarter symmetric model of size 0.45 m × 0.45 m × 0.6 m was discretized into 10,320 zones. Sensitivity analyses were carried out to determine the mesh density and based on which, the relatively coarse mesh was chosen for the analysis. Preliminary analyses carried out revealed that

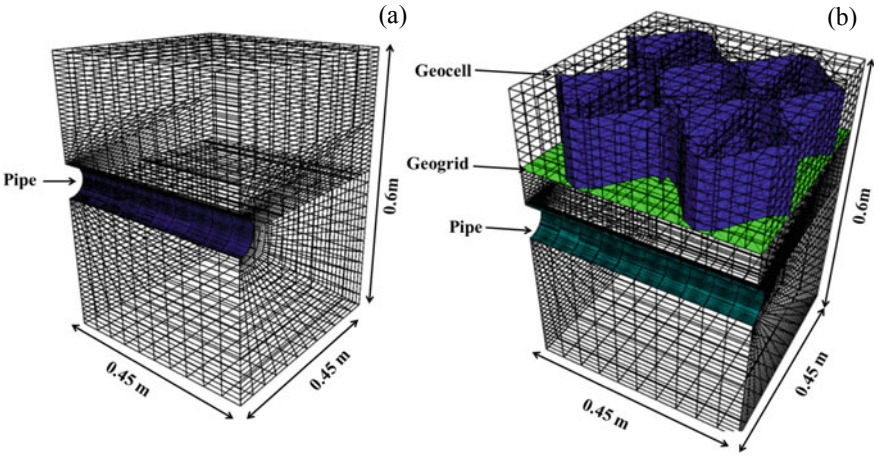

Fig. 13.12 **a** and **b** Skeleton view of the FLAC3D model: **a** unreinforced case; **b** geocell and geogrid reinforced case. Sourced from Hegde and Sitharam (2015c)

the boundary distances did not influence the results as deformations and stresses were contained within the boundaries. The displacement along the bottom boundary (which represents tank bottom) was restrained in both horizontal as well as vertical directions. The side boundaries (which represent tank side) were restrained only in the horizontal direction, such that the displacements were allowed to occur in the vertical direction.

Table 13.4 represents the properties of different materials used in the numerical simulations. Shear strength properties (C and φ) of the sand were determined from the direct shear test. The dilation angle was taken as 2/3rd of the friction angle as suggested by the earlier researchers in similar studies in FLAC (Ghazavi and Lavasan

Table 13.4 Properties of different materials used in numerical modeling. Courtesy Hegde and Sitharam (2015c)

Parameters	Values
Sand	
Shear modulus, G (MPa)	5.77
Bulk modulus, K (MPa)	12.5
Poisson's ratio, μ	0.3
Cohesion, C (kPa)	0
Friction angle, φ (°)	36
Dilation angle, Ψ(°)	24
Unit weight, γ (kN/m^3)	20
Geocell	
Young's modulus, E (MPa)	275
Poisson's ratio, μ	0.45
Interface shear modulus, k_i (MPa/m)	2.36
Interface cohesion, c_i (kPa)	0
Interface friction angle, φ_i (°)	30
Thickness, t_i(mm)	1.5
Basal Geogrid	
Young's modulus, E (MPa)	210
Poisson's ratio, μ	0.33
Interface shear modulus, k_i (MPa/m)	2.36
Interface cohesion, c_i (kPa)	0
Interface friction angle, φ_i (°)	18
Thickness, t_i(mm)	1.5
Pipe	
Young's modulus, E (GPa)	3.1
Poisson's ratio, μ	0.4
Thickness, t_i(mm)	1.4

2008; Madhavi and Somwanshi 2009). The elastic modulus (initial tangent modulus) of the sand was determined from the consolidated undrained triaxial compression test. The test was carried out at three different confining pressures of 100, 200, and 300 kPa. Initial tangent modulus was determined from the stress–strain curve corresponding to the confining pressure of 200 kPa. From the elastic modulus, the shear modulus and the bulk modulus values were determined by assuming the Poisson's ratio of 0.3. The elastic modulus of the geocell, geogrid, and the pipe was determined from tensile stress–strain curve shown in Fig. 13.3. The secant modulus corresponding to 2% axial strain was considered while calculating the modulus. Similarly, the Poison's ratio values provided by the manufacturer were used. The interface shear strength properties (c_i and φ_i) for both geocells and geogrid were obtained from the modified direct shear tests. In case of the geocells, the reported interface properties are corresponding to the interface between the sand and the geocell wall. In the modified direct shear test, the reinforcement was glued to a wooden plate and was placed in the lower half of the shear box such that the top surface of the reinforcement was along the horizontal shear plane (Srinivasa Murthy et al. 1993). The interface shear modulus value (k_i) of 2.36 MPa/m was considered in the analysis for geocells and geogrids (Itaska 2008).

Figure 13.13 represents the comparison of the experimental and numerical bearing pressure-settlement curves for unreinforced and geocell with additional basal geogrid reinforced case, when the pipe was placed at a depth 1.5*B* below the loading plate. A good agreement in the results was obtained between the experimental and numerical studies. Numerical studies also revealed that the no failure of the sand bed, even up to large settlements in the presence of geocells. Figure 13.14 shows the vertical stress

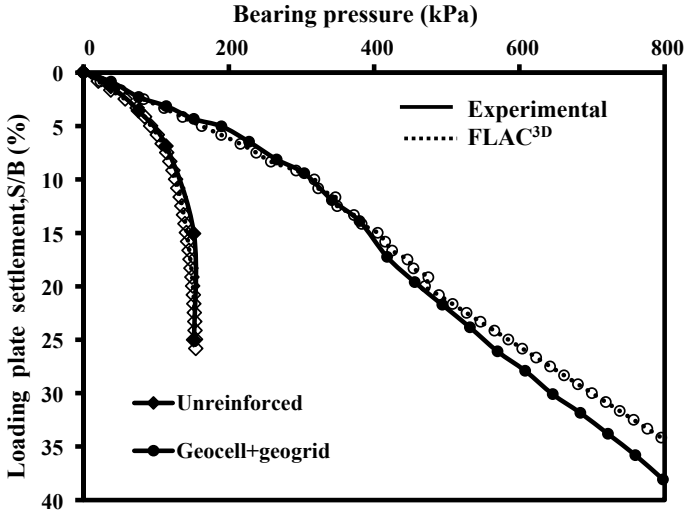

Fig. 13.13 Comparison of experimental and numerical bearing pressure-settlement curve. Sourced from Hegde and Sitharam (2015c)

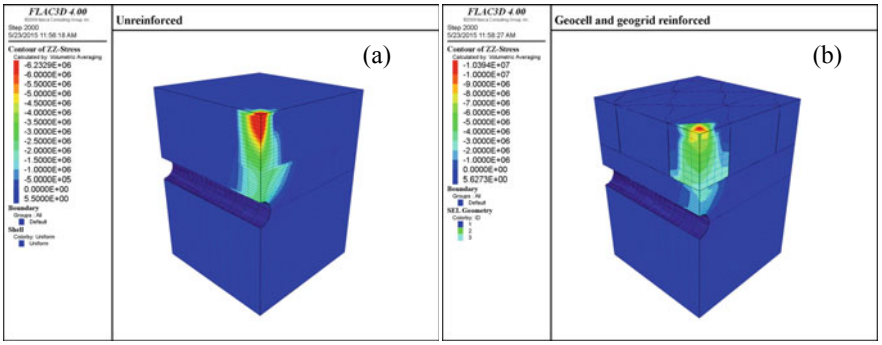

Fig. 13.14 **a** and **b** Vertical stress distribution (N/m^2): **a** unreinforced case; **b** geocell and geogrid reinforced case. Sourced from Hegde and Sitharam (2015c)

distribution contours for unreinforced and the reinforced cases. These contours are corresponding to the settlement of $S/B = 33\%$. The tank boundaries found to have no influence on the results as the measured stresses adjacent to the boundary were equal to zero. A substantial reduction in the pressure transferred to the pipe was observed in the presence of the reinforcements. In case of the unreinforced soil, stress was found to distribute to a greater depth in the form of a narrow band. However, in case of geocells, the stress was found to distribute in the lateral direction to a shallow depth. Similar observations were also made by Saride et al. (2009) and Hegde and Sitharam (2015d, e) during the numerical simulations of the geocell reinforced soil beds. Since geocell distribute the load in the lateral direction, the intensity of the stress will reduce the soil existing blow the geocells. Therefore, the pipe will also experience less stress in the presence of reinforcement as compared to the unreinforced beds.

Figure 13.15a and b shows the distribution of the vertical displacement contours on the surface of the pipe for unreinforced and the reinforced cases. The reported displacements are acting in the downward direction. From the figure, it is evident that the deformation of the pipe significantly reduces the presence of the geocells and geogrids. From the maximum value of the observed deformation, the strain on the pipe was deduced for both unreinforced and reinforced cases. The strain values thus calculated were 0.93% and 0.58%, respectively, for unreinforced and reinforced cases. As compared to experimentally obtained strain, the numerically obtained strain values were found to be 8 to 9% higher for both the cases. This difference may be due to the material properties used in the numerical simulations.

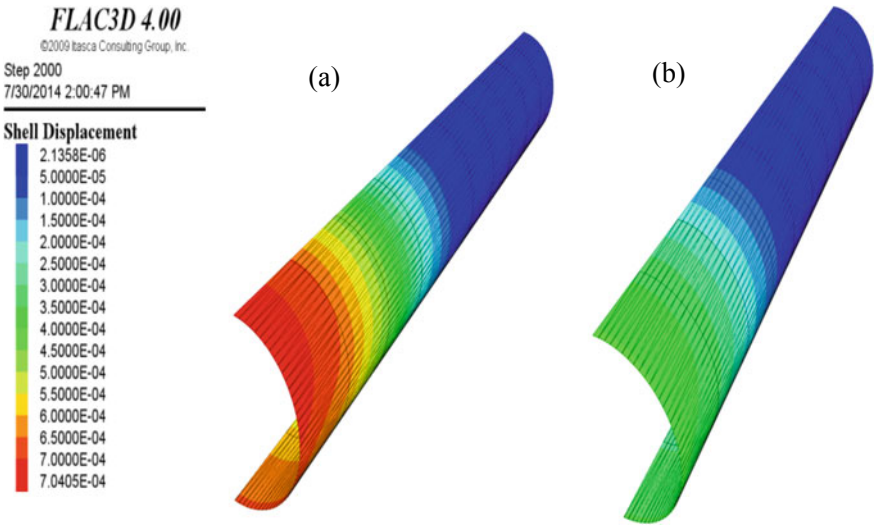

Fig. 13.15 **a** and **b** Deformation on the pipe (m): **a** unreinforced case; **b** geocell and geogrid reinforced case. Sourced from Hegde and Sitharam (2015c)

13.5 Clay Bed Test Results

Hegde et al. (2016) performed the test on pipe embedded in the clay bed as shown in Fig. 13.16a, b. Similar to sand bed, the pressure and strain on the pipe were measured at the different depth of placement of the pipe. The reinforcement type, properties, and infill soil properties are similar to the one reported by Hegde and Sitharam (2015c). Figure 13.17 represents the comparison of the measured strains at the top

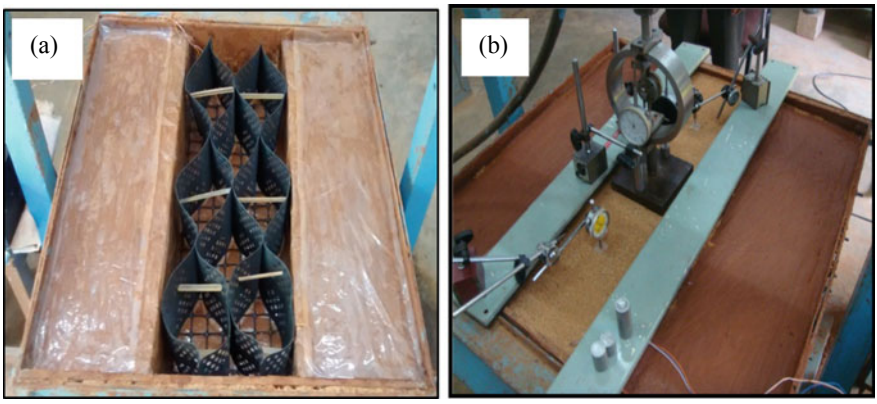

Fig. 13.16 **a** anf **b** Photographs of the clay bed tests: **a** model preparation; **b** load application. Sourced from Hegde et al. (2016)

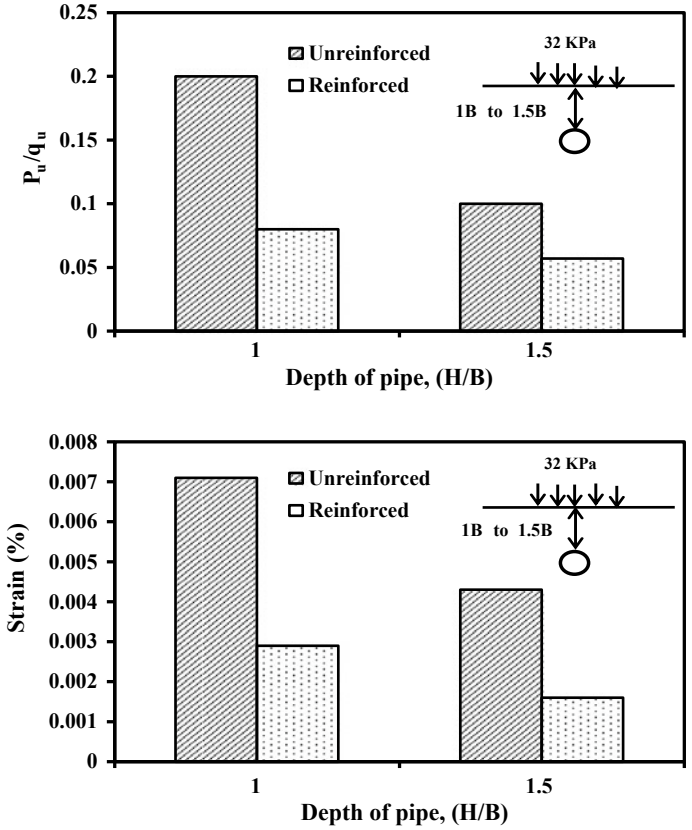

Fig. 13.17 Pressure and strain values measured at the top of the pipe embedded in clay bed for different depth of placement of pipe. Sourced from Hegde et al. (2016)

surface of the pipe at two different depths of placement. The reported strain values are compressive in nature and measured at the center of the pipe, exactly below the footing. The measured vertical strains in a pipe wall could vary a great deal, depending on the point on the periphery at which strain is measured (Brachman et al. 2008). Another key factor that affects the accumulation of the strain is the stiffness of the pipe. As the stiffness of the pipe decreases, the strain increases. In the present case, at both the depths, more than 60% reduction in the strain was observed in the presence of geocell and geogrid reinforcement as compared to unreinforced bed.

Figure 13.17 shows the variation of the vertical pressure on the top of the pipe. For convenience, the measured pressure value (P_u) was normalized with applied footing pressure (q_u). The reported P_u/q_u values corresponding to the applied footing pressure value (q_u) of 32 kPa, which is nothing but the ultimate bearing pressure of the unreinforced soft clay bed. In the present case, at both the depths, more than 45%

reduction in the pressure experienced by the pipe was observed in the presence of the combination of geocell and geogrid.

13.6 Environmental Impact

Buried pipelines form a complex network in the underground space and are often laid below the pavements and the temporary structures. These pipeline networks are used to transport a variety of liquid and gases, including water, sewage, petroleum, natural gases, etc. Often, these pipelines are buried at shallow depths in trenches. These pipes may undergo breakage due to the application of repeated traffic loads or heavy static loads from temporary structures. The damage of the pipelines will cause disturbances to the users of these facilities and also leads to a variety of environmental pollutions. Breakages of the sewer lines cause water and land pollutions leading to the epidemic of the diseases. Air pollution and the fire causalities may take place in the case of the petroleum or natural gas pipe breakages. As revealed by the present study, the geocells and geogrid can be used to protect the buried pipelines and the utility lines. Hence, the use of the geocell and the geogrid reduces the environmental pollutions caused by the pipeline breakage. In addition, use of the geocells and the geogrid increases the bearing capacity of the fill soil and reduces the differential settlement. Hence, it also helps to minimize the surface disturbances and the related socioeconomic concerns.

13.7 Scale Effects

Though full-scale model tests are the most reliable means of studying the behavior of the prototypes, at times these tests become cumbersome. In those cases, reduced scale model tests are performed at 1-g condition. 13.1-g model tests help to obtain the approximate information about the general behavior of the prototypes quicker than the full-scale testing with closer control over the key parameters. However, the results of 1-g model tests are prone to scale effects. Hence, the results obtained from the 1-g model tests are not directly applicable to the prototype case.

As suggested by Fakher and Jones (1996), the results of the small scale model tests can be extrapolated to prototype cases by carefully applying the scaling laws. Dimensional analysis can be used to deduce the scaling laws involving the relationship between the parameters that could affect the phenomenon that is being modeled. The theory of dimensional analysis is explained in detail elsewhere by Buckingham (1914). Generally, the dimensions of the variables are expressed in the combinations of three fundamental units, namely, length (L), mass (M), and time (T). However, Butterfield (1999) highlighted that application of dimensional analysis can produce misleading results in some cases unless the alternative grouping for force [$MLT^{-2} =$

F] is used as a member of the fundamental system. Hence, in most of the geotechnical problems force (F) and length (L) are used as the two fundamental dimensions.

In the present case, the major influencing parameters are, B, D, H, h, d, b, u, S, K_g, K_p, G, γ, φ, q_r, $q_{u,}$ where K_g and K_p are the stiffness of the geocell and the pipe, respectively; G is the shear modulus of the sand; S is the settlement of the loading plate; γ is the unit weight of the sand; φ is the friction angle of the sand; q_r and q_u are the ultimate bearing capacity of the reinforced and unreinforced case, respectively. Please refer Fig. 13.5 for the description of remaining geometric properties used in the study.

The function (f) that governs the present system can be represented as

$$f(B, D, H, h, d, b, u, S, K_g, K_p, G, \gamma, f, q_r, q_s) = 0 \tag{13.1}$$

There are 15 influencing parameters present in Eq. (13.1) and the model involves only two fundamental dimensions, i.e., force (F) and length (L). Hence, the present system might be studied by a complete set of 13 independent dimensionless parameters as described below.

$$g(\pi_1, \pi_2, \pi_3, \pi_4 \ldots \pi_{13})$$

$$= g\left[\left(\frac{D}{B}\right), \left(\frac{H}{B}\right), \left(\frac{h}{B}\right), \left(\frac{d}{h}\right), \left(\frac{d}{B}\right), \left(\frac{b}{B}\right), \left(\frac{u}{B}\right), \left(\frac{S}{B}\right), \left(\frac{K_g\gamma}{G^2}\right), \left(\frac{K_p\gamma}{G^2}\right), \left(\frac{G}{\gamma B}\right), \left(\frac{q_s}{q_u}\right), \phi, \right] = 0 \tag{13.2}$$

where g is the function that governs the system. The π terms (π_1 to π_{13}) reported in Eq. (13.2), should be same for model and prototype. Considering the width of the prototype plate will be N times higher than the model plate,

$$\frac{B_p}{B_m} = N \tag{13.3}$$

where N is the scaling factor; subscripts p and m refer to prototype and model, respectively. Equating, $(\pi_{11})_p = (\pi_{11})_m$.

$$\left(\frac{G}{\gamma B}\right)_p = \left(\frac{G}{\gamma B}\right)_m \tag{13.4}$$

It is very important to maintain the soil properties the same in both model and prototype in order to avoid the particle size effect. Hence, the unit weight of the soil (γ) must be the same in model and prototype. Equation (13.4) can be re-written as,

$$\left(\frac{G_p}{G_m}\right) = \left(\frac{B_p}{B_m}\right) = N \tag{13.5}$$

Similarly, equating, $(\pi_9)_p = (\pi_9)_m$

$$\left(\frac{K_g \gamma}{G^2}\right)_p = \left(\frac{K_g \gamma}{G^2}\right)_m \tag{13.6}$$

Rewriting the Eq. (13.6),

$$\left(\frac{K_{g_{(p)}}}{K_{g_{(m)}}}\right) = \left(\frac{G_p^2}{G_m^2}\right) = N^2 \tag{13.7}$$

As per Eq. (13.7) the stiffness of the reinforcement to be used in the prototype should be N^2 times the stiffness of the reinforcement used in the model. Sireesh et al. (2009) observed that the stiffness of the geocell joint that decides the performance of the geocell than the stiffness of the material from which it is made. In the same line, it is possible to obtain the stiffness of the pipe to be used in the prototype as N^2 times the stiffness of the pipe used in the model.

Based on the scaling law deduced above, the results are extrapolated to the prototypical case of the shallow pipeline below the pavement. Generally, the diameter of the tire contact is about 0.3 m. The steel plate width used in the present study is 0.15 m. Hence, the scale factor can be deduced as,

$$\frac{B_p}{B_m} = \frac{0.3}{0.15} = 2 = N \tag{13.8}$$

The ultimate tensile strength of the prototype reinforcement should be 80 kN/m (20 kN/m $\times$ 4). Generally, bamboo will have the ultimate tensile strength in that range. Three-dimensional cells prepared from the bamboo strips known as bamboo cells could be used in the prototype pavement applications. The beneficial aspects of the bamboo cells and other details are explained elsewhere by Hegde and Sitharam (2015f). Similarly, the diameter and the thickness of the prototype pipe turns out to be 0.15 m (2 $\times$ 0.075) and 2.8 mm (1.4 mm $\times$ 2), respectively. The ultimate tensile strength of the prototype pipe should be 168 kN/m (42 kN/m $\times$ 4). Generally, cast iron pipes will have the tensile strength in that range. Fakher and Jones (1996) warned that it is not feasible to use complete similarity between model and prototype due to involvement of several complex factors. It should be left to the judgment of the researchers to decide about the factors to scale up considering the accuracy and the nature of the problem. In the present study, the scaling laws suggested using the geocell of bigger pocket size, i.e., 0.5 m in the prototype applications. However, it is recommended to use the geocells of smaller pocket size in the prototype applications similar to the model studies.

13.8 Conclusions

Experimental studies have been conducted to explore the possibility of using the geocells in protecting the underground utilities and buried pipelines. Results suggest that the use of geocells with additional basal geogrid significantly reduces the deformation of the pipe as compared to other types of reinforcements used in the study. Further, the depth of the placement of the pipe was varied between 1*B* to 2*B* below the loading plate in the presence of geocells and geogrids. The measured pressure/strain values in the reinforced case were compared with the pressure/strain values measured at the same depth for the unreinforced case. More than 50% reduction in the pressure and more than 40% reduction in the strain values were observed in the presence of reinforcement at all the depths. The pressure on the pipe becomes almost negligible (i.e., $P_u/q_u < 0.1$) beyond the depth of 1.5*B* below the loading plate in the presence of geocells. The observed pressure and strain values indicate that the provision of the geocells significantly reduces the depth of placement of the pipe. From a broader perspective, these findings will help to reduce the installation costs of the buried pipelines in large projects, where pipelines are laid along several hundreds of kilometers. Further, numerical simulations were carried out using FLAC3D to understand the distribution of the stresses and strains in the pipe. Modeling results revealed that the geocells distribute the load in the lateral direction to a shallow depth, thus reducing the pressure on the pipe. A good agreement in measured strain values on the pipe was observed between the experimental and numerical studies.

The study has some limitations. Only one type of backfill soil and only one type of pipe were used in the study. Hence, it should be noted that the results are applicable to limited cases. Further studies are necessary with different types of pipe, soil, and the loading conditions. It should be noted that the observed results may vary significantly for the pipes with different stiffness values.

Acknowledgements The first author is thankful to Mr. Sharan Kadabinakatti (graduate research student) for his help in carrying out the laboratory model tests in the initial stage of this study.

References

Almeida M, Hosseinpour I, Riccio M, Alexiew D (2014) Behavior of geotextile encased granular columns supporting test embankment on soft deposit. J Geotech Geoenviron Eng. https://doi.org/10.1061/(ASCE)GT.1943-5606.0001256,04014116

Arockiasamy M, Chaallal O, Limpeteeparakarn T (2006) Full-scale field tests on flexible pipes under live load application. J Perform Constructed Facil 20(1):21–27

ASTM D638 (2010) Standard test method for tensile properties of plastics. ASTM International, West Conshohocken, PA, USA

ASTM D4885 (2011) Standard test method for determining performance strength of geomembranes by wide strip tensile method. ASTM International, West Conshohocken, PA, USA

ASTM D6637 (2011) Standard test method for determining the tensile properties of geogrid by the single or multi-rib tensile method. ASTM International, West Conshohocken, PA, USA

Bia X-H, Huang X-Z, Zhang W (2013) Bearing capacity of square footing supported by a geobelt-reinforced crushed stone cushion on soft soil. Geotext Geomembr 38:37–42
Brachman RWI, Moor ID, Rowe RK (2000) The design of a laboratory facility for evaluating the structural response of small diameter buried pipe. Can Geotech J 37(2):281–295
Brachman RWI, Moore ID, Munro SM (2008) Compaction effects on strains within profiled thermoplastic pipes. Geosynthetics Int 15(2):72–85
Buckingham E (1914) On physically similar systems; illustrations of the use of dimensional equations. Phys Rev 4(4):345–376
Butterfield R (1999) Dimensional analysis for geotechnical engineers. Geotechnique 49(3):357–366
Dash SK, Krishnaswamy NR, Rajagopal K (2001) Bearing capacity of strip footings supported on geocell reinforced sand. Geotext Geomembr 19:235–256
Demir A, Laman M, Yildiz A, Ornek M (2013) Large scale field tests on geogrid reinforced granular fill underlain by soft clay. Geotext Geomembr 38:1–15
Fakher A, Jones CJFP (1996) Discussion on bearing capacity of rectangular footings on geogrid reinforced sand, by Yetimoglu T, Wu JTH, Saglamer A, 1994. J Geotech Eng 122:326–327
Ghazavi M, Lavasan AA (2008) Interference effect of shallow foundations constructed on sand reinforced with geosynthetics. Geotext Geomembr 26(5):404–415
Hegde A, Sitharam TG (2013) Experimental and numerical studies on footings supported on geocell reinforced sand and clay beds. Int J Geotech Eng 7(4):347–354
Hegde A, Sitharam TG (2015a) Joint strength and wall deformation characteristics of a single cell subjected to uniaxial compression. Int J Geomech 15(5):04014080
Hegde AM, Sitharam TG (2015b) Effect of infill materials on the performance of geocell reinforced soft clay beds. Geomech Geoengineering 10(3):163–173
Hegde A, Sitharam TG (2015c) Experimental and numerical studies on protection of buried pipelines and underground utilities using geocells. Geotext Geomembr 43:372–381
Hegde A, Sitharam TG (2015d) 3-dimensional numerical modeling geocell reinforced sand beds. Geotext Geomembr 43(2):171–181
Hegde AM, Sitharam TG (2015e) 3-Dimensional numerical analysis of geocell reinforced soft clay beds by considering the actual geometry of geocell pockets. Can Geotech J 52(9):1396–1407
Hegde A, Sitharam TG (2015f) Use of bamboo in soft ground engineering and its performance comparison with geosynthetics: experimental studies. Mater Civil Eng 27(9):04014256
Hegde A, Kadabinakatti S, Sitharam TG (2014) Protection of buried pipelines using a combination of geocell and geogrid reinforcement: experimental studies. Ground Improvement and Geosynthetics, Geotechnical Special Publication-238, ASCE, pp 289–298
Hegde A, Kadabinakatti S, Sitharam TG (2016) Use of geocells to protect buried pipelines and underground utilities in soft clayey soils. Geotechnical Spaecial Publication 271 ASCE (Geo-Chicago 2016), pp 914–924
Indraratna B, Nimbalkar S, Christie D, Rujikiatkamjorn C, Vinod J (2010) Field assessment of the performance of a ballasted rail track with and without geosynthetics. Geotech Geoenviron Eng 136:907–917
Indraratna B, Biabani M, Nimbalkar S (2014) Behavior of geocell reinforced subballast subjected to cyclic loading in plane strain condition. J Geotech Geoenviron Eng. https://doi.org/10.1061/(ASCE)GT.1943-5606.0001199
Itaska (2008) Fast lagrangian analysis of continua (FLAC3D 4.00). Itasca Consulting Group Inc, Minneapolis, USA
Lambert S, Nicot F, Gotteland P (2011) Uniaxial Compressive behavior of scrapped tire and sand filled wire netted geocell with a geotextile envelop. Geotext Geomembr 29:483–490
Madhavi LG, Somwanshi A (2009) Effect of reinforcement form on the bearing capacity of square footing on sand. Geotext Geomembr 27:409–422
Mehdipour I, Ghazavi M, Moayed RZ (2013) Numerical study on stability analysis of geocell reinforced slopes by considering the bending effect. Geotext Geomembr 37:23–34
Mir Mohammad Hosseini SM, Moghaddas Tafreshi SN (2002) Soil structure interaction of embedded pipes under cyclic loading conditions. Int J Eng 15(2):117–124

Moghaddas Tafreshi SN, Dawson AR (2010) Behavior of footings on reinforced sand subjected to repeated loading comparing use of 3D and planar geotextile. Geotext Geomembr 28:434–447
Moghaddas Tafreshi SN, Khalaj O (2008) Laboratory tests of small-diameter HDPE pipes buriedin reinforced sand under repeated-load. Geotext Geomembr 26:145–163
Moghaddas Tafreshi SN, Khalaj O, Dawson AR (2014) Repeated loading of soil containing granulated rubber and multiple geocell layers. Geotext Geomembr 42:25–38
Palmeira EM, Andrade HKPA (2010) Protection of buried pipes against accidental damage using geosynthetics. Geosynthetics Int 17(4):228–241
Pokharel SK, Han J, Leshchinsky D, Parsons RL, Halahmi I (2010) Investigation of factors influencing behavior of single geocell reinforced bases under static loading. Geotext Geomembr 28(6):570–578
Rowe RK, Taechakumthorn C (2011) Design of reinforced embankments on soft clay deposits considering the viscosity of both foundation and reinforcement. Geotext Geomembr 29:448–461
Saride S, Gowrisetti S, Sitharam TG, Puppala AJ (2009) Numerical simulations of sand and clay. Ground Improv 162(GI4):185–198
Sireesh S, Sitharam TG, Dash SK (2009) Bearing capacity of circular footing on geocell sand mattress overlying clay bed with void. Geotext Geomembr 27(2):89–98
Sitharam TG, Hegde A (2013) Design and construction of geocell foundation to support the embankment on settled red mud. Geotext Geomembr 41:55–63
Srinivasa Murthy BR, Sridharan A, Bindumadhava (1993) Evaluation of interfacial frictional resistance. Geotext Geomembr 12:235–253
Srivastava A, Goyal CR, Raghuvanshi A (2012) Load settlement response of footing placed over buried flexible pipe through a model plate load test. Int J Geomech 13(4):477–481
Tavakoli Mehrjardi Gh, Moghaddas Tafreshi SN, Dawson AR (2012) Combined use of geocell reinforcement and rubber soil mixtures to improve performance of buried pipes. Geotext Geomembr 34:116–130
Tavakoli Mehrjardi Gh, Moghaddas Tafreshi SN, Dawson AR (2013) Pipe response in a geocell-reinforced trench and compaction considerations. Geosynthetics Int 20(2):105–118
Thakur JK, Han J, Pokharel SK, Parsons RL (2012) Performance of geocell-reinforced recycled asphalt pavement (RAP) bases over weak subgrade under cyclic plate loading. Geotext Geomembr 35:14–24
Yang X, Han J, Pokharel SK, Manandhar C, Parsons RL, Leshchinsky D, Halahmi I (2012) Accelerated pavement testing of unpaved roads with geocell reinforced sand bases. Geotext Geomembr 32:95–103

Chapter 14
Guidelines for the Use and Design of Geocells in Road Reinforcement Applications

Yitzchak Schary

Abstract The use of geocells in flexible pavement reinforcement applications lagged behind other geosynthetics due to a number of factors, one of which is the lack of standards and guidelines. Recent advances, however, in research, innovative technology as well as market acceptance and growth may have closed the gap. The latest milestone is the development of new guideline standards for geocells. This includes recently published standards in the Netherlands, as well as those under development by the ISO and ASTM organizations. These standards cover geocell applications, support mechanisms, and design principles; and emphasize the importance of geocell material attributes –and their influence on long-term reinforcement factors. The test standards for evaluating geocell performance cited in the Dutch, ISO and ASTM standards are also described. The discussion translates (as necessary) and reviews these standards to help designers and engineers worldwide realize the potential contribution of geocell reinforcement in transportation and infrastructure.

Keywords Geocell standards · Geocell guidelines · Geocell attributes · Base reinforcement · Reinforcement geosynthetics · Stabilization geosynthetics · Design with geocells

14.1 Introduction

14.1.1 Geocells Versus Geosynthetics

The goal of standards is to improve the design and manufacturing quality of processes and products. This enables products to compete in the international marketplace by attesting that they are comparable, compatible and fit their intended use. While standards and guidelines abound for geosynthetic solutions, there were no such standards for geocells. This is due to several historical and market/industry-related reasons

Y. Schary (✉)
PRS Geo-Technologies, 4 Kaufman St., Tel Aviv, Israel
e-mail: yitzchak@prs-med.com

T. G. Sitharam et al. (eds.), *Geocells*, Springer Transactions in Civil and Environmental Engineering,
https://doi.org/10.1007/978-981-15-6095-8_14

and evidenced in publications of geosynthetics in pavement reinforcement, where geocells are not part of the discussion (Christopher et al. 2006; Berg et al. 2000; AASHTO 2010; Zornberg and Gupta 2010; European Committee for Standardization 2004).

Furthermore, there is a fragmentation of the existing knowledge over several publications and borders. Many publications are geotechnically oriented, making the connection with the road construction sector more challenging. The result is that designers, contractors and managers of transportation infrastructure do not make optimal use of the geocell road reinforcement technology (Vega et al. 2018). A further challenge to standardization of geocells in the construction industry, particularly in the fields of road and rail design, is the regulatory gap between national vs. international standards (Hughes and Laryea 2009). Until now there were no international guidelines for the design and use of geocells in road design. This lack of standardized guidelines or knowledge about how to utilize this technology in road design impeded widespread adoption by the engineering and construction community.

Fortunately, all this has changed in recent years (as evidenced by the publication of this book). There has been an enormous surge in geocell basic and applied research, materials and technology, field investigations and growing market and engineering recognition of the utility of geocell reinforcement in transportation and infrastructure projects (Hegde 2017). Standards for geocells, performance, testing and certification are under development by government and industry institutes worldwide, in Holland, Israel, Russia, India, South Africa, Canada, Indonesia, Philippines, Colombia, Vietnam, Dominican Republic, Chile and others (PRS Geo-Technologies 2018).

The latest milestone in the evolution of geocells is the development and publication of guideline standards. These are intended to disseminate the most updated knowledge about the best design methods and practices for implementing geocell technology in soil stabilization and road base reinforcement applications. The guidelines also reflect recent changes in road construction specifications (and contracts!) that stipulate performance-based factors rather than actual material properties, emphasizing function over form (Vega et al. 2018).

The national road research-standards institutes in the Netherlands recently published the *Geosynthetics for Reinforcement of Unbound Base and Subbase Pavement Layers* Guidelines. This comprehensive standard is translated and reviewed here for the benefit of the wider engineering community. In addition, international guidelines for reinforcement geosynthetics, basically geogrid and geocells, currently being prepared by the ISO and ASTM organizations, respectively, are also briefly reviewed.

14.2 New Guideline for Geocell Road Base Reinforcement, Netherlands

14.2.1 Introduction

Geosynthetics for Reinforcement of Unbound Base and Subbase Pavement Layers is a new Guideline Standard published in the Netherlands in 2018 (Vega et al. 2018) published by SBRCURnet/CROW—renowned research institutes that produce standards and regulations in the fields of civil engineering, transportation and construction. The goal of the Standard is to determine the added value of reinforcement geosynthetics in road building, based on improvement factors and pavement design (para 1.1). The document collates the currently available design methods, knowledge and experience to optimize geosynthetic reinforcement for pavements, for both 2D Geogrids and 3D Geocells. The Standard is published in Dutch; in the interest of bringing this Guideline to a wider audience, this chapter provides a brief overview in English of sections (referenced by paragraph no.) relevant to geocells (all rights reserved by SBRCURnet/CROW).

Terminology. The following are several assumptions used in this Standard:

- **Reinforcement Geosynthetics**—the Standard focuses on mechanical stabilization by both—2D Geogrids, which work by means of interlock between the aggregate and the grid, and—3D Geocells, which work by confinement stress on the aggregate to improve the strength of the entire layer.
- **Reinforcement versus stabilization**—although there is a fine distinction between the function of base reinforcement and mechanical stabilization, in practice, both are often used interchangeably.
- **Base Reinforcement**—in this Standard, "base" reinforcement refers to reinforcement of the subbase and soil, as well as the base layer.
- **Selecting Reinforcement**—The Standard stresses that the selection of the reinforcement geosynthetic should be based on the design criteria; the following review discusses content relevant to Geocells.

14.2.2 Purpose of Base Reinforcement

As defined in the Standard: "**Base reinforcement** is the reinforcement of the bearing capacity and integrity of bases supporting roads. By applying base reinforcement, the designer, contractor or construction manager attempt to improve the structural behavior of an unbound base, either by having to apply less material, or by achieving a longer life span in an unpaved road, or in a road paved with asphalt, concrete or paving stone. Base reinforcement may also be applied when considering working with an inferior or lightweight base material with less than optimal stability and stiffness properties." (para. 1.2.1). The relevant properties of geosynthetics for reinforcement are shown below (Table 14.1):

Table 14.1 Relevant properties of geosynthetics for reinforcement function

Benefit	Dynamic stiffness modulus subgrade		
	<30 MPa	30–80 MPa	>80 MPa
Limited digging for replacement of subgrade	●	◗	○
Reduced layer thickness of subbase for reduced tension on subgrade	●	◗	○
Reduced disruption of subgrade during road construction	●	◗	○
Reduced total layer build-up of road construction through subbase reinforcement	●	◗	○
Reduced total layer build-up of road construction through base reinforcement	◗	●	◗
Extension of road construction design life through reinforcement of subbase	◗ geogrid ● geocell	◗ geogrid ● geocell	◗ geogrid ● geocell
Extension of design life by reinforcing base	●	●	●

Source Geosynthetics for Reinforcement Guideline Standard (Vega et al. 2018)
● = usually benefit; ◗ = benefit under certain circumstances; ○ = usually no benefit

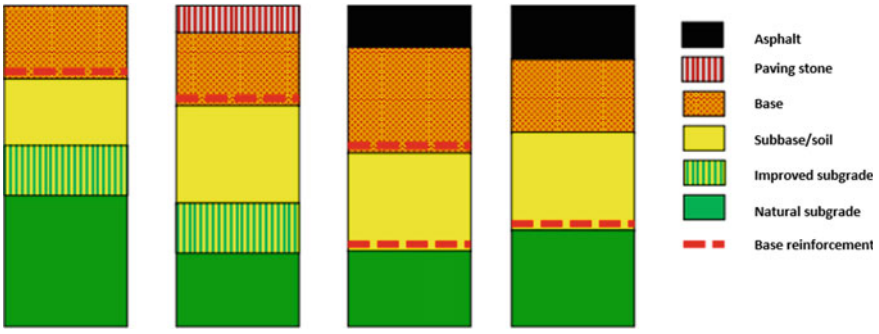

Fig. 14.1 Examples of base reinforcement application in base and subbase. *Source* Geosynthetics for Reinforcement Guideline Standard (Vega et al. 2018)

The following figure shows (from left to right), a schematic application of base reinforcement in the base of an unpaved road, base reinforcement of a block pavement, reinforcement of the subbase and base of an asphalt pavement and reinforcement of only the subbase of an asphalt pavement (Fig. 14.1). (para. 1.2.2)

14.2.3 Reinforcement Versus Stabilization

Terminology. Although the two terms are often used interchangeably, the standard attempts to make a fine distinction between the two: "**Mechanical (stabilization)**

means that a product is applied in the unbound base material to increase the contact pressure on the surfaces between the particles of the mineral aggregate and with 3D **base reinforcement** to increase the confinement stress on the mineral aggregate to improve the overall strength of the entire layer." (para. 1.2.4)

Reinforcement is dependent upon material properties. This is one of the main points in the Standard: "(In addition to the structure of the road construction), the extent of the reinforcing or stabilizing effect is determined by the material from which the product is made and the geometry. The most important material properties are the elastic stiffness and the resistance to permanent deformation (creep)…. **Materials that exhibit a lot of creep will gradually lose their reinforcing capacity over time**." (para 1.2.4)

The reinforcement mechanism is summarized as follows: "When using a geocell, Interlock occurs through the geocell walls, as well as the activation of tensile forces in the geocell, Under the vertical traffic load and the load of the overlying layers, horizontal stresses in the mineral aggregate in the geocell are generated by load distribution. This horizontal ground pressure is controlled by the cell walls, in which "hoop" tensions are generated. The "hoop" tensions and passive ground pressure in the adjacent cells prevent lateral deformation of the mineral aggregate…. As a result, shear deformation in the mineral aggregate is slowed down or prevented and the entire paving construction behaves more rigidly." (para. 1.2.4)

The limit on plastic deformation for reinforcement synthetics is defined as low deformation, e.g., **less than 2%, as elongation more than that will lead to much larger degradation of the pavement.** (para. 1.2.4)

14.2.4 Geocells

Raw Materials. "The polymers polyamide (PA) and polyethylene (PE, HDPE) are less suitable for reinforcement and stabilization in view of the higher elongation at break and lower stiffness. Because the behavior of small deformations is decisive for application in road bases, the PA and PE plastics will not be discussed in this publication. There are also products available that use different types of polymers to optimize their combined benefits in the end product." (para. 2.1)

Physical Description. This section describes geocells and their physical construct. Geocells are "hardly dependent on the grain size and on the mineral aggregate…" (para. 2.2.4). The effect of confinement, lateral stress and hoop stress in the cell walls is described. The geocell mechanism provides an improved spread angle through the so-called "beam effect" (see Fig. 14.2).

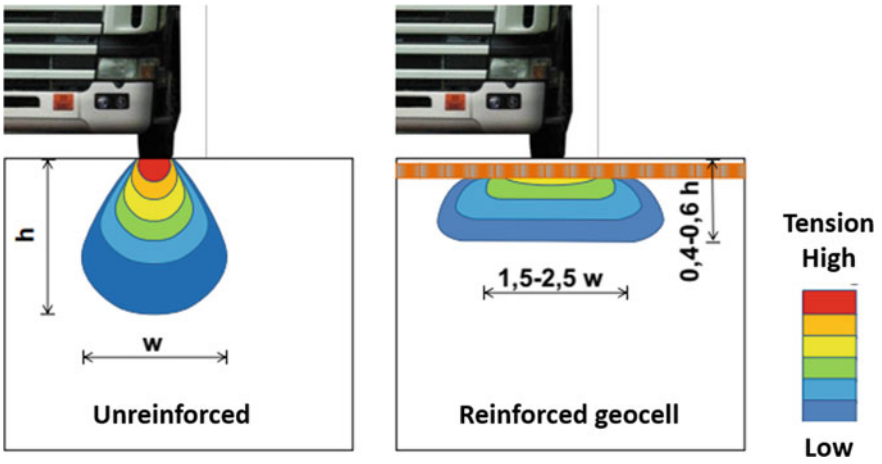

Fig. 14.2 Improvement of load distribution by geocell in upper structural layer *Source* Geosynthetics for Reinforcement Guideline Standard (Vega et al. 2018)

14.2.5 Geocell Material Properties

Geocells must also have the right properties in all directions when it comes to **dynamic stiffness, resistance to plastic deformation and tensile strength** (para. 2.2.4) (Table 14.2).

Table 14.2 Required global properties of geocells for road base reinforcement[a]

Property	Unit	Testing method	Value
Dynamic stiffness modulus (net) (DMA-test)	MPa	EN-ISO 6721-1 ASTM E2254	[b]
Cumulative plastic distortion (creep) (SIM test)	% m/m	ASTM D6992	<3
Tensile force, non-perforated cell wall (wide width)	kN/m	EN-ISO 10319	20–29
Tensile force, perforated cell wall (wide width)	kN/m	EN-ISO 10319	16–25
Adhesion strength internal connections	kN/m	NEN-EN-ISO 13426-1 (part 1 method C)	>17
Height cell wall	mm	–	50–200
Distance between internal connections	mm	–	330–720

Source Geosynthetics for Reinforcement Guideline Standard (Vega et al. 2018)
[a]Available only for Novel Polymeric Alloy (NPA) Geocells
[b]Values depend on application

The Standard defines the following as key properties for design with geocells and how they are verified:

Tensile strength and elasticity at maximum load. "Tensile strength is the force in kN/m that a geosynthetics produces at a certain stretch that is measured in accordance with NEN-ISO 10,319. Elasticity at maximum load is the distortion of that material under maximum tensile load. Details regarding tensile force are particularly useful for the evaluation of the reinforcement function…." (para. 3.6.4)

Stiffness modulus. "The stiffness modulus of a material is a measure of its elastic deformation behavior. The stiffness modulus is an indication of the relationship between the force exerted on a material and the associated elastic deformation. **For all types of bases, from unbound to bound, the elastic deformation behavior is the main mechanical property**. The same applies to subbase reinforcement…. In geocells, the net Dynamic stiffness modulus (DMA-test) is determined in accordance with NEN-ISO 6721-1 or ASTM E2254." (para. 3.6.5)

Creep resistance. "Creep means the non-elastic deformation, which increases with time, of a material under unchanged load. Creep in non-reinforced bound bases is described in (European Committee for Standardization 2004). Creep is unimportant in non-reinforced, self-binding and unbound bases. **If base reinforcement is applied, this material must be examined for its creep properties…** For geocells, the Stepped isothermal method (SIM) in accordance with ASTM D6992 is often used to determine the resistance to creep. (para. 3.6.10)

Tensile force of seams and joints. "Data on the tensile strength of seams and internal joints are necessary for the evaluation of the reinforcement function…. For geocells, the testing method is described in NEN-EN-ISO 13426-1 part 1, with method C1 used. Two cells connected to each other are positioned in an optimal opening condition, after which the cell connection is tested…. The test determines the tensile strength of a joint or seam between geosynthetics." (para. 3.6.6)

14.2.6 Design with Geocells

The design factors and methods relevant to geocell stabilization are discussed in detail in the guideline, including examples; only brief highlights are presented in the following sections.

Base Layer thickness and Reduction. "The layer thickness requirement of a base is always linked to the resistance of a construction (or component thereof) to the applied mechanical load and the dimensional stability of the construction…" (para. 3.5.11) a principle that applies to basic design as well as to reinforcement geosynthetics. Road design with base reinforcement seeks to optimize the base thickness, with the quantity of materials and material properties.

Design Methods: Design Aspects by Mechanical Stress. An inventory study of 17 design methods was carried out and analyzed. The pluses and minuses of each method for each type of design method were evaluated. The following checklist was used (para. 4.2.1):

- Background;
- Model validated to practice measurements, laboratory measurements or otherwise;
- Input parameters;
- Calculation results; output of the method;
- Applicability;
- Type of design method (numerical, empirical or analytical);
- Possibility of input of axle load repetitions.

Unpaved Roads. Resistance to permanent deformation is the most important design criterion. Empirical models are used to determine the base thickness to limit rutting. Both the Giroud-Noiray and the Giroud-Han (Han 2015) models are recommended for the design of base reinforcement of unpaved roads and paving blocks. These models utilize correction factors to express the performance in unpaved roads of specific geocell product, based on experimental studies (para. 4.5.1). The Standard includes a detailed discussion of how to use these models. (para. 4.5)

Asphalt Pavements. "In the design calculation of asphalt pavements, a stiffness modulus is assigned to each construction layer. This load capacity indicator is in many cases not constant but depends on the stiffness of the underlying layers and the layer thickness. **The contribution of base reinforcement is therefore expressed in an increased stiffness modulus**." (para. 4.1) "In this publication, the AASHTO model was (chosen), with some adjustments that take into the account the reinforcement product, the bearing capacity of the substrate or substructure and the stiffness of the layer in which the product is applied." (para 4.2.2). The Standard includes a detailed discussion of how to use these models. (para. 4.7)

Additional Design Factors. The discussion describes the factors to be taken into account, which are beyond the scope of this review: traffic load, importance of construction phase ("The quality of the base is highly dependent on the degree of compaction"), subgrade stiffness, base aggregate stiffness, and substructure stiffness.

Substructure Stiffness. For the subbase, the stiffness modulus is increased by the application of geocells. The improved confinement increases the stiffness of the subbase over the height of which the geocell is effective. **The degree of stiffness increase will depend on the validated Support improvement factor (SIF) and Modulus improvement factor (MIF) values indicated by the relevant supplier (see description below)**

Support Improvement Factor. The reinforcing effect of base reinforcement depends on: (para. 4.4.3)

- the characteristics of the geosynthetics
- the mineral aggregate in which the product is used
- location in the structural pavement.

Limits to the stiffness of a granular layer depend on the thickness and stiffness of the layer under the granular layer. With the Shell pavement design method for asphalt roads, the stiffness of an unbound granular layer is at most four times as large as that of the underlying layer. "The same principle also applies to granular layers with

base reinforcement. The relative stiffness increase will be greater than when using an unreinforced granular layer because of the beam effect (see Fig. 14.2) … The maximum improvement factor of the reinforced layer in relation to the underlying layer is indicated by the Support Improvement Factor." (para. 4.7.2)

For example, "if for a reinforcement product in the subbase, the support improvement factor SIF = 5, this means that the stiffness of the subbase over the effective height of the reinforcement product is up to 5 × the stiffness of the underlying medium. If the base has a stiffness of 30 MPa and the reinforcement is directly on the subgrade, then the stiffness of the reinforced part of the subbase on the basis of the SIF is maximum 150 MPa. For most reinforcement products, the value of SIF is independent of the stiffness of the underlying medium." (para. 4.7.2)

Modulus Improvement Factor. For a geocell with a MIF = 3, this means that the stiffness of the subbase over the effective height of the geocell is three times the stiffness of the mineral aggregate in the unreinforced situation. "The stiffness of mineral aggregate in an unreinforced subbase depends on the bearing capacity of the subgrade and the layer thickness of the subbase. With increasing values of bearing capacity of underlying medium and increasing layer thickness of the subbase, the stiffness of a subbase in an unreinforced situation increases. Figure 14.3 clarifies this relationship." (para. 4.7.2)

Zone of Confinement. "Geocells with rigid walls have a reinforcing effect over the entire height of the geocell…. the height of the geocell (is) the effective height plus two cm of mineral aggregate above the geocell. Above that, the reinforcing effect slowly decreases and at a distance of six to eight times the maximum grain diameter from the top geocell, it will no longer be detectable or present. If this type of geocells is placed somewhere halfway in the (sub)base, the direct reinforcing effect is also

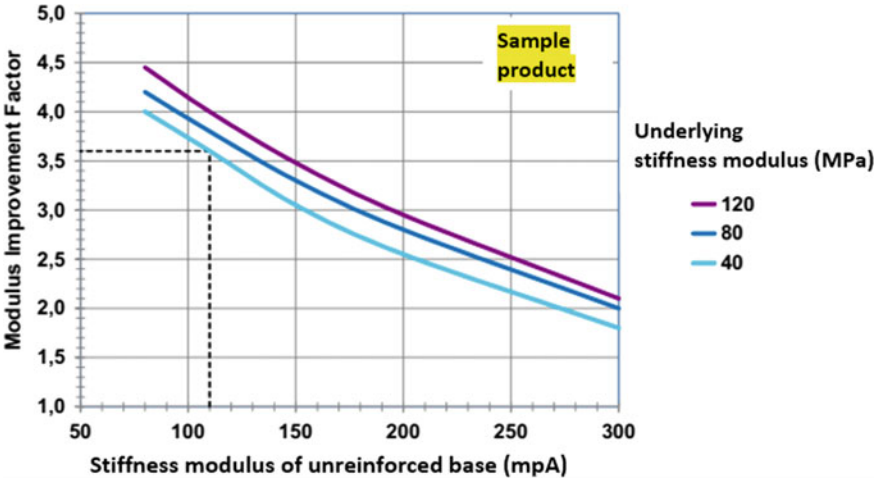

Fig. 14.3 Relationship of MIF and stiffness of substructure and base. *Source* Geosynthetics for Reinforcement Guideline Standard (Vega et al. 2018)

visible and can be added to the two cm under the cells. In geocells with flexible walls, the full reinforcing effect usually extends over the total height of the geocell minus the upper cm." (para 4.7.2)

14.2.7 Design Example—Mechanical Stabilization of Subbase

The subbase or base or both can be mechanically stabilized by applying base reinforcement. The stiffness modulus of a subbase or base is increased by the application of geocells…. The design procedure is similar for both. The extent to which reinforcement in the subbase can increase the stiffness modulus of that layer depends on the working height of the reinforcement and the factors SIF and MIF.

The definition of the reinforcing effect of the subbase is explained by the example in Fig. 14.4 (para. 4.7.3).

- The product is applied to the subgrade, i.e., in the lowest part of the subbase.
- The effective working height of the geocell is 200 mm.
- The manufacturer of a rigid geocell sets the SIF = 5 and MIF = 3.
- The dynamic stiffness of subgrade is 40 MPa.
- The stiffness modulus of the sand can be up to 200 MPa.
- Compacted sand of 750 mm (C1) and 500 mm (C1) for control sections.

***NOTE**: The values for SIF and MIF given in the example serve solely to clarify the design procedure. In practice, products are available with both higher and lower values for SIF and MIF.*

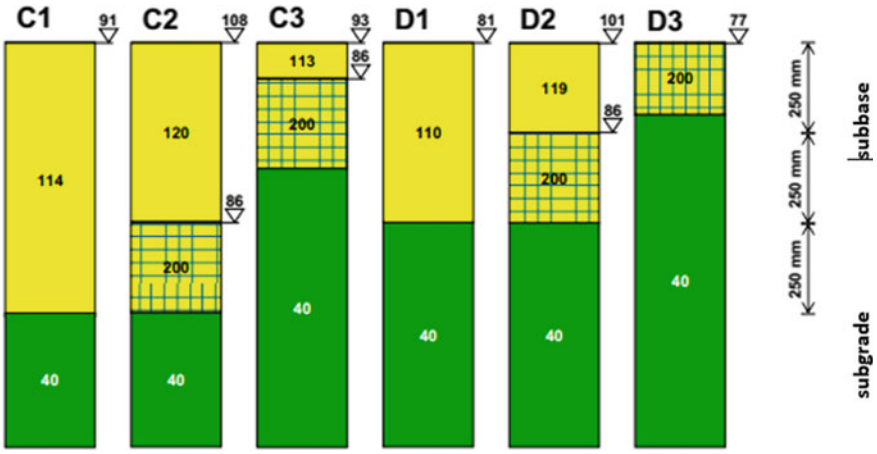

Fig. 14.4 Example of subbase stabilization. *Source* Geosynthetics for Reinforcement Guideline Standard (Vega et al. 2018)

***NOTE**: The numbers indicate the dynamic stiffness moduli of the sublayers, subbase and the subgrade in MPa. The value in the triangle is the equivalent stiffness modulus of the entire substructure.*

Discussion. The equivalent stiffness (measure for bearing capacity of substructure) for the both subbase thicknesses (C2, D2) increases by 20% with geocell reinforcement. However, sections C3 and D3 show that layer thickness of the subbase can be halved with equal total load bearing capacity. In practice, it is of course possible to opt for an interim solution between improving the bearing capacity and reducing the layer thickness of the subbase. Once the stiffness moduli are per layer, these can be used in pavement design software as input variables to further complete the design of reinforced asphalt pavement. (para. 4.7.3)

***Note**: this applies to the example presented. In practice, far better performance may be achieved by optimally showing the performance of the base reinforcement in the design.*

Additional examples are given in the Standard for both geocells and geogrids showing the impact of reinforcement in different locations in the pavement structure. The optimal location of the (sub) base reinforcement depends strongly on local conditions and if the design objectives are to reinforce soft subgrade, increase base layer stiffness and/or reduce layer thickness. The design calculation of mechanical stabilization in the base is done the same way as for the subbase.

14.2.8 Summary

The previous section presented translated highlights of the new "groundbreaking" Geosynthetics for Reinforcement Guideline Standard for reinforcement geosynthetics. The Standard consolidates the current knowledge about Geocell design principles, properties and mechanisms of reinforcement to bring a more unified understanding of the use of Geocell technology in roadway reinforcement.

The following two sections present an unofficial glance of geosynthetic/geocell guidelines under development by the ISO and ASTM organizations.

14.3 ISO/TR 182828 Working Document: Design Using Geosynthetics: Part 5—Stabilization

14.3.1 Introduction

The ISO Technical Committee TC 221 is currently developing an all-inclusive Design Using Geosynthetics Standard that covers the gamut of functions from separation and drainage, through stabilization, erosion control to asphalt overlays (Corbet and Cazzuffi 2016). Stabilization Geosynthetics are described in Part 5, which includes

both geogrids and geocells, despite their differing stabilization mechanisms (ISO Standard WD TR 18228-5 1822). The ISO standard defines the fundamental principles of stabilization as "improving the mechanical properties of unbound granular material by geosynthetic layers that reduce deformation of applied loads." While not yet published, a brief unofficial overview of the draft Guide is presented below (all rights reserved by ISO).

14.3.2 Main Principles and Mechanisms

Stabilization is achieved by **confinement** of particle movement (or tensioned membrane effect for planar geosynthetics). According to the ISO Standard, confinement is **internal**, via soil-friction interlock for a Geogrid, or **external** via lateral restraint that mobilize hoop tension forces on Geocell walls.

The concepts of serviceability and ultimate limit states are incorporated in the principles. The goal is to effectively withstand service loading, control deformation within service requirements, and do so over time. The design life of the project is proposed as a key design consideration, which means limiting the rate and level of deformation of the geosynthetic stabilization accordingly. The standard states that confinement operates most effectively at relatively low levels of strain 1–2%. Geocells have shown to stiffen granular materials by 3D confinement, thereby increasing the modulus of the stabilized layer; this is the Modulus improvement factor (MIF).

14.3.3 Principles of Design

The Standard describes a number of different **design scenarios** for the stabilization of the base and/or subbase for pavements, rail track bed and working platforms. Whereas geosynthetics are not generic, their inclusion in empirical design methods needs to be based on empirically obtained evidence, e.g., layer modulus improvement factor provided by field and full-scale laboratory testing of the specific product using the relevant aggregate and loading for the application.

The discussion of design objectives includes: bearing capacity improvement, settlement control, reduction in deformation from trafficking (elastic stiffness, modulus improvement), reduction in aggregate degradation and extension of design life. These should be based on full-scale validation and calibration of geosynthetic, e.g., via Accelerated pavement testing (APT), and integration in design approaches.

- **Design factors** are product and project specific, and normally evaluated by performance testing. This includes a wide range of properties and parameters of the cell material, but not limited to cell geometry, infill, loading, location in pavement

and distribution of lateral and vertical stresses (which depends on initial geocell properties and long-term resistance to deformation).

- **Design methods** for unpaved roads and railway aggregate on soft soils include Giroud-Han (2004), Leng-Gabr (2006) and Rimoldi (2012) modified for geocells, while the paved road may be based on Mechanistic-Empirical Design method using the layer elastic model, incorporating the MIF– obtained through performance testing.

14.3.4 Key Properties for Geocells

In addition to the geocell geometry, the ISO Standard cites the material properties of the geocell as a key attribute in design, which seeks to maximize the magnitude of mechanical stabilization for the project design life. The two essential performance properties are elastic stiffness and resistance to permanent deformation, in addition to the regular properties of junction strength, friction, etc. The stiffer the geocell, the higher the hoop tensile strength will be and thus the higher the MIF.

The Standard states that the key properties should be validated by standard test methods to ensure the design performance for the entire project design life:

- Strip Tensile Strength—wide width with perforated cell walls (ISO 10319) and junction strength (ISO 13426-1 Part 1, Method C)
- Dynamic Stiffness—elastic modulus by Dynamic Mechanical Analysis (ISO 6721-1/ASTM E2254)
- Accelerated Creep Deformation using Stepped Isothermal Method (SIM) (ASTM D6992 modified for geocells)
- UV, Durability (HPOIT—ASTM D5885 @ 150 °C), and Seam test is also included (ISO 13426-1 Part 1, Method C).

To ensure the design life of the geocell-stabilized layer these material properties (tensile, dynamic stiffness and creep) must ensure low deformation of the cell walls, i.e., less than accumulated 2%. A higher value may invalidate stabilization. The influence of geometry, texture and perforation pattern and their impact on the magnitude of mechanical stabilization is also discussed.

The Standard emphasizes that the performance testing should include laboratory test, large-scale moving wheel test and on-site monitored field trials. The improvement factors are based on the tests for each specific geocell type (material and geometry).

14.4 ASTM Working Document K61159: Standard Guide for Use of Geocells in Geotechnical and Roadway Projects

14.4.1 Introduction

Recognizing that there is currently no guide for the use of geocells in geotechnical projects, the ASTM D35.01 technical subcommittee is developing a standard guideline for use and design of geocells in ground improvement and earth stabilization applications (D8105-18 2018). The guide presents the key Geocell design principles, properties, mechanism, and methodologies for geotechnical applications. "This guide is intended to cover basic considerations for the use of geocells in various geotechnical and roadway projects to bring a more unified understanding of the most efficient and appropriate ways to utilize this type of ground improvement technology for a variety of geotechnical-related applications." While not yet published, a brief unofficial overview of the draft Guide is presented below (all rights reserved by ASTM).

14.4.2 Overview of Technology

The primary benefit of geocells according to the ASTM Standard is to increase the stiffness of a stabilized layer by the addition of tensile strength at low strain levels. The geocell dimensional stability limits volumetric changes to prevent settlement. This is achieved by limiting accumulated permanent strain of the cell walls for the entire project design life.

In addition to the description of the geocell characteristics and how it works, the Standard states that the material properties of the geocell are key parameters in geocell design. These include: (1) dynamic tensile stiffness, (2) tensile wall strength, (3) resistance to permanent deformation, and (4) environmental durability. Resistance to permanent deformation depends upon the long-term retention of these key properties and geometry. Adequate tensile stiffness of the geocell polymeric material ensures that elastic deformations under loading are limited.

The geocell properties are determined by standard test procedures and performance testing, including accelerated methods to ensure long-term performance: These are presented as the following: (1) elastic/dynamic tensile stiffness of the polymeric material (ISO 6721-1, ASTM E2254); (2) tensile strength of the cell wall with and without perforations (ISO 10319, ASTM D4595) and seam connection strength (ISO 13426-1); resistance to accumulated permanent deformation (i.e., creep resistance) of the cell wall (ASTM D6992); and resistance to ultra-violet degradation (ASTM D7238) and oxidation degradation (ASTM D3895 or ASTM D5885) by accelerated methods.

14.4.3 Design for Applications

The guideline describes the major considerations associated with the design of geocell in the main application areas: load support, retaining walls, slope and channel protection. The key attributes of the geocell for design and the magnitude of confinement in all the applications are: dynamic elastic stiffness and tensile strength, resistance to permanent deformation, geometry, and environmental durability. Permanent hoop strain should not exceed 2% over the design life to maintain sufficient stiffness, stabilization and limit settlement. The role of additional influencing factors, such as friction, perforations, infill and compaction are discussed for each application as well.

Load Support. The discussion of load support function—road, railway, heavy-duty pavement and embankment applications—begins with the primary support mechanism. This is described in short as lateral restraint of the soil particles subject to vertical stress from vehicles. The geocells add tensile strength (apparent cohesion) to unbound infill materials thereby creating a stiffer stabilized layer. Stress to layers below the stabilized layer is decreased while support to the layers above is increased. Vertical deformations and settlements are limited.

An example is given that illustrates the significance of limiting hoop strain to 2% on the geocell walls, by showing how the increase of the geocell wall perimeter increase in vertical settlement of infill material. Additional factors in the design of geocells for load support applications include the location in the pavement, load spread angle, cell dimensions and density, zone of influence, aggregate confinement and the slab/mattress effect.

Retention Walls. For retaining structures in unstable slopes, the Standard defines the primary support geocell mechanism is mechanical soil stabilization. This creates a stable soil mass that resists soil pressure, loads and seismic forces through tensile hoop forces developed on the geocell walls. The geocell attributes for design are similar as those listed above for load support applications—tensile stiffness and strength, resistance to permanent deformation and geometry. Environmental durability is also required to ensure the protection of these three parameters throughout the design life. Whereas the long-term resistance to strain accumulation is critical in retaining wall structures, testing including accelerated methods is necessary to characterize the geocell long-term deformation properties. The Guidelines also discuss in influence of cell geometry, geocell creep resistance (limited to less than 2%), and benefits of planar reinforcement.

Erosion Control and Channel Protection. The primary support geocell mechanism on inclined slopes is mechanical soil stabilization acting that holds infill soil in place against sliding and tractive water forces. The same key attributes are used to determine the suitability of the geocell to the design: tensile stiffness and strength, resistance to accumulated permanent deformation, geometry and environmental durability. The constraint to limit creep strain to 2% over the design life is included here as well, in order maintain geometry and confinement.

14.5 Performance Testing Methods

The Geocell Standards described above recommend specific performance testing to validate the long-term capability of the geocell. These include the following, which are described below:

- Elastic/dynamic tensile stiffness of the polymeric material (ISO 6721-1, ASTM E2254)
- Resistance to accumulated permanent deformation (i.e., creep resistance) of the cell wall (ASTM D6992)
- Wide-width tensile strength of the cell wall—with and without perforations (ISO 10319, ASTM D4595); tensile strength of seam connection strength at an opening angle representative of the installed angle (ISO 13426-1, Part 1—Method C)
- Resistance to UV and oxidation degradation by accelerated methods (ASTM D5885).

14.5.1 Elastic/Dynamic Tensile Stiffness of the Polymeric Material (ISO 6721-1, ASTM E2254)

Dynamic mechanical analysis DMA is a technique that measures the viscoelastic properties of polymeric materials as a function of temperature, frequency, stress and/or time. This method is widely used in the automotive, electronic, military as well as other geosynthetics industries, and is supported by ASTM and ISO standards.

Simulating elastic versus plastic behavior is important to ensure performance in long-term applications, as polymers tend to lose elastic modulus (stiffness) over time, particularly under dynamic loading, and enter the plastic (viscous) range (Pokharel et al. 2018).

A geocell system must maintain its stiffness and elastic properties without permanent deformation or loss of geometry, which could result in a loss of confinement, settlement, fatigue and/or failure.

The DMA determines the pure stiffness in the elastic region of a polymer plastic, that is the ability to apply loads on the system without permanent deformation. This accelerated method validates that the elastic modulus of a geocell is sufficient for stable elastic behavior under dynamic cyclical loads typical of roadways, railways and heavy-duty applications. A high dynamic elastic behavior allows the engineer to design a geocell application with higher stress, lower settlements, higher resistance to fatigue and higher Modulus improvement factor (MIF) (Corbet and Cazzuffi 2016).

14.5.2 Resistance to Accumulated Permanent Deformation (Creep Resistance) of the Cell Wall (ASTM D6992—SIM)

The Stepped isothermal method (SIM) was developed for the space, military, automotive industries to predict the creep rate of polymers based on Time-temperature superposition (TTS). The test measures the cumulative plastic deformation of a polymer product at constant load by incrementing the temperature (representing time) in steps. For example, in Step 5 at 51 °C, one (1) test hour = 100,000 h of use (4166 days or 11 years). The creep reduction factor is extrapolated from the time-temperature data in the test by means of master curves. Time-temperature models are useful to extrapolate the results of the creep test to creep values for design purposes (Koerner et al. 2016).

In a modified version of the test to make it simpler, faster and cheaper, the accumulated plastic deformation of a geocell is measured under constant load. The test is limited to three temperature steps, from 44 °C through 51 to 58 °C. The test load depends on the typical loads in the application of the geocell (unpaved road, highway pavement, railway ballast, etc.).

The SIM tests the accumulative permanent strain on the material, with a constant load, in incremental changes in temperature (steps) from 23 °C (ambient) to 65 °C in increments of 7 °C. Each step lasts 167 min, after temperature ramp up time and is plotted. Results for permanent deformation can now be generated in a day or less.

Creep is permanent deformation over time. Unlike elastic behavior, permanent (creep) deformation does not occur suddenly under the application of stress. Instead the strain accumulates as a result of sustained stress. Thus, permanent (plastic) deformation is the **time dependent** strain of the stressed material under evaluation.

The SIM test gives the ability to test, measure and calculate how a material will perform over an extended period, representing tens of years of service life. The relationship between (tension) creep and project design life and infill settlement can be plotted. The test sample is modified for geocells to a full wide-width section, which includes the entire strip width (height of cell) to include the perforation pattern in its entirety (Fig. 14.5).

Failure is defined as >3% total creep due to the loss of confinement of the cell and subsequent loss of compaction. Creep in typical HPDE geocells can be acute and may reach failure within 1.9 years in moderate loads, while other geocells made from novel polymeric alloys exhibit less than 3% creep well beyond 75 years (PRS Geo-Technologies 2016).

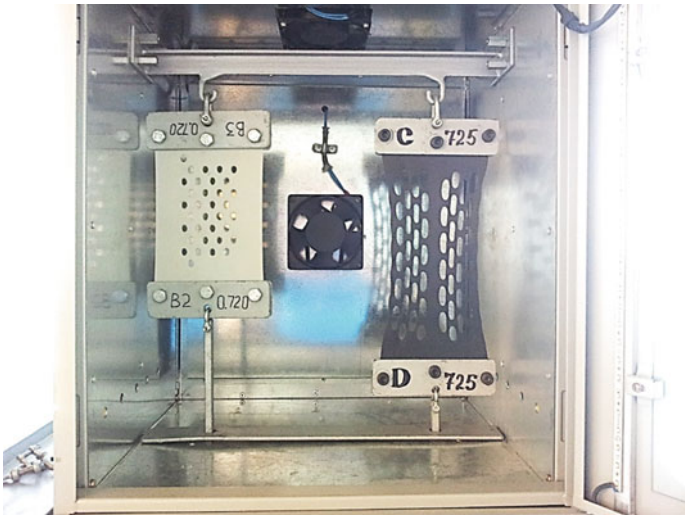

Fig. 14.5 Two geocell types in SIM environmental test chamber: Novel polymeric alloy geocell on left, HDPE geocell on right showing permanent deformation in temperature superposition. *Source* PRS Geo-Technologies

14.5.3 Wide-Width Tensile Strength of the Cell Wall—with and without Perforations (ISO 10319, ASTM D4595); Tensile Strength of Seam Connection Strength (ISO 13426-1, Part 1—Method C)

The tensile strength test is performed by standard extensometer device and test methods. The tensile strength and strain at maximum load (in %) are recorded and normalized for the thickness. This procedure is modified for geocells by using "wide-width" sample size-dimensions that include the representative distribution of the strip wall perforations (from seam to seam). A longitudinal force is applied to the test specimen at a constant strain rate at 100 mm/min—until the specimen ruptures. The test is carried out until the yield point, which indicates the geocell material strength.

The seam weld (joint/connection) strength uses Part 1 method C: SPLIT of the ISO 13426-1. This method best simulates the actual vectors of stresses the tested product is subject to in the field. An *X*-shaped sample is cut from the geocell and wrapped round two rollers in a jig apparatus clamped to the tensile test machine. The test is conducted at rate of 100 mm/min until a tensile split failure of the weld occurs.

14.5.4 Resistance to UV and Oxidation Degradation by Accelerated Methods (ASTM D5885)

Stabilizers (from the Hindered amine light stabilizers (HALS) family) are added to geocells to intercept the oxidation reaction within the polymer and prevent polymer degradation, and degradation of the mechanical properties. The stability of the additives to resist environmental conditions that can deplete the stabilizers—UV radiation, high temperature, and oxidative processes in air, water and soil—is measured by ASTM D5885: High-Pressure Oxidation Induction Time (HPOIT). This method is similar to OIT testing on a small sample strip but heated only to 150 °C under elevated pressure in a High-Pressure Differential Scanning Calorimetry (HP-DSC). As the heat consumes the stabilizers, the material begins to combust. The more stabilizer in the product, the longer the reaction time—and service life—will be.

14.6 Conclusion

Recently published and soon-to-be published standard guidelines for the design and use of geocells in road base reinforcement are a significant milestone. The design factors, principles and methodologies in these standards enable design engineers to determine the added value of reinforcement geosynthetics (geocells and geogrids) to subgrade/subbase soil stabilization and base layer reinforcement.

Although developed independently, the discussions guidelines and conclusions of all three reviewed standards are quite similar. A key conclusion of all three is that the extent of the reinforcing or stabilizing effect is determined by the material from which the product is made (and its geometry). The standards are in agreement that the most important material properties of geocells are elastic stiffness and resistance to permanent deformation (creep), as well as tensile strength. This is due to the limit on plastic deformation for reinforcement synthetics defined as less than 2%. The actual effectiveness of geocell reinforcement is reflected in the Support improvement factor (SIF) and the Modulus improvement factor (MIF). In addition to describing the specific geocell properties and functions of geocell reinforcement, the standards cite the recommended international tests to evaluate geocell performance parameters.

These standards will make current knowledge and experience available to private industry and government professionals to optimize geosynthetic reinforcement for pavements in general, and geocell reinforcement in particular, to help achieve the goal of more reliable, cost-effective and sustainable infrastructure for tomorrow today.

References

AASHTO (2010) Standard practice for geosynthetic reinforcement of aggregate base course of flexible pavement structures, R50-09, Standard specifications for transportation materials and methods of sampling and testing, 31st edn, American Association of State Highway and Transportation Officials, Washington, DC, 4 p

Berg RB, Christopher BR, Perkins S (2000) Geosynthetic reinforcement of the aggregate base/subbase courses of pavement structures—GMA White Paper II; AASHTO Technical Committee 4E, Geosynthetics Materials Association, Roseville, MN, 176 p

Christopher BR, Schwartz C, Boudreau R (2006) FHA/NHI-05-037 Geotechnical aspects of pavements (132040). https://doi.org/FHWANHI-05-037. https://www.fhwa.dot.gov/engineering/geotech/pubs/05037/index.cfm

Corbet SP, Cazzuffi D (2016) CEN/TC189 and ISO/TC 221—European geosynthetics: the current developments and international standards for CEN/TC189 et ISO/TC 221—Normes Européennes et Internationales Pour Géosynthétiques: Les 2493–2496

ASTM D8105-18 (2018) Standard guide for use and application of geosynthetic reinforcement reduction factor test results, ASTM International, West Conshohocken, PA, 2018, https://www.astm.org. Unpublished document under development

European Committee for Standardization (2004) Eurocode 7—Geotechnical design—part 1: general rules. En 1997-1 1, 168. https://doi.org/10.1680/igeng.1997.28998

Han J (2015) Principles and practice of ground improvement. Wiley, Hoboken, NJ

Hegde A (2017) Geocell reinforced foundation beds-past findings, present trends and future prospects: a state-of-the-art review. Constr Build Mater 154:658–674. https://doi.org/10.1016/j.conbuildmat.2017.07.230

Hughes WP, Laryea S (2009) Standardization of procurement: national or international? In: Cerić A, Radujković M (eds) CIB joint international symposium: construction facing worldwide challenges. Dubrovnik, pp 742–751

ISO Standard WD TR 18228-5 (2018) Design using geosynthetics—part 5: stabilization. In: International Organization for Standardization, Geneva, Switzerland. Unpublished document under development

Koerner R, Koerner G, Hsuan Y (2016) Creep tension testing of geosynthetics (610)

Pokharel SK, Schary Y, Kief O (2018) Evaluation of the elastic modulus of geocells for structural contribution in pavement stabilization. Unpublished manuscript

PRS Geo-Technologies (2016) Internal QA lab test data, 10 Jan 2016

PRS Geo-Technologies (2018) Internal correspondence, Oct 2018

Vega E, Van Gurp C, Kwast E (2018) Geokunststoffen als funderingswapening in ongebonden funderingslagen (geosynthetics for reinforcement of unbound base and subbase pavement layers), SBRCURnet (CROW), Netherlands. CRW C1001 (in Dutch)

Zornberg JG, Gupta R (2010) Geosynthetics in pavements: North American contributions. In: 9th international conference on geosynthetics, Brazil, vol 1:379–98

Chapter 15
Case Studies on Geocell-Based Reinforced Roads, Railways and Ports

Yitzchak Schary

Abstract Although geocells have been around for more than half a century, only recently were they adopted for heavy-duty infrastructure projects. This is due to a better understanding of geocell technology and to the creation of a novel polymeric alloy (Neoloy®) for geocells with high elastic modulus, low permanent deformation and high tensile strength. Case studies of Neoloy-based geocells used in airport, feeder road, railway and port projects demonstrate their suitability for long-term base reinforcement of heavy-duty pavements. These geocells show an improved engineering performance in terms of subgrade bearing capacity, layer stiffness and fatigue resistance beyond conventional geocells. The result is sustainable, stronger and stiffer pavements with an extended lifespan and lower maintenance.

Keywords Airport pavement · Rural road · Railway · Port platform · Heavy-duty pavements · Base reinforcement · Soil stabilization · Neoloy · Geocells

15.1 Introduction to Neoloy Geocells

Geocells are a proven soil stabilization and reinforcement solution used for over five decades for problematic soils, challenging environs and where aggregate is scarce. Yet their adoption by the civil engineering community was not widespread due to a lack of basic research, testing standards, design methodologies and R&D in advanced polymeric materials. This changed about 15 years ago with the introduction a novel polymeric alloy, Neoloy® that improved the key geocell performance factors, accompanied by a surge in experiential and field studies, published papers, the development of design methodologies, and more recently, international guidelines and testing standards. The Neoloy Geocell was developed specifically with performance properties to meet the demands of heavy-duty pavements: high elastic modulus, creep resistance and tensile strength. These provide the geocell with reliable dimensional stability,

Y. Schary (✉)
PRS Geo-Technologies, 4 Kaufman St., Tel Aviv, Israel
e-mail: yitzchak@prs-med.com

T. G. Sitharam et al. (eds.), *Geocells*, Springer Transactions in Civil and Environmental Engineering,
https://doi.org/10.1007/978-981-15-6095-8_15

Table 15.1 Neoloy parameter properties evaluated by standard testing procedures (source PRS Geo-Technologies)

Performance parameter	Value	Description	Standard
Elastic stiffness (dynamic modulus)	>500 MPa @ 60 °C	DMA—dynamic mechanical analysis	ASTM E2254, ISO 6721-1 (DMA)
Permanent deformation (creep resistance)	<3% deformation at 75 years	SIM—stepped isothermal method	ASTM D-6992
Tensile strength	>19 kN/m	Wide-width method	ISO 10319:2015
Environmental durability	>1600 min	HPOIT—high pressure oxidative induction time	ASTM D5885 @ 150 °C

confinement and compaction for the entire lifespan of infrastructure projects (Table 15.1) (Kief et al. 2014).

Four case studies of Neoloy-based geocell reinforcement of heavy-duty, permanent pavements are provided in the following sections for airport, unpaved feeder road, railway and port platform projects.

15.2 Case Study A: Ground Reinforcement for New International Airport Roadways, Mexico

See Figs. 15.1, 15.2 and Table 15.2.

15.2.1 Introduction

Construction of the New International Airport Mexico City (NAICM) airport—one of the world's largest—on unstable, saturated and sinking clay mud of the ancient Lake Tenochtitlan lakebed is an enormously challenging geotechnical engineering project. Conventional soil stabilization and construction methods were insufficient, too costly or time consuming. After extensive trials, Neoloy Geocells were selected as the best qualified solution with the required performance that met the soil conditions.

15.2.2 Soil

The soil has high-water content with little capacity to support large loads. In addition, the area is seismic, and the effects of ground movement are magnified by the soil

Fig. 15.1 Soil stabilization of poor subgrade with Neoloy Geocells. *Photo credit* Innovater

Fig. 15.2 Neoloy Geocell stabilized asphalt pavement roadways. *Photo credit* Innovater

type in the area. Finally, the site is subject to substantial settlement over time, from groundwater extraction for the drinking water supply of the city.

The upper layer of this soft soil is a very thin layer (20–25 cm) of clay with a 1% CBR. Under this, is a 30–60-m deep layer of clay mud with a 0.6% CBR. This consolidated mud layer makes road building extremely difficult, the soil is extremely soft, saturated and highly plastic with wet-dry cycles that cause extensive potholes and cracking of the surface. A high groundwater level, coupled with high seasonal

Table 15.2 Case Study A: Project Snapshot

Description	Neoloy Geocell ground reinforcement and soil stabilization for heavily trafficked asphalt paved roads on very soft soil
Subgrade soil	20–25 cm clay with 1% CBR 30–60 m layer of clay mud with 0.6% CBR
Client	New International Airport, City of Mexico (NAICM) Authority
Project design	Innovater, Innovciones en Terracerias S.A. DE C.V., Mexico
Achievements	• Soil stabilization on extremely weak soil • Use of local volcanic rock for structural infill lowered weight of pavement by 60% • Reduced construction time by at least one year • Eliminated need for soil replacement • Lower construction costs
Date	Phase I and II—September 2015–June 2017
Keywords	Airport, clay mud, geocell, stabilization

Source PRS Geo-Technologies

rains, creates even more complicated ground conditions, limiting the mobility of construction trucks and equipment.

15.2.3 Conventional Solutions

Due to the extremely soft and deep clay soils, conventional road pavements were unfeasible—the weight of a pavement thick enough for the required traffic and loads on the compressible soil would actually cause it to sink, not to mention the costs.

Soil removal and replacement were also unfeasible as the 4.4-ha size of the site and the extreme 30–60 m depth of the problematic subgrade would have meant years of earthmoving, and unacceptable delays in the project timeline (Fig. 15.3).

Chemical soil stabilization was also ruled out due to problematic application—the application equipment breaks the upper crust and sinks in the soft mud—as well as concerns about curing time, durability, environmental impact and high costs.

Geosynthetic mechanical soil reinforcement appeared to be the only feasible choice. A geogrid-based solution comprised of a non-woven geotextile and two geogrid layers were tested in field trial sections. However, these also failed: the geogrids ruptured, the surface developed multiple potholes and loaded trucks sunk in the soil unable to traverse the road surface.

High-density polyethylene (HDPE) geocells were considered. The geocell confinement restricts lateral movement and deformation of the infill resulting in increased stiffness of the layer. However, questions arose about the suitability of HDPE-based geocells for this project as the design life was for a perpetual pavement– 50-year lifespan. HDPE geocells have low elastic stiffness (<600 MPa @ 45 °C), high creep and relatively low tensile strength (<11 kN/m).

Fig. 15.3 Loaded truck in section reinforced with geogrids (left) versus section reinforced with Neoloy Geocell (right). *Photo credit* Innovater

15.2.4 Neoloy Geocell Solution

A geocell based on Neoloy was proposed to the ground engineering experts of the NAICM airport authority by Innovater—Innovciones En Terracerias S.A. DE C.V, as the best available solution. Neoloy® is an advanced polymeric alloy developed by PRS, based on polyimide in a polyolefin matrix. The NAICM authorities examined the key properties for geocell reinforcement:

- Dynamic stiffness for cyclic loading at low-level elastic deformation
- Creep resistance for low-level accumulated plastic deformation less than 2%
- Radial tensile strength to withstand hoop stresses.

These properties are similar to those cited in a recently published guideline standard for geocells in road building, published by the SBRCUR/CROW road building and transportation research and standard institutes, Netherlands (Vega et al. 2018): "The most important material properties are the elastic stiffness and the resistance to permanent deformation (creep)…. Materials that exhibit a lot of creep will gradually lose their reinforcing capacity over time."

The Neoloy Geocell properties enable an optimum performance of the airport pavement for the entire 50-year design life: For example, the improvement factor in geocell design is based on a maximum deformation of cell wall less than 2–3%. A volumetric increase of the cell beyond that may cause infill to settle, thereby invalidating the design.

Engineering proofs of testing were conclusive. Results of a comparative stepped isothermal method (SIM) accelerated-creep test (ASTM D6992 modified) under heavy loading (6.1 kN/m) show that permanent elastic deformation of a high-quality HDPE geocell was 22.5% after only 4.5 months, as compared to deformation of a Neoloy Geocell of 1.2% after 75 years (see Fig. 15.4).

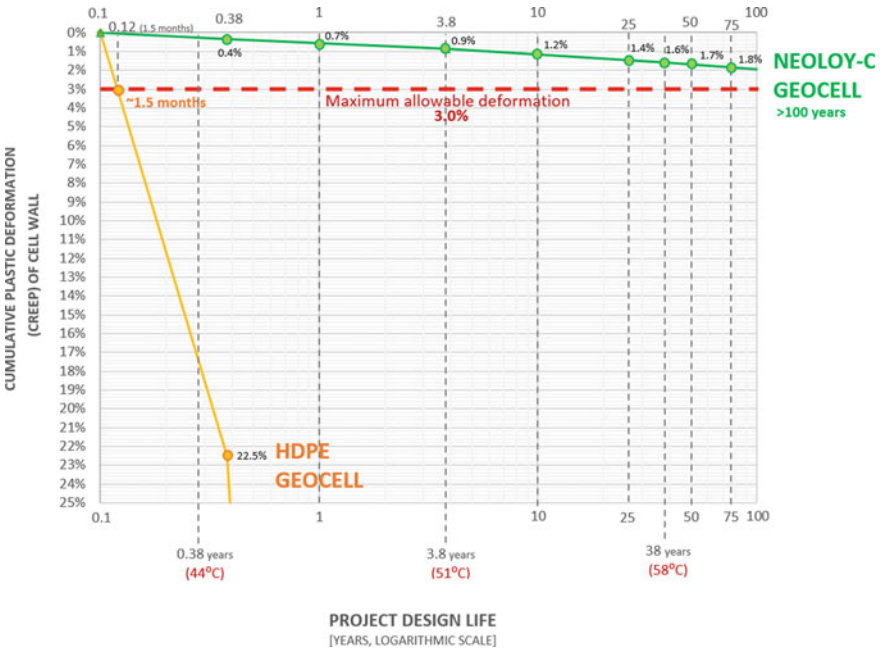

Fig. 15.4 SIM test results showing time (temperate) versus plastic deformation (max. allowable = 3%) under constant heavy-duty load (6.1 kN/m); test method ASTM D6992 (SIM). *Source* PRS Geo-Technologies

Of significance to the NACIM project is the locally available but low strength, ungraded, lightweight Tezontle volcanic rock. The Neoloy Geocell improves the modulus of Tezontle by a factor of 3.5 enabling its use as infill material. This very lightweight of the volcanic stone contributes to a significant reduction in the overall weight of the pavement and optimizes the entire design.

In addition, the Neoloy Geocell with Tezontle infill had previously demonstrated excellent results in apron and platform pavements in the current Mexico City Airport. Consolidated settlements were reduced from an annual average of 18 cm to zero settlement over a period of 4 years.

After a four-month field trial by NAICM involving 45-ton loaded trucks × 60 passes per day, the Neoloy Geocell-reinforced roads evidenced no surface deformation, potholes or settlement. Based on the trial and the factors described above, the NAICM authorities concluded that Neoloy Geocells were the best available solution for soil stabilization and ground improvement (Fig. 15.5).

Fig. 15.5 Compaction of volcanic rock infill, during installation of NPA Geocell in swampy soil. *Photo credit* Innovater

15.2.5 Design and Construction

The design of a typical pavement section is illustrated below (Fig. 15.6).

A "sacrificial" geogrid layer on the subgrade is a key component of the NAICM solution. The geogrid acts as a working platform, to improve the reinforcement factor

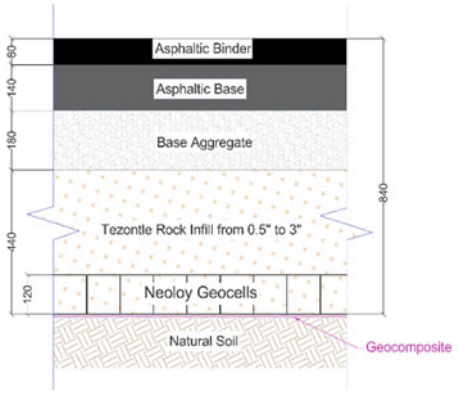

Pavement Structure Design (typical)

- 8 cm Asphalt Wearing Surface
- 14 cm Asphalt Base
- 18 cm Aggregate Base Layer
- 32 cm Tezontle rock infill
- 12 cm Neoloy-330-120-C
- Biaxial Geogrid
- Non-woven Geotextile

Fig. 15.6 Typical Neoloy Geocell-reinforced pavement section for NAICM. *Source* Innovater

of the geocell installed above it. This hybrid geosynthetic combination exceeds the sum of its separate parts to maximize the reinforcement factor.

The first phase of 34 km of the airport road networks was built in 2016–2017. After clearing and grading, the geotextile and geogrid are installed over the subgrade layer. Next, the Neoloy Geocell sections were unfolded, fastened, expanded and staked on both sides of the roadway routes. The geocells were then infilled with 12 cm of Tezontle rock infill (0.5″ to 3″) with an additional 3 cm minimum overfill and compacted by standard procedures. The remaining subbase layer and base layer with high-quality aggregate were then constructed, with the asphalt concrete surface layer paved on top. Standard road construction quality control tests were used.

It is important to note that Neoloy Geocells were installed in all-weather conditions and continued throughout the 6-month rainy season—adding more economic value to the solution.

15.2.6 Results

The performance of the newly constructed asphalt roads exceeded the design requirements of the airport engineering—negligible settlements, with no evidence of rutting, hollows or bumps.

Quality control testing on the asphalt layer (surface deflection) verified that pavement structural layer stiffness and modulus increased by 3.5 times. This results in less deformation, thereby increasing the time between maintenance cycles by four times.

The use of local Tezontle rock as infill material increased the sustainability of the project immensely. It lowered the environmental impact of the construction—less quarrying, hauling, fuel pollution, carbon—aligning it with the NAICM goal to achieve the world's first sustainable airport.

The above case study demonstrated how innovative Neoloy Geocell technology and its contribution to building sustainable roads, highways and infrastructures.

15.3 Case Study B: Stabilization Feeder Roads, UN, South Sudan

See Figs. 15.7, 15.8 and Table 15.3.

Fig. 15.7 Installation of Neoloy Geocell on rural feeder road project, UN. *Photo Credit* UNOPS

Fig. 15.8 Neoloy Geocell-reinforced rural feeder road, UN. *Photo Credit* UNOPS

15.3.1 Introduction

One of the least developed countries in the world, the new country of South Sudan faces enormous challenges. Large parts of the country lack basic road infrastructure,

Table 15.3 Case Study B: Project Snapshot

Description	Creation of basic road infrastructure to provide security, aid and opportunity in remote regions of South Sudan characterized by poor site conditions, undeveloped markets, and political and food insecurity
Subgrade soil	Sand, loam and clay soils, 7% CBR, isolated marshland
Client	UNOPS—United Nations Office of Project Services, South Sudan
Project design	WSP|Parsons Brinckerhoff, South Africa
Results	• Helping people—sustainable access for food, aid, security and regional development • Permanent road achieved using local soil materials • 50% cost savings compared to conventional design • 35% reduction in installation time—all-weather construction (and all-weather use) • Sustainable objectives achieved—environmental and social
Date	December 2016 through February 2017
Keywords	Gravel road, road design, Sudan, UNOPS

Source PRS Geo-Technologies

which severely impacts all aspects of life: farming and economic opportunities are impeded, political-security situation becomes more perilous and displaced people and ensuing food crisis are more acute.

A vital strategy to address the chronic food insecurity, improve livelihoods and stimulate rural development is to improve the rural road infrastructure and provide sustainable access to markets. It is also critical for essential aid to get to those in need.

The United Nations Office of Project Services (UNOPS) together with the South Sudan government and the European Union (EU) established the 'Feeder Road Construction Project.' The goal is to increase small farmer's food production and sustainable livelihoods with access to market; an unforeseen but increasingly urgent goal is to enable safe, reliable access into these regions by international aid organizations for aid to displaced populations in distress.

The engineering firm of WSP|Parsons Brinckerhoff working as consultants for UNOPS arrived at an optimized pavement design for 225 km of roads that crossed four regions. Conditions included poor subgrade, high traffic loading and a lack of quality aggregate, all in a very remote and underdeveloped region, subject to tribal conflict and food insecurity.

After extensive investigations and road design analysis, WSP proposed soil stabilization with Neoloy Geocells. "*Considerable distances between the project road and approved gravel borrow areas also contributed to the selection of this solution.*" The subsequent UNOPS tender specifications for the type of geocells were based on the following design considerations (UNOPS 2016):

- Mechanistic design analysis
- Use of low-quality infill material

- Overall stiffness required for expected stresses and strains
- Limited allowable creep for pavement life cycle.

The UNOPS tender stated that "*the application of (Neoloy or approved equivalent) geocells on this project is for a* ***permanent*** *solution, rather than a* ***temporary*** *solution, as is often the case with haul roads or access roads. This project specifically requires a long-term stabilization of the layer to withstand high traffic loads, which correspond to the upper allowable envelope for gravel roads. This is the reason for the specification for long-term creep of the geocell material*."

UNOPS awarded the tender for the supply and delivery of 1/2 million sqm of Neoloy Geocells, which met or exceeded the UNOPS tender minimum technical requirements for elastic stiffness, creep resistance and tensile strength.

15.3.2 Soil

The subgrade is generally characterized by sand, loam and clay with no rock outcrops. Black clayey loam and sedimentary material occupy the isolated marshlands. A significant part of the roads is in areas with poor subgrade material and/or poor drainage conditions, including marshlands. Average CBR of these soils is 7%. Seasonal rain causes flooding and makes large sections of road impassable due to poor design, construction and maintenance.

15.3.3 Conventional Solution

The road design includes a wearing course, a base (formation) layer and in situ material roadbed (subgrade layer). WSP considered several types of conventional solutions. A conventional pavement design according to the South African Pavement design manual comprised the following:

- 200 mm gravel wearing course
- No subbase
- Local fill material (CBR >7%).

However, the conventional pavement design was not feasible due to the considerable distance between the borrow area for the gravel wearing course borrow area and the project road. This distance, coupled with large haulage fees, made this design option unfeasible.

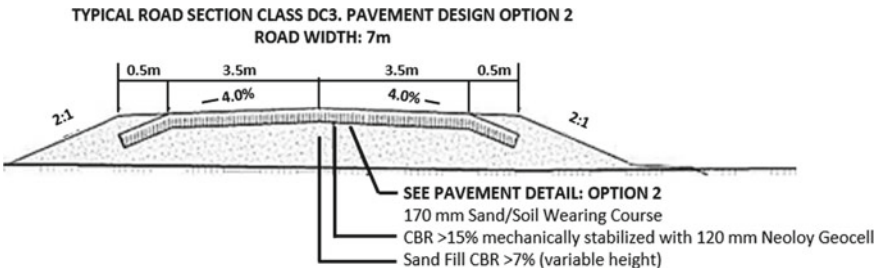

Fig. 15.9 Typical road section drawing with Neoloy Geocell base reinforcement. *Source* WSP

15.3.4 Neoloy Geocell Design

In order to reduce the amount of gravel required for the wearing course, only two geocell pavement design options were analyzed (see Fig. 15.9). The Neoloy Geocells confine the in situ material and improve compressive strength. The 330 mm small cell size and 120 mm height were chosen as the most effective configuration. The Neoloy Geocell design improved the subgrade elastic modulus between 1.5 and 5 times, while the subgrade elastic modulus was improved by a factor of at least two times.

The Average annual daily traffic (AADT) was less than 300; therefore, this road has been classified as a Low volume road (LVR) of design class DC4 with an intended level of service C. This road category provides for a DV4 design vehicle which is equivalent to a truck and semi-trailer. The design standards applied to this road are:

- Design speed: 50 km/h
- Road width: 7.0 m
- Minimum stopping site distance: 125 m
- Horizontal radius: 250 m
- Gradient: <2%
- Superelevation: 4%
- Camber: 4%.

The design and tender included a non-woven, needle-punched continuous-filament synthetic geotextile for separation, filtration, drainage and to reduce construction times over soft ground.

15.3.5 Installation

Over 1/2 million sqm of Neoloy Geocells were delivered in 16 weeks to Nairobi port, from which they were distributed overland to the UNOPS logistics centers and then to the local road sites. The project included knowledge management transfer, which included training local work crews in the use of Neoloy Geocells. The involvement of

Fig. 15.10 Installation and infill of Neoloy Geocell on rural feeder road project. *Photo Credit* UNOPS

the local population was a key aspect of the project, as stakeholders in the construction and maintenance.

The Neoloy Geocells were incorporated in the wearing course of the 7.0 m wide road with significant overfill. The road is basically constructed from sand, with the higher quality sandy-gravel infill limited to the wearing course. It should be noted that unforeseen delays were caused by the unstable security situation in the region (Figs. 15.10 and 15.11).

15.3.6 Results

The UNOPS, WPS, local government officials and the local contractors involved in the project expressed full satisfaction with the product, the installation and the stabilized road performance. The project was submitted by the UNOPS project management team to the annual UNOPS project of the year award. Additional tenders for geocell soil stabilization were issued, for example, in airfield pavement rehabilitation in South Sudan.

A key achievement of the project was a 50% cost savings compared to conventional design: due to the reduction in construction costs—reduced pavement thickness, less hauling (use of local sand, faster construction and reduced maintenance). This also helped achieve UNOPS sustainable objectives due to the road's durability, low environmental impact (using local materials) and employing the local populace in the road construction and maintenance. Installation time, costs and resources were

Fig. 15.11 Finished feeder road. *Photo Credit* UNOPS

also reduced by an estimated 35% due to reduced pavement thickness and in situ placement.

Finally, this project literally stabilizes an unstable world and helps people and improves their lives. The roads are literally a live-saving artery in the short term for the reliable delivery of food aid to get to those in need; and a key element enabling the development of a rural economy and opportunity for a better life in the long run.

15.4 Case Study C: Neoloy Geocell Soil Stabilization for High-Speed Passenger Rail Operations, Amtrak, USA

See Figs. 15.12, 15.13 and Table 15.4.

15.4.1 Introduction

Maintenance of track geometry is a key expenditure for railways, particularly, for high-speed passenger operations with strict geometry tolerances. Degradation of geometry requires frequent and expensive surfacing, tamping and downtime. A section in Maryland of Amtrak's high-volume Northeast corridor (NEC), which carries 2200 high-speed commuter and freight trains daily, suffered mud pumping and severe ballast fouling from problematic soils.

Fig. 15.12 Poor clay subgrade conditions on Track C (before rebuild). *Photo Credit* PRS Geo-Technologies

Fig. 15.13 Installation of Neoloy Geocell stabilized track (rebuild). *Photo Credit* PRS Geo-Technologies

Table 15.4 Case Study C: Project Snapshot

Description	Neoloy Geocells were used to stabilize subgrade on main line conditions of the Amtrak high-speed Northeast corridor, which suffered significant mud pumping and track geometry degradation from poor subgrade. Measurements demonstrated 50% less subgrade pressure and a reduction of the track geometry degradation/ extension of track surface maintenance by factor of 6.7
Subgrade soil	Highly plastic clay—1.2 MPa as per DCP Ballast strength was 30–40% (13.8 MPa) of normal resistance (34 to 41 MPa)
Client	Amtrak, National Railroad Passenger Corporation (USA) with research supported by US Federal Railway Administration (FRA), Department of Transportation (DOT)
Project design	Amtrak
Achievements	• Reduced track maintenance by factor of 6.7 • Reduced vertical pressure on substructure by 50% • Improved Track Quality Index by up to 10 times • Economically viable solution for high-speed rail systems
Date	September 2015
Keywords	Railroad track, track geometry, subgrade stabilization, geocells, track maintenance

Source PRS Geo-Technologies

Amtrak undertook a subgrade renewal project utilizing Neoloy® Geocells. The aim of the total track rebuild was to rectify the frequent geometry track degradation, insufficient substructure and weak subgrade. The project was part of a US Federal Railway Administration (FHA) program to promote innovative railway technologies for high-speed passenger operations.

A comprehensive full-scale in-track field and performance evaluation were conducted on this section of high-speed rail track, including long-term monitoring by the Harsco Rail Consulting Group and researchers from the Universities of Delaware and Colombia, in addition to the FHA and Amtrak.

The goal was to assess the impact of Novel polymeric alloy (NPA) Neoloy Geocells on the track geometry performance as a potential solution for other locations with subgrade problems and high track geometry degradation. Comprehensive analysis of the data qualified the efficacy of Neoloy Geocells in reducing the rate of degradation, which translates into reduced surfacing cycles and maintenance compared to a conventional structure (Palese et al. 2017; Zarembski et al. 2017) (Fig. 15.14).

15.4.2 Soil

The cause of ballast fouling the high-speed rail section in Maryland stemmed from undercutting operations in the 1990s on the middle of three tracks. This disturbed the underlying highly plastic clay layer causing migration in saturated conditions into

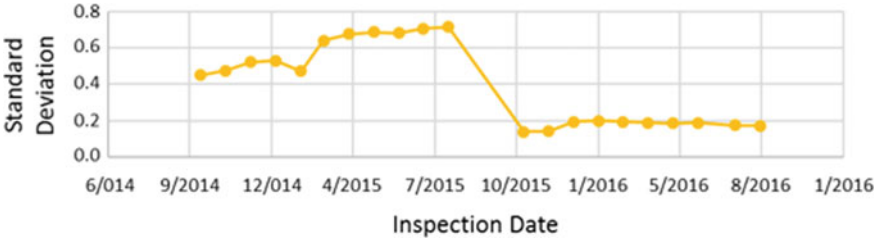

Fig. 15.14 Track geometry degradation rate before and after geocell installation (10/2015) measured in TQI—track quality index. *Source* Amtrak

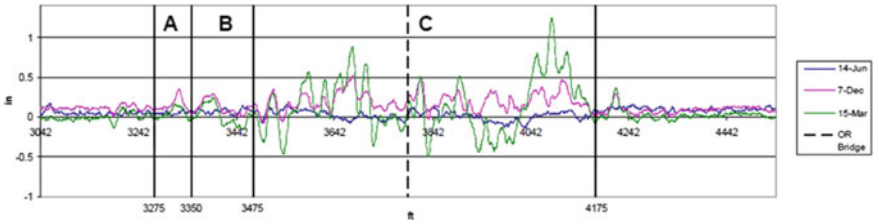

Fig. 15.15 Cross-level measurements before rebuild. *Source* Amtrak

the track's ballast layer. Soil investigation verified that the overall track substructure in general and the subgrade clay were very weak. Tip resistance measurements showed that the top 1.5 m of the ballast were at a maximum 13.8 MPa instead of the expected tip resistance of 34–41 MPa. Track geometry measurements over an 8-month period prior to the rebuild showed significant degradation of cross-level and surface geometry (see Fig. 15.15). Frequent surfacing was required to maintain track geometry.

15.4.3 Design with Neoloy Geocell

The test site is an FRA Class 7 high-speed 200 kph (125 mph) passenger track with 20–25 Million gross tons of traffic (MGT), but which often deteriorates to a Class 6 (176 kph) or even Class 5 (144 kph).

The goal of the rebuild was to stabilize the weak subgrade and eliminate the factors fouling the ballast. The rebuild for all three tracks in the section included removing track and substructure. The subballast was recompacted, and additional drainage and clean ballast were installed. Neoloy Geocells were installed on the middle track only to compare the performance of the reinforced (geocell) vs. control (unreinforced) zones of track.

After a comparative analysis, Amtrak chose the Neoloy (Novel polymeric alloy—NPA) Geocell category type, small cell (330 mm), 150 mm height, heavy-duty category D, due to the following long-term performance properties:

- High elastic stiffness (>600 MPa @ 60 °C)
- High resistance to permanent (plastic) deformation (<3%)
- High tensile strength (>26 kN/m).

A "hybrid" solution was used, which include a Tensar BX Type 2-450 geogrid installed on the subgrade. The geogrid acts as a stable working platform, which enables the stiff NPA geocell layer embedded in the ballast layer to achieve a higher Modulus improvement factor (MIF). The stiff geocell in the subballast layer acts like an "I" shape steel girder. Its high resistance to swelling renders it unaffected by moisture variations in the clay subgrade. This hybrid solution has been proven effective in preventing heaving from expansive clay soils in railway applications (Kief 2016).

Pressure load cells (force transducers) (20 cm diameter) with a capacity of 500 kPa were installed at the top of the subbase layer to measure vertical loading resistance over time in both the reinforced and unreinforced sections (see Fig. 15.16).

The Neoloy Geocells were filled in with subballast 2A 2-in. max. size stone with many fines for good compaction and drainability. Standard Amtrak quality 3-in. max. size AASHTO #57 open graded, clean stone was used for the ballast layer. The immediate impact of the Neoloy was visually noticeable by those present on-site. For example, haul trucks loaded with ballast infill caused severe rutting to the wet mud subgrade as they approached the site, but easily traversed the areas in which geocell was already installed with no noticeable rutting whatsoever.

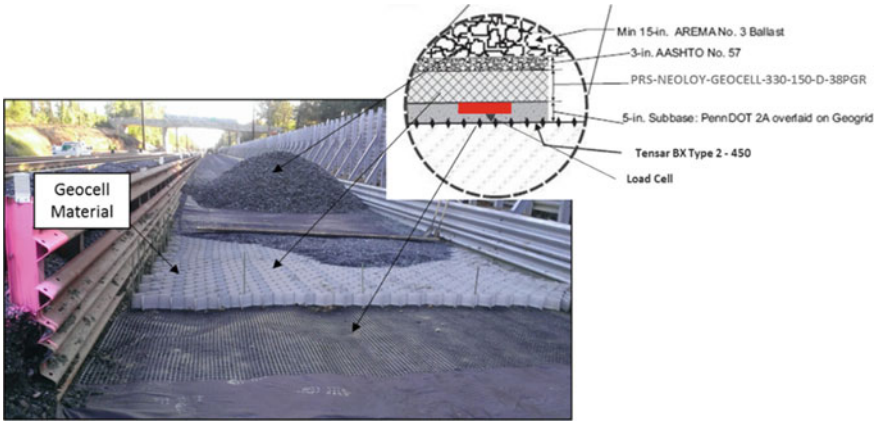

Fig. 15.16 Cross-section of the geocell-reinforced substructure. *Source* Amtrak

15.4.4 Results

Track geometry data was collected by Amtrak track geometry vehicles, from pre-build and post-build measurements including data from the pressure load cells installed in the track subgrade. Data include surface (vertical), cross-level (elevation of two tracks), gauge and twist (change in cross-level). Measurements from the control section (rebuild without geocell reinforcement) showed significant degradation in the track geometry within 6-7 months after the rebuild.

Data from the Neoloy stabilized section showed that the subgrade pressure was consistently 50% of that in the control zone (no geocell). Track geometry variations in the NPA geocell zone were significantly smaller—for left and right track, cross-level data and the TQI standard deviation (shown in Fig. 15.17).

The data results show that the NPA geocell improved track support, reduced bearing pressures on the subgrade and provided improved track geometry performance over time. The rate of track geometry degradation was reduced, thereby extending the time between surfacing maintenance cycles by a factor of 6.7. This results in marked maintenance savings to Amtrak and an exceptional ROI on the project.

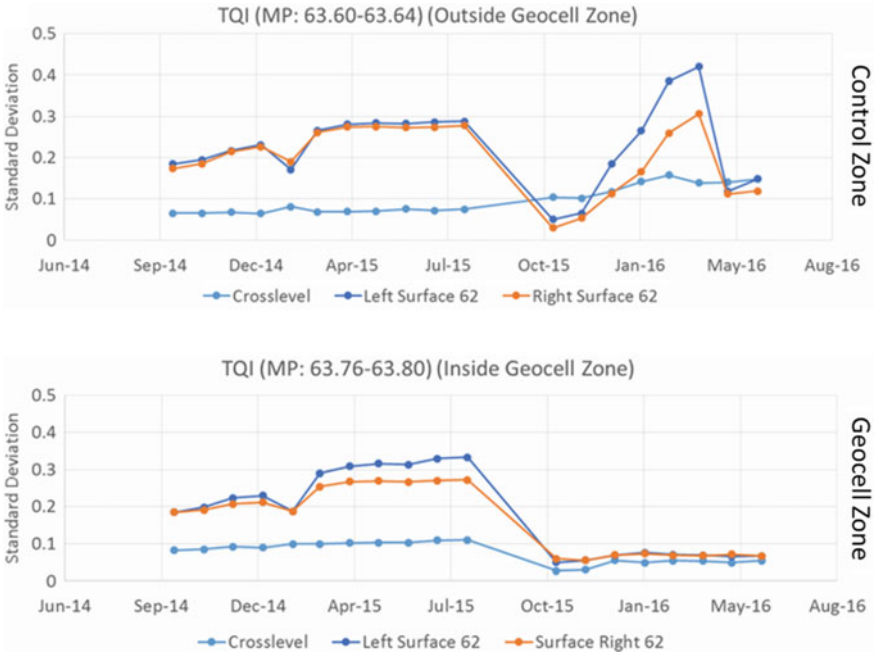

Fig. 15.17 TQI standard deviation variation before and after track rebuild (Oct 15) in unreinforced control zone (top) and geocell zone (bottom). *Source* Amtrak

15.5 Case Study D: Load Transfer Platforms for Vertical Columns, Manzanillo Port, Mexico

See Fig. 15.18 and Table 15.5.

15.5.1 Introduction

A new 50,000 m^2 multiple use terminal (MUT) was planned for Manzanillo port to handle 2.5 million tons of general purpose cargo and bulk minerals per year. The objective was to build five 10,000 m^2 platforms within a year. Design was to be according to the highest international standards with a goal to exceed the planned handling capacity. A stated objective was to utilize the best available environmental-friendly and sustainable infrastructure.

Marine port terminals are often constructed as Load transfer platforms (LTP) to resolve the typically challenging site and subgrade conditions on one hand with the heavy-duty loading requirements from port operations on the other. LTPs mobilize soil arching to transfer the applied loads onto vertical pile columns. If the layer thickness is decreased, the arching effect decreases as well. Therefore, geogrids, concrete base plates or hydraulic-bonded layers are needed to increase the soil stiffness to mobilize the load transfer from the soil to the vertical elements.

Fig. 15.18 Installation of Neoloy Geocell layer in load transfer platform, Manzanillo Port, Mexico. *Photo credit* Innovator

Table 15.5 Case Study D: Project Snapshot

Description	Neoloy Geocells provided stabilization for Load transfer platform (LTP) on saturated silty sand, for heavy port platform, in Manzillo Port, enabling a reduction pavement thickness and significant cost savings
Subgrade soil	Saturated silty sand with CBR <2%
Client	Group Hazesa—contractor with experience in multiple use terminal (MUT) construction
Project design	Ancora Ingenieria—structural pavement designers, Mexico, Innovater, Innovciones en Terracerias S.A. DE C.V., Mexico
Achievements	• Optimized pavement—modulus improved by 2–3 times, total pavement thickness reduced by 37%, including 17% reduction in concrete surface layer • Eliminated need and time for soil consolidation • Locally available used for structural infill • Fast, simple and all-weather installation • Significant cost savings
Date	Q4 2014—Q2 2015
Keywords	Load transfer platforms, port, platform, geocell reinforcement

Source PRS Geo-Technologies

Neoloy Geocells were chosen to reinforce the earth LTP for their excellent load distribution mechanism, due to their very stiff, strong and low creep properties. The Neoloy Geocells act as a flexible beam (or slab), distributing vertical loads widely. This effectively transfers applied loads directly to the vertical columns via soil arching instead of the soft soils.

15.5.2 Soil

Extreme site conditions for the terminal platform included soft marine foundation soils of saturated silty sand with a CBR of <2%. Bulk handling of lead and zinc minerals on the dock could reach loads of 35 ton/m^2. The foundation for the terminal was constructed on vertical columns; therefore, the reinforcement solution had to function as a load transfer platform as well.

Load transfer platforms of concrete, hydraulic-bonded or composite geosynthetic (geogrid) layers are too expensive or insufficient, while unreinforced solutions are too heavy and costly. The thickness of a conventional unreinforced platform would have been thick and costly in terms of the concrete surface layer and the high-quality aggregate required for the base and subbase layers.

15.5.3 Neoloy Geocell Design

The project design included a 5 × 5 m grid of vertical columns (piles), each approximately 10 m high and 1 m diameter for each platform. Research demonstrated that geocells can be directly placed above vertical columns; the load transfer mechanism significantly stiffens the geocell stabilized soil and applied loads are transferred from the soft soil directly into the columns (Emersleben and Meyer 2012; Collin et al. 2018).

To meet the challenging site conditions and project requirements, Innovator, Ancora Engineering and PRS Engineering developed a design for a geocell-reinforced load transfer platform (LTP). MePADS pavement design software was used to compare the vertical static stresses on the subgrade surface from the applied load (35 tons/m^2) in the conventional design vs. the Neoloy Geocell-reinforced design to determine the modulus improvement factor, based on an equivalent performance. The maximal vertical stress (σ_{zz}) at the subgrade surface was 315.7 kPa for the unreinforced pavement vs. 266.5 kPa for the Neoloy Geocell-reinforced pavement with a pavement thickness 37% less.

Neoloy Geocells were selected as they were the only geocell offering high elastic stiffness (>500 MPa @ 63 °C), low permanent degradation (<1.5% at 50 years) and high tensile strength (>19 kN/m). These properties are crucial for heavy-duty loading over the 30-year pavement design life. The Neoloy-based Geocell gave the design engineers the confidence to meet the following three key project challenges:

- Geotechnical—the 3D mechanical stabilization technology acts as a flexible mattress with a wide load distribution angle (~35°) for maximum load distribution in each layer.
- Engineering—optimized load transfer by improving the modulus by 2.3 times; enabling 60% reduction in subgrade layer thickness, 30% in base layer and 17% of concrete thickness.
- Economics—cost-effective, sustainable solution, eliminating the need for consolidation and expediating construction.

15.5.4 Installation

The first step involved creating a 5 cm working platform of poured lightweight concrete to create a stable working foundation, after natural subgrade excavation and capping. Two layers of Neoloy Geocell 330–120 (330 mm cell size, 120 mm height) with 12 cm of 1″ gravel fill were installed directly over the working platform and compacted to 3 cm overfill. A layer of 115 cm controlled subgrade undercut was placed with quality-controlled compaction every 15 cm. The Neoloy Geocell reinforcement enabled a reduction in the subgrade thickness by approximately 50%, while increasing the elastic modulus of the subgrade layer by 1.4 times. It also caused a “jump” in the modulus of the granular base layer above it by more than three times.

Fig. 15.19 Installation of Neoloy Geocells on subgrade of LTP. *Photo credit* Innovator

The additional layer of Neoloy Geocells was installed in the base layer filled with base quality granular aggregate (+3 cm overfill), with a calculated Neoloy Geocell Modulus improvement factor (MIF) of 3.1. This increased the base layer modulus by a factor of 2.3 while enabling a 17% reduction in the Portland concrete cement slab from 30 to 25 cm with no reduction in performance (Fig. 15.19).

15.5.5 Results

This reinforced load transfer platform structure was very cost-effective. It resolved problems with settlement and consolidation, enabled a thickness reduction in the platform structural layers, and used locally available dredged sand for structural infill. The Neoloy Geocell reinforcement also increases the efficiency of LTP design so that the number of piles can be decreased.

The geocell cellular confinement system works as load distribution system and is therefore well suited to a load transfer platform above vertical columns (piles). Neoloy Geocells were selected for this heavy-duty pavement due to their high modulus and low creep characteristics. Dual layers of Neoloy Geocells above the piles work as a composite that distributes the pressure bulbs generated by the piles into a larger area to successfully resist penetration. Deformations between the center

grid of the piles is not significant. The top Neoloy Geocell layer distributes the pressure bulbs generated by the loading of the mineral ore (35 ton/m_2) into a larger area as well. Vertical stresses on the subgrade are reduced as is settlement between the load distribution platform and the subgrade material. The increased bearing capacity of Neoloy Geocell reinforcement of the subgrade had additional benefits for the project: significant decrease in the overall pavement thickness, the ability to use local materials and a demonstrated decrease in the construction time.

15.6 Conclusions

The use of geocells to reinforce heavy-duty pavements was demonstrated in four case studies involving demanding project requirements and challenging soil and site conditions: (a) stabilize asphalt pavements in a Mexican airport built on extremely soft soil; (b) use low-quality infill to build a permanent pavement in a very remote region of Africa; (c) reduce maintenance of high-speed track by 82% over problematic soils; (d) stabilization of marine port load transfer platforms in Mexico while reducing pavement thickness by 50%.

The use of Neoloy-based geocells led to significant engineering improvements in each project: higher modulus, increased soil bearing capacity and reduced deformation more than any other geocell or geosynthetic reinforcement; and enabled optimization of the pavements in terms of layer thickness, infill materials and lifespan.

The extended lifespan and reduced maintenance were critical factors in each of these projects. Therefore, it was essential that the elastic modulus and resistance to permanent deformation of the geocell would maintain dimensional confinement, compaction and reinforcement for the entire design life of the project—up to 50 years.

In addition to the extensive engineering proofs provided by Neoloy-based geocells test methods, methodologies, research and field trials, the use of these geocells had significant economic benefits. This included road construction using locally available but marginal quality soils for structural infill, and extended service life with less maintenance. These same economic benefits are aligned with the sustainability goals for each of the projects in terms of environmental footprint and durable construction.

These case studies validated the important contributions advanced geocells made to large-scale, heavy-duty transportation and infrastructure projects.

References

Collin JG, Han J, Huang J (2018) Geosynthetic-reinforced column-support embankment design guidelines

Emersleben A, Meyer N (2012) The use of vertical columns in combination with geocell stabilized load transfer platforms for the construction of roadways over soft soils. 1302–1309. https://doi.org/10.1061/9780784412121.134

Kief O (2016) Rail track pavements on expansive clay restrained by hybrid geosynthetic solution. In: Geosynthetics 2016 conference proceedings. Miami Beach, USA. April

Kief O, Pokharel S, Schary Y (2014) High modulus geocells for sustainable highway infrastructure. Indian Geotech J 45. https://doi.org/10.1007/s40098-014-0129-z

Palese JW, Zarembski AM, Thompson H, Pagano W, Ling HI (2017) Life cycle benefits of subgrade reinforcement using geocell on a highspeed railway—a case study. In: AREMA conference proceedings (American Railway Engineering and Maintenance-of-Way Association). Indianapolis, Indiana, USA

UNOPS (2016) Invitation to Bid (ITB) for supply and delivery of geocells material delivered to Mombasa, Kenya and/or Kangi, Achol Pagong and Gok Machar in Greater Bahr el Ghazal Region, South Sudan. Section II: Schedule of Requirements. ITB Ref No: UNOP/SSOC/88050/ITB/GOODS/2016-001-Rebid

Vega E, Van Gurp C, Kwast E (2018) Geokunststoffen als funderingswapening in ongebonden funderingslagen (geosynthetics for reinforcement of unbound base and subbase pavement layers), SBRCURnet (CROW), Netherlands. CRW C1001 (in Dutch)

Zarembski AM, Palese JW, Hartsough CM, Ling HI, Thompson H (2017) Application of geocell track substructure support system to correct surface degradation problems under high-speed passenger railroad operations. Transp Infrastruct Geotechnol 4:106–125. https://doi.org/10.1007/s40515-017-0042-x

Chapter 16
An Overview of Natural Materials as Geocells and Their Performance Evaluation for Soil Reinforcement

Sreevalsa Kolathayar, Renuka Sai Gadekari, and Prof. T. G. Sitharam

Abstract This chapter presents a review of studies on the performance of both natural and polymer-based geogrids and geocells as reinforcement in the foundation bed. An attempt was made to lay out identified research gaps and to present future directions for research to explore the potential of geocells made from natural materials. The performance of a variety of natural products, like areca leaf sheath, sisal leaf sheath, coir mat, and jute mat, as reinforcement was evaluated and compared with that of polymer-based geocells. A series of model footing plate load tests were conducted to evaluate the influence of different cell layers on the strength and stability behavior of the soil. Tests were performed on unreinforced soil as well as soil reinforced with areca leaf cells, sisal leaf cell, coir cell, jute cell, and polyethylene geocell for comparison. The settlement-bearing pressure behaviors were plotted, and it was observed that natural geocells perform at par with polyethylene geocells. The leaves and fibers can be chemically treated before application for extending its durability.

Keywords Geocell · Areca cell · Coir cell · Jute cell · Sisal cell · Load-settlement · Footing

16.1 Introduction

The development of infrastructure is a very important need in the present time and investment in the infrastructure can enhance economic growth considerably. New

S. Kolathayar (✉)
Department of Civil Engineering, National Institute of Technology Karnataka, Mangaluru, Karnataka, India
e-mail: sreevalsakolathayar@gmail.com

R. S. Gadekari
Department of Civil Engineering, Amrita Vishwa Vidyapeetham, Coimbatore, India
e-mail: rnksai@gmail.com

Prof. T. G. Sitharam
Department of Civil Engineering, Indian Institute of Technology Guwahati (IITG), Surjyamukhi Road, North, Amingaon, Guwahati, Assam 781039, India
e-mail: sitharam@iisc.ac.in

T. G. Sitharam et al. (eds.), *Geocells*, Springer Transactions in Civil and Environmental Engineering,
https://doi.org/10.1007/978-981-15-6095-8_16

multi-story buildings, high-speed rail tracks, highways, bridges, electric towers, dams, and airports are required to be constructed to fulfill the needs of the growing population. In recent decades, the construction of buildings has increased rapidly though the space available for construction is limited. Due to this, situations have arisen where the engineers have to construct on weak soils. Construction over weak soils poses challenging situations to civil engineers as they are susceptible to differential settlements, poor shear strengths, and high compressibility. Thus, the replacement of weak soils by strong soils or improvement of the engineering properties of the weak soil by different ground improvement techniques is recommended in such situations. In situations where the replacement of soil is uneconomical, the soil improvement techniques are preferred at the site.

Soil reinforcement technique is the most popular ground improvement techniques used for the improvement of the properties of soil. Addition of fibers to the soil, use of metal bars, sheets, and strips were the traditional ways of reinforcing soil. In recent times, the use of geosynthetics has become more prominent in the field of civil engineering for soil stabilization. Geosynthetics, one of the main techniques of soil reinforcement, have been widely used as construction materials in civil engineering projects. Geosynthetics are man-made polymeric materials which are usually provided for soil confinement to increase the shear strength of the soil which in turn increases the bearing capacity of the soil. It also functions as separators, hydraulic barriers, filters, reinforcement, protectors, and erosion control system in the field of geotechnical engineering. Today, the geosynthetic products like geocell, geogrid, geotextile, geomembrane, etc., are available in the market. The shear resistance between soil and geosynthetics limits the lateral deformation of the soil. Each product is designed to solve a specific type of civil engineering problems.

Cellular confinement systems, also known as geocells, are widely used in construction for soil stabilization on slopes, channel protection, and structural reinforcement for load support and for retaining earth. Geocells consist of a series of interconnected single cells that are manufactured from different types of polymers. The cell walls of geocells completely encase the infill material and provide all-around confinement. The soil–geocell layers act as a stiff mat and distribute the vertical loads over a much larger area of the subgrade soil. At present, geocells are commonly made of high-density polyethylene (HDPE), polypropylene, or polyester. In the construction field, geocells are used for laying roads, slope stabilization, retaining walls, canals, railways, and embankments, etc. The plastic and polymer-based geocells are not degradable for many years, and also they may act as a hindrance for the rooting of plants and trees. This fact navigates us toward looking for a much more eco-friendly, cost-efficient, and easily available alternative material. Hence, geocells made out of natural fibers such as sisal fiber, jute fiber, and coir fibers are effective alternatives to polymer-based geocells, and they can be adopted for cost-effective ground improvement technique. These natural leaves and fibers are very strong, natural, and found widely in South Asian countries.

16.2 Review of Literature

During the past few decades, a number of experimental and numerical investigations have been reported by various researchers to evaluate the performance of cellular confinement in soil using commercially available geocells and different infill materials. An attempt has been made in this chapter to review the available literature on the cellular confinement of soil using polymeric as well as natural materials.

16.2.1 Studies on HDPE and NPA Geocells

Rajagopal et al. (1999) conducted a series of triaxial tests on geocells made up of woven and nonwoven polypropylene geotextiles. They found that the infill soil imparts cohesive strength even though it is cohesionless soil. This cohesive strength depends upon the tensile modulus of geosynthetic material used to form geocells. The stiffness of composite increases by providing geocell reinforcement. Minimum of three interconnected geocells are required to understand the performance of the interconnected geocells layer bed. With geocell, soil can withstand high tensile stresses. The frictional strength of both reinforced and unreinforced soil samples will remain the same, and the failure envelopes of these samples will be parallel to each other.

Dash et al. (2003a, b) performed model footing tests on a circular footing supported on geocell made of polypropylene and observed that the encapsulated sand which was used as infill material owed to the confinement effect from the geocell walls and behaved as a relatively rigid member. This rigid member supports the footing load by distributing the frictional resistance over its outer periphery throughout the height of the geocell wall. By this, it reduces the pressure on the underlying soft soil and increases sand bed performance. Surface heaving can be reduced by increasing the width of the geocell layer. This leads to the development of rupture planes in the soil bed by inducing a better composite behavior. The basal geogrid layer besides geocell further improves the performance of the footing both in terms of stiffness and load-carrying capacity of the soil bed. The geogrid layer resists the downward deflection of the geocell mattress under footing load by its strength and membrane action. At higher settlements, the geocell layer deflects more and induces higher deformation in the geogrid layer at its base. By this action, the geogrid layer gets strained more and hence mobilizes higher strength that gives rise to higher-performance improvement. On the other side, an increase in the height of the geocell mattress increases the rigidity. This gives more uniform settlement at the base of the geocell mattress and reduces the contact pressure on the underlying soil. Load-bearing capacity of planar-reinforced soil reduces, when the soil between two successive layers gets squeezed out. In the case of geocell reinforcement, the cells infilled with soil provide all-round confinement. This makes the geocell mattress behave as a composite body, even at larger footing settlement.

Pokharel et al. (2010) experimentally investigated the stiffness and bearing capacity of single geocell-reinforced bases, including shape, type, embedment, height of geocells, and quality of infill materials. Four types of geocells (HDPE geocell and three Novel Polymeric Alloy (NPA) geocells with different tensile strengths) were used with Kansas River sand and quarry waste as infill materials. The elliptical-shaped geocells failed suddenly, and the infilled soil in it escaped from the geocell from the bottom of it. Due to this, the confinement effect of geocell was lost. But, this loss was not seen in circular-shaped geocells as they fail gradually. The stiffness and bearing capacity of reinforced base depend on elastic modulus of geocell sheet. The geocell without infill material had shown poor performance due to the breakage of weld under the application of load. The average stress was reduced, and the load capacity was increased when there was an increase in the lateral expansion of cross section of the geocell. In the confined geocell, the deformation in the loaded cell was minimized, and the rupture of the weld was immobilized due to the presence of the surrounding sand. The cohesion existing in the base material minimizes the benefit of the geocell for lateral confinement under static loading.

The provision of the geocell reinforcement significantly increases the load-carrying capacity, reduces the footing settlement, and decreases the surface heave of the footing bed as compared to that of the planar reinforcement with the same characteristics and mass. Increase in the number of planar reinforcement layers and increase in the height and width of geocell reinforcement increase the bearing pressure of the foundation bed and decrease the footing settlement (Tafreshi and Dawson 2010). The presence of reinforcing layer in the soil mass enhances the load-settlement behavior and the ultimate bearing capacity (Selvadurai and Gnanendran 1989).

Various parameters such as reinforcement embedment length, length, number of layers, and number of piles of braided coir rope affect the strength characteristics of reinforced bed. A sixfold increase in the strength and ninety percent reduction in the settlement are proved in the study made (Vinod et al. 2009). The tests on soil beds using rubber shreds as soil reinforcement were performed. These were distributed on the soil bed uniformly. The optimum value of the parameters considered in this study was found out (Tafreshi and Norouzi 2012).

Chen et al. (2013) performed triaxial compression tests on high-density polyethylene (HDPE) geocells of various shapes (circular, rectangular, and hexagonal), size and number of cells to evaluate compression strength of samples, and stress–strain behavior of soil samples. It was found that the shear strength of granular soil can be improved by the confinement effect of geocells. Due to the number of corners, hexagonal cells showed a higher friction angle than circular and rectangular cells.

Tafreshi et al. (2016) manufactured geocell and geotextile layers from the same geosynthetic material. The tests were conducted on these geocells to study their performance when circular footing is placed on it. The multiple geocell layers were laid under the footing. They observed that the first layer of geocell makes the stress field to pass into the deeper layers of the soil, and the next two layers provide the tensile capacity to oppose the outward shear even under low settlements. Due to this reason, more than three layers of geocell did not show any effect. The geotextile layers act sequentially, whereas the geocell layers act at a time to resist the load. The

same or greater improvement in vertical stiffness can be achieved by geocell layers than by planar sheets.

Kargar et al. (2017) described the influence of geocell geometrical properties on the improvement in bearing capacity and settlement of footing by loading strip footing model to the ultimate failure level. Compared to the unreinforced sand, the failure zones on the surface of reinforced soil were extended to a considerably larger distance beyond the edge of strip footing. The geocell mattress acted as a secondary foundation, and it redistributes the footing stresses over a wider area in the bottom of the geocell cushion with a dispersion angle. The overall frictional resistance on the geocell wall, the moment of inertia, and the bending rigidity of the geocell mattress increased, with increase in the height of the geocell wall. The lateral movements of soil particles inside the geocell will be restrained with the confinement of geocells. The membrane effect of the geocell reinforcement develops a tensile force in the reinforced bed and reduces the settlement. The points below the middle axis of geocell walls, under the footing center, undergo large strains up to the ultimate strain for geocells with $h/B > 0.5$ (h is the height of the geocell, and B is the width of the footing). Consequently, a sudden shear failure takes place leading to a large heave in the soil surface beside the footing width, and the infill soil of the geocell moves out of the pockets. As the diameter of geocell pocket increases, the number of cells under the loading area decreases leading to less confinement effect. Footing loads will be distributed over a larger area due to the rigidity of the geocell layer. This can be achieved by increasing geocell width. The extension of geocell width to two times of footing width in each side of the footing provides anchorage from both sides of the loaded area due to the frictional and passive resistance developed at the soil–geocell interfaces.

The parameters such as the bearing capacity, heave, depth to the first layer of reinforcement from footing, the spacing between reinforcements, and number of layers of geogrid reinforcements were studied, and the optimum values for all were found out (Harikumar et al 2016). The effect of multilayered geosynthetic reinforced granular fills above soft clay was analyzed by using rectangular footings and by comparing the bearing capacity improvement factor, settlement reduction factor, and load dispersion angle (Roy and Deb 2017).

16.2.2 Studies on Natural Geocells

Hegde and Sitharam (2015) proved analytically and experimentally that the bamboo geocells and geogrids (Fig. 16.1) together provide higher bearing capacity than commercially available geocells and geogrids. The soil infilled bamboo cell acts as a beam and disperses the loads acting on them to the wider areas. The basal geogrid ceases the downward movement of soil and reduces the settlement of the bed. The lateral confinement, vertical dispersion, and membrane effects are the three mechanisms which contribute to increasing the bearing capacity of soil bed. The Neoloy and Bamboo geocells reduce the surface heave due to their interlocking effect.

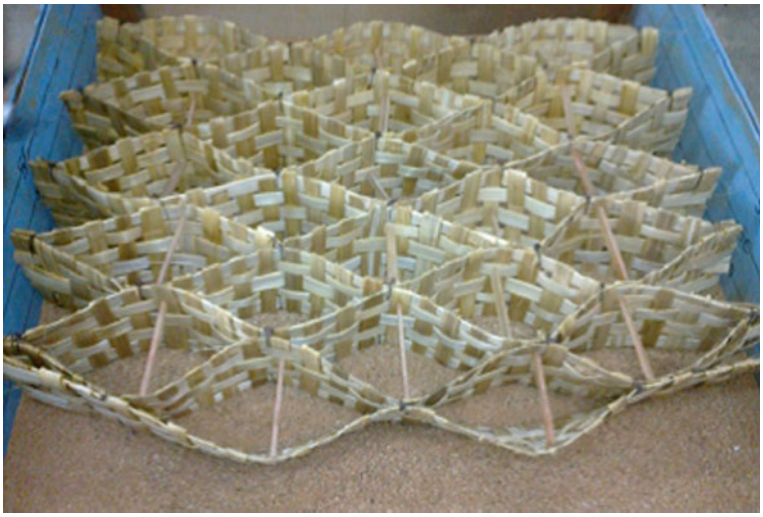

Fig. 16.1 Bamboo geocell *Source* Hegde and Sitharam (2017)

Lal et al. (2017) studied that coir geocells perform well than coir geotextiles under static loading. This is due to the frictional resistance in coir geocells. The performance of coir geocell will not be affected by the degradation of geocell as the soil attains the required strength with time due to applied pressure. They further specified that the coir coated with cement or bitumen will be more durable than uncoated coir. Further increase in width and no. of layers of geocell does not show any effect on the bearing capacity. In recent studies, Kolathayar et al. (2019, 2020) demonstrated the performance of geocells made of areca leaf sheath and coir mat through a series of model footing tests.

It is observed that there are limited studies on performance evaluation of geocells made from natural materials. This chapter makes an attempt to evaluate the performance of different natural geocells to improve the strength of the soil as the foundation medium.

16.3 Materials

16.3.1 Soil

The clay soil which was used for forming the foundation bed in this study was obtained from a construction site situated in Coimbatore region, Tamil Nadu. The sand, i.e., normal fine aggregate was used as the infill material for the geocell in this study to improve the shear strength which in turn increases the bearing capacity. The properties of soils are summarized in Tables 16.1 and 16.2.

Table 16.1 Clay soil properties

Characteristic properties	Value
Liquid limit (%)	64
Plastic limit (%)	34
Optimum moisture content (%)	28.73
Maximum dry density (kN/m^3)	1.42
Specific gravity	2.32
Differential swell test	77.78
Plasticity index	30

Table 16.2 Infill soil properties

Characteristic properties	Value
Specific gravity	2.65
Fineness modulus	3.62
Effective size, D10 (mm)	0.215
The coefficient of uniformity, Cu	3.67
The coefficient of curvature, Cc	0.919
Grading zone	GRADE II

16.3.2 Geocells

The areca leaf sheath was soaked in water for 10–15 min and cut into thin strips of width 5 mm. The strips were woven together to form areca grids by maintaining the same grid size as that of the polypropylene geogrid. The areca leaf sheath belongs to the species Areca catechu. The coir fibers were extracted from the husk of the coconut. The husks of the coconut were taken and cured in an environment that facilitated the action of microbes. The fibers were extracted from the husks by the process of defibring. These fibers were made into yarns which were woven into mats on handlooms or power looms. The strips were hand-stitched and were made into a geocell network. The coir strips were cut from a coir mat woven with the processed coir fibers. The jute geocells were stitched from the jute geotextile. Sisal fibers were extracted from the leaves of the sisal plant. The sisal geocells stitched from the sisal geotextile were used in the experimental analysis. Commercially available HDPE geocells of pocket size 250 mm × 210 mm were bought and sized down to the pocket size of 125 mm × 105 mm. The specifications of the geocells are listed in Table 16.3.

Figures 16.2, 16.3, 16.4 and 16.5 show typical geocells made of natural material such as areca leaf sheath, coir fiber, jute fiber, and sisal fiber.

Table 16.3 Properties of geocells

Material	Areca	Coir	Jute	Sisal	HDPE
Opening size (mm)	125 × 105				
Maximum tensile strength (kN/m)	44	30.3	13.7	62.7	11.5
Opening shape	Honeycomb				
Cell depth (mm)	75				
Strip thickness (mm)	2	6.18	4.28	3.25	1.53

Fig. 16.2 Areca geocell

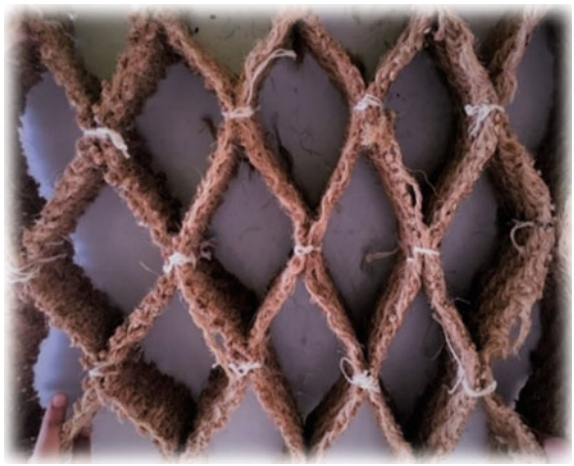

Fig. 16.3 Coir geocell

Fig. 16.4 Jute geocell

Fig. 16.5 Sisal geocell

16.4 Laboratory Model Tests

The laboratory model footing tests were conducted in a tank of dimensions 700 mm × 700 mm × 700 mm which is made of steel plates with glass on the front side. The tank was assembled with a loading frame and a hydraulic jack. The sides of the tank walls were covered with polyethylene sheets to avoid side friction. The clay which is used as the foundation bed was uniformly compacted 25 times using a metal rod in 50 mm layers, and the infill sand was filled by maintaining a constant fall of height. The same method of compaction was carried out for all the tests. The footing is placed on the sand bed such that it coincides with the center of the axis of

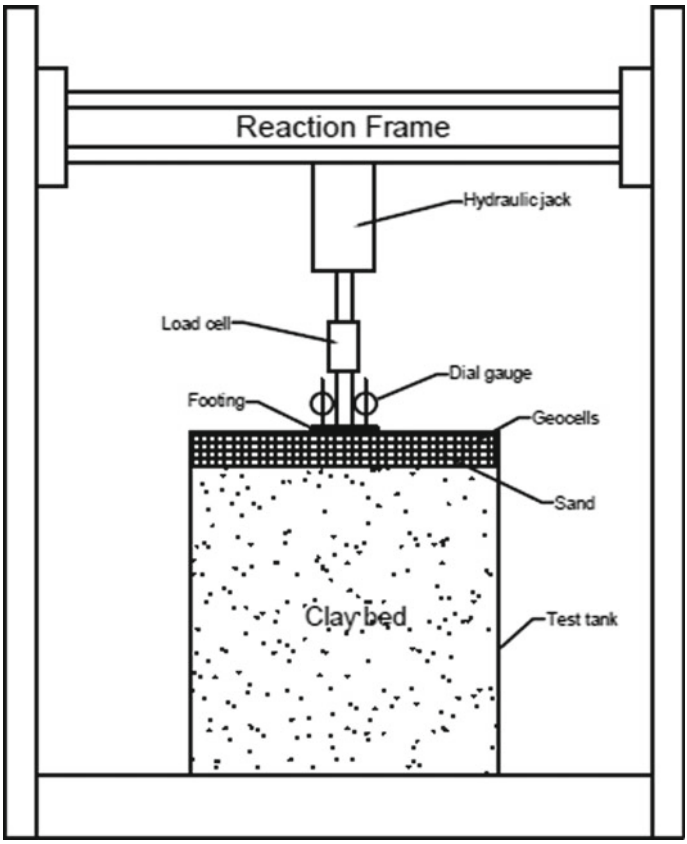

Fig. 16.6 Schematic diagram of model footing test setup

the bed and hydraulic jack. A load cell is connected between the hydraulic jack and the footing to measure the load applied on the footing. The settlements were noted using the two dial gauges of 50 mm capacity placed on either side of the footing. Figure 16.6 represents the experimental setup of the model footing tests.

16.5 Results and Discussions

The tests were independently done as mentioned in the procedure. Various values of the settlement of soil corresponding to different values of the load were noted, and a graph between bearing pressure and settlement was plotted as shown in Fig. 16.7.

A substantial increase in the bearing capacity was observed due to the provision of reinforcements as compared to unreinforced clay bed. A gradual failure was observed when the areca material was used as the soil reinforcement. It yielded a higher bearing

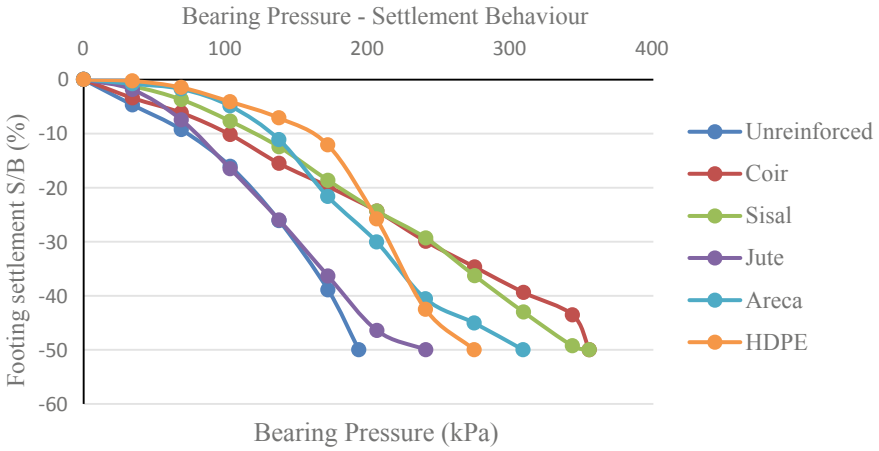

Fig. 16.7 Bearing pressure versus settlement curve for different geocell materials

capacity as compared to that of the commercially available geocells. When the soils are reinforced with coir geocell, it was observed that the settlement arrived at large loads. This observation could be attributed to the fact that the coir material is elastic, irrespective of its form. This implies that the elastic nature of coir material is primarily contributing to the result, giving less weight to the packing type.

From Fig. 16.7, it can be seen that, even though soil reinforced with HDPE geocells withstand initial loads at low settlements, with increasing loads, the settlement observed increases drastically. However, in the case of natural fiber geocells, i.e., jute and sisal, increase in the settlement with increasing loads is uniform. This could be due to the brittle nature of HDPE geocell material in contrast to the natural fibers jute and sisal, which are elastic in nature. Owing to their elastic properties, natural fiber geocells could withstand larger stresses (bearing pressure) at the same strain (settlement) when compared with those of HDPE geocell.

Further, a series of tests were conducted to understand the behavior of soil reinforced with geocells along with geogrids with both synthetic as well as natural materials. Areca leaf sheath was chosen to compare the performance with HDPE geocell and geogrid. The tests were conducted on HDPE geocell + geogrid-reinforced clay bed and areca cell + Areca grid-reinforced clay bed. The bearing pressure-settlement behavior is represented in Fig. 16.8.

The test on unreinforced soil shows a sudden failure after 10% of the footing settlement. But due to the provision of reinforcements, a gradual failure was observed, and when the areca material was used as the soil reinforcement, it yielded a higher bearing capacity as compared to that of the commercially available geocells. As observed from the previous researches, an increase in the bearing capacity was observed due to the provision of two-dimensional grids in addition to the three-dimensional cells. From the above results, the soil confined with areca cell and areca grid is found to have maximum bearing capacity when compared to all the others. The bearing capacity

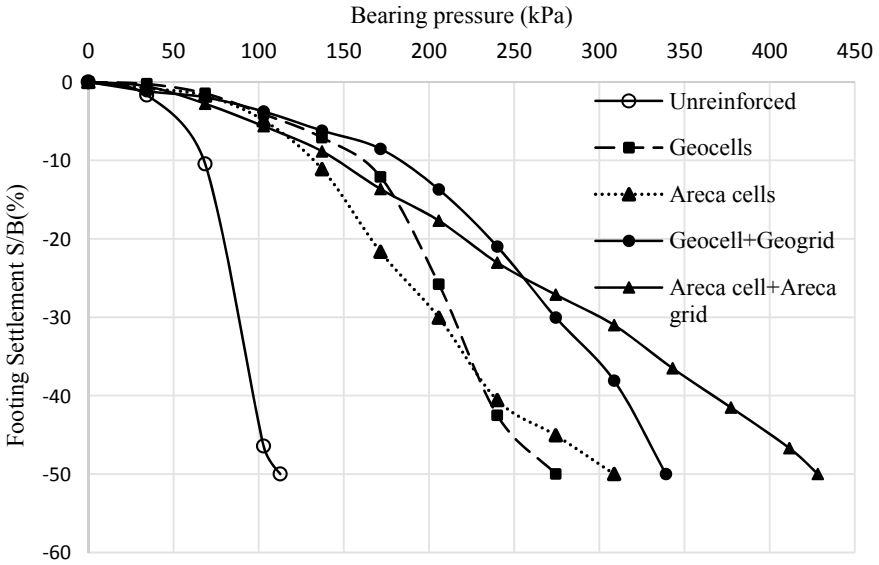

Fig. 16.8 Bearing pressure versus settlement behavior of soft soils

of the combination—areca cell and areca grid—is found to be approximately 1.25 times greater than that of the geocell and geogrid combination.

The bearing capacity ratio (BCR) was defined to indicate the bearing capacity increase as a result of providing different confinement materials to the soil. This term was put forward by Binquet and Lee (1975) and is defined as the bearing capacity ratio of the confined soil (BC_c) to the unconfined soil (BC_u),

$$\text{BCR} = \frac{BC_c}{BC_u}$$

The bearing capacity ratio factor for confinements provided in the soil with areca and HDPE systems is shown in Fig. 16.9. The maximum value is found for the areca cell and areca grid-reinforced foundation beds.

16.6 Conclusions

This paper reviewed several studies on the performance of geocells (both synthetic and natural) under static loading. It is observed that geocell performs better than geogrids due to the cellular confinement effect. The sufficient strength and stiffness of HDPE geocell provide the long-term performance of a structure with smaller displacements. A three-dimensional geocell which is infilled with soil or gravel will have both shear and bending moment resistance. This makes the geocell-reinforced

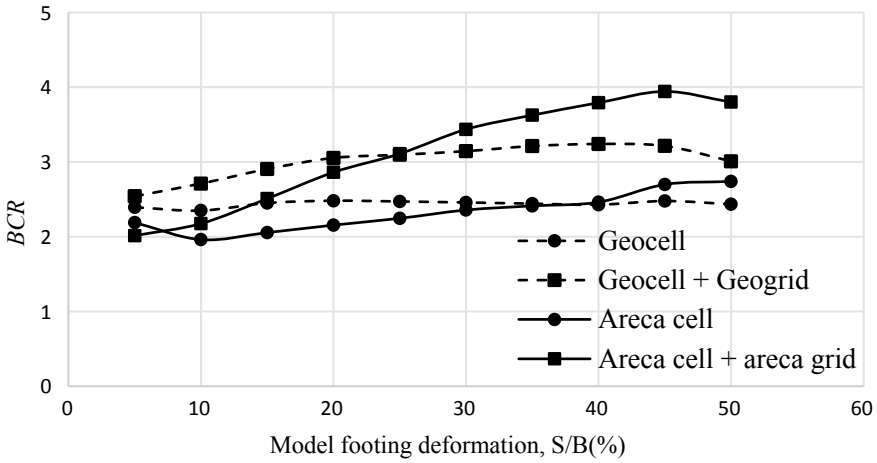

Fig. 16.9 Bearing capacity ratio versus deformation

bed to exhibit a higher capacity to absorb and dissipate energy from side to side and up-down motion as well. The chapter presented experimental investigations of different types of natural geocells in comparison with HDPE geocells as cellular confinement in clayey soil.

The major findings from this study are listed below:

1. The soil confined with the commercially available geocells proved to have 2.5 times higher bearing capacity as compared with the unreinforced soil, whereas for the areca cells it was found to be increased by 2.8 times. The performance of coir and sisal geocells was also promising, whereas jute was not efficient to provide the reinforcing effect.
2. The load-bearing capacity of the soil was observed to be maximum in case of soil reinforced with coir geocell.
3. From this experimental study, it can be concluded that the settlement versus load plot for natural fiber geocells—coir, jute, and sisal—are linear, and therefore, a reliable reinforcement material when compared to HDPE geocell material fails abruptly.
4. The bearing capacity of the soil reinforced with natural fiber geocells is about 3–4 times larger than that of unreinforced soil, and therefore, it can be used as an effective alternative material to the HDPE material.
5. The tensile strength of the areca woven geocells is four times greater than that of the HDPE geocell. However, the strain percentage is less in areca as compared to the HDPE geocells, and hence, areca cells can be recommended to use only in low strain geotechnical applications.

Natural cells were found to be highly cost-effective and environmentally friendly material that can be used in place of the polymer-based commercially available

HDPE geocells. Reinforcing the soil with abundantly available, eco-friendly, and cost-efficient coir material, areca leaf and sisal fibers woven into geocells prove to be a better way to increase the bearing capacity of the weak soils and thereby enhance the construction above the weak soils. However, the performance of jute geocell was not so promising as compared to areca, coir, and sisal. Usage of areca, coir, and sisal materials will most likely build a business arena for the farmers and cottage industries. In addition to HDPE geocells, geocells made out of natural materials have great scope for potential applications in ground engineering.

References

Binquet J, Lee KL (1975) Bearing capacity tests on reinforced earth slabs. J Geotech Eng Div ASCE 101(GT12):1241–1255

Chen R-H, Huang Y-W, Huang F-C (2013) Confinement effect of geocells on sand samples under triaxial compression. Geotext Geomembr Elsevier 37(2013):35–44. https://doi.org/10.1016/j.geotexmem.2013.01.004

Dash SK, Sireesh G, Sitharam TG (2003a) Model studies on circular footing supported on geocell reinforced sand underlain by soft clay. Geotext Geomembr 21:197–219

Dash SK, Sireesh G, Sitharam TG (2003b) Model studies on circular footing supported on geocell reinforced sand underlain by soft clay. Geotext Geomembr Elsevier 21(2003):197–219. https://doi.org/10.1016/S0266-1144(03)00017-7

Harikumar M, Sankar N, Chandrakaran S (2016) Behaviour of model footing resting on sand bed reinforced with multidirectional reinforcing elements. Geotext Geomembr 44:568–578

Hegde A, Sitharam TG (2015) Experimental and analytical studies on soft clay beds reinforced with bamboo cells and geocells. Int J Geosynthetics Ground Eng 1:(1–13). https://doi.org/10.1007/s40891-015-0015-5

Hegde A, Sitharam TG (2017) Experiment and 3D-numerical studies on soft clay bed reinforced with different types of cellular confinement systems. Transp Geotech 10:73–84

Kargar M, Mir Mohammad Hosseini SM (2017) Effect of reinforcement geometry on the performance of a reduced-scale strip footing model supported on geocell-reinforced sand. Trans A: Civil Eng Scientia Iranica A 24(1):96–109

Kolathayar S, Aravind CA, Sitharam TG (2019) Model tests and analytical studies on performance of areca leaf cells as cellular confinement in soil. Geomech Geoengin 1–12

Kolathayar S, Narasimhan S, Kamaludeen R, Sitharam TG (2020) Performance of footing on clay bed reinforced with coir cell networks. Int J Geomech 20(8):04020106

Lal D, Sankar N, Chandrakaran S (2017) Effect of reinforcement form on the behaviour of coir geotextile reinforced sand beds. Soils and Found 57(2017):227–236. https://doi.org/10.1016/j.sandf.2016.12.001

Pokharel SK, Han Jie, Leshchinsky Dov, Parsons RL, Halahmi I (2010) Investigation of factors influencing behavior of single geocell-reinforced bases under static loading. Geotext Geomembr Elsevier 28(2010):570–578. https://doi.org/10.1016/j.geotexmem.2010.06.002

Rajagopal K, Krishnaswamy NR, Madhavi Latha G (1999) Behaviour of sand confined with single and multiple geocells. Geotext Geomembr Elsevier 17:171–184. https://doi.org/10.1016/S0266-1144(98)00034-X

Roy SS, Deb K (2017) Bearing capacity of rectangular footings on multilayer geosynthetic-reinforced granular fill over soft soil. Int J Geomech 17(9):04017069

Selvadurai APS, Gnanendran CT (1989) An experimental study of a footing located on a sloped fill: influence of a soil reinforcement layer. Can Geotech J 26:467–473

Tafreshi MSN, Dawson AR (2010) Comparison of bearing capacity of a strip footing on sand with geocell and with planar forms of geotextile reinforcement. Geotext Geomembr 28:72–84
Tafreshi MSN, Norouzi AH (2012) Bearing capacity of a square model footing on sand reinforced with shredded tire—an experimental investigation. Constr Build Mater 35:547–556
Tafreshia MSN, Sharifia P, Dawsonb AR (2016) Performance of circular footings on sand by use of multiple-geocell or -planar geotextile reinforcing layers. Soils and Found 56(2016):984–997
Vinod P, Ajitha B, Sreehari S (2009) Behavior of a square model footing on loose sand reinforced with braided coir rope. Geotext Geomembranes 27:464–474

Chapter 17
Performance of Bamboo Geocells in Soft Ground Engineering Applications

Amarnath M. Hegde and Prof. T. G. Sitharam

Abstract This chapter presents the results of the laboratory investigation performed on clay bed reinforced with natural (bamboo) and commercial (geosynthetics) reinforcement materials. 3D cells (similar to geocells) and 2D grids (similar to geogrids) were formed using bamboo known as bamboocells and bamboogrids, respectively. The performance of bamboocells and bamboogrids reinforced clay beds were compared with that of reinforced geocells and geogrids. Bearing capacity of the clay bed is increased by 6 times due to the provision of combination of geocell and geogrid. The ultimate bearing capacity of the bamboocell and bamboogrid reinforced clay bed was found to be 1.3 times that reinforced with geocell and geogrid. Also, substantial reduction in the footing settlement and the surface deformation was observed. The tensile strength and surface roughness of the bamboo were found to be 9 times and 3 times higher than geocell materials. The bamboo was treated chemically to increase the durability. The performance of the bamboo was reduced by 15–20% after the chemical treatment; still the performance was better than its commercial counterparts.

Keywords Soft soil · Geosynthetics · Footing · Bearing capacity · Bamboo · Geocell · Geogrid · Settlement

17.1 Introduction

Due to the rapid urbanization in the twenty-first century, the construction in the soft ground has almost become inevitable. Soft ground engineering offers enormous challenges to the engineers across the globe. Ground improvement techniques are

A. M. Hegde (✉)
Department of Civil and Environmental Engineering, Indian Institute of Technology Patna, Patna 801106, India
e-mail: ahegde@iitp.ac.in

Prof. T. G. Sitharam
Department of Civil Engineering, Indian Institute of Technology Guwahati (IITG), Surjyamukhi Road, North, Amingaon, Guwahati, Assam 781039, India

T. G. Sitharam et al. (eds.), *Geocells*, Springer Transactions in Civil and Environmental Engineering,
https://doi.org/10.1007/978-981-15-6095-8_17

the largely preferred techniques in soft soils for low-to-moderate loading conditions. Engineers and scientists are constantly looking for new ground improvement techniques which are cheaper (compared to the present techniques) and more amenable to the field construction. Geocells are three-dimensional expandable panels made up of high-density polymers which are specially designed for load-bearing applications in soft soils. Many researchers have reported the beneficial effects of geocells (Madhavi et al. 2009; Dash 2010, 2012; Han et al. 2011; Moghaddas Tafreshi et al. 2013, 2014; Hegde and Sitharam 2013, 2015b, c Mehdipour et al. 2013; Leshchinksy and Ling 2013; Sitharam and Hegde 2013; Tanyu et al. 2013; Hegde et al. 2014). This study intends to explore the possibility of using naturally available bamboo to construct three-dimensional cells and uses it in soft soils as an alternative to the commercially available geocells. Bamboos are one of the fastest-growing plants and been heavily used as the building materials in the construction industry.

Coincidently, the regions which are facing the problems pertaining to the soft soils also have abundant sources of bamboo (e.g., Southeast Asia, India, etc.). Generally, short-term stability is the major governing factor in the design of the geotechnical structures in the soft soils. The soil gains the strength with the time due to the continuous process of consolidation. Bamboo is a biodegradable material which imparts the required short-term stability to the soil before it slowly breaks down and mixed with the soil. However, nowadays techniques are available to increase the durability of the bamboo through impregnation of the preservatives by various means.

The use of wood in the foundation construction is not a new concept. World-famous monument Taj Mahal was built on the gigantic wooden slabs made of ebony wood supported on the deep wall foundations www.scientifichistory.blogspot.in (Dec 4, 2013). The massive solid foundation of the Taj Mahal including the wooden shock absorbers has defied the onslaught of time keeping the superstructure stable for more than three and a half centuries without any deterioration. Generally, in geotechnical engineering applications, bamboo is used in two ways. One is to use bamboo directly to build a foundation as illustrated in the case of Taj Mahal. The other way is to use bamboo to reinforce the soft soil to increase its bearing capacity. This paper deals with the latter case, where bamboo is used to increase the bearing capacity of the soft soil. Hence, reported findings are applicable to all those geotechnical problems in which bearing capacity of the soil is major concern, e.g., foundations, embankments, pavements, etc.

Many researchers have studied the different engineering properties of the bamboo in the past in both natural and laminated forms (e.g., Mitch et al. 2010; Madhavi et al. 2011; Ramirez et al. 2012; Sinha and Miyamoto 2013). The concept of using natural and artificial fibers to reinforce the soil is not a new concept, and there are instances where these fibers were used to enhance the strength and stiffness of soil (Sivakumar Babu and Vasudevan 2008; Jiang et al. 2010). However, very few works have been reported on the direct use of bamboo to increase the strength of the soil. Khatib (2009) conducted the laboratory plate load tests to evaluate the effectiveness of bamboo poles in increasing the bearing capacity of the soft soil. Researchers observed 1.8 times increase in bearing capacity due to the provision of the bamboo pole as compared to

unreinforced clay beds. The recent trend is to use bamboo along with other materials such as geotextiles and bitumen. Marto and Othaman (2011) compared the performance of the bamboo geotextile composite (BGC) reinforced embankments with the high-strength geotextile (HSG) reinforced embankments in soft soil through large-scale model tests. Researchers observed that BGC reinforced embankments conceded lesser settlements and lateral movements than the HSG reinforced embankments. Similarly, Prasad et al. (2010) studied the performance of the reinforced granular subbase layers with different reinforcing materials such as bitumen-coated bamboo, waste plastic, and waste tire rubber. Researchers rated bitumen-coated bamboo mesh (BCBM) superior to waste plastic and waste tire rubber. Toh et al. (1994) reported a case history of the use of geotextile-bamboo fascine mattresses to support a huge earth fill on the very soft soil in Kuala Lumpur, Malaysia. The authors observed that use of bamboo not only provided the stable platform to place the geotextile but also substantially increased the bearing capacity.

The general tendency is to use bamboo poles itself to reinforce the soil as reported in the most of the literature (e.g., Khatib 2009). Contrary to previous research, in the present study a unique attempt has been made to use bamboocells and bamboogrids to reinforce the soft soil. Bamboocells and bamboogrids resemble their commercial counterparts, namely geocells and geogrids, but are made out of bamboo strips. The bamboo strips were prepared in the laboratory from the locally available bamboo. The results of laboratory plate load tests conducted on soft soil reinforced with bamboocells and bamboogrids are discussed in the manuscript. The performances of the bamboocells and grids are compared with the geocells and geogrids. In addition, the bamboo strips were treated chemically using copper chrome arsenic (CCA) solution to improve the durability. The reported results also include the comparison of the performances of treated and untreated bamboocells and bamboogrids.

17.2 Experimental Setup

Plate load tests were conducted in an existing test tank cum loading apparatus in our laboratory. The test tank was having a dimension of 900 mm in length, 900 mm in width, and 600 mm in height. A square-shaped steel plate with 20 mm thick and 150 mm sides was used as the model footing. The base of the footing was made rough by coating a thin layer of sand using epoxy glue. Footing was loaded with hand-operated hydraulic jack supported against self-reacting frame. The load applied to the footing was measured through a pre-calibrated proving ring, which was placed between hydraulic jack and the footing with a ball bearing arrangement. Schematic and photographic views of the test setup are shown in Fig. 17.1.

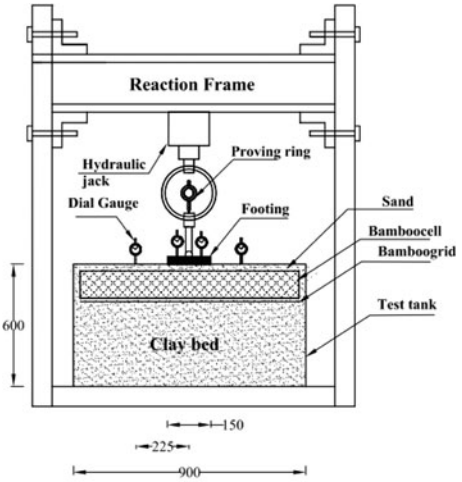

(a)

(b)

Fig. 17.1 Test setup: **a** schematic view; **b** photographic view (sourced from Hegde and Sitharam 2015a with permission from ASCE)

17.3 Materials Used

Natural silty clay with medium compressibility (CI) was used to prepare the foundation bed. The liquid limit, plastic limit, and the specific gravity of the soil were 40%, 19%, and 2.66, respectively. The maximum dry density and the optimum moisture content of the soil in the Standard Proctor test were 18.2 kN/m^3 and 13.2%, respectively. The silty clay was made of kaolinite clay mineral. The sand infill used in the experiment was classified as the poorly graded sand (with symbol SP as per unified

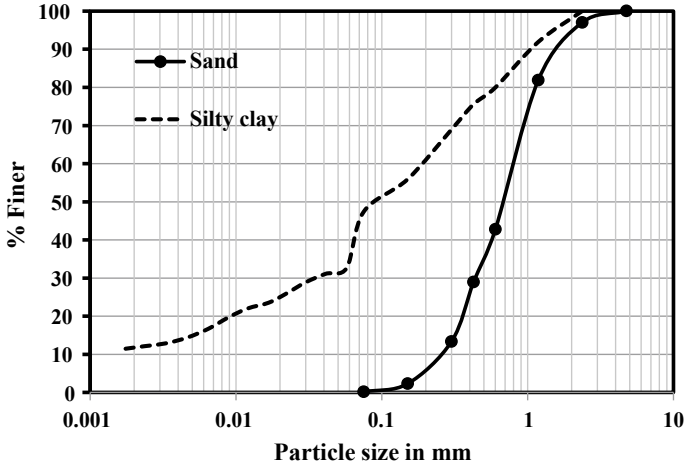

Fig. 17.2 Grain size distribution of the materials (sourced from Hegde and Sitharam 2015a with permission from ASCE)

soil classification system). Sand was having specific gravity, 2.64; effective particle size (D_{10}), 0.26 mm; coefficient of uniformity (C_u), 3.08; coefficient of curvature (C_c), 1.05; maximum void ratio (e_{max}), 0.81; and minimum void ratio (e_{min}), 0.51. The friction angle (φ) value of the sand as obtained from the triaxial compression test was found to be 36°. Grain-size distributions of the sand and silty clay are presented in Fig. 17.2.

The geocell used in the study was made up of Neoloy (Novel polymeric alloy). Each cell is 250 mm in length, 210 mm in width, and 150 mm in height. A biaxial geogrid made up of polypropylene which was used at the base of the geocell. The bamboo used in the study belongs to the Belgaum region in Karnataka State in India. The relatively fresh green bamboo was cut into pieces to obtain a strip of 20 mm width of required length. Then the strips are woven together to form a grid. These grids are tied together using galvanized steel wire to form a shape which resembles the geocells. The joint distances were maintained so as to give the pocket size of the bamboocells equivalent to that of commercial geocells used in the study. The properties of the different reinforcement materials used in the study are listed in Table 17.1.

17.4 Treatment of Bamboo

Generally, the durability of the natural bamboo is up to 5 years in the moist conditions (Gnanaharan 2000). The biodegradation of the bamboo with the time is a major concern in the geotechnical engineering applications. The biodegradation takes place

Table 17.1 Properties of different reinforcement materials used in the study (sourced from Hegde and Sitharam 2015a with permission from ASCE)

Parameters	Quantity
Geocell	
Material	Neoloy (Novel polymeric alloy)
Cell size (mm)	250 × 210
No. of cells/m^2	40
Cell depth (mm)	150
Strip thickness (mm)	1.53
Ultimate tensile strength (kN/m)	20
Seam peal strength (N)	2150 (±5%)
Density (g/cm^3)	0.95 (±1.5%)
Short-term yield strength (kN/m)	20
Perforations on the wall (%)	12% of the surface area
Surface roughness (μm)	1.12
Geogrid	
Polymer	Polypropylene
Aperture size (MD × XMD) mm	35 × 35
Ultimate tensile strength (kN/m)	20
Mass per unit area (g/m^2)	220
Shape of aperture opening	Square
Bamboo	
Species	Bambusa bambos
Water content (%)	23
Density (g/cc)	0.97
Ultimate tensile strength (kN/m)	253
Secant modulus at 2% strain (MPa)	5500

due to various sources in the form of moisture, fungi, and insect attacks. The biodegrading of the bamboo severely affects the strength and structural performance. To ensure the long-term structural performances, bamboo must be protected from the natural predators. Depending upon the state of the bamboo (green or dry), various techniques are available to preserve the bamboo. Steeping, diffusion process, and sap displacement are the commonly adopted methods for the treatment of fresh bamboo. The generally used methods for the treatment of the dry bamboo are soaking, pressure impregnation, and hot and cold process. In the present case, the bamboo was dry and hence soaking technique was chosen considering the simplicity and efficiency of the method. In soaking method, the air-dried bamboo girds were immersed in the preservative solution for a fixed duration. The commonly used chemical preservatives are boron containing compounds, zinc chloride, sodium pentachlorophenate (NaPCP), copper chrome arsenic (CCA), and copper chrome boron (CCB). However,

the most widely used preservative for dry bamboo is CCA www.bambootech.org (Nov 26, 2013). A typical composition of this preservative comprises of copper sulfate ($CuSO_4$. $5H_2O$), arsenic pentoxide (AS_2O_5. $2H_2O$), and sodium or potassium dichromate ($Na_2Cr_2O_7.2H_2O$ or $K_2Cr_2O_7$. $2H_2O$) in the proportion of 3: 1: 4 conforming to ASTM D 1625-71 & IS 10013 (Part 2). CCA is a fixing-type preservative with chromium acting as a fixing agent, and copper is effective against fungi and soft rot, while the arsenic acts against termites and insects. The bamboogrids were immersed in the CCA solution for 7 days. The grids were dried in the sunlight before the use. Figure 17.3 shows the CCA treatment of the bamboo.

Chemical composition test was carried out using energy dispersive X-ray analysis (EDAX) to ascertain the effectiveness of the treatment. It is an extensively used

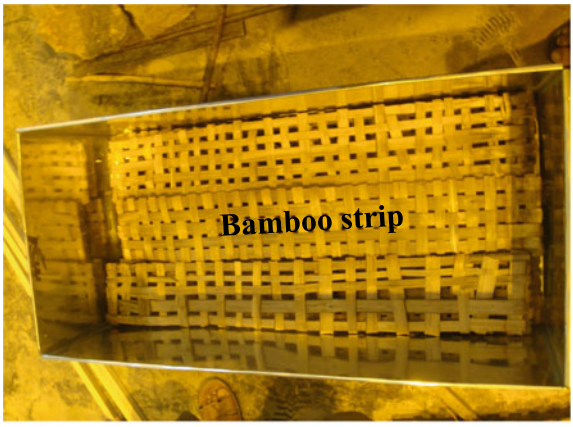

(a)

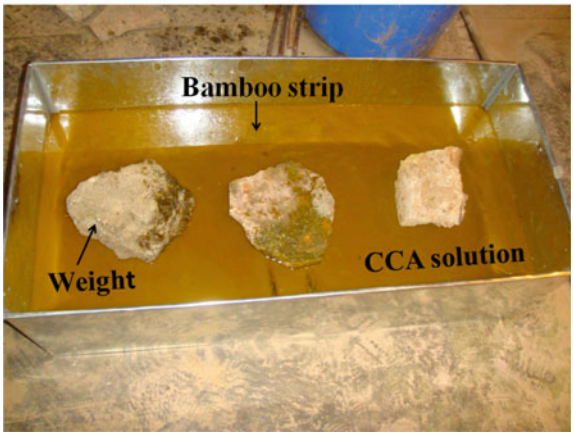

(b)

Fig. 17.3 **a** and **b** CCA Treatment: **a** bamboo strips before immersing; **b** bamboo strips after immersing in CCA (sourced from Hegde 2015)

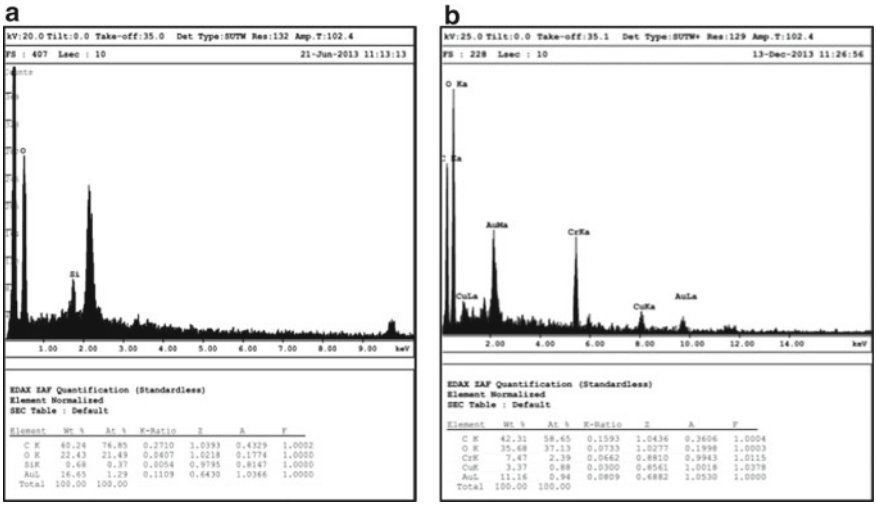

Fig. 17.4 EDAX Images: **a** untreated bamboo; **b** treated bamboo (Sourced from Hegde and Sitharam 2015a with permission from ASCE)

technique to analyze the chemical components of a material. In this method, an electron beam is allowed to focus on the sample in a scanning electron microscope. The electrons will penetrate into the sample and interact with the atoms with which it is made. This interaction will lead to the generation of X-rays. The generated X-rays are captured by an energy dispersive detector. By analyzing these X-rays, the concentrations of the elements are quantified. A sample size of 5 mm × 5 mm was used for the EDAX analysis. Before the test, aurum (A_u) coating of thickness 10 nm was applied to increase the conductivity of the sample. Figure 17.4 shows the EDAX results for untreated and treated bamboo. The result shows (Fig. 17.4a) that the carbon content (C) of 60% and oxygen (O) content more than 20% are present in the untreated bamboo. In the case of treated bamboo, the presence of chromium (C_r) and copper (C_u) was found (Fig. 17.4b) in addition to the carbon and the oxygen. The presence of chromium and copper content is due to the treatment with CCA solution. It indicates that the immersion technique adopted for treatment has successfully injected CCA into the bamboo strips.

17.5 Comparison of Properties of Geocell and Bamboo

17.5.1 Tensile Strength

Figure 17.5 represents the comparison of tensile stress–strain behavior of the different materials. In case of geocell and bamboo, the test sample of width 25 mm cut from

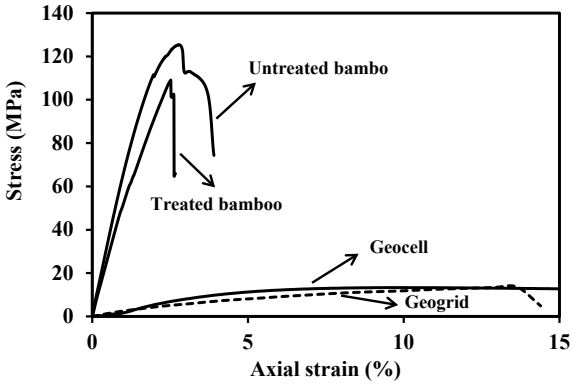

(a)

(b)

Fig. 17.5 Tensile test: **a** stress–strain behavior of different material (Sourced from Hegde and Sitharam 2015a with permission from ASCE); **b** bamboo sample during testing (sourced from Hegde and Sitharam 2015d)

seam-to-seam was used for tensile testing. The strain rate applied was 0.1% of the gauge length of the sample per sec. Multi-rib tensile strength test was carried out as per ASTM D 6637-11 to determine the tensile properties of the geogrid. The tensile strength of the bamboo found to be 9 times higher than the geocell and geogrid materials. After the treatment, the ultimate tensile strength of the bamboo was reduced by 15%. The nature of the stress–strain behavior indicates that the bamboo is brittle compared to geocells and geogrids.

It is well-known fact that the soil is very weak in resisting the tension load and can perform better under the action of compression load. The very concept behind the soil reinforcement is to insert those materials into soil which are good in tension, such that soil can take both tension and compression loads. Hence, higher tensile strength is one of the basic characteristics that soil reinforcement should possess with.

17.5.2 Surface Roughness

Figure 17.6 shows the scanning electron microscopy (SEM) images of the geocell and the bamboo. The image shows the unique texture on the surface of both geocell and the bamboo. These surface textures are responsible for the interface friction between the material and the soil. The geocell surface has the cup-shaped textures made up of the polymeric resins. In case of the bamboo, the horizontal strips of natural fibers contribute to the roughness of the surface.

The features of the surface texture were quantified using the surface roughness value (Ra). The surface roughness of the samples was estimated using Talysurf CCI Lite optical profilometer. The Talysurf CCI Lite is a non-contact type of profilometer, which uses an innovative correlation algorithm to find the coherence peak and the phase position of the interference pattern. It pictorially reproduces the minute textures present on the surface of the material in three-dimensional form. It computes the height difference between the peak and the valley at the different points on the surface before averaging it to arrive at one value called surface roughness value (R_a). In a way, roughness is nothing but the average height of the textures present on the surface. The Talysurf CCI Lite is extensively used in many applications requiring high precision 3D profile analysis. The instrument can measure the roughness of the variety of materials, including the glass, metals, polymers, etc. Figure 17.7 represents the 3D surface profiles of the different samples. A small strip of the sample of size 5 mm × 5 mm was used for surface profiling. The surface roughness values observed for commercially available geocell, treated, and untreated bamboos were 1.12 μm, 3.86 μm, and 3.08 μm, respectively. The surface roughness of the natural bamboo is about 3.5 times higher than that of the geocell. With treatment, the roughness value was found to be reduced by 20%.

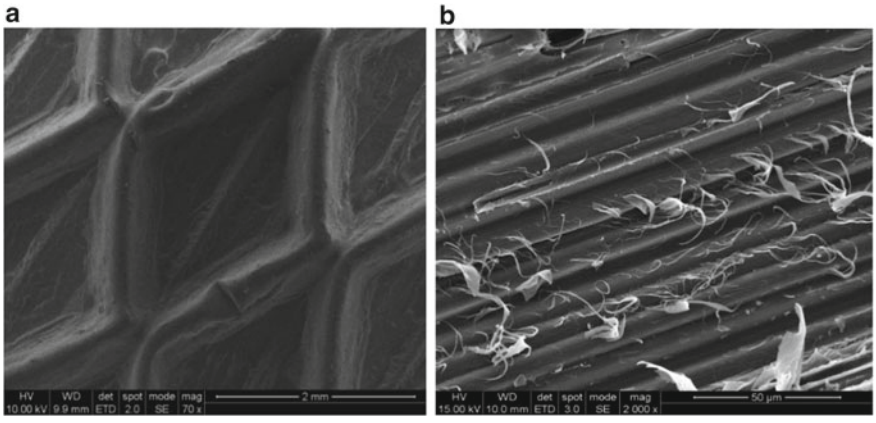

Fig. 17.6 SEM images: **a** geocell; **b** bamboo (sourced from Hegde and Sitharam 2015a with permission from ASCE)

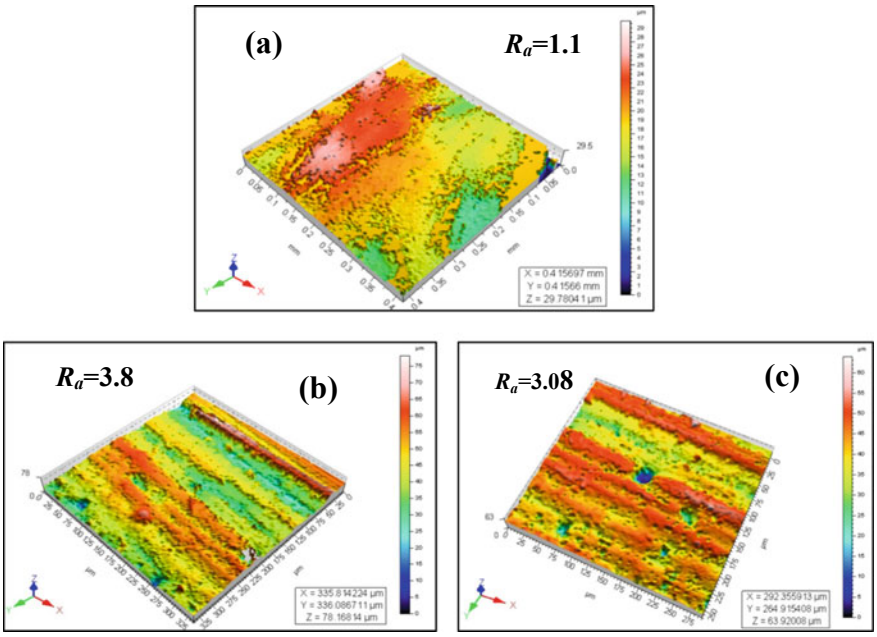

Fig. 17.7 3D surface roughness profile: **a** geocell; **b** untreated bamboo; **c** treated bamboo (sourced from Hegde and Sitharam 2015a with permission from ASCE)

Roughness of the surface has the significant effect on the performance of the reinforcement. Generally, roughness is the indication of the textures present on the surface of the reinforcement. It is understood that geocell/bamboocell pockets are filled with granular material like sand. When these granular materials come in contact with the surface textures, friction force will generate at the interface. These friction forces act in the upward direction and will help to resist the imposed load (Koerner 1998; Hegde and Sitharam 2015b). Hence, surface roughness of the reinforcement has the substantial influence on the bearing capacity of the reinforced foundation bed.

17.6 Laboratory Plate Load Tests

17.6.1 Clay Bed Preparation

The clayey soil was first pulverized and then mixed with a predetermined amount of water. The moist soil was placed in the airtight container for 3–4 days for allowing uniform distribution of moisture within the sample before kneading again. Soil was uniformly compacted in 25-mm-thick layers to achieve the desired height of the

foundation bed. A manually operated plate compactor was used for the purpose. The sides of the tank were coated with polyethylene sheets to avoid the side friction. By carefully controlling the compaction effort and the water content of the test bed, a uniform test condition was maintained in all the tests. The fall cone apparatus was used to measure the undrained cohesion of the bed. Undisturbed samples were collected at different location of the test bed to determine the properties of the test bed. The test bed was having unit weight, 18.63 kN/m^3; moisture content, 26%; degree of saturation, 91%; undrained shear strength, 5 kPa; and average dry density, 14.81 kN/m^3.

17.6.2 Test Procedures

Above the clay bed, the reinforcements were placed to the full width of the tank. Figure 17.8 represents the geocells and bamboocells in the expanded from inside the test tank. The cell pockets were filled up with the clean sand using pluviation technique to maintain the uniform density. A layer of geotextile was used as a separator between soft clay bed and the sand overlaying it. Upon filling the geocell with the sand, the fill surface was leveled and footing was placed in a predetermined alignment in such a way that the load from the jack would act at the center on the footing. The load transferred to the footing was measured through the pre-calibrated proving ring placed between ball bearing and hydraulic jack. Loads were applied in steps with equal load increments in each step. The magnitude of each load increment was equal to 0.34 kN, and it was equivalent to 15 kPa in terms of footing pressure. Footing settlements were measured through two dial gauges ($D1$ and $D2$) placed on either side of the centerline of the footing. The deformations of the soil surface were measured by dial gauges ($S1$ and S2) placed at a distance $1.5B$ (B is the width of the footing) from the centerline of the footing on either side. The footing settlement (S) and the surface deformation (δ) were normalized by footing width (B) to express them in non-dimensional form as S/B (%) and d/B (%). In all the plots, settlements are reported with the positive sign and heave with the negative sign.

17.6.3 Testing Program

The size of the footing (B = 150 mm), height of the geocell/bamboocell (H = 150 mm), pocket size of the geocell/bamboocell (250 mm × 210 mm), and thickness of the clay bed (t = 400 mm) were maintained constant thought the testing program. In reinforced tests, the reinforcement was placed for the full width of the tank leaving the small distance between the tank wall and the reinforcement to avert the boundary effects. In other words, the width of the reinforcement is about the 6 times the width of the footing. Dash et al. (2001) reported the optimum depth of geocell placement as 0.1 B (where B is the width of footing) from the bottom of the footing. Similarly,

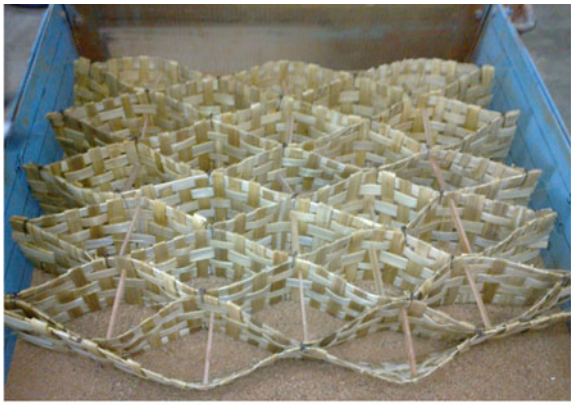

(a)

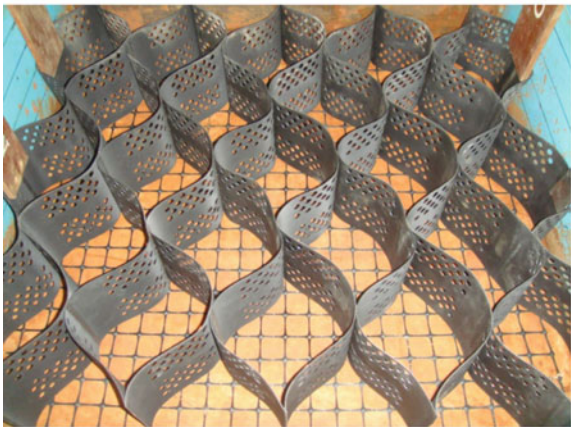

(b)

Fig. 17.8 **a**-**b** Photographs: **a** bamboocell; **b** geocell (sourced from Hegde and Sitharam 2015d)

many researchers reported the optimum depth of placement of the planar geogrid from 0.30 B to 0.37 B (e.g., Huang and Tatsuoka 1990; Omar et al. 1993; Khing et al. 1993). Hence, in the present investigation, the geocell/bamboocell was placed at the depth of 0.1 B (u) and the geogrid/bamboogrid was placed at the depth 0.3 B (v). Details of the tests are summarized in Table 17.2. The geometry of the test configuration is shown in Fig. 17.9.

Table 17.2 Test details (sourced from Hegde and Sitharam 2015a)

Test series	Type of test	Test details
A	Unreinforced	–
B	Test with geosynthetics	Only geogrid, only geocell and geocell + geogrid
C	Test with untreated bamboo	Only bamboogrid, only bamboocell and bamboocell + bamboogrid
D	Test with treated bamboo	Only bamboogrid, only bamboocell and bamboocell + bamboogrid

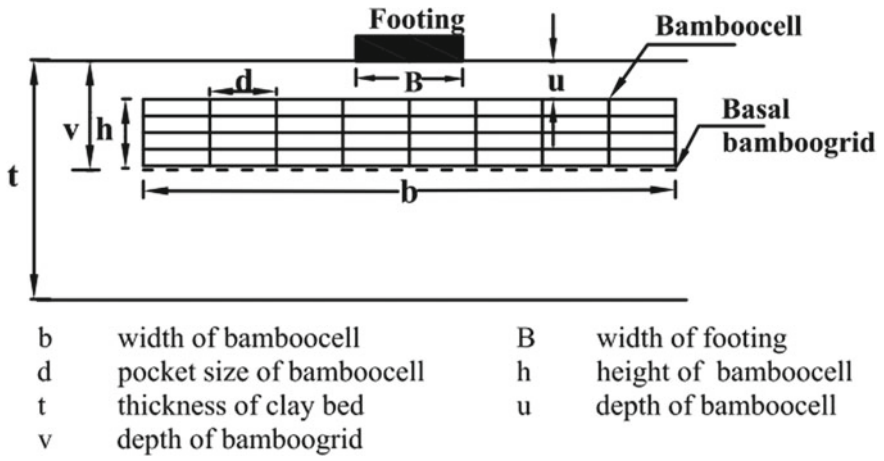

Fig. 17.9 Geometry of the test configuration (sourced from Hegde and Sitharam 2015a with permission from ASCE)

17.7 Results and Discussion

Figure 17.10 represents the bearing pressure-settlement behavior of the clay bed reinforced with different types of reinforcements. A substantial increment in the bearing capacity was observed due to the provision of reinforcements as compared to unreinforced clay bed. In case of unreinforced bed, load settlement curve becomes almost vertical beyond $S/B = 5\%$ indicating the failure of the bed. However, there was no clear cut failure was observed in the presence of reinforcement. As expected, ultimate bearing capacity of the clay bed reinforced with 3D reinforcements is much higher than that reinforced with planar reinforcements. In 3D reinforcements also, bamboocells provided much higher bearing capacity than the geocells. From the load settlement curve, it is obvious that the use of combination of geocell and geogrid or combination of bamboocell and bamboogrid yields a better performance than using geocell or bamboocell alone. Out of all tested combinations, the performance of the combination of untreated bamboocells and bamboogrids is found to be better than any other type or combination of reinforcements. The bearing capacity of the clay

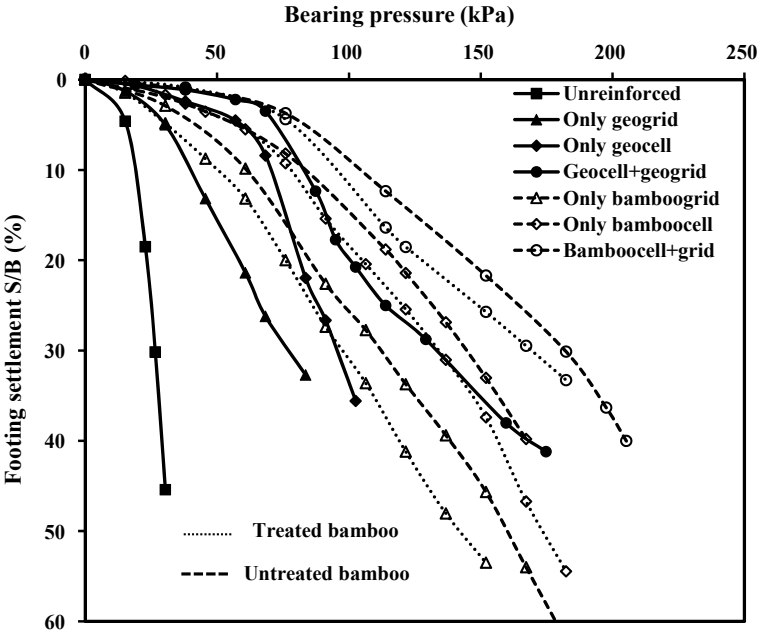

Fig. 17.10 Bearing pressure-settlement curves for different tests (sourced from Hegde and Sitharam 2015a with permission from ASCE)

bed reinforced with bamboocell and grid found to be 1.2–1.5 times higher than that reinforced with geocells and geogrids.

The increase in the bearing capacity due to the provision of the reinforcement can be measured through a non-dimensional parameter called bearing capacity improvement factor (I_f), which is defined as,

$$I_f = \frac{q_r}{q_o} \tag{17.1}$$

where q_r is the bearing pressure of the reinforced soil at the given settlement and q_o is the bearing pressure of unreinforced soil at the same settlement. Binquet and Lee (1975) reported that the improvement factor is similar to the bearing capacity ratio. When the ratio is beyond the ultimate bearing capacity of the unreinforced soil, the ultimate bearing capacity (q_{ult}) is used instead of q_0. Variations of bearing capacity improvement factors with footing settlement for different tests are shown in Fig. 17.11. I_f value is found to be increased with the increase in footing settlement. The maximum value of If, i.e., $I_f = 7$ was observed in the case of combination of bamboocell and the bamboogrid. $I_f = 7$ means the seven time increment in the load-carrying capacity of the foundation bed as compared to the unreinforced bed. From the figure, it is evident that the even bamboocell alone in both treated and untreated from can yield the same performance as that of the combination of geocell

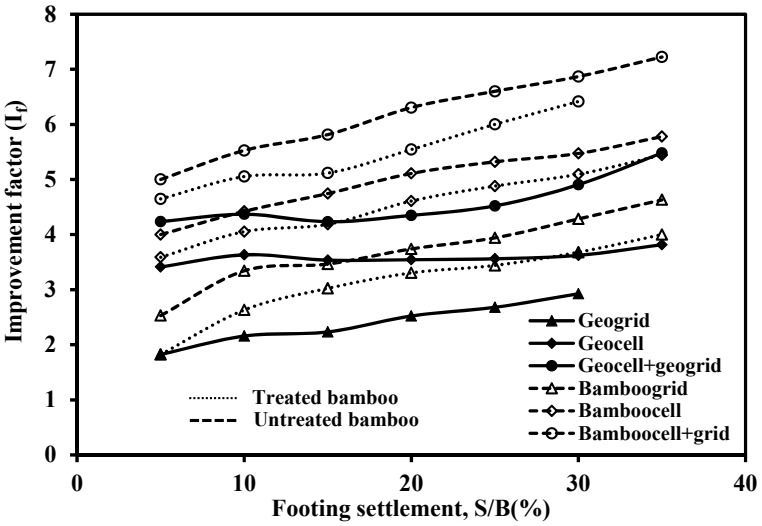

Fig. 17.11 Variation of bearing capacity improvement factor with footing settlement (sourced from Hegde and Sitharam 2015a with permission from ASCE)

and geogrid. Similarly, the performance of the untreated bamboogrid is as good as the geocells. It was found that the load-carrying capacity of the bamboo was reduced from 15 to 20% after the treatment. But still the treated bamboo products can produce better performance (1.1–1.3 times in terms of load-carrying capacity) than their geosynthetic counterparts.

The performance improvement of the foundation bed due to geocell reinforcement can also be quantified in terms of the reduction in the settlement of the footing using the parameter called percentage reduction in settlement (PRS). PRS is defined as,

$$\text{PRS} = \left(\frac{S_o - S_r}{S_o}\right) \times 100 \tag{17.2}$$

where S_o is settlement of the unreinforced foundation bed corresponding to its ultimate bearing capacity. The double tangent method (Vesic 1973) was used to estimate the ultimate load bearing capacity of the unreinforced clay bed. As per this method, the ultimate bearing capacity is defined as the pressure corresponding to the intersection of the two tangents: one at the early part of the pressure-settlement curve and the another at the latter part. In the present case, the ultimate bearing capacity was obtained at a settlement equal to 10% of the footing width ($S/B = 10\%$). S_r is settlement of reinforced foundation bed corresponding to the footing pressure equal to the ultimate bearing pressure of unreinforced foundation bed. Table 17.3 lists the PRS values for different forms and combination of the reinforcement. The maximum PRS = 97% was observed in the case of the clay bed reinforced with bamboocell and bamboogrids. PRS = 97% means, 97% reduction in the settlement in the reinforced

Table 17.3 PRS values observed at different test series (sourced from Hegde and Sitharam 2015a with permission from ASCE)

Test series	Type of test	Test details	PRS (%)
B	Test with geosynthetics	Only geogrid	72
		Only geocell	89
		Geocell + Geogrid	93
C	Test with untreated bamboo	Only bamboogrid	81
		Only bamboocell	92
		Bamboocell + bamboogrid	97
D	Test with treated bamboo	Only bamboogrid	73
		Only bamboocell	90
		Bamboocell + bamboogrid	95

bed as compared to the unreinforced clay bed. Bamboocells due to its beam action disperse the load to wider area. Due to this, the loading intensity on the soil will be lesser than what it supposed to be. This action leads to the reduction in the settlement of the bed. In addition, basal bamboogrid further reduces the settlement of the bed by arresting the downward movement of soil.

Figure 17.12 represents the variation of the surface deformation (settlement/heave) with footing settlement for different types of reinforcements. Surface

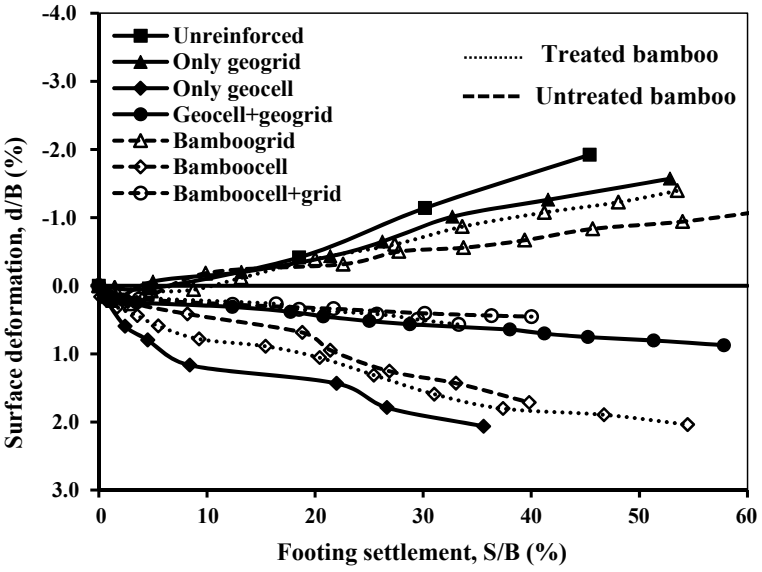

Fig. 17.12 Variation of surface deformation with footing settlement (sourced from Hegde and Sitharam 2015a with permission from ASCE)

deformation measurements were made through the dial gauges placed at the distance of 1.5*B* from the centerline of the footing. Chummar (1972) observed that the surface heaving extends up to 2*B* from the centerline of the footing in case of the unreinforced bed and with maximum heaving occurring at a distance of 1.5*B*. Surface deformation in the form of heaving equal to 2% of the footing width was observed in case of the unreinforced clay bed. Generally, surface heaving can be attributed to the shear failure of the soil mass. Heaving was also observed in the case of only geogrid and only bamboogrid reinforced beds. However, the amount of heaving was lesser as compared to unreinforced bed. Surface heaving was completely eliminated when the clay bed was reinforced with geocell or bamboocell in both treated and untreated forms. Instead, the settlement of the fill was observed. Maximum fill settlement up to 2% of the footing width was observed in case of the only geocell. The settlement of the fill was reduced when additional geogrid was provided at the base of geocells. The least settlement of the fill was observed in the case of combination of bamboocell and bamboogrid in the untreated form. Not much difference in the fill settlement was observed in case of the treated bamboocells and grids as compared to their untreated counterparts.

In addition to its performance benefits as a reinforcing material, bamboocells have got two other main advantageous over commercial geocells. Firstly, bamboo is environmental friendly. Bamboocells are not responsible for the emission of greenhouse gases and also not leave any carbon footprint. Secondly, the bamboo is cost-effective. Generally in a project, the total cost associated with installation of geocells includes many factors. In addition to maximum retail price (MRP) or market price of the geocells, the costs due to transportation (from selling point to a site) and costs due to installation also largely contribute to the overall cost of the project. The market price of a geocell covers, its raw material cost, manufacturing cost and the transportation cost from the manufacturing unit to selling point. However, if bamboocells are used in a place where it is available in a large quantity, the raw material cost and all types of transportation costs become negligible. In addition, the production cost also considerably on the lower side since bamboocells are fabricated at the site itself using local labors. The installation cost may be the same for both bamboocells and geocells. With the treatment, the overall cost of the bamboo may increase by 13–20%, depending on the type of treatment, but the durability will be increased by more than two times (Sharma et al. 1998). Hence, even with the treatment, the bamboocells are much cheaper compared to commercial geocells.

17.8 Summary

The results of the laboratory investigation performed on a clay bed reinforced with natural (bamboo) and commercial (geosynthetics) reinforcement materials are reported in the present chapter. In order to use the bamboo effectively, 3D cells (similar to geocells) and 2D grids (similar to geogrids) are formed using bamboo

known as bamboocells and bamboogrids, respectively. The performance of bamboocells and bamboogrids reinforced clay beds were compared with the clay bed reinforced geocells and geogrids. Bearing capacity of the clay bed increased by 4–5 times due to the provision of combination geocell and geogrid. The ultimate bearing capacity of the bamboocell and bamboogrid reinforced clay bed was found to be 1.5 times the bearing capacity of the clay bed reinforced with geocell and geogrid. Also, substantial reduction in the footing settlement and the surface deformation was observed. The tensile strength and surface roughness of the bamboo were found to be 9 times and 3 times higher than geocell materials. The bamboo was treated chemically to increase the durability. The performance of the bamboo was reduced by 15–20% after the chemical treatment; still the performance was better than its geosynthetic counterparts. The study has its own limitations. Only one type of geocell was used in the study. Hence, the results are applicable to limited cases only. One should be careful while applying these results directly to the prototype conditions. Considering the 1-*g* model tests, the results presented in the study are prone to scale effects. Hence, further studies recommended with either using centrifuge model tests or full-scale model tests. The 1-*g* model tests are conducted only to understand the basic mechanism and overall trends in the results. These results will be of use in providing guidelines for design and construction of bamboocell-reinforced clay foundations, conducting large-scale model tests, and developing numerical models. The 1-*g* model tests conducted in the present study are successful enough to highlight the efficacy of treated and untreated bamboo products in improving the strength of the soft soils.

References

Binquet J, Lee LK (1975) Bearing capacity tests on reinforced earth slabs. J Geotech Eng Div 101(12):1241–1255

Chummar AV (1972) Bearing capacity theory from experimental results. J Geotech Eng Div 12:1257–1276

Dash SK (2010) Influence of relative density of soil on performance of geocell reinforced sand foundations. J Mater Civ Eng 22(5):533–538

Dash SK (2012) Effect of geocell type on load carrying mechanism of geocell-reinforced sand foundations. Int J Geomech 12(5):537–548

Dash SK, Krishnaswamy NR, Rajagopal K (2001) Strip footing on geocell reinforced sand beds with additional planar reinforcement. Geotext Geomembr 19:529–538

Gnanaharan R (2000) Preservative treatment methods for bamboo: a review. Technical report 177 (ii), Kerala Forest Research Institute, Trissur, pp 1–20

Han J, Pokhrel SK, Yang X, Manandhar C, Leshchinsky D, Halahmi I, Parsons RL (2011) Performance of geocell reinforced RAP bases over weak subgrade under full scale moving wheel loads. J Mater Civ Eng 23(11):1525–1534

Hegde A, Sitharam TG (2013) Experimental and numerical studies on footings supported on geocell reinforced sand and clay beds. Int J Geotech Eng 7(4):347–354

Hegde A (2015) Ground improvement using 3d-cellular confinement systems: experimental and numerical studies. Ph.D. thesis submitted to Indian Institute of Science Bangalore, India.

Hegde A, Sitharam TG (2015a) Use of bamboo in soft ground engineering and its performance comparison with geosynthetics: Experimental studies. J Mater Civ Eng ASCE 27(9):04014256

Hegde A, Sitharam TG (2015b) Joint strength and wall deformation characteristics of a single cell subjected to uniaxial compression. Int J Geomech 15(5):04014080
Hegde AM, Sitharam TG (2015c) Effect of infill materials on the performance of geocell reinforced soft clay beds. Geomech Geoengineering 10(3):163–173
Hegde A, Sitharam TG (2015d) Experimental and analytical studies on soft clay beds reinforced with bamboo cells and geocells. Int J Geosynthetics Ground Eng 1(2):1–13
Hegde A, Kadabinakatti S, Sitharam TG (2014) Protection of buried pipelines using a combination of geocell and geogrid reinforcement: experimental studies. Geotechnical Special Publication-238, ASCE, Ground Improvement and Geosynthetics, pp 289–298
Huang CC, Tatsuoka F (1990) Bearing capacity of reinforced horizontal sandy ground. Geotextiles and Geomembranes 9(1):51–82
Jiang H, Cai Y, Liu J (2010) Engineering properties of soils reinforced by short discrete polypropylene fiber. J Mater Civ Eng 22(12):1315–1322
Khatib A (2009) Bearing capacity of granular soil overlying soft clay reinforced with bamboo-geotextile composite at the Interface. (PhD. thesis) Department of Geotechnics and Transportation, Faculty of Civil Engineering, University Technology Malaysia
Khing KH, Das BM, Puri VK, Cook EE, Yen SC (1993) The bearing capacity of a strip foundation on geogrid reinforced sand. Geotext Geomembr 12:351–361
Koerner RM (1998) Designing with geosynthetics. Prentice Hall, New Jersey-07632
Leshchinsky Ben, Ling Hoe (2013) Effects of geocell confinement on strength and deformation behaviour of gravel. J Geotech Geoenviron Eng 139(2):340–352
Madhavi Latha G, Dash SK, Rajagopal K (2009) Numerical simulations of the behaviour geocell reinforced sand in foundations. Int J Geomech 9(4):143–152
Mahdavi M, Clouston PL, Arwade SR (2011) Development of laminated bamboo lumber: review of processing, performance, and economic considerations. J Mater Civ Eng 23(7):1036–1042
Marto A, Othman BA (2011) The potential use of bamboo as green material for soft clay reinforcement system. In: International Conference on Environment Science and Engineering, Singapore. IPCBEE, 8, 129–133
Mehdipour Iman, Ghazavi Mahmoud, Moayed RZ (2013) Numerical study on stability analysis of geocell reinforced slopes by considering the bending effect. Geotext Geomembr 37:23–34
Mitch D, Harries KA, Sharma B (2010) Characterization of splitting behavior of bamboo culms. J Mater Civ Eng 22(11):1195–1199
Moghaddas Tafreshi SN, Khalaj O, Dawson AR (2013) Pilot-scale load tests of a combined multilayered geocell and rubber-reinforced foundation. Geosynthetics Int 20(3):143–161
Moghaddas Tafreshi SN, Khalaj O, Dawson AR (2014) Repeated loading of soil containing granulated rubber and multiple geocell layers. Geotext Geomembr 42:25–38
Omar MT, Das BM, Puri VK, Yen SC (1993) Ultimate bearing capacity of shallow foundations on sand with geogrid reinforcement. Can Geotech J 30:545–549
Prasad DSV, Anjan Kumar M, Prasada Raju GVR (2010) Behavior of reinforced sub bases on expansive soil sub grade. Global J Res Eng 10:2–8
Ramirez F, Correal JF, Yamin LE, Atoche JC, Piscal CM (2012) Dowel-bearing strength behavior of glued laminated guadua bamboo. J Mater Civ Eng 24(11):1378–1387
Sharma NM, Venmalar D, Vani CN, Rao SP (1998) Studies on the treatment of green Bambusa Arundinacea by sap displacement method. My Forest 34(1):685–696
Sinha A, Miyamoto BT (2013) Lateral load carrying capacity of laminated bamboo lumber to oriented strand board connections. J Mater Civ Eng 26(4):741–747
Sitharam TG, Hegde A (2013) Design and construction of geocell foundation to support embankment on soft settled red mud. Geotext Geomembr 41:55–63
Sivakumar Babu GL, Vasudevan AK (2008) Strength and stiffness response of coir fiber-reinforced tropical soil. J Mater Civ Eng 20(9):571–577
Tanyu BF, Aydilek AH, Lau AW, Edil TB, Benson CH (2013) Laboratory evaluation of geocell-reinforced gravel sub-base over poor subgrades. Geosynthetics Int 20(2):46–71

Toh CT, Chee SK, Lee CH, Wee SH (1994) Geotextile-bamboo fascine mattress for filling over very soft soils in Malaysia. Geotext Geomembr 13:357–369
Vesic AS (1973) Analysis of ultimate loads of shallow foundations. J Soil Mech Found Div 99:45–69

Chapter 18
Coir Geocells

K. Balan

Abstract Behaviour of geocells made of woven coir geotextiles, placed over soft soil, was studied by varying the width, height and cell size through model tests. The studies have shown that, with the provision of geocell-reinforced sand cushion, there is a substantial reduction in settlement of the underlying soft soil due to modified stress distribution. The beneficial effect in terms of increased bearing capacity and reduced settlement is proportional to the width, height and cell size of coir geocell mattress. Optimum width, height and cell size of coir geocell were derived from the model tests. A tenfold increase in bearing capacity of soft clay is obtained by the provision of geocell reinforcement in the system. The performance of coir geocell with synthetic geocell having same width, height, cell size and shape were also evaluated and found that for 10 cm high geocell, the bearing capacity of synthetic geocell is 1.73 times more than that of coir geocell. In the case of 20 cm high geocell, the average increase in bearing capacity of synthetic geocell is 2.29 times that of geocell with coir.

Keywords Coir · Coir geocell · Natural geotextiles · Soft soil · Reinforcement

18.1 Introduction

Geotextiles made of coir and jute are used for non-critical civil engineering applications such as erosion control, silt fence and separation layer. In the geosynthetic market, geotextiles/composites made of natural fibres such as coir, jute sisal hemp and straw are occupying their share. But the extent of their usage even today is limited to 2–3% of the total quantity of geosynthetics used in civil engineering and is being used mainly for erosion control application. India is the first largest country (66% of the world production) producing coir fibre. Coir fibres can be converted into fabric both by woven and non-woven (stitched, needle punched, adhesive bonded) process.

K. Balan (✉)
Rajadhani Institute of Engineering and Technology, Attingal, Trivandrum, Kerala, India
e-mail: drkbalan@gmail.com

T. G. Sitharam et al. (eds.), *Geocells*, Springer Transactions
in Civil and Environmental Engineering,
https://doi.org/10.1007/978-981-15-6095-8_18

Table 18.1 Natural fibre properties as a percentage of polyester values [Bisanda and Anselm (1992)]

Type of natural fibre	Tenacity	Failure elongation	Tensile modulus
Abaca	156	12	278
Coir	33	20	33
Cotton	76	20	78
Flax	111	12	211
Hemp	100	12	222
Henequen	56	20	167
Jute	89	8	189
Ramie	118	16	167
Sisal	89	12	222
Viscose	44	80	56
Wool	33	140	22
Polyster (Base 100)	100	100	100

It can be easily blended with man-made fibres too. Its low cost makes it attractive for geotechnical applications.

The ultimate strength, extension at failure and tensile modulus of various natural fibres have been expressed as a percentage of the values for polyester are presented in Table 18.1 to understand the similarity of technical characteristics. From the table, it is clear that;

1. Many natural fibres have similar ultimate strengths to polyester.
2. The rupture strain of natural fibres is much smaller than that of polyester.
3. The tensile moduli of many natural fibres are significantly higher than that of polyester.

However, in order to utilize the foregoing advantageous properties in engineered design, the biodegradability behaviour should be accounted for within any design methodology. Hence, the real key to developing geosynthetics from biodegradable natural fibres is the concept of designing by function, i.e., identifying the functions and characteristics required to overcome a given problem and then selecting appropriate fibres and manufacturing the product accordingly.

The potential of coir as a geocell material, made of closely woven coir mat, especially to reinforce the soft subsoil to carry the embankment load has been reported in this chapter. In this study, investigation is carried out on the reinforcing efficiency of coir geocells within a homogeneous soft clay bed supporting a square footing. The dimensions of geocells such as total width, height and pocket size were varied with respect to the size of footing to arrive at the most effective dimensions of coir geocells in improving the bearing capacity of soft soil. The behaviour of coir geocell in improving the bearing capacity of soft soil is compared with that of synthetic geocells of similar dimensions.

Table 18.2 Nomenclature used

Nomenclature	
b	Width of geocell layer
B	Width of footing
s	Settlement
h	Thickness of the overlying fill layer
u	Thickness of the cover layer
d	Pocket width of geocell
I_f	Bearing capacity improvement factor

The nomenclatures used in this chapter are presented in Table 18.2.

18.2 Materials and Test Set-Up

18.2.1 Materials

In this study, geocells made of coir geotextiles were used to confine the soil above the soft clay bed made of kaolinitic clay. Geocell was filled with river sand.

The properties of materials used for the study are given in Tables 18.3, 18.4, 18.5, 18.6 and 18.7. Geocells with coir geotextiles were made similar to the size and shape of the synthetic geocells as shown in Table 18.7 (Balan and Sreelekha 2016, 2018, Jency and Balan 2014, 2015).

Table 18.3 Properties of kaolinitic clay

Description	Value
Specific gravity	2.43
Soil classification	MH
Liquid limit (%)	54.5
Plastic limit (%)	44.0
Plasticity index (%)	10.5
Percentage of clay (%)	74.5
Maximum dry density (g/cc)	1.30
Optimum moisture content (%)	34.0
Coefficient of consolidation (cm^2/sec)	1.03×10^{-3}
Coefficient of compressibility (m^2/kN)	0.66×10^{-4}
Compression index	0.23

Table 18.4 Properties of sand

Description	Value
Specific gravity	2.61
Coefficient of uniformity (C_u)	1.80
Coefficient of curvature (C_c)	1.04
Effective particle size, D_{10} (mm)	0.28

Table 18.5 Properties of coir geotextile

Description	Value
Coir geotextiles specification	Woven; Panama weave; M2R3 as per Coir Board Specification.
Thickness (mm)	7.77
Mass per unit area (gsm)	1267
Opening size (cm × cm)	0.538 × 0.28
Tensile strength (kN/m)	11.28

Table 18.6 Properties of synthetic web

Description	Value
Material	Compound of various Polyethelenes
Polymer density (g/cm^3)	0.935–0.965
Environmental stress crack resistance (hrs)	>500
Nominal sheet thickness (mm)	1.30 (minimum)

Table 18.7 Cell/section properties of synthetic geocell

Synthetic cell/section properties					
Property		Unit	SW330	SW356	SW445
Cells			3 × 3	3 × 3	2 × 2
Weld spacing		mm	330	356	445
Cell depth		mm	100 and 200		
Expanded cell dimensions	Width	mm	244	259	320
	Length	mm	210	224	287
Overall dimension	Width	mm	732	777	640
	Length	mm	630	672	574

18.2.2 Test Set-Up

Model tests were conducted in a test bed-cum-loading frame assembly in the laboratory. The soil beds were prepared in a test tank with inside dimensions of 1000 mm ×

1000 mm × 1000 mm. The model footing used was made of a rigid square steel plate and measured 200 mm size (L × B) and 20 mm thickness. The footing was loaded with a hydraulic jack supported against the reaction frame. A schematic diagram of the test set-up is shown in Fig. 18.1. A specimen of coir geocell developed to ascertain the optimum size is depicted in Fig. 18.2. Synthetic and coir geocell are shown in Figs. 18.3 and 18.4.

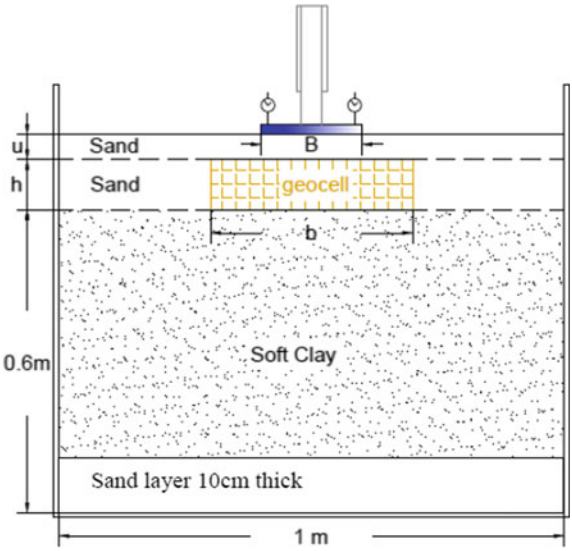

Fig. 18.1 Schematic diagram of test set-up

Fig. 18.2 Sample of geocell with coir geotextile for optimum size determination

Fig. 18.3 Synthetic geocell as reinforcement

Fig. 18.4 Coir geocell similar to synthetic geocell as reinforcement

Preparation of clay beds

For the entire experiment programme, the height of soft soil bed is kept constant at 60 cm. Sand layer of 10 cm thickness was formed at the bottom of the tank for allowing drainage from the clay bed above. Clayey soil was first pulverized and then mixed with water. The water content was kept near to the liquid limit so that the soil is used in soft condition. The density of soil at this water content was considered as the average of loose and compacted densities of soil with the same water content. Soil mixed with water was placed in the tank in layers. For each layer, the required amount of soil to produce the calculated density was found out and compacted up to the required height. By carefully controlling the water content and compaction, a fairly uniform test condition was achieved throughout the test programme. The properties of clay bed are given in Table 18.8.

Table 18.8 Properties of clay bed

Description	Value
Moisture content (%)	50
Unit weight (kN/m^3)	16.3

Preparation of reinforced beds

To prepare the natural geocell mattress, coir geotextile was cut into strips of required length and height from full rolls, and then sides of strips were stitched. After placing the geocell mattress on top of the compacted clay bed in the correct position, the geocells pockets were filled with fine to medium sand at 70% relative density and a unit weight of 15.6 kN/m^3 using sand raining technique. The height of fall to achieve the desired relative density was determined by performing a series of trials with a different height of fall.

Test Procedure

Surface of the fill was levelled and the footing plate was placed at the centre of the tank. Loads were applied through a hydraulic jack and the load transferred to the footing was measured using a pre-calibrated proving ring. Footing settlements were measured using two dial gauges placed on either side of the centre line of the footing.

Four different series of tests were carried out by varying different parameters such as width (b), height (h) and pocket size (d) of geocell mattress. The height of sand layer above the geocell mattress (u) was kept constant in all the tests as 0.1 times the width of footing as it gives maximum performance [Dash et al. (2001)]. Two different series of tests were conducted to evaluate the comparative performance of coir geocell with similar synthetic geocells.

The details of laboratory model tests are given in Table 18.9.

18.3 Results and Discussion

The performance improvement and comparison due to the provision of synthetic and natural fibre geocells are made using a non-dimensional improvement factor (I_f) which is defined as the ratio of footing pressure (q_c) with fill material or geocell at a given settlement to the corresponding pressure on unreinforced soil (q_0) at the same settlement. If the footing on unreinforced soil has reached its ultimate capacity at a certain settlement, the bearing pressure (q_0) is taken as the ultimate value (q_{ult}) while calculating I_f at higher settlements.

Table 18.9 Details of laboratory model tests

Test series	Type of reinforcement	Details of test parameters	Remarks
A	Unreinforced	Variable parameter:$h + u$ = 0 cm, 7 cm, 12 cm, 17 cm, 22 cm, 27 cm constant parameter: ID = 70%	Medium to fine sand layer of varying thickness
B	Geocell mattress	Variable parameter: b = 20 cm 40 cm 60 cm, 80 cm, constant parameters: h = 10 cm, d = 10 cm, u = 2 cm	Geocell of varying width
C	Geocell mattress	Variable parameter: h = 5 cm, 10 cm, 15 cm, 20 cm constant parameters: b = 60 cm, d = 10 cm, u = 2 cm	Geocell of varying height
D	Geocell mattress	Variable parameter: d = 5 cm, 10 cm, 15 cm, constant parameters: b = 60 cm, h = 20 cm, u = 2 cm	Geocell of varying pocket size
E	Geocell mattress with planar geotextiles	b = 60 cm, h = 20 cm, u = 2 cm, d = 10 cm.	Geocell with 60 × 60 × 20 cm with pocket size 10 × 10 cm
F	SW330, SW356 and SW445 of synthetic geocell and with coir geocell of similar dimensions	$h + u$ = 12 cm (height of geocell h = 10 cm)	Fill material medium to fine sand
G	SW330, SW356 and SW445 of synthetic geocell and with coir geocell of similar dimensions	$h + u$ = 22 cm (height of geocell h = 20 cm)	Fill material medium to fine sand

18.3.1 Effect of Width of Geocell Mattress—Test Series B

The bearing capacity improvement factor (I_f) with respect to 12 cm thick sand cushion against foundation settlement ratio (s/B) for test series B, varying the width of geocell, is shown in Fig. 18.5. For geocell of total width 20 cm, equals to the size of plate (b/B = 1), bearing capacity improvement is found to be less than that of 12 cm thick sand layer. Bearing capacity increases with increase in total width of geocell. When the (b/B) ratio is greater than 3, the improvement is found to be marginal. Hence, the ideal situation has been taken as b equal to 3 B, i.e., the total width of the geocell is 60 cm. The improvement factor becomes almost asymptotic after 15% of foundation settlement.

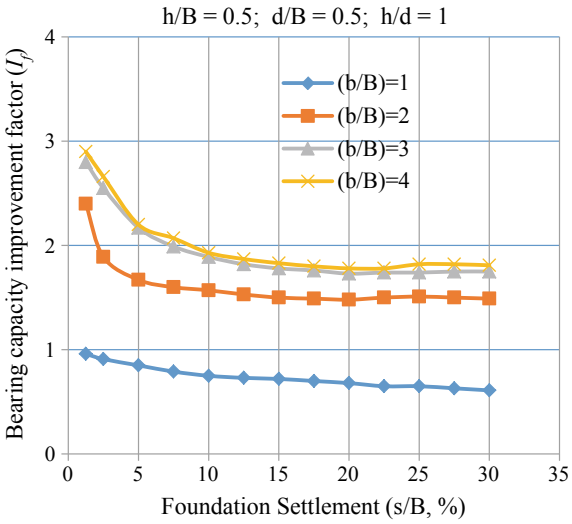

Fig. 18.5 BC improvement factor with foundation settlement for test series B

The bearing capacity has been increased by about 1.80 times that of 12 cm sand cushion alone. The increase in bearing capacity with 3 B size of geocell was found to be 4.90 times that of soft soil alone. Geocell made from synthetic geogrid has shown an increase inI_f of about 3 times that of sand cushion bed of equivalent size as reported by Dash et al. (2003). However, it can be noted that geocells made from geogrid gives the above performance when the total width of geocell is 4 times that of loading plate. In the case of geocell made of coir, the increase in I_f by 1.80 times is achieved with geocells having a total width of 3 times that of loading plate. Even though such a difference has been noticed between synthetic and natural fibre geocells, a clear comparison has its own limitations owing to the difference of soft clay bed used in both studies.

The settlement and heave of the clay bed from the centre line of loading plate for various width of geocell under 20 kPa load are shown in Fig. 18.6. As the total width of geocell increases, the settlement and heave decreases. The decrease in settlement and heave between the 60 and 80 cm wide geocell is found to be marginal. From the above results, the total width of geocell was fixed as 60 cm for further studies.

18.3.2 Effect of Height of Geocell Mattress—Test Series C

In this series, the height of geocell has been varied from 5 to 25 cm with a sand cushion of 2 cm above the geocell. The bearing capacity improvement factor with respect to corresponding sand layer thickness against foundation settlement ratio for test series C is shown in Fig. 18.7. From Fig. 18.7, it can be observed that as the height of geocell increases the bearing capacity improvement factor also increase till

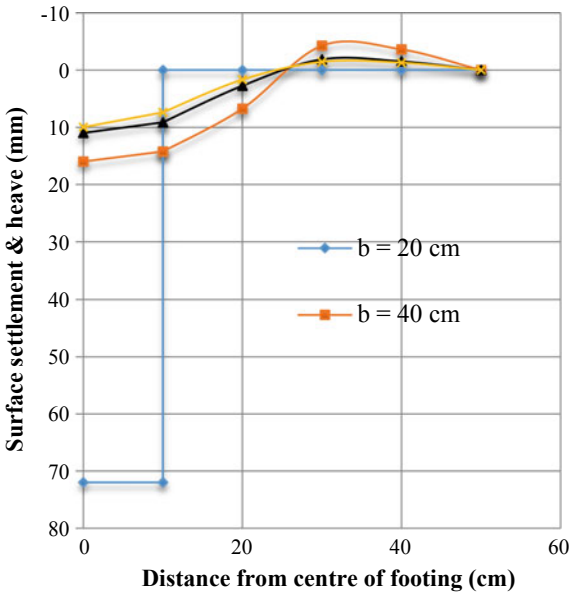

Fig. 18.6 Settlement and heave of clay bed at 20 kPa—test series B

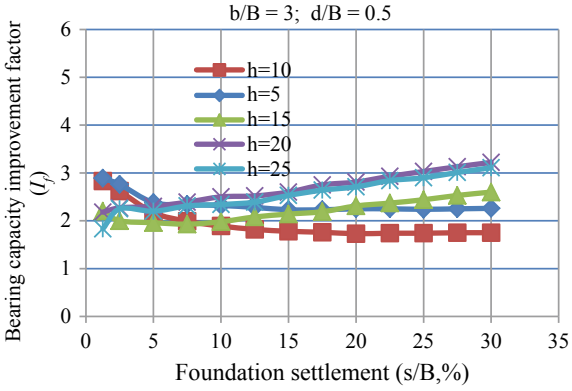

Fig. 18.7 BC improvement factor with foundation settlement for test series C

the height of geocell (h) is 20 cm, i.e., h/B equal to 1 and h/d equals 2. The maximum improvement for 20 cm height geocell at 15% settlement was found to be 2.6 times with that of 22 cm thick sand layer and about 10.5 times with that of clay layer alone. As per Sitharam et al. (2005) and Dash et al. (2001), the carrying capacity of the soft soil has been increased by 4.8 times and 8 times that of the unreinforced soil in the case of synthetic geocells.

Settlement and heave of clay bed at 50 kPa load are shown in Fig. 18.8. From the figure, it can be seen that surface heaving and settlement reduces with increase in height of geocell mattress. The settlement and heave effect seems to be similar for 20 and 25 cm height of geocell. Hence, the optimum height of coir geocell is fixed

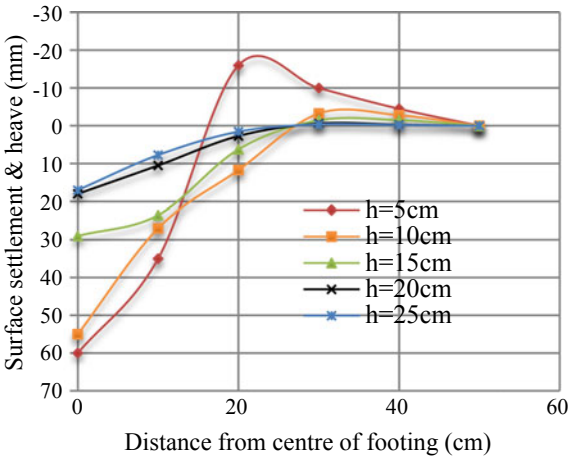

Fig. 18.8 Settlement and heave of clay bed at 50 kPa—test series C

as width of loading plate. In the case of synthetic geocell, the optimum obtained was 2 times the width of loading plate Dash et al. (2003).

18.3.3 Effect of Pocket Size of Geocell Mattress—Test Series D

From the above two series of testing the coir geocell size has been fixed as follows; total length and width of 60 cm, height of 20 cm. In this series, the size of pocket has been changed keeping the other parameters constant. The bearing capacity improvement factor with respect to 22 cm thick sand cushion against the settlement ratio is given in Fig. 18.9.

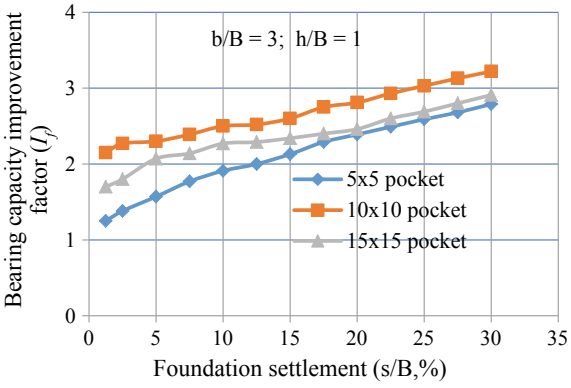

Fig. 18.9 BC improvement factor with foundation settlement for test series D

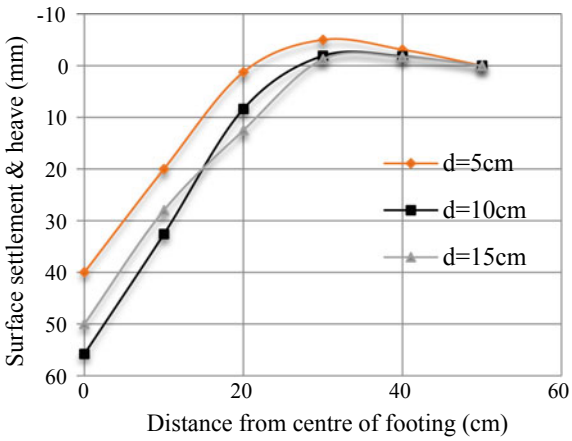

Fig. 18.10 Settlement and heave of clay bed at 120 kPa—test series D

The bearing capacity improvement factor found to increase as the pocket size increases from 5 × 5 cm and reaches a maximum at 10 × 10 cm, i.e., d equal to half the size of loading plate (0.5 B). In the case of synthetic geocells, it has been reported as 0.8 B. Hence, the ideal size of coir geocell can be fixed as follows; length, 60 cm; width, 60 cm; cell size of 10 × 10 cm and height 20 cm.

Settlement and heave of clay bed for various pocket size is shown in Fig. 18.10. Heaving is observed in the clay layer at the outer edges of coir geocell in all the three cases. However, the heave occurred for pocket size of 10 cm and 15 cm were almost the same.

In all the above cases, no failure of geocell was observed even up to a settlement of 30% of footing width. The carrying capacity of the soft soil has been increased by 10.5 times with coir geocell of 600 mm × 600 mm × 200 mm having cell size of 100 mm × 100 mm.

18.3.4 Effect of Planar Geotextile with Geocell—Test Series D

The effect of providing a planar geotextile under the geocell, at the interface of the clay bed and sand cushion, was studied in this series.

The load-carrying capacity of coir geocell (60 × 60 × 20 cm with pocket size of 10 × 10 cm) with respect to that of a planar coir geotextile at the interface of clay bed and sand layer has been explored. Figure 18.11 shows the bearing capacity improvement factor (I_f) with respect to the foundation settlement. Planar reinforcement with coir improves the bearing capacity factor (I_f) by about 1.9 times with that of sand 22 cm sand bed. The figure also shows the improvement in bearing capacity factor (I_f) when the coir geocell is provided with a planar coir geotextile at the base. It can be

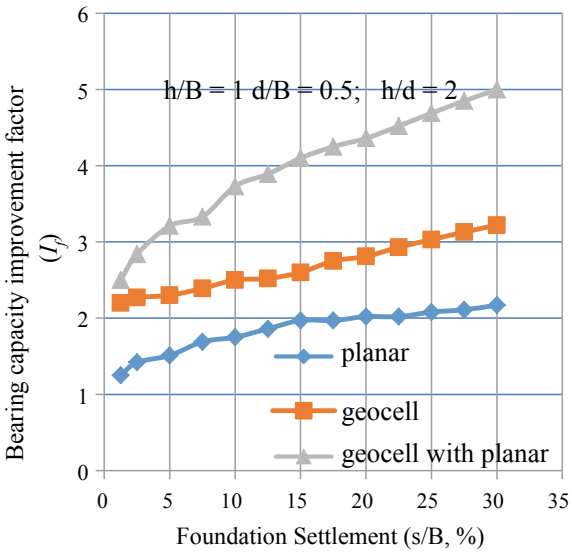

Fig. 18.11 BC improvement factor with foundation settlement for geocell with planar reinforcement—test series E

observed that the bearing capacity factor is improved by 4 times that of sand bed and 16 times with that of clay bed alone.

Settlement and heave of clay bed with planar coir geotextile is shown in Fig. 18.12. Heaving of the sand bed was observed near the edge of the loading plate when planar geotextile alone was used. Whereas, for coir geocell and geocell with planar geotextile, no heaving of sand bed was observed.

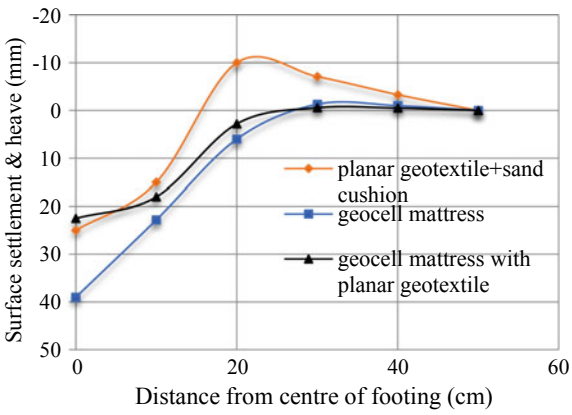

Fig. 18.12 Settlement and heave of clay bed at 90 kPa—test series E

18.3.5 Comparative Performance of Geocells of SW330; 100 Mm High

Geocell of SW330 has 3 × 3 cell and having an overall size of 732 mm (L) × 630 mm (B) and 100 m height. Cell size of 244 mm × 210 mm. Bearing capacity improvement factor (I_f) with respect to sand bed, and that for both the geocells of SW330 is shown in Fig. 18.13. Settlement and heave at the surface of the clay layer after the test is given in Fig. 18.14.

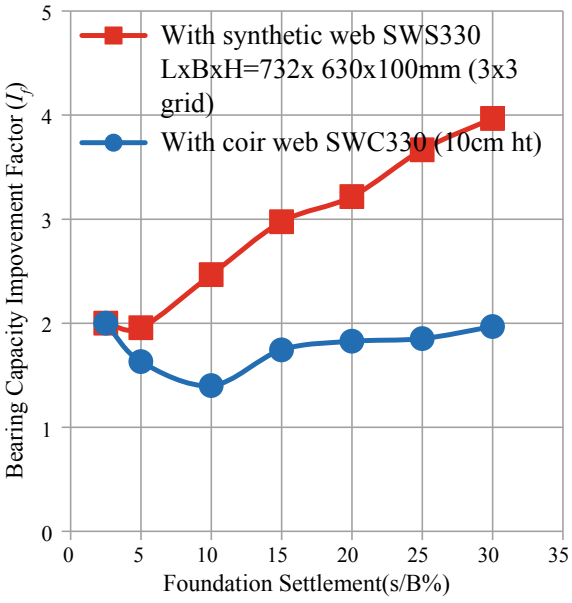

Fig. 18.13 Bearing capacity improvement factor (I_f) for soil bed reinforced with SWS330 and SWC330 of 10 cm height with respect to unreinforced sand bed

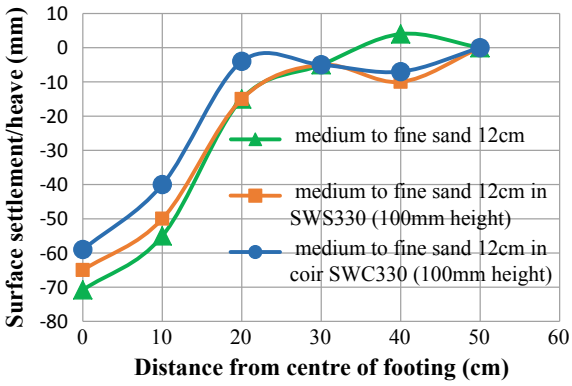

Fig. 18.14 Settlement or heave at surface of clay bed for SW330; 100 mm

From Fig. 18.13, it can be seen that synthetic geocell with fine to medium sand as fill material has a higher bearing capacity factor with respect to the fill material. The bearing capacity improvement factor was found to be 2 and 4 for coir and synthetic geocells, respectively. The increase in bearing capacity factor was marginal after a settlement of 15% of the size of footing in coir geocells, whereas in synthetic geocell, it goes on increasing with increase in percentage of settlement. No heaving on the surface of clay bed is observed for both synthetic and coir geocells. Heaving was observed without geocell reinforcement in the fill material. Provision of geocell of both synthetic and coir reduces the settlement compared to that of fill material alone. Settlement was found to be higher in synthetic geocell than that due to coir geocell.

18.3.6 Comparative Performance of Geocells of SW356; 100 Mm High

Geocell of SW356 has 3 × 3 cell and having an overall size of 777 mm (L) × 672 mm (B) and 100 m heigh. Overall size of the geocell was higher than SW330. Cell size of 259 mm × 224 mm, i.e., cell size is larger than SW330. Bearing capacity improvement factor (I_f) against settlement and settlement or heave at the surface of the clay bed are shown in Figs. 18.15 and 18.16.

As the cell size increases; the bearing capacity improvement factor reduces for both synthetic and coir geocells as established by earlier studies. Up to 15% of footing settlement in coir geocell, bearing capacity improvement factor varies, and thereafter it is almost constant. For synthetic geocell, a steady increase in bearing capacity factor is visible as the settlement increases. Bearing capacity improvement factor is 2.85 and 1.80, respectively, for synthetic and coir geocells, i.e., a reduction of 29 and 10% in the improvement factor, respectively, for synthetic and coir geocell, when the cell size is increased by 6% than that of SW330. Settlement and heaving behaviour was similar to SW330, with coir geocell showing a lesser settlement compared to synthetic geocell.

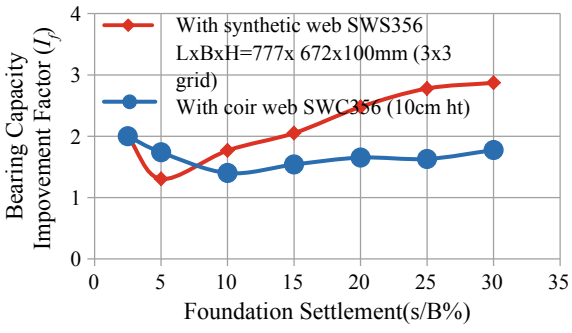

Fig. 18.15 Bearing capacity improvement factor (I_f) for soil bed reinforced with SWS356 and SWC356 of 10 cm height with respect to unreinforced sand bed

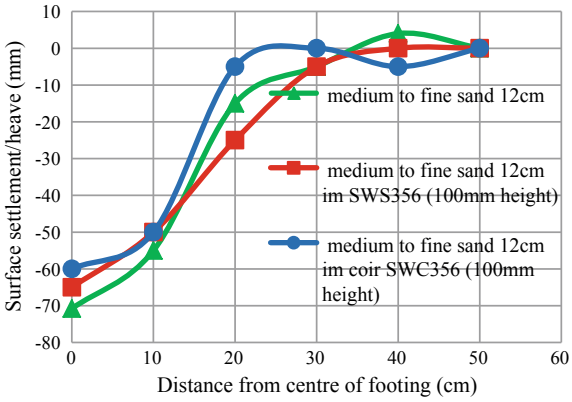

Fig. 18.16 Settlement or heave at surface of clay bed for SW356; 100 mm

18.3.7 Comparative Performance of Geocells of SW445; 100 Mm High

Geocell of SW445 has 2 × 2 cell and having an overall size of 640 mm (L) × 574 mm (B) and 100 m heigh. Overall size of the geocell was less than SW330 and SW356. Cell size of 320 mm × 287 mm, i.e., cell size is larger than SW330 and SW356 series. Cell size is about 33% higher than SW330 and 25% with that of SW356. Bearing capacity improvement factor (I_f) against settlement, and settlement or heave at the surface of the clay bed, are shown in Figs. 18.17 and 18.18, respectively.

The behaviour of both synthetic and coir geocell is same as in the previous cases, with higher bearing capacity improvement factor for synthetic geocell. However, the

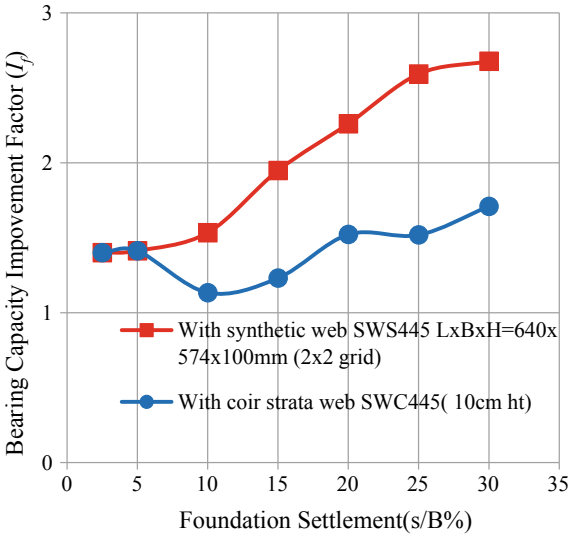

Fig. 18.17 Bearing capacity improvement factor (I_f) for soil bed reinforced with SWS445 and SWC445 of 10 cm height with respect to unreinforced sand bed

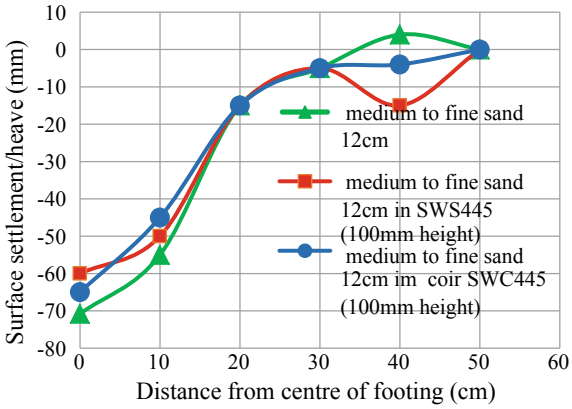

Fig. 18.18 Settlement or heave at surface of clay bed for SW445; 100 mm

improvement factor for both the cases was less than that of SW330 and SW356. It was 2.68 and 1.71 for synthetic geocell and coir geocell, respectively. With respect to SW330, the decrease in improvement factor was about 33% for an increase in cell size of about 33%, whereas with SW356, it was about 6% for an increase in cell size of 25%. For coir geocells, the improvement factor was less by 14 and 5% compared to SW330 and SW356, respectively. Though a general conclusion can be made for the relation between bearing capacity improvement factor and cell size of geocell, a definite relationship could not be established. However, the reduction in bearing capacity improvement factor with increase in cell size and is more predominant in synthetic geocell than coir geocell. Settlement behaviour was found to be same as in the previous cases and there was no heaving at the surface of the clay bed.

18.3.8 Comparative Performance of Geocells of SW330; 200 Mm High

The influence of height in bearing capacity improvement is investigated with same varieties of synthetic and coir geocells with a height of 200 mm.

Figures 18.19 and 18.20 show the bearing capacity improvement factor, and settlement and heave at the surface of clay bed, for SW330 with 200 mm height, respectively. When the height of geocell is increased to double, the bearing capacity improvement factor is increased to 6 times that of unreinforced fill material, i.e., an increase of 50% with that of 100 mm high geocell. In the case of coir geocell, it was increased by 2.44 times, i.e., an increase of 22% when the height of geocell is made to double. The increase in bearing capacity improvement factor with height of geocell is predominant in the case of synthetic geocell than coir geocell. Settlement was found to be less in the case of synthetic geocell than coir geocell when height is doubled. As in the earlier cases, heave was not occurred when the fill is reinforced with geocells.

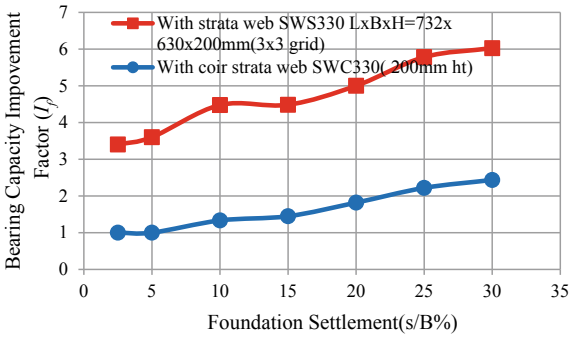

Fig. 18.19 Bearing capacity improvement factor (I_f) for soil bed reinforced with SWS330 and SWC330 of 20 cm height with respect to unreinforced sand bed

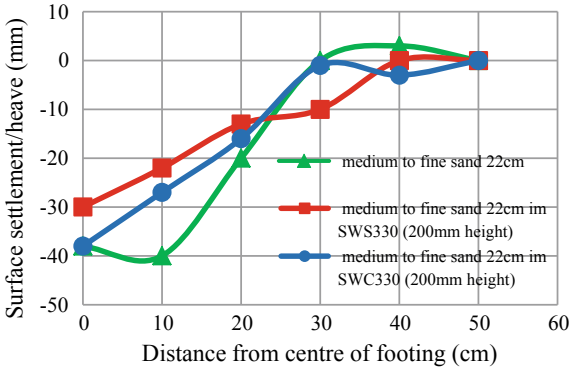

Fig. 18.20 Settlement or heave at surface of clay bed for SW330; 200 mm

18.3.9 Comparative Performance of Geocells of SW356; 200 Mm High

For SW356, for a height of 200 mm, the bearing capacity improvement factor and settlement and heave at surface of clay bed is shown in Figs. 18.21 and 18.22. Synthetic geocell improved the bearing capacity improvement factor to 5.33 and that by coir geocell to 2.28. When the height of geocell is doubled, the bearing capacity is

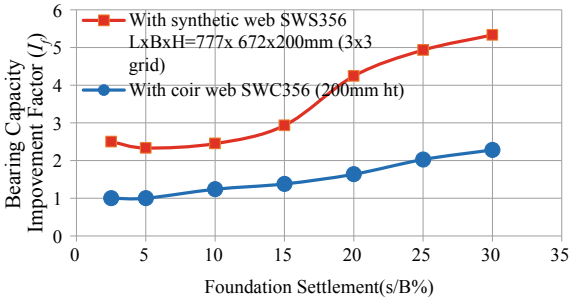

Fig. 18.21 Bearing capacity improvement factor (I_f) for soil bed reinforced with SWS356 and SWC356 of 20 cm height with respect to unreinforced sand bed

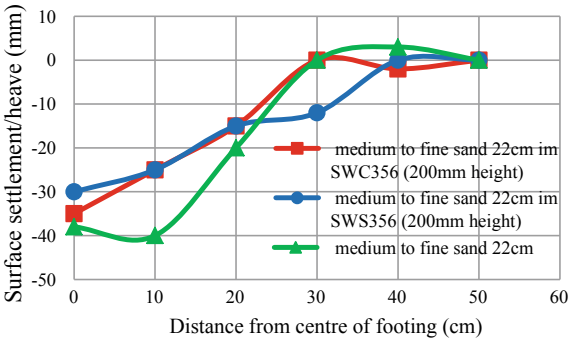

Fig. 18.22 Settlement or heave at surface of clay bed for SW356; 200 mm

increased by 87% and 27%, respectively, by synthetic and coir geocells. The increase in improvement factor is predominant in the case of synthetic geocells. Settlement and heave of surface of clay bed were similar to the previous cases.

18.3.10 Comparative Performance of Geocells of SW445; 200 Mm High

The bearing capacity improvement factor for SW445 when the height is doubled is shown in Fig. 18.23. Settlement and heave at the surface of clay bed are depicted in Fig. 18.24. Bearing capacity improvement factor was found to be 4.50 and 2.20 for synthetic and coir geocells, respectively, when the height of cell is increased to double. The increase was about 68% for synthetic geocell and 27% for coir geocell. As the cell size is increased with 200 mm height, for synthetic geocell, the bearing

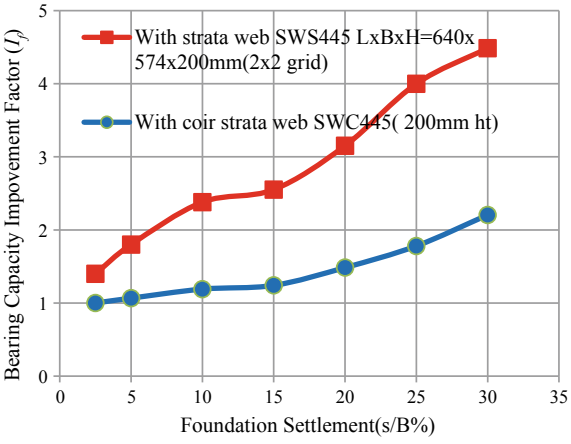

Fig. 18.23 Bearing capacity improvement factor (I_f) for soil bed reinforced with SWS445 and SWC445 of 20 cm height with respect to unreinforced sand bed

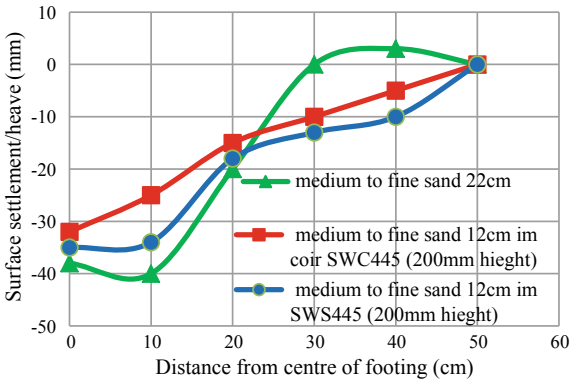

Fig. 18.24 Settlement or heave at surface of clay bed for SW445; 200 mm

capacity was reduced by 33% and 18% with respect to SW330 and SW356, respectively. For coir geocell it was found to be less by 11% with SW330 and almost the same factor for SW356. Settlement was less in coir geocell compared to synthetic geocell and no heave was observed at the surface of clay bed.

18.4 Conclusion

From the model studies, the following conclusions about coir geocells are arrived at;

- Coir geocells with width 3 times the width of loaded area, having height 20 cm and square pockets of 10 cm × 10 cm is the ideal dimension to have the maximum bearing capacity improvement factor.
- It improves the bearing capacity by about 2.6 times with that of the unreinforced sand cushion and 10.5 times that compared with soft clay bed.
- A woven planar coir geotextile at the base of the coir geocell improves the bearing capacity by about 4 and 16 times with that of unreinforced sand cushion and soft clay bed, respectively.
- The effect of cell size and depth of geocell on bearing capacity is more predominant in synthetic than coir geocell.
- Settlement in coir geocell seems to be less compared to that of synthetic geocell.
- Synthetic geocell improves the bearing capacity by 2.5 times more than that by coir geocell.

References

Balan K, Sreelekha B (2016) Effect of coir geocell and fill material on bearing capacity improvement of soft clay—an Experimental Study. Indian J Geosynthetics Ground Impro 5(1):31–37. Indian Chapter of International Geosynthetic Society, CBIP, New Delhi

Balan K, Sreelekha B (2018) Comparative evaluation of geocells with synthetic and natural fibres. In: Proceedings of 11th international conference on geosynthetics, Seoul, Korea

Balan K, Jency A (2015) Improvement of bearing capacity of soft soil using coir geocells. In: International Conference on Geotechnical Engineering ICGE, Colombo, pp 415–418

Bisand ETN, Anselm MP (1992) Properties of Sisal—CNSL composite. J Mater Sci 27:1690–1700

Dash SK, Krishnaswamy NR, Rajagopal K (2001) Bearing capacity of strip footing supported on geocell reinforced sand. J Geotextiles Geomembranes 19:235–256

Dash SK, Sireesh S, Sitharam TG (2003) Model studies on circular footing supported on geocell reinforced sand underlain by soft clay. J Geotextiles Geomembranes 21:197–219

Jency A, Balan K (2014) Behaviour of geocells made of coir in improving the bearing capacity. Indian geotechnical conference, Kakkinada, Andhra Pradesh, India, pp 1498–1505

Sitharam TG, Sireesh S, Dash S K (2005) Model studies of a circular footing supported on geocell reinforced clay. Can Geotech J 42(2):693–703

Appendix

Leading Geocell Manufacturers

1. **A.G.H. Industries, Inc.**
   1103 Stanley Dr.
   Euless, TX. 76040
   Call or fax us:
   Phone (817) 284-1742
   Fax (817) 284-1745
   info@aghindustries.com

2. **ATARFIL EUROPE**
   Ctra. Córdoba km 429
   18230 Atarfe(Granada), Spain
   Tel: +34 958 43 92 00
   Email: comercial@atarfil.com

3. **BOSTD Geosynthetics**
   Qingda Industrial Zone, Chengyang District, Qingdao, Shandong, P.R. China
   Zip Code: 266111
   TEL: +86-532-87806919
   E-mail: marketing@bostd.com

4. **HANES GEO COMPONENTS**
   815 Buxton Street, Winston-Salem, NC 27101-1310, USA
   Toll Free: 888.239.4539 | T: 336.747.1600

5. **HongXiang New Geo-Material Co., LTD.**
   Economic Development Zone of Lingxian County,
   Shandong Province, P.R. China
   Mobile: 0086-18866093555

T. G. Sitharam et al. (eds.), *Geocells*, Springer Transactions
in Civil and Environmental Engineering,
https://doi.org/10.1007/978-981-15-6095-8

6. **Maccaferri**
   Via Kennedy 10
   40069, Zola Predosa (Bologna), Italy
   Ph: +39 051 6436 000
   Fax: +39 051 6436 201
   E-mail: info@hq.maccaferri.com

7. **NAUE GmbH & Co. KG**
   Gewerbestr. 2
   D-32339 Espelkamp-Fiestel
   Germany
   Tel.: +49 5743 41 0
   Fax.: +49 5743 41 240

8. **Presto GeoSystems**
   670 N Perkins Street, PO Box 2399
   Appleton, Wisconsin 54912-2399, USA
   Phone: 800-548-3424: 920-738-1328
   Fax: 920-738-1222
   Email: info@prestogeo.com

9. **PRS Geo Technologies Ltd.**
   66 Prescot Street, E1 8NN London, United Kingdom
   E-mail: info@prs-med.com

10. **Strata Systems**
    1831 North Park Avenue
    Glen Raven, NC 27217-1100 USA
    Phone: 800.680.7750

11. **Taian Road Engineering Materials Co., Ltd.**
    Taiwen Road, Taian City, Shandong, China Tai'an, Shandong, P.R. China
    Phone: 86-538-6626578

12. **TENAX SPA,**
    Via dell'Industria 3, I-23897 Viganò (Lecco), Italy
    Tel. +39 039 92191—Fax +39 039 9219290

13. **TERRAM Global Office**
    A Berry Plastics Company
    Fiberweb Geosynthetics Ltd.
    Blackwater Trading Estate
    The Causeway, Maldon, Essex, UK, CM9 4GG
    Tel: +44(0) 1621 874200
    Fax: +44(0) 1621 874299
    Email: info@terram.com

14. **TMP GEOSYNTHETICS**
No. 32, Jinniushan Road Taian City,
Shandong Province P.R. China 271000
Tel: +86-538-8560690
Fax: +86-538-8560690
info@tmpgeosynthetics.com

15. **TYPAR**
Berry Global, Inc.
70 Old Hickory Blvd.
Old Hickory, TN 37138, USA
800-541-5519
Email: geos@typar.co

16. **Wall Tag Pte Ltd.**
23 Serangoon North Ave 5, #01-01, BTH Centre
Singapore 554530
Tel: (65) 6398 0308
Fax: (65) 6398 0309
Email: enquiries@walltag.com.sg